MSC - 05937

4th ANNUAL EARTH RESOURCES PROGRAM REVIEW

VOLUME II
UNIVERSITY PROGRAMS

Presented at the
Manned Spacecraft Center
Houston, Texas

January 17 to 21, 1972

FOREWORD

A review of various aspects of the Earth Resources Program was held at the Manned Spacecraft Center, Houston, Texas, January 17 to 21, 1972. Particular emphasis was placed on the results of analysis of data obtained with the Manned Spacecraft Center and other aircraft which have contributed data to the program.

The review was divided into the disciplinary areas of Geology, Geography, Hydrology, Agriculture, Forestry, and Oceanography. Program investigators presented the results of their work in each of these areas. The material presented is published in five volumes:

VOLUME I - NATIONAL AERONAUTICS AND SPACE ADMINISTRATION PROGRAMS N72-29302

VOLUME II - UNIVERSITY PROGRAMS

VOLUME III - U.S. GEOLOGICAL SURVEY PROGRAMS N72-29355

VOLUME IV - NATIONAL OCEANIC AND ATMOSPHERIC ADMINISTRATION PROGRAMS AND U.S. NAVAL RESEARCH LABORATORY PROGRAMS N72-29378

VOLUME V - AGRICULTURE AND FORESTRY PROGRAMS N72-29407

The review provided a current assessment of the program for both management and technical personnel. Note that the material presented represents the current status of ongoing programs and complete technical analyses will be available at a later date.

Where papers were not submitted for publication or were not received in time for printing, abstracts are used.

FRONT COVER

The map on the front cover depicts the NASA Earth Resources aircraft coverage of the United States through June 1971.

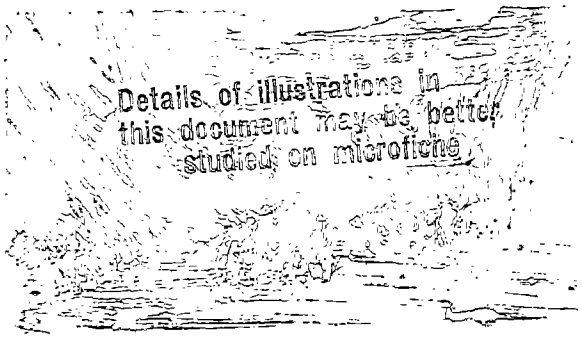

CONTENTS OF VOLUME I

CONTENTS OF VOLUME II

CONTENTS OF VOLUME III

CONTENTS OF VOLUME IV

CONTENTS OF VOLUME V

SECTION 28

A SUMMARY OF MICHIGAN PROGRAM FOR EARTH RESOURCES INFORMATION SYSTEMS

N72-29328

by

Jon D. Erickson
Willow Run Laboratories
The University of Michigan
Ann Arbor, Michigan

INTRODUCTION

This paper is a summary of and guide to the NASA-sponsored program carried out in 1971 at The University of Michigan's Willow Run Laboratories in earth resources information systems which employ multispectral remote sensing. The objectives of this program are to improve automatic techniques for extracting information from multispectral scanner data about the amount, location, and condition of remotely sensed objects of user interest and to reduce the costs of achieving such information on an operational (or research) basis from aircraft and satellites such as ERTS or SKYLAB - in short, to achieve a practical tool for planners and decision makers.

The program has four major areas of activity as shown in the table below:

1. Improved Throughput Parallel Processing Systems
2. Improved Processing Techniques
3. Show Practical Use in User Applications
4. Improved Sensors

The first area is a program to achieve substantially improved throughput from special purpose, parallel processing systems for multispectral data. The second area consists of a series of investigations directed at improving the machine processing techniques and our understanding of them. The third area is a series of programs with various investigators from user agencies to exploit the techniques developed to date in demonstration applications of practical interest to users, which also generally extend the usefulness of these techniques. Finally, the fourth area is improving experimental sensors for earth resources applications, both multispectral scanners in the 0.4 - 14 μm region and multispectral imaging radar with X- and L- bands.

In this paper I will summarize the status of these four areas of research, the activities of the past year in the area of improved throughput processing systems, and cite one result from the processing techniques improvement area. Four of the papers following this one by authors from the Willow Run Laboratories (WRL) will present results from this information extraction technique development area. As shown in Table I these are the papers by W. Malila, G. Suits, R. Nalepka, and R. Vincent. Results from the user applications of data processing will be presented in the paper by F. Thomson. Improved experimental sensors are discussed in the papers by P. Hasell and L. Porcello.

Eleven reports [Ref. 1 - 11] will be issued on the work of this past year, in addition to journal articles and papers. During the course of the paper, I shall refer to these reports so that those interested in details will have the references.

IMPROVED THROUGHPUT PARALLEL PROCESSING SYSTEMS

The assessment of current multispectral processing systems to meet the needs of keeping pace with multispectral data acquisition which occurs typically at rates of hundreds of kiloHertz or megaHertz is given in the table below:

1. Sensor capability exceeds processing capability by large factors

2. Digital and analog implementations of present techniques will not keep pace with needs of many operational-prototype information systems

3. Multiple computer approach may be too costly

4. Hybrid implementation of special purpose parallel processing with improved techniques appears promising from both throughput and cost aspects but requires development

Presently available conventionally organized digital computers are too slow (with current algorithms) by orders of magnitude so that even many computers per sensor are still inadequate. A parallel processing analog computer at Michigan meets the data rate requirement, but is slow to set up reducing the average throughput. Parallel processing all-digital computers may become useful and practical for image processing in the future but are not yet competitive. However, the programmability of the digital computer combined with the high throughput calculation rate of parallel channel analog computers in a hybrid multispectral processor, which we are beginning to build at the WRL with NASA support, appears to offer a realistic way now to breakup the processing bottleneck caused by data collection capability far outstripping processing capability in terms of both throughput and cost. Figure 1 indicates the present and projected multispectral data capability as various sensors begin to operate, [Ref. 12].

These are the Michigan multispectral scanner (M-5) and new Michigan single aperture scanner (M-7), the NASA 24-channel Multispectral Data System, and the ERTS-A multispectral scanner. The maximum planned rates are about 10-15 billion data elements per week.

Data quantities of this rate are impressively large but the cost to process the data is not well known. Some rough idea of the costs of data processing per element and per square mile are shown in Figure 2. The Corn Blight Watch multispectral processing costs using analog and digital computers separately were somewhere between $100 and $200 per square mile indicating the achievement of a feasibility type processor system. The impact of these costs can be assessed if some typical applications are analyzed. Some are given in Figure 3. The Corn Blight multispectral processing costs for 50 square miles were not $42,000/week but about $5,000 to $10,000 per week again indicating progress beyond research processor costs. The practical impact of cost reduction by proceeding to prototype or operational equipment is easy to project and will be quite dramatic. I feel that costs of a few dollars per square mile for processing are achievable. Using the projected data capacities and research processing costs of $420 per square mile, Figure 4 shows the cumulative cost picture where the continued rise in costs is the accumulated cost as various sensors are introduced and used. The 2 breaks in the cost curve in 1972 and 1973 indicate the cost leveling effect of the introduction of prototype processor at either of these points in time. Development of a prototype processor is expected to take two years, however.

We have investigated the possible design alternatives for such a prototype processor of the hybrid parallel processing type and are beginning its implementation. Figure 5 shows a component diagram for such a system which indicates the various types of units that are involved. Figure 6 indicates the various functions that are performed and some estimate of the time required in terms of factors of real time meaning acquisition rate for a typical multispectral scanner. One of the major variables which we need experience with to bring under control is the man-machine interaction with this type of processor. Some of the benefits derived from achieving such a prototype processor are listed below:

1. Facilitate research and development
2. Meets the needs of prototype data processing demands
3. Allows projection of operational costs
4. Defines operational requirements for personnel and equipment
5. Reduces present costs

It will facilitate further research and development, making it dramatically quicker and less costly to experiment with different techniques and applications. Because this parallel processor meets the needs of prototype data processing demands, projected data collection over the near future can be processed in a timely fashion. Projection of operational requirements and costs will be more accurate and present costs can be reduced. We see the hybrid as an improvement, not necessarily a breakthrough or panacea, but a needed improvement nonetheless. It may also speed the day of on-board processing for aircraft and satellites.

A particular point of view must be preserved: that of the information needs of the problem-oriented user. The fact that the user of such data is not directly concerned with the techniques or physical parameters of sensing and processing but is, rather, interested in mapping, identifying and studying specific objects on the surface of the earth and the interrelationships of these objects, must be foremost in the conception and implementation of these information systems. The user would like to know, for example, how many bushels of wheat and corn will be produced in a county of so many acres, how many ducks will be successfully raised in the prairies, how much water is needed to preserve the Everglades and where are and what are the various sources of pollution for Lake Michigan, Lake Ontario, or Chesapeake Bay.

Data processing, it should be noted here, refers to the procedures, algorithms, and computations which are applied to the raw sensor output data to transform it into useful information to the user. Data processing includes the combination of (1) data formatting, handling, editing, digitizing, or film printing with (2) data reduction and analysis consisting of image enhancement, spectral analysis, signature correlations, and recognition computations. Care in understanding the scope of data processing is required because the term can mean only (1) above, thereby leaving out data reduction, analysis and recognition (or classification) which are critical to the user as information extraction processes.

IMPROVED INFORMATION EXTRACTION TECHNIQUES

I would like to proceed now to summarize my assessment of the status of the 2nd area of activity in our program, namely processing techniques or information extraction techniques. The table below indicates the judgement that a variety of useful techniques have been demonstrated to be feasible in various applications under limited conditions appropriate to showing feasibility but not generally appropriate to prototype or pilot operational conditions.

1. Variety of techniques are feasible in many applications under limited conditions

    a. Constrained data collection to minimize effects of resolution, atmosphere, and changing illumination

    b. Little or no time constraint for processing

    c. Maximum ground observation

2. These limitations are being lessened to the point where operational-prototype information systems are feasible in some applications

This transferral of present techniques to prototype environments is needed and requires effort to solve problems which arise that are not otherwise evident. The Corn Blight Watch pressured conditions (1b) and (1c) in the table above by imposing a time constraint of less than one day per 10 square mile segment processed and reported and reducing the amount of ground data collected. Aircraft data collection costs can be reduced by relaxing the constraints on sun angles and cloud cover percentage presently imposed by processing techniques limitations.

Further technique development is clearly required. The thrust of our activities in this area has been the development of techniques that allow the reduction of required ground observations and that extend spectral signatures in space and time away from these known areas. The fundamental barrier to signature extension to large areas has been variations in the environment. These variations are manifested, both spatially and temporally, as changes in atmospheric transmission, illumination of the scene, bidirectional properties of the materials, and atmospheric path radiance or backscatter. The table below outlines several areas where we are working at improving processing techniques:

1. Extending the Applicability of Training Sets
2. Spectral Signatures and ERSIS
3. Modeling and Simulation
4. Ratio Processing
5. Parameter Mapping
6. Proportions of Classes
7. Adaptive Techniques
8 Mensuration and Mapping

Extending the applicability of training sets away from known areas has been studied previously at WRL using 3 approaches: (1) the use of preprocessing transformations on the remotely collected multispectral data aimed at reducing systematic variations; the intent of these transformations is to make the data invariant despite variations in transmission, illumination, and path radiance, (2) the use of ancillary sensors in the data collection platform such as the sun sensor to measure illumination, transmission, or path radiance variations, and (3) the use of in-scene references which provide a calibration in the scene that permit corrections to the data are all useful in signature extension and reducing the amount of ground observation required. This year we have extended these studies to modification of the decision parameters, decision rules, and adaptive classifiers.

We have continued our efforts to understand the basic spectral characteristics of various materials so that spectral signatures can be better understood and have added data to the Earth Resources Spectral Information System (ERSIS) installed on the Univac 1108 at the MSC which will aid other investigators in understanding the spectral reflectance, emission, or transmission of natural materials, in determining the spectral channels likely to be of interest in their application, or in devising an appropriate processing technique. Dr. David Pitts of the Earth Observations Division at the NASA/MSC has responsibility for user requests for laboratory or field spectral data in ERSIS.

ERSIS also provides basic data as input to models and simulations of various problems in remote sensing applications. Dr. Suits' model for predicting the directional reflectance from vegetative canopies given in a following paper is an example of the use of spectral reflectance data as an input to derive important insight. Our efforts in each of the other areas listed in the table above and the significant progress made will be discussed in papers following, except for the adaptive techniques area which I will turn to now.

ADAPTIVE MULTISPECTRAL PROCESSING

I would like to present one preliminary result of some interest from the work on adaptive classifier techniques by Bob Marshall, Frank Kriegler, and Wyman Richardson of our staff, [Ref. 13]. Figure 7 shows a comparison between two different classifiers recognizing wheat (shown as the darkest tones) in a 4 or 5 mile long agricultural scene. The map on the left half shows the result of using a single distribution (that from field A) in a maximum likelihood classifier to recognize wheat and shows a gradual deterioration in recognition over the run from bottom (South) to top (North). The reason for this deterioration was determined to be a change in illumination due to changeable atmospheric conditions. A simple algorithm to adapt the means of the distribution in an exponentially weighted fashion when points are recognized as wheat was added to the maximum likelihood classifier. The results of this adaptive multispectral

processing are shown on the map on the right half. The improvement in recognition accuracy using this adaptive classifier is apparent.

Some increase in false classification occurs in two oat fields just below the two small wheat fields in the left center of the run. Since only the means of wheat were being adapted rather than all distributions some capture of the process by other distributions was expected and exists.

A simple experiment was also conducted to determine the ability of the algorithm to recover, given a transient error. The set of means obtained at the end of the run in field B were used as an initial estimate for field A and a classification run was made which is shown in Figure 8. No difference exists after 600 points, twice the weighting constant of 300.

While not all sources of error in classification are correctable by adaption those remaining after preprocessing transformations have reduced the systematic variations may be largely corrected. It appears that a considerable processing gain may be obtained from adaption of distribution parameters and we intend to pursue this vigorously. In terms of a digital classifier, the speed of classification may be improved as a direct function of the number of distributions eliminated from the classifier in exchange for a simple mean adapting computation. For analog and hybrid processors, the complexity and size of the machine may be reduced.

It is possible to relate the results obtained in modeling the scene and the radiative transfer in the atmosphere to the adaptive recognition process. This makes it possible to use models to describe the general trends for the trajectories of distributions and to make corrections as functions of the agreement between observed changes and the predicted trajectories.

PRACTICAL USE OF EXISTING TECHNIQUES IN USER APPLICATIONS

I now want to assess the status of the 3rd area of our program, user applications. It is the benefits in user applications which is the raison de etre of the entire Earth Resources Survey Program. As shown in the table below the potential of multispectral sensing and automatic processing has been demonstrated.

1. Many applications in a variety of user disciplines have been demonstrated to be feasible under limited conditions.
2. Operational-prototypes may be feasible in some applications from both technical and cost aspects
3. No operational use is yet being made of information

A large number of user applications of Multispectral Earth Resources Information Systems have been demonstrated to be feasible in scaled down programs and we are ready to examine ERTS data with confidence of what has been accomplished from aircraft. Some applications are further advanced than others and operational prototypes should be exercised next for some of these. However, no operational use is yet being made of any information system on Earth Resources employing multispectral sensing, I believe largely because they must become cost effective first.

IMPROVED SENSORS FOR EARTH RESOURCES APPLICATIONS

The status of multispectral sensors technology is assessed in the table below:

1. Improved experimental airborne MS scanners are now in use and the quality of data in the UV, visible, near IR, and thermal IR is generally excellent

2. Operational airborne MS scanners are commercially available

3. Spaceborne MS scanners will be utilized for the first time in ERTS and SKYLAB

4. Experimental airborne multispectral imaging radar is being developed

5. Experimental laser scanners are planned

The comments here basically indicate the mature and advanced state of this area. However, despite the attempts that have been made to date at systems engineering of complete information systems including user needs, sensors, and processors a more complete systems approach will be needed for multispectral sensing based information in the future.

CONCLUSIONS

Despite making substantial progress in achieving improved processing techniques, improved throughput parallel processing systems, improved experimental sensors for multispectral sensing, and showing the practical use of multispectral sensing in various earth resources applications, there is still much to be accomplished before the Earth Resources Survey Program spins off successful, operational user information systems. Potential benefits of information will remain largely "potential" until this is done.

The most critical need is for processing systems capable of keeping pace with the sensors so that unprocessed data does not have to be accumulated and stored. Greatly reduced costs of processing are also likely to result with an attendant increase in interest on the part of potential users.

But greatly reduced dependency on ground observations is also needed to reduce both the costs of collection and processing. For this reason continued research in pursuit of improved processing techniques which allow less ground data and multi-stage sampling approaches are required. Our signature extension and other information extraction technique development is aimed at this goal.

Spectral reflectance, emittance, and transmittance data on a great variety of natural materials are available to the remote sensing community through ERSIS. This data can be used to define the approach to many remote sensing problems by understanding the spectral basis of discrimination.

We are ready to examine ERTS and Skylab EREP data with confidence of what can be done from aircraft.

REFERENCES

(1) J. Erickson, "Research on Operational Earth Resources Information Systems Using Multispectral Sensing", 31650-89-P, in publication.

(2) W. Malila, et.al., "Information Extraction Techniques", 31650-74-T, in publication.

(3) W. Malila, "Discrimination Techniques Employing Both Reflective and Thermal Multispectral Signals", 31650-75-T, in publication.

(4) R. Nalepka, et.al., "Estimating Proportions of Objects From Multispectral Data", 31650-73-T, in publication.

(5) R. Vincent, "Rock-Type Discrimination From Ratio Images of the Pisgah Crater, California Test Site", 31650-77-T, in publication.

(6) V. Leeman, "NASA Earth Resources Spectral Information System: A Data Compilation, Supplement", 31650-69-T, in publication.

(7) V. Leeman, "NASA/MSC Earth Resources Spectral Information System Procedures Manual, Supplement", Informal Technical Report, 31650-72-T.

(8) R. Vincent, "Investigation of Theoretical Methods for the Optical Modeling of Agricultural Fields", 31650-78-T, in publication.

(9) F.J. Thomson & R.F. Nalepka, "Contribution to the Corn Blight Watch Final Report", 31650-104-L, January 1972.

(10) W.G. Burge, "Summary of Ground Observations of Selected Corn Blight Segments in Indiana", 31650-105-L, in publication.

(11) L. Larsen & P. Lambeck, "Performance of MSDS as of 18 August 1971", 31650-82-T, September 1971.

(12) R.E. Marshall & F.J. Kriegler, "An Operational Multispectral Surveys System", Proceedings of the 7th International Symposium on Remote Sensing of Environment, Ann Arbor, Michigan, May 1971, 10259-1-X.

(13) R.E. Marshall, et.al., "Adaptive Multispectral Recognition of Wheat Fields", 31650-86-S, EAI Symposium on Automatic Photointerpretation, Washington, D.C., December 7-8, 1971.

TABLE I.- PAPERS IN THE UNIVERSITY OF MICHIGAN SESSION OF FOURTH ANNUAL EARTH RESOURCES PROGRAM REVIEW

IMPROVED PROCESSING TECHNIQUES

W. Malila	-	Information Extraction Techniques for Multispectral Scanner Data
G. Suits	-	Prediction of Directional Reflectance of a Corn Field Under Stress
R. Nalepka	-	Classification of Spatially Unresolved Objects
R. Vincent	-	Experimental Methods for Geological Remote Sensing

SHOW PRACTICAL USE IN USER APPLICATIONS

F. Thomson	-	User-Oriented Multispectral Data Processing at The University of Michigan

IMPROVED SENSORS

P. Hasell	-	Michigan Experimental Multispectral Scanner System
L. Porcello	-	Multispectral Imaging Radar

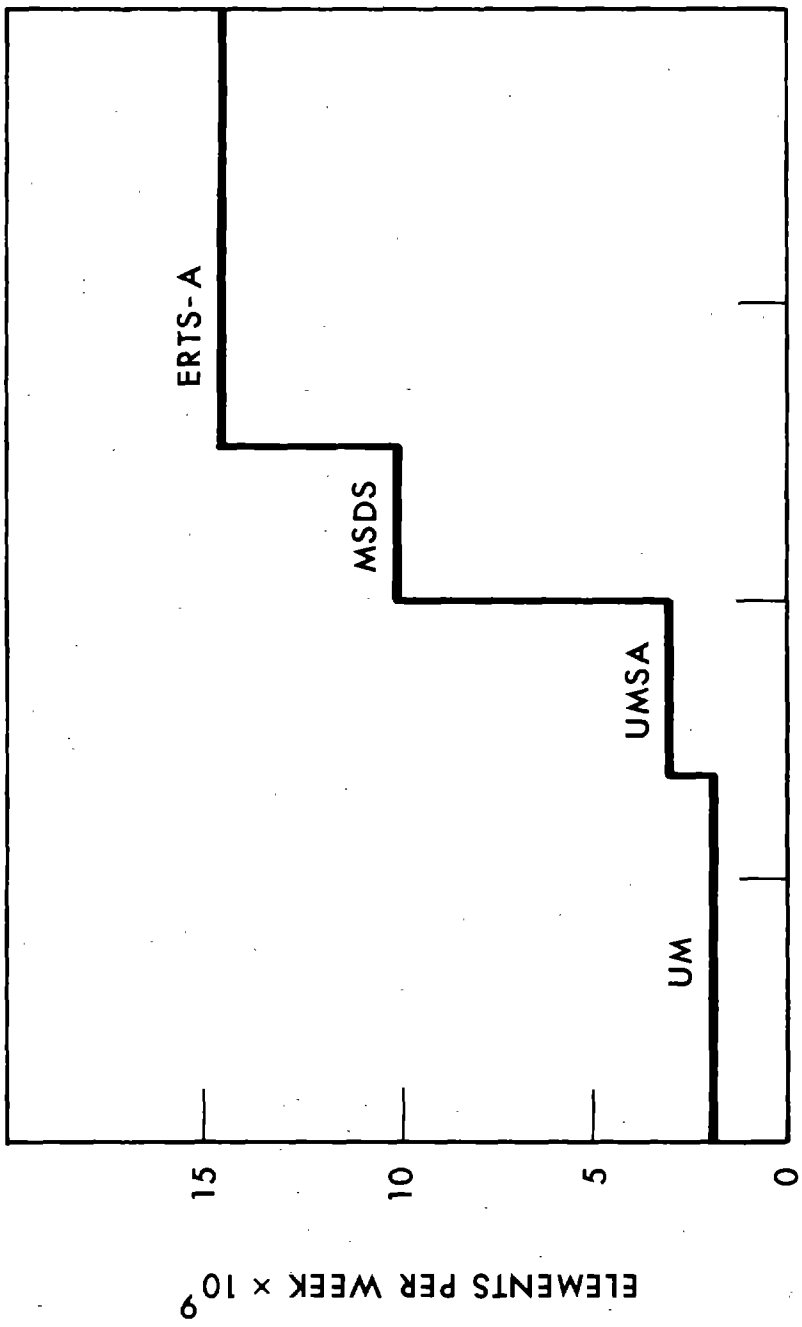

FIGURE 1. MULTISPECTRAL SCANNER DATA RATE CAPABILITIES

FIGURE 2. OPERATING COST OF PROCESSING

	$/ELEMENT	$/MI^2	HOURS/MI^2
RESEARCH	130×10^{-6}	420	2
FEASIBILITY	60×10^{-6}	195	1
PROTOTYPE	3×10^{-6}	10	0.05
OPERATIONAL	1×10^{-6}	3	0.02

JOB	AREA SIZE	RESEARCH PROCESSOR COST	PROTOTYPE PROCESSOR COST
SURVEY AGRICULTURAL COUNTY	36 sq. mi.	$15,000	$360
CORN BLIGHT SURVEY	100 sq. mi./wk.	$42,000/wk.	$1000/wk.
EVERGLADES SURVEY	4000 sq. mi./yr.	$1,680,000/yr.	$40,000/yr.
TYPICAL USER REQUEST	20 sq. mi./wk.	$8400/wk.	$200/wk.

FIGURE 3.

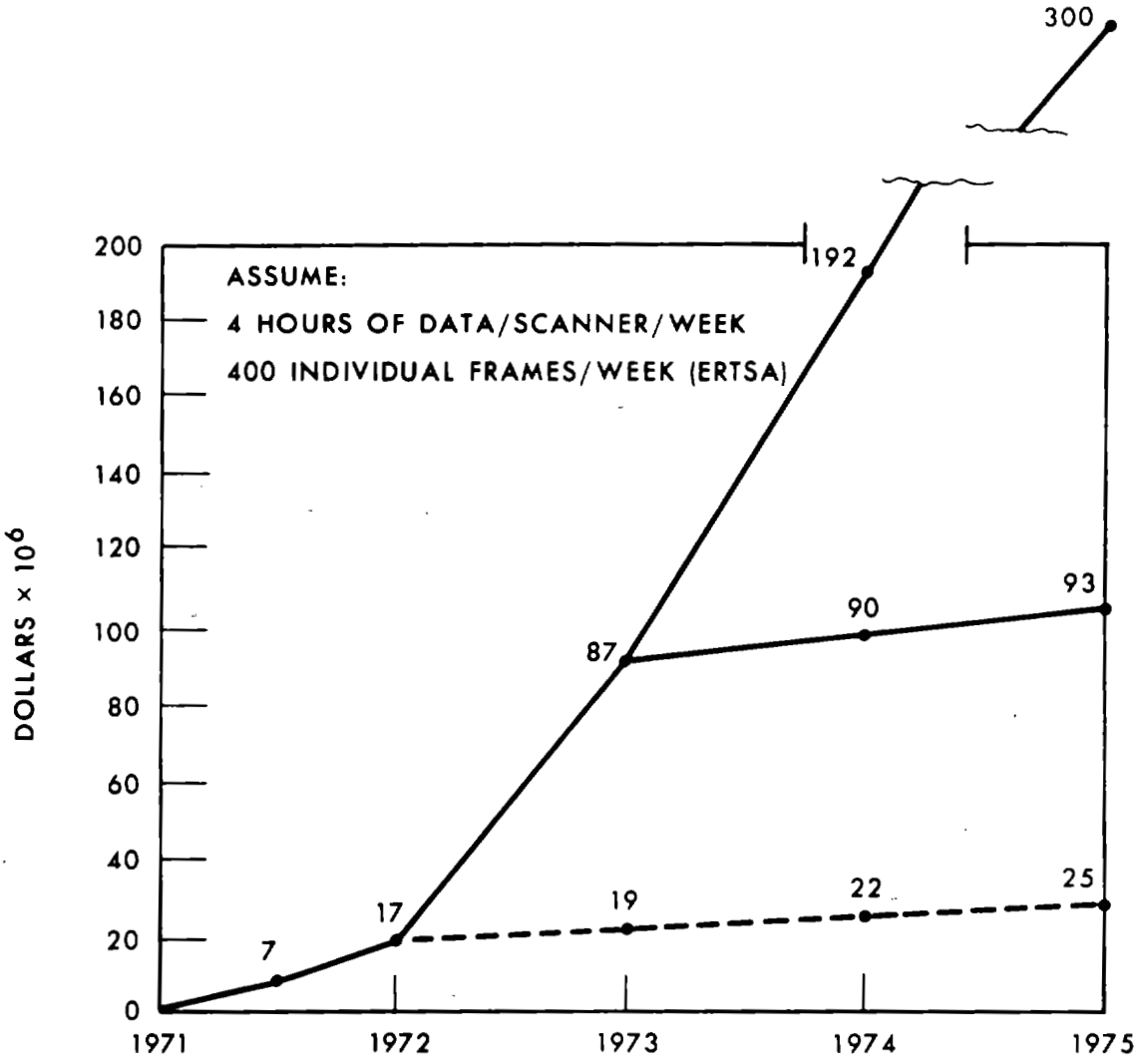

FIGURE 4. CUMULATIVE PROCESSING COST OF MULTISPECTRAL DATA

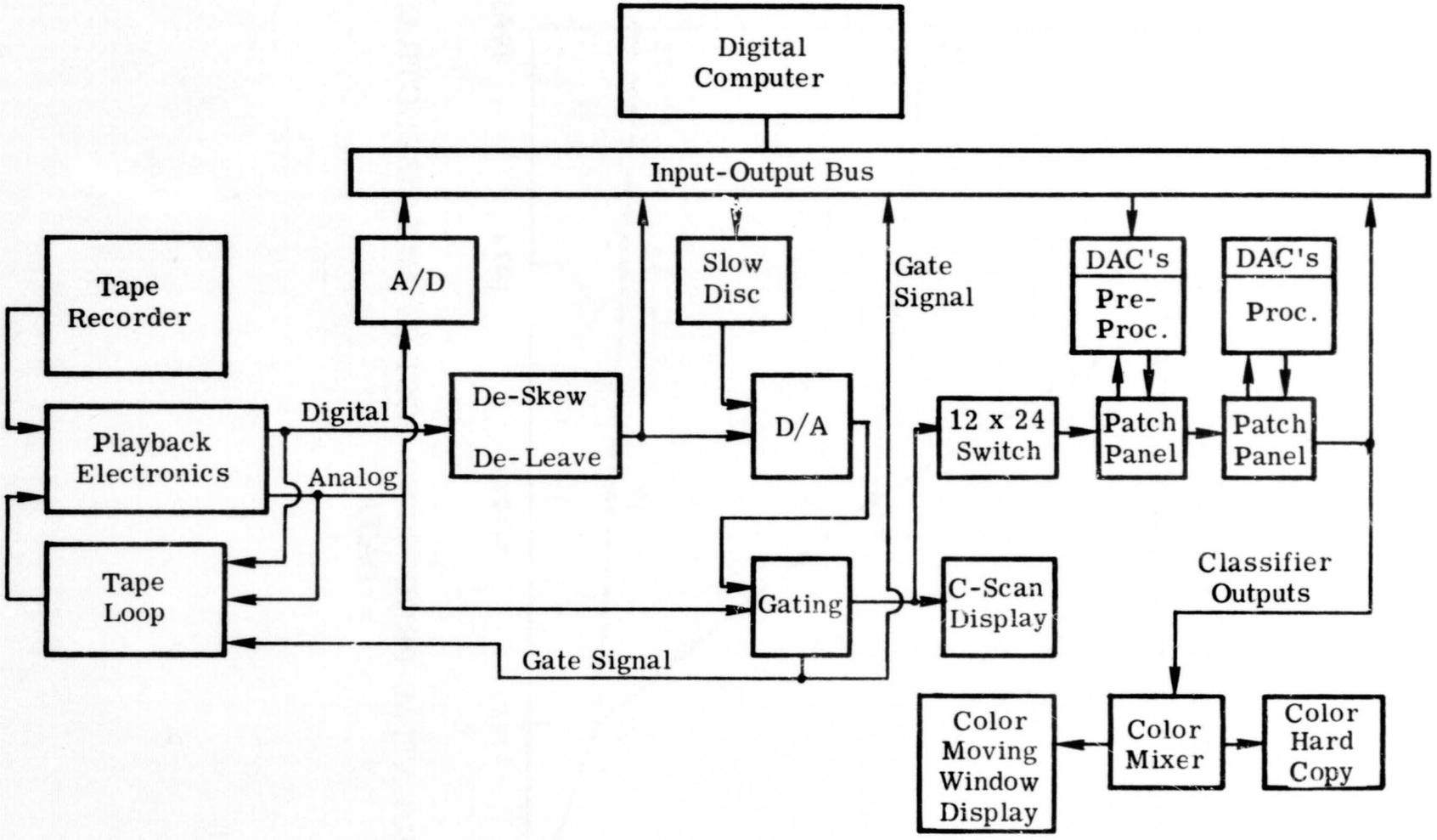

FIGURE 5. BLOCK DIAGRAM OF COMPLETE HYBRID PROCESSING SYSTEM

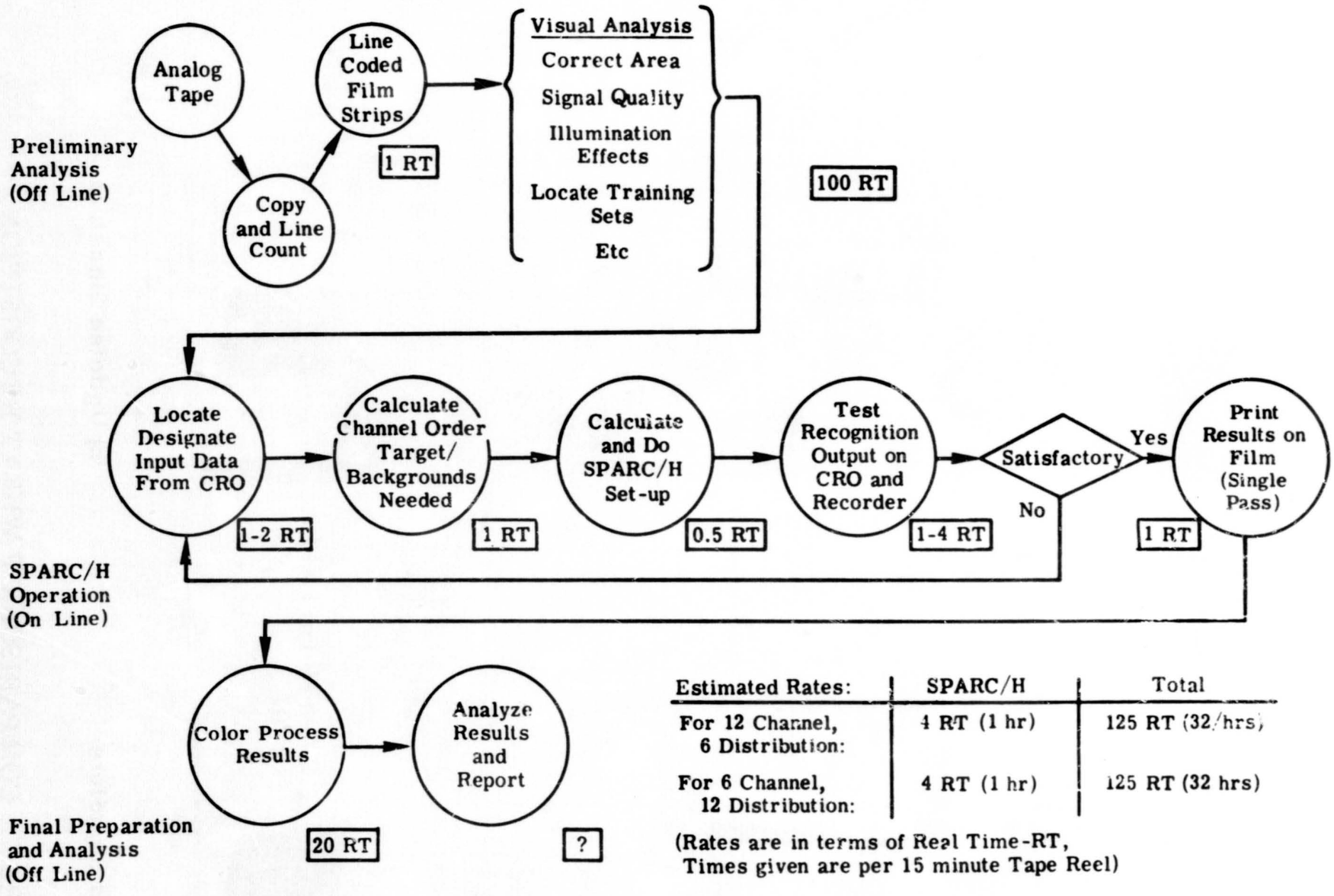

Estimated Rates:	SPARC/H	Total
For 12 Channel, 6 Distribution:	4 RT (1 hr)	125 RT (32 hrs)
For 6 Channel, 12 Distribution:	4 RT (1 hr)	125 RT (32 hrs)

(Rates are in terms of Real Time-RT, Times given are per 15 minute Tape Reel)

FIGURE 6. SPARC/H PROCESSING FLOW AND TIMING CHART

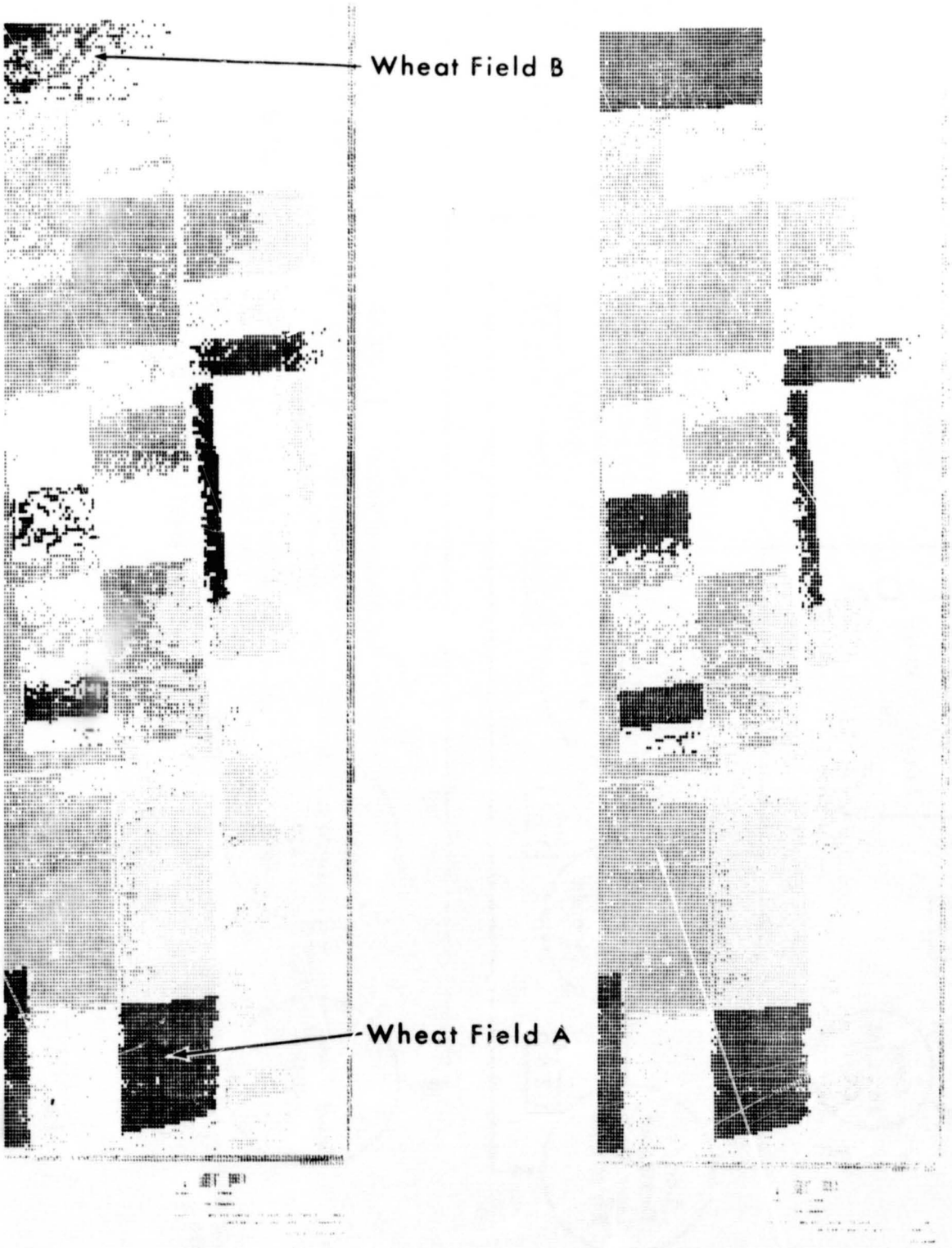

(a) Fixed Signature (b) Updated Signature

FIGURE 7. COMPARISON OF WHEAT RECOGNITION RESULTS FOR FIXED AND ADAPTED SIGNATURES

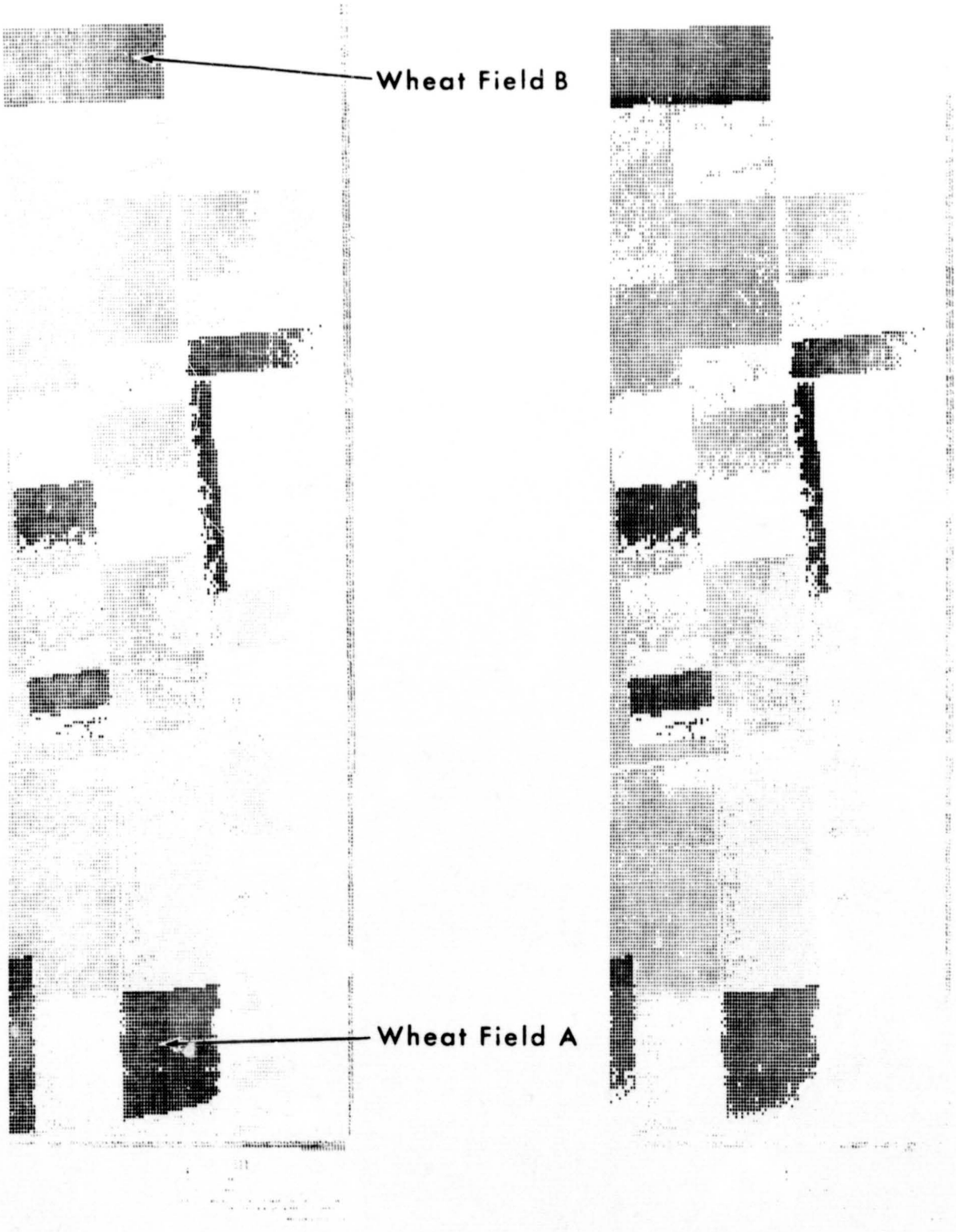

(a) Initial Signature From Wheat Field A

(b) Initial Signature Using Previous Update

FIGURE 8. WHEAT RECOGNITION RESULTS SHOWING THE CONVERGENCE OF THE ADAPTED SIGNATURE

INFORMATION EXTRACTION TECHNIQUES FOR MULTISPECTRAL SCANNER DATA

by

William A. Malila, Robert B. Crane,
Wyman Richardson, Robert E. Turner
Willow Run Laboratories
The University of Michigan
Ann Arbor, Michigan

INTRODUCTION

This paper summarizes some of the work during 1971 at the Willow Run Laboratories that has been directed toward four information extraction problems: (1) signature extension for improved recognition processing over large areas, (2) the choice of density functions for recognition decision rules, (3) channel selection for cost reduction, and (4) radiation balance mapping for interpretation of wide-spectrum scanner data. The details of these studies are reported in References 1 and 2.

Signature extension and cost reduction are problems that must be solved if the promise of large-area surveys of Earth resources and man's impact on his environment are to be realized. The techniques presently in use are limited in their ability to provide recognition and other information extraction with sufficient accuracy, timeliness, and cost effectiveness to make operational uses a practical reality. These techniques should be improved and refined for use on data from both aircraft and spacecraft.

A two-pronged approach is being followed in the development of techniques to overcome the degradation of recognition accuracy that occurs because systematic variations in scanner data cause the signatures obtained from training areas to be different from data collected farther in time and/or space from the training areas. The first is a theoretical approach to examine the sources of variation in scanner data and gain insight for improved techniques by the simulation of scanner radiance signals. The second is a more empirical approach for the development of preprocessing techniques to remove systematic effects from scanner data so that large areas can be surveyed accurately with a minimum of ground-truth information.

Preprocessing has been under development at Michigan as one method for removing systematic effects from scanner data before recognition processing (Fig. 1). During last year's meeting, Mr. Legault discussed some of the methods that we have explored [3]. These include the transformation of data (such as by ratioing signals), the use of data from a sky sensor on

the aircraft, and the use of in-scene reference areas to develop corrections for signature extension. At Michigan, preprocessing was used during 1971 in the processing and analysis of Corn Blight data [4] and in data processing tasks for various users [5]. In this paper, a generalized preprocessing technique that has been developed and tested during 1971 is discussed [1,6].

Multispectral recognition decision rules use likelihood functions of the various material classes. Our second area was an investigation into the suitability of the normal (Gaussian) likelihood functions for these decision rules as opposed to empirical likelihood functions.

In the third problem area, cost reduction, we improved our procedures for selecting a subset of channels or features for use in the recognition processor. Our digital channel selection procedures use a criterion that can be formulated as an average probability of misclassification, a quantity with direct physical interpretation. Our most exact procedure is time consuming and this negates some of the cost advantage gained by reducing the number of processing channels. However, we have recently developed a much faster method by making use of a linear approximation in our calculations.

In the fourth area, we endeavor to use the full spectrum of scanners for interpretation aspects of multispectral remote sensing. Energy budgets are of interest in many studies of natural and agricultural areas, and they also are being used increasingly in urban studies. Since net radiation is the most important component of an energy budget and the scanner measures the apparent outgoing radiation, procedures for producing maps of the outgoing radiation, and the net radiation or radiation balance were developed and applied.

EXAMINATION OF SYSTEMATIC VARIATIONS BY SIMULATION

Figure 2 lists some sources of variation in multispectral scanner signals that are associated with conditions of measurement (such as atmospheric haze and the position of the sun) and parameters of measurement (such as the scan geometry and the sensor characteristics). Although not listed, there also are variations associated with the characteristics of the surface materials being observed, such as inhomogeneities and bidirectional reflectance characteristics. While both systematic and random variations are listed, the systematic variations are the ones that most seriously reduce the recognition accuracy away from the training areas.

Last year, a theoretical radiative transfer model was developed at Michigan to simulate multispectral scanner signals [7]. This model characterizes the spatial and spectral distribution of radiation in Earth's atmosphere as a function of several parameters and conditions of measurement. During the past year, the model was improved, extended, and used to simulate scanner radiance signals and other radiometric quantities and their systematic variations under a wide variety of conditions [1,8].

One of the major improvements made in the model was the incorporation of time as an independent parameter which allows us to simulate temporal variations that would be present in area survey data. Another is the use of exact scattering phase functions in our calculation procedure which has increased the accuracy to the point where our calculations agree well with measurements of sky radiance and with theoretically exact calculations based on Chandrasekhar's theory.

The next nine figures present graphs that are representative of the model's ouput and illustrate the sources of systematic variation in scanner data. Figure 3 shows the dependence of transmittance on scan angle for four different visual ranges. V=2 km corresponds to a dense haze and V=23 km represents a normal clear day (bordering on a light haze). The airborne scanners generally collect data at scan angles of ±45° or smaller, and it is clear that the path transmittance for these angles varies substantially. The transmittance and all other quantities depend on the altitude of the observer, and the data in this figure are for an altitude of 3 km. While all of the data presented herein are for aircraft altitudes, the model also can be used to simulate data collected from spacecraft.

Irradiance is another quantity of interest. Figure 4 shows the spectrum of the irradiance that would be detected by a sky sensor on an aircraft flying at an altitude of 1 km. Note the increase in levels for the hazy condition, that is, for short visual ranges. Information of this sort is of value in using the sky sensor signals for signature extension.

Next consider the downlooking scanner. Not all the radiation that reaches the scanner originates at the surface element being viewed. There is a quantity called path radiance, which is extraneous radiation that is scattered into the field of view by the atmosphere.

Figure 5 shows that path radiance depends strongly on visual range and wavelength. The wavelength dependence is much different than that for the irradiance shown in Figure 4. The reason for this difference is that path radiance depends on the reflectance spectrum of the material being viewed. In this instance, the spectrum is that of green vegetation.

Path radiance also depends on the nadir scan angle and the location of the sun. Figure 6 shows the scan-angle dependence of path radiance for three different sun positions on a very hazy day. The scan plane includes the sun, and one readily can see the characteristic peak in backscattered radiance at the antisolar angle. When the scan plane does not include the sun, the path radiance is a much more symmetric function of scan angle. Figure 7 shows how path radiance would vary throughout one day if the aircraft were flying East or West at an altitude of 1 km on a medium hazy day. The scan is in the North-South plane. Note the increase and decrease of the radiance at any given scan angle as the time changes throughout the day. Also note the increase in path radiance at noon when the sun moves into the scan plane. This type of information is useful for planning flight lines.

A scanner measures the total radiance from the view direction; thus, the atmospheric effects of path radiance and transmittance are both present in its signals. Figure 8 simulates the total radiance that would be received by the scanner from a diffusely reflecting surface with the reflectance spectrum of green vegetation. A comparison of Figures 7 and 8 shows that the path radiance is a substantial component of the total received radiance. Both figures show the large and systematic changes in signal level that are associated with time of day, that is, with sun position.

Now, let us examine the scan angle dependence more closely. Figure 9 presents a comparison between experimental measurements of sky radiance and calculated values for three different surface albedos. Note the excellent agreement between the shapes of the experimental and the calculated curves of sky radiance. We also compared total radiance calculated with the model and total radiance measured by our scanner for several fields of soybeans. The data are presented in Figure 10. One immediately notes the difference in angular response. We believe that much of this difference is due to the surface reflectance characteristics. The simulation model assumed a perfectly diffuse, or Lambertian, surface, whereas results presented in this volume on reflectance modeling of corn [9] and results of other investigators show that agricultural crops, like soybeans, do have definite bidirectional reflectance characteristics. We are presently modifying our model to include such reflectances.

To complete this part of the discussion, two graphs that depict interdependencies of radiation quantities as functions of time of day are presented. Figure 11 presents the ratio of the total downward irradiance at an altitude of 5 km to the total irradiance at the Earth's surface. We see that the irradiance at the aircraft is slightly greater than on the ground, and becomes more so with an increase in haze below the aircraft. There is relatively little change in the ratio for two hours either side of solar noon when conditions are clear (V=23 km), but the time dependence for that interval increases for shorter visual ranges. In all cases, there is strong time dependence during early morning and late afternoon hours. This type of information can be helpful in using sky sensor signals for signature extension.

The second interdependence, presented in Figure 12, is the ratio of path radiance to total radiance. These curves clearly show that path radiance is a large fraction of the total radiance, especially for very hazy conditions. The important point of Figure 12 is that, for reasonably clear days, the ratio of path radiance to total radiance is essentially constant for several hours at mid-day for a given atmospheric condition and a fixed surface albedo. This fact should be of value in the development of techniques to remove atmospheric effects from data. It is worth noting that the difference between atmospheric effects at an altitude of 5 km and at low altitude is greater than between 5 km and space altitudes.

TECHNIQUES FOR OVERCOMING SYSTEMATIC VARIATIONS

The simple physical model that has been used in our analysis is as follows:

$$L(\theta, i, j) = \rho'_{ij} E_j(\theta) T_j(\theta) + L_{pj}(\theta) + L_{nj} \qquad (1)$$

where L is the radiance signal,
i denotes the class of ground cover being scanned,
j denotes the spectral channel,
θ is a vector that describes the parameters and conditions of the measurement,
ρ'_{ij} is the bidirectional reflectance of the surface (for a diffuse surface, $\rho'_{ij} = \rho_{ij}/\pi$, where ρ_{ij} is the diffuse or directional reflectance),
E_j is the irradiance in channel j,
T_j is the corresponding atmospheric transmittance,
L_{pj} is the path radiance in channel j, and
L_{nj} is the noise-equivalent radiance in channel j.

Equation (1) has exact physical meaning only when the reflectance of the surface is diffuse and, consequently, has no angular dependence. However, for preprocessing, one can define a generalization in which angular dependence is allowed.

As can be seen in Equation (1), the atmosphere contributes both an additive term, L_p, the path radiance, and a multiplicative term, T, the transmittance. From this, we conclude that, in general, a preprocessing transformation should include both additive and multiplicative correction functions. Our general preprocessing transformation, called the U-V transformation, meets this requirement.

The operating principle of this transformation is one of adjusting a signal, $L(\theta)$ to $L(\theta_o)$, the value it would have had, had it been measured under a reference set of conditions represented by θ_o. That is,

$$L(\theta_o) = L(\theta)U(\theta) + V(\theta) \qquad (2)$$

where $L(\theta_o)$ is the radiance at reference condition, θ_o,
θ is a vector quantity that denotes conditions and parameters of measurement, and
$U(\theta)$ and $V(\theta)$ are correction functions that are independent of the material classes.

Clearly, $V(\theta)$ is the additive correction function and $U(\theta)$ is the multiplicative one.

There are several systematic or deterministic effects for which the technique potentially can correct; these include scan angle effects, illumination changes along the flight line, cloud shadows, altitude effects, and day-to-day changes in conditions. We will discuss and show examples of corrections only for scan angle effects and altitude effects.

The correction functions, $U(\theta)$ and $V(\theta)$, can be determined either from the data or from model calculations. The simplest empirical procedure for scan angle correction is to select two relatively uniform fields of different reflectance that extend over a common range of scan angles. The solution of simultaneous equations yields the U and V functions. More general ways have been developed and applied.

We determined angle correction function for a data set collected under hazy conditions (at a visual range of $\sim$6 km). Figure 13 presents plots of average signal vs. scan angle for six soybean fields before angle correction was applied. The data cover a scan angle interval roughly $\pm 25°$ from nadir. Even though the ordinate scale accentuates differences, a substantial scan angle effect is evident in all fields. These within-field angle variations mask the between-field differences present in this data set. Figure 14 shows the same six fields after U-V angle corrections were applied. The within-field angle variations have now been reduced to the point where the between-field differences dominate the data set.

An indirect method for testing the ability of preprocessing techniques to remove systematic variations is to perform recognition on data sets with and without preprocessing. Differences between fields used for training and those in other parts of the data set, however, can mask or obscure the improvements produced by the techniques in such a test.

Figure 15 presents a comparison of recognition errors for different treatments of the data sets where, like golf, the smaller numbers signify better performance. The left-hand three data columns are for data collected at an altitude of 1,000 ft and processed with training areas selected from within that data set. The first column gives recognition errors without data smoothing and without preprocessing. The fact that 48% of the fields had less than half their elements identified correctly is a feature of the data set and the way in which the training areas were selected. Only 14% of the fields were incorrectly classified when the majority decision was assigned to the field. As shown in the second column, a smoothing to reduce system noise and element-to-element variation did not appreciably affect the recognition performance here, although it has been useful in other instances. Then, when we examine column 3, we see that the application of the U-V preprocessing transformation produced a substantial reduction in classification errors according to both criteria.

The two columns on the right of Figure 15 represent data collected at an altitude of 5,000 ft. The first of the two used training areas from the 5,000-ft data and no preprocessing. The second used the U-V preprocessing transformation in two ways, one to remove scan angle effects and one to extend training signatures from 1,000 ft to 5,000 ft. The recognition errors resulting from use of 1,000-ft signatures are comparable with those for 5,000-ft signatures. Although the comparison would be less favorable had the 5,000-ft data been preprocessed, the signature extension demonstration is still encouraging.

SUITABILITY OF THE NORMAL LIKELIHOOD FUNCTION FOR RECOGNITION DECISION RULES

Likelihood functions are used in classification decision (i.e., recognition) processes on multispectral scanner data. These functions are usually represented by multivariate normal (Gaussian) density functions, whose statistical parameters are determined for the various decision classes from subsets of the data. Last year, we tested the normality of individual subsets of data corresponding to single fields, and all were found to be non-normal at the 1% level of significance using a standard chi-square goodness of fit test [7]. During the year just ended, we compared two maximum likelihood decision rules on the basis of paired receiver operating characteristic (ROC) curves, one member of each pair representing a multivariate normal decision rule and the other a rule based on an empirical density function. For each data set, an alternative hypothesis was assumed, and the Type I vs. Type II errors (probability of miss vs. false alarm) were plotted for different decision levels for each decision rule; see Figure 16 for a typical pair of ROC curves. From such curves a direct comparison can be made between the two likelihood function decision rules.

The choice of an alternative hypothesis is an important consideration. If we consider the data to be points in a hyperspace, of which each coordinate corresponds to a transformed spectral channel, then the question becomes one of: where in the hyperspace shall we locate the alternative hypothesis? The location and shape of the alternative distribution can be expected to affect the decision errors. A distribution was chosen that was uniformly located in the hyperspace and corresponds to the use of many different separate distributions located uniformly in the hyperspace. Thus, the results correspond to an average of the performance that would be obtained using a large number of separate distributions. This choice of an alternative distribution has the additional advantage of making it possible for one to test each data set individually.

The Type I errors were found by selecting a decision level and counting the percentage of points that were rejected by using first one, then

the other, decision rule. The Type II errors were found by direct calculation. Data points for the alternative were assumed to be located uniformly throughout a hyper-rectangular parallelepiped, the dimensions of which were set so that 0.9995 of the volume of the Gaussian distributions would be included.

As a result of our tests, we have decided that the use of the normal likelihood function for individual fields is justified for recognition processing of multispectral scanner data. This function is much quicker to generate and use than the histogram function. Also, the improvement in performance that would result from using a histogram likelihood function and all of the channels is not believed to be significant. More promising approaches, we believe, are (1) to preprocess the data to compensate for scan angle and similar systematic effects and/or (2) to compensate by changing the decision rule parameters. By using the first approach, we would expect the transformed data to have distributions that are more nearly normal and at the same time, have reduced variances.

CHANNEL SELECTION

Digital recognition processing costs are proportional to the square of the number of channels used for quadratic decision rules so a reduction in the number of channels reduces costs. Analog and hybrid systems can maintain a high throughput rate for any number of channels, but their flexibility and capacity for different material classes are reduced when many information channels are used for recognition.

The principal features of our channel selection procedure are listed in Figure 17. First, we have chosen the Bayesian criterion, average expected loss. It can be formulated as an average probability of misclassification and has a direct physical interpretation.

To make the calculation of this criterion practical, we have had to make a number of assumptions which are straightforward and have been analyzed and verified. First, we assume normal (Gaussian) statistics. Second, we use a pairwise method of calculation, and third, we use a stepwise procedure that successively adds the one channel which gives the lowest average probability of misclassification when used with those already selected.

Recently, we developed a much faster procedure that assumes a linear approximation to the quadratic decision surface which results in a much simpler calculation of the probability of misclassification. The new linear method is 50 times faster than the quadratic method, and its use results in substantial savings while retaining the interpretation feature of the older method. Figure 18 presents a comparison of results obtained with the two procedures for a data set with nine signatures and ten data channels. Note first the difference in time - one hour for the quadratic

method and only 70 seconds for the linear method. Next, we see that the ordering of the channels is the same in both cases for the first six channels. Finally, we see that the average probabilities of misclassification computed by the linear method are in very good agreement with those of the other method.

RADIATION BALANCE MAPPING

Our final study results from the fact that synchronous reflective and thermal data have become available. We now can explore an interpretive use of scanner data in analyzing the energy budgets of vegetation and other surface materials, both man-made and natural. An energy budget is simply a statement of the fact that materials maintained balance in the exchange of energy with their environment. As shown in Figure 19, there is a net amount of radiant energy absorbed by an object, like a plant, from its surroundings. This energy is partitioned into several components. The first component is used in evaporating water such as in transpiration. Other components heat the air around the plant and soil or represent energy conducted away from them. Finally, there is a net energy conversion component which usually is small by comparison. From this partitioning of net absorbed radiant energy, it is clear why net radiation is of interest for irrigation and water stress studies.

The instantaneous net rate at which radiant energy is absorbed by a surface also is made up of several components as shown in Figure 20. A fraction, ρ, of the short-wavelength irradiance, E_s, is reflected leaving a net amount absorbed equal to $(1 - \rho)E_s$. Next, there is a substantial amount of thermal radiation from the atmosphere and surroundings that is absorbed. Finally, the surface itself emits thermal radiation.

A multispectral scanner measures the outgoing radiance of a surface, in many channels, through the atmosphere. Figure 21 is a map of the apparent outgoing radiation or exitance from an agricultural area. It was produced by weighting and summing the contributions from the various scanner channels. The atmospheric effects (path radiance and transmittance) must be removed to obtain the actual exitance of each surface with the assumed spatial distribution of exitance. The small dark spots in the lower left hand corner are young trees in an orchard. The dark circular area above them is wet bare soil, surrounded by dry bare soil. Less radiation is leaving the wet soil because it is darker and because the energy used to evaporate the water keeps its temperature lower. At the right of the map, we have two corn fields; the lower one is darker; it was more mature, reflected less near-IR radiation, and had more evapotranspiration than the upper field.

Upon estimating the incoming power density at both short and long wavelengths, a map of net radiation or radiation balance can be produced and

would appear as shown in Figure 22. Here, the relative tones are reversed from those of the previous slide. The wet soil and vegetation which have the highest net radiation values are here displayed in light tones.

CONCLUDING REMARKS

Four aspects of techniques for extracting useful information from multispectral scanner data are discussed above. Our major emphasis is on the problems that have held back the use of scanner data for large-area surveys, for instance, problems of extending recognition performance away from areas used to train the recognition computers,

Sources of systematic variation have been examined by use of a simulation model and some valuable insights have been gained. These insights, through techniques based on the model calculations, will be applied to real scanner data during the coming year. The model is applicable to both aircraft and space data.

Preprocessing is one method for removing these systematic effects so as to improve recognition performance. We have developed a general technique and demonstrated its ability to reduce scan angle variations and to extend signatures from one altitude to another. We also have studied the extension of the technique to two dimensions and must now develop it to remove systematic variations that occur along the direction of flight as the sun changes position and atmospheric conditions change. This is an important problem for area survey operations.

While preprocessing is an efficient method for removing systematic variations, it transforms all signals in exactly the same way regardless of their material class. More flexibility in processing, such as the use of adaptive techniques, would be possible if the decision rule parameters were changed in addition to changing the data.

A study of the usefulness of empirical density functions as opposed to the normal (Gaussian) density function for recognition processing led to the conclusion that the normal assumption for individual fields is justified for processing multispectral scanner data,

We have developed a rapid method for choosing subsets of information channels to use for processing. While thus far it has been applied only for selecting among scanner channels, it can be used to select among other features extracted from these original data channels. The theory developed during this effort should also be applicable to other areas of processing.

Finally, in the area of interpretive techniques, we have developed procedures for producing radiation balance maps from the wide spectrum covered by the new multispectral scanners. This type of map and variants of it should prove useful in agriculture, meteorology, hydrology, geography, and other disciplines in which energy budget relationships are of interest.

REFERENCES

1. Malila, W.A., R.B. Crane, & R.E. Turner, "Information Extraction Techniques", Willow Run Laboratories, Institute of Science & Tech., University of Mich., Ann Arbor, Mich., Report No. 31650-74-T, in publication.
2. Malila, W.A., R.B. Crane, & W. Richardson, "Discrimination Techniques Employing Both Reflective and Thermal Multispectral Signals", Willow Run Laboratories, Institute of Science & Tech., University of Mich., Ann Arbor, Mich., Report No. 31650-75-T, to be published.
3. Legault, R.R., "Summary of Michigan Multispectral Investigations Program", Section 37, Third Annual Earth Resources Program Review, Volume II, Dec. 1-3, 1970, NASA/MSC, Houston, Texas.
4. Nalepka, R.F., J.P. Morgenstern, & W.L. Brown, "Detailed Interpretation and Analysis of Selected Corn Blight Watch Data Sets", 4th Annual Earth Resources Program Review, NASA/MSC, Houston, Texas, 17 January 1972.
5. Thomson, F.J., "User Oriented Multispectral Data Processing at The University of Michigan", Fourth Annual Earth Resources Program Review, NASA/MSC, Houston, Texas, 17 January 1972.
6. Crane, R.B., "Preprocessing Techniques to Reduce Atmospheric and Sensor Variability in Multispectral Scanner Data", Proceedings of Seventh International Symposium on Remote Sensing of Environment, Ann Arbor, Michigan, June 1971, pp. 1345-1356.
7. Malila, W.A., R.B. Crane, C.A. Omarzu, & R.E. Turner, "Studies of Spectral Discrimination", Willow Run Laboratories, Institute of Science & Tech., University of Michigan, Ann Arbor, Mich., Report No. 31650-22-T, May 1971.
8. Turner, R.E., W.A. Malila, & R.F. Nalepka, "Importance of Atmospheric Scattering in Remote Sensing, or Everything You've Always Wanted to Know About Atmospheric Scattering But Been Afraid to Ask", Proceedings of Seventh International Symposium on Remote Sensing of Enviornment. Ann Arbor, Mich., June 1971, pp. 1651-1698.
9. Suits, G.H., G. Safir, & A. Ellingboe, "Prediction of Directional Reflectance of a Corn Field Under Stress", Fourth Annual Earth Resources Program Review, NASA/MSC, Houston, Texas, 17 January 1972.

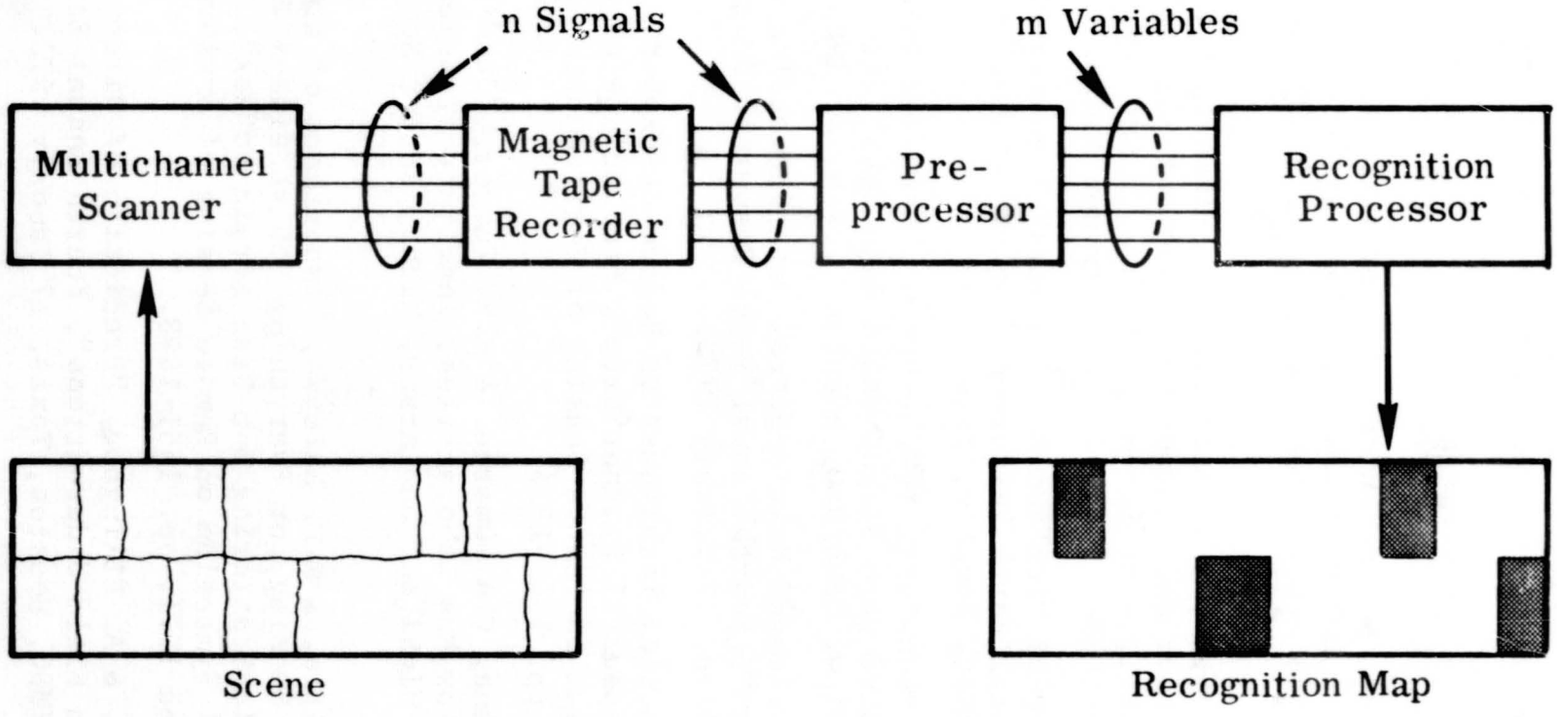

FIGURE 1. MULTISPECTRAL REMOTE SENSING AND PROCESSING SYSTEM

CLASS	SYSTEMATIC	RANDOM
Atmosphere	Path length Geometry	Inhomogeneities Clouds
Sun Position	Time, Date Location	
Scan Geometry	Nadir angle Azimuth w.r.t. sun Altitude	Angle errors Terrain profile
Sensor	Aperture effects Gain changes	System noise

FIGURE 2. SOURCES OF VARIATIONS IN MULTISPECTRAL SCANNER SIGNALS

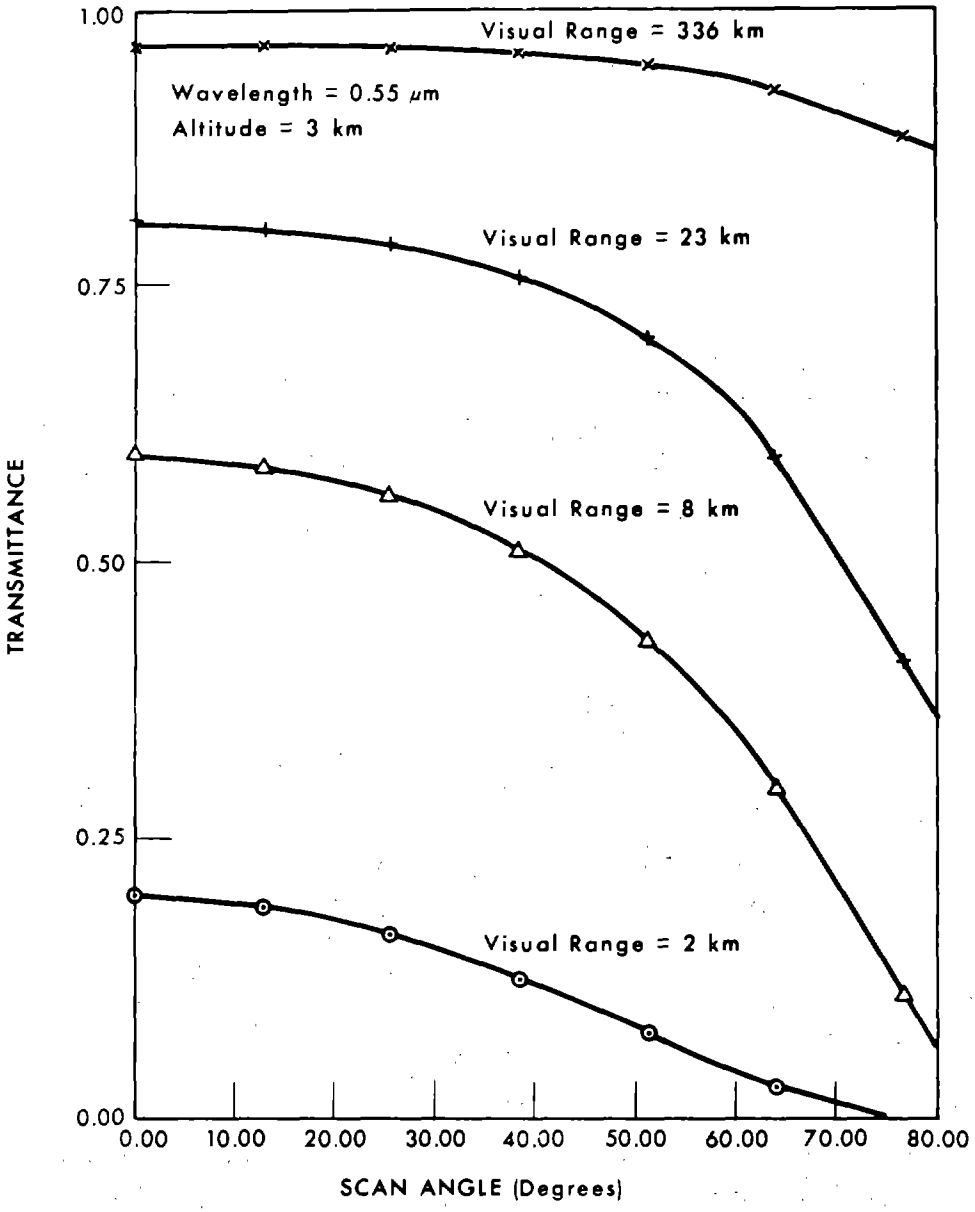

FIGURE 3. DEPENDENCE OF TRANSMITTANCE ON NADIR SCAN ANGLE FOR VARIOUS VISUAL RANGES

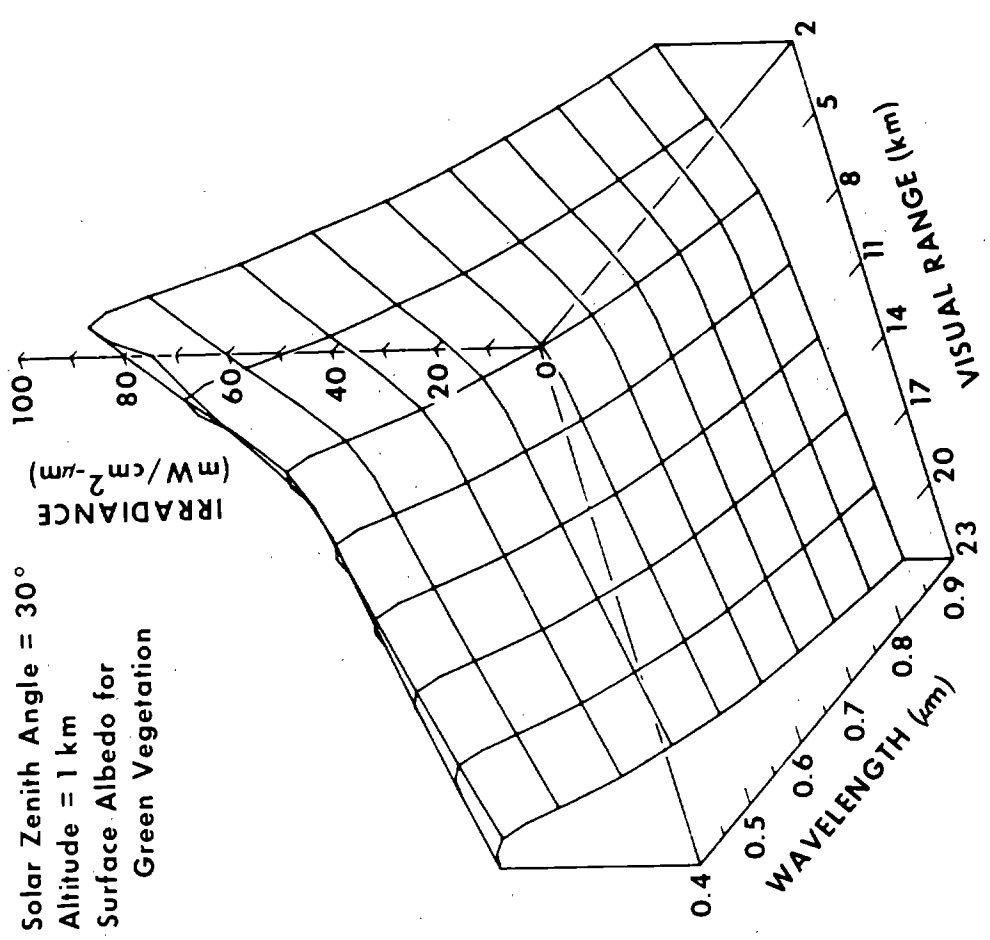

FIGURE 4. DEPENDENCE OF DIFFUSE DOWNWARD IRRADIANCE ON VISUAL RANGE AND WAVELENGTH

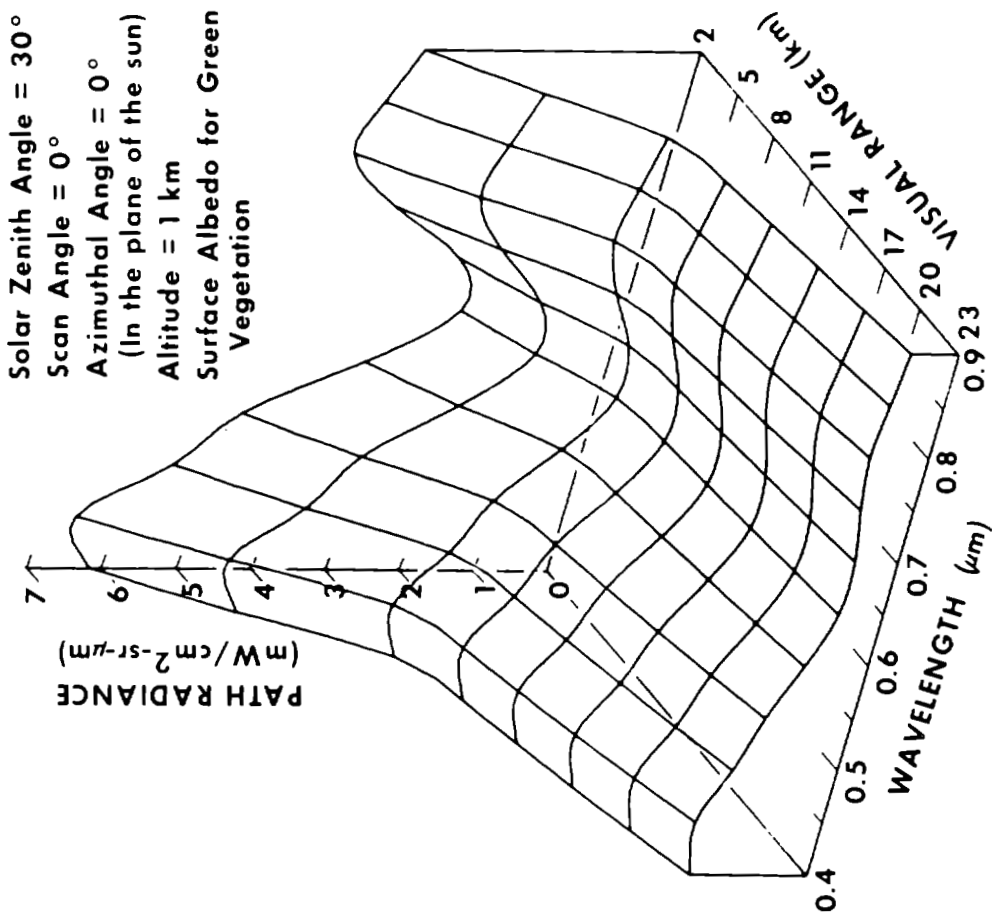

FIGURE 5. DEPENDENCE OF PATH RADIANCE ON VISUAL RANGE AND WAVELENGTH

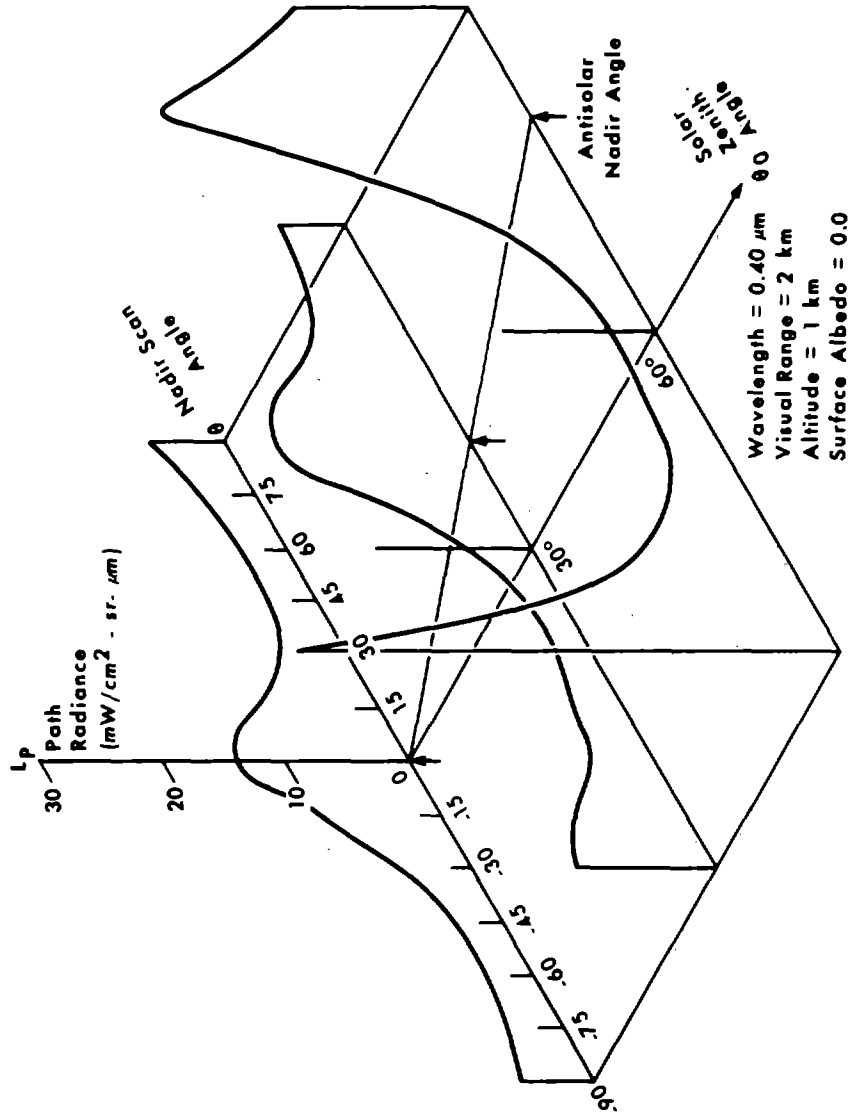

FIGURE 6. PATH RADIANCE VERSUS SCAN ANGLE AND SOLAR ZENITH ANGLE

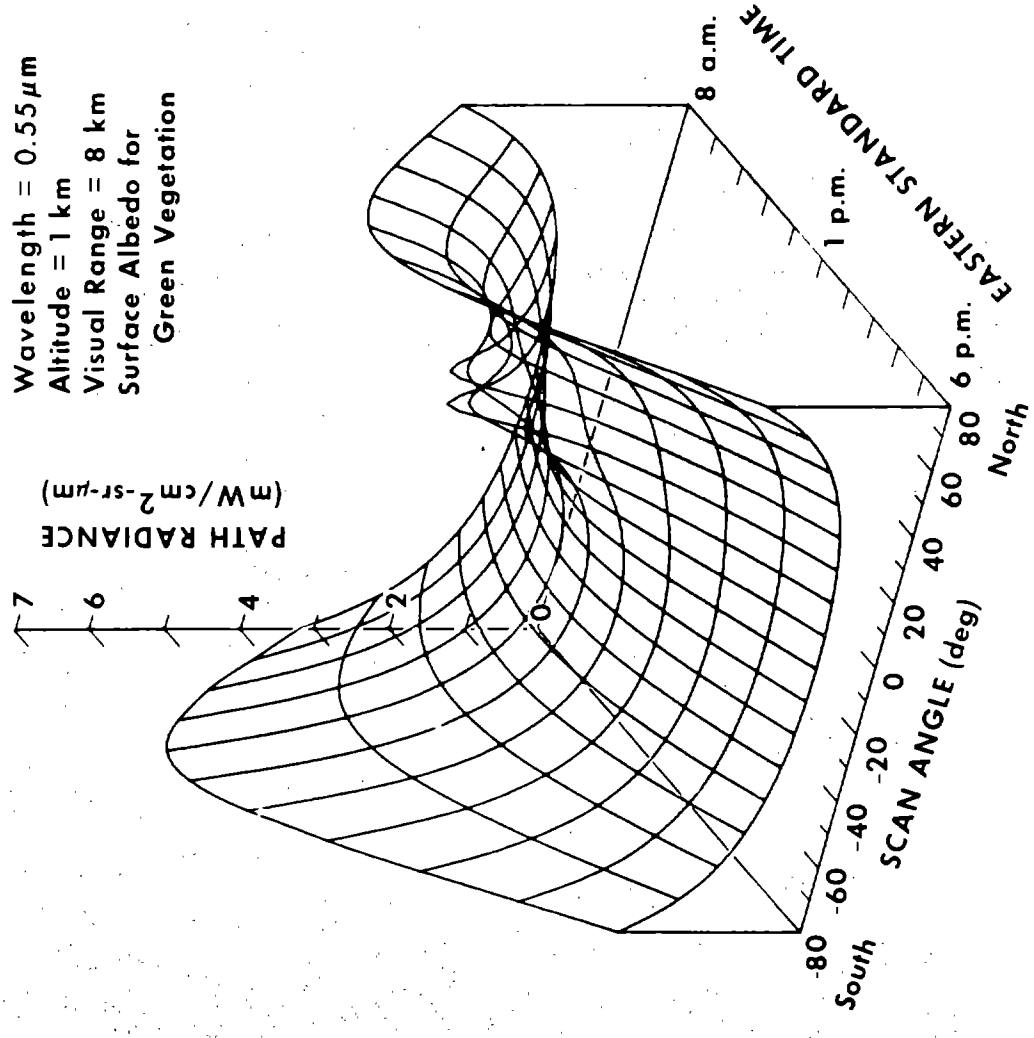

FIGURE 7. DEPENDENCE OF PATH RADIANCE ON TIME AND SCAN ANGLE. Southeastern Michigan, 1 September 1971.

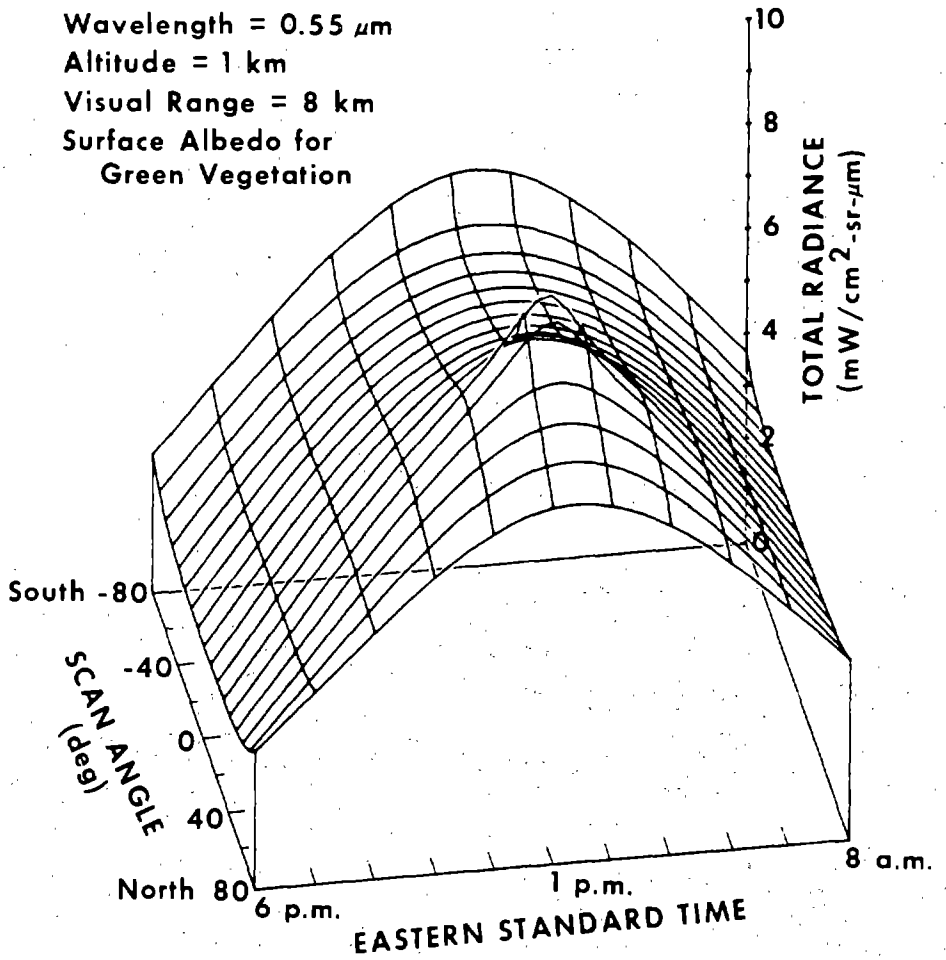

FIGURE 8. DEPENDENCE OF TOTAL RADIANCE ON TIME AND SCAN ANGLE. Southeastern Michigan, 1 September 1971

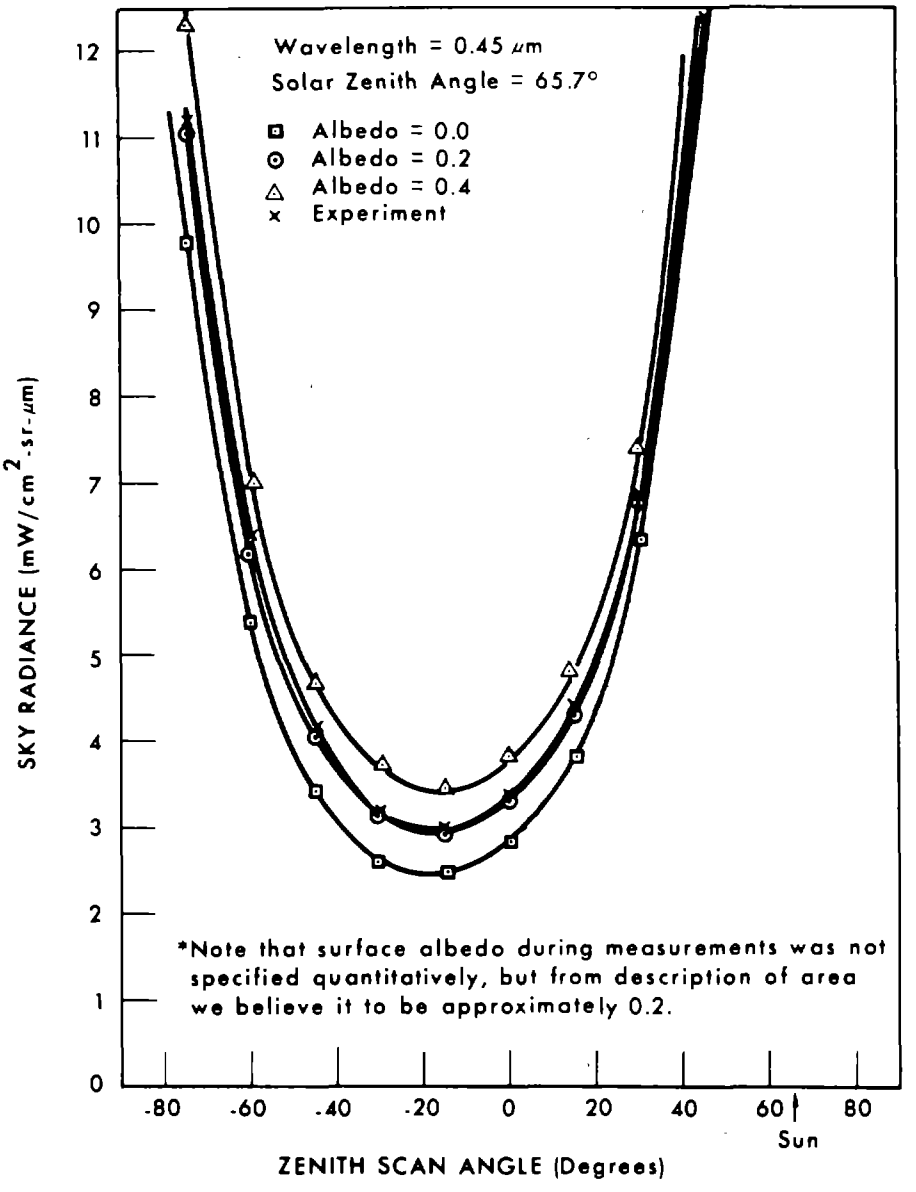

FIGURE 9. DEPENDENCE OF SKY RADIANCE ON ZENITH ANGLE IN SOLAR PLANE FOR CLEAR SKY CONDITIONS

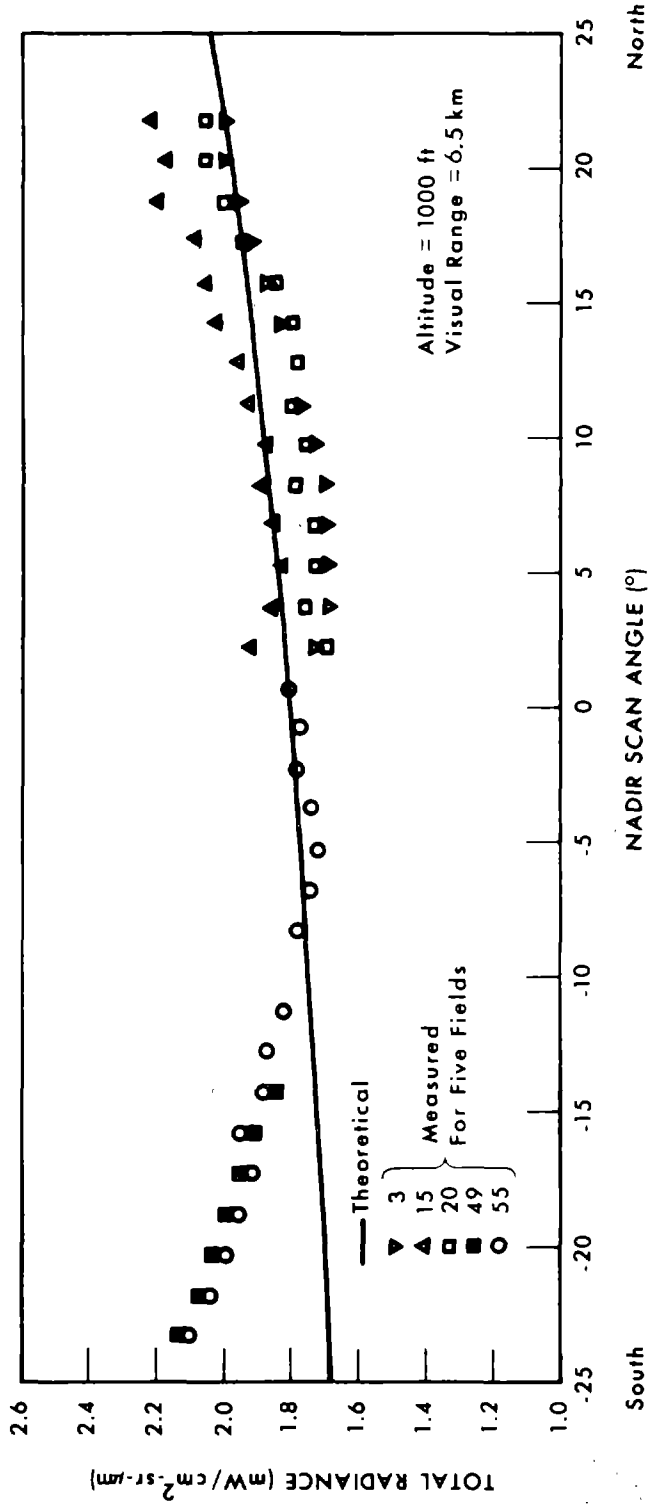

FIGURE 10. COMPARISON OF CALCULATED AND MEASURED RADIANCE DATA FOR SOYBEAN FIELDS (WAVELENGTH OF 0.42 μm)

C.2

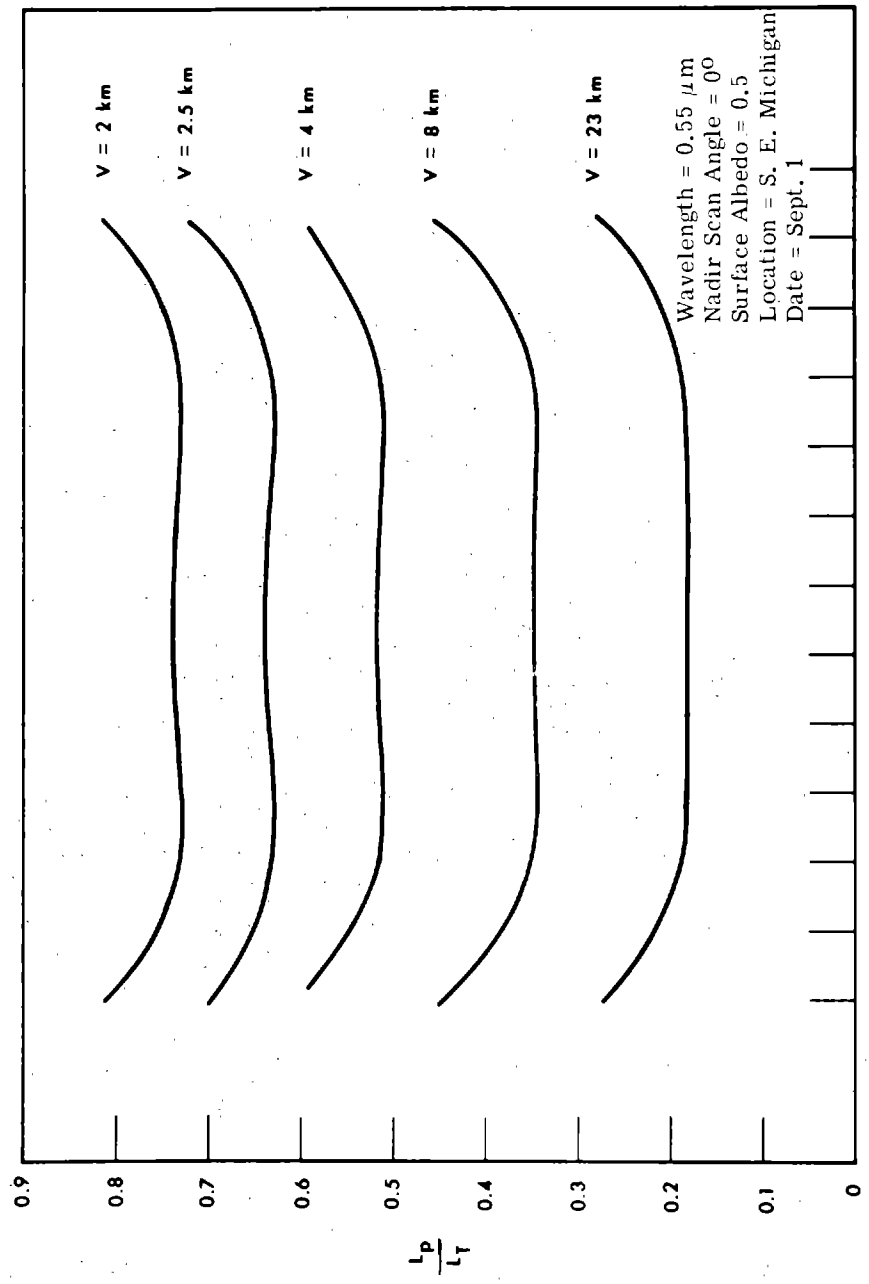

FIGURE 11. RATIO OF PATH RADIANCE TO TOTAL RADIANCE AT AN ALTITUDE OF 5 km AS A FUNCTION OF TIME

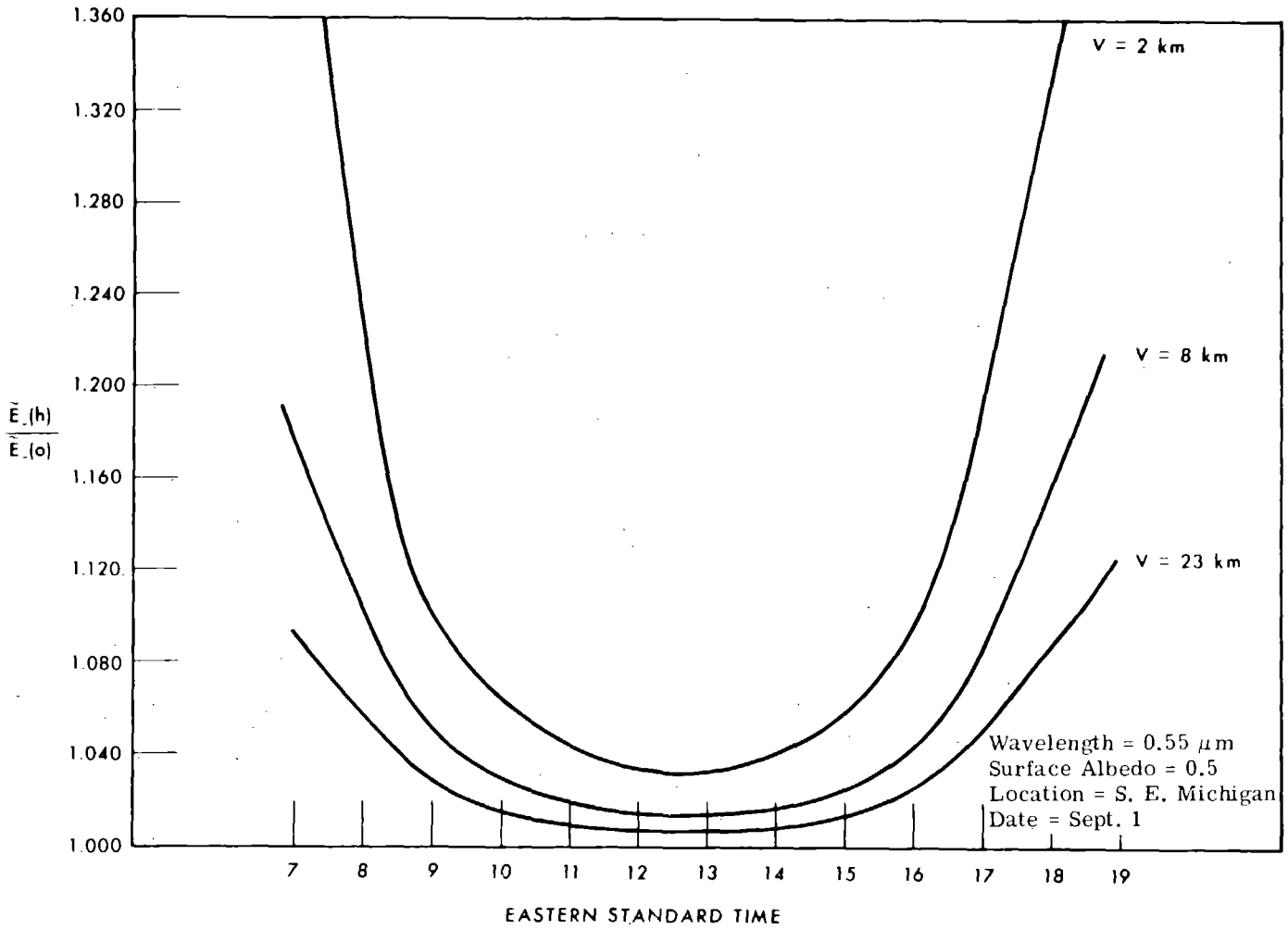

FIGURE 12. RATIO OF TOTAL DOWNWARD IRRADIANCE AT AN ALTITUDE OF 5 km TO TOTAL DOWNWARD IRRADIANCE AT EARTH'S SURFACE AS A FUNCTION OF TIME

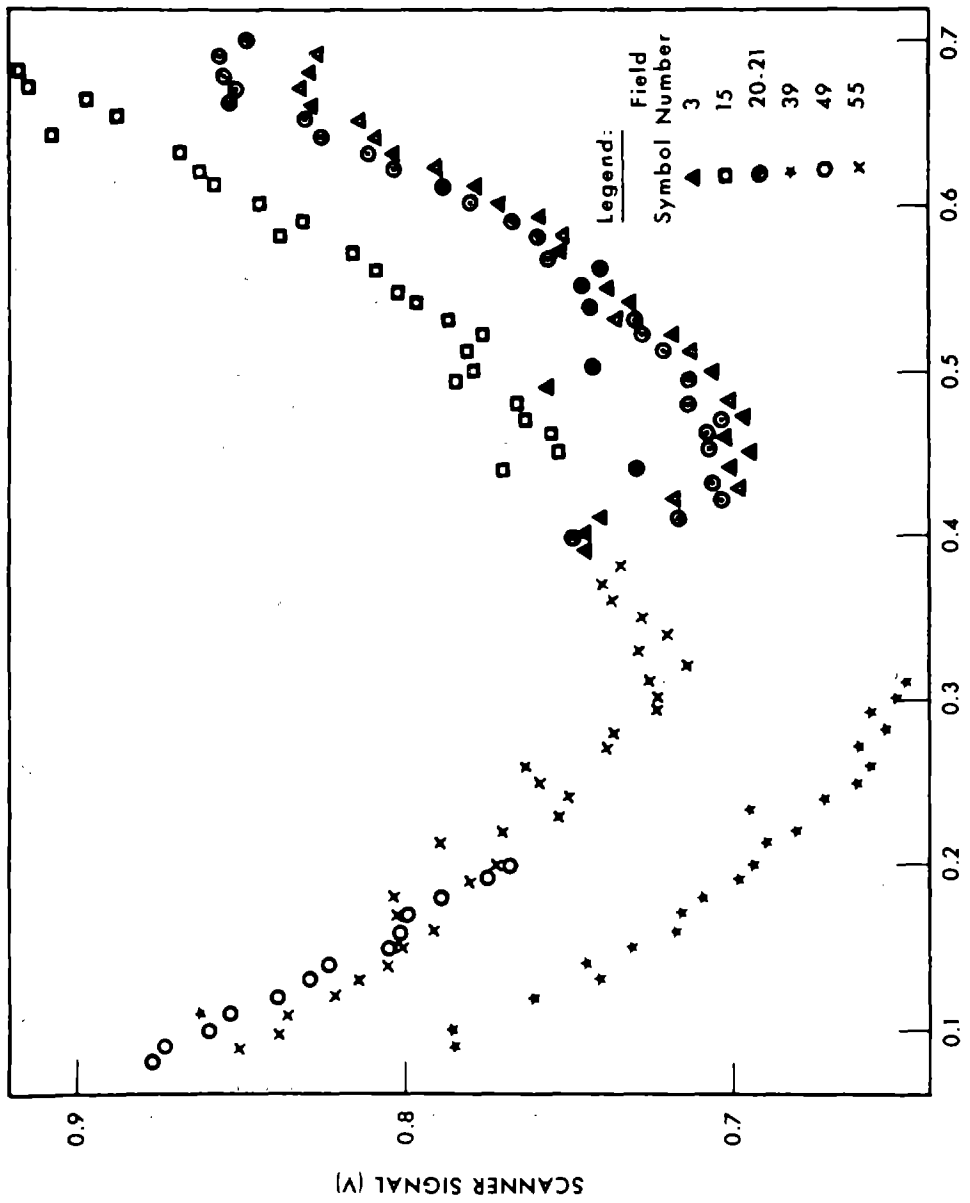

FIGURE 13. SCAN ANGLE EFFECT IN 6 SOYBEAN FIELDS (UNCORRECTED)

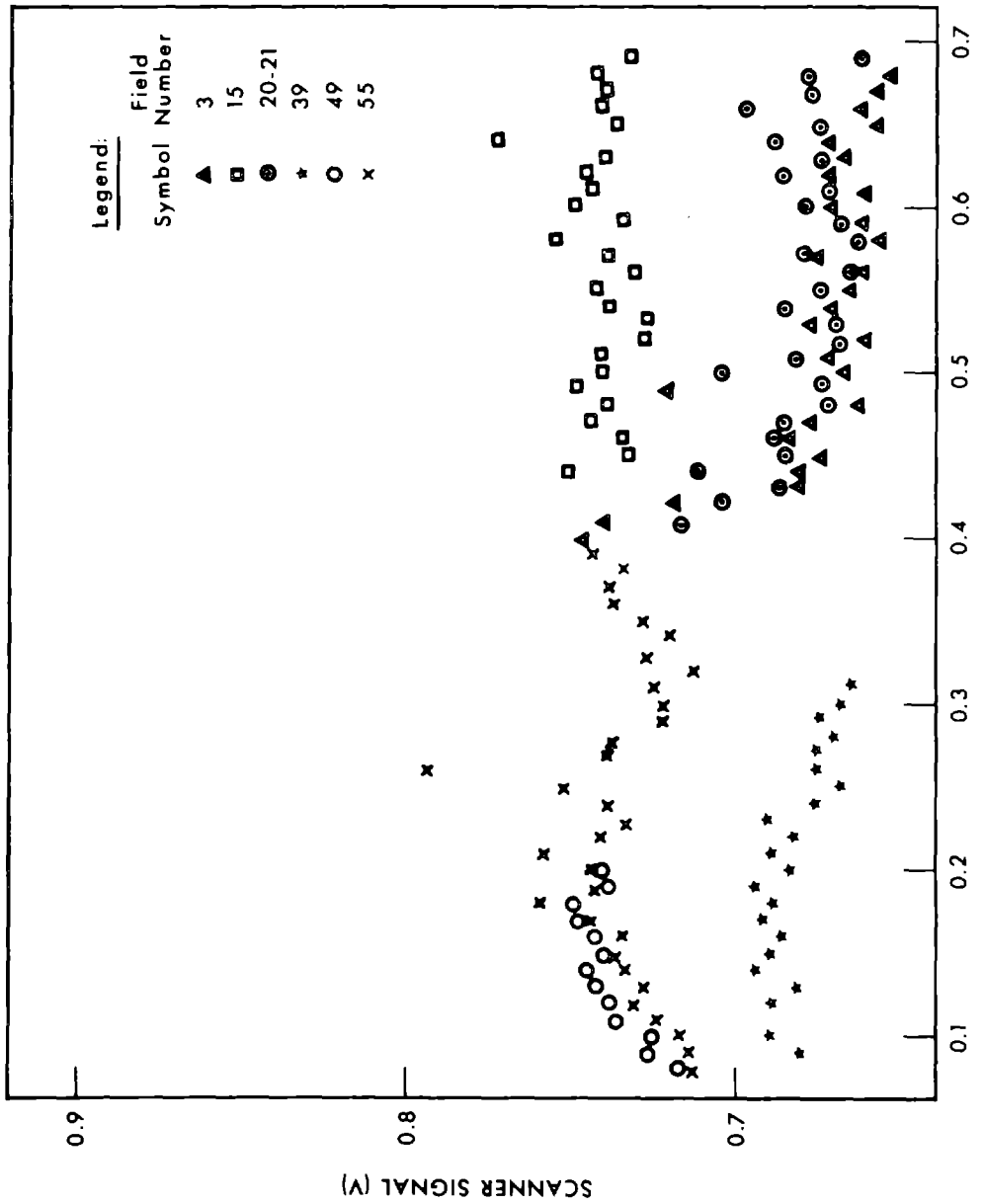

FIGURE 14. SCAN ANGLE EFFECT IN 6 SOYBEAN FIELDS AFTER QUADRATIC UV CORRECTION

Data Description					
ALTITUDE	1Kft	1Kft	1Kft	5Kft	5Kft
SMOOTHING	--	Yes	Yes	--	Yes
PREPROCESSING	--	--	U-V	--	U-V
TRAINING ALT.	1Kft	1Kft	1Kft	5Kft	1Kft
Pct. Fields with Pcorrect < 0.5	48	45	24	48	45
Percent Fields with Majority Decision Incorrect	14	14	3	24	17

FIGURE 15. COMPARISON OF RECOGNITION RESULTS

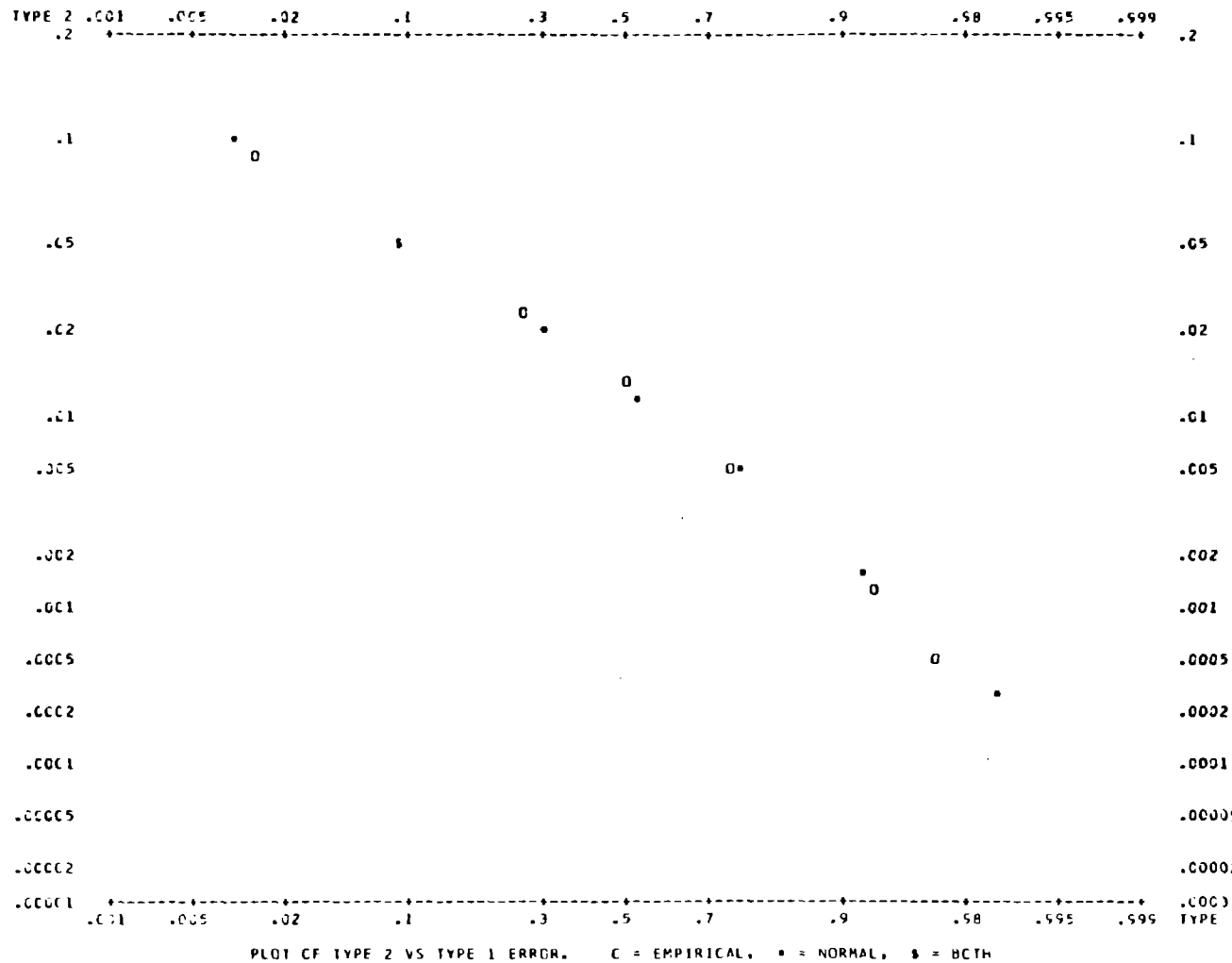

FIGURE 16. EFFECT OF LIKELIHOOD FUNCTION ON OPERATING CHARACTERISTICS (TYPICAL FOR THE FIRST THREE VARIABLES)

- Criterion is average expected loss (probability of misclassification)
- Stepwise procedure
- New linear approximation is 50 times faster than quadratic method

FIGURE 17. FEATURES OF CHANNEL SELECTION PROCEDURE

QUADRATIC METHOD (1 HOUR)

Channel Order	4	10	1	9	7	5
Avg. Prob. Miscl.	0.119	0.054	0.031	0.025	0.023	0.021

LINEAR METHOD (70 Sec)

Channel Order	4	10	1	9	7	5
Avg. Prob. Miscl.	0.122	0.059	0.034	0.028	0.025	0.024

FIGURE 18. COMPARISON OF CHANNEL SELECTION PROCEDURES
(9 signatures, 10 data channels)

$$R_N = ET + H + S + P$$

where

R_N is Net Incoming Radiant Energy

ET is Energy for Evapotranspiration

H is Energy for Heating Air (Sensible Heat)

S is Energy Conducted (e.g., Soil Heat Flux)

P is Net Energy Conversion (Photosynthesis minus respiration for Plants)

FIGURE 19. ENERGY BUDGET

$$E_{net} = (1 - \rho)E_S + \epsilon E_L - M_L$$

where

E_{net} is Net Irradiance
(Net Incoming Radiant Power Density)

E_S is Irradiance at Short Wavelengths
(Direct Sunlight + Skylight)

ρ is Reflectance of Surface (Albedo)

E_L is Irradiance at Long Wavelengths
(Incoming Thermal Radiation)

ϵ is Thermal Emittance of Surface

M_L is Exitance at Long Wavelengths
(Emitted Thermal Radiation)

Typical Units: watts/m^2

cal - cm^{-2}/min = ly/min

FIGURE 20. RADIATION BALANCE

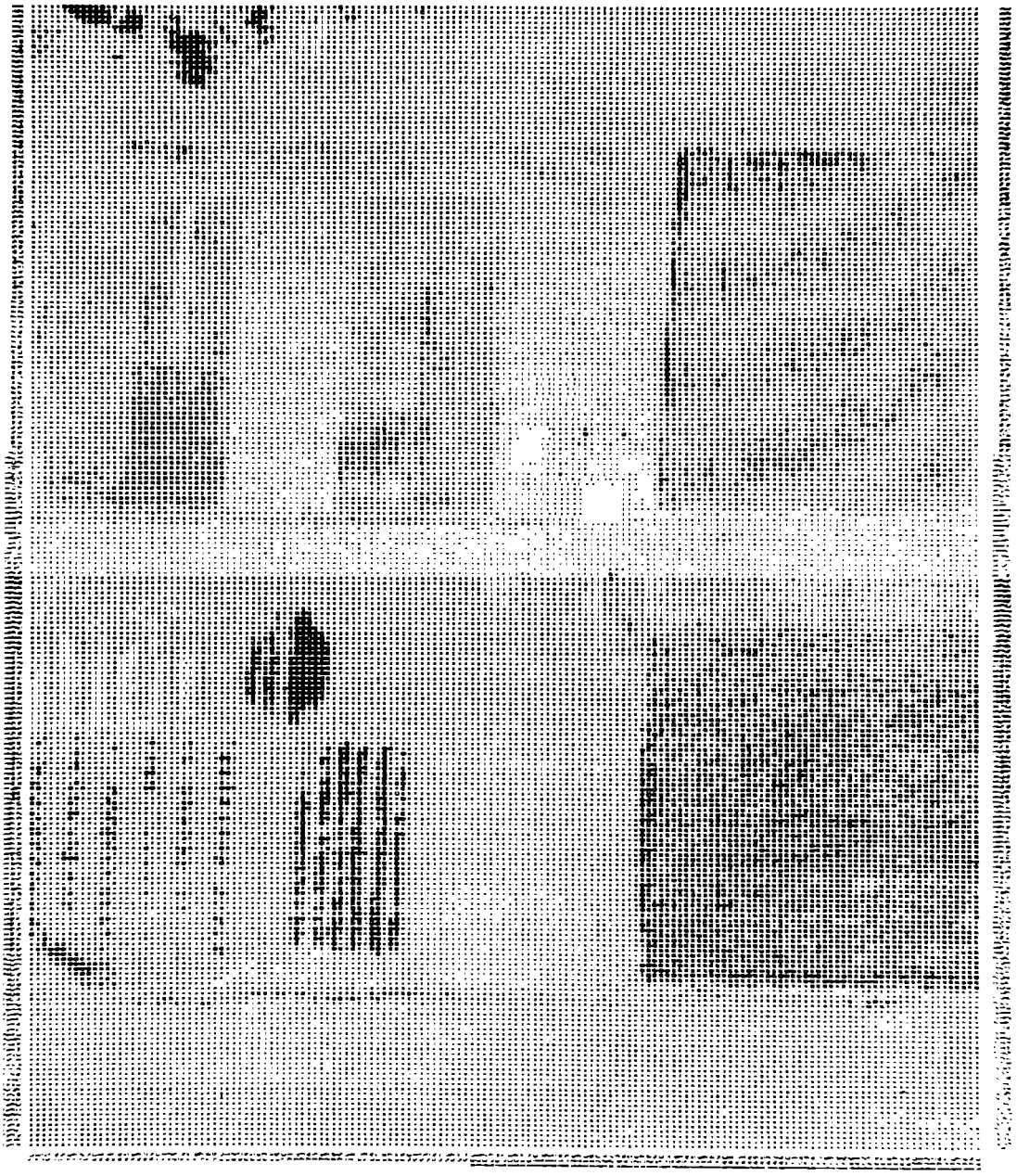

FIGURE 21. EXAMPLE EXITANCE MAP

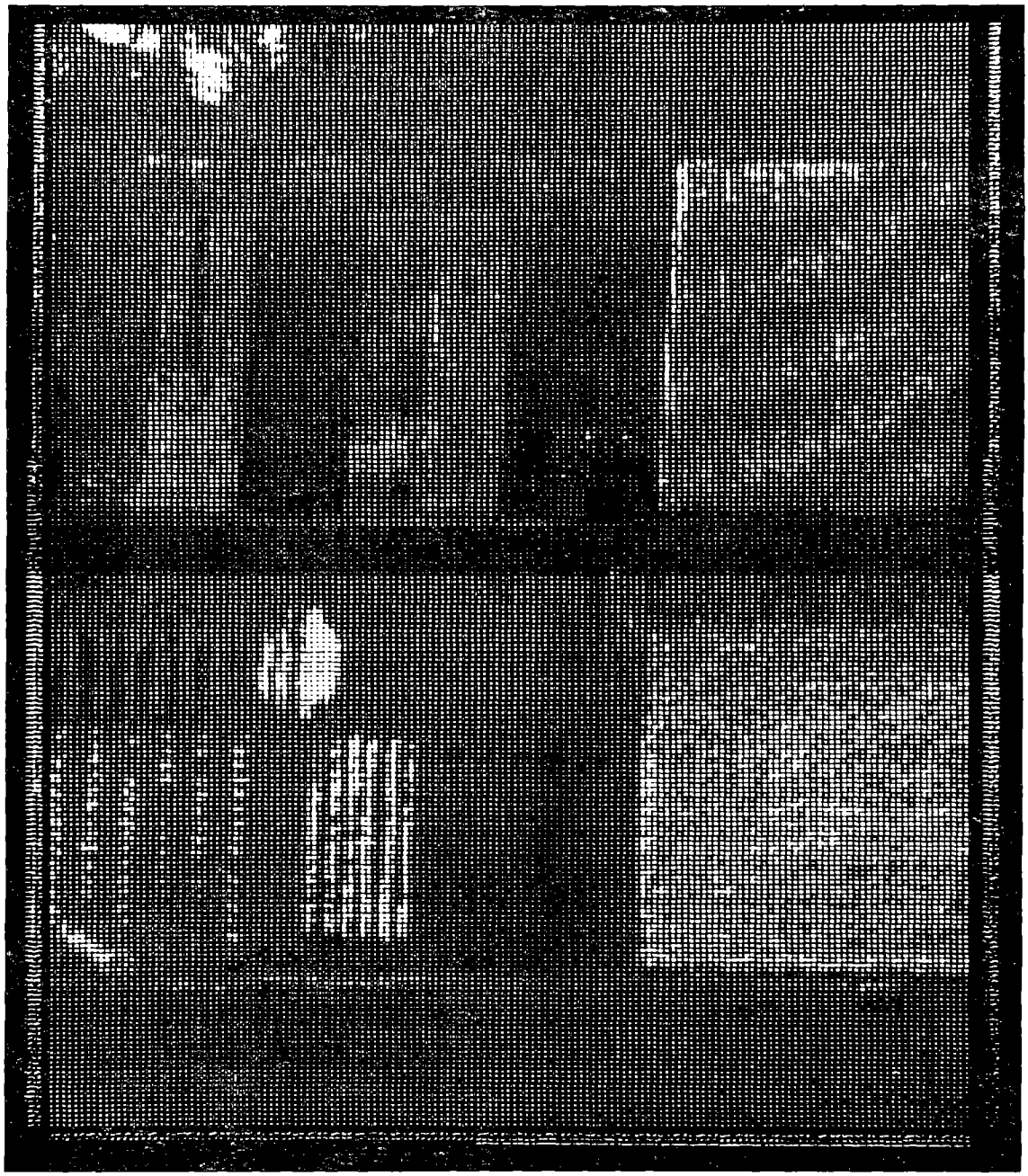

FIGURE 22. EXAMPLE RADIATION BALANCE MAP

SECTION 30

USER ORIENTED MULTISPECTRAL DATA PROCESSING AT THE UNIVERSITY OF MICHIGAN*

by

Frederick J. Thomson
University of Michigan
Ann Arbor, Michigan

INTRODUCTION

This paper discusses the results of the second year of a coordinated program of application of proven and promising multispectral data processing techniques to practical problems posed by NASA center, government agency, and university investigators. The two goals of this program are to assess the feasibility of solving practical problems with available processing techniques, and to identify areas where more technique development is required. For the past two years, this program at the University of Michigan has been funded by NASA through the Manned Spacecraft Center at Houston.

During the past five years of working with investigators on practical problems, a number of processing techniques have been found useful. These techniques, summarized in Figure 1 and 2, have been called Type I and Type II techniques. The Type I techniques are simpler processing techniques usually applied to single or few channels of data. They include imagery, contouring and quantization, false color films, duplicate analog tapes, digitized data tapes, and canvas calibration panel reflectance measurements. The Type II processing techniques are more sophisticated techniques applied to the multispectral data set. They include signature extraction, optimum channel determination, likelihood ratio processor performance prediction (by computing probabilities of misclassification), object reflectance or radiance determination, preprocessing analysis, analog and digital implementations of the likelihood ratio classification map, and ratio maps.

This paper discusses several technical accomplishments of this year's data processing. Two new processing techniques (parameter mapping and ratio mapping) were developed in response to user requests. Under this contract we also processed half of the multispectral data collected for the Corn Blight Watch Experiment. Remaining sections of this paper will discuss technical highlights, the scope of this year's effort, and a list of cooperating agencies, NASA centers, and university personnel. It will conclude with suggested areas of further investigation.

---

* This report has the Willow Run Number 03165-100-S

TECHNICAL HIGHLIGHTS

The data processing effort was highlighted by two kinds of technical achievements. First, two new processing techniques (parameter mapping and ratio mapping) were developed to solve specific investigator-posed problems. Second, our participation in the Corn Blight Watch experiment gave us the opportunity to evaluate the capabilities of existing multispectral data processing technques applied to semi-operational investigation.

While the parameter mapping and ratio mapping techniques were developed to solve specific problems, we feel that they have general applicability, and thus warrant fairly complete discussion here. Because of the scope of the Corn Blight Watch effort, it is discussed in the next section.

PARAMETER MAPPING

Parameter mapping, closely related to likelihood ratio pattern recognition, was implemented on SPARC to test a hypothesis offered by A.E. Coker of USGS-Tampa. He was attempting to assess pollution of ground water in central Florida occurring when fluoride rich, high pH, effluents from phosphate processing ponds seep through dikes and mix with the ground water supply. Large seepages of effluents from diked ponds can be detected because the surrounding vegetation is killed and a white salt crust appears on the soil surface. The problem is to detect small seepages of the dangerous and toxic effluent when concentrations are not large enough to kill vegetation.

Coker hypothesized that the reflectance spectra of the plants affected with fluoride would be modified, and that the amount of this modification was possibly proportional to the amount of fluoride pollution. To test this hypthesis we proposed a two step process. First, using conventional likelihood ratio techniques, all areas of a given vegetation type, affected or not, are recognized. Second, using a signature from a known normal area of vegetation, the distance between the signature of each scene point previously recognized and this "normal" signature is computed. The distance is displayed on black and white film as a continuous tone display with film density proportional to distance. Only points recognized as vegetation are printed on the film as various shades of gray. In this case, the parameter which is being mapped is the fluoride content of the plants. It is being mapped through the effect that this fluoride content has on the vegetation reflectance signature. This is illustrated in Figure 3, where a two dimensional, color-space plot of the signatures, decision boundaries, and distance is shown.

The implementation of this technique on the SPARC is shown in Figure

4. The likelihood ratio, formed from the probability density functions of the total vegetation signature and background signatures, is thresholded to form a conventional recognition signal. This is used to gate the signal from circuitry computing the statistical distance from the normal vegetation signature to the signature of the point being processed. This procedure is repeated for every point on the scan line, and processing proceeds at a real time rate.

Although the parameter mapping was developed for assessing the fluoride content of vegetation, we feel that the technique has general applicability in cases where stresses subtly alter the reflectance spectrum of vegetation. One such example is corn blight, where the stress, although not systemic, still modifies the reflectance of the corn through changes in plant geometry and in leaf spectra. Another example is the change in reflectance spectra of trees correlated with copper and molybdenum content of the soil reported by Canney (1).

Compared with likelihood ratio mapping techniques, where a training set for each degree of stress must be found, the parameter mapping offers a reduction of training set requirements. Only a training set for the class as a whole and for the "normal" condition must be found. The output is not a recognition map because no decision as to the degree of stress is made by the computer. We are anxious to apply this processing technique to other stress conditions to test its effectiveness.

RATIO MAPPING

Ratio mapping is a technique developed in response to an application proposed by Robert Vincent of the University of Michigan (2). For this technique, the ratio of two suitably calibrated channels is printed on either 70mm film or on computer paper in the form of a graymap.

Vincent found, after analysis of laboratory and field spectra collected by R.J.P. Lyon, that a ratio of radiances in two narrow wavelength intervals in the 8-14μm window could be correlated with the silica content of rocks. The basis for this conclusion was that all silica containing minerals display decreases in emissivity in reststrahlen bands in the 8-10μm region, and the position of these bands shifts to longer wavelengths with decrease in silica content (see Vincent and Thomson (3)). Ratios of radiance locate the position of the reststrahlen band because the emissivity directly affects the observed emitted radiation.

To test this technique, we developed both digital and analog ratio map capabilities. The analog ratio maps, shown in Figure 5, are produced by dividing the two signals in an analog divider which is part of the SPARC preprocessor. The resultant ratio is printed on 70mm film.

The digital implementation of the ratio map is slightly more sophisticated than the SPARC implementation and offers the advantage of easily obtained quantitative output at the disadvantage of slightly coarser and physically larger display. The CDC-1604 digital computer program RAITEM was developed to calibrate two channel thermal infrared data from the Honeywell layered detector (flown in Michigan's M-5 scanner system), form the ratio of the two channels' data, and correct the ratio for effects of varying object temperature. The correction is done by obtaining a radiometric estimate of temperature in a third thermal band, then using a table lookup procedure to determine the correction factor.

Although the ratio map technique was developed in response to a geology problem, the concept of ratio maps may be generally useful for other types of investigations. For example Pearcy (4) has proposed a blue - green ratio to delineate water masses in the Pacific Ocean off Oregon. Vincent has proposed a green-infrared ratio to indicate the presence of ferrous and ferric iron in rocks. There are indications that ratio maps may be useful in delineating plant stress.

Ratio maps are not recognition maps. No decisions are made by the computer before the results are printed. The output of ratio processing applied to visible data is relatively insensitive to changing illumination conditions--this is the basis of the ratio preprocessing techniques. Ratio techniques have yielded important information for geological investigations, and we look forward to applying them to other types of investigations.

FURTHER DEVELOPMENTS IN SIMULATION OF OTHER SENSORS

The simulation of other sensors is an important part of multispectral processing operations. Frequently, investigators want to evaluate how much better the multispectral data and processing performs a job than a more conventional photographic sensor and human processor. The question usually arises--what if the photography were processed in the same way as the scanner data. To help answer this question we have developed spectral simulations of photographic and other sensors.

Many investigators have been interested in determining whether problems can be solved using ERTS data. Last year we simulated the spectral response of ERTS-MSS channels (see Figures 6 and 7 where simulated responses are shown as dashed lines and assumed ERTS-MSS responses are shown as solid lines). This year we also simulated the spatial response of the ERTS system. This was accomplished by smoothing the scanner data to achieve 80m resolution element size. This smoothing was accomplished by averaging over points and scan lines of the original scanner data.

Figure 8 shows two digital graymaps of a 2 x 8 mile portion of Biscayne Bay data for which ERTS spectral and spatial simulations were performed.

The bottom map in Figure 8 is of spectrally simulated ERTS-MSS channel 3(0.7-0.8μm) at the original scanner data resolution of 10m. Prominent land features of southern Biscayne Bay are identified. The top map in Figure 8 is a simulation of the ERTS-MSS 80m. spatial resolution using the same data set. The important land features can still be identified. This suggests that at least, features of the size of Mangrove Point, Turkey Point, and Arsenicker Key will be delineated on the ERTS data.

No aircraft sensor can adequately simulate the 100 x 100 mi field of view of the ERTS sensor. The data shown in Figure 8 comprise about 0.16% of the data in an entire ERTS frame. Even a single RB-57 photograph covering 18 x 18 miles covers less than 4% of the area of an ERTS frame. It is clear that some of the problems being attacked with aircraft data will not be feasible from ERTS because of the lower spatial resolution. By simulating this lower resolution, some estimate of the feasibility may be obtained before getting ERTS data. Further, by simulating spatial resolutions intermediate between ERTS and scanner, we can assess the utility of various levels of resolution for solving problems.

CORN BLIGHT WATCH PARTICIPATION

In early May, we were asked to assist the Laboratory for Applications of Remote Sensing (LARS) in processing multispectral data collected as part of the Corn Blight Watch Experiment. Data were collected every two weeks over thirty segments of the intensive study area in western Indiana. We were asked to process half of this data, delineate levels of corn blight severity, and report results to LARS within two weeks after having received the data. This effort commenced in early July and continued through the middle of October, and some originally scheduled processing for investigators had to be deferred.

At the outset, we realized that the processing of the data would have to keep pace with the collection. Both LARS and we estimated that one segment per day was a suitable data processing rate for each facility. The aircraft program was thus scaled to collect thirty segments' data every two weeks.

To meet the goal of processing one segment's data each day, we organized a team of four supervisors and six SPARC operators. Supervisors selected corn and background training sets from available biweekly ground information, color IR film collected by the C-47, and previous processing experience with the segment. The SPARC and preprocessor were setup in the 8 target, 6 channel configuration. LARS selected separate sets of six channels for northern, central, and southern Indiana segments from an analysis of the previous mission's data.

Loops of data were prepared by the SPARC operators. These operators then setup the SPARC, implemented preprocessing where required, and trained SPARC. Despite careful planning of the aircraft data collection program to minimize the variations of observed radiance with scan angle, those effects were prominent enough to require preprocessing correction in about 80% of the data. These data were collected at about 5000 ft. above terrain under visibility conditions greater than 6 miles. Because these are quite reasonable conditions under which to collect data in operational programs, we conclude that preprocessing (or other accounting for angle-dependent variations of observed radiance) must be considered in the design of processors for operational applications.

Recognition maps of each corn blight class were produced and area counts were accumulated of each blight level detected by SPARC. The area counts were reported to LARS on standard forms. Also, supervisors analysed each recognition map, estimating the fraction of each corn field detected as each blight level. This information was reported to LARS every two weeks.

Some typical Corn Blight Watch SPARC maps are shown in Figures 9 and 10. In Figure 9, SPARC results from segment 212, Mission 43M (8/17/71) are color coded to portray corn of blight levels 0-3 (light) in green, corn of blight levels 4 and 5 (heavy) in red, and other areas as white. Fields in this figure are either predominantly green or red, with very few fields with a sizable mixture of green and red, indicating that there is a small range of blight levels within any one field, and that different fields are affected quite differently by southern corn leaf blight (SCLB), depending on cytoplasm type and location.

One source of confusion in the data analysis is illustrated by Figure 10. In this figure a portion of a corn recognition map for segment 211 is presented, along with color IR photography. There are several roughly circular areas of no recognition within corn field boundaries that were identified as weedy patches or areas of low corn growth from examination of the color IR photo. The processor failed to detect corn in these areas because there was little or no corn. If one is interested in estimating the acreage planted in corn by remote sensing means, some account will have to be made of areas within corn fields which do not contain corn. Per field classification is one possible solution to this problem.

QUANTITATIVE ASPECTS

Shown in Figure 11 is a list of investigators we have collaborated with this year, their affiliation, and the general nature of the problems investigated. The list is quite varied and indicates the general interest in multispectral data collection and processing within the user community. Shown in Figures 12 and 13 are the numbers of each of the Type I and Type II processing jobs performed. A considerable amount of both digital and

SPARC analysis work was accomplished. A great majority of the 102 SPARC jobs completed last year were for the corn blight watch experiment, but SPARC maps were also prepared for other investigators.

CONCLUSIONS

The first semi-operational test of multispectral data collection and processing techniques was conducted this year--Corn Blight Watch Experiment. From this valuable experience, as well as work with other investigators, we draw some conclusions and make recommendations for the course of future research.

We have demonstrated that multispectral data processing can solve a number of important and relevant problems under restricted data collection conditions and with few constraints on processing time. Because the investigations to date have been primarily feasibility studies, no agency is currently making use of processed multispectral data in decision making. To make this use feasible, we will have to expand proven techniques to larger data sets, process these data sets more efficiently, and identify and provide the information that decision makers want. We have previously noted that the signature extension problem is crucial to the extension to larger data sets. At the University of Michigan, we have obtained some encouraging results in this area (reported in this symposium by Nalepka), and work here should continue to be vigorously pursued. Two other areas should also be considered--processor efficiency and cost and post-processing information extraction.

Our Corn Blight Watch experience has taught us that the aircraft is able to gather high quality data much faster than current, research oriented processors are able to digest it. The C-47, flying four days per month, generated enough high quality data to keep both LARS and Michigan processors busy for the whole month. If the potential of the aircraft and spacecraft sensors are to be realized, faster more efficient processors will have to be built. We see the hybrid computer as such a system. By designing and constructing such an improved throughput system, results can be generated faster more cheaply. This will benefit both operational programs and feasibility studies.

The generation of processed results more cheaply and faster will not alone insure their acceptance by potential decision making users. We need to consider the post processing information extraction. An important start has been made in this area with the extraction of pond acreage and perimeter statistics for wildlife managers setting duck hunting limits in North Dakota. More of this effort must be undertaken. One part of this area which needs attention is mensuration. For some investigators, the desired final output is a map. Because of distortions introduced in the scanning process and because of aircraft platform instabilities, maps of the required

fidelity have been difficult, if not impossible, to generate. Further, some investigators desire accurate acreage measurements of crops or other ground materials. This problem is linked with the problem of scanner cartography because the same kinds of distortions must be accounted for. It is clear that some unified approach to sensor platform and processor design is required to solve this problem most efficiently.

Collection of data from ERTS and Skylab sensors will impose new demands upon existing processing facilities, for data quantities will be sizably larger. We face the ERTS data with a number of processing technique proven useful for processing aircraft data. It is clear that many of these processing techniques will be useful for ERTS data, but that other processing techniques may be required to optimally exploit the unique characteristics of this data. Some of these techniques are now under development at Michigan, and will be discussed in other papers in this section.

REFERENCES

(1) Canney, F.C., Wenderoth, Sondra, Yost, Edward, December 1 to 3, 1970, "Relationship Between Vegetation Reflectance Spectra and Soil Geochemistry: New Data From Cathreart Mountain, Maine", Third Annual Earth Resources Program Review, Volume II Agriculture, Forestry, and Sensor Studies.

(2) Vincent, Robert K.,Horvath, Robert, Thomson, Fred, Work, Edgar A, April 1971, "Remote-Sensing Data-Analysis Projects Associated with the NASA Earth Resources Spectral Information System",NASA CR-WRL 3165-26-T.

(3) Vincent, Robert K., Thomson, Frederick J., May 1971, "Discrimination of Basic Silicate Rocks by Recognition Maps Processed from Aerial Infrared Data", Proceedings of the Seventh International Symosium on Remote Sensing of Enviroment, Vol. 1, pp. 247-252.

(4) Pearcy, W.G. (Dr.), Oregon State University, private communication.

TYPE I PROCESSING SERVICES

* Imagery
* Contouring and Quantization
* False Color Films
* Digital Tape
* Canvas Panel Reflectance Measurements
* Duplicate Analog Tape

INFRARED AND OPTICS LABORATORY
INSTITUTE OF SCIENCE AND TECHNOLOGY
WRL
THE UNIVERSITY OF MICHIGAN

Figure 1

TYPE II PROCESSING SERVICES

* Signature Extraction and Analysis
  - Optimum Channel Analysis
  - Processor Performance
  - Reflectance or Radiance
* Preprocessing Analysis
* Digital Recognition Map
* SPARC Recognition Map
  - Likelihood Ratio
  - Parameter Map
* Ratio Map

INFRARED AND OPTICS LABORATORY
INSTITUTE OF SCIENCE AND TECHNOLOGY
WRL
THE UNIVERSITY OF MICHIGAN

Figure 2

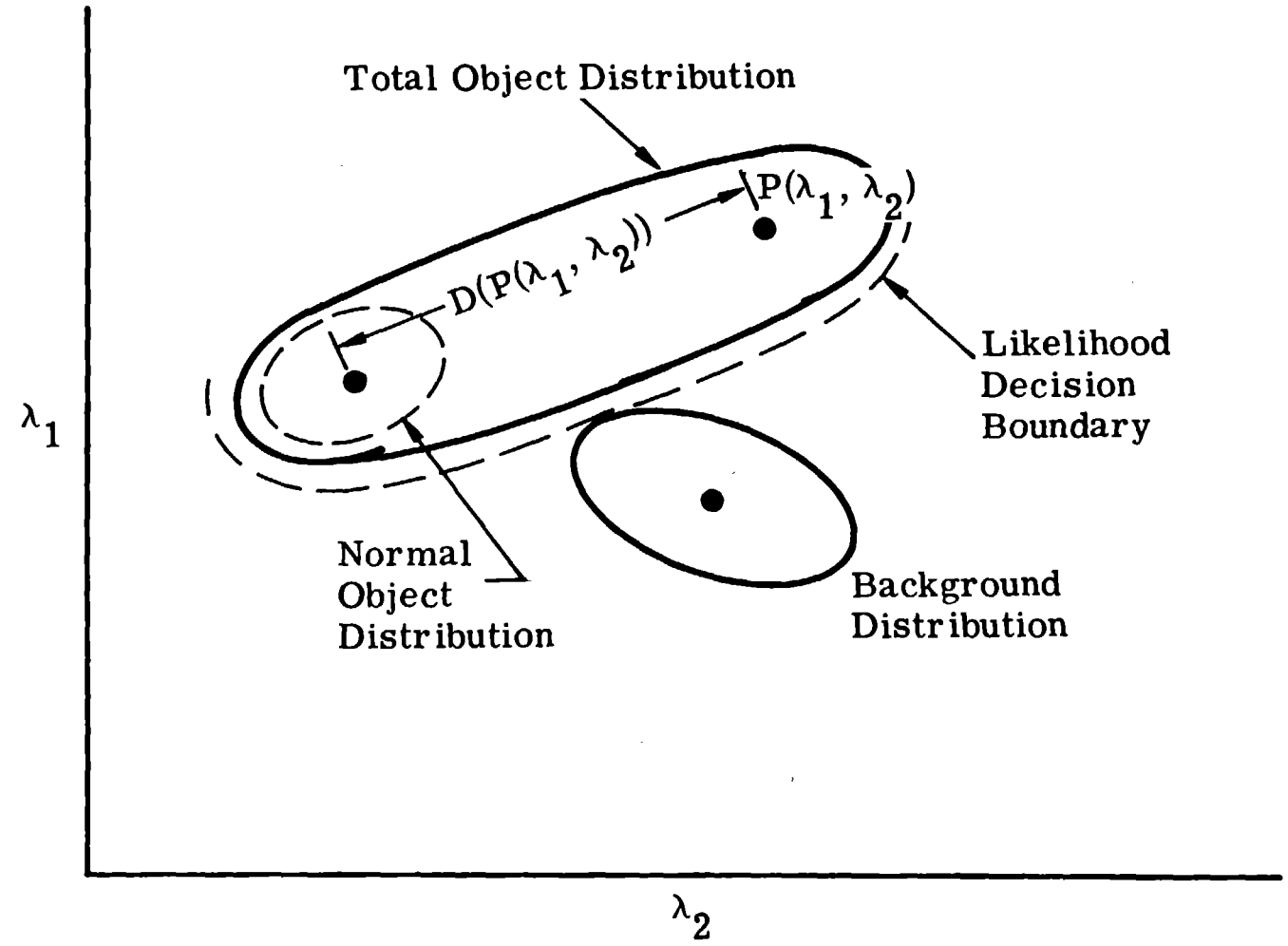

FIGURE 3. DEFINITION OF SIGNATURES FOR PARAMETER MAPPING

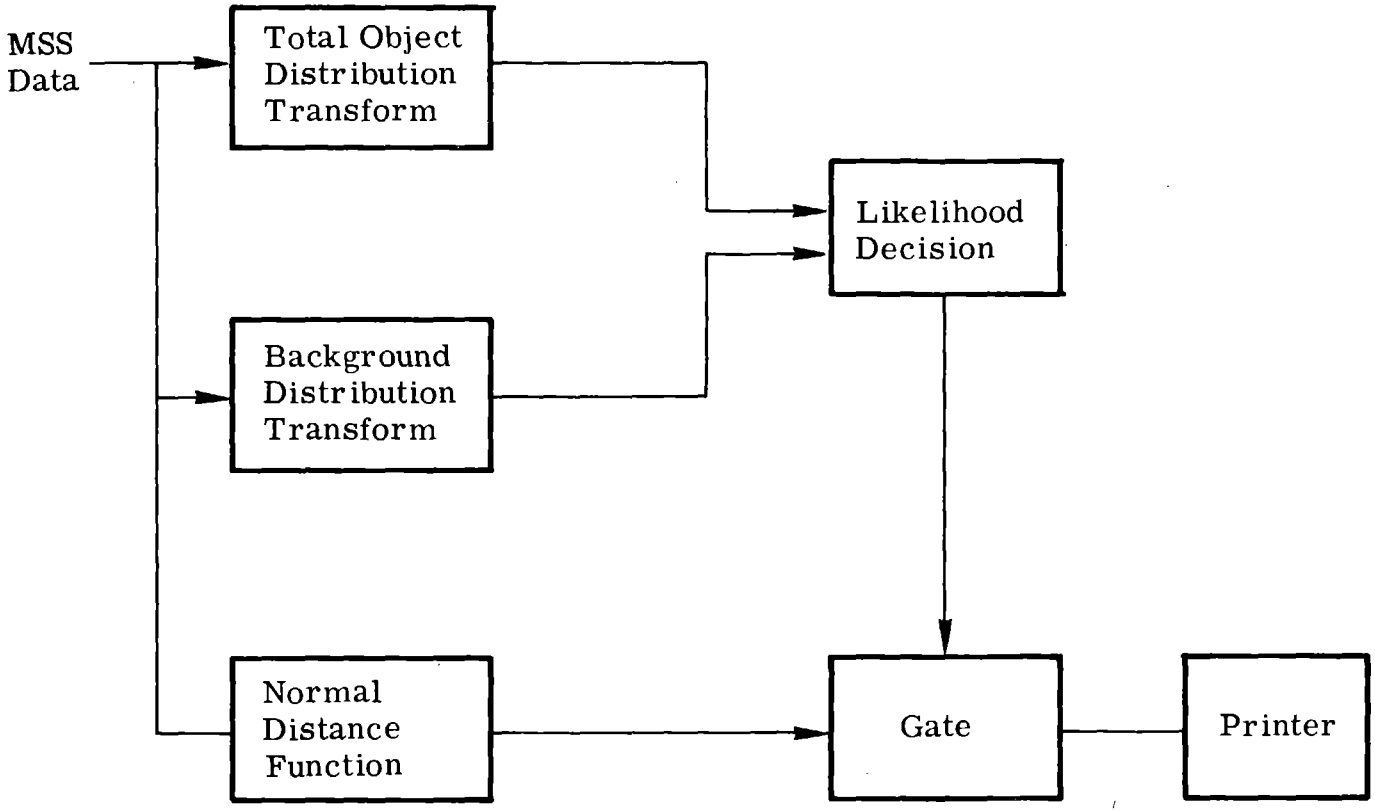

SIMPLIFIED BLOCK DIAGRAM OF SPARC SETUP FOR PARAMETER MAPPING

Figure 4

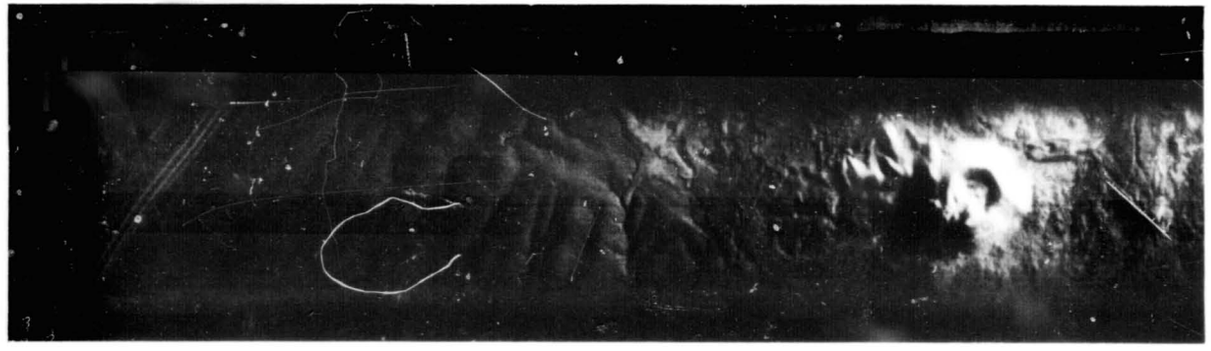

Channel 1: 8.2 - 10.9 μm

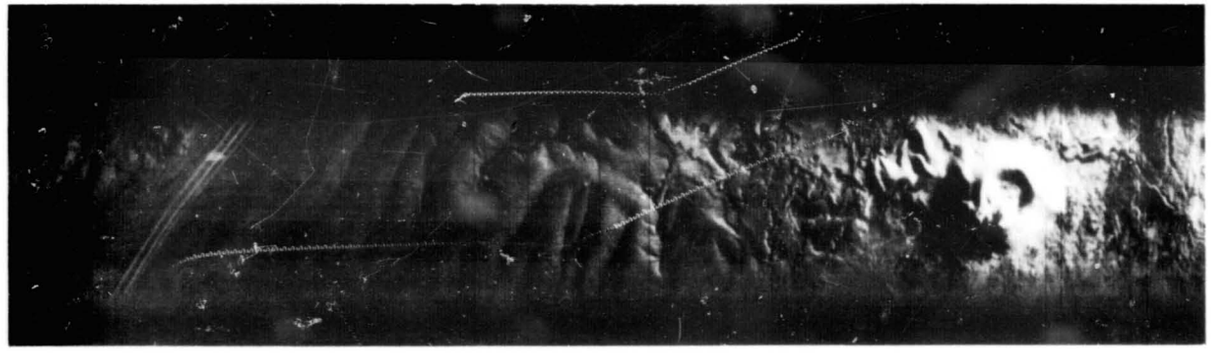

Channel 2: 9.4 - 12.1 μm

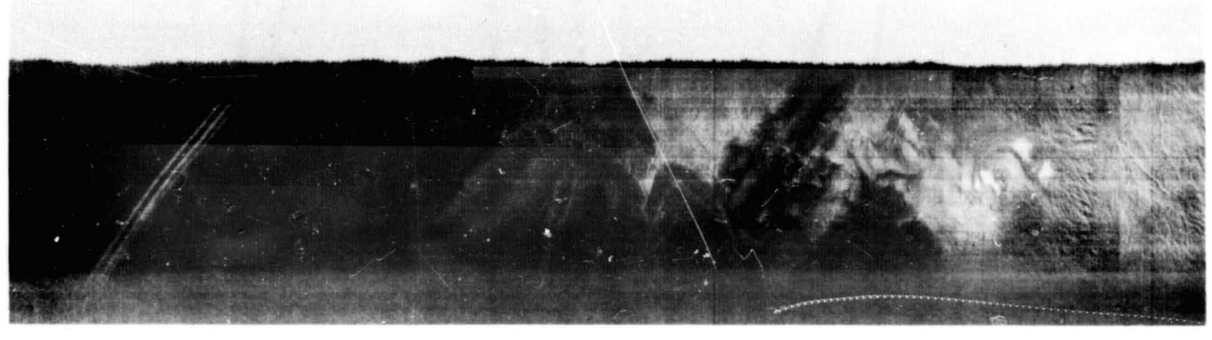

Ratio: $\frac{\text{Channel 1}}{\text{Channel 2}}$

ANALOG INFRARED IMAGES OF FLIGHT LINE 1, SECTION A
NEAR PISGAH CRATER, CALIFORNIA

INFRARED AND OPTICS LABORATORY
WRL

Figure 5

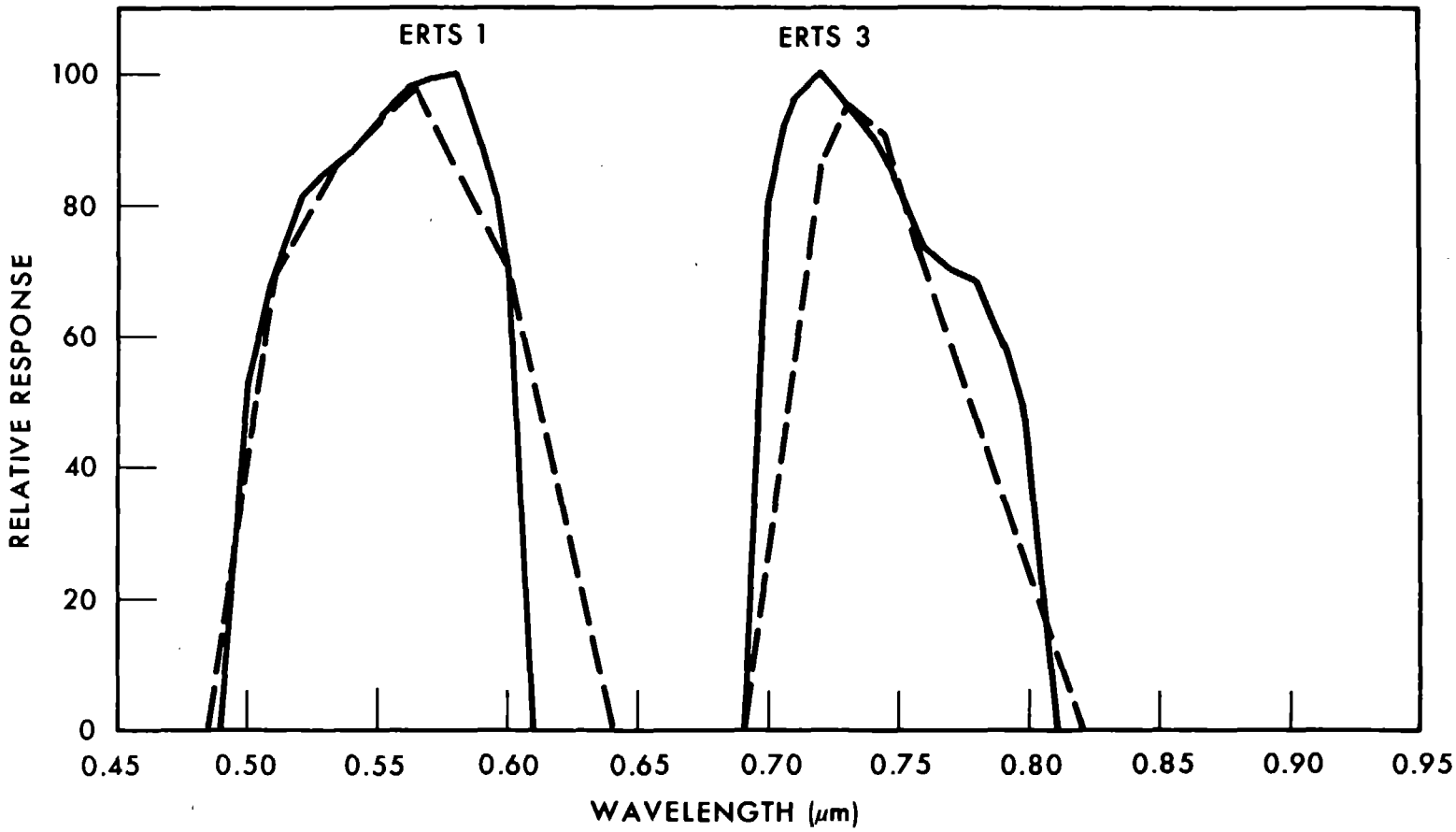

ACTUAL AND SIMULATED ERTS SENSITIVITY

Figure 6

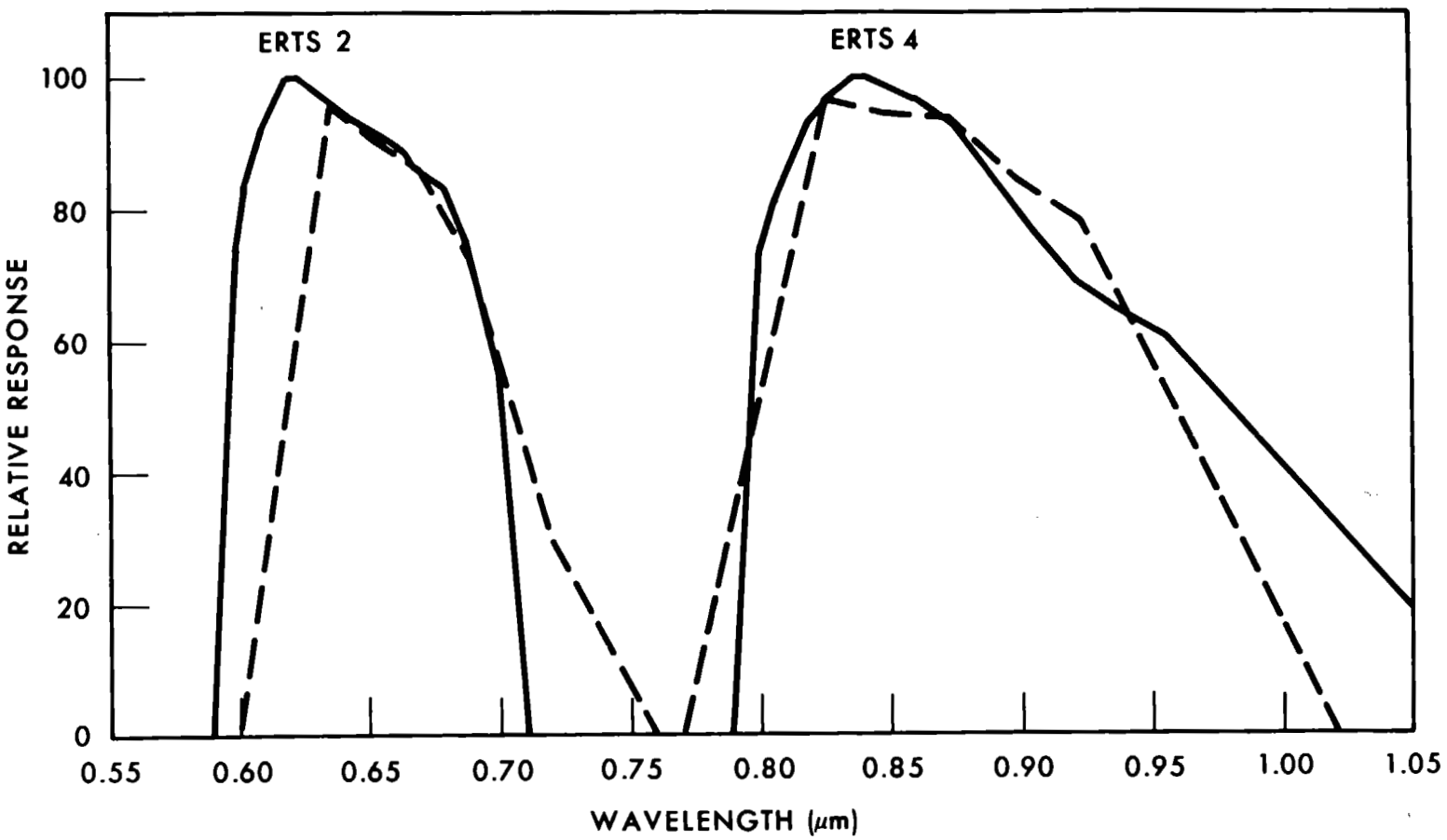

ACTUAL AND SIMULATED ERTS SENSITIVITY

Figure 7

INFRARED AND OPTICS LABORATORY
INSTITUTE OF SCIENCE AND TECHNOLOGY
WRL
THE UNIVERSITY OF MICHIGAN

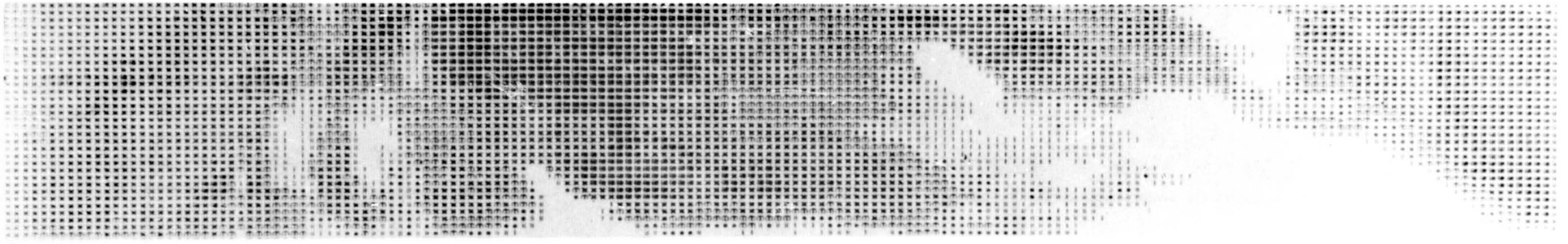

← N —

Simulated 80m Resolution ERTS Data

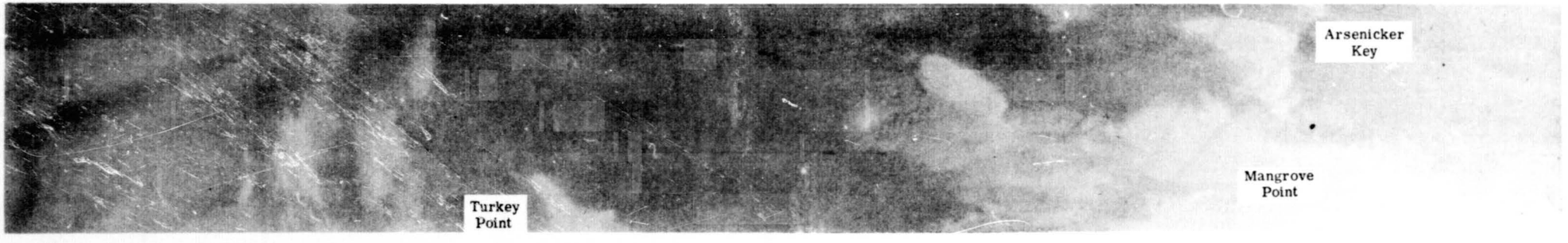

Scanner Data-10m Resolution

ERTS-MSS CHANNEL 3 SPATIAL RESOLUTION SIMULATION

Figure 8

0.72-0.92 μm Imagery

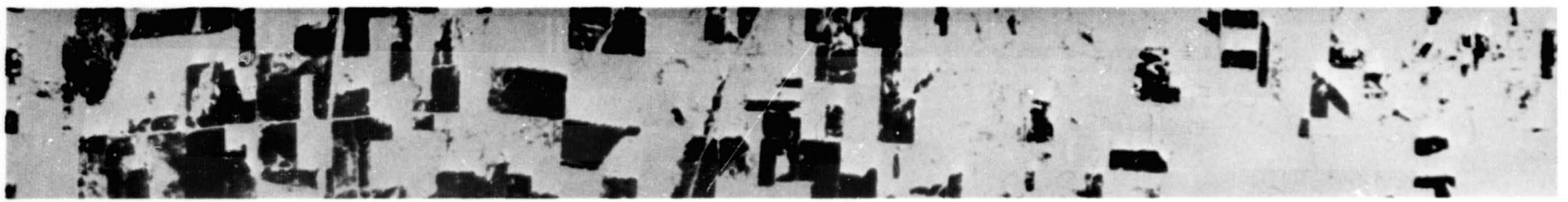

Color Coded Recognition Map

COLOR CODED RECOGNITION MAP OF CORN BLIGHT FOR SEGMENT 212 MISSION 43.
8/17/71, 1030 hrs.

Color	Material	Optimum Channels (μm)
Green	Corn, Blight levels 0-3	0.50-0.54
Red	Corn, blight levels 4 and 5	0.58-0.65
White	Not recognized	0.66-0.76
		0.72-0.92
		1.0 -1.4
		9.3 -11.7

Figure 9

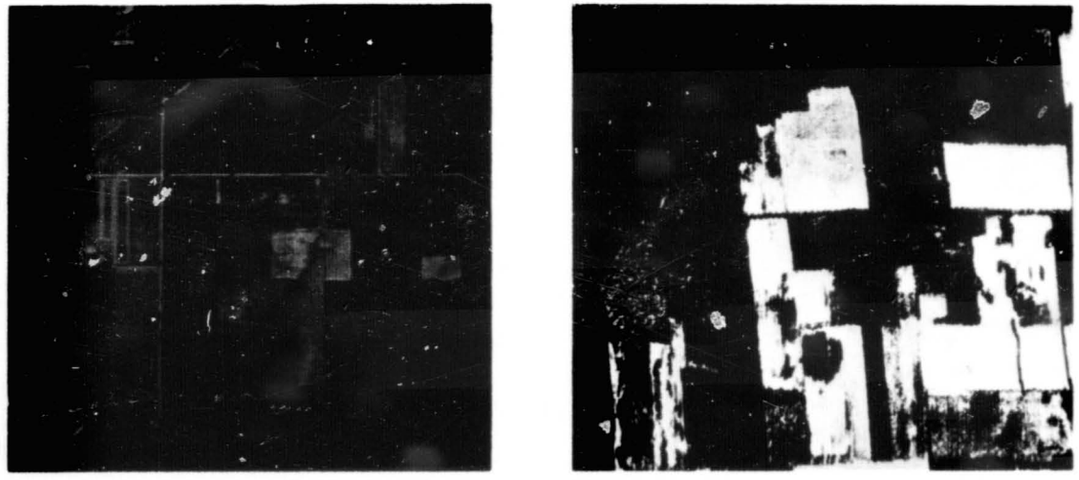

Color IR Photo Recognition Map

ILLUSTRATION OF DETECTION FAILURES IN CORN FIELDS.
Segment 211, 7/16/71, 0916 hrs., 5000 ft above terrain. Six channel likelihood ratio processing.

Figure 10

Investigator	Affiliation	Area	Problem
Frank Canney	USGS-Denver	Catheart Mtn., Maine	Delineate copper and molybdenum stressed trees.
A.E. Coker	USGS-Tampa	Central Florida	Delineate Vegetative indicators of fluoride pollution of ground water.
Richard Driscoll	USDA-Ft. Collins, Colorado	Manitou Nat'l Forest	Map forest, rangeland, and wetland sites
Milton Kolipinski	USGS-Miami	Biscayne Bay, Florida	Study ability of spectrally and spatially simulated ERTS data to map underwater plant communities.
Robert Johnson	USDA-Bemidji, Minnesota	Chippewa Nat'l Forest Minnesota	Map forest species and ponds in Chippewa Nat'l Forest.
Harvey Nelson	BSFW-Jamestown, North Dakota	North Dakota	Map pond water distribution and surrounding vegetation indicative of waterfowl productivity.
William Pearcy	Oregon State University	Oregon Coast	Delineate ocean water types by measurements of water spectral radiance.
Robert Vincent	University of Michigan	Pisgah Crater, California	Delineate exposed rock types using thermal ratio - reststrahlen technique.

Figure 11

Investigator	Affiliation	Area	Problem
Kenneth Watson	USGS-Denver	Mill Creek, Oklahoma	Map exposed sedimentary rocks using visible data, provide rock reflectance statistics, and provide temperature statistics for correlation with thermal model.
Craig Wiegand	USDA-Weslaco	Weslaco, Texas	Map soil and vegetation using spectrometer, near infrared, and simulated photographic data.

Figure 11. - Concluded.

TYPE I PROCESSING 1970-71

* Imagery — 3100 miles
* Contouring and Quantization — 14 jobs
* False Color Films
* Digital Tape — 2 jobs
* Panel Reflectance Measurements — 2 jobs
* Duplicate Analog Tape — 1 job

INFRARED AND OPTICS LABORATORY
INSTITUTE OF SCIENCE AND TECHNOLOGY
WRL
THE UNIVERSITY OF MICHIGAN

Figure 12

TYPE II PROCESSING 1970-71

* Signature Extraction and Analysis
  - Optimum Channel Analysis — 7 jobs
  - Processor Performance — 4 jobs
  - Reflectance or Radiance — 6 jobs
* Preprocessing Analysis — 11 jobs
* Digital Recognition Map — 13 jobs
* SPARC Recognition Map
  - Likelihood Ratio — 102 jobs
  - Parameter Map — 1 job
* Ratio Map — 2 jobs

INFRARED AND OPTICS LABORATORY
INSTITUTE OF SCIENCE AND TECHNOLOGY
WRL
THE UNIVERSITY OF MICHIGAN

Figure 13

SECTION 31

N72-29331

PREDICTION OF DIRECTIONAL REFLECTANCE OF A CORN FIELD UNDER STRESS

by

Gwynn H. Suits
The University of Michigan
Willow Run Laboratories
Ann Arbor, Michigan

Gene Safir
A. Ellingboe
Michigan State University
East Lansing, Michigan

INTRODUCTION

The remote sensing of symptoms of pathological conditions in vegetative canopies such as Southern Corn Leaf Blight depends upon a consistent relationship between the pathological symptoms and the remotely sensed effects. The use of training sets show only that in particular cases, and at a particular time, a certain pathological condition occurs concurrently with some remotely sensed effect. There may be no necessary connection between them. The use of a mathematical model to predict the remotely sensed effect from the fundamental biological causes allows one to establish the expected consistency between the conditions and the sensed effects as well as to provide insight leading to the best remote sensing techniques to use for a particular application.

A new method of calculating the directional reflectance of a vegetative canopy (1) has been used to calculate the directional spectral reflectance of a corn canopy under stress. The comparison of predicted reflectance with field measurements indicate that the model is sufficiently accurate when applied to corn fields to warrant the use of the model for application to other conditions. The prediction of the expected reflectance differences between a healthy and a blighted one-month old corn field illustrates the application to other conditions.

THE CANOPY MODEL CONCEPTS

A vegetative canopy has been idealized by assuming that any vegetative canopy, such as an agricultural crop, can be represented by several layers of uniform but randomly distributed biological components as shown

in Figure 1. For example, a corn field might consist of three layers, the top layer contains tassels, the second layer contains the main body of the corn plant, and the bottom layer contains a dead leaf region or a blighted region. The canopy is bounded on the bottom by the soil.

The biological components which exist in these layers are idealized as shown in Figure 2. The horizontal and vertical projection of leaves, for example, replace the actual leaf. The accumulative horizontal projection leads to the quantity called the horizontal leaf area index while the accumulative vertical projection leads to a quantity called the vertical leaf area index for each layer. The spectral properties of the projections are obtained from the spectral properties of the biological components. These vertical and horizontal indices, their spectral properties, the number of layers and the soil reflectance provide an idealized physical description of the vegetative canopy which is all that is required to calculate the spectral reflectance of the canopy under any conditions of illumination and for any angles of view.

VERIFICATION OF THE MODEL PREDICTION

The structure and contents of two mature corn fields at Michigan State University were measured and the calculation of the expected directional spectral reflectances were made on the basis of these measurements. Three sample plants in each field were used for measurements. Figure 3 shows the summary of the measurements. Field B data is on the left and Field G data is on the right. Each field is divided into two layers; the data for the top layer (number one) is on the left and the bottom layer (number two) is on the right. Each layer contains an accumulative horizontal index on the left and a vertical index on the right. Finally, each index type is divided into the spectral types; the green healthy leaf material is shown in cross hatch bar on the left, the chlorotic material is shown by the clear bar, the necrotic material is shown by the black bar, and the stalk material is shown by the vertical lined bar.

Both fields are Texas-male-sterile corn with about 21,000 plants per acre. Field B is an unblighted field but is under drought stress which was the prevailing condition in southern Michigan during the growing season of 1971. Field G is blighted by Southern Corn Leaf Blight to an estimated blight level of 3 but the field is also under irrigation. The difference in character of these two types of stress are made manifest by these structural measurements. Note the extensive necrotic material in layer two of field G caused by the blight. Compare, also, the vigor of layer one of field G to layer one of field B. This difference is due to the effects of irrigation in field G.

It is not difficult to foresee the consequences of this structure in influencing the spectral reflectance of the canopy. The top layer will tend to be dominant so that field G will have a spectrum of a nearly healthy undroughted field while field B will have a spectrum in which the lower layer and soil will contribute,

The comparison between the predicted directional reflectance and the measured directional reflectance for two polar viewing angles, 0° and 45°, are shown in Figure 4 for field B and Figure 5 for field G. The correspondence is good between predicted and measured spectra indicating that the model of biological structure and content accounts for the major causes of the remotely sensed effects.

APPLICATIONS TO HYPOTHETICAL CASES

In order to illustrate what can be done with a predictive directional reflectance model, suppose one wished to know what the reflectance of a blighted field of Texas-male-sterile corn would be like one month after planting and in what way that reflectance would differ from the reflectance of a similar but unblighted field. The procedure which was followed by the authors was to grow greenhouse samples, to make geometric measurements on these plants, and to introduce this data into the predictive model. Naturally, for realistic results, these sample plants must be grown under such conditions that they will be physiologically equivalent to field grown plants.

The structural measurements of representative plants at the age of one month were begun on April 5, 1971, twenty-four hours after inoculation with *Helminthosporium maydis* (Southern Corn Leaf Blight). Data from a control plant which remained uninoculated were also taken. Figure 6 shows the progression of these measurements as obtained on April 5, 9, and 12. The data labeled C-2 is obtained from control plant number two; the data labeled I-2 is from inoculated plant number two. Total leaf areas are plotted to the right of the corresponding data graphs. The cross-hatch coding is the same as used before in Figure 3. The vigorous growth of the healthy plant, C-2, is in sharp contrast to the retarded growth of I-2. Note also the change in the ratios of horizontal to vertical leaf areas indicative of important geometrical orientation changes of the leaves in I-2.

The comparison of predicted reflectances of a field of C-2 and a field of I-2 with 21,000 plants per acre is shown in Figure 7. In the infrared range, the difference in reflectance is modest but significant; however, notice that the difference due purely to polar viewing angle is greater than the difference between blight and healthy fields. While blighted fields viewed at 0° are darker than healthy fields at that same viewing

angle, the blighted field viewed at 50° polar angle is brighter than the downward view of healthy fields. Thus, a remote sensing system, which is based upon the assumption that blighted fields are always darker in the infrared than healthy fields, would misclassify fields if the healthy field were at 0° and the blighted fields were at 50°.

The reflectances in the chlorophyll absorption band near 0.67 μm behave quite differently. In this band, the difference between reflectances of blighted fields and healthy fields is greater than the differences due to viewing angle so that one could rely upon the blighted fields always being brigher than the healthy fields by a considerable margin.

SUMMARY

A new way of calculating the directional spectral reflectance of a vegetative canopy has been applied to corn fields under stress conditions. The predicted and field measured spectra are in good agreement so that predicted spectra for hypothetical cases can be trusted to indicate significant directional spectral reflectance properties which may be useful in applying remote sensing techniques to a variety of vegetative canopies and aid in interpreting the results.

REFERENCE

(1) G. Suits, "Calculation of the Directional Reflectance of a Vegetative Canopy," Remote Sensing of Environment, Vol. 2.2, in publication, American Elsevier.

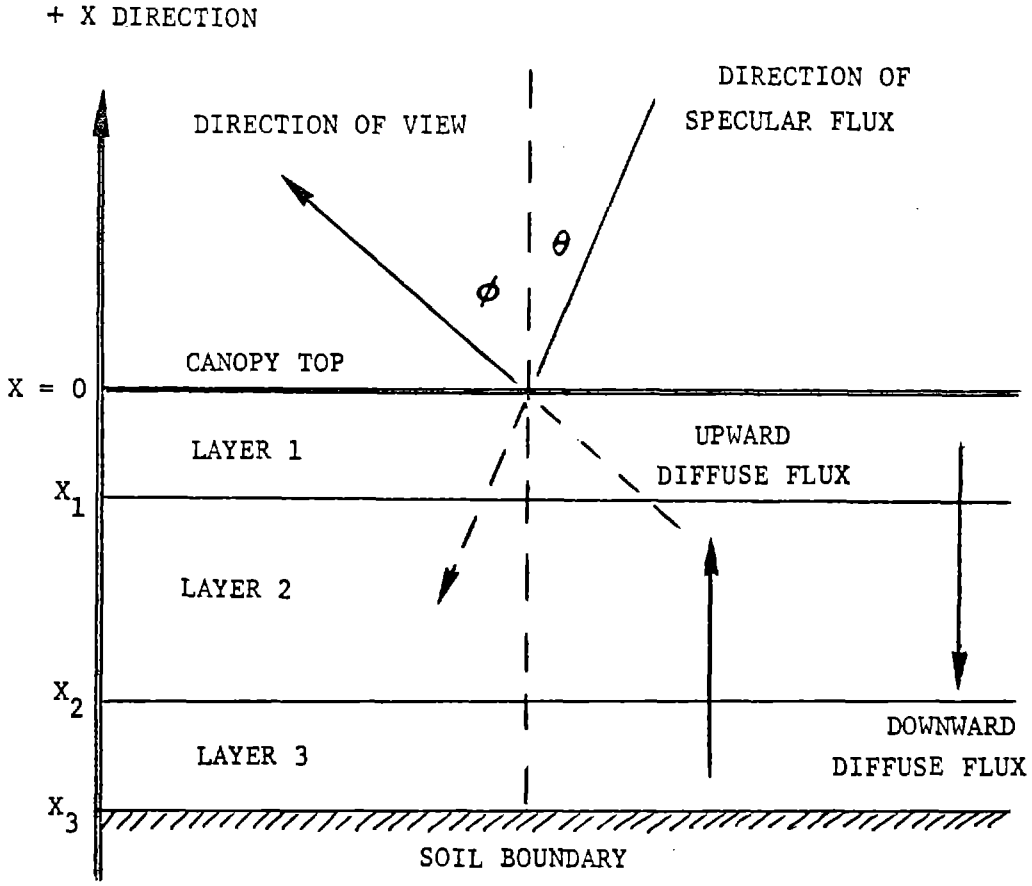

FIGURE 1. IDEALIZED LAYER STRUCTURE OF A CANOPY. Each layer represents a uniform mixture of biological elements normally found at that level in the vegetative canopy.

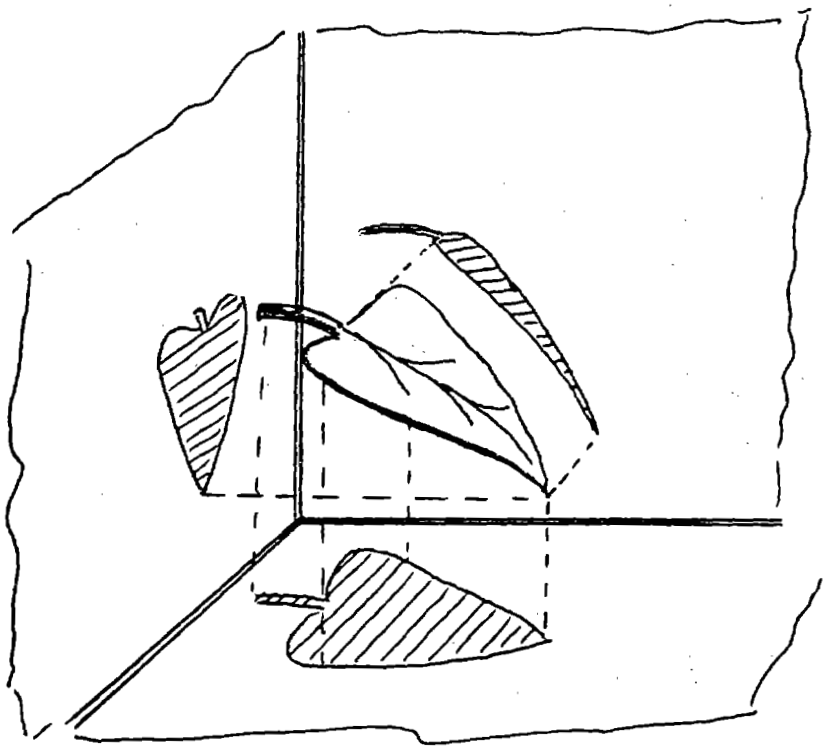

FIGURE 2. ORTHOGONAL PROJECTIONS MAKING IDEALIZED BIOLOGICAL COMPONENTS. The horizontal projections taken together lead to a quantity called the horizontal leaf area index. The vertical projections taken together lead to a quantity called the vertical leaf area index.

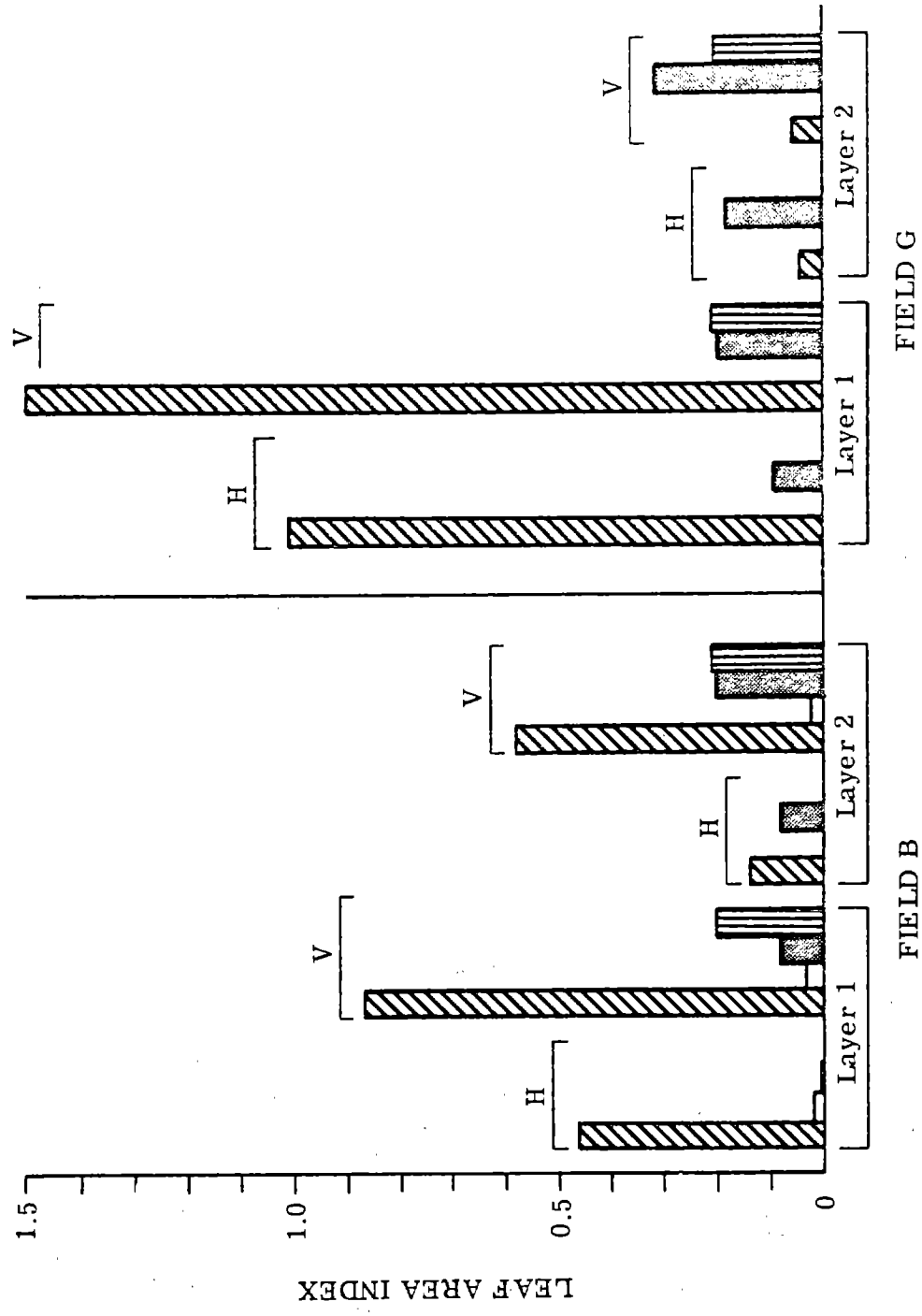

FIGURE 3. STRUCTURAL MEASUREMENTS OF TWO MATURE CORN FIELDS. Layer 1 is the top layer; layer 2 is the bottom layer. The horizontal and vertical leaf area indices for each layer are shown by bar graph. Cross hatched is green healthy material; clear is chlorotic material; black is necrotic material; and vertical hatched is stalk material.

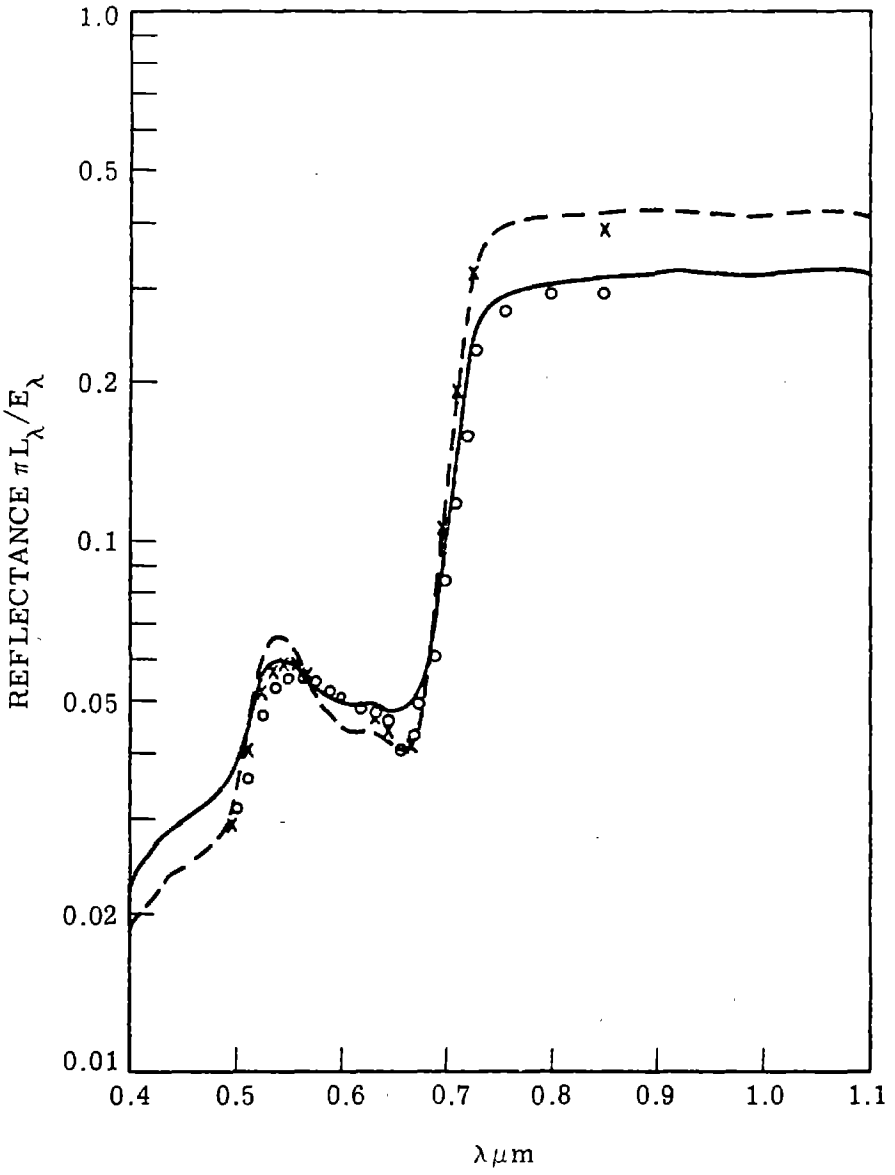

FIGURE 4. FIELD B SPECTRAL REFLECTANCE. The predicted and measured directional spectral reflectance of MSU corn field B is shown for the day 8-24-71. The field is under drought stress. It contains Texas-male-sterile corn with about 21,000 plants per acre. The canopy is about 2 meters high. The sun is 38^{o} from zenith. The azimuth of view is 160^{o} relative to the sun (azimuth of 0^{o} means sun at observers back). The calculated solid curve is for polar view angle of 0^{o}; the calculated dashed curve is for polar view angle of 45^{o}. Field measurements corresponding to the 0^{o} view angle are designated by 0. The field measurements for the 45^{o} view angle are designated by x.

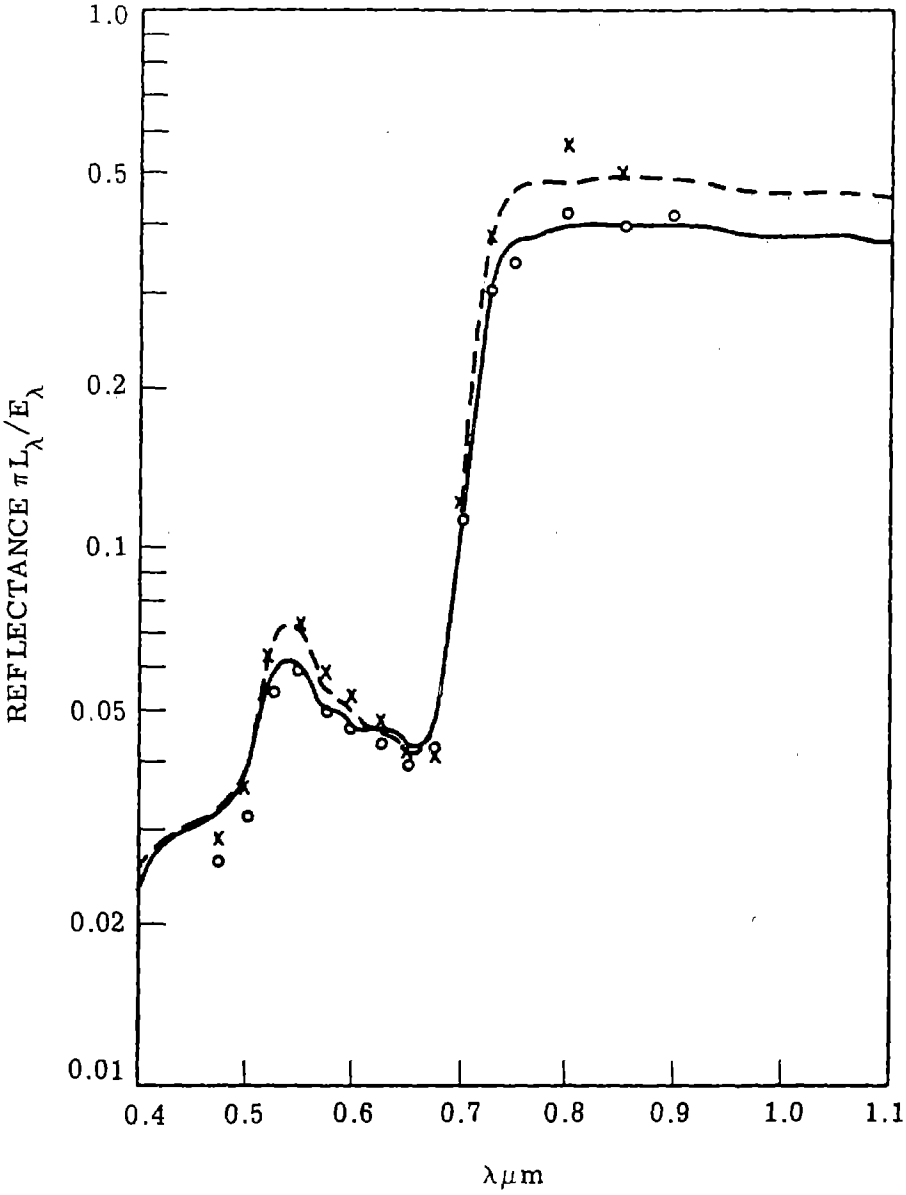

FIGURE 5. FIELD G SPECTRAL REFLECTANCE. The predicted and measured directional reflectance of MSU corn field G is shown for day 8-13-71. The field is under irrigation but also under level 3 Southern Corn Leaf Blight stress. It contains Texas-male-sterile corn, 21,000 plants per acre at a height of about 2 meters. The sun is 38° from zenith. The azimuth of view is 90° (at right angles to the direction of solar flux). The calculated solid curve is for polar view angle of 0°; the calculated dashed curve is for polar view angle of 45°. Field measurements corresponding to view angles of 0° and 45° are designated by 0 and x respectively.

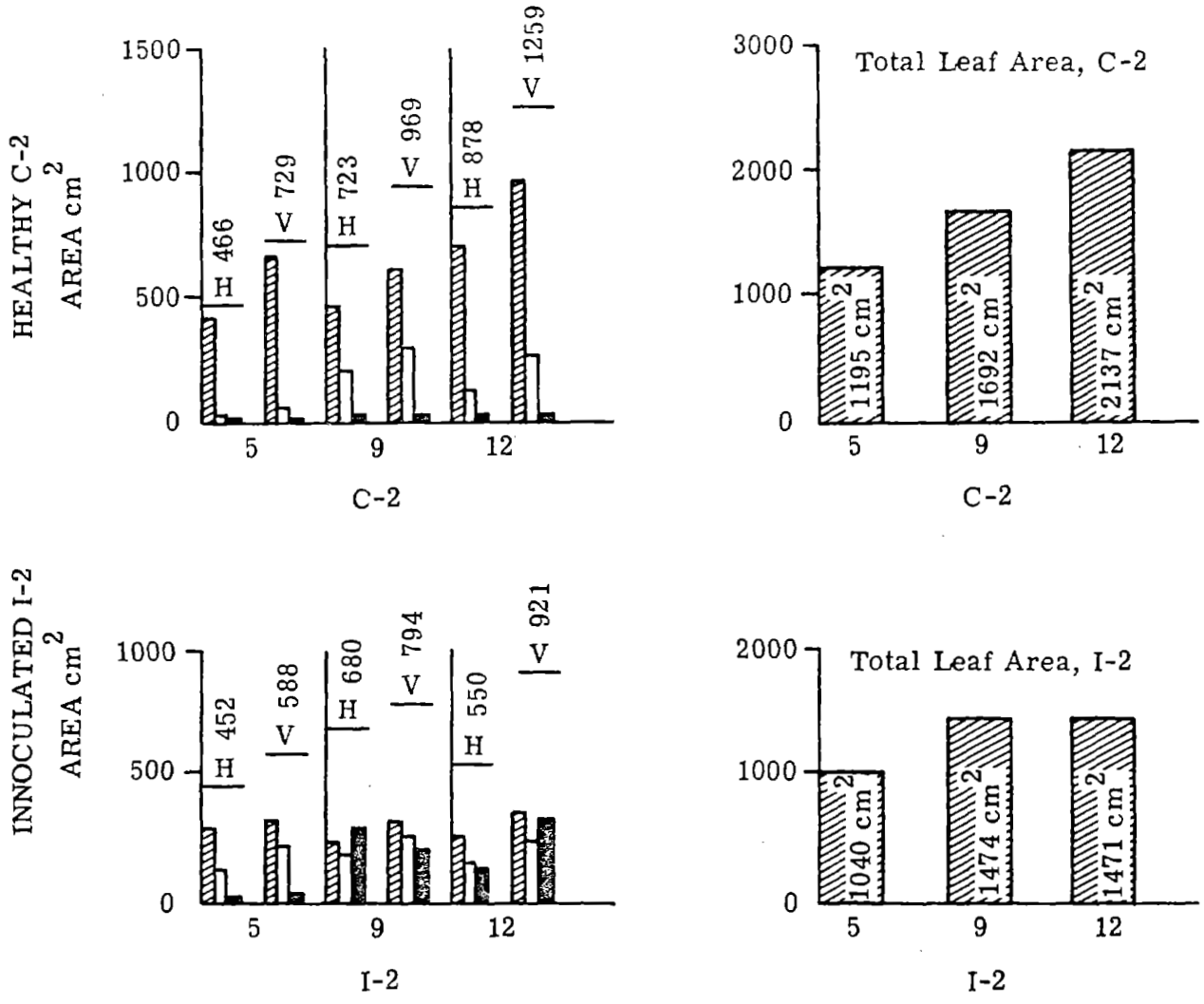

FIGURE 6. STRUCTURAL PROGRESSION OF GROWTH OF YOUNG CORN. Two one month old corn plants, C-2 and I-2, were measured beginning one day after I-2 was innoculated with Southern Corn Leaf Blight, April 5, 9, and 12. Cross hatched bars show areas of green healthy material; clear bars show areas of chlorotic material, and black bars show acres of necrotic material.

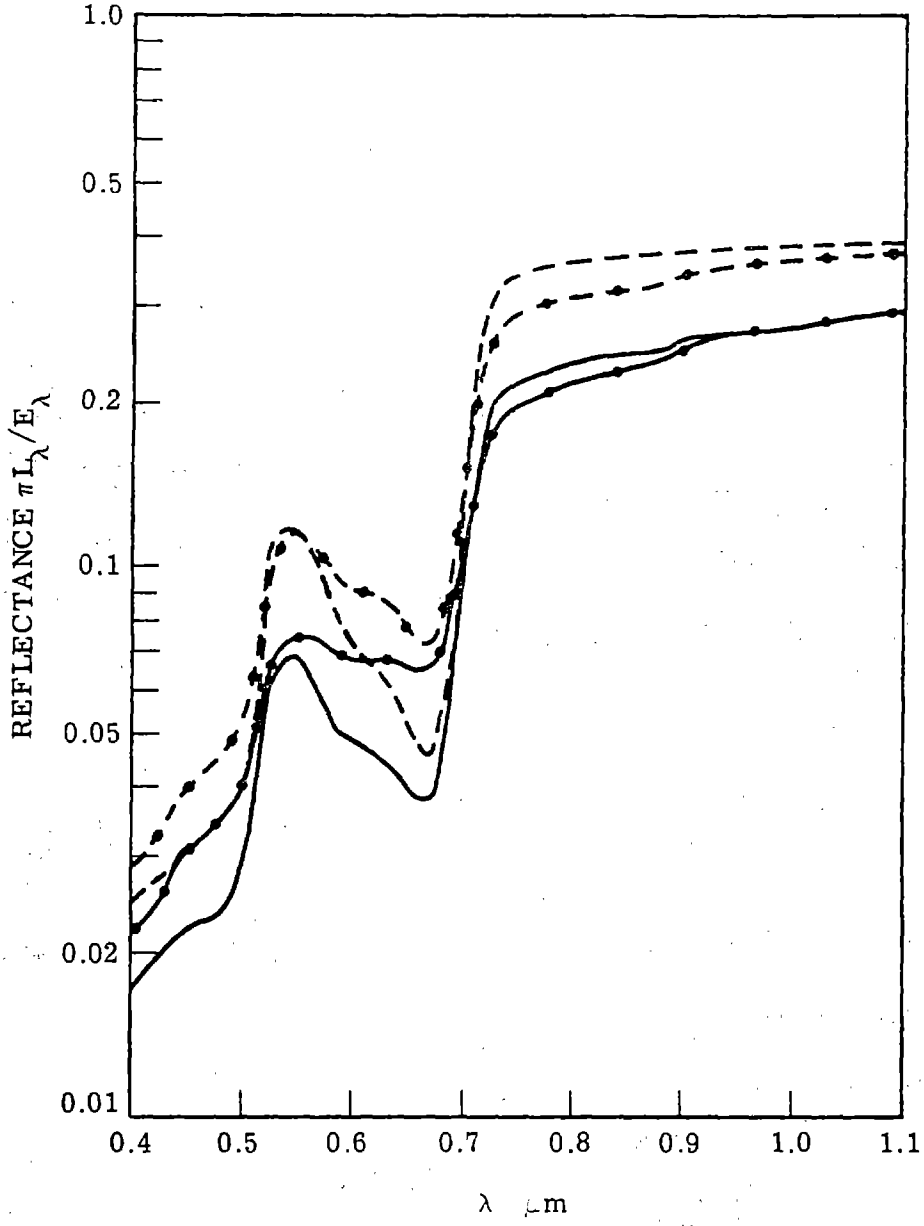

FIGURE 7. PREDICTED SPECTRAL REFLECTANCES OF YOUNG CORN. The calculations assumed a polar sun angle of 50°, a polar view angle of 0° (solid curves) and 50° (dashed curves) and a viewing azimuth relative to the sun of 45°. The smooth curves are for a field of plants like C-2; the rough curves are for a field of plants like I-2 8 days after innoculation. Plant density is assumed to be 21,000 per acre on the soil type found at the Michigan State University Agricultural Experiment Station.

N72-29332

SECTION 32

CLASSIFICATION OF SPATIALLY UNRESOLVED OBJECTS*

by

Richard F. Nalepka
Harold M. Horwitz
Peter D. Hyde
James P. Morgenstern
Willow Run Laboratories
University of Michigan
Ann Arbor, Michigan

The practical utility of multispectral scanner data is often restricted by the limited spatial resolution of the sensor gathering the data. Restrictions of this sort will exist in the data to be gathered by the multispectral scanners in the ERTS-A and SKYLAB satellites. These scanners will view the ground with an instantaneous field of view (IFOV) covering a ground patch about 300 feet on a side. The radiation detected when scanning portions of a scene containing objects smaller than this size will be composed of a mixture of radiation from all objects within the IFOV. Similarly, when the field of view overlaps the boundary between two larger objects, the radiation detected will be a mixture from the two objects. The signals generated by the sensor in both of these cases will not be representative of any one object.

The effect of viewing more than a single object class is illustrated in Figures 1 and 2. In Figure 1 the reflectance spectra are depicted for corn and bare soil as they would appear individually. If the sensor was to simultaneously view both corn and bare soil the effective reflectance spectrum would be quite different. This is shown in Figure 2 for the combinations 20% corn - 80% bare soil and 50% corn - 50% bare soil. These spectra are simply weighted combinations of the pure spectra of Figure 1.

The use of standard multispectral recognition processing techniques on data points which result from viewing two or more objects will likely result in the improper classification of those data points. Given a

* The work reported in this paper was supported by NASA under Contract NAS9-9784.

sufficient number of improper classifications of this sort the results of such efforts as might be applied in crop acreage determination, for example, would be greatly in error.

It might be useful, at this point, to provide some idea of the seriousness of this effect. Figure 3 illustrates the effect of sampling and reconstructing a scene using a sensor whose resolution is approximately the size of the structure in the scene. For illustrative purposes the scene is composed of black and white squares arranged as on a checkerboard. Obviously if the resolution of the sensor was significantly smaller than the dimensions of the square, the scene could be reconstructed with very good fidelity. However, this will generally not be the case for either the ERTS or SKYLAB multispectral sensors.

In Figure 3 we consider two situations. One in which the resolution is one half that of the squares and another in which the resolution exactly equals the square size. Now, it is possible for both these situations to perfectly reconstruct the scene. The probability of this occurring, however, is very slim since the samples must be taken only at those times during which the sensor is viewing portions of all of either the black or the white square. It is much more likely that in an attempt to sample the entire scene, that is leave no voids between samples in either direction, many samples would be extracted when the sensor was viewing some portion of each of two or more adjacent squares. In this case the scene could not accurately be reconstructed.

In the lower portion of Figure 3, we depict the reconstruction of the scene for the resolution being one half the square size (lower left) and equal to the square size (lower right). Here we consider the worst situation that may exist since we can have no assurance beforehand that this will not in fact be the case for an arbitrary scene for which the sampling scheme has not been specifically designed. For the resolution of one half the square size, the samples which fall totally within each square fall precisely in the center of the squares. All other samples, therefore, are extracted when half the sensor field of view covers white squares and the other half covers black squares. The sensor signals generated in this situation are not characteristic of either of the objects in the scene. In this case the use of standard automatic processing techniques for classification and determination of the ground area covered by each of the two objects in the scene, would result in significant errors. In this particular case 50% of the scene area would be improperly classified. For the situation where the resolution equaled the square size the error would be 100% since not a single sample would be classified correctly.

We have carried out some calculations to get a feeling for how serious this problem may be for spaceborne sensors viewing an instantaneous ground patch 300 feet on a side. The results of the calculations are plotted in Figure 4 which illustrates the effect of field area and shape on the multispectral training and classification operations. Just as before we consider fields which are square in shape, however in addition, we also consider rectangular fields. The dimensions of both square and rectangular fields are integral multiples of 300 feet and all sampled areas which occur at field boundaries are assumed to fall one half (at the corners this is three quarters) outside the field. For the rectangular fields the small dimension is limited to 600 feet. Square fields and rectangular fields of this sort define the limiting conditions (best and worst) for regularly shaped areas.

Two pairs of curves are plotted in Figure 4. The curves depicted as dashed lines relate the number of acres in a field to the number of 300 by 300 foot elements totally within the field. This relationship is significant when considering the requirements for training a recognition computer. The number of samples generally considered necessary for an adequate determination of the statistics defining a multispectral signature is ten times the number of spectral channels being utilized. If the four ERTS channels were considered, a minimum of 40 representative samples would be required. To assure this number of samples in a single field would require a square field of at least 110 acres and a 2 x n element rectangular field of 170 acres or so.

If, however, training of the computer had already been accomplished, it would be desirable to know what errors might be expected in automatically determining the area covered by a selected set of object classes. This information is also plotted in Figure 4. The curves depicted as solid lines relate the number of 300 by 300 foot elements in the field to the percentage of the field area which is seen in combination with portions of adjoining fields. It is this area which would probably be classified incorrectly and produce the errors in area computed. For the 110 acre square field described before, 40 elements were totally within the field and a 25% error in the determination of the area of that field could be expected. A 51% error in the area of the 170 acre rectangular field could be expected.

Not only are these errors of significant size, but if one is considering carrying out agricultural surveys, the field sizes considered above are somewhat larger than is typical in many agricultural areas. As shown in Figure 4 larger errors would result for smaller fields.

In order to reduce the restrictions on the utility of remotely sensed multispectral data, personnel of the Willow Run Laboratories have been conducting theoretical studies to develop special processing and information extraction techniques which will enable the accurate and timely estimation of the proportions of objects and materials appearing within the IFOV of a remote multispectral sensing device.

It is the fact that the radiation emanating from each scene element is detected simultaneously in several spectral bands which offers the possibility for classifying and estimating the proportions of spatially unresolved objects. The model that we have used to describe the signature generated in viewing a mixture of objects is as follows:

$$A_X = \sum_i X_i A_i$$

$$M_X = \sum_i X_i M_i$$

where the signature of Type i material is a Gaussian distribution with mean A_i and covariance matrix M_i and the proportion of Type i material is X_i.

As long as the radiation spectra generated by objects within the IFOV are linearly independent, i.e., a unique radiation spectrum results for each combination of objects, a satisfactory solution will usually be possible. This requirement is somewhat more limiting than that imposed for standard recognition processing. In Figure 5 we illustrate two separate plots of the means and distribution contours (signatures) of three objects as seen in two spectral bands. In each case the signatures of the three objects are sufficiently separate so that if any one of them was viewed in its pure state it could easily and properly be classified. For the case depicted in the upper portion of the figure, combinations of the three objects would produce points generally falling within the triangle and using the specially developed techniques the proportions of these objects could be determined. The lower portion of the figure, however, depicts a situation where the pure signature for object A_1 exhibits characteristics very similar to a combination of the other two objects. In this case the proportions of a mixture of these objects could not be accurately determined. Although all possible sets of objects and materials of interest may not meet the requirements for linear independence, it is believed that the requirements are met often enough to make the solutions now being investigated potentially very useful.

During the last year our primary efforts have been directed towards searching for computational algorithms which could both efficiently and accurately estimate the proportions of mixtures of objects. Three potentially useful algorithms were located, implemented via digital

computer programs, and tested. In order to provide the control necessary for the proper testing of these algorithms all tests were carried out using artificially generated mixtures. In some cases the pure signatures used to generate the artificial mixtures were extracted from data gathered by The University of Michigan multispectral scanner while in other situations totally artificial signature sets were constructed.

The latter was the case when tests were run to compare the processing time of the three computational methods as a function of the number of signatures employed. Here the pure signatures were arranged to form a symmetric set exhibiting identity covariance matrices and separated from each other by a unit distance. Two sets of 100 data points were generated. One set was distributed normally about the centroid of the signatures (the equal proportion situation) while the other set was similarly distributed about one of the signature means.

In Figure 6 we see that the computation time is a function of the location of the data points with respect to the pure signatures for all three methods considered. For two of the three methods (the F and the C methods) the computation time required for data points at or near the centroid exceeds that for points at or near the vertex. The opposite is true for the T method. These differences are a result of differences in the manner in which proportions are estimated in each method.

It is clear that as the number of signatures increases the computation time also increases. The best overall method seems to be the C method. However, for small numbers of signatures and data points near the centroid the T method would do just as well. As illustrated in Figure 6, the computation of proportions for each data point is a relatively time consuming task. The time required is approximately an order of magnitude greater than standard processing and four orders of magnitude greater than data collection. Some reductions in processing time could be achieved by utilizing larger and more up to date computer facilities but still the time required would be significant.

In many applications, proportions for each data point may not be required. For these cases a reduction in computation time can be achieved by averaging many data points and then carrying out a single computation of the proportions of the objects appearing in the entire region which was averaged. This approach is not only much faster but it also provides the possibility for improved accuracy. Improved accuracy might result since averaging would reduce the effect of the variability of sensor signals due to the natural variation of the radiation received from any object class in the scene. In addition, the effects of random noise would be reduced.

In order to test the averaging approach, signatures for bare soil, weeds, alfalfa, and barley were extracted from multispectral scanner data gathered by The University of Michigan. A total of 400 data points were generated with each set of 100 being normally distributed about the mean of artificial mixtures indicated in columns 2-5 of Table I. These 400 data points were averaged and an estimate of the proportions for the single average data point was computed. The results of the computation are given in column 7. Upon comparison with the average of the specified proportions shown in column 6 it is obvious that the estimated proportions are quite accurate, exhibiting a maximum error of 1.5%.

We are now preparing to apply these proportion estimation techniques to real data to identify any unforeseen problems which may arise in operating on real data sets, to refine or modify the approach to overcome these problems, and to provide a more realistic demonstration of the potential of these techniques.

TABLE I. TEST OF AVERAGING APPROACH TO ESTIMATE PROPORTIONS
(Artificial Mixtures)

MATERIAL	SPECIFIED PROPORTIONS 100 PTS.	SPECIFIED PROPORTIONS 100 PTS.	SPECIFIED PROPORTIONS 100 PTS	SPECIFIED PROPORTIONS 100 PTS.	AVE. SPECIFIED PROPORTIONS 400 PTS.	ESTIMATED PROPORTIONS	ERROR
BARE SOIL	0.25	0.35	0.10	0.20	0.225	0.234	0.009
WEEDS	0.25	0.20	0.50	0.35	0.325	0.320	0.005
ALFALFA	0.25	0.15	0.20	0.30	0.225	0.210	0.015
BARLEY	0.25	0.30	0.20	0.15	0.225	0.236	0.011

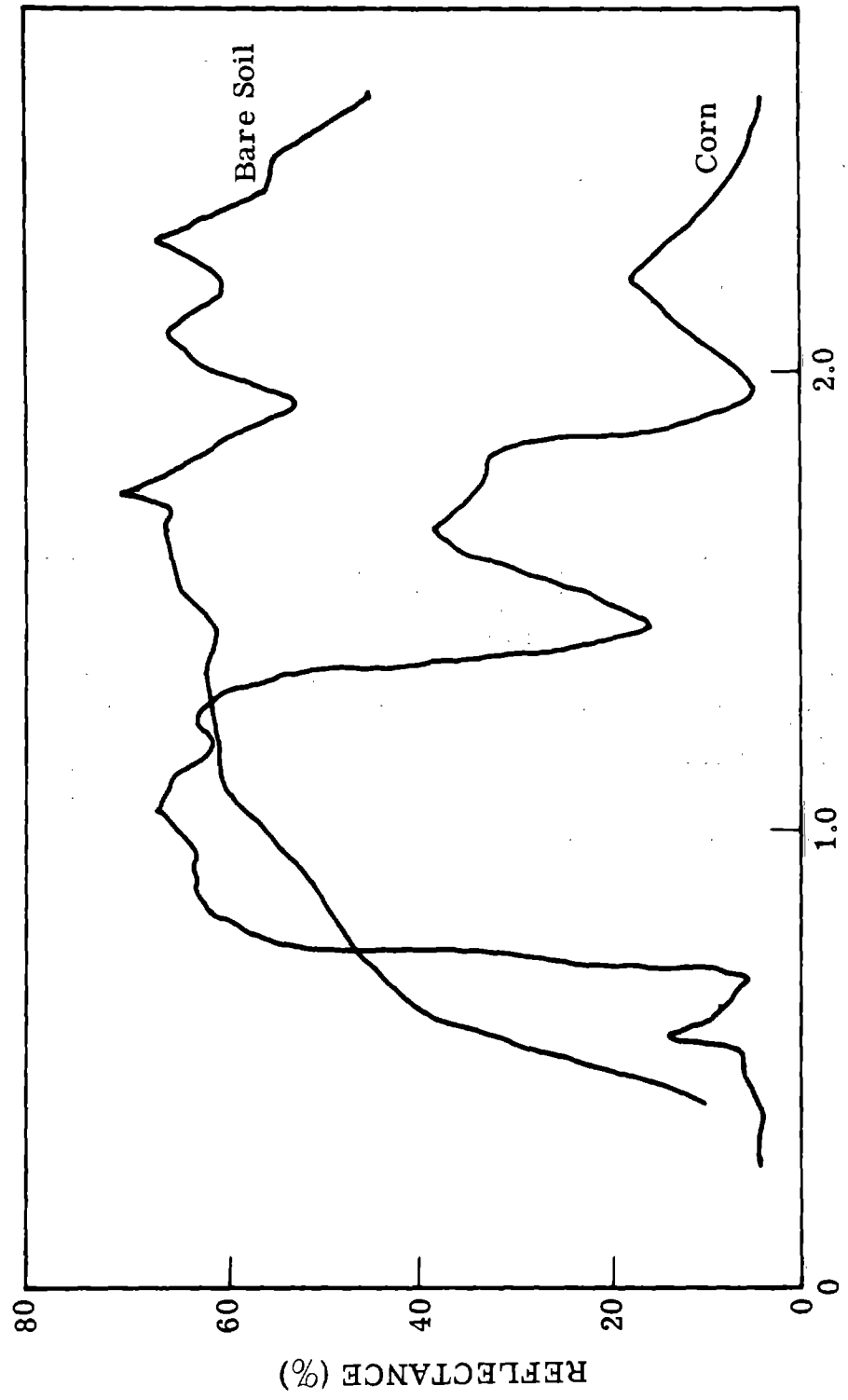

FIGURE 1. REFLECTANCE SPECTRA

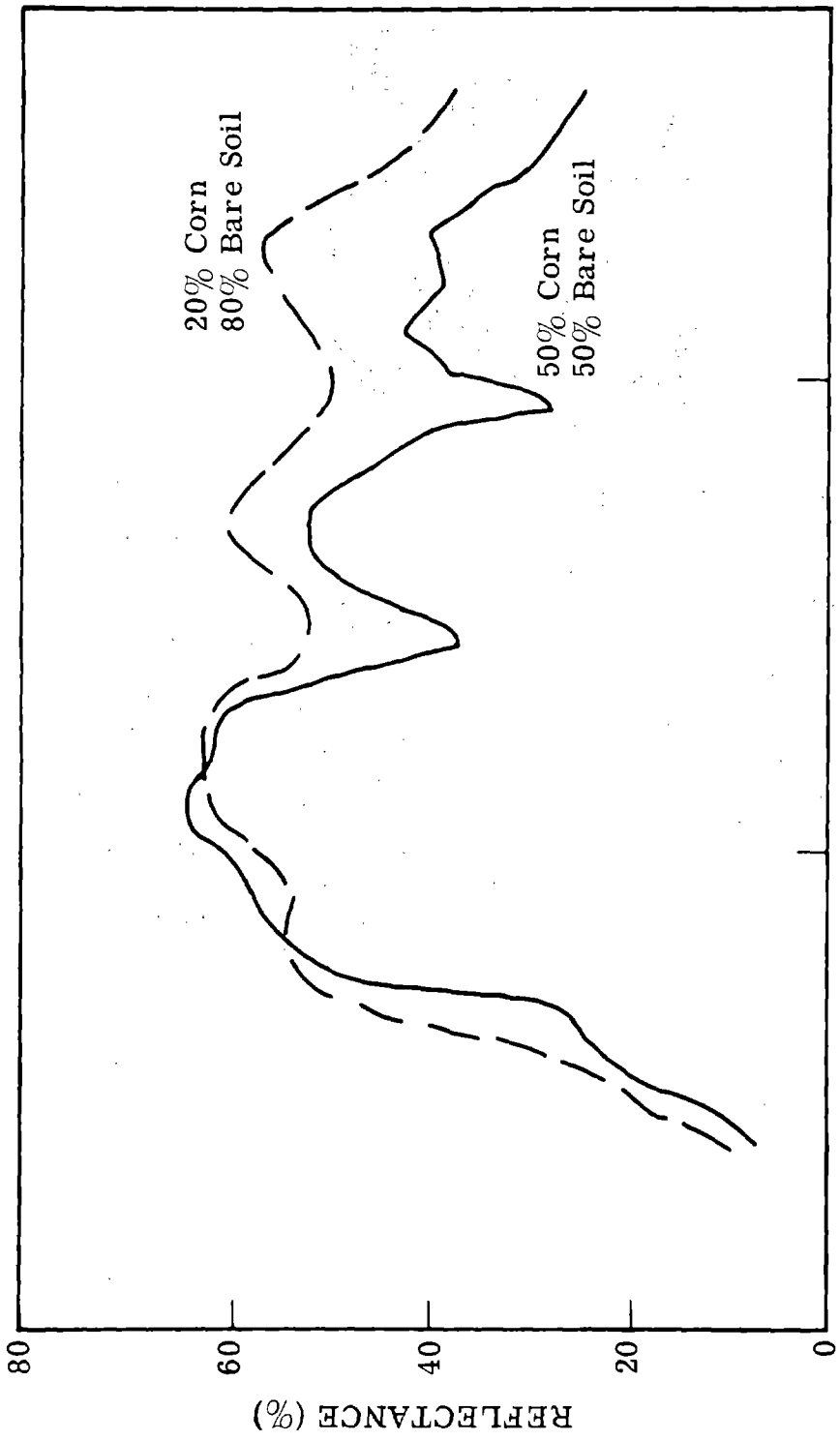

FIGURE 2. REFLECTANCE SPECTRA OF MIXTURES

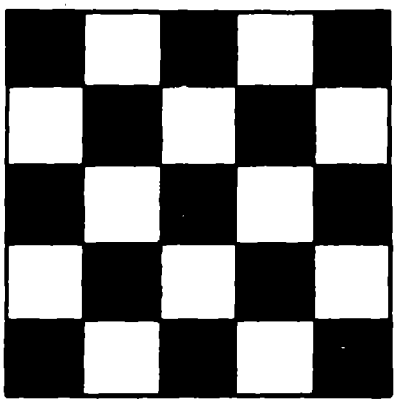

Checkerboard Scene

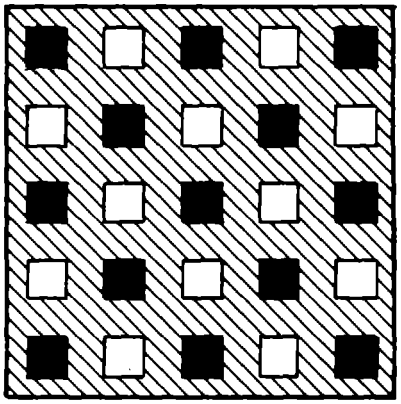

Reconstructed Scene
Optical Resolution Equals
One Half Checkerboard
Cell Size (Worst Case)

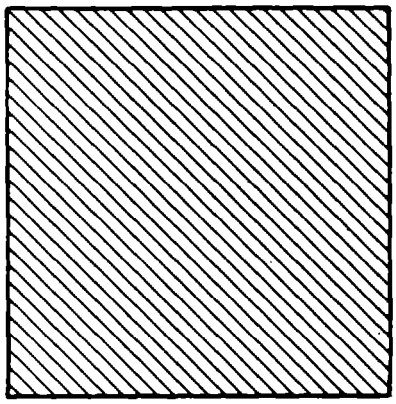

Reconstructed Scene
Optical Resolution Equals
Checkerboard Cell Size
(Worst Case)

FIGURE 3. EFFECT OF SAMPLING AND RECONSTRUCTING A SCENE WITH OPTICAL RESOLUTION APPROACHING THE SCENE STRUCTURE SIZE

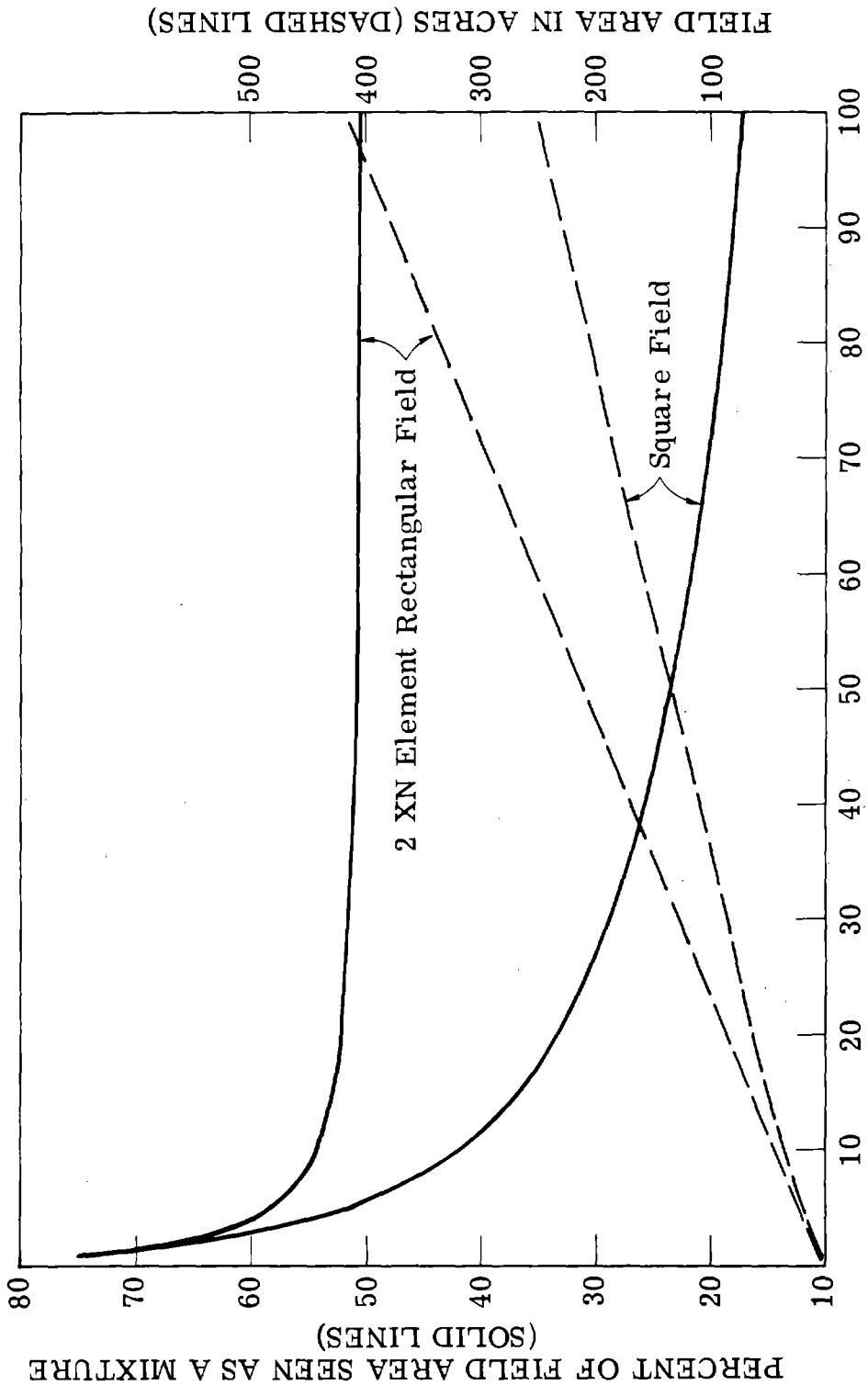

FIGURE 4. THE EFFECT OF FIELD AREA AND SHAPE ON MULTISPECTRAL TRAINING AND CLASSIFICATION FOR 300 X 300 ft. OPTICAL RESOLUTION

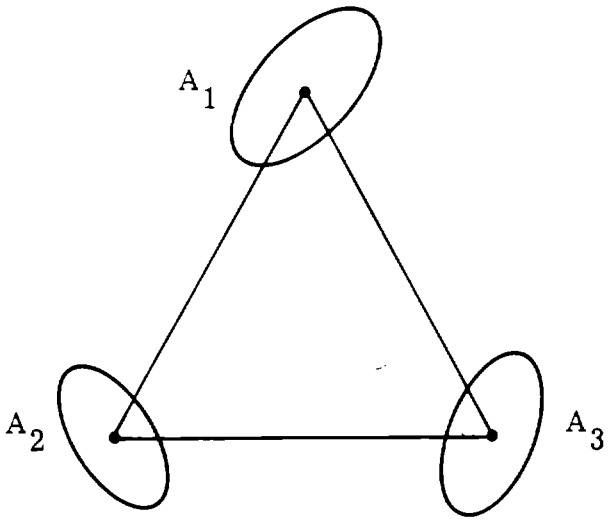

(a) Signature Simplex with Unit Contour Ellipsoids

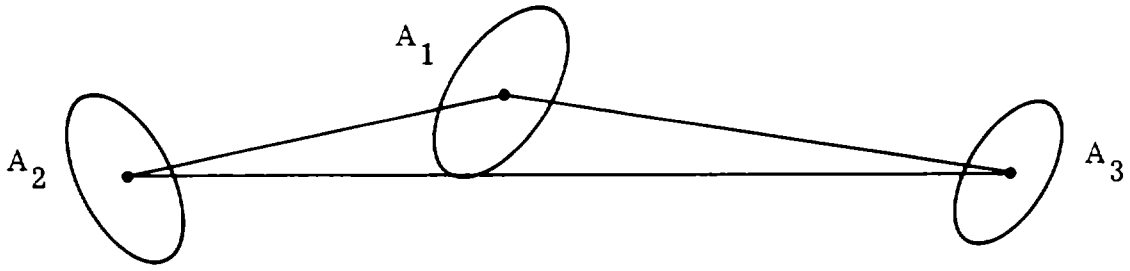

(b) Nearly Degenerate Signature Configuration

FIGURE 5. GEOMETRIC CONFIGURATION FOR THREE SIGNATURES AND TWO CHANNELS

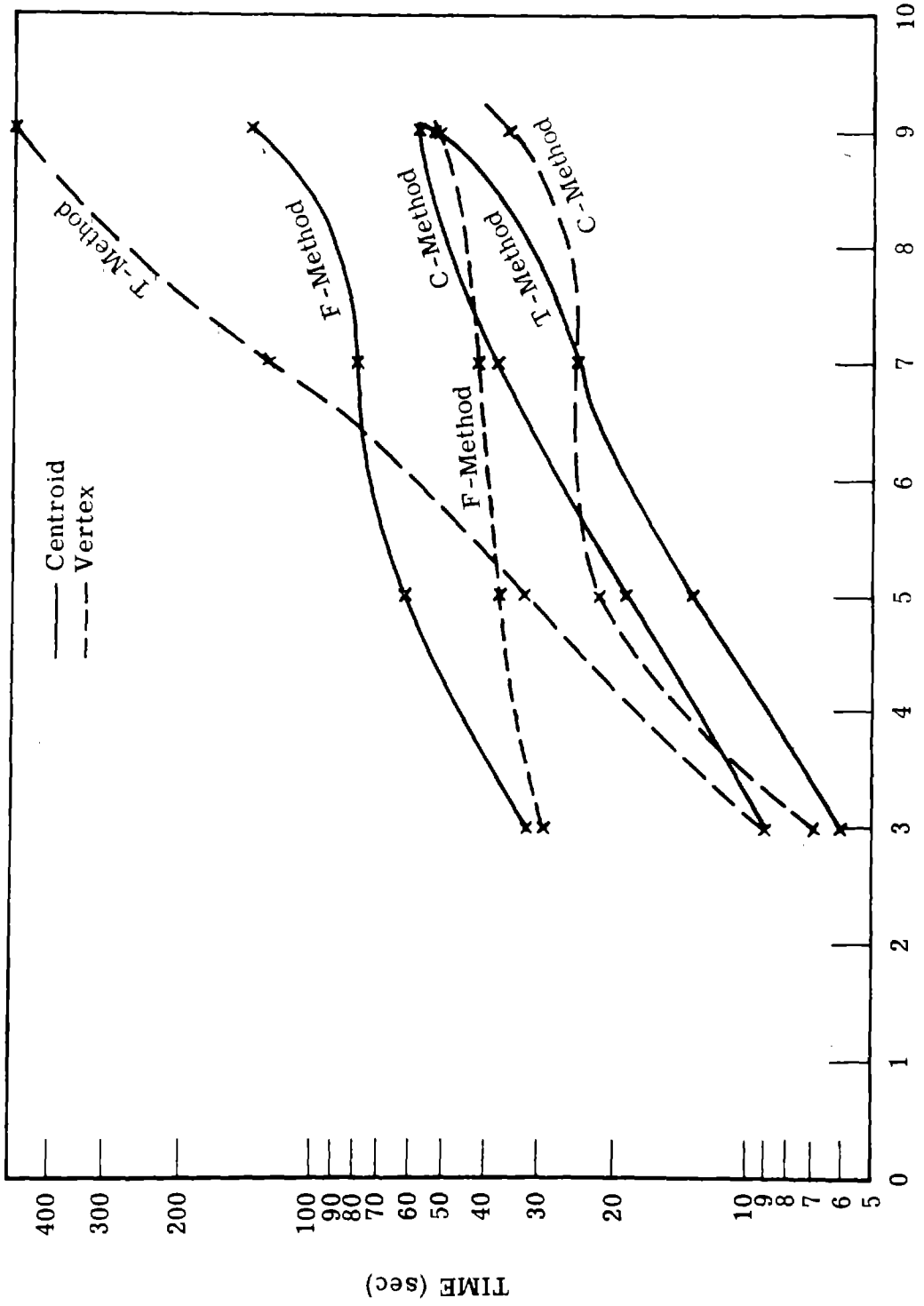

FIGURE 6. PLOTS OF RUNNING TIME VERSUS NUMBER OF SIGNATURES (CENTROID AND VERTEX)

EXPERIMENTAL METHODS FOR GEOLOGICAL REMOTE SENSING

by

Robert K. Vincent
The University of Michigan
Willow Run Laboratories
Ann Arbor, Michigan

INTRODUCTION

At Willow Run Laboratories in 1970, under NASA Contract 9-9784, a two channel analog ratio technique in the thermal IR wavelength region for mapping gross compositional variations in silicate rocks was developed which successfully produced automatic ratio recognition maps of quartz sand and sandstone near the Mill Creek, Oklahoma sand quarry. In the report which describes that effort [1], a three channel IR technique was hypothesized for a more refined version of this ratio method, whereby the third channel is used for correction of temperature variations across the target scene. It was also hypothesized that the resulting temperature-corrected ratios would be at least crudely correlated with SiO_2 content of the geological targets encountered.

During 1971, the state-of-the-art of geological remote sensing was further advanced by the processing of data from an aircraft flight over Pisgah Crater, California. There are four major results from the Pisgah Crater data. First, the two-channel thermal IR analog ratio method from last year has been successfully used to map relative differences among various silicate rock types. Secondly, the three-channel thermal IR technique, hypothesized last year, has been implemented successfully to make digital temperature-corrected ratio maps which are more sensitive than the two-channel ratio maps to true compositional variations in geological targets. Thirdly, a new technique involving the ratio of radiances in visible green to reflective IR channels has been theorized and qualitatively tested for the purpose of mapping variations in iron oxides on the surfaces of exposed rocks.

The Pisgah Crater area in San Bernardino County was chosen as a test site for three reasons: there are many silicate rock types in close proximity, the semiarrid terrain is very sparsely vegetated, and considerable ground truth data was already available about the area from other reports and geologic maps [2,3]. The flight took place on 30 October 1971 between 0800 (approximately 1 hour after sunrise) and 0840 hours, local time, at above-ground altitudes of 500 ft and 3000 ft. Only the 3000 ft data was processed through to the final stages because of monetary limitations. The morning was clear, with relative humidity less than 25% and a ground-level air temperature of approximately 5°C. This time of day was chosen because

temperature variations across the scene due to compositional effects (albedo, thermal conductivity, etc.) were small, yet enough solar illumination was available for visible and reflective IR data collection.

Dr. Larry C. Rowan, a U. S. Geological Survey geologist from the Regional Geophysics Office in Denver, and Ben Drake, a geology Ph.D. candidate at The University of Michigan, greatly assisted the author in field checking these images.

DESCRIPTION OF APPARATUS AND METHOD OF ANALYSIS

The data were collected by The University of Michigan multispectral scanner (4) and a Honeywell two-element Hg:Cd:Te detector filtered (5) to the approximate 10% cutoff points of 8.2 μm - 10.9 μm and 9.4 μm - 12.1 μm, which will be called channels 1 and 2, respectively, aboard the University's C-47 aircraft. The two methods of analysis for the thermal IR data are described in references 1 and 5. Briefly, in the first method, the ratio of radiances in channel 1 to channel 2 was made the "signal" to the University's analog computer. The resulting "ratio images" are bright where this R_{12} ratio is high and dark where R_{12} is low. Silicate rocks display various spectral emittance minima in the 8 μm - 14 μm region, caused by reststrahlen bands (molecular vibrational modes). Generally speaking, felsic (silica-rich) rocks tend to have spectral emittance minima at shorter wavelengths than mafic (silica-poor) rocks. Hence, there is a tendency for the R_{12} ratio to be lower for felsic rocks (dark in the ratio image) than for mafic rocks (bright in the ratio image).

The second thermal IR method involves the correction of R_{12} for temperature variations across the scene. The spectral emittance of the geologic target in a channel 3 (11.4 μm - 14.4 μm at 15% points) is assumed to be a constant value for all silicates, which is a reasonably good assumption in that wavelength region. From the channel 3 radiance, the rock temperature is determined (within 5°K), and a ratio correction factor, R_g, is calculated. The R_{12} ratio is then corrected for temperature variations across the scene to yield the temperature-corrected ratio

$$R = R_g R_{12} \tag{1}$$

This three-channel scheme is done digitally. Laboratory emittance spectra and a theoretical atmospheric model are then used to calculate expected R ratios for various rock types. The measured values of R from the scanner data can be compared with these theoretical values to determine broad classifications of rock type. A simpler two-channel scheme for temperature correction, which has proved qualitatively successful, will be implemented quantitatively during the coming year.

The method for the visible-reflective IR ratio images involves a simple ratio of radiances in channel 5 (0.50 μm - 0.52 μm) to channel 7 (0.74

μm - 0.85 μm). Electronic transitions of iron oxides produce a relatively large rise in spectral reflectance from 0.5 μm to .80 μm, compared with lesser or no rise in spectral reflectance over the same spectral region for felsic rocks, and with a drop in reflectance for unoxidized mafic rocks. Thus, generally speaking, iron oxides appear dark, felsic rocks appear a medium gray tone, and unoxidized mafic rocks appear bright on the R_{57} ratio image.

RESULTS AND DISCUSSION

A demonstration of the two-channel IR ratio method is given in figure 1, which shows from top to bottom the analog images of channel 1 (8.2 μm - 10.9 μm), channel 2 (9.4 μm - 12.1 μm), and R_{12} (the ratio of radiances in the two channels) for section 2A of the Pisgah data. This is a region approximately 5 miles south-southeast of Pisgah Crater. North is to the top of the images. The ratio image shows emittance variations which are indicative of rock type differences. The felsic mountains (D) and alluvium (A) appear darker than the mafic lava (LA), and the playa material is contrasted sharply against the alluvium. The topographically higher dacitic mountains (D) are warmer than other parts of the scene, which makes the ratio for that region higher than it should be on the sole basis of reststrahlen position. The patchy appearance of the playa is primarily caused by emittance variations, because the gray level of the single channel images are almost uniform across the floor of Lavic Lake, of which this is a part. The most important fact about this figure, however, is that felsic and mafic lithological units are clearly discriminated in the ratio image.

The three-channel IR technique corrects the R_{12} ratio for temperature variations across the scene via equation (1). It is demonstrated by the digital ratio map in figure 2, which includes almost all of the region shown in figure 1. The ratio R from equation (1) is divided into the following 5 levels:

Level 1	$R \leq .969$
Level 2	$.969 < R \leq .973$
Level 3	$.973 < R \leq .981$
Level 4	$.981 < R \leq .992$
Level 5	$.992 < R$

The lowest recorded R in level 1 is .941 and the highest level recorded level 5 is 1.024. These values for R can be compared directly with the graph in figure 3, which plots R versus $\%SiO_2$ as calculated from laboratory rock emittance spectra of Lyon [6] and an atmospheric model of Anding, et. al. [7]. Levels 1 and 2 are primarily felsic (acidic) silicates and levels 4 and 5 are primarily mafic (basic) silicates. A graybody with constant emittance $\varepsilon = 0.94$ throughout the 7 μm - 14 μm region would yield a ratio value of R = 0.975, which would appear in level 3, along with some of the

intermediate rocks. Graybodies of that type can be distinguished from silicates by ratioing the sum of radiances in channels 1 and 2 to the radiance in channel 3 for the purpose of determining the presence or absence of reststrahlen bands, which was not done here. More and different ranges in R could have been printed, but these ranges and symbols were chosen for printing because they produced a more pleasing figure for demonstration purposes. The estimated error in R is ± .007.

The primary effect of the temperature-correction can be seen in a comparison of R for dacitic mountains (D) with R for the alluvium (A) in figures 1 and 2. Figure 1, which is not temperature-corrected, shows the alluvium as having a lower R_{12} ratio (darker in the R_{12} ratio image) than the adjacent dacitic mountains, even though the alluvium has a chemical composition similar to the mountains (the former consists primarily of rock fragments from the latter). However, the mountains, which are topographically higher, were warmer than the alluvium at this time of morning (see the single channel images of figure 1), which biased the R_{12} ratio toward a higher value in the mountains. Figure 2, on the other hand, shows nearly equal values for R, the temperature-corrected ratio, in the alluvium and in the mountains. This is a good indication that the temperature corrections have been successful.

As a more stringent test of the quantitative accuracy of this method, the ratios of the dacite and plagioclase basalt samples of Lyon, plotted as data points in figure 3, can be compared with ratios for the dacitic mountains (D) (also for the dacitic fragments in the alluvium) and basalts of the Sunshine lava flows (LA) in figure 2. Lyon's dacite yields a theoretical ratio of R = .947, which falls into level 1, a ratio frequently measured in the mountain (D) and alluvium (A) regions of figure 2. Lyon's plagioclase basalt yields a ratio of R = 1.015, which falls into level 5, a commonly measured level in the Sunshine basalt flows (LA) of figure 2. Therefore, the laboratory and scanner data quantitatively agree within reasonable limits (perhaps as small as the estimated ± .007 error in R).

To demonstrate the third ratio technique, ratio images of radiances in the visible green, channel 5 (0.50 μm - 0.52 μm), to reflective IR channel 7 (0.74 μm - 0.85 μm) were processed in a manner similar to the two-channel thermal ratio method discussed above, for approximately the same areas as shown in figures 1 and 2. Figure 4 shows, from top to bottom, analog scanner images of channel 5, channel 7, and the ratio R_{57}. The ratio image shows gray level variations unlike the single channel images. Theoretically, iron oxide will appear dark in the ratio image. The two eruptive phases (labeled 1 and 2) of Sunshine lava display various shades of gray, which are darker than the alluvium (A) on the west side. The younger phase 2 Sunshine lava appears darker in the ratio image than the older phase 1 lava. The greater presence of calcium carbonate on joint planes and in local minor depressions on the phase 1 Sunshine lava accounts, in part, for the lighter color of this unit in the single channel images. This may also partly account for the slightly brighter gray level

in the ratio image.

The alluvial deposits (A) on either side of the Sunshine lava appear quite different in the ratio image. It is probable that the drainage patterns carry more ferric oxides from the Pisgah and Sunshine lava flows to the eastern alluvium (surrounded by basalt) than to the western alluvium (basalt only on one side). This would explain the darker gray level of the eastern deposits in the ratio image. However, the playa and alluvium east of the Sunshine flows appear to have similar spectral properties in these two channels of information, as evidenced by similar gray levels in the ratio image, which may indicate almost equal amounts of surficial ferric oxide in or on both types of material.

Probably the most significant features in the ratio image of figure 4, however, are the dark linear regions in the dacitic mountains on the left side of the image. The two prominent, dark, linear features running northwest to southeast are andesitic dikes in the predominantly dacitic mountain range. The longer dark feature, north of the alluvium inlet, is shown as an andesite dike on T. W. Dibblee's geologic map of the area [8]. The shorter dark feature is an andesitic dike which cuts across the dacitic peninsula on the southern border of the alluvium inlet. This short dike, which is not on Dibblee's map, may be a slightly offset continuation of the more prominent, longer dike. If so, there may be a west-to-east fault below the alluvium in the inlet. The andesitic dikes appear rusty brown to the naked eye of a field geologist on the ground, and, if not in shadow, are easily recognized by ground observers. However, the dikes do not show up well in the single channel images. Contrarily, the ratio image produces excellent contrast between oxidized surfaces of andesite and the surrounding dacite, whether in shadow or bright solar illumination. Finally, the small dark spot at the top of the ratio image on the mountain-alluvium border is a darkly weathered biotite quartz monzonite outcropping that shows up equally well in the ratio or single-channel images.

Generally speaking, acidic (felsic) rocks should contain less ferric oxide than basic (mafic) rocks, because the latter have more iron available for oxidation. Thus, there should be some correlation between R_{12} and R_{57} with respect to silicate rock type. This implies that, low R_{12} and high R_{57} indicate acidic silicates, whereas high R_{12} and low R_{57} indicate basic silicates. Although desert varnish (ferric oxides) can cover any type of rock, it does not seem to prevent the acidic rocks from appearing brighter than basic rocks in the R_{57} ratio of figure 4, except for cases where the felsic rocks contain appreciable amounts of biotite (biotite quartz monzonite in figure 4). The weathered andesite in the dikes of figure 4 is an intermediate rock with relatively high iron content; hence, it has a higher Fe_2O_3 content and appears dark in the R_{57} ratio image, even though it is not bright in the R_{12} image of figure 1.

There are several indications in the Pisgah data that the thermal infrared R_{12} ratio is not very affected by the amount of ferric oxides on

the rock surfaces. For instance, R_{57} variations within Pisgah lava flows (not shown) are not accompanied by similar variations in R_{12}. Laboratory tests are needed to confirm or deny this hypothesis. However, the iron oxide reststrahlen bands occur near 20 μm and greater, which hints that they may be relatively transparent in the silicate reststrahlen region between 8 μm and 12 μm.

CONCLUSIONS

During the past year a 2-channel IR technique for discrimination among silicate rocks was tested for a second time, a three-channel IR method was tested for the first time, and a new visible-reflective IR ratio method was hypothesized and qualitatively tested for iron-oxide recognition. Both the two-channel and three-channel IR ratios methods were capable of discriminating felsic from mafic rock types near Pisgah Crater, California. The three-channel ratio values measured by the scanner were found to agree, within reasonable limits, with the values of R calculated from laboratory data. The capability of the three-channel method to obtain absolute ratios is accompanied by a costly processing routine. The two-channel technique is superior for low thermal contrast scenes ($\Delta T \leq 5°C$) about which some ground truth is available because of its speed and economy ($3400 for data processing of the first 150 data-miles and $750 for each additional 150 data-mile set; this does not include data collection costs).

The reflective channel ratio method was found capable of enhancing the contrast of iron oxides in the presence of unoxidized or iron-deficient rock surfaces. Photographic IR methods can duplicate some of these visible-reflective IR ratio results [9,10] with less image distortion and lower cost. However, this scanner ratio technique (which costs the same as the 2-channel thermal ratio processing) is superior for suppressing shadowing and atmospheric effects.

All three techniques can be useful for geologic mapping. For example, the thermal ratio method should assist in the mapping of volcanic ash flows, which are sometimes indistinguishable to the naked eye from sedimentary material, and glacial tills, which can vary significantly in SiO_2 content. Similarly, the visible-reflective IR ratio should be useful in the exploration for gossans or other iron and nickel ore bodies, as well as for the mapping of iron-rich (lateritic) soils. These and other applications can be tested with esiting equipment and computer software.

REFERENCES

1. R. K. Vincent, R. Horvath, F. Thomson, and E. Work, Remote Sensing Data-Analysis Projects Associated with the NASA Earth Resources Spectral Information System, The Univ. of Mich. Tech. Report 3165-26-T, NASA Contract NAS9-9784, Ann Arbor, Michigan, (1971).

2. T. W. Dibblee, Jr., U.S.G.S., Misc. Geol. Inv. Map I-472 (1966).

3. S. J. Grawarecki, NASA Earth Resources Aircraft Program Status Review, 1, 10-1(1968).

4. L. M. Larsen and P. G. Hasell, Jr., Calibration of an Airborne Multispectral Optical Sensor, The Univ. of Mich. Report No. 6400-137-T, Contract DA 28-043-AMC-00013(E), AD 842419, Ann Arbor, Michigan, (1968).

5. R. K. Vincent, Rock-Type Discrimination from Ratio Images of Pisgah Crater, California Test Site, The Univ. of Mich. Report No. 31650-77-T, Contract NAS9-9784, Ann Arbor, Michigan,(1972).

6. R. J. P. Lyon, Evaluation of Infrared Spectrophotometry for Compositional Analysis of Lunar and Planetary Soils: Rough and Powdered Surfaces, Final Report - Part II under NASA Contract NASr-49(04), Stanford Research Institute, Menlo Park, California, (1964).

7. D. Anding, R. Kauth, and R. Turner, Atmospheric Effects on Infrared Multispectral Sensing of Sea Temperature from Space, The Univ. of Mich. Report 2676-5-P, Ann Arbor, Michigan, (1970).

8. T. W. Dibblee, Jr., Op. Cit.

9. L. Rowan and R. K. Vincent, Abstracts, Annual Meeting of the Geological Society of America, Washington, D. C., p. 739, (1971).

10. R. K. Vincent, Op. Cit.

FIGURE CAPTIONS

FIGURE 1: Analog Infrared images of flightline 2 section A of a west-east flight about 5 miles south of Pisgah Crater. North is toward the top. Channel 1, channel 2, and the R_{12} ratio image are at top, middle, and bottom, respectively. From left to right are dacitic mountains (D), alluvium (A), Sunshine lava flows (LA), alluvium (A), playa material (P) of Lavic Lake, and Pisgah lava (LA) of phase 1.

FIGURE 2: Temperature-corrected digital recognition map of silicate rocks for most of flight line 2, section A (including most of the area covered in figure 1) about 5 miles south of Pisgah Crater. North is to the top. The top and bottom maps are contiguous. Felsic rocks (high $\%SiO_2$) appear yellow and mafic rocks (low $\%SiO_2$) appear blue.

FIGURE 3: Temperature-corrected ratio R versus %SiO2 for 25 rock samples of Lyon [6].

FIGURE 4: Analog visible and reflective IR images of flight line 2 section A of a west-east flight about 5 miles south of Pisgah Crater (same area as in figures 1 and 2). North is toward the top. Channel 5, channel 7, and R_{57} ratio are at top, middle and bottom, respectively. From left to right are dacitic mountains (D) with dark (low ratio) andesitic dikes, alluvium (A), Sunshine lava (LA) of two eruptive phases, alluvium (A), playa material (P), and phase 1 Pisgah lava (1).

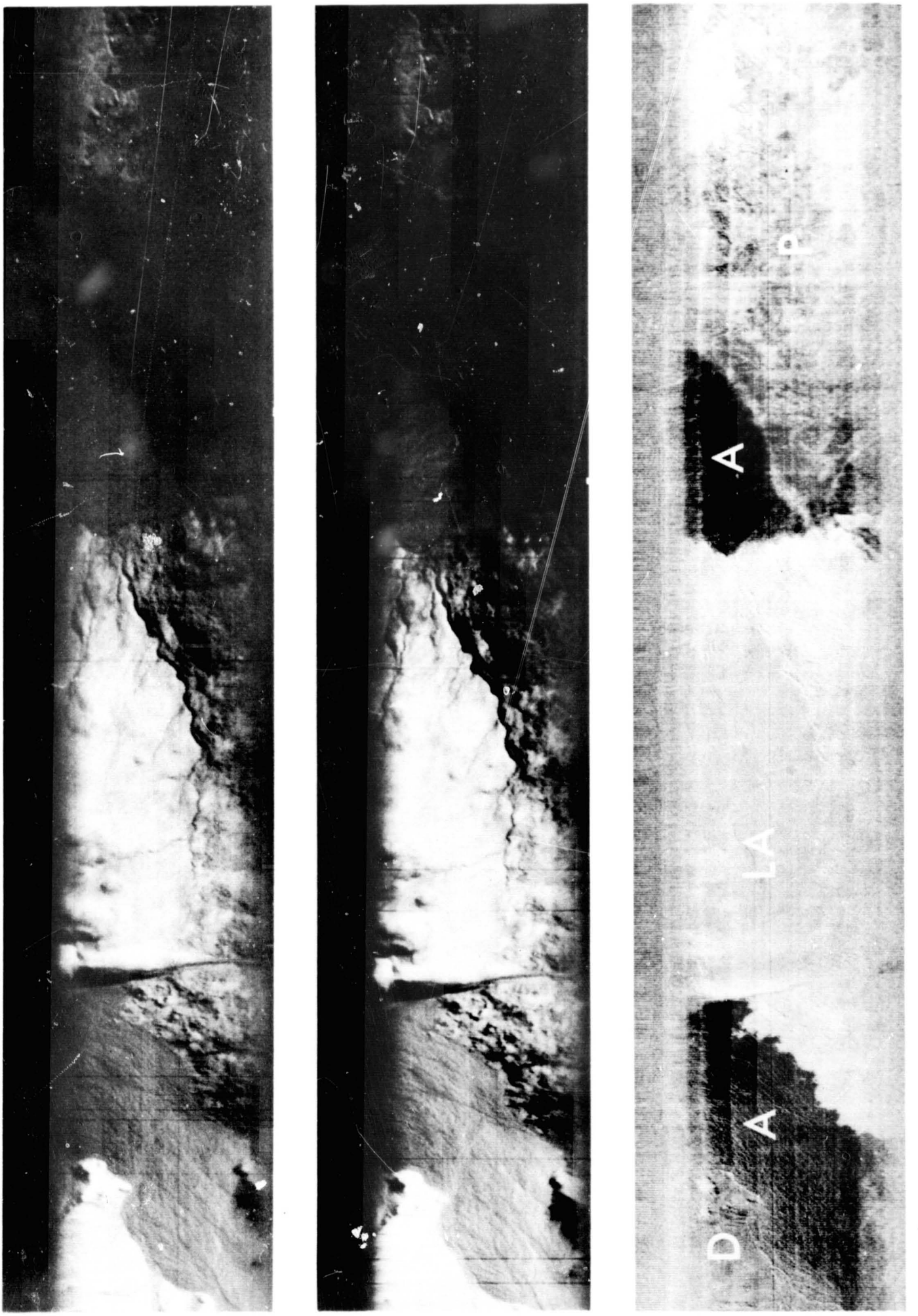

FIGURE 1

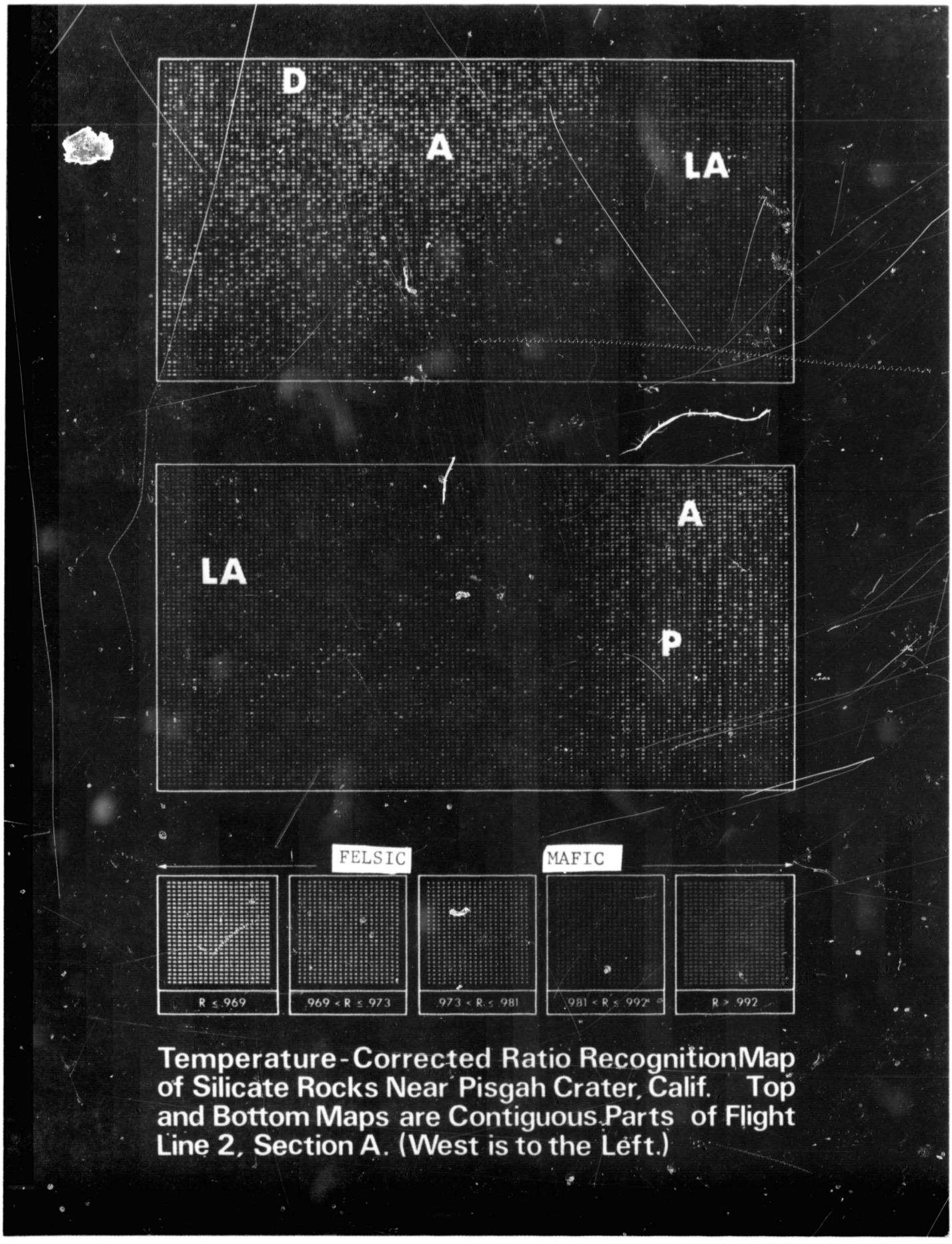

Temperature-Corrected Ratio Recognition Map of Silicate Rocks Near Pisgah Crater, Calif. Top and Bottom Maps are Contiguous Parts of Flight Line 2, Section A. (West is to the Left.)

FIGURE 2

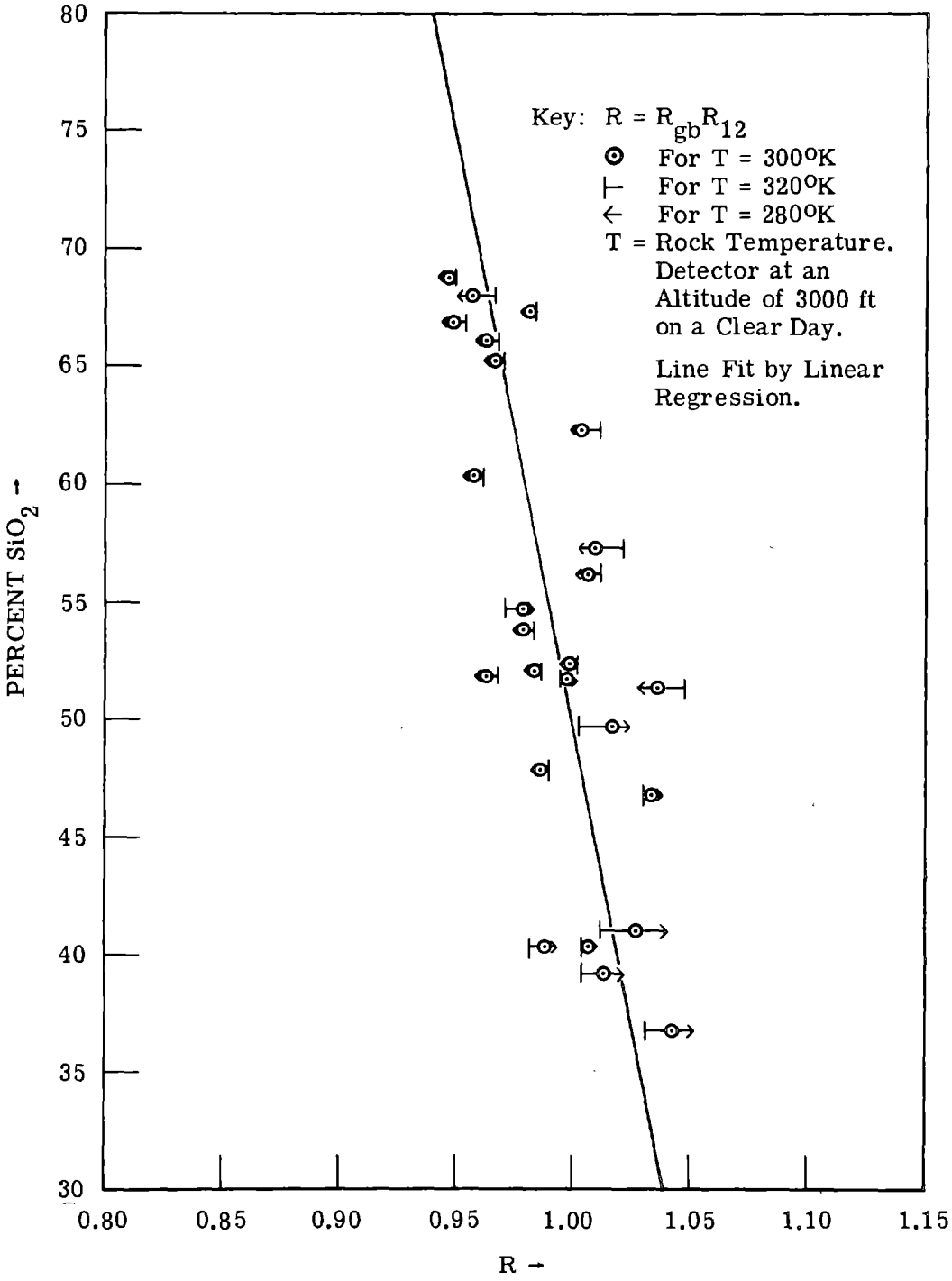

FIGURE 3. TEMPERATURE-CORRECTED RATIO VERSUS PERCENT SiO_2

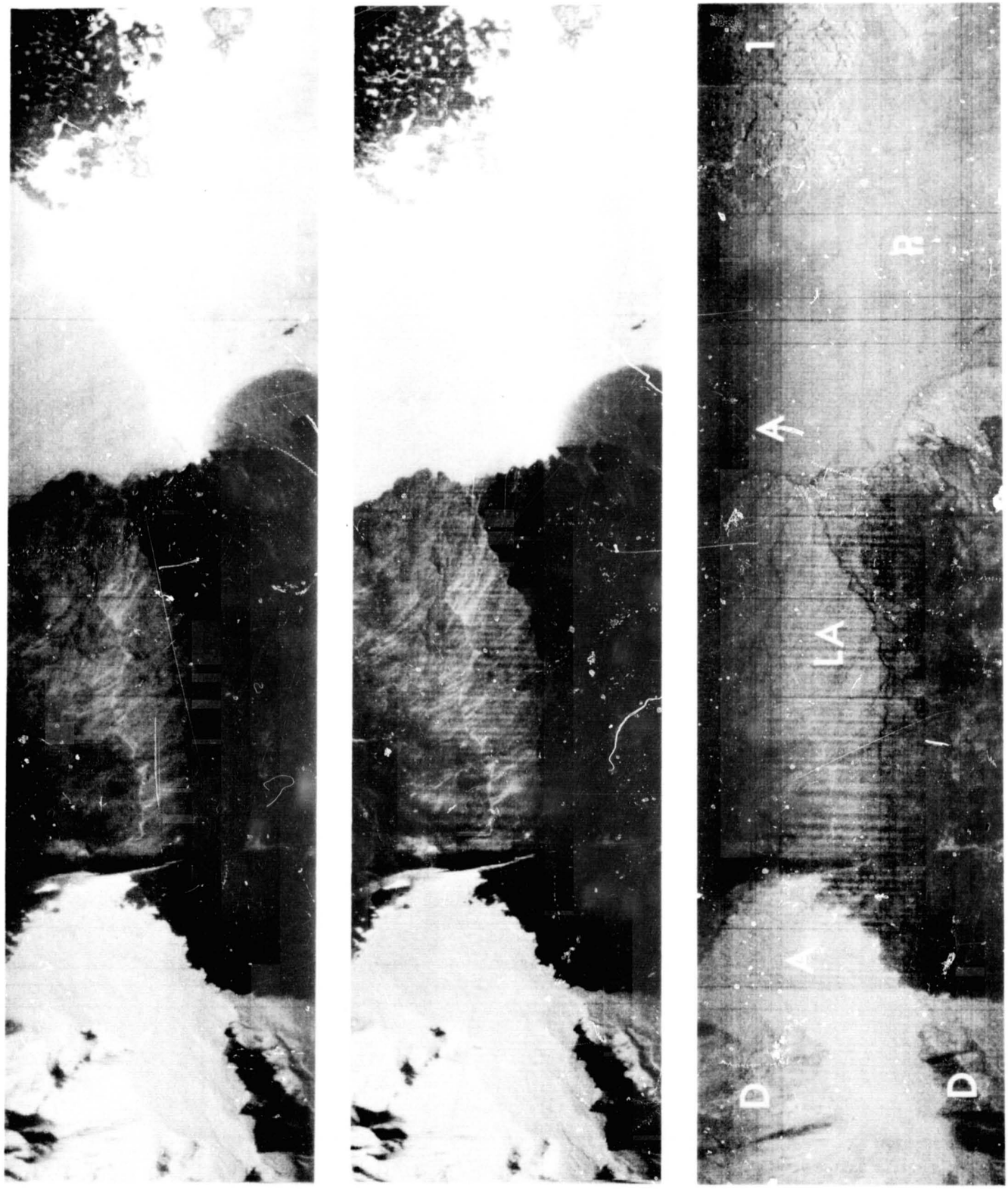

FIGURE 4

SECTION 34

N72-29334

MICHIGAN EXPERIMENTAL MULTISPECTRAL SCANNER SYSTEM

by

Philip G. Hasell, Jr.
The University of Michigan
Ann Arbor, Michigan

The research laboratories of The University of Michigan pioneered the application of multispectral mapping techniques to earth resources problems with experimental hardware developments beginning in the mid sixties. During FY71 under NASA/MSC support, Michigan modified its original multipath multispectral airborne scanner system to provide the same spectral bands along a single optical line of sight. Previous to this modification, the choice of spectral bands for machine processing was limited to those few grouped in one of four separate optical paths. After the modification, any of the multispectral bands selected from throughout the ultraviolet, visible and infrared regions could be processed together. The modified system became operational in late June 1971, only six months after contract go ahead and just in time for use in the Corn Blight Watch experiment.

The Michigan experimental system has supplied all of the multispectral scanner data processed and analyzed by Michigan, Purdue, NASA/MSC and others during the past five years. The system can generate up to eighteen different spectral bands over a wavelength range of from 0.33 to 14.0 microns. Twelve of these bands can be selected for tape recording at any one time on a fourteen track analog tape machine. The scanner includes provisions for five separate radiation reference sources. These sources are viewed in sequence by each radiation detector as part of each line scan of the terrain beneath the aircraft.

For those not familiar with airborne scanners, a functional description of line scanning will be presented with reference to Figure 1, The Geometry of Airborne Scanning. As shown in the optical schematic at the top of the figure, the airborne scanner consists of an optical telescope with its narrow field of view directed by a rotating flat mirror to scan in a plane perpendicular to the longitudinal axis of the aircraft. In place of the usual eyeball at the eyepiece of the telescope, there is a radiation detector, or detectors, which converts the radiation to electrical signals. Again referring to Figure 1, the telescope field of view or ground resolution element scans laterally across the aircraft ground track through an opening in the bottom of the aircraft. Then it scans radiation references internal to the scanner before making the next ground scan. By the time the next ground scan begins, the aircraft has

moved forward so that subsequent line scans form a continuous strip image of the terrain beneath the aircraft. The electrical voltage representation of a single line scan is shown in Figure 2, Scanner Voltage Output vs Time. Note that while the detectors for all wavelength bands view in phase each of the radiation references as well as the terrain, not all references apply to each wavelength band. Although the thermal ambient and dark level references may be a common radiation source, the other sources are associated with either thermal or non thermal bands as shown. A synchronization reference is generated by the scanner for recording with the video signals for indexing purposes. The marker pulse refers to the scan position relative to internally mounted radiation references and the roll stabilized pulse refers to ground scan nadir with aircraft roll motion removed.

The complete airborne scanner system is shown in schematic block diagram form in Figure 3, Michigan Experimental Multispectral Scanner System. The terrain radiation enters the scanner at the bottom left and is registered by the radiation detectors in the scanner assembly along with operator controlled reference sources. The output of the radiation detectors are electrical signals which are amplified in preamplifiers before being transmitted to an operator console for further amplification in postamplifiers. The operator monitors the video signals and adjusts them to the proper level for tape recording. During recording he monitors the signals reproduced from the tape record to confirm satisfactory recording. The system makes a linear transformation of input radiation to voltage recorded on the analog magnetic tape. The boresight camera which is part of the system records visible radiation on film for use in the analysis of the scanner data.

The system modification completed in June 1971 amounted to the substitution of the single scanner assembly shown on the left of the figure for two double ended military surplus scanners originally used in the system. The radiation references, detector assemblies, electronics, operator displays and the tape machine remained the same. However, the system configuration is a dynamic one which is continually changing to accept new detector assemblies and electronic components with improved performance. Figure 4, M7 Scanner Performance Characteristics, shows the gross parameters of the current system which is formed around the Michigan designated M7 scanner.

Figure 5, Optical Schematic of Michigan Experimental Multispectral Scanner, shows the optical configuration of the M7 scanner. Figure 6, Michigan Experimental Multispectral Scanner, shows a similar view of the actual scanner with inspection panels removed. The key feature to note in the design is the flexibility to easily accept different radiation reference sources and new detector assemblies. Weight and space savings were sacrificed to provide this flexibility which allowed the immediate use of references and detector assemblies from the original system with the understanding that they would eventually be replaced as time and

funds permitted. Also, the scan motor drive shaft was extended beyond the aft end of the motor housing in order that illumination sources (such as lasers) might later be added to the system in time phase with the scan mirror.

The radiation intercepted by the five inch diameter collecting aperture is directed into the Dall-Kirkham telescope which has a three inch diameter secondary mirror. The incoming radiation blocked from the telescope by this secondary is directed upward to detector position number one. This nominal three inch diameter collecting aperture is broadband (0.3 to 14.0 microns). Currently a focusing lens designed for 8.0 to 14.0 microns is used at this position with a HgCdTe detector to provide thermal data. In work is a modification to use a dichroic mirror in this position to divert UV radiation onto a photomultiplier detector while maintaining the thermal detector in the same position. A wide variety of detector assemblies can be used in this position.

The radiation collected by the effective four inch aperture of the telescope is folded into a dichroic mirror which reflects the radiation below a nominal 0.9 micron and transmits the energy beyond. The radiation beyond 0.9 microns is focused onto three separately filtered InAs detector elements by a lens optimized for transmission in the 1.0 to 2.6 micron region. This dichroic and lens can be changed relatively easily for different detector configurations at this detector position number two.

The radiation at wavelengths shorter than 0.9 microns is focused onto the entrance slit of a prism spectrometer at detector position number three. This spectrometer disperses visible and near infrared radiation through fiber optic bundles onto as many as twelve photomultiplier tubes. The sixteen fibers are directed onto nine separate photomultiplier detectors in the current configuration.

The radiation reference sources currently in use with the system are: (1) an NBS lamp packaged to simulate a point source, (2) two temperature controlled greybody thermal references which fill the collecting aperture, and (3) a sky illumination reference consisting of an opal glass diffusing plate mounted in the top of the aircraft. The operator has control of the radiation from all reference sources through electronic control of the lamp and greybodies and attenuating optical filters for the sky illumination. The calibrated output of these sources are monitored and recorded manually by the operator during data collection. These internal references are calibrated periodically against external standards in the laboratory.

Figure 7, Detector Configurations for M7 Scanner, shows the detector assemblies currently available for use in the system and those planned for the near future. All data collected during the last half of 1971 used the specific detectors listed in the top row of the chart.

A 9.3 micron long wavelength pass filter was used with the HgCdTe detector in position one to provide thermal coverage. Some of the future detectors will be available for use by the spring of 1972 and all should be operational by the summer of 1972. It is interesting to note that the most useful wavelength bands of those available for processing the corn blight data were the thermal IR (9.3 to 11.5 microns), two in the mid IR (1.0 to 2.6 microns) and three in visible and near IR (0.4 to 0.9 microns). The specific bands in the non thermal wavelengths varied with the changing crop conditions. It was fortunate that the system was modified in time to make these bands available for multispectral processing of corn blight.

Figures 8 and 9 show an external view of the Michigan C47 aircraft which normally transports the multispectral mapping system and an internal view of the instrumentation installed in the aircraft. The internal view looks forward in the aircraft from the rear. The M7 scanner with reference sources and radiation detectors removed is in the lower right hand corner of the figure. The scanner rests in an instrument well through the floor of the aircraft. The supporting electronics and operator positions for the system are forward of the scanner position. At the time of this photograph most of the original multispectral system was still installed in the aircraft including one of the double ended military surplus scanners. The modified multispectral system weighs about 1200 pounds which is about half the instrumentation payload of the C47 aircraft. Therefore other systems may be installed and operated in conjunction with the multispectral mapping functions.

The M7 multispectral system can also be installed in the Michigan C46 aircraft which contains a high resolution, side looking airborne radar (SLAR) system. This SLAR system is also used for earth resource applications. However, the two systems cannot be operated simultaneously and the aircraft data collection time is reduced from four to two hours because of reduced fuel capacity with both systems installed. This combined system installation in the C46 is usually a temporary one which provides for IR and radar mapping with one aircraft on the same field trip.

Aside from continued development of new detector assemblies and electronic components to improve scanner performance, several other items are scheduled for investigation in the near future. One is to make provision for scanning in an oblique instead of a vertical plane across the aircraft track. The oblique view of vegetation should show more vegetation and less ground in a resolution element. This mix of soil and crop in a common resolution element has been a problem in remotely identifying farm crops in the past and the technique may benefit other applications. The other new technique of potential benefit is to actively scan in selected wavelength bands which will be recorded along with passive bands. Laser radiation sources can be coupled with line scanners to provide this capability.

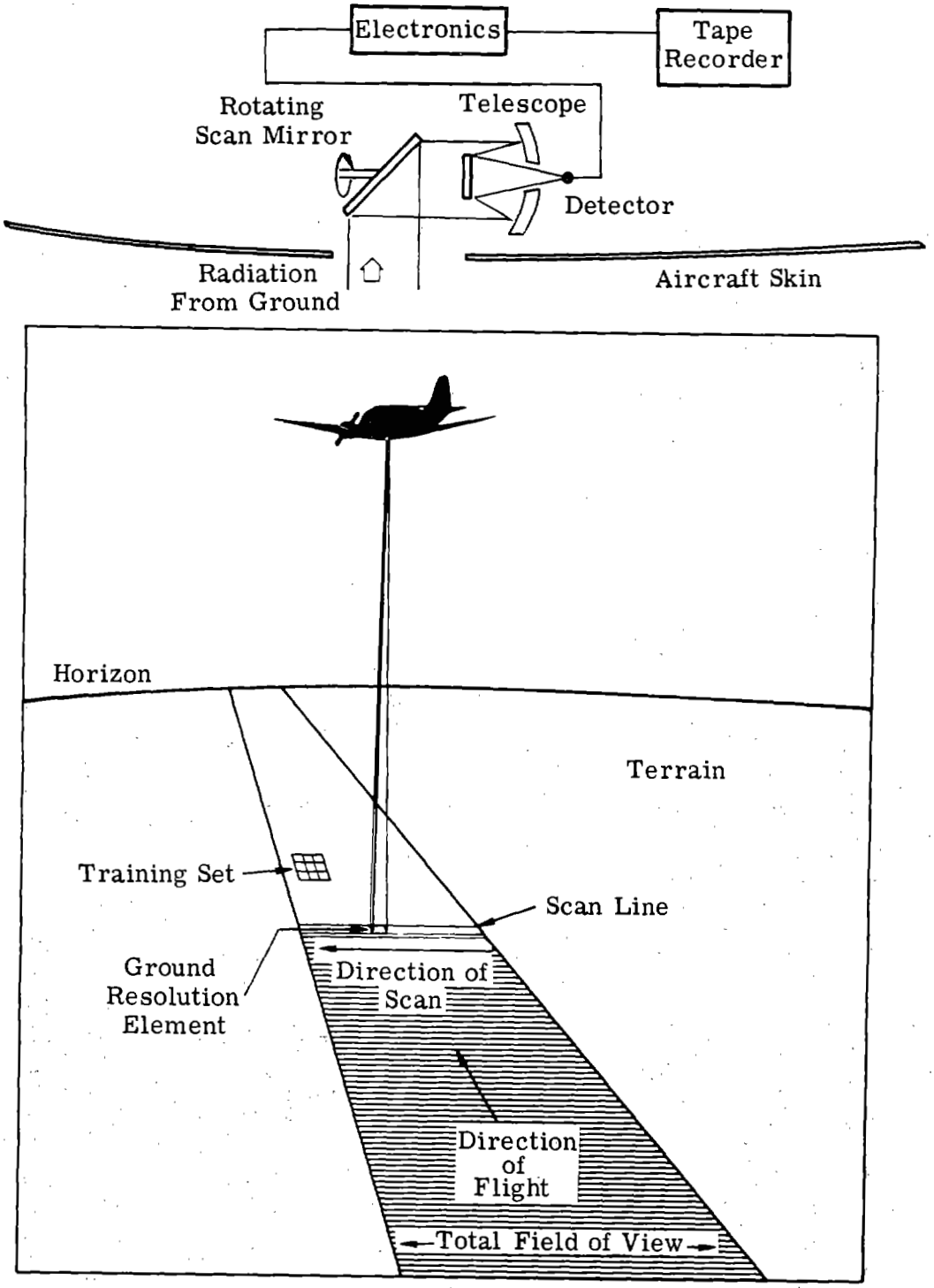

FIGURE 1. THE GEOMETRY OF AIRBORNE SCANNING

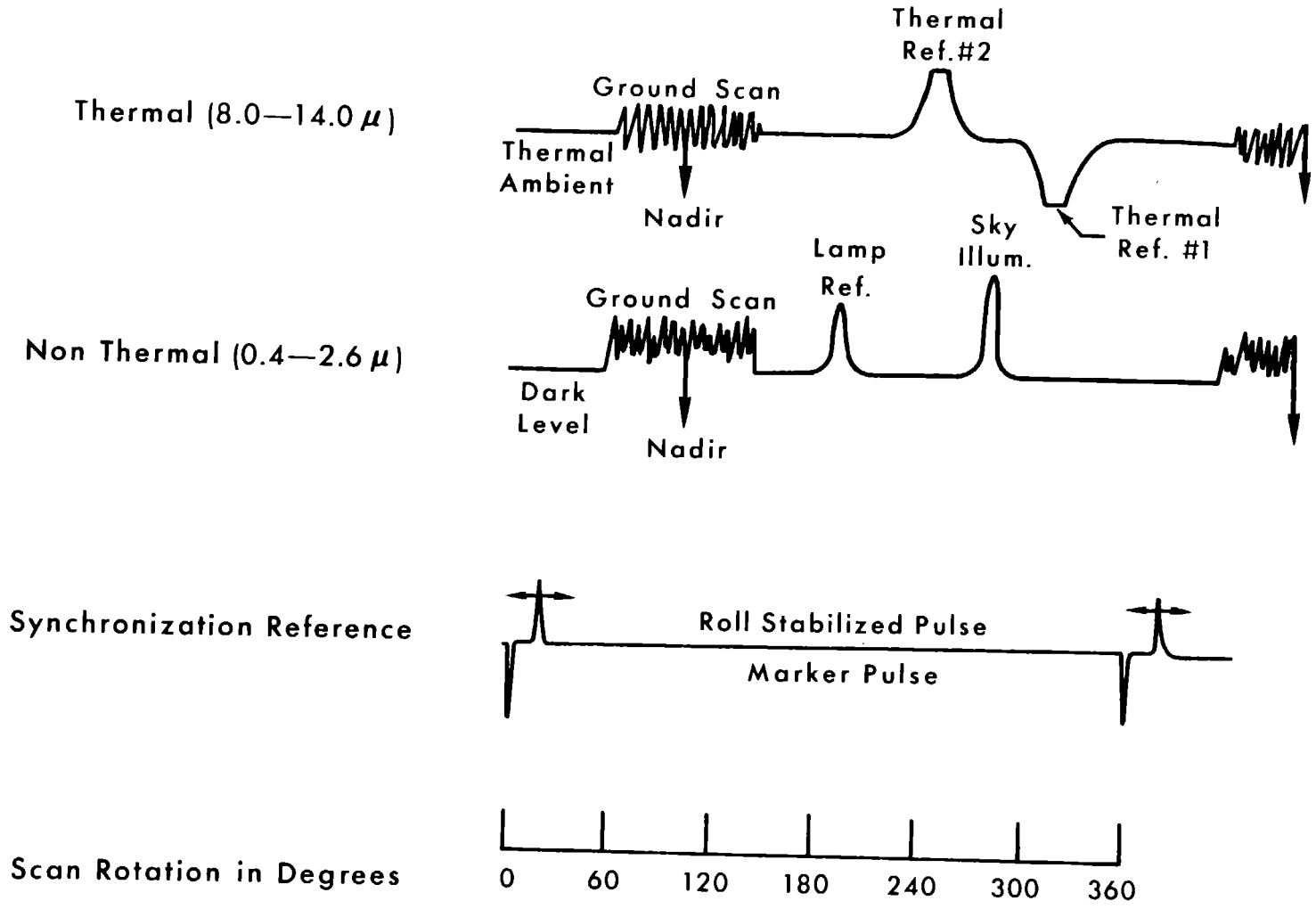

FIGURE 2. SCANNER VOLTAGE OUTPUT VERSUS TIME

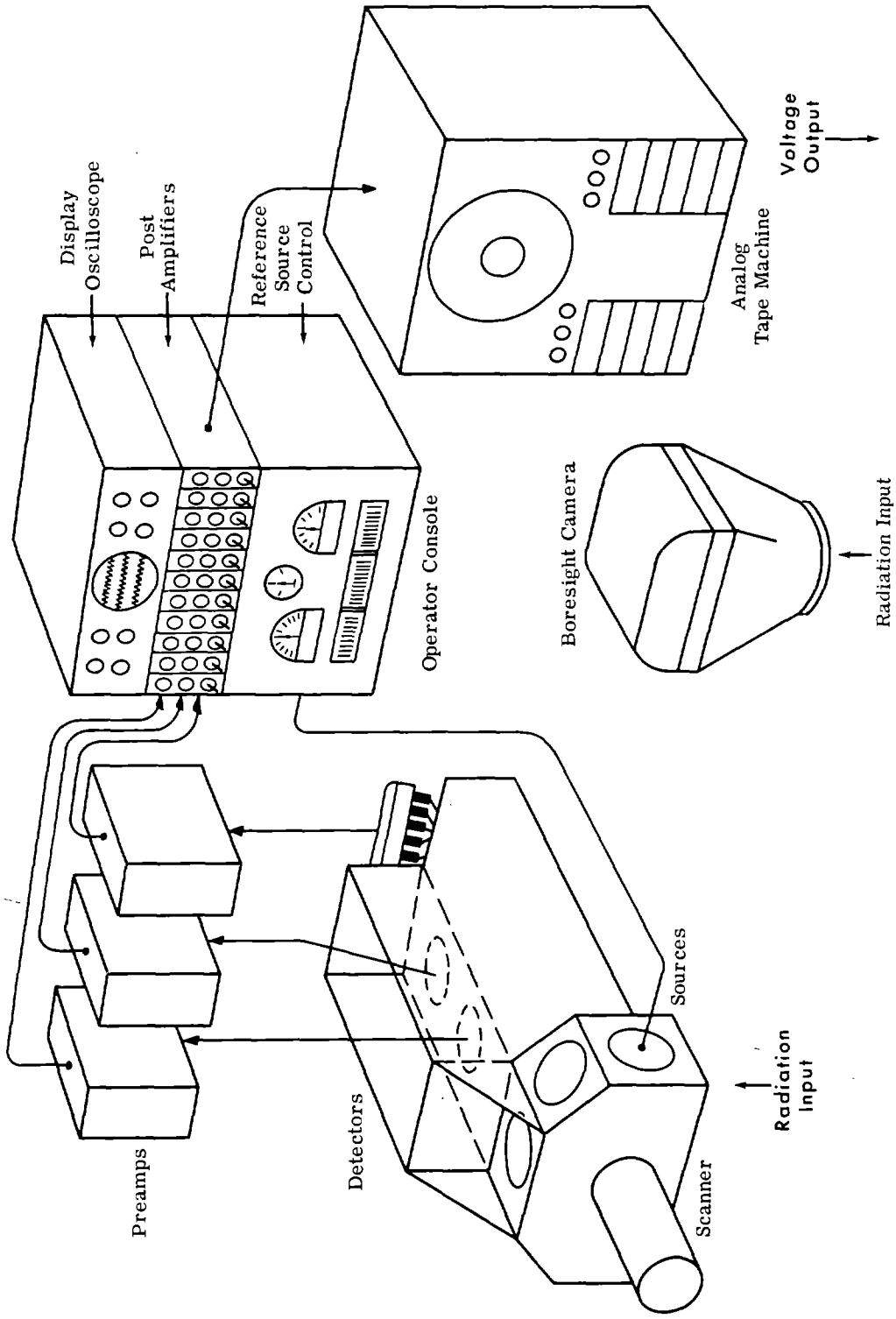

FIGURE 3. MICHIGAN EXPERIMENTAL MULTISPECTRAL SCANNER SYSTEM

- 12 Spectral Bands in UV, Vis, IR
- 90^{o} External FOV ($\pm 45^{o}$ from nadir)
- 2 mr. Max. Spatial Resolution
- 0.3^{o}C Nominal Thermal Resolution
- 1% Nominal Reflectance Resolution
- 5 Radiation Reference Ports
- 5 in. Diameter Collector Optics
- 60 or 100 scans/sec. Scan Rate
- DC to 90 KHz Electronic Bandwidth
- Roll Stabilized Imagery

FIGURE 4. M7 SCANNER PERFORMANCE CHARACTERISTICS

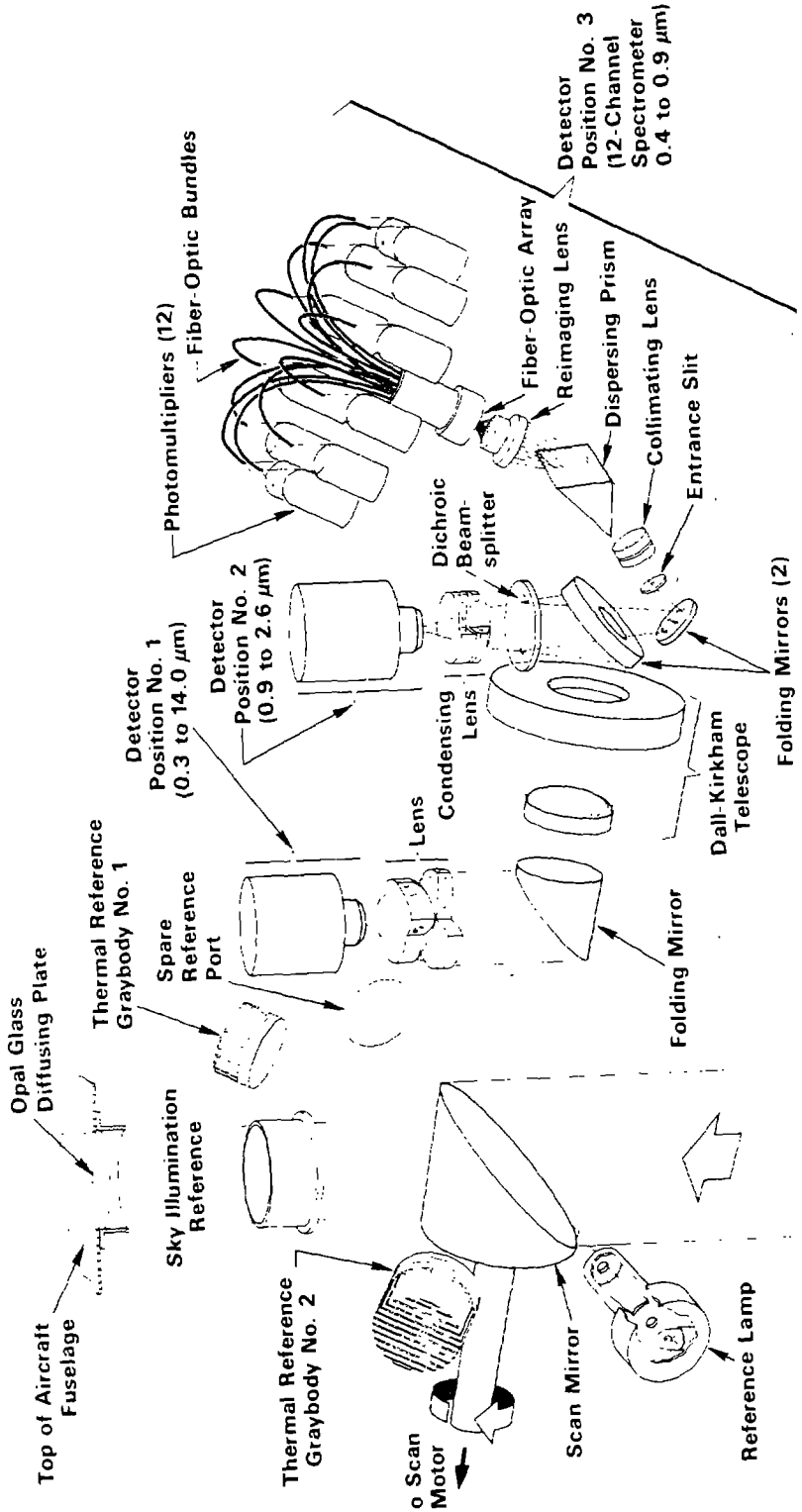

FIGURE 5. OPTICAL SCHEMATIC OF MICHIGAN EXPERIMENTAL MULTISPECTRAL SCANNER

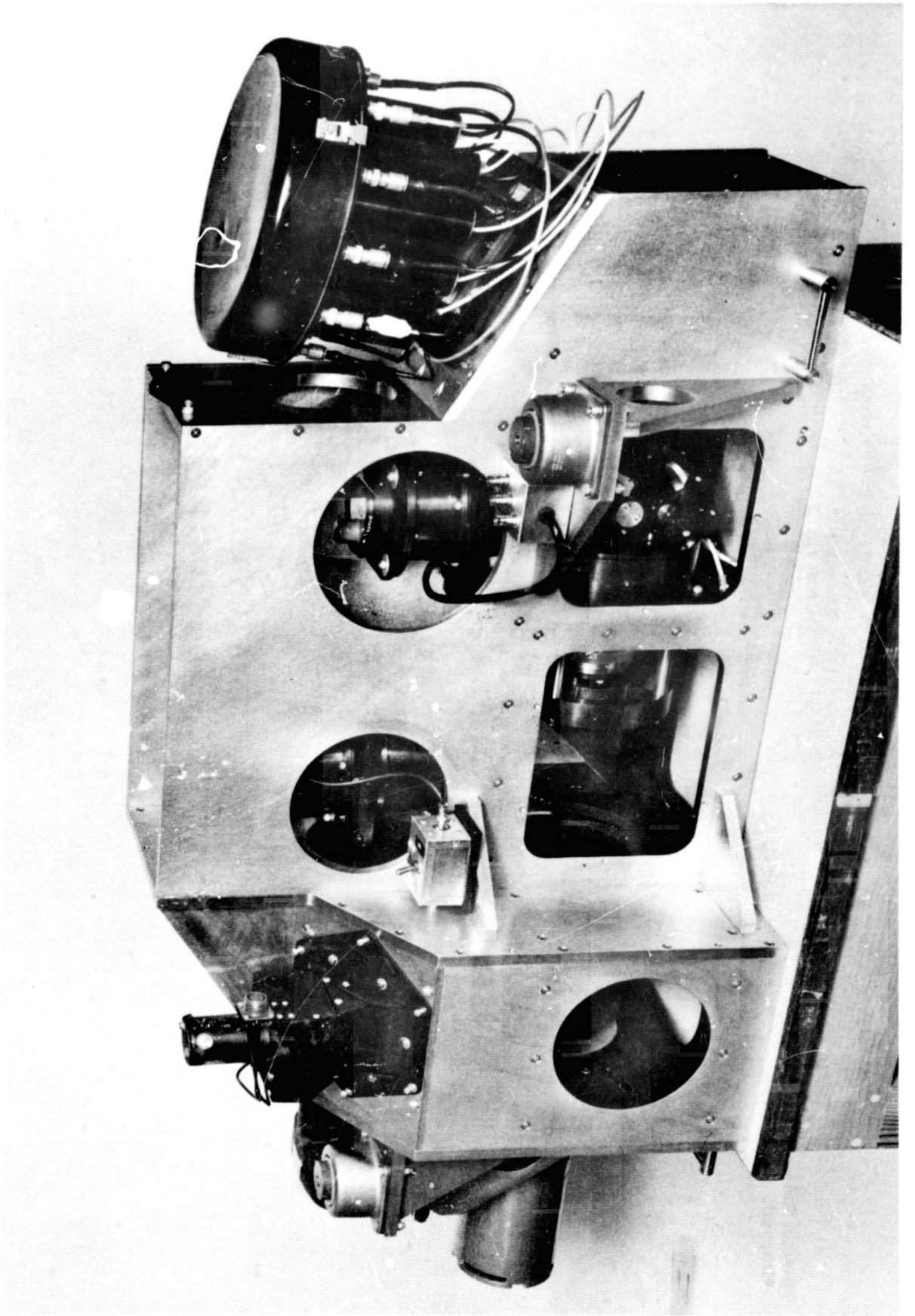

FIGURE 6. MICHIGAN EXPERIMENTAL MULTISPECTRAL SCANNER.
(View with inspection panels removed.)

	Position 1 (14.0 to 0.3 μ)			Position 2 (2.6 to 0.9[1] μ)			Position 3 (0.9[1] to 0.4 μ)		
CURRENT	Det.SN	Spec. Band (μ)	Spat. Res. (mr)	Det. SN	Spec. Band (μ)	Spat. Res. (mr)	Det. SN	Spec. Band (μ)	Spat. Res. (mr)
	HgCdTe1-3	1.0-11.5[2]	3.3×3.3	InAs3-5	2.0-2.6	2.0×4.0	PM12-1	.67-.94	2.0×2.0
					1.5-1.8	2.0×4.0		.62-.70	2.0×2.0
	HgCdTe1-2	1.0-14.0[2]	6.6×6.6		1.0-1.4	2.0×4.0		.58-.64	2.0×2.0
								.55-.60	2.0×2.0
				InSb3-6	2.0-2.6	2.0×4.0		.52-.57	2.0×2.0
					1.0-1.4	2.0×4.0		.50-.54	2.0×2.0
								.48-.52	2.0×2.0
								.46-.49	2.0×2.0
								.41-.48	2.0×2.0
FUTURE	HgCdTe3-1	8.2-9.3	6.6×6.6	InAs3-6	2.0-2.6	2.0×4.0	PM10-1	.90-1.1	3.0×3.0
		10.2-11.3	6.6×6.6		1.5-1.8	2.0×4.0		.67-.94	3.0×3.0
		11.7-13.8	6.6×6.6		1.0-1.4	2.0×4.0		.62-.70	3.0×3.0
								.58-.64	3.0×3.0
	HgCdTe1-4	1.0-14.0[2]	3.0×3.0	HgCdTe2-3	2.0-2.6	3.0-3.0		.55-.60	3.0×3.0
	UVPM1-3	0.3-0.7[2]	3.0×3.0		1.5-1.8	3.0×3.0		.52-.57	3.0×3.0
								.50-.54	3.0×3.0
	UVPM1-3	0.3-0.7[2]	3.0×3.0	InAs1-2	1.0-2.6[2]	3.0×3.0		.48-.52	3.0×3.0
								.46-.49	3.0×3.0
								.41-.48	3.0×3.0

Note: 1. Cutoff established by replaceable dichroic mirror.
2. Bandpass established by external optical filter.

FIGURE 7. DETECTOR CONFIGURATIONS FOR M7 SCANNER

FIGURE 8. MICHIGAN C-47 REMOTE SENSING AIRCRAFT

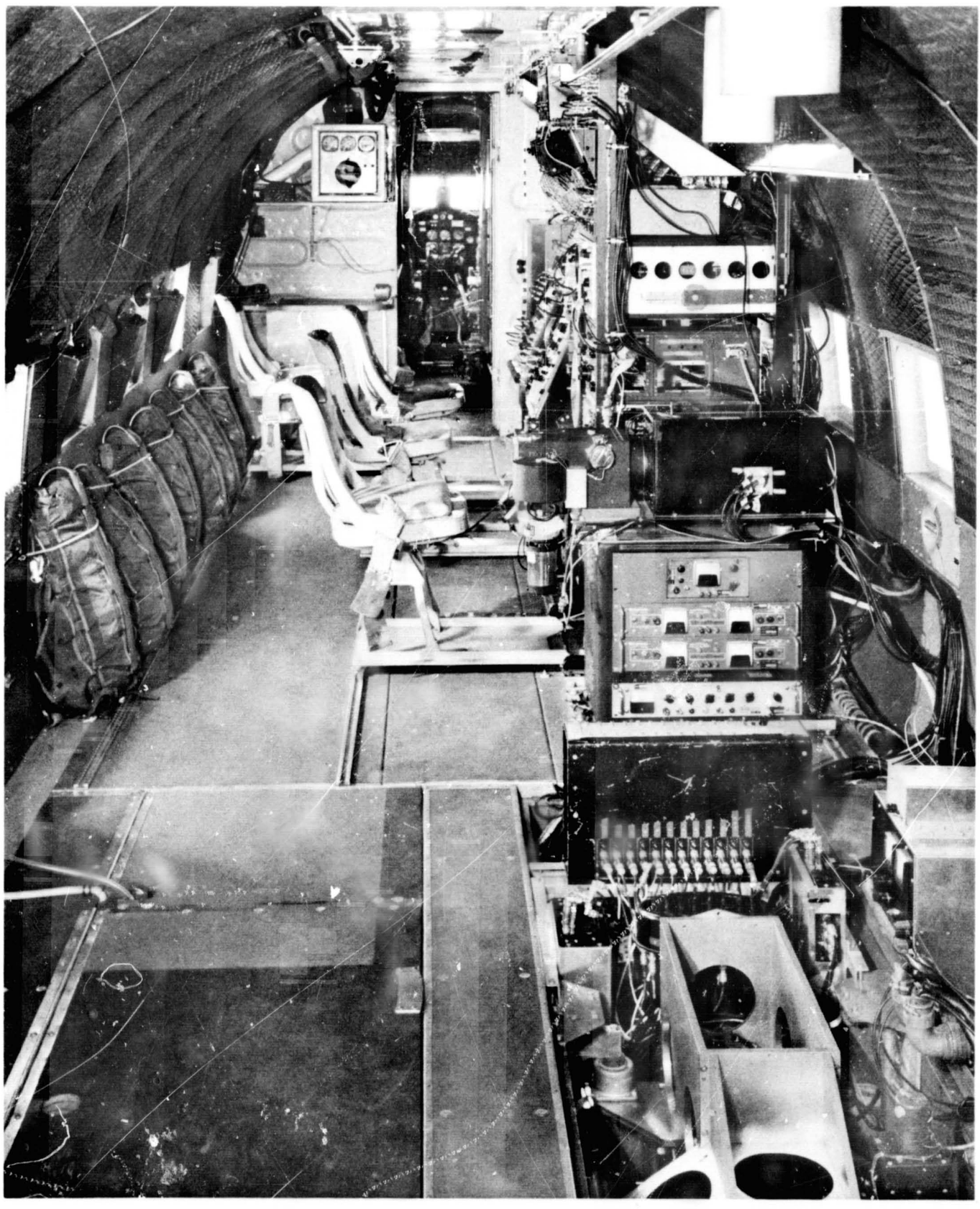

FIGURE 9. INTERIOR VIEW OF C-47 REMOTE SENSING AIRCRAFT SHOWING MULTISPECTRAL MAPPING SYSTEM

SECTION 35

MULTISPECTRAL IMAGING RADAR

by

L. J. Porcello
R. A. Rendleman
Radar and Optics Division
Willow Run Laboratories
Institute of Science and Technology
The University of Michigan
Ann Arbor, Michigan

ABSTRACT

During calendar year 1971 a University of Michigan fine-resolution sidelooking radar, installed in a C-46 aircraft, was modified to provide it with an initial multispectral imaging capability. The radar is capable of radiating at either of two wavelengths, these being approximately 3 cm and 30 cm, with either horizontal or vertical polarization on each wavelength. Both the horizontally- and vertically-polarized components of the reflected signal can be observed for each wavelength/polarization transmitter configuration. At present, two-wavelength observation of a terrain region can be accomplished within the same day, but not with truly simultaneous observation on both wavelengths. A multiplex circuit to permit this simultaneous observation has been designed. A brief description of the modified radar system and its operating parameters is presented. Emphasis is then placed on initial flight test data and preliminary interpretation. Some considerations pertinent to the calibration of such radars are presented in passing.

INTRODUCTION

In this report, we describe results achieved by the Radar and Optics Division of The University of Michigan's Willow Run

Laboratories under a NASA-supported* multispectral radar program. A fine-resolution airborne synthetic-aperture radar system, originally designed to operate at a wavelength of 3 cm (X-band), was modified such that, on any pass of the aircraft, the radar could be operated either at 3 cm or at 26 cm wavelength (L-band). Although funding did not permit provisions to be made for simultaneous two-wavelength operation, duplication of flight paths on successive passes was adequate to permit images generated at each of the two wavelengths to be examined in reasonable geometric registration. At each wavelength, it was possible to transmit one linear polarization — either horizontal or vertical — and to receive both the parallel-polarized and the cross-polarized components of the reflected signal. Because the two operating wavelengths differ by almost an order of magnitude, the roughness scales to which the radar is sensitive in its two operating modes likewise differ by a like amount. This feature, coupled with the greater transparency of vegetation at the longer wavelength provides us with a "two-color", two-polarization view of overflown terrain which is a potentially significant step in the direction of a multispectral microwave remote sensor.

After completion and checkout of the hardware, this simple multispectral system was then operated at Garden City, Kansas, and in the Lavic Lake/Pisgah Crater region of California. In this paper, we describe the radar system itself, and include some preliminary samples of multispectral radar imagery. The agricultural and geologic interpretation of the Garden City and Pisgah data respectively are the responsibility of University of Kansas investigators and are not treated formally in this paper.

SYSTEM DESCRIPTION

The multispectral radar consists of a synthetic-aperture radar (SAR) system which, in its basic form, operates at 3 cm wavelength. The 26-cm capability is provided by means of a down-converter inserted between the transmitter and antenna, and an up-converter inserted between the antenna and receiver. The basic 3-cm radar

---

* Contract NAS 9-11036

has the following key properties:

Type:	Focused synthetic aperture
Pulse:	Dispersed, linear FM
Antenna:	Dual-polarization slotted guide array with 6 in. × 60 in. aperture, and 25 db isolation between polarization
Data storage:	CRT/film recorder
Data processor:	Coherent optical correlator

The system is operated in a C-46 aircraft (Fig. 1). For the purpose of this program, the overall system, including the data processor, yields imagery with slant-range and along-track resolutions both equal to 30 feet. Since the system is a focused synthetic-aperture radar, both values of resolution are independent of slant range at the ranges of interest to this program.

When 26-cm operation is required, the down-converter/up-converter circuitry is inserted into the radar signal chain. The RF bandwidth of the radar is not altered, although the radiated nominal center frequency is translated from 9.4 GHz to 1.265 GHz. Therefore, the range resolution of 30 feet is preserved. The 30 foot along-track resolution is likewise preserved, since synthetic-aperture systems have a theoretical resolving capability which is λ-independent. The motion-compensation circuitry which frequently is employed in SAR systems must be rescaled when λ is changed, since the inertial sensing subsystem is sensitive to aircraft translation or its derivatives, and a given translation inserts a phase error which varies as λ^{-1}. The required rescaling is provided by a gain change in an amplifier. The conversion of the system from 3-cm to 26-cm or vice versa can be accomplished in the air between passes since it was feasible to mount both the 3-cm and the 26-cm dual polarization antennas within the C-46 radome. (Figure 2) Changeover time for the RF circuitry and motion compensation scaling is about 30 minutes, considerably shorter than one day changeover time initially specified by MSC. Once the conversion from X-band to L-band is complete, the basic performance parameters are as listed earlier for the 3-cm case.

A comment is in order on the reasons why a heterodyne approach was employed to provide the multispectral capability. One fundamental reason was cost. The operating X-band system, prior to modification, contained nearly all the expensive and technically difficult components which a SAR system requires; i.e.,

Phase coherence circuitry
Broad-band pulse generation circuitry
Motion sensing and compensation
Broad-band receivers and video gain
Optical data recorders

The only new components which were required were the up/down converters, the L-band transmitter and the antennas. In addition to minimizing cost, this approach provided high probability of success, since the basic X-band system had been well proven.

PRELIMINARY RESULTS

The two-frequency radar was operated in Kansas and in California during the latter half of 1971. Figure 3 shows comparative X/L band images of a portion of the Garden City Agricultural Test Site, Kansas, generated July 23, 1971. As mentioned above, University of Kansas investigators will provide detailed interpretation of this imagery and thus only comments based on brief inspection of the data and no ground truth are presented here. The two fields called out by arrows in the four images provide an interesting illustration of the reflectivity differences to be expected at the two wavelengths and polarizations. The X-band images show some fine structure in the ground cover, possibly related to water content, while the normal polarized L-band energy probably penetrated the vegetative cover and was reflected by the residual cultivation furrows which are perpendicular to the radar line-of-sight and was reflected relatively less by the furrows parallel to the line-of-sight.

Figure 4 shows comparative X/L band images of Pisgah Crater, California, generated in October 1971. An interesting feature of these images is the relative reflectivity of the lava area left (west northwest) of the crater. This demonstrates the multifrequency radar's ability to differentiate surface roughness changes from

slope changes as the relative reflectivity would remain approximately constant from wavelength to wavelength if the higher return in this area were due to slope effects.

Figure 5 shows comparative X/L band imagery of Lavic Lake, California, generated in October 1971. Once again surface roughness effects are evident with particular emphasis in the left (southwest) portion of the image.

CONCLUDING REMARKS

The radar described above satisfies the basic program objective of providing a capability for imaging terrain, with fine resolution, in two spectral regions separated by approximately one order of magnitude in wavelength. However, this system, as implemented, has several glaring weaknesses:

a) It cannot observe on both wavelengths simultaneously. Therefore, even if flight lines are repeated precisely, other natural changes may occur between observations which alter the apparent reflection properties of the surface. As one example, enough rain fell on the surface at Lavic Lake between two of the passes so that the lake surface was dry on one pass and liquid on the other (these are not the passes illustrated in Fig. 5).

b) Differences in flight path for the 3-cm and 26-cm observations result in changes of aspect and depression angle of the observation for flat terrain and differential errors in ground range/slant range transformations over hilly or mountainous terrain. As a result, λ-dependences are mixed with viewing angle dependences, and this complicates the interpretation/recognition process.

c) The two-wavelength radar is not amplitude-calibrated on either operating wavelength.

Many of the multispectral recognition concepts now being developed and applied in the IR and visible portions of the electromagnetic spectrum show promise, if suitably modified, in the

microwave portion of the spectrum. A full assessment of the applicability of these techniques to radar imaging is very difficult without a calibrated and simultaneous observation system. The Michigan X/L band SAR system, while not adequate for this larger assessment, does provide a good start toward establishment of a data base which is a necessary step in the direction of multispectral radar sensing.

Figure 1. - C-46 radar testbed.

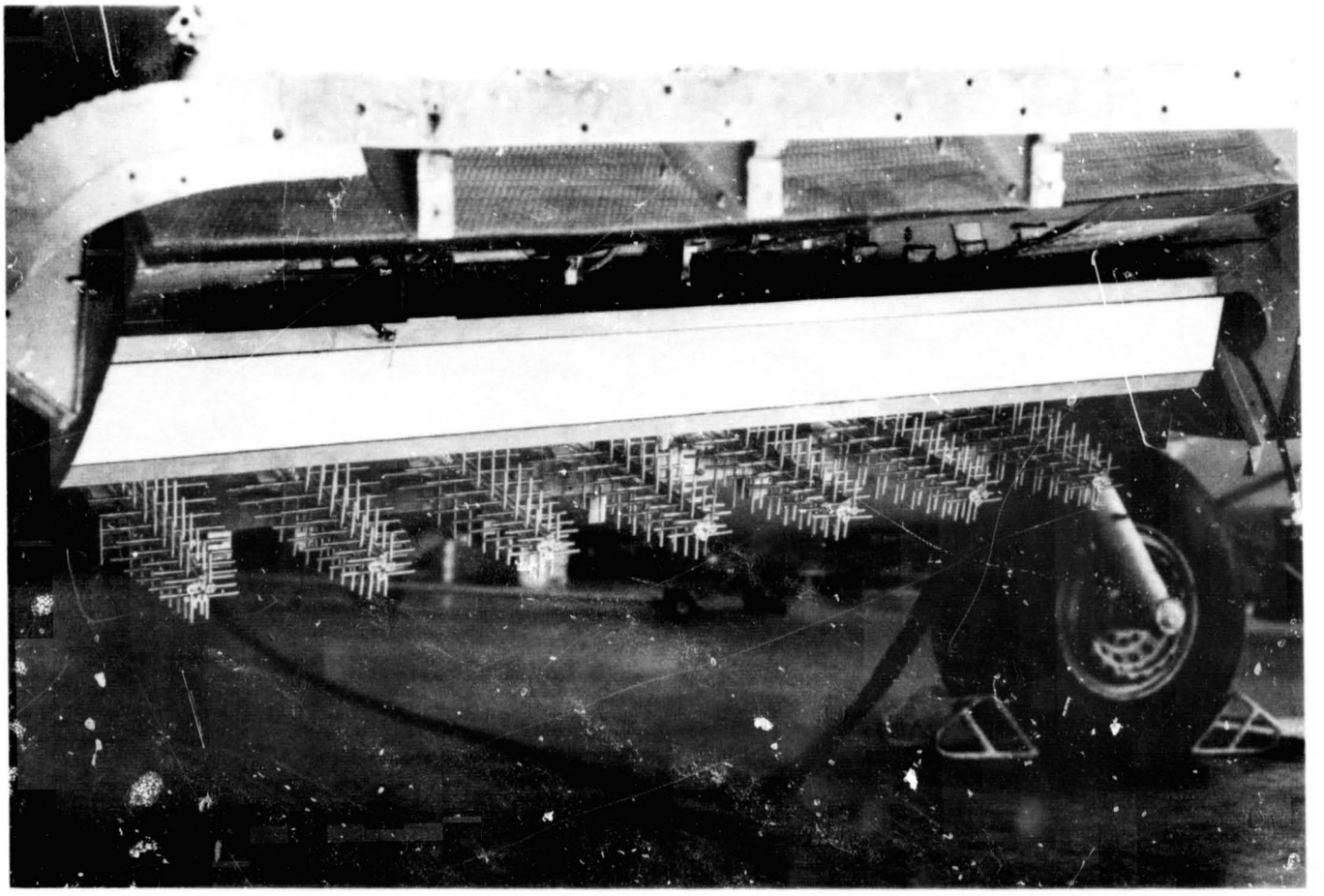

Figure 2. - X-band (above) and L-band (below) antenna installation on C-46 aircraft (radome removed).

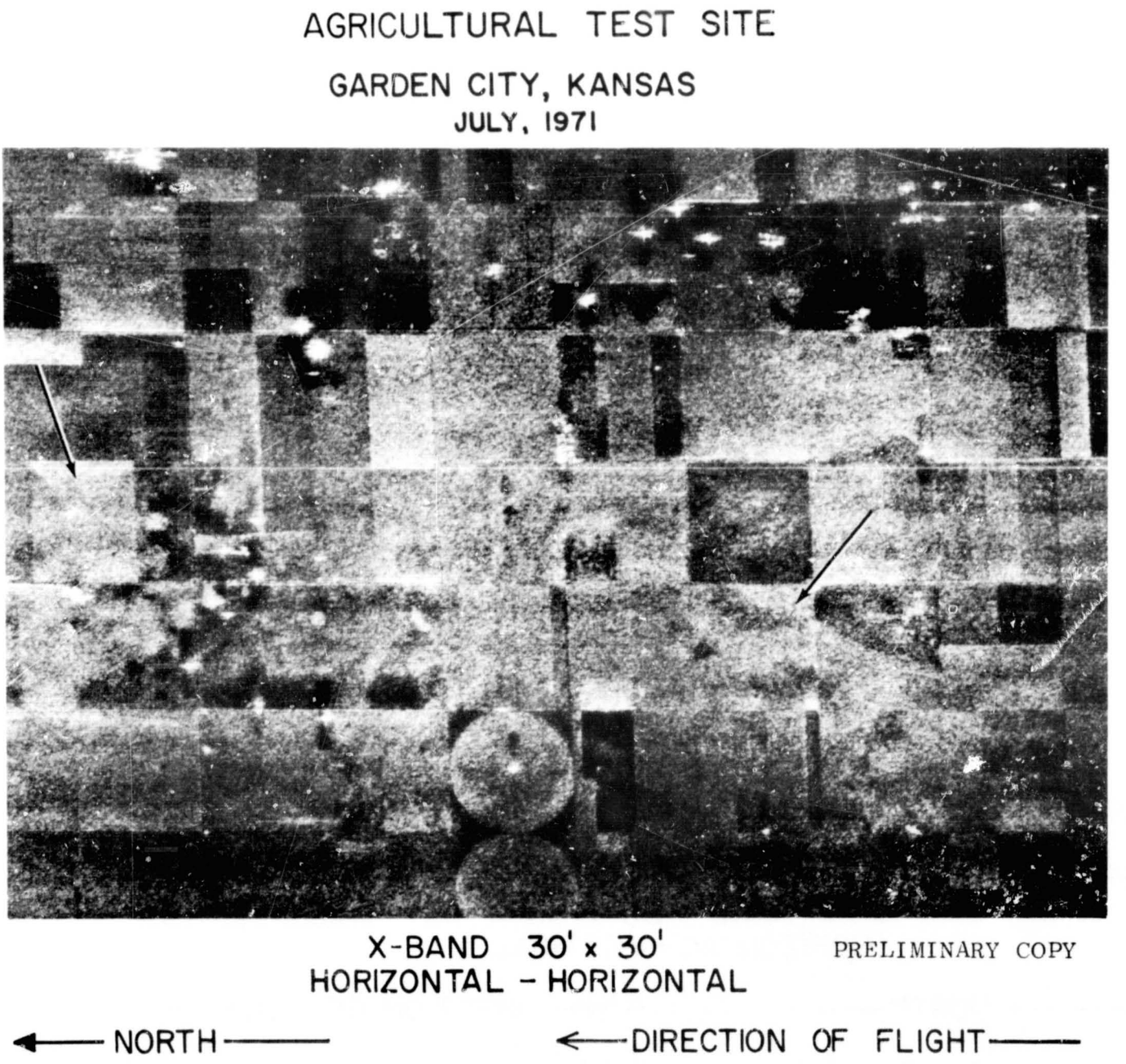

Figure 3. - Multifrequency, multipolarization imagery of agricultural test site.

AGRICULTURAL TEST SITE

GARDEN CITY, KANSAS

JULY, 1971

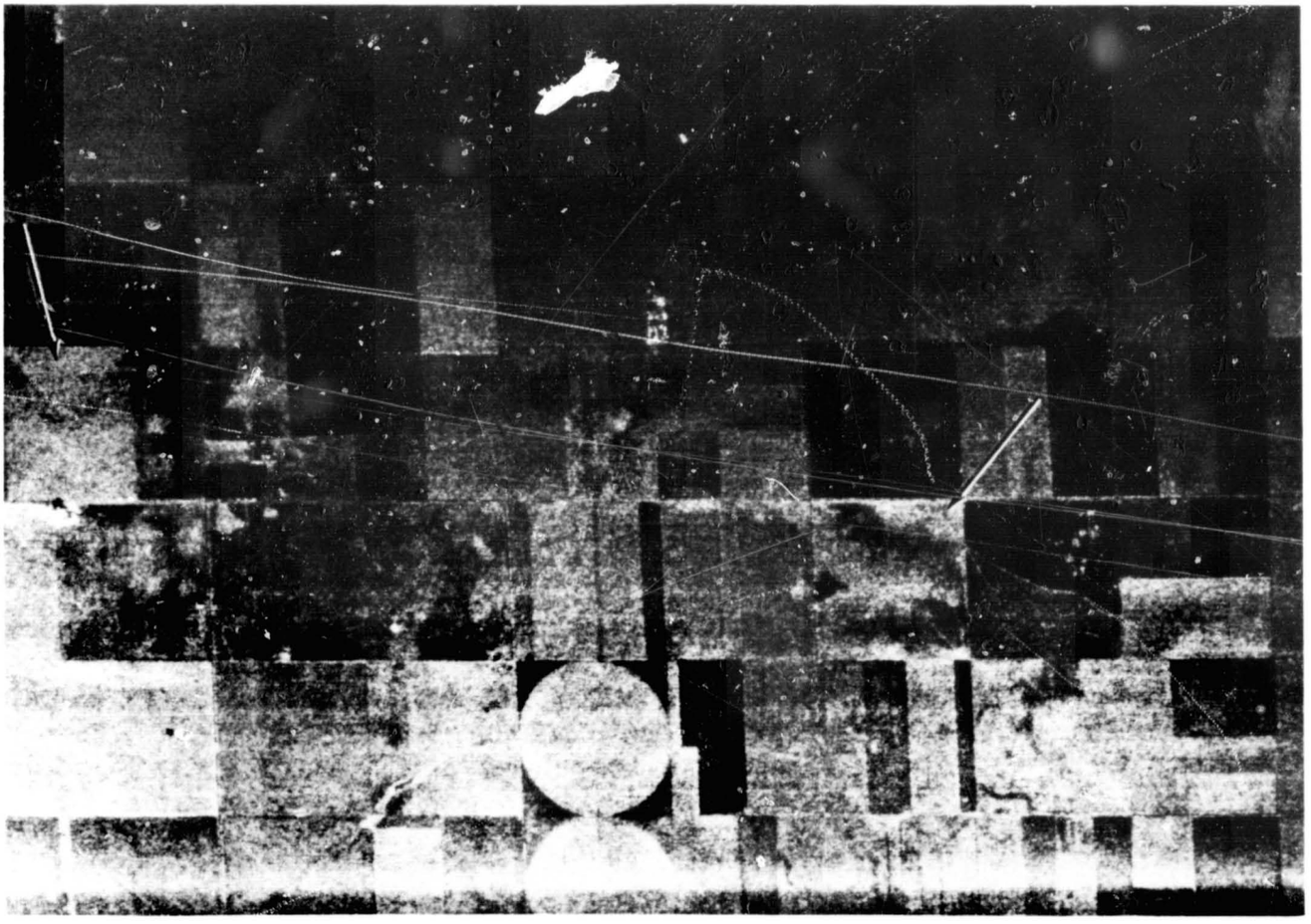

X-BAND - 30' x 30'
HORIZONTAL - VERTICAL

PRELIMINARY COPY

← NORTH —

← DIRECTION OF FLIGHT —

Figure 3. - Multifrequency, multipolarization imagery of agricultural test site (continued).

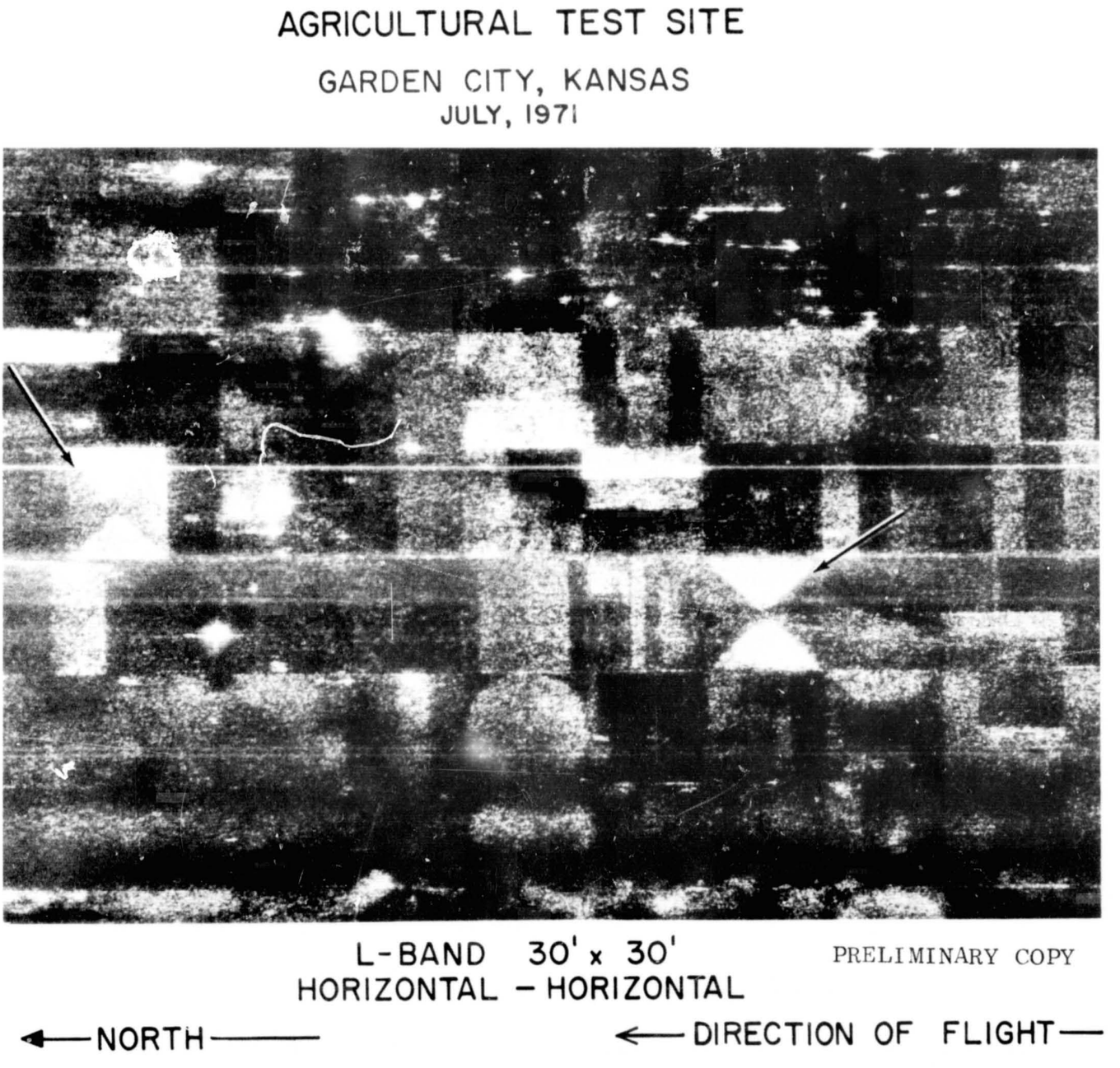

Figure 3. - Multifrequency, multipolarization imagery of agricultural test site (continued).

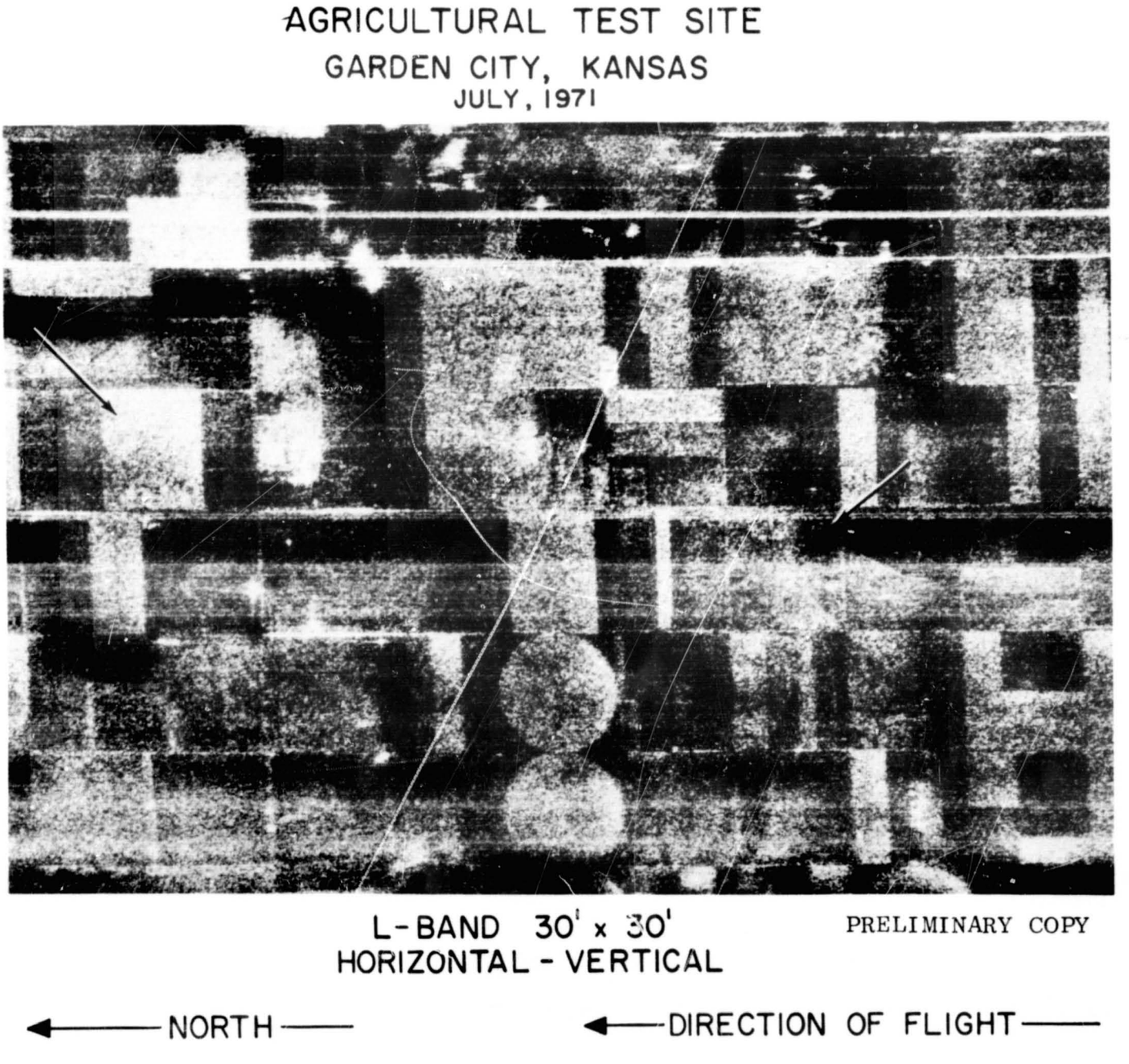

Figure 3. - Multifrequency, multipolarization imagery of agricultural test site (concluded).

Figure 4. - Multifrequency, multipolarization imagery of Pisgah Crater area.

Figure 4. - Multifrequency, multipolarization imagery of Pisgah Crater area (continued).

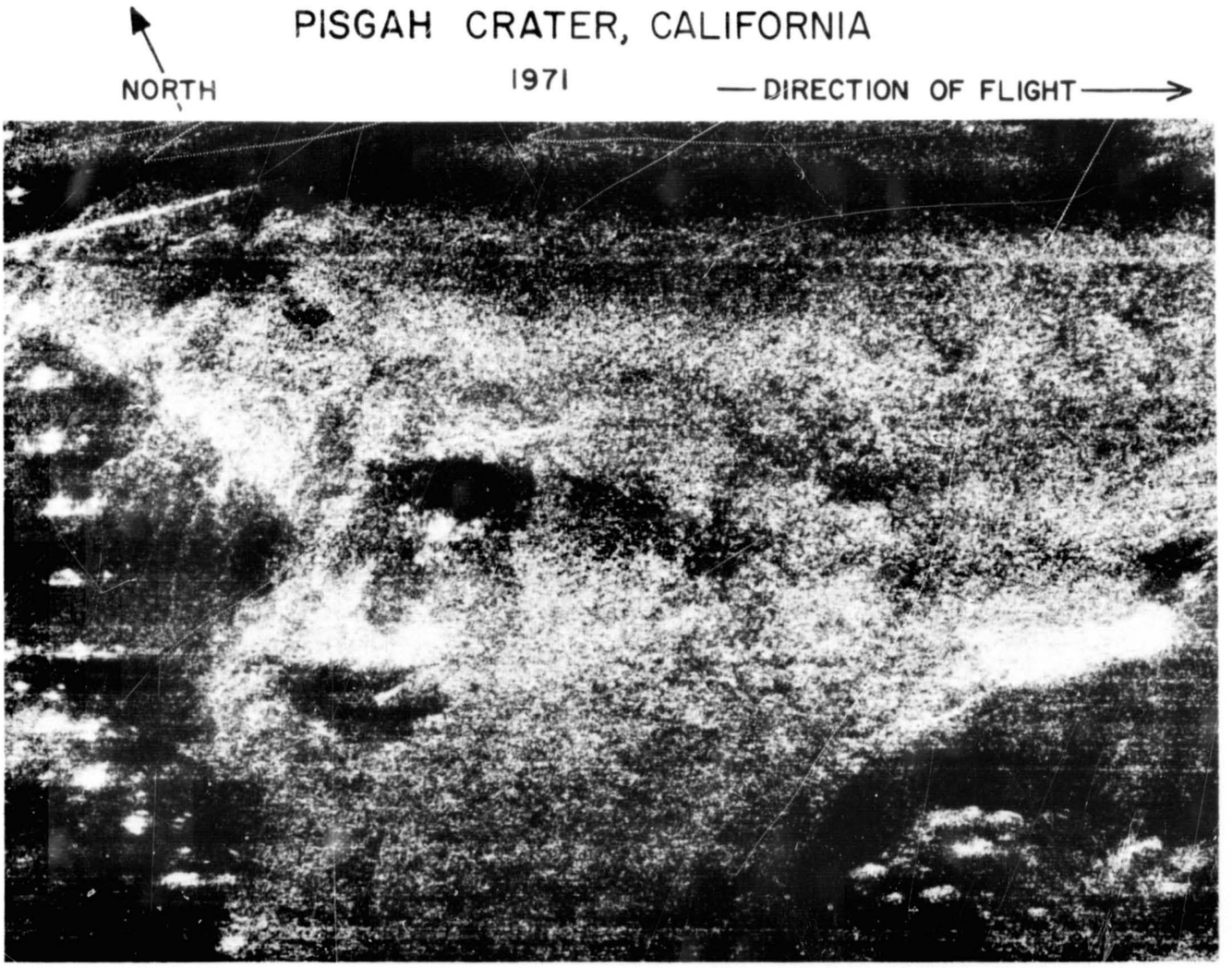

Figure 4. - Multifrequency, multipolarization imagery of Pisgah Crater area (continued).

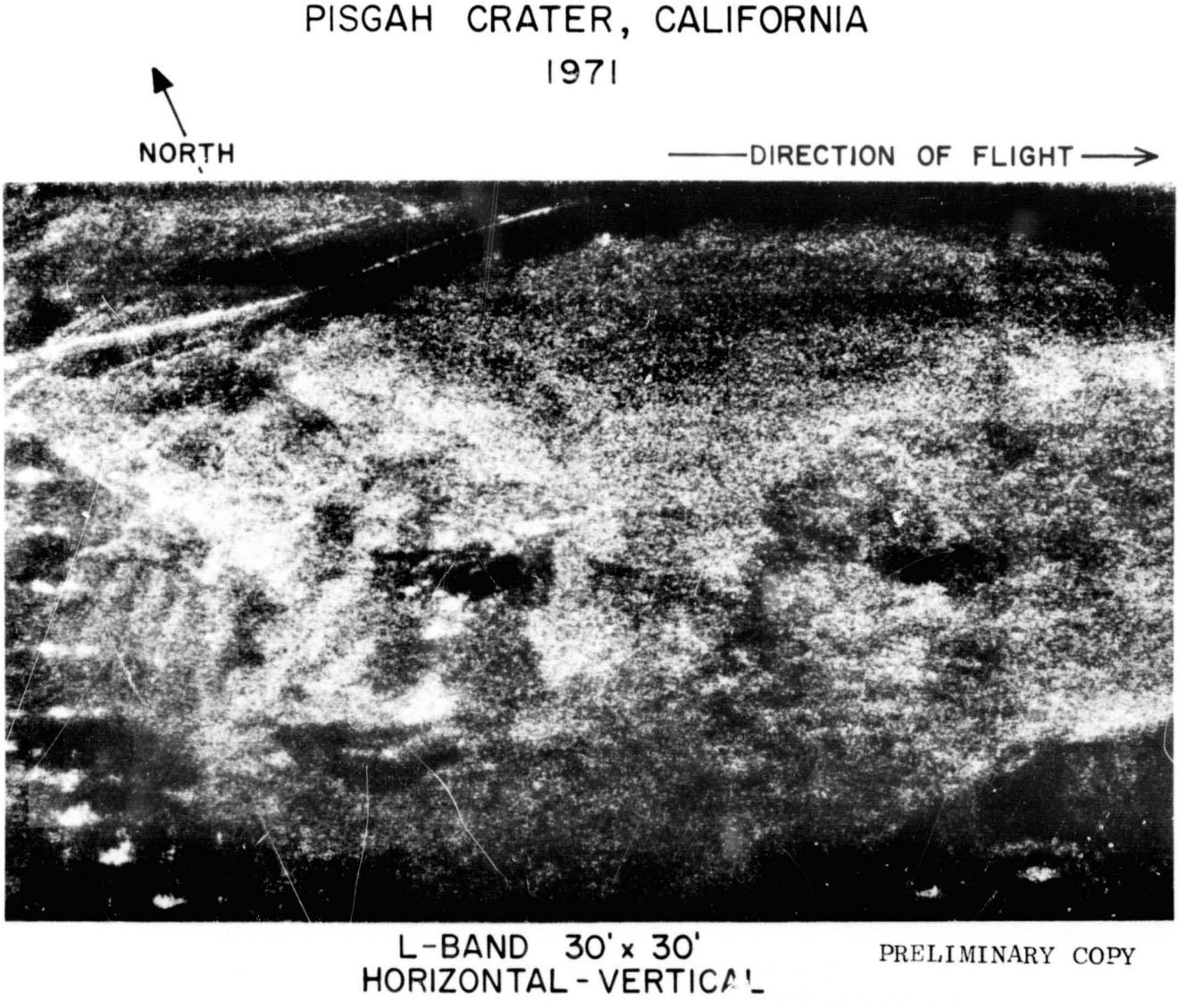

Figure 4. - Multifrequency, multipolarization imagery of Pisgah Crater area (concluded).

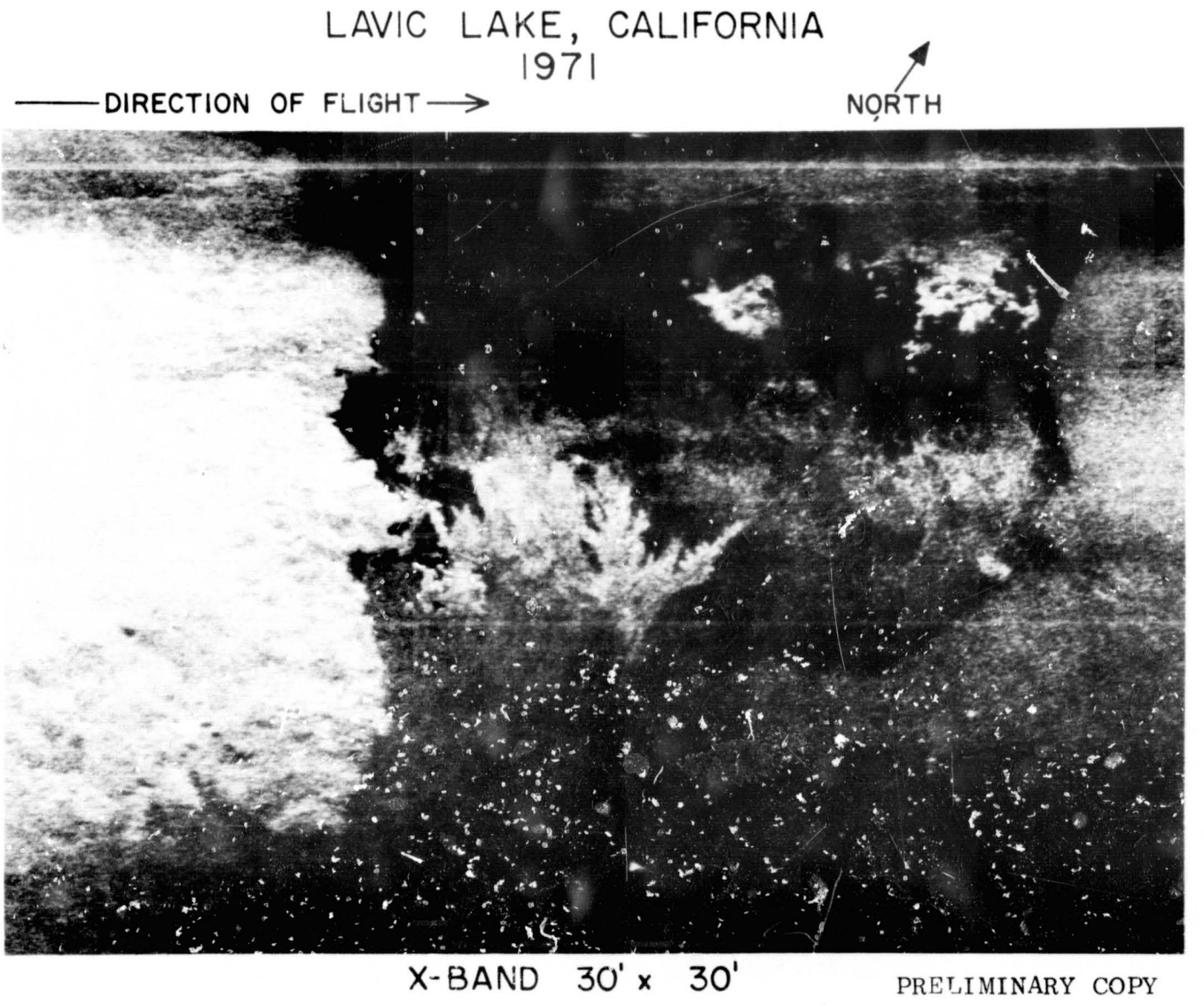

Figure 5. Multifrequency imagery of Lavic Lake.

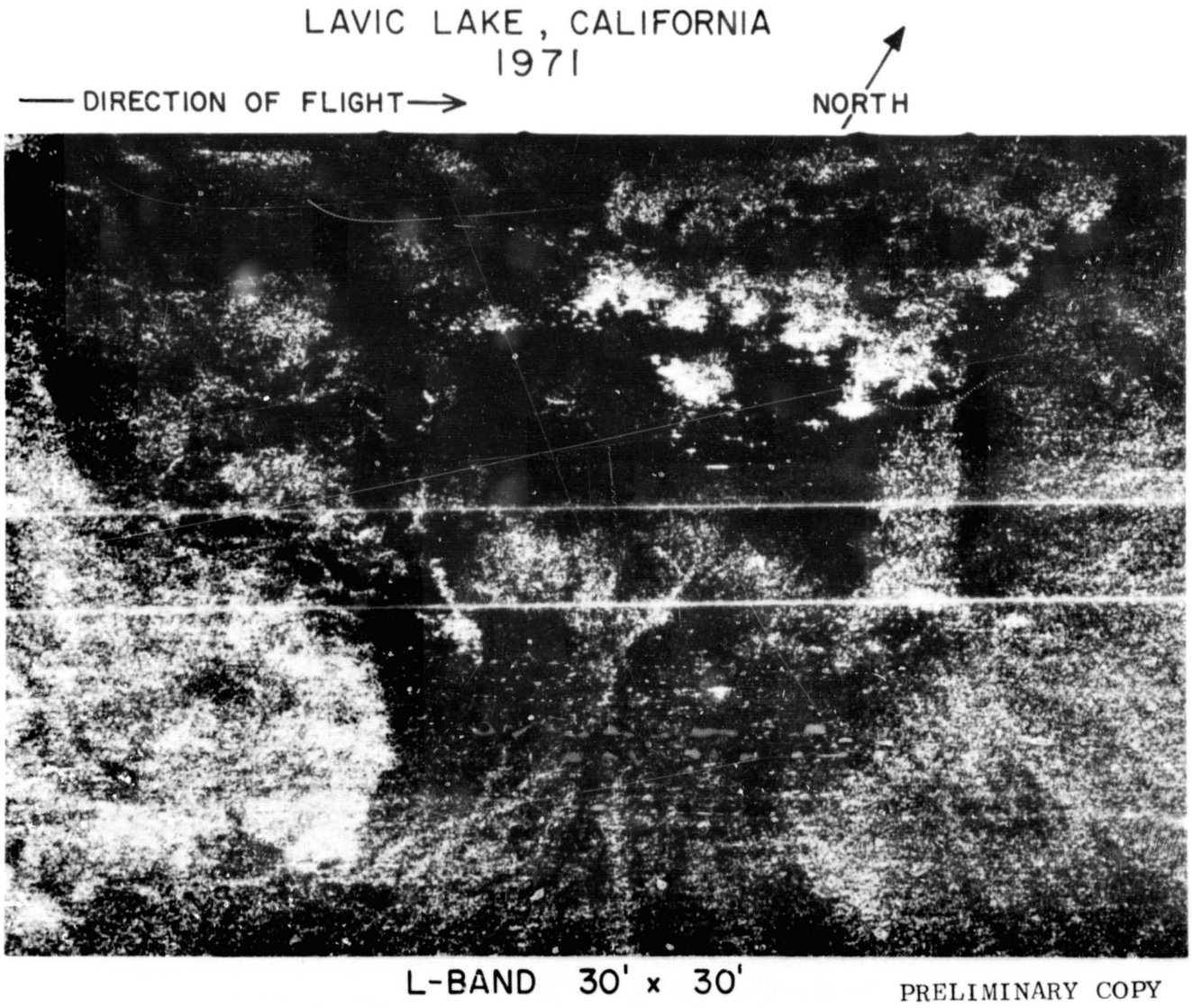

Figure 5. Multifrequency imagery of Lavic Lake (concluded).

SECTION 36

SURFACE CONFIGURATION AS AN EXPLANATION FOR LITHOLOGY-RELATED CROSS-POLARIZED RADAR IMAGE ANOMALIES

by

James R. McCauley
Center for Research, Inc.
Remote Sensing Laboratory
University of Kansas
Lawrence, Kansas 66044

INTRODUCTION

With the development of multipolarized side-looking radar systems, it became possible to record two orthogonal components of the backscattered radiation in the form of two congruent and simultaneously produced radar images, a like-polarized image, either HH or VV and corresponding cross-polarized image, HV or VH. Study of Westinghouse AN/APQ-97 Ka-band multipolarized imagery acquired in 1965 and 1966 as part of the Earth Resources Program has uncovered various targets that appear differently on the like- and cross-polarized images. One group of polarization anomalies has concerned geologists for some time, namely the significantly lower cross-polarized returns produced by certain volcanic rocks.

An explanation of these lower cross-polarized returns is the subject of the present investigation conducted at the Remote Sensing Laboratory of the Center for Research, Inc. at the University of Kansas with funding by NASA Contract NAS 9-10261.

The first geologic evaluation of simultaneously produced like- and cross-polarized images was performed by Dellwig and Moore (1966) in the Pisgah Crater area of Southern California. The area is a NASA test site and was imaged in 1965 with the AN/APQ-97 SLAR system using its full polarization capacity together with several look directions. Geologically, the area is composed of two Quaternary basalt flows, a playa, and large areas of alluvial fans. Studies of the imagery revealed that whereas the flows associated with Pisgah Crater and the areas of alluvium retained much the same appearance on all images regardless of polarization, the other basalt flow (Sunshine flow) produced images that were distinctly darker on cross-polarized returns than on like-polarized returns. This reversal in tone by the Sunshine flow allowed the easy discrimination of adjacent rock types on cross-polarized images that were difficult to separate on the like-polarized image. These and other polarization-related differences lead the authors to state that "In simultaneously produced like- and cross-polarized imagery, as exemplified by the Pisgah Crater area, the geologist finds information previously unattainable from only like-polarized radar imagery," (Dellwig and Moore, 1966, p. 3601).

About the same time, Cooper (1966), conducting a preliminary evaluation of K-band imagery in the Twin Buttes area of Arizona, (see Figure 2A), noted two areas of low return on the HV image that were not delineated on the corresponding HH image or aerial photographs. Subsequent field investigation established these areas as being previously unmapped outcrops of pyroxene rhyodacite. Noting no important differences in surface roughness between the outcrop and surrounding areas, Cooper suggested the high glass content of the rhyodacite as a possible cause for the differing radar returns.

Gillerman (1967) tested the preliminary hypothesis of Cooper concerning glass content by searching the K-band imagery of the Western United States for areas with lower return (darker) on the cross-polarized image than on the like-polarized image. A number of such areas were uncovered. All consisted of Tertiary or Quaternary volcanic rocks with wide ranging compositions and glass contents. This lead Gillerman to conclude that glass content was not the determining factor in producing lower returns on the cross-polarized imagery.

PROCEDURE

When the present study was undertaken, certain generalizations could be made concerning the nature of the anomalous returns.

1. These anomalies always produced bright like-polarized and dark cross-polarized images.
2. In test sites where the full polarization capability was used; the lower cross-polarized returns occurred independently of the polarization of the transmitted signal, that is darker VH images were produced as well as darker HV images.
3. In these same sites, lower cross-polarized returns appeared independently of look-direction.
4. The lower cross-polarized returns were apparently associated with volcanic rocks although they occurred independently of composition and glass content since both factors vary widely in the rocks producing such returns.

A further search of available multipolarized radar was conducted to uncover additional polarization anomalies. These were documented with respect to rock-type using published literature and maps. Aerial photos of many of these areas were obtained and studied, and finally, several areas were investigated in the field where samples were collected and ground truth was obtained. No single hypothesis was tested, many lithologic properties were considered in hopes of uncovering consistencies which may be responsible for the lower cross-polarized returns.

RESULTS

Search of the radar uncovered a number of cross-polarized anomalies which were not associated with volcanic rocks but were apparently caused by outcrops of certain sandstone formations, namely, the Navajo Sandstone of Utah and its time

equivalent in southern Nevada, the Aztec Sandstone. Extensive outcrops of thick Tertiary clastics in the Imperial Valley of California also produced images with distinctly lower cross-polarized returns.

Gross lithologic differences between sandstones and volcanic rocks discounted many early hypotheses concerning various volcanic phenomena. Field investigation, however, has led to the conclusion that surface configuration of the outcrops involved is responsible for their appearance on multipolarized imagery. The manner in which these anomalous returns are produced is by specular non-depolarized reflection from planar rock surfaces.

In general, the rocks producing anomalous cross-polarized returns can be grouped into three general types: (1) certain geologically recent lava flows (late Pleistocene and Holocene), (2) some Tertiary volcanics and (3) certain massive sandstones. These three rock types, for differing reasons, produce terrains in which radar return is dominated by specular reflection from planar surfaces.

For a specular reflector to be recorded on a SLAR image, its orientation must be normal to the path of the impinging radar, and for such an orientation, Fung (1965) has shown that the depolarized component of the reflected radar energy is at a minimum. This results in a higher return onthe like-polarized image and a lower return on the cross-polarized image; which is in compliance with the observed multi-polarized behavior of the three rock types. When planar surfaces are normal to the path of the incident radar, both horizontally and vertically polarized radar behave the same since both are oscillating in the plane of the reflecting surface. This explains the fact that lower cross-polarized returns occur independently of the original polarization direction.

The planar rock surfaces are large with respect to the wavelength of the Ka-band AN/APQ-97 system (0.86 cm.) yet are small in comparison to the resolution. The outcrops involved represent highly faceted surfaces with facets of varying orientations. However only those of the proper orientation produce significant returns. Because there may be many facets so oriented in any given resolution cell, the observed radar images are averaged returns showing the dominance of specular reflectors in the production of the returns. In addition, the omnidirectional attitude of the facets and their wide distribution on the outcrops studied explains the independence of look-direction that the flat lying anomalous outcrops exhibit in production of darker cross-polarized images.

DISCUSSION

The first group of rocks, the young lavas, all have one characteristic in common — blockiness. This blockiness results from the actual eruption of the lavas. With dacites and rhyolites, the low temperature and high viscosity of the lava results in domes and thick stubby flows with surfaces littered by large blocks that yielded to the stresses of eruption. The rhyolitic domes and flows of the Mono Craters in east-central California are good examples. Some basaltic eruptions result in blocky flows

because of rapid cooling of the lava while still in motion. The youthful lava associated with S. P. Crater in the San Francisco volcanic field of Arizona is a very blocky basalt that produces anomalous returns on multipolarized imagery. In both bases, the terrain is dominated by blocky fragments with planar surfaces that are much larger than the wavelength of the radar. Because of the youthfulness of the lavas, the effects of weathering are not much in evidence; soils and regolith are lacking and vegetation is minimal. Because of the large size of these flows as well as their well-defined boundaries, they are easily resolved on K-band imagery.

Figure 1a is a radar image of the Mono Craters recorded with an easterly look-direction. The top image is a like-polarized image (VV) whereas the lower image is cross-polarized (VH). Numerous parts of the north-south chain of extinct volcanoes appear darker on the cross image. These areas are all blocky domes and flows of recent geologic age composed of obsidean and punice of rhyolitic composition.

Figure 1b is a view of the small flow at the northern end (right) of the chain, which shows a sharply lower return on the cross-polarized image. The picture was taken on the younger flow looking in a northwesterly direction. Large angular blocks of punice are evident in the foreground. In the middle distance, an older flow can be seen which has been buried by an intervening episode of ash erruption. As a result, the blocky nature of the older flow is concealed and vegetation is developed which together with the puffy ash covering produces a diffuse and depolarized return.

Figure 1c is a close-up view of the angular blocks of pumice which make up the surface of the flow. The smoothness of these surfaces is apparent. In addition the vesicles of the pumice are small and evenly distributed. Thus there are no discontinuities in the blocks to produce internal reflecting boundaries. As a result most of the return from these blocks is produced by reflection from the surface, which in this case is specular. In other areas, particularly in the flows to the south, obsidian makes up the blocks which dominate the surfaces. For the same reason as in the case of pumice, similar low cross-polarized returns are produced.

The second group of rocks are also volcanic including some shallow intrusives but are older, generally tertiary in age and thus have undergone more extensive weathering. The cause for differential depolarization by this class of rocks is again blockiness. In this case, however, the blockiness is due to weathering which produces blocky outcrops and extensive areas of rubble. However, because of the age of the outcrops, soils and vegetation have also developed. Thus it is only in dry climates such as in the southwestern part of the country that soil development and vegetation cover is suppressed sufficiently to permit the blocky rubble to contribute significantly to the radar return. Because the radar return from these rocks is only partially due to specular reflection, the differences between the like- and cross-polarized returns are usually less than those observed with the first class of rocks.

Figure 2a shows HH and HV images of the Twin Buttes area. Arrows indicate the outcrops of pyroxene rhyodacite studied by Cooper. Figure 2b is a view of the large northern outcrop. The difference in vegetation is largely due to the blocky surface which hinders root development of larger plants such as the mesquite trees in the foreground. Figure 2c is a view of blocks of rhyodacite which protrudes above the sparse cover of short grasses.

The third rock type accountable for differential depolarization are the thick massive sandstones particularly those of a friable nature that are easily physically weathered. Such sandstones are swept clean with each rain, thus extensive bare rock outcrops are capable of forming. Because these sandstones weather into broad smoothly rounded forms, there are limited surfaces in a given area that have the proper attitude to reflect radar energy back to the receiver. This accounts for the speckled return these rocks produce on the like-polarized image with the bright specks representing surfaces of the proper orientation. The cross-polarized image is almost completely black. The Navajo Sandstone of the Colorado Plateau behaves in this manner as does its time equivalent in southern Nevada, the Aztec Sandstone.

Figure 3a is a radar image in southern Nevada to the north of Lake Mead. Numerous bright specks on the HH image appear completely dark on the HV image. These returns are produced by outcrops of the Aztec Sandstone such as pictured in figure 3b. Such outcrops are devoid of soil and vegetation and present extensive areas of bare sandstone surfaces which are quite smooth, as shown in figure 3c. As in the case of fine-grained volcanics, fine-grained massive sandstone presents a homogeneous medium to the incident radar, as a result, the returning signal is dominated by reflection from the surface which again is specular and maintains its original polarization.

The three rock types discussed are not the only ones capable of producing dark cross-polarized images, however they are the only ones thus far uncovered which do so on Ka-band imagery. Scale and resolution appear to be the limiting factor; since an ideal surface has to be of sufficiently uniform and sufficiently large in area to be delineated on small scale Ka-band imagery. With the employment of higher resolution multipolarized radar systems this type of radar return may become more important in the interpretation of radar imagery and may be found to be produced by additional rock types.

Non-depolarized reflection is dependent upon smooth surfaces, as a result the production of dark cross-polarized images by rock surfaces is frequency dependent. The interrelationships of frequency and polarization in the production of radar images of various natural surfaces is an area that needs further study. The possibility exists that the combination of a multipolarization capability with one or two different frequencies could provide the same amount of terrain information as the use of several frequencies with the same polarization configuration.

CONCLUDING REMARKS

Three rock types: (1) geologically recent blocky lavas, (2) some Tertiary volcanics and (3) certain massive sandstones produce radar images characterized by bright like-polarized returns and dark cross-polarized returns. Outcrops of the three rock types discussed share certain features; planar rock surfaces that are large in comparison with the wavelength of the incident radar are abundant and detrital material and vegetation are of secondary importance; the planar surfaces appear to significantly contribute to the returning radar energy with this energy maintaining a

constant polarization; the outcrop areas are of sufficient size and sufficiently uniform character to be delineated on small scale K-band imagery. In addition, this mode of reflection may become of more importance inthe design and utilization of future radar systems.

REFERENCES

1. Dellwig, L. F. and R. K. Moore (1966) The Geological Value of Simultaneously Produced Like- and Cross-Polarized Radar Imagery: Journal of Geophysical Research, vol. 71, no. 14, pp. 3597-3601.

2. Cooper, J. R. (1966) Geologic Evaluation - Radar Imagery of Twin Buttes Area, Arizona: U. S. Geological Survey Unpublished Report.

3. Gillerman, E. (1967) Investigation of Cross-Polarized Radar on Volcanic Rocks: Kansas University Center for Research, Inc. (CRINC), Technical Report 61-25, 11 pp.

4. Fung, A. K. (1965) Scattering and Depolarization of Electromagnetic Waves by Rough Surfaces: Kansas University Center for Research, Inc. (CRINC), Technical Report 48-5, 22 pp.

5. Moore, R. K. (1969) Radar Return from the Ground: University of Kansas Publication, Bulletin of Engineering No. 59, 87 pp.

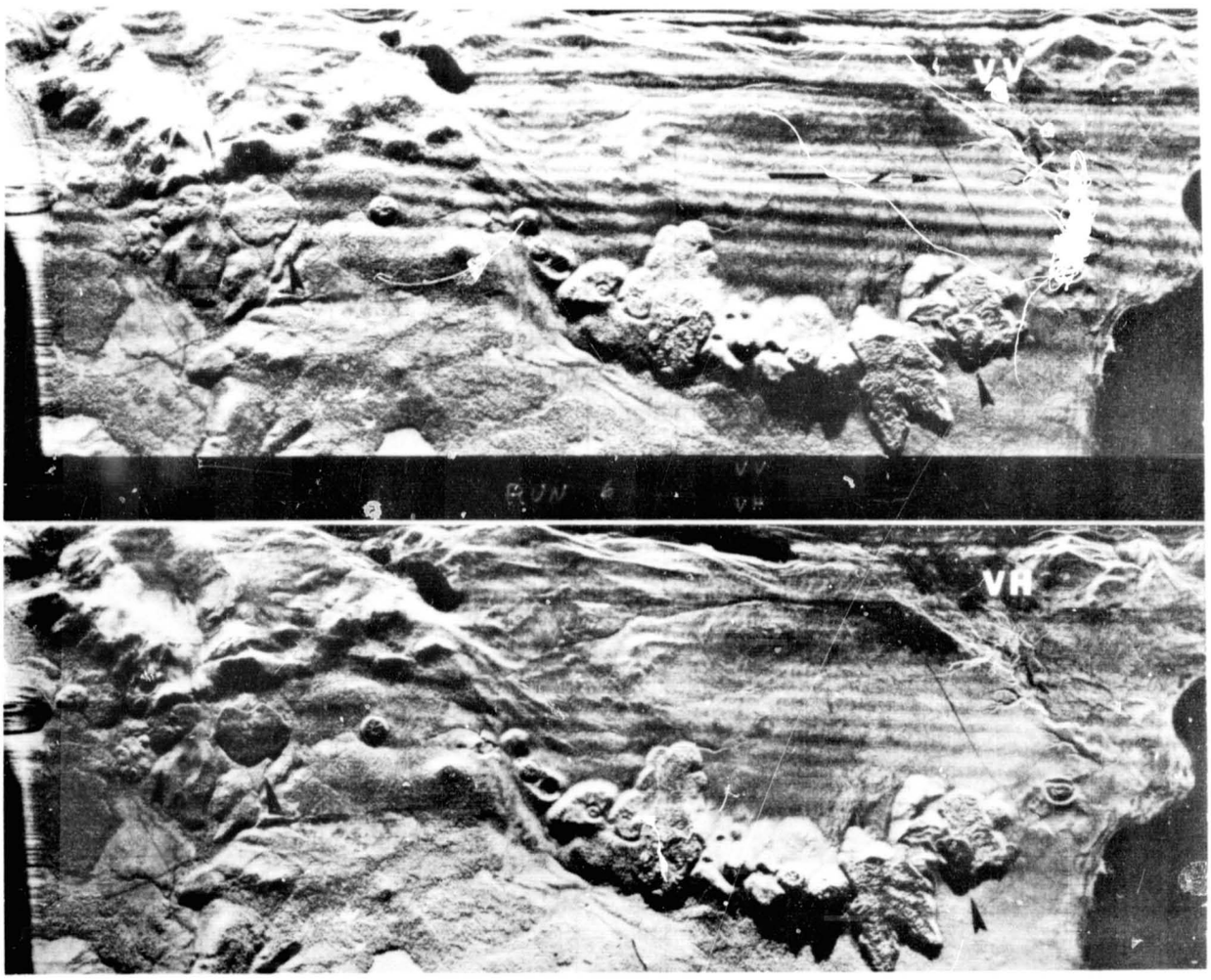

1a VV and VH images of Mono Craters, showing tonal reversals associated with recent blocky flows.

1b View on northern-most anomalous flow looking northwest.

1c Close-up of pumice blocks.

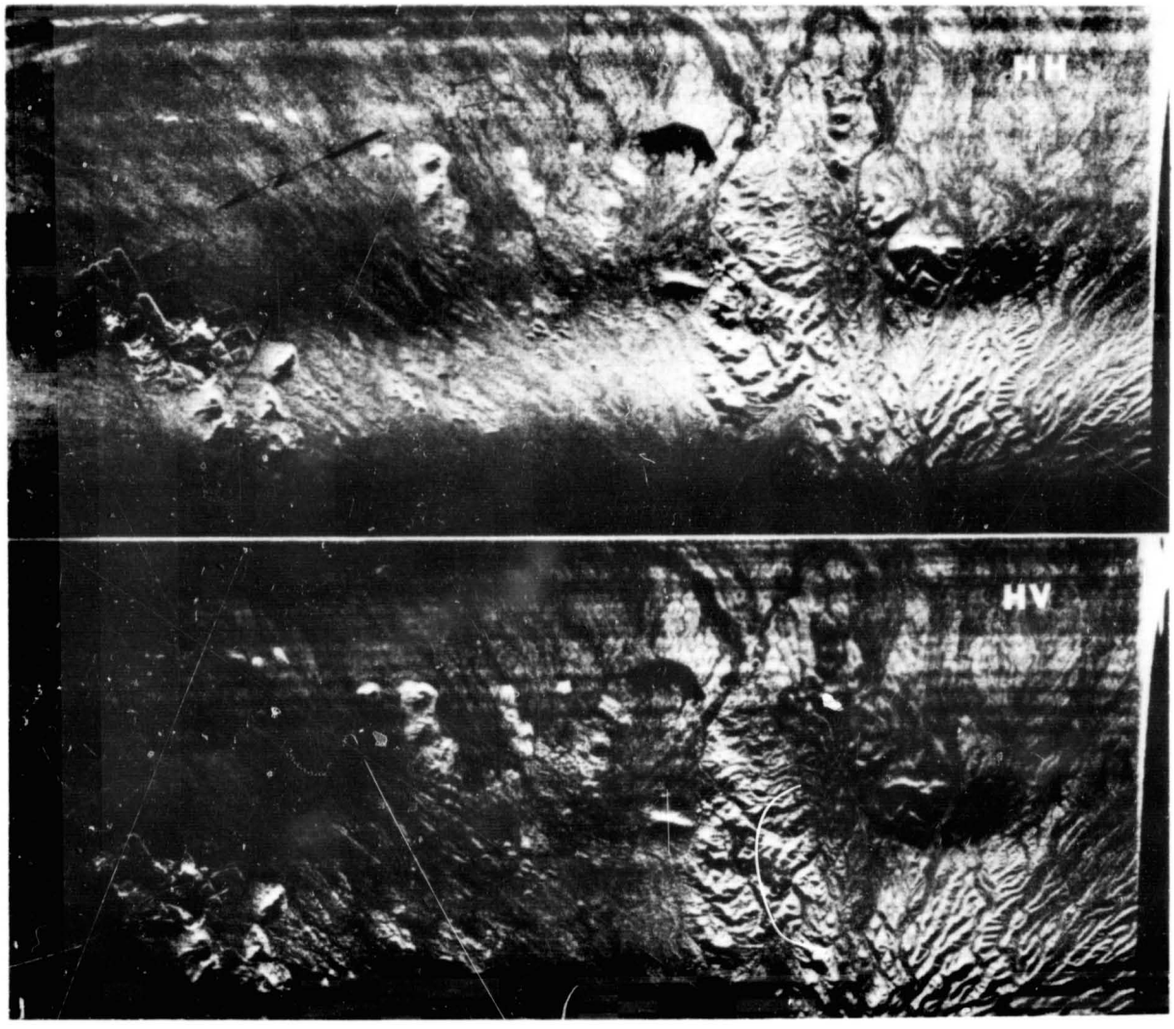

2a HH and HV images of Twin Buttes mining district, Arizona showing anomalous returns from pyroxene rhyodacite.

2b Distant view of northern-most outcrop

2c Close-up showing blocks of pyroxene rhyodacite.

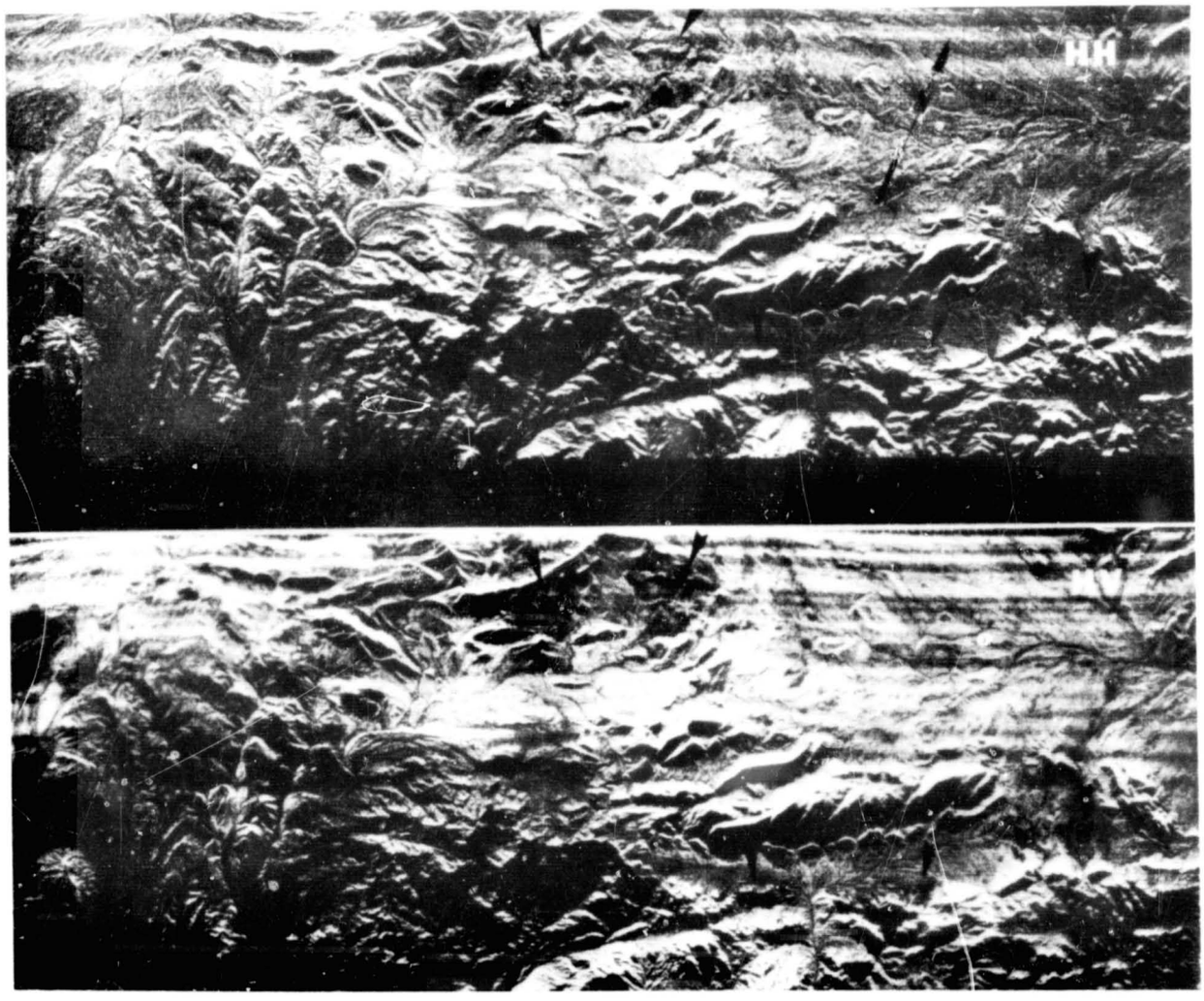

3a HH and HV images of southern Nevada showing numerous tonal reversals caused Aztec Sandstone.

3b Typical outcrop of Aztec Sandstone.

3c Close-up of surface of Aztec Sandstone.

SECTION 37

N72-29337

THE STATUS OF PARAMETRIC STUDIES IN RADAR AGRICULTURE

by

Stanley A. Morain
Center for Research, Inc.
University of Kansas
Lawrence, Kansas

A brief overview of geoscience tasks under NASA Contract NAS9-10261 is given, followed by a report on the status of parametric studies for radar agricultural determinations. The overview will outline this year's progress on 1) an information system for agriculture based on the use of remote sensor data by county agents; and 2) the design, testing and implementation of interpretation keys for agriculture.

The task of crop identification from radar imagery is a complex problem involving the intersecting geometries of two "real worlds:" that of SLAR design parameters and that of biotic parameters. Through appropriate design strategy we are able to conduct a series of semi-controlled experiments on combinations of radar variables to evaluate their influence on radar return from crops. To illustrate the approach, approximate σ^{o} values for sorghum are presented for two frequencies each having two polarizations and a range of viewing angles. Analyses are underway to simultaneously evaluate all parameters measurable from the imagery for each crop type and growth stage. Our greatest needs at present are 1) to expand the data base in both the frequency and angular domains; 2) to improve quality control in the signal-to-image-to-digitizer transformations; and 3) to speed up data extraction from computer maps.

INTRODUCTION

Radar agricultural studies at the University of Kansas are being conducted by geographers, consequently the interest is aimed more at spatial information (the introduction and diffusion of phenomena into an agricultural scene) than to other types of agricultural information. With this in mind we will present a scenario of how we view the role of radar in an agricultural monitoring program. For a more complete statement of our overall program goals and progress, see Morain (1972). All of the work in this report is funded under Contract NAS9-10261.

IMAGE INTERPRETATION

Our research approach is directed along two lines: the development of interpretation strategies using radar imagery; and, the evaluation of signal/terrain interactions to aid in crop identification. These lines of effort are complimentary to one another though not mutually dependent. Among the most important aspects of the interpretation approach is our recommended strategy for information extraction and dissemination and our studies into the use and development of radar dichotomous keys.

The Information System

Figure 1 is a first approximation of an information system designed solely for agriculture. It is an "information system" in the strictest sense of the word rather than a data acquisition system. In the presentation of Figure 1 data are returned from some form of agricultural satellite to a data return facility from which it can be disseminated to counties as needed. Our strategy really begins with what happens at the county level. We envision the capability for automatic data processing of both image and digital data and that automated dicotomous keys will be among the available algorithms. Since the county agents are most familiar with their own particular area (of the number of acres in production, the local weather conditions for crop production, the nature of local diseases, etc.), they should be in the best position to accurately and closely interpret data returns from remote sensors. In addition they are in a position to very quickly disseminate information at the local information user's level. Such users are indicated in the diagram.

From the initial interpretation and acquisition of information at the county level, the diagram shows a flow upward through the agricultural hierarchy through state and regional offices to the national and international scene. At the state and regional level, data from counties can be aggregated and put into a broadened frame of reference. At these levels we find a somewhat different user group, with different information needs, so what was earlier considered "information" at the county level reverts to data for the region. Finally, at the highest levels in the agricultural hierarchy, we can see still another user group with different needs than the previous group. This information can be created by further aggregation and reprocessing results from lower levels. The diagram in Figure 1 is really no different from the agricultural system as it now exists, but it represents a change of thinking for remote sensing. To the author's knowledge other so-called "information systems" have assumed a beginning point at the top and disseminate information downward. Clearly this is not the most efficient strategy if information needs are tied to higher frequency data acquisition. To illustrate the concept of a county agricultural interpretation center, Figure 2a, showing an artist conception of ADP hardware, has been extracted from the work of Lorsch (1969). Figure 2b is essentially the same idea but shows what might evolve at the Regional Data Center.

Figures 3a and 3b represent the pattern of idle land as it might appear in the year 1980. These drawings are modified from an article by Mayer and Heady (1969) and are included here to suggest the possible economic-geographic uses of agricultural information extracted from a future remote sensing system. Figure 3a shows the pattern of idle land based on acreage quotas. One can see that the distribution of idle land is fairly well distributed throughout the country and that no particularly large areas are idled from agricultural production. Figure 3b, however, shows the pattern of idle land based on a free market economy. In this case we see that the distribution of idle land has shifted significantly and that the spring wheat belt in the Dakotas, as well as much of the agricultural land of the South, are taken out of production. Presumably, under the acreage quota system these two areas can compete in the market place, but under a free market economy they cannot successfully compete.

These kinds of trends could, and we think eventually will, be monitored by remote sensing systems. They will serve a function not only in telling us where the major areas of idle land may reside but they may also be useful in guiding our decision making process regarding the kind of policies we want in the agricultural community. In each part of the country the appearance and characteristics of idle land will change and it would be very difficult, indeed, for a system based on the dissemination of information from the top downward to ever monitor idle land. If, on the other hand, we work from the county level upward, we can be rest assured that the county agent knows what attributes to look for in identifying idle land and these data can then be aggregated at regional and national levels into the kinds of maps represented in Figure 3.

Dichotomous Keys

To aid in the implementation of the information system described above we are pursuing a number of interpretation strategies to aid the county agents in information extraction. Amongst the most useful of the strategies so far investigated is the dichotomous key. These were reported last year at the 3rd annual review. In the meantime we have prepared keys for Ka-band, X-band, and Ku-band radar imagery, for both natural and cultural vegetation categories. When reported last year we had just begun to automate one of the Ka-band keys from the Westinghouse 1965 overflight of Garden City. At that time we were achieving on the order of 50% correct idenfication of crops using a set of Yes/No decisions based on human interpretation of the imagery. Since our preliminary trials, we have improved the keys as well as our ability to make and automate them, to the extent that we can now correctly identify between 75 and 80% of the cropped fields at Ka-band in September. We are confident that we can push this level even higher but we are reaching an impass because agricultural data come in county size blocks.

In order for us to really test the utility of these keys, and of this approach, we are nowin critical need of radar imagery for the whole of Finney County and at specified times of the year so that we can compare our results with those of the county agriculturalists and the state statistician. From the standpoint of the information system,keys are potentially extremely useful because they can be created by county agents, who, as we have already indicated, know the situation in their county very well. We hope to have a final report out on the use and implementation of dichotomous keys by June, 1972. In this report we will include the general algorithm for automating keys on IDECS-like hardware. In the algorithm now in use, keys for specific identification problems are inserted as subroutines. In this way subroutines based on any type of imagery, any time of the year, or for the identification of particular terrain conditions, can be inserted for rapid analysis. Figure 4 is an example of the October 1969 X-band key which illustrates the concept of keys for agricultural landscapes. Figure 5 is a "matrix" key for the identification of forest types at Yellowstone. In the forthcoming report on keys we discuss the relative merits of each of these approaches and the degree to which they can be successfully automated.

PARAMETRIC STUDIES

Under the radar agricultural subtasks of NAS9-10261 we are engaged in a number of studies aimed at evaluating signal/terrain interactions for agricultural

scenes. A brief review of these studies was given at the 3rd annual review a year ago and need not be repeated here. Progress on these experiments has either been reported, or will be reported shortly, in the form of technical reports. Rather than outline all of the material here it would be more useful to summarize our progress on parametric studies.

Background

Almost all of the radar parametric studies to date have been conducted using one of three or four frequencies: the Westinghouse Ka-bond imagery from 1965; the NASA Ku-band imagery flown at various times in 1969, 70 and 71; and X-band imagery flown by Michigan in 1969 and 1971. In all of these frequencies, for the entire range of look angles represented and polarizations obtained, we can extract image densities for every crop type and state at Garden City. What we are attempting to do in N-dimensional space is isolate those particular combinations of frequency, polarization, look angle and time which give us the best discrimination of particular crop types or crop states. This strategy is diagramed in Figure 6 on which is shown only three parameters: frequency, look angle and polarization. Intuitively, given two nearly identical crops such as corn and sorghum, one would expect that somewhere in this data space corn and sorghum could not be discriminated. In another sector, however, these two crops may be partially identifiable and in yet another part, the two may be entirely distinguishable. We are looking for those areas where crops can be identified. It does not mean that, should we find such combinations, all crops will be identifiable with that combination of parameters, merely those under particular scrutiny. This reasoning argues strongly in favor of polyfrequency radar so that we can acquire a full compliment of frequencies look angles, and times in the growing season. Under the present array of data available to us, as shown in Figure 7, it is clear that we cannot achieve our goal without a more complete data set. Working with single frequencies is exactly the same as working with an extremely narrow band filter, and we cannot even be sure that the frequencies available are the optimum "filters" for viewing the kinds of terrains we want to view. For all we know, we may be looking at agricultural landscapes through the equivalent of a blue filter.

Image-based Studies

All of the available imagery from the systems described above, with the exception of the Michigan X-band data, have been digitized by Optronics at a 50 micron cell size. From these data we are extracting means, standard deviations, and other measures for each field in the agricultural scene. Dr. Haralick has been working with the same digitized data in his pursuit of image texture. Progress on that work is reported in the next paper.

Initially we began these studies using only the high quality fields as described by our field teams. In order to increase the data set, however, we more recently began using all of the information for each crop type, irrespective of the crop quality. We know this injects terrain "noise" into our results, but there seems to be little alternative.

Results. - To illustrate the kind of results we are getting, Figure 8 represents a 3-dimensional plot for sorghum in July. We have plotted the image density

against viewing angle and frequency, using the Ka and Ku-band systems. The results seem to indicate that for these two frequencies there is no particular best viewing angle where image density variations are minimized. The addition of other image parameters might improve the situation as regards this particular crop and certainly such N-dimensional approaches should be pursued. At the present time we are engaged in similar kinds of investigations for other crop types using this 3-dimensional model in hopes that when one crop is overlayed on another we will see the extent to which their data spaces overlap. Space does not permit even a beginning to a discussion of this topic. For further information the interested reader is referred to Morain, 1972.

Non-Image Based Studies

The only system presently available to us that is capable of obtaining backscatter values across a range of frequencies is the polypanchromatic system developed at the University of Kansas. This system operates in the 4-8 GHz region over a range of viewing angles from nadir out to 70°. As part of the initial tests of this system last summer, the geography group was engaged in two separate studies. The first focused on backscatter returns from soils under different conditions and the second focused on returns from corn.

Soil Studies.- Previous soil studies together with observations from the imagery suggest there is almost certainly a moisture/roughness trade-off in backscatter from soils. That is to say, a dry/rough surface may give exactly the same return as a moist/smooth surface. In our use of the polypan system, therefore, we rototilled a small field near the Center for Research to 3 broad roughness classes (roughness here characterized in terms of micro-relief rather than in soil texture). After obtaining backscattering cross sections from these three different roughness categories in their dry state (about 15% moisture by volume) we wetted the fields by hand to bring their moisture content up to near field-capacity (about 30% moisture by volume). Thus we had three different roughness categories and two moisture conditions for which we obtained data.

Results: In Figure 9 we have plotted the backscattering cross sections from a few spot frequencies within the 4-8 GHz range at selected viewing angles. The results clearly illustrate the tendency for returns to "string out" at any given frequency and look angle. There is no suggestion in the diagram that any one frequency or look angle is best for discriminating these soil conditions. On the other hand we must remember that not all of the data have been plotted and that there may be other frequencies and look angles in the 4-8 region where the data might cluster. It might, in fact, be possible, using these more or less continuous data, to create a mean trend surface for each of the six soil conditions to see whether or not they are discriminable.

Corn Studies.- The corn experiment was aimed precisely at evaluating the contribution of moisture in crop backscatter. At the time microwave data were taken, field members took measurements of soil moisture and temperature. Stratified plant samples were collected and later processed for their moisture content. We have partitioned the moisture measurements into two categories: 1-foot whole plant increments; and stalk, leaf, and cob increments.

Results: We have not finished our analysis of these moisture data. However, there is a preliminary suggestion (which needs further evaluation) that at particular frequencies and look angles moisture in corn is highly detectable. The implications of this are exciting and far reaching. The diagram in Figure 10 represents the backscattering coefficients from corn looking diagonally across the rows for the same set of frequencies and look angles as presented in Figure 9. We see the same kind of stringing out in the returns, except that in the case of corn there seem to be some frequencies and look angles where the data cluster rather nicely. Whether or not these frequencies and look angles would be useful as identifiers for corn remains to be seen. We need to carry out similar studies with related crops such as sorghum and with grossly different crops such as soy bean or sugar beet. Our experiments this coming summer will, in fact, be along these lines.

CONCLUDING REMARKS

In general the radar agriculture work can be divided into two broad sectors: The development of interpretation strategies for imagery, in which our emphasis so far has been on dichotomous keys; and the search for frequency, angular and other microwave dependencies of crops for use in discrimination. These two sectors are not mutually exclusive because many of the ideas generated from the parametric studies can, and are, being used in the development of interpretation strategies. In assessing our overall progress we seem to be making more headway in the area of interpretation strategies than in the parametric studies. We hope in the upcoming growing season to divorce ourselves a little more from the Garden City test strip and begin to obtain data on a county wide basis. This is critical because agricultural data come in county-size units. Unless we get information on this scale there will be no basis for comparing our results with those obtained by standard USDA techniques. So far we have had one flight over the whole of Finney county in June of 1971 (NASA 16-5 system). We have produced a mosaic from that imagery (Figure 11) and we will be able to use it for preliminary studies of acres in wheat and total acres in production. The mosaic will provide us a temporal base-point which will be useful in monitoring the spread of such phenomena as circular irrigation, the spread of crops such as sugar beets, and many other phenomena. In closing I might also point out that only by obtaining imagery on a county wide basis and comparing our results with traditional techniques will we be able to cost evaluate the ability of radar as an agricultural remote sensor.

REFERENCES

1. Lorsch, Harold G., 1969, "Agricultural Resources Information Systems - The Users Point of View", American Astronautical Society, 15th Annual Meeting, Denver, Colorado.

2. Mayer, L. V. and E. O. Heady, 1969, "Projected State and Regional Resource Requirements for Agriculture in the United States in 1980", Iowa Agriculture and Home Economics Experiment Station, Iowa State University of Science and Technology, Research Bulletin 568.

3. Morain, S. A., (ed.), 1972,"Radar Applications in Agriculture/Forestry Annual Report on Subtasks 2.5.2 and 2.5.3 of NASA Contract NAS9-10261."

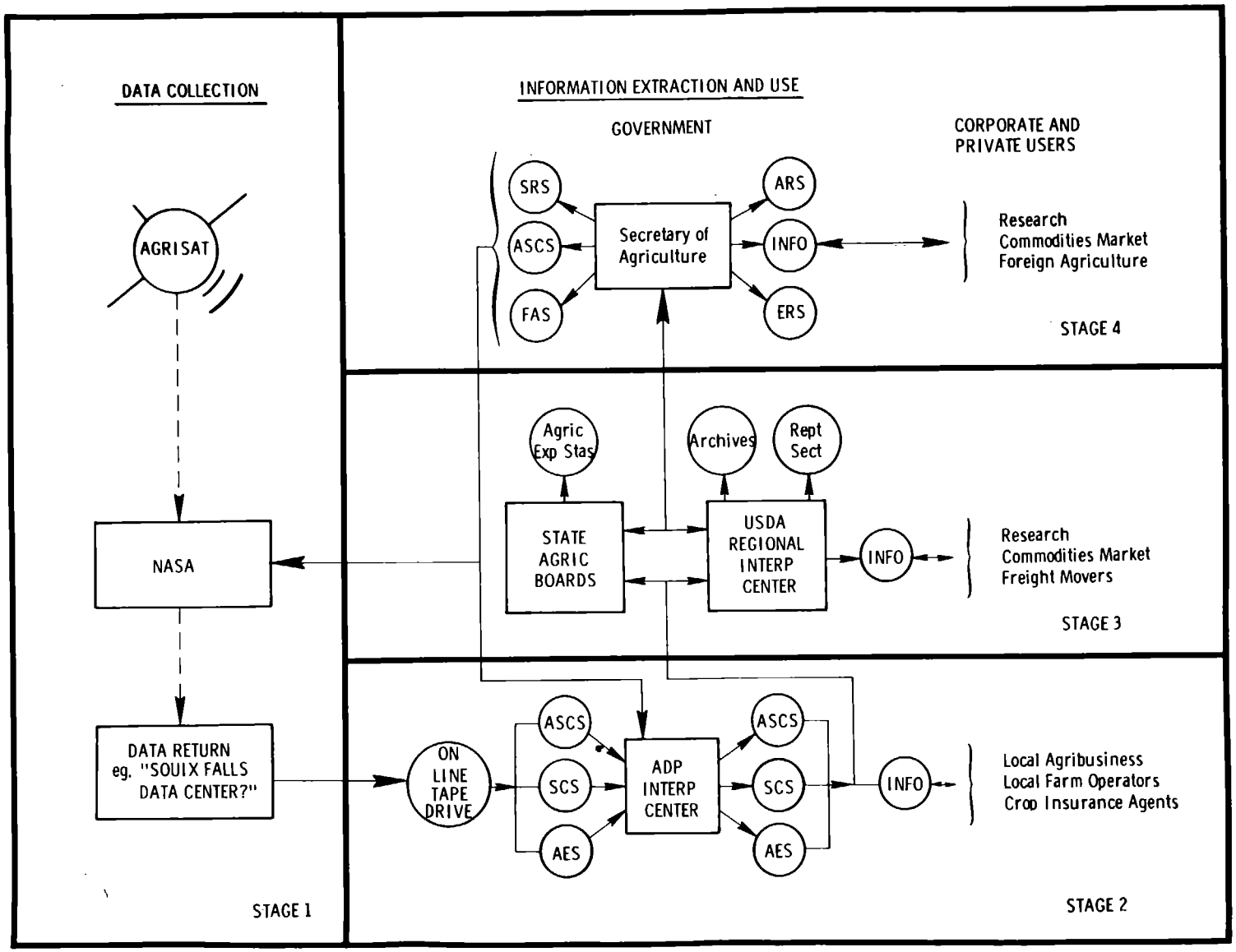
DATA COLLECTION
INFORMATION EXTRACTION AND USE
GOVERNMENT
CORPORATE AND PRIVATE USERS
AGRISAT
SRS
ASCS
FAS
Secretary of Agriculture
ARS
INFO
ERS
Research
Commodities Market
Foreign Agriculture
STAGE 4
Agric Exp Stas
Archives
Rept Sect
NASA
STATE AGRIC BOARDS
USDA REGIONAL INTERP CENTER
INFO
Research
Commodities Market
Freight Movers
STAGE 3
DATA RETURN eg. "SOUIX FALLS DATA CENTER?"
ON LINE TAPE DRIVE
ASCS
SCS
AES
ADP INTERP CENTER
ASCS
SCS
AES
INFO
Local Agribusiness
Local Farm Operators
Crop Insurance Agents
STAGE 1
STAGE 2

FIGURE 1.

a.

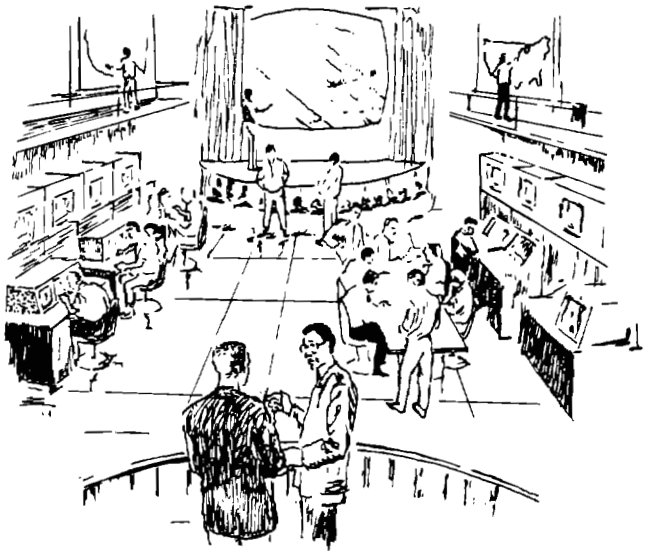

b.

Data Processing Facilities in Agriculture
a) The County Agent's Office; b) The Regional Office.
(After Lorsch, 1968)

FIGURE 2.

C.4.

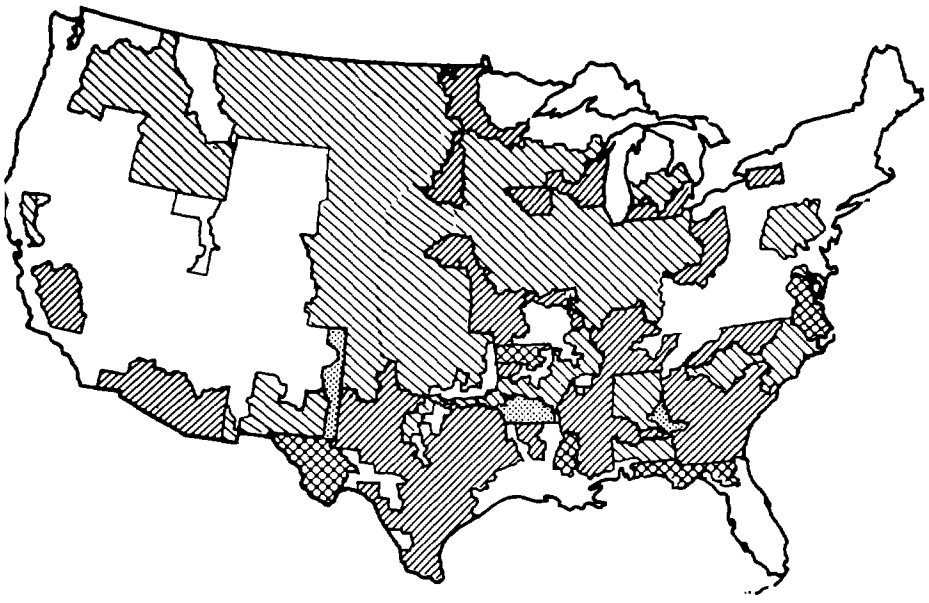

a. PROPORTION OF TOTAL CROPLAND UNUSED FOR MAJOR CROPS IN EACH OF THE 144 CROP PRODUCING REGIONS UNDER AN ACREAGE QUOTA PROGRAM WITH TREND LEVEL EXPORTS IN 1980.

b. PROPORTION OF TOTAL CROPLAND UNUSED FOR CROPS IN EACH OF THE 144 PRODUCING REGIONS UNDER A FREE MARKET WITHOUT COTTON QUOTAS AND WITH TREND LEVEL EXPORTS IN 1980.

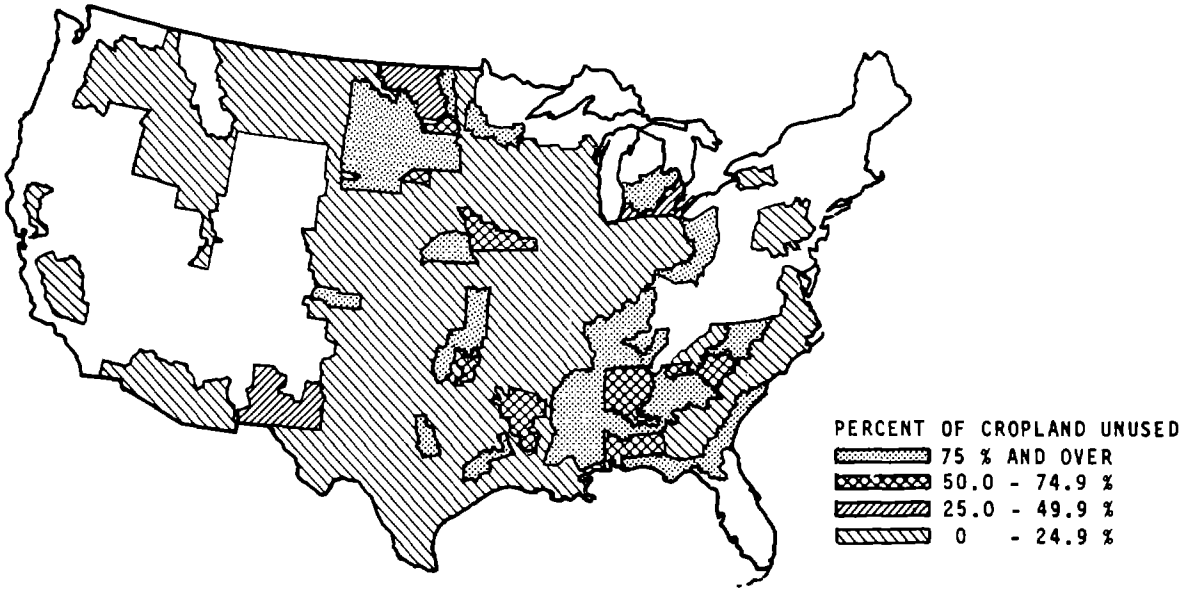

FIGURE 3.

FIGURE 4.

PROBABILITY* KEY FOR CROP TYPES AT GARDEN CITY, KANSAS

for

OCTOBER
(Derived from Radar Imagery)

A. Field has a moderately high to high return (light grey to white on radar positive) (with respect to HH)
  B. Field has a homogeneous** tone (with reference to HH)
    C. Field displays a shift in tone from HH (lighter) to HV (darker)
      D. Amount of tone shift is relatively unpronounced
        E. HV tone is homogeneous ---------- sugar beets; or wheat > 3"
        EE. HV tone is not homogeneous ---------- fallow
      DD. Amount of tone shift is relatively pronounced
    CC. Field does not display a tone shift HH (lighter) to HV (darker)
      F. Field displays a tone shift from HH (darker) to HV (lighter)
        G. Field has evident lineations ---------- cut alfalfa
        GG. Field does not have evident lineations
      FF. Fields does not display a tone shift from HH (darker) to HV (lighter)
  BB. Field does not have a homogeneous tone
AA. Field does not have a moderately high to high return
  H. Field has medium low to moderate return (medium dark to medium light on radar positive)
    I. Field has a homogeneous tone (with reference to HH)
      J. Field has lineations parallel to long axis of field
        K. Tone shift is evident from HH (dark) to HV (light) ------- maturing alfalfa (flood irrigated)
        KK. Tone shift is not evident
      JJ. Field does not have lineations
        L. Field displays medium coarse texture (particularly on HV image) ---- grain sorghum (rows ⊥ flight line)
        LL. Field has no obvious image "texture"
          M. Field has a moderate tone shift (HH to HV) -------- alfalfa > 12"
          MM. Field has an unpronounced tone shift ---------- wheat > 3"
    II. Field does not have a homogeneous tone
      N. Cultivation pattern is observable (particularly on HV image) --- emergent wheat
      NN. Cultivation pattern is not observable
        O. Boundary shadowing is observable ---------- mature corn
        OO. Boundary shadowing is not observable
  HH. Field does not have moderately low to moderately high return
    P. Field has very low return (very dark grey to nearly black on radar positive)
      Q. Field has a homogeneous appearance ---------- recently tilled
      QQ. Field does not have a homogeneous appearance
    PP. Field does not have very low return

*This key is experimental. It is based on only one look-direction (and for a narrow range of incidence angles) for one flight during October 1969 - almost at the end of the growing season for that year. It is a probability key in the sense that only the most likely, economically important crops are indicated for any given spot in the listing. To use it the interpreter must make a series of yes/no decisions until a logical end point is reached. For example, the first decision relates to image tone: does the field have a high or moderately high return (A) or does it not have such a return (AA)? If the answer is AA, then for subsequent decisions, that portion of the key above AA can be ignored, and the interpreter's attention focused on material listed below AA. The second decision would then be whether or not the field had a medium low or moderate return (HV vs. HH in the key). The process continues in this fashion until no further choices can be made. Notice that, if the location PP is reached, an error in judgment has been made. When this happens the entire process must be repeated. Similar reasoning applies to points BB, DD, GG, FF, KK, OO, and QQ, though future revisions of the key may provide information at these locations.

**"Homogeneous" refers to the uniformity of return intensity within the boundaries of a given field, i.e., there is no evident mottling of tone.

VERBAL KEY TO THE VEGETATION OF
YELLOWSTONE NATIONAL PARK

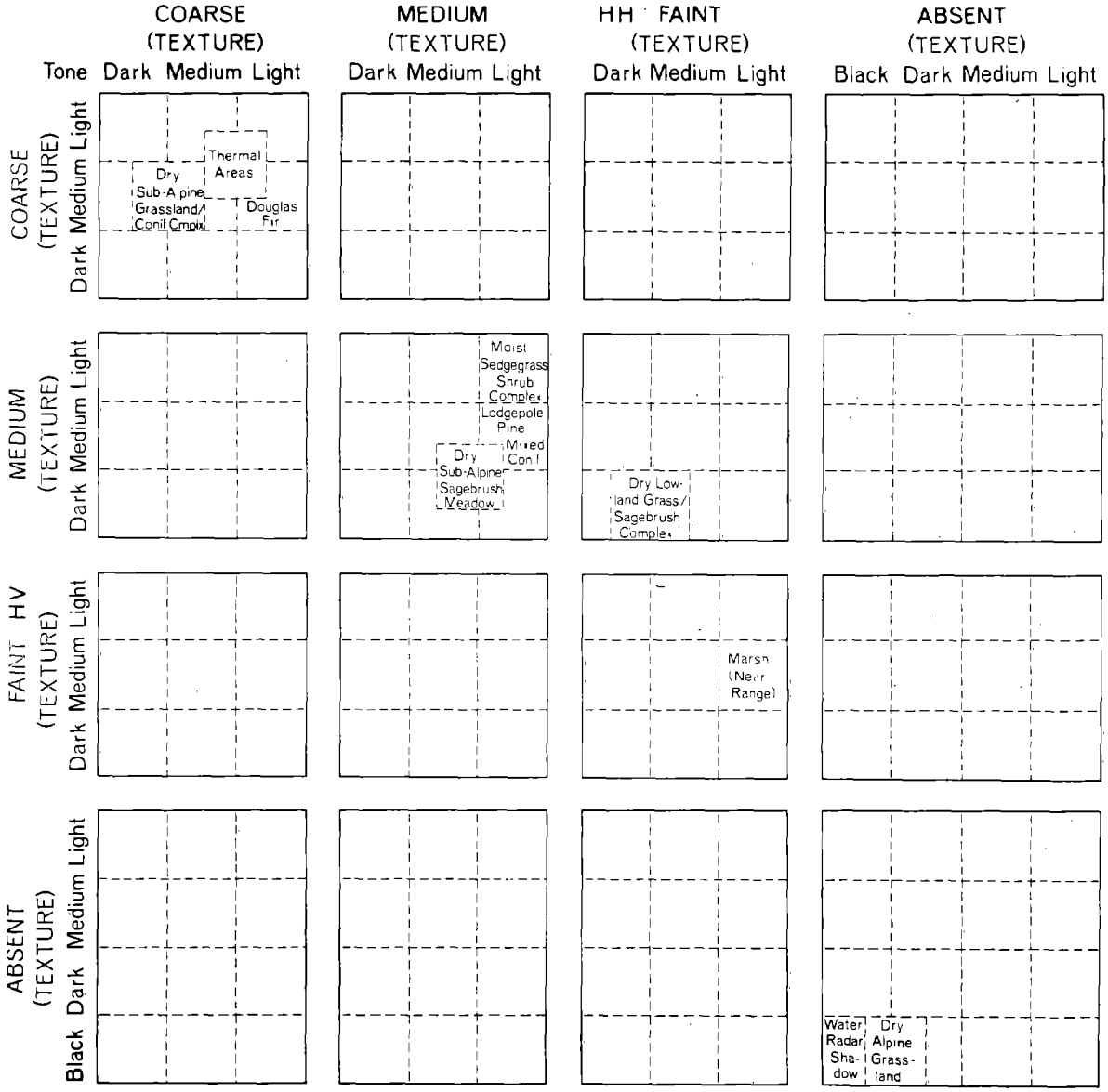

Figure 5 . Verbal matrix key to the various vegetation communities which were developed from radar imagery. This key allows ready comparison of HH and HV radar polarizations.

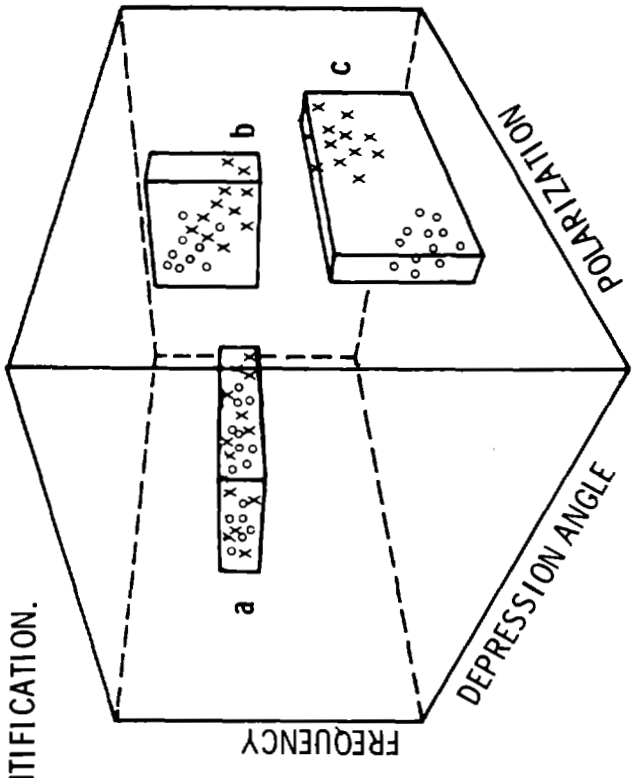

FIGURE 6
DATA CELLS IN SYSTEM DESIGN SPACE SHOWS NEED FOR WIDE SWATH, POLY FREQUENCY DEVICE FOR MAKING AGRICULTURAL IDENTIFICATION.

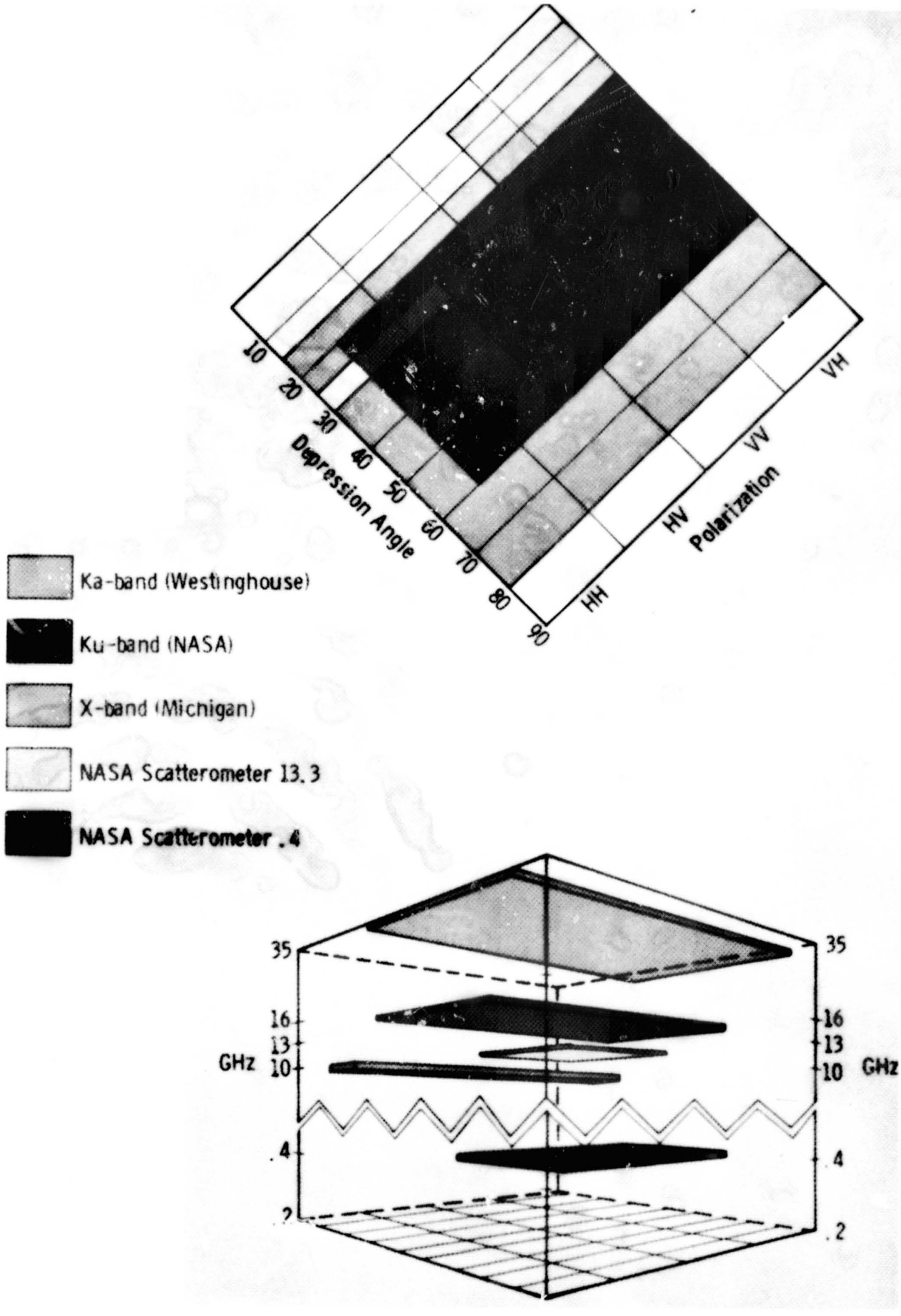
10
20
30
40
50
60
70
80
90
Depression Angle
HH
HV
VV
VH
Polarization
Ka-band (Westinghouse)
Ku-band (NASA)
X-band (Michigan)
NASA Scatterometer 13.3
NASA Scatterometer .4
35
16
13
10
GHz
.4
.2
35
16
13
10
GHz
.4
.2

FIGURE 7.

IMAGE DENSITY FOR SORGHUM
In July

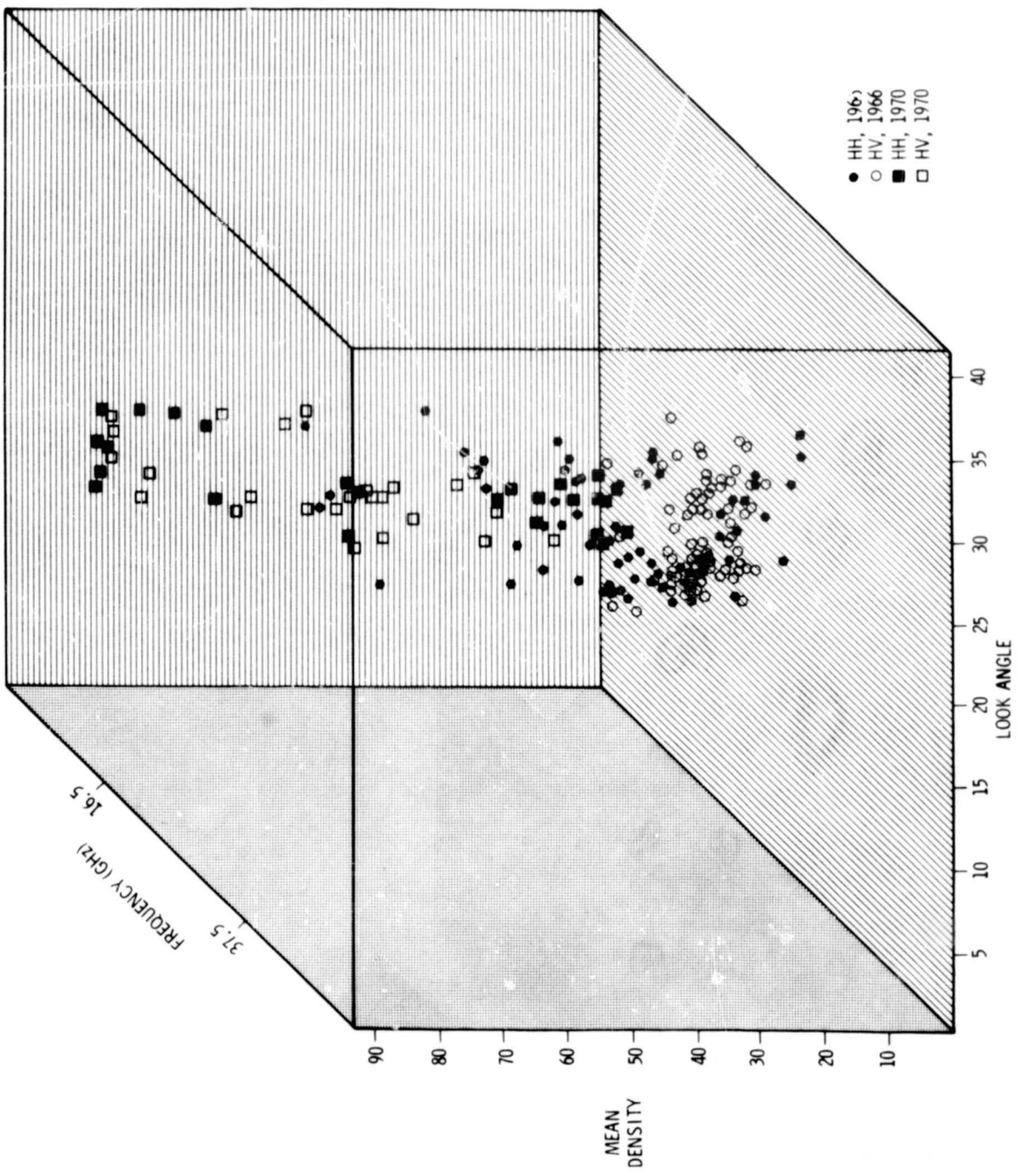

FIGURE 8.

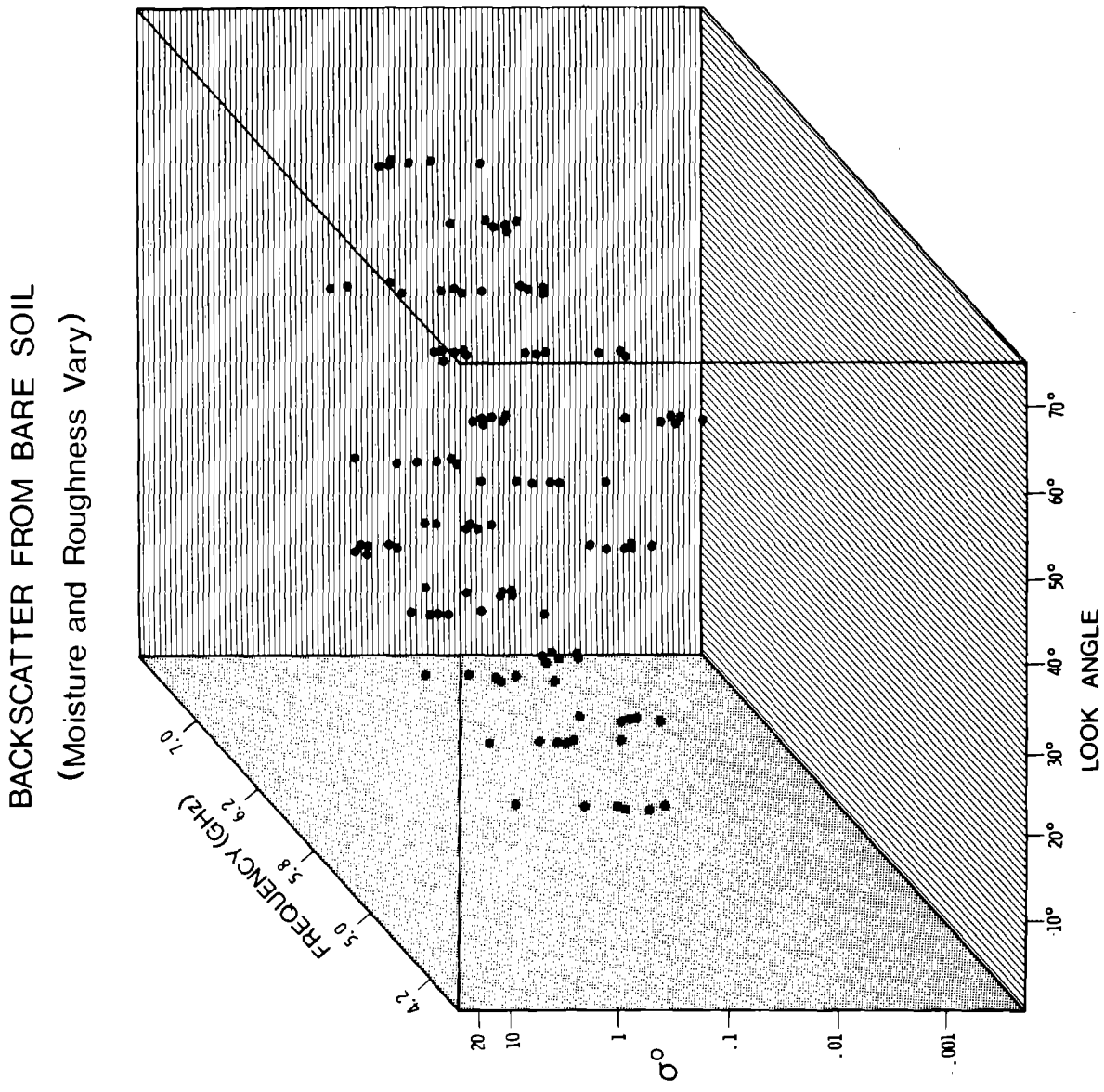
BACKSCATTER FROM BARE SOIL
(Moisture and Roughness Vary)
FREQUENCY (GHz)
4.2
5.0
5.8
6.2
7.0
σ°
20
10
1
.1
.01
.001
LOOK ANGLE
10°
20°
30°
40°
50°
60°
70°

FIGURE 9.

BACKSCATTER FROM CORN

(Look Direction Diagonal to Row Direction)

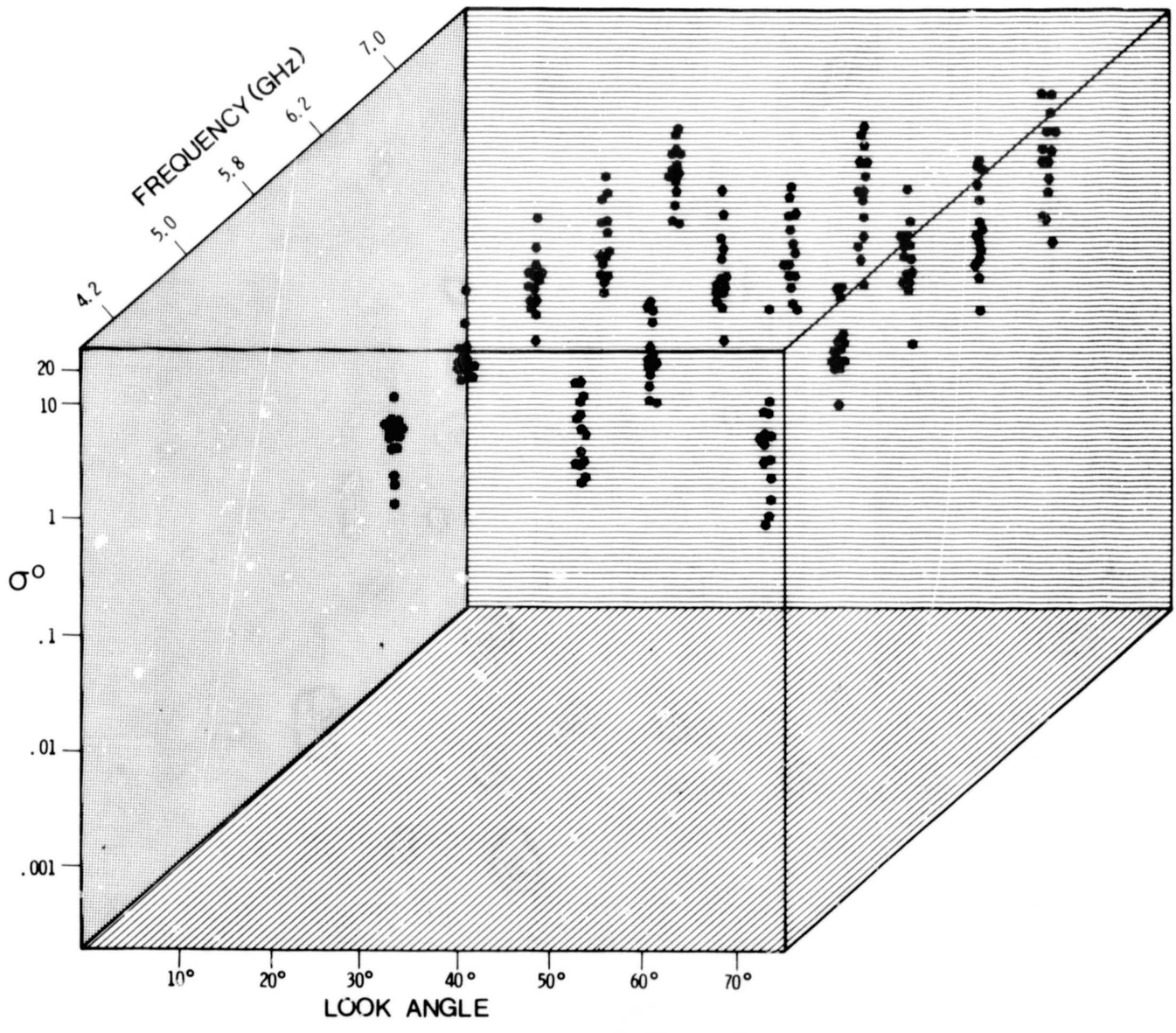

FIGURE 10.

FINNEY COUNTY, KANSAS
JUNE, 1971
NASA DPD-2 SIDE-LOOKING AIRBORNE RADAR

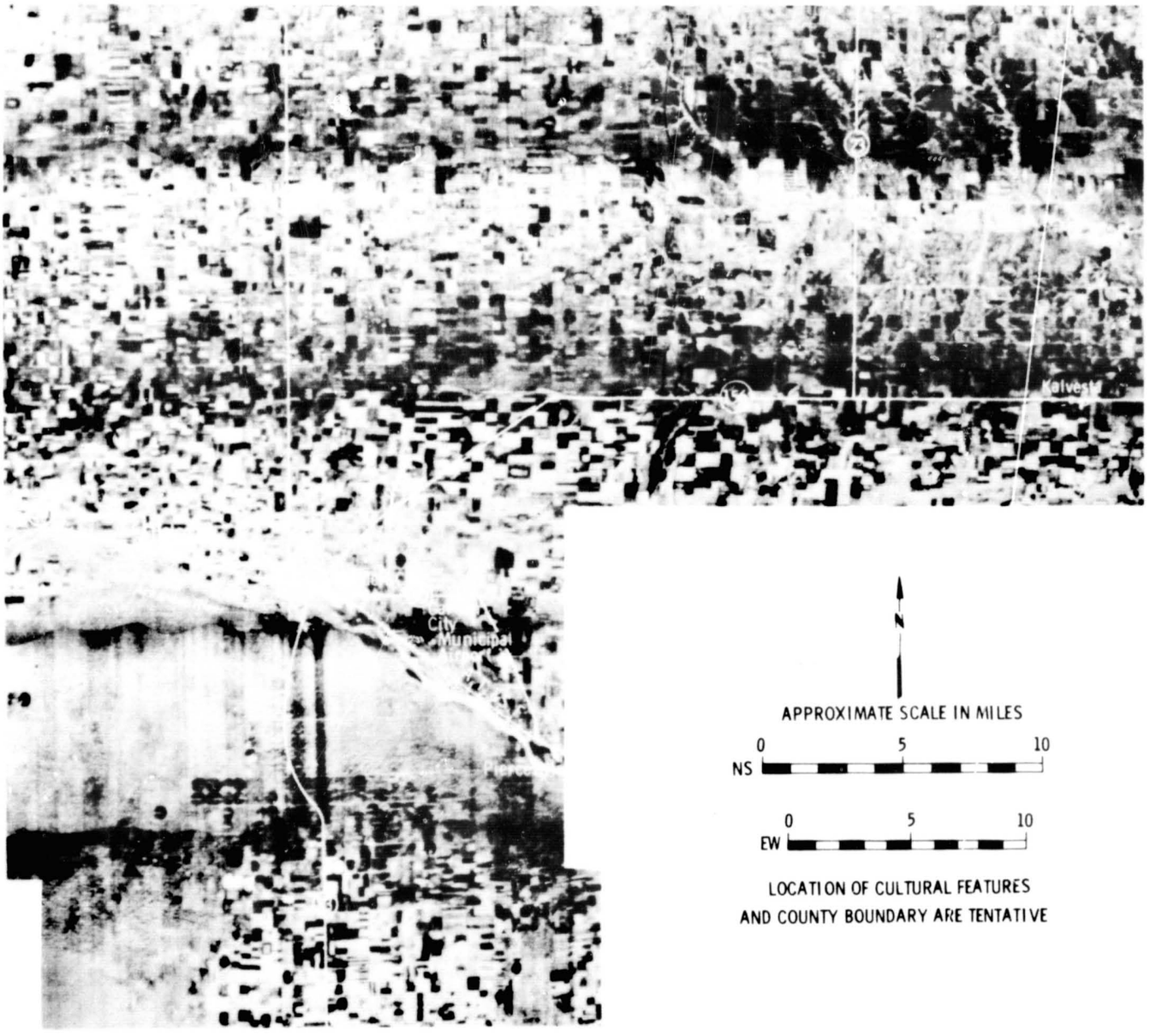

FIGURE 11.

SECTION 38

DATA PROCESSING AT THE UNIVERSITY OF KANSAS

by

Robert M. Haralick
Center for Research, Remote Sensing Laboratory
University of Kansas
Lawrence, Kansas

The University of Kansas has taken a two-fold approach to the data processing of remotely sensed imagery. Our approach has been based upon the need to have a special purpose hardware facility for the near-real time processing of multi-image data and the need to have a general purpose digital computer facility for the more sophisticated non-real time processing. Our near-real time facility is called IDECS (Image Discrimination Enhancement Combination System) and our non-real time facility is called KANDIDATS (Kansas Digital Image Data System). These facilities have been funded from both NASA and DOD sources.

THE NEED FOR A DUAL APPROACH

During the next decade there is a large amount of research yet to be done on data processing methods in order to bring the maturity of data processing up to the maturity of sensor technology. Yet, while this research is being done, many remotely sensed data sets from both aircraft and satellite platforms will have to be processed. Important constraints are, therefore, imposed on the remote sensing data processing center. It must have a flexible enough computational facility to implement and evaluate new ideas so that basic long range research on effective processing algorithms can be done; and for those data sets which now have to be processed quickly, it must have near real-time equipment to process and display those image sets economically.

For the near real-time equipment, it is extremely important that the man-machine interface be as convenient as possible for the interpreter since all image data is ultimately utilized by a human interpreter in some form. A color display is very useful for presenting image data to an interpreter since the human eye can distinguish differences in colors more readily than differences in grey levels. IDECS is one of the first systems to utilize a color display for presenting remote sensing data and it is described in the next section.

A HARDWARE SYSTEM FOR MULTI-IMAGE PROCESSING: IDECS

The IDECS (Image Discrimination, Enhancement, and Combination System) is an analog-digital near real-time image processing system and has been in continual development at the University of Kansas Center for Research, Inc., since 1964. The IDECS is a unique facility for performing a wide variety of enhancements, measurements, and category discriminations on single and multiple images. Currently, the input images must be in photographic form, but their source may be aerial and

space photography, airborne radar, infrared, multi-spectral scanners, medical and industrial X-rays, or maps. The primary IDECS output is on a color display unit; however, other outputs include a black-and-white monitor, area measurements on a counter, and a pseudo three-dimensional display.

A photograph of the IDECS is shown in Figure 1, and a block diagram of the total system is shown in Figure 2. The input to the IDECS consists of three flying-spot scanners suitable for inputting image transparencies from 3 x 4 inches to 35 mm format, a vidicon camera utilized for map or photographic inputs, and a congruencing unit which can rotate, translate, and scale images. The image scanners have the following three modes of operation:

(1) a continuous scan where the horizontal and vertical deflections for the CRT are driven by ramps which are synchronized with the display units,

(2) a staircase or dot scan where deflections are determined by the output of two digital-to-analog converters driven by two binary counters which are synchronized with the display unit, or

(3) a PDP-15/20 computer controlled slow-scan, where the scanning dot is moved horizontally and vertically to specific location.

Modes (1) and (2) are used when real time processing is desired, and the program controlled scan is used to gather information from specific areas of the film for training purposes and also to obtain a more accurate analog-to-digital conversion when necessary. Images to be scanned are positioned above the raster with an enlarging lens placed between. A condenser lens focuses the light transmitted through the image onto the cathode of a video photomultiplier tube. A reference photomultiplier tube and an automatic gain control (AGC) loop to modulate the cathode of the CRT are used to assure uniformity of light level over the entire area of the image being scanned. The reference photomultiplier tube is placed beside the enlarging lens and senses the light output from the raster at full value. The desired signal is used as an input into the AGC amplifier which is an error amplifier with a voltage reference. The resultant error signal is level shifted and is used as the signal to modulate the cathode of the CRT.

The operator can congruence multiple images by adjusting the position and size for horizontal and vertical position and rotating one image with respect to another image as the two images are electronically flickered. When the images are aligned, the displeasing interference pattern which occurs for misaligned images disappears.

Once the images are congruenced, they may be processed and enhanced by IDECS. There are a variety of processing and enhancing functions available. One function is a linear combiner unit which performs a linear transformation on a multi-image set in 1/30 of a second. This unit may be used for coordinate rotation if the coefficients of the linear transformation are selected appropriately. Another function is level selection. A level selector produces a binary output for an image

if and only if the input video signal is between two adjustable thresholds. The level selectors can be operator controlled or computer controlled. In addition, two more level selectors can be logically combined producing an output if and only if each one has an output, thus implementing a MIN-MAX decision rule.

The automatic classifier is a unit (not computer controlled) which is used to select and display all points on a video image whose levels fall within the same range of level as those detected in a small rectangular training area of the image. The position and size of this training area is selected using a small joy stick to determine position, and control pots are used to adjust vertical and horizontal size. To accomplish this operation, a rectangular training area is first defined on the image. Then peak detectors sample and hold the positive and negative signal peaks within the range of the training area. The remaining portion of the video signal is then compared with the peak levels of the training area; whenever the video signal falls within the training voltage range, a digital output is produced for processing or display.

Other functions include a unit to measure the area of any displayed category or grey level, a variable time constant differentiation unit to enhance edges and a pseudo three-dimensional display unit which permits one to view the three-dimensional surface generated by the grey tone density of an image. Soon to be implemented is a near real-time (1/30 of a second) table lookup pattern classifier which assigns categories on the basis of the digitized levels of two video signals and stored parameters for a Bayes decision rule.

A recently acquired PDP-15/20 computer is being interfaced to the system so that the IDECS can be program controlled and have a wider capability in performing image enhancements and category identifications. In effect, the PDP-15/20 will perform the task of generating a decision rule from data gathered by the IDECS, and the IDECS implements the resulting rule (in near real-time) on data derived by scanning the images. In general, five steps will be required in performing category identifications for images:

(1) the images must be congruenced,

(2) training data must be obtained by the computer from the images by directing the IDECS to scan appropriate areas,

(3) from the training data, the PDP-15/20 is programmed to determine the parameters for the chosen decision rule,

(4) the calculated parameters are used to set control voltages in the analog processing subsystems in the IDECS, and

(5) the specified category identifications are made and displayed by IDECS.

The PDP-15/20 will control the image processing steps of the IDECS by issuing commands to the IDECS central processing unit (CPU). The CPU in turn directs data flow and processing in the IDECS. The system configuration can be digitally selected utilizing a twenty by twenty video configuration matrix.

A digital disc memory having twenty-four channels and containing 24,000,000 bits of storage is also utilized in the system. There is an interface between the disc and computer capable of transferring at the rate of 18,000,000 bits per second. Also, there is an interface between the disc and the color display unit of the IDECS with the capability of up to three six-bit digital-to-analog converters or any number of binary outputs between one and twenty-four. The color selector is a unit such that any of the twenty-four channels of the disc can be assigned any of ten fixed colors and any of ten textures. The textures are merely series of horizontal and vertical lines superimposed on the displayed information. Figure 3 illustrates one image from a radar image pair and the IDECS processed image.

A SOFTWARE SYSTEM FOR DIGITAL IMAGE PROCESSING: KANDIDATS

KANDIDATS (Kansas Digital Image Data System), currently being developed, is a software package consisting of a monitor and a set of multi-image processing programs designed to run on a GE-635 computer. The multi-image processing programs are all written in FORTRAN IV and allow for image editing, registering, congruencing, quantizing, clustering, feature extraction, image size and/or dimensionality reduction, image texture analysis, image pattern recognition. It has a variety of decision rules, data display capability with scatterograms and histograms, grey-tone image display with overprinting or digital image color map display. The KANDIDATS monitor is a GMAP assembly language program designed to integrate the multi-image processing programs by handling all bookkeeping type and I/O operations and to minimize the cost of processing image data by speeding up I/O time and overlapping I/O time with execute time. Figure 4 illustrates a block diagram of the basic KANDIDATS organization.

The KANDIDATS monitor inputs in free-format all instructions required by the image processing program, supervises the execution of the programs, provides error processing, and dynamic storage allocation and tape input and output for the programs. The monitor has been written so that during a single activity of KANDIDATS many processing programs may be sequentially executed using many different data sets. The monitor does this by treating each program as a separate task and by allocating and releasing data tapes as necessary.

Once remotely sensed data is converted to digital type format, it is necessary to check the digitized tape to see of the conversion was made successfully. Preliminary checking can be done by dumping the first few records on the tape; however, this is by no means a complete check. The KANDIDATS image display program can make a complete check by outputting the tape in picture format on the digital printer creating the grey-tones by overprinting. If the image has so many resolution cells as to make the digital picture printing awkward, a program may be utilized which reduces the image size by averaging blocks of N x N resolutions or by selecting every N^{th} row and every N^{th} column.

Examination of this picture output will indicate what kind of editing will have to be done on the sides and top and bottom of the image as well as indicate skewing

and A/D conversion distortion. (Skewing can occur because it may be impossible to start digitizing each line of the image in exactly the same place. A/D conversion distortion can occur when jitter or noise internal or external to the A/D conversion makes the conversion go awry.) If necessary, a KANDIDATS deskewing program may have to be used to remove skew and a special smoothing-replacement program may have to be used for those resolution cells which were improperly converted.

When multi-image data is being processed, it is often necessary to align the individual images to the same place. To do this KANDIDATS employs a registering program. When different sensors or the same sensors with different look directions are involved it may be necessary to bring the images to the same geometry. In this case a congruencing program must be used.

When the geometries on the images to be congruenced are quite different, the congruencing job may be quite hard. However, where only minor geometric distortions are involved, congruencing may be done by a KANDIDATS program which treats the image as a rubber surface and expands or contracts it to best match up a set of given corresponding points.

There are two formats by which multi-image data may be stored on taps by KANDIDATS. In the photo format all the grey-tones from the first image are stored on a matrix followed by the grey-tones from the second image and so on. In the corresponding point format the grey-tone from image one resolution cell (1,1) is followed by the grey-tone from image two resolution cell (1,1) and so on. Editing and congruencing imagery from different sensors is usually done with data in photo form as is image display and texture analysis. Most of the other programs work most easily with the data in corresponding point format. KANDIDATS has programs which convert multi-image data from one format to the other.

After initial editing and congruencing it is convenient to obtain an intuitive idea of what is happening in the data. To help with this, programs are available which pick out specified regions on the image and display the data points in scatterogram or histogram fashion. The scatterograms or histograms may be indexed by ground truth categories when the ground truth is available. The axes of the scatterograms may be combinations of pairs of the different sensor signals or the axes of a rotated coordinate system. Rotation can be accomplished from principal component analysis or from linear discriminant functions and there are programs available for these operations. Either of these operations will allow a significant reduction of dimensionality and, therefore, allow a reduction in storage and display of data, especially in 12 or 24 channel multi-spectral scanner data.

Before pattern discrimination or clustering is done, a feature extraction is performed which selects the relevant variables or which combines the original variables in some optimum way. Sometimes as part of the feature extraction process quantizing is done to normalize the data as well as to reduce the memory required for storage of the data. KANDIDATS has available programs which do equal interval, equal probability, minimum variance, and spatial quantizing.

When texture is an important feature for a category of interest, the dimensionality of the images may be augmented by a texture analysis program which adds dimensions providing texture type information.

Probably, the major workhorse of image data analysis consists of pattern discrimination and clustering techniques. With pattern discrimination techniques, a training set of data is gathered for which the correct category identification of each distinct entity in the data is known. Then estimates are made of the required category conditional probability distributions and a decision rule is determined from them. The decision rule can then be employed to identify any other data set gathered under similar conditions. With clustering techniques there is no training data set or decision rule. Rather, the natural data structures are determined. Distinct structures are then interpreted as corresponding to distinct objects or environmental processes.

The advantage of the discrimination techniques is that the scientist is able to decide the types of environmental categories among which he wishes to distinguish. The decision rule then determines as best as possible, to which environmental category an arbitrary data entity belongs. The disadvantage of the discrimination techniques is that they are sensitive to mis-calibrations. Any slight difference between the sensor calibrations or state of environment for the training data and the new data will cause error.

The advantage of the clustering techniques is that they are not sensitive to calibration problems. Two small-area patches of corn growing in the same field are going to be detected as being similar because they have similar grey tone associated with them. The disadvantage of the clustering techniques is that they are not able to identify the distinct environmental structures they determine.

KANDIDATS has available iterative and chaining clustering programs and pattern discrimination programs. The pattern discrimination programs use a variety of decision rule types including a distribution-free Bayes rule which can only be used on coarsely quantized data, a Bayes decision rule assuming the category conditional probabilities are of some given type of multivariate distribution, a linear decision rule, or a nearest neighbor decision rule.

Appendices I, II, and III summarize a few of the things we are doing with KANDIDATS.

CONCLUDING REMARKS

Two systems for processing remotely sensed image data have been discussed. The first system, IDECS, is a near real-time hardware system oriented towards processing multi-image data sets quickly and economically. The IDECS has convenient film input and color display output capabilities and implements simple kinds of decision rules. The second system, KANDIDATS, is a software system capable of performing many of the more sophisticated processing methods. Because of its monitor which handles all bookkeeping and its modular design, KANDIDATS easily allows

the testing of new automatic processing techniques. After a new technique has been proven on KANDIDATS, it may be simplified and hard-wired in IDECS, thereby keeping the volume processing of remotely sensed data always up to the current state-of-the-art.

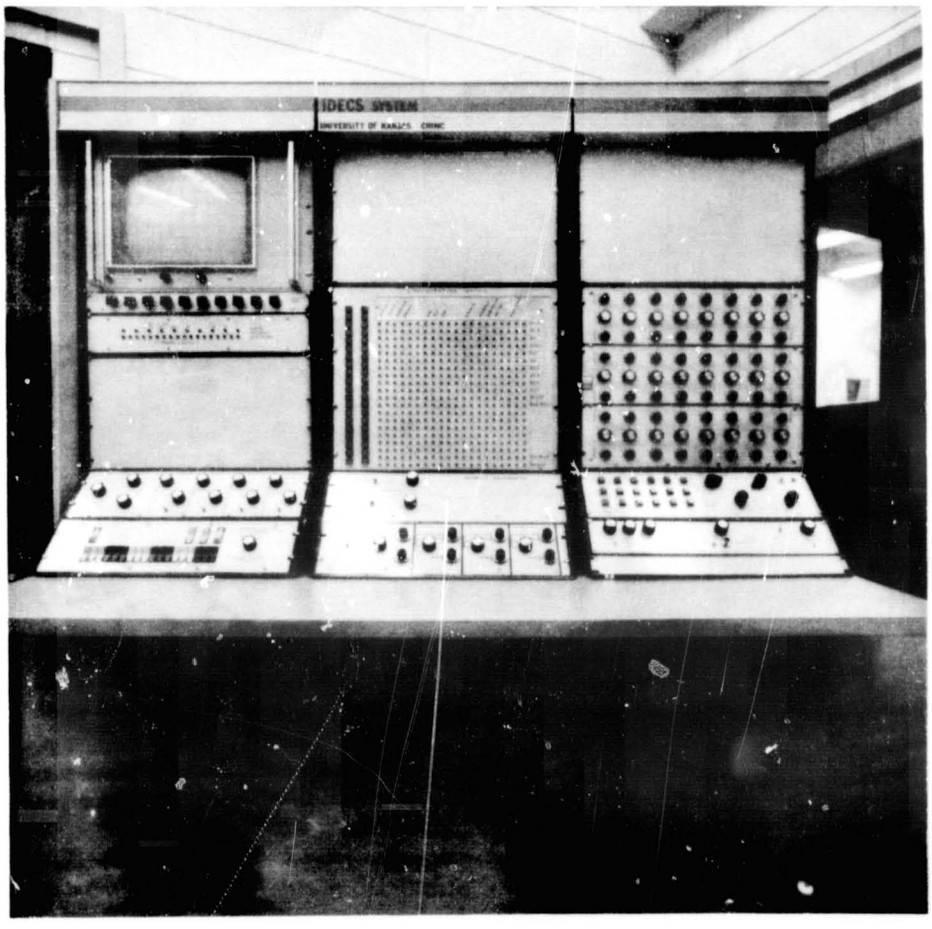

FIGURE 1. IDECS

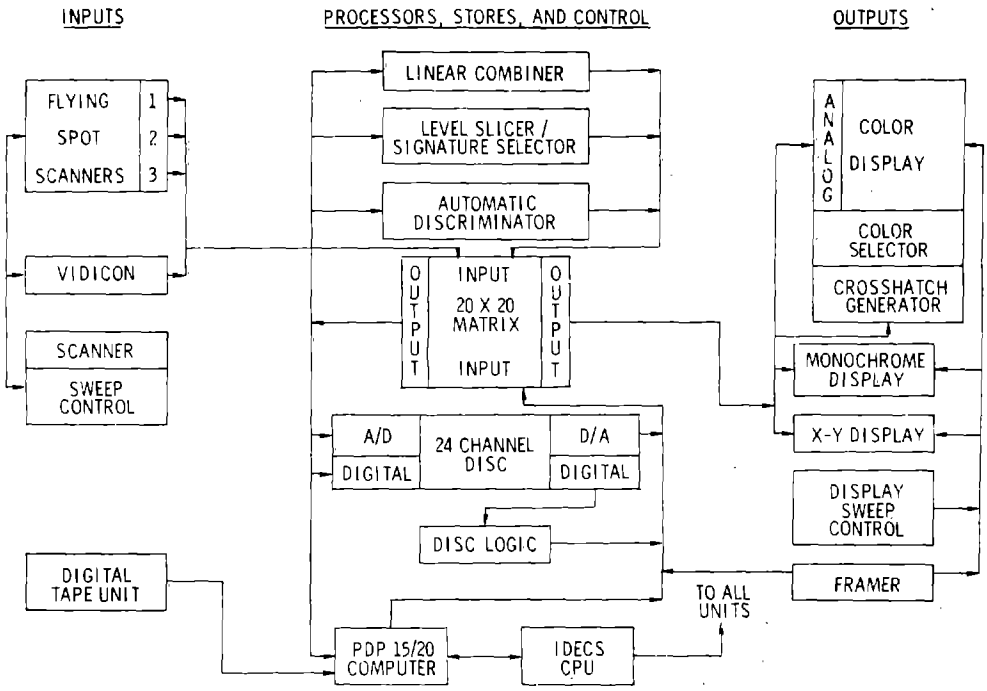

FIGURE 2. IDECS FUNCTIONAL BLOCK DIAGRAM

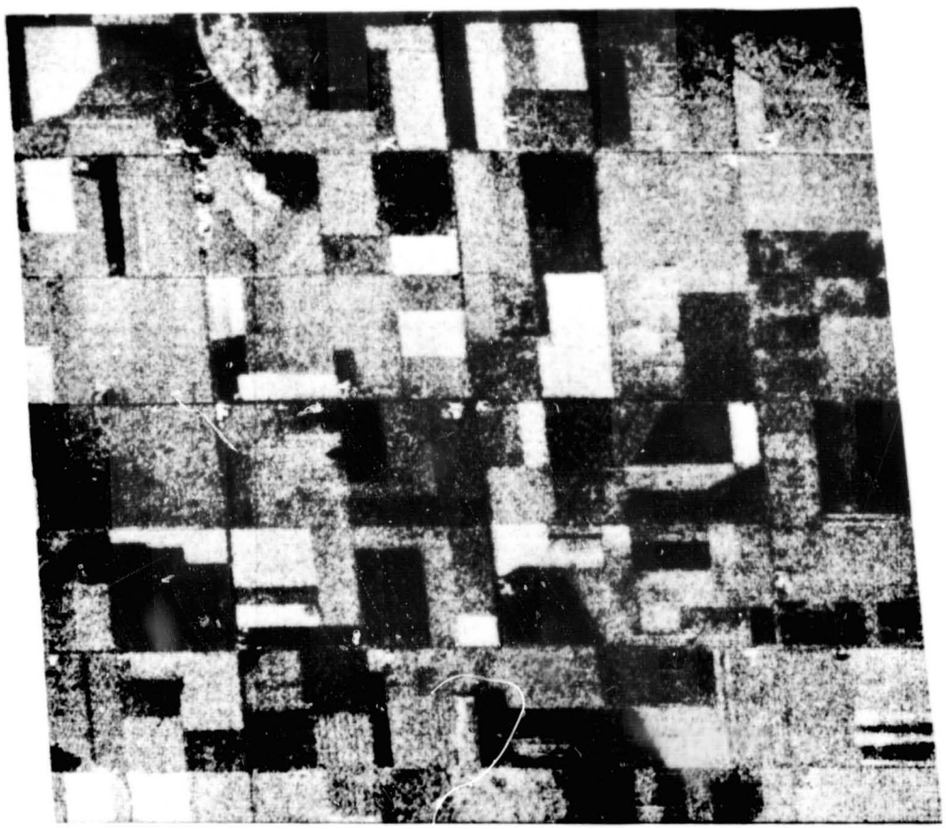

FIGURE 3a. RADAR IMAGE, HH POLARIZATION TAKEN OVER GARDEN CITY, KANSAS, JULY, 1966 BY WESTINGHOUSE AN/APQ 97.

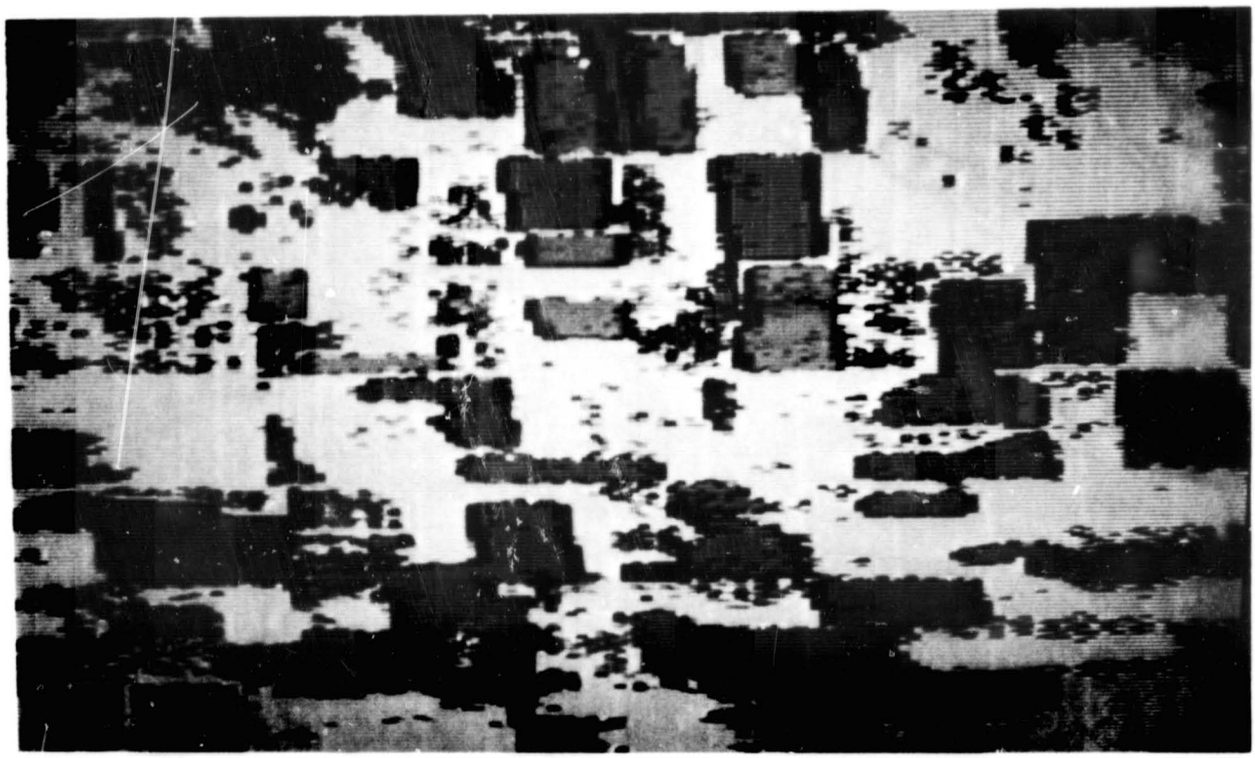

Green Bare Ground

Blue Sugar Beets

Purple Sorghum and Alfalfa

Black No Decision

FIGURE 3b. THEMATIC LAND USE MAP PRODUCED BY IDECS FOR AN HH HV RADAR IMAGE PAIR TAKEN OVER GARDEN CITY, KANSAS, JULY, 1966, BY A WESTINGHOUSE AN/APQ 97. THE RESULTS SHOW 100% CORRECT IDENTIFICATION ON SUGAR BEETS AND BARE GROUND AND 85% CORRECT IDENTIFICATION ON SORGHUM AND ALFALFA.

BASIC KANDIDATS ORGANIZATION

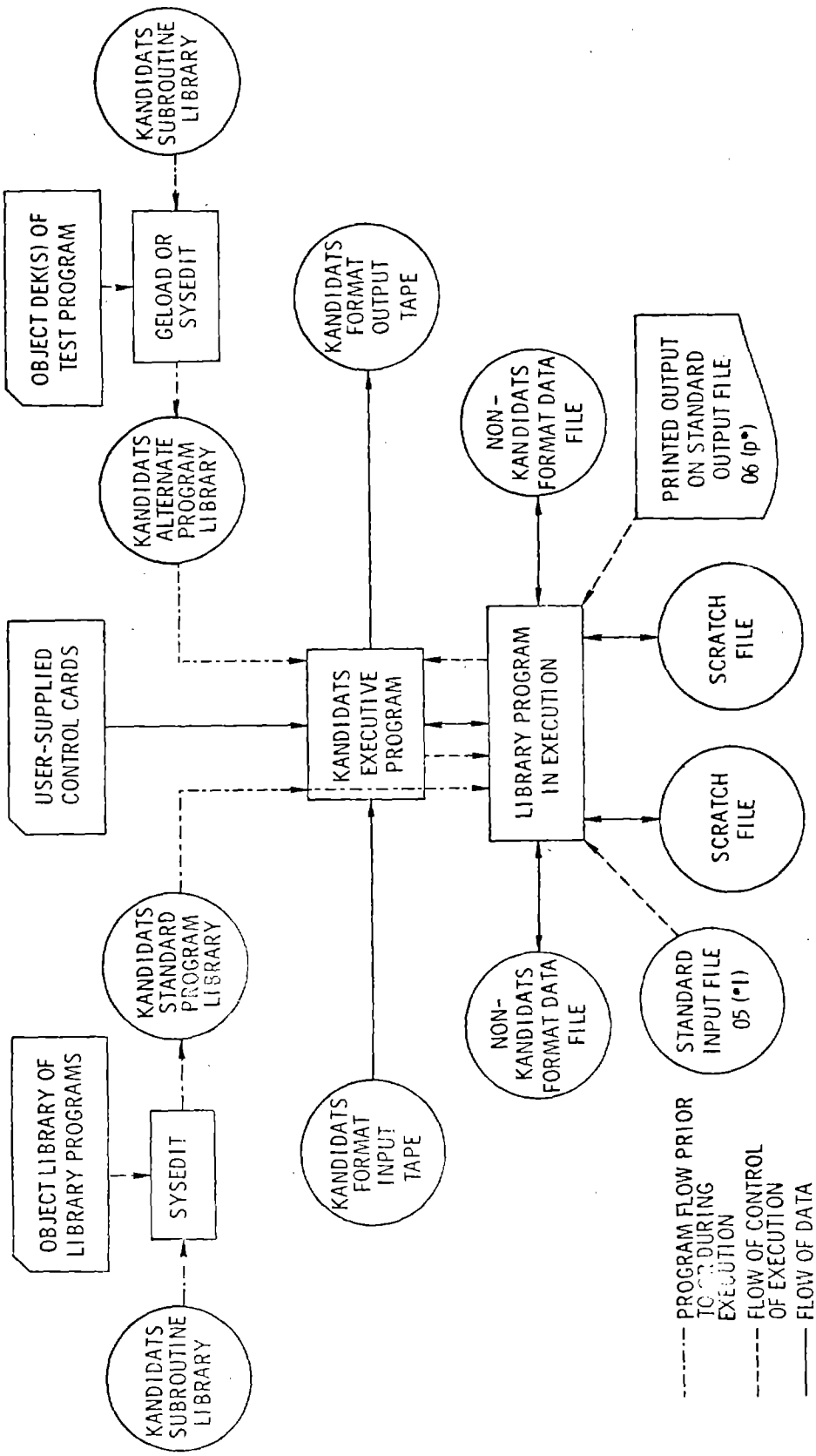

FIGURE 4.

APPENDIX I

by

Percy Batlivala
Center for Research, Remote Sensing Laboratory
University of Kansas
Lawrence, Kansas

ENHANCEMENT AND NORMALIZATION OF RADAR IMAGE TEXTURE

Texture has been of interest to engineers and geoscientists alike because of its potential as a useful discriminant in image category identification. Hence, one important preprocessing operation must be concerned with the enhancement and normalization of image texture. Such an operation must bring out in normal form grey tone variation due to texture and exclude grey tone variations due to look angles or flight parameter fluctions.

Antenna patterns and flight parameter fluctuations have been two factors most responsible for degradation of radar imagery. If we regard the degradation as additive noise, enhancement of the image would, in a sense, be appropriate if there were means of removing the added noise. The 'streaks' parallel to the line of flight in an image could be due to flight parameter fluctuations, scratches caused by handling of the image before digitization, or due to antenna pattern and perpendicular 'streaks' could be due to scan lines.

Given below is a mathematical formulation, which in essence is the enhancement technique.

Let Lx and Ly be the x and y spatial domains, G be the set of grey tones and $P: Lx \times Ly \rightarrow G$ be some digital picture function of some more or less "homogeneous' object O, $O : Lx \times Ly \rightarrow G$.

The relationship between P and O is assumed to be of the following form:

$$P(i,j) = O(i,j) + \alpha(i) + \beta(j) \qquad (1)$$

where $\alpha(i)$ and $\beta(j)$ can be thought of as additive row and column distortion respectively. If we are interested in the texture of O, the average grey tone is not important and a function $\hat{P}(i,j)$ can be determined such that

$$\hat{P}(i,j) = P(i,j) - \hat{\alpha}(i) - \hat{\beta}(j) \qquad (2)$$

where

$$\sum_{i=1}^{I} \sum_{j=1}^{J} \left[\hat{P}(i,j)\right]^2 \qquad (3)$$

is minimized.

The problem now is to estimate $\alpha(i)$ and $\beta(j)$ by $\hat{\alpha}(i)$ and $\hat{\beta}(j)$ so that (3) is minimized.

Let

$$F = \sum_{i=1}^{I} \sum_{j=1}^{J} [P(i,j) - \hat{\alpha}(i) - \hat{\beta}(j)]^2 \qquad (4)$$

To minimize F with respect to $\hat{\alpha}(i)$ and $\hat{\beta}(j)$ we take the partial derivatives, thus

$$\frac{\partial F}{\partial \hat{\alpha}(i)} = \sum_{j=1}^{J} [P(i,j) - \hat{\alpha}(i) - \hat{\beta}(j)](-2) \quad ; \; i = 1, 2, \cdots I \qquad (5)$$

and

$$\frac{\partial F}{\partial \hat{\beta}(j)} = \sum_{i=1}^{I} [P(i,j) - \hat{\alpha}(i) - \hat{\beta}(j)](-2) \quad ; \; j = 1, 2, \cdots J \qquad (6)$$

Setting the partial derivatives to zero.

$$P_{i\cdot} - J\hat{\alpha}(i) - \hat{\beta}_{\cdot} = 0 \quad ; \; i = 1, 2, \cdots, I \qquad (7)$$

$$P_{\cdot j} - \hat{\alpha}_{\cdot} - I\hat{\beta}(j) = 0 \quad ; \; j = 1, 2, \cdots, J \qquad (8)$$

Summing (7) over all i and multiplying (8) by J, we have

$$P_{\cdot\cdot} - J\hat{\alpha}_{\cdot} - I\hat{\beta}_{\cdot} = 0 \qquad (9)$$

$$JP_{\cdot j} - J\hat{\alpha}_{\cdot} - JI\hat{\beta}(j) = 0 \quad ; \; j = 1, 2, \ldots, J \qquad (10)$$

Subtracting equation (10) from (9) we have

$$-JP_{\cdot j} + I[J\hat{\beta}(j) - \hat{\beta}_{\cdot}] = 0 \quad ; \; j = 1, 2, \cdots, J \qquad (11)$$

Similarly by multiplying (7) by I and summing (8) over all j, we have

$$IP_{i\cdot} + J[I\hat{\alpha}(i) - \hat{\alpha}_{\cdot}] = 0 \quad ; \; i = 1, 2, \cdots, I \qquad (12)$$

The solutions to equations (11) and (12) are found to be

$$\hat{\alpha}(i) = \frac{P_{i\cdot}}{J} - \frac{\gamma P_{\cdot\cdot}}{IJ} \quad , \quad \hat{\beta}(j) = \frac{P_{\cdot j}}{I} - (1-\gamma)\frac{P_{\cdot\cdot}}{IJ} \qquad (13)$$

for any arbitrary γ.

Hence

$$\hat{\alpha}(i) + \hat{\beta}(j) = \frac{P_{i\cdot}}{J} + \frac{P_{\cdot j}}{I} - \frac{P_{\cdot\cdot}}{IJ} \tag{14}$$

and the enhanced image $\hat{P}(i,j)$ is then obtained by substituting equation (14) into equation (2) and

$$\hat{P}(i,j) = P(i,j) - \frac{P_{i\cdot}}{J} - \frac{P_{\cdot j}}{I} + \frac{P_{\cdot\cdot}}{IJ} \tag{15}$$

The enhanced image $\hat{P}(i,j)$ is found to have a zero mean, and also each row and column mean is zero.

Figure 1 shows a simulated 5 x 5 'homogeneous' image to which the enhancing technique has been applied. The 5 x 5 image shown in (c) of Figure 1 is the model with additive noise. The 5 x 5 enhanced image shown in (d) of Figure 1 clearly shows a 'diffusion' of the additive noise. For simplicity of representation, image (d) has been quantized, and therefore does not have a zero mean.

Figure 2 shows the enhancement technique applied to a radar image. Part (a) shows a digitized radar image of a sorghum field. This field was isolated from the radar image of a test site selected at Garden City, Kansas. The mission was conducted on September 15, 1965, by Westinghouse. Part (a) of Figure 1 shows a computer output of the original. Streaks running vertically and horizontally show up very clearly on the image. Part (b) shows the pictorial view of the 'noise' which was subtracted out of (a). Part (c) shows the enhanced image. All three images are represented by 13 grey tones and are quantized using an equal probability routine.

Figure 3 shows a larger area of the same test site and is made up of 14 fields. The images shown in the figure are positioned the same, relative to one another, as they were on the ground. Each image in the figure is a representation of the noise subtracted out from it. The streaks occurring in one field carry on into the neighboring fields. The vertical streaks (perpendicular to the line of flight) are almost periodic and, as stated earlier in this section, could be due to scan lines. The horizontal streaks may have been caused due to scratches on the negative or due to antenna pattern, but to pinpoint their cause at this stage, without further research, would be difficult.

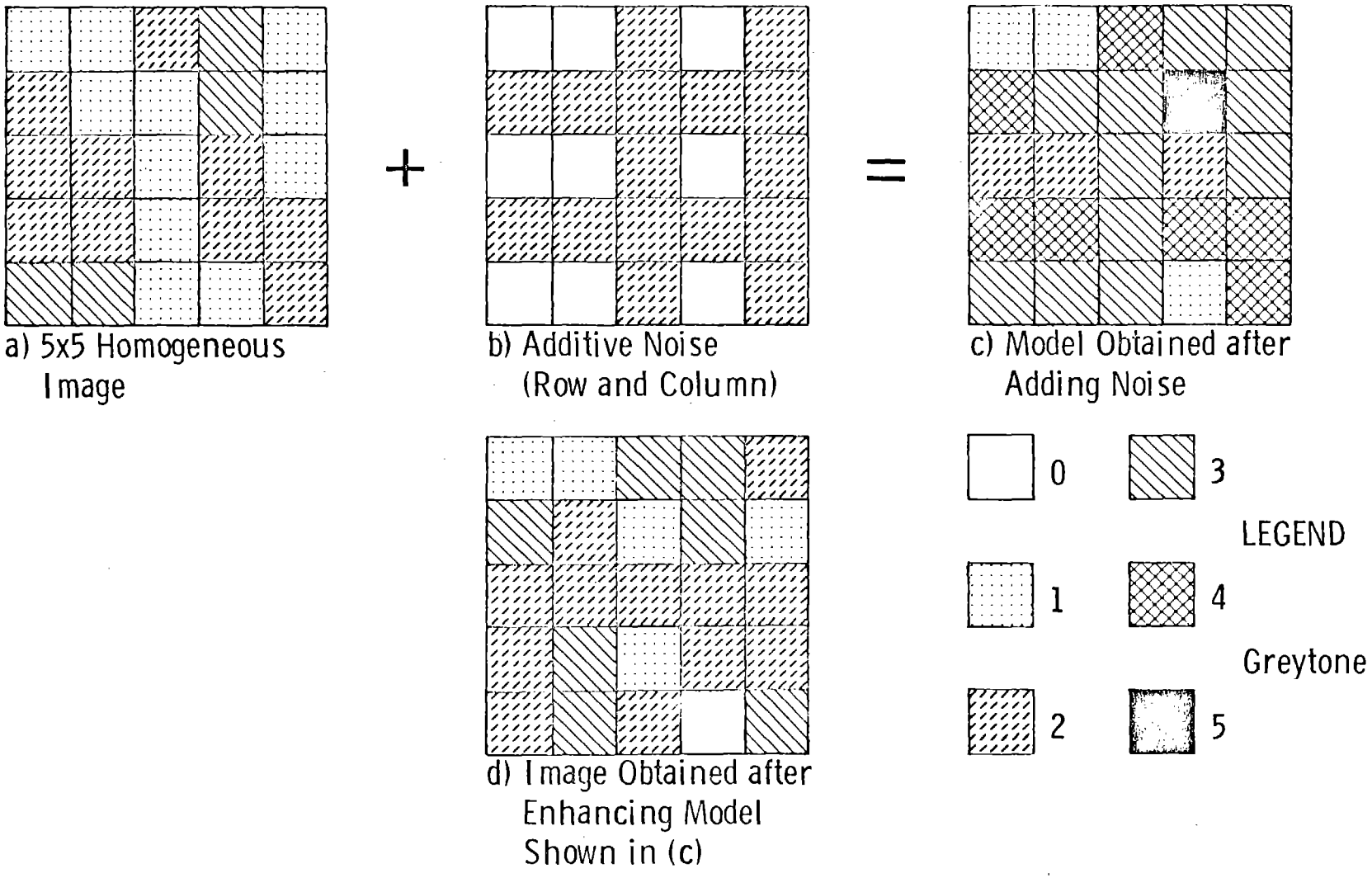

Figure 1, Shows a simulated 5x5 homogeneous image with additive noise (row and column) and its removal by the enhancement technique.

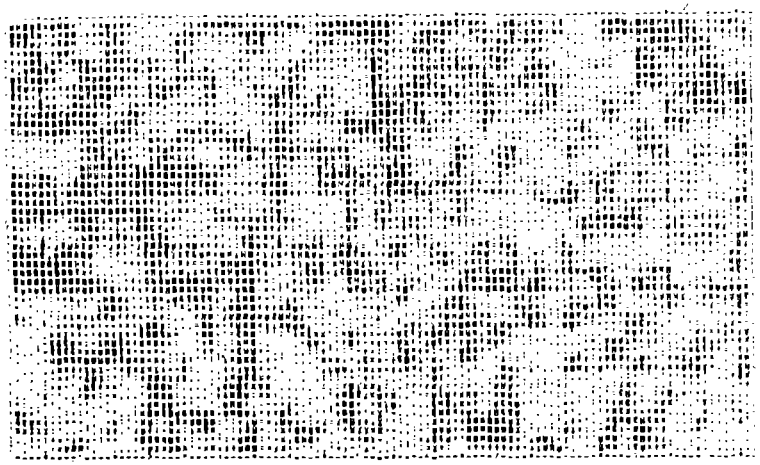

(a) Original image.

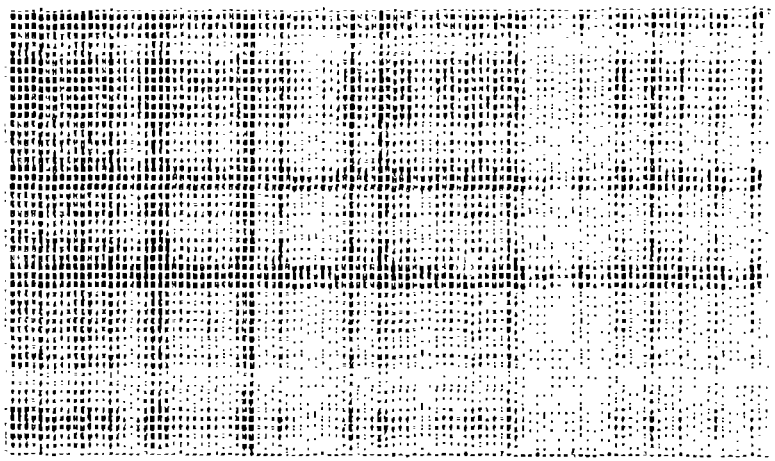

(b) Noise subtracted out of original.

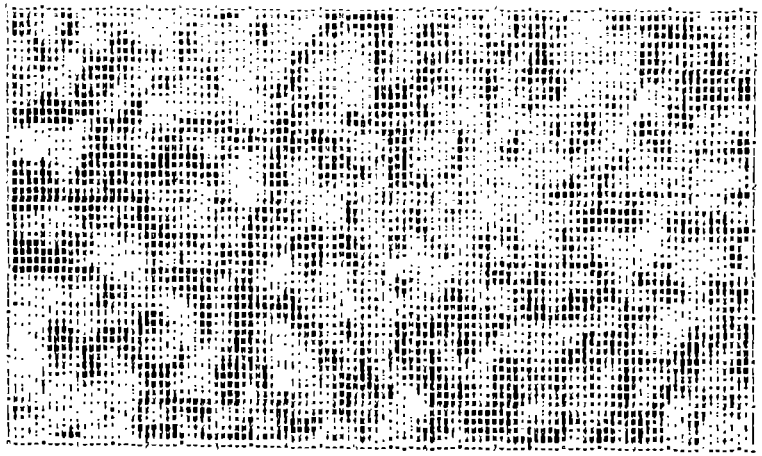

(c) Enhanced image

Figure 2, Texture enhancement technique applied to a digitized radar image of a sorghum field (Garden City,Sept.,1965)

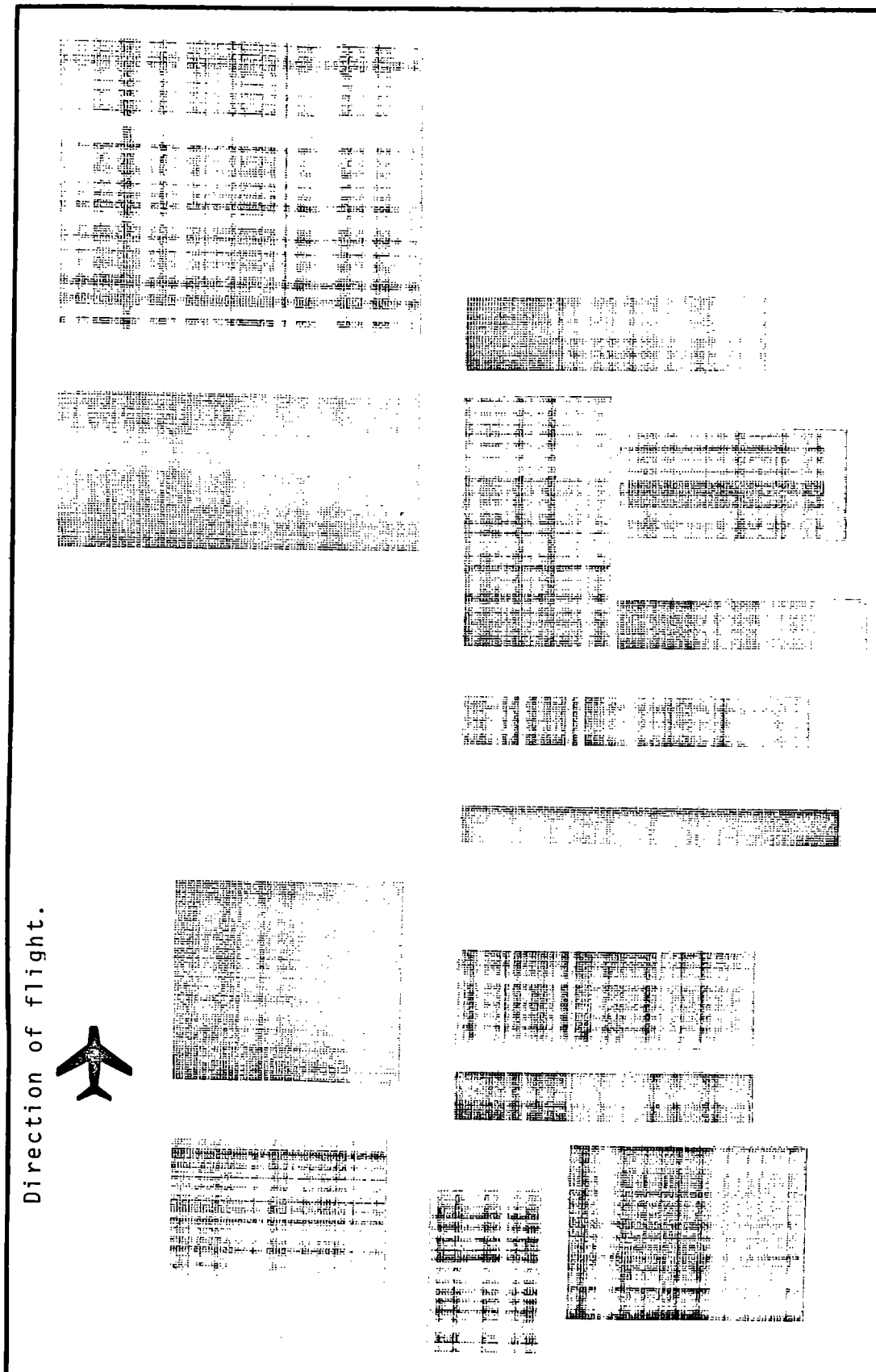

Figure 3, Part of the Garden City test site showing the 'noise' subtracted out of the 14 fields.

APPENDIX II

ON A TEXTURE-CONTEXT FEATURE EXTRACTION ALGORITHM FOR REMOTELY SENSED IMAGERY

R. M. Haralick
Center for Research, Inc.
Remote Sensing Laboratory
University of Kansas
Lawrence, Kansas 66044

ABSTRACT

An image data set of 54 scenes was obtained from 1/8" by 1/8" areas on a set of 1:20,000 scale photography. The scenes which consisted of 6 samples from each of the nine categories scrub, orchard, heavily wooded, urban, suburban, lake, swamp, marsh, and railroad yard was analyzed manually and automatically.

For the automatic analysis, a set of features measuring the spatial dependence of the grey tones of neighboring resolution cells was defined. On the basis of these features and a simple decision rule which assumed that the features were independent and uniformly distributed an identification accuracy of 70% was achieved by training of 53 samples and assigning an identification to the 54th sample and repeating the experiment 54 times. This identification accuracy must be compared with the average 81% correct identification which five photointerpreters achieved with the same scenes, although the 81% correct identification is the accuracy achieved when they used the 9" x 9" photograph to interpret from. Note that the photograph is data of considerably higher resolution having much more context information on it than the small digitized 1/8" x 1/8" area the automatic analysis had available.

INTRODUCTION

The main problem facing us is that of feature selection of textural-contextual information. The features that we may use are limited not only by the catholic constraint of practicality*, but also by our heuristic idea of texture-context information.

In the next section we briefly go over the feature selection problem in general and in subsequent sections present the intuitive ideas behind what we have termed 'texture-context' features. The mathematical details of these features are then explained and some simple examples are shown. The decision making algorithms that were used are discussed; results, including comparison with interpretations by expert photointerpreters, and conclusions are in separate sections.

For this study the data sets were comprised of 54 digitized 1/8" x 1/8" sections of standard 1:20,000, 9" x 9" aerial photography supplied by the United States Army Engineer Topographic Laboratories. Each image was digitized into a 64 x 64 resolution cell matrix (and later into a 58 x 58 one because of some dark border effects encountered from the mask used in the digitization process), and the levels of digitization ranged from 63 to zero. There were six data sets per category and 9 general categories: scrub, orchard, heavily wooded, urban, suburban, lake, marsh, swamp, and railroad yard.

*With regard to this point, it seems appropriate to note here that all feature selection and decision making algorithms were written in FORTRAN IV and implemented on a PDP 15/20 digital computer with 12K core and two DEC tape drives.

PREPROCESSING AND FEATURE SELECTING

The 'classical' black-box description of an automated pattern recognition system is based on four main, not necessarily distinct, subsystems:

(1) the sensors or measuring instruments
(2) the preprocessors
(3) the feature selectors
(4) the categorizor or decision maker.

The data which the sensors or instruments produce are not always in the kind of normalized form with which it makes sense to work. For example, many sensors or measuring instruments produce relative measurements, i.e. the measurements are correct up to an additive or multiplicative constant. Despite calibration efforts, this is particularly true for the camera-film-digitizer system which produce the digital magnetic tape containing the digitized image. Variations in lighting, lens, film, developer, and digitizer all combine to produce a grey tone value which is an unknown but usually monotonic transformation of the "true" grey tone value. Under these conditions we would certainly want two images of the same scene, one image being a grey tone monotonic transformation of the other, to produce the same results from the pattern recognition process. It has been shown that normalization by equal probability quantizing guarantees that images which are monotonic transformations of one another produce the same results. Hence, all the images we used were quantized to 16 levels.

The sensors usually produce many measurements. Simple sensors such as an EKG machine produce $10^3 - 10^4$ sampled values while image sensors produce $10^4 - 10^7$ sensed grey tones. Compared to the huge amount of data produced by the sensors, the category distinctions we need to make are relatively few, say a choice of one out of ten to a hundred categories. This suggests that the pattern recognition system should be able to reduce the data to a more succinct form, eliminating much extraneous information (that information which is, in general, not relative to the discrimination of the given categories). This sort of data reduction which produces the initial features is called preprocessing or feature selecting and unfortunately there exists little or no theory to aid in establishing what this preprocessing or feature selecting should consist of. Rather, this operation is determined intuitively, rationalized heuristically and justified later progmatically and empirically. In the case of our texture-context problem, the use of various moments of the spatial grey tone dependence matrices corresponds to this sort of preprocessing or initial feature selecting.

Research was supported by U.S. Army Engineer Topographic Laboratories, Fort Belvoir, Virginia, CONTRACT DAAK02-70-C-0388.

It is important to note that a primary characteristic of preprocessing or feature selecting is the number of operations needed to be performed in order to obtain the features. Quick procedures are characterized by a number of operations proportional to the number of data points needing to be processed. All procedures which we develop here are quick in that sense.

The next stage in feature selecting consists of removing redundancies from the initial features. If the initial features are N-dimensional vectors in Euclidean N-space, as they are in our study, then it might be that all the vectors lie in some K-dimensional flat where K is much smaller than N. In this case there are N-K linear constraints to which the initial feature vectors are subject and it is possible to essentially maintain all the information in the features vectors by representing them by their coordinates in the smaller dimensional subspace or flat. Such redundancy removal can be done by principal component analysis or by not using those features which do not contribute additional information for the identification of the given categories. It is this latter approach which we take here.

The various features which we suggest are all a function of distance and angle. The angular dependence presents a special problem. Suppose image A has features a,b,c,d for angles $0^\circ, 45^\circ, 90^\circ, 135^\circ$ respectively and image B is identical with image A except that image B is rotated by say 90° with respect to A. Then B will have features c,d,a,b for angles $0^\circ, 45^\circ, 90^\circ, 135^\circ$ respectively. Since the texture-context of A is the same as B, any decision rule using the angular depence features a,b,c,d must produce the same results for c,d,a,b (a 90° rotation) or for that matter b,c,d,a (a 45° rotation) and d,a,b,c (a 135° rotation). To guarantee this we do not use the angular dependent feature directly. Instead, we use some symmetric function of a,b,c,d: their average, range, and mean deviation.

SPATIAL GREY TONE DEPENDENCE

Let $L_x = \{1,2,\ldots N_x\}$ and $L_y = \{1,2,\ldots,N_y\}$ be the x and y spatial domains and $L_y \times L_x$ be the set of resolution cells. Let $G = \{0,1,\ldots,N_g\}$ be the set of possible grey tones. Then a digital image I is a function which assigns some grey tone to each and every resolution cell; $I: L_y \times L_x \rightarrow G$.*

An essential component of our conceptual framework of texture is a measure, or more precisely, four closely related measures from which all of our texture-context features are derived. These measures are arrays termed angular nearest neighbor grey tone spatial dependence matrices, and to describe these arrays we must re-emphasize our notion of adjacent or nearest neighbor resolution cells themselves. We consider a resolution cell -- excluding those on the periphery of an image, etc.—to have eight nearest neighbor resolution cells as in Figure 1.

*The spatial domain $L_y \times L_x$ consists of ordered pairs whose components are row and column respectively. This convention conforms with the usual two subscript row-column designation used in FORTRAN.

We assume that the texture-context information in an image I is contained in the over-all or "average" spatial relationship which the grey tones in image I have to one another. More specifically, we shall assume that this texture-context information is adequately specified by the matrix of relative frequencies P_{ij} with which two neighboring resolution cells separated by distance d occur on the image, one with grey tone i and the other with grey tone j. Such matrices of spatial grey tone dependence frequencies are a function of the angular relationship between the neighboring resolution cells as well as a function of the distance between them. Figure 2 illustrates the set of all horizontal neighboring resolution cells separated by distance 1. This set along with the image grey tones would be used to calculate a distance 1 horizontal spatial grey tone dependence matrix. Formally, for angles quantized to 45° intervals the unnormalized frequencies are defined by:

$$P(i,j,d,0^\circ) = \#\{((k,l),(m,n)) \in (L_y \times L_x) \times (L_y \times L_x) \mid k-m=0,\ |l-n|=d,\ I(k,l)=i,\ I(m,n)=j\}$$

$$P(i,j,d,45^\circ) = \#\{((k,l),(m,n)) \in (L_y \times L_x) \times (L_y \times L_x) \mid (k-m=d,\ l-n=-d) \text{ or } (k-m=-d,\ l-n=d),\ I(k,l)=i,\ I(m,n)=j\}$$

$$P(i,j,d,90^\circ) = \#\{((k,l),(m,n)) \in (L_y \times L_x) \times (L_y \times L_x) \mid |k-m|=d,\ l-n=0,\ I(k,l)=i,\ I(m,n)=j\}$$

$$P(i,j,d,135^\circ) = \#\{((k,l),(m,n)) \in (L_y \times L_x) \times (L_y \times L_x) \mid (k-m=d,\ l-n=d) \text{ or } (k-m=-d,\ l-n=-d),\ I(k,l)=i,\ I(m,n)=j\}$$

Note that these matrices are symmetric; $P(i,j;d,a) = P(j,i;d,a)$. The distance metric ρ implicit in the above equations can be explicitly defined by $\rho((k,l),(m,n)) = \max\{|k-m|, |l-n|\}$.

Consider Figure 3-a, which represents a 4 x 4 image with four grey tones, ranging from 0 to 3. Figure 3-b shows the general form of any grey tone spatial dependence matrix. For example, the element in the (2,1)-st position of the distance 1 horizontal P_H matrix is the total number of times two grey tones of value 2 and 1 occurred horizontally adjacent to each other. To determine this number, we count the number of pairs of resolution cells in R_H such that the first resolution cell of the pair has grey tone 2 and the second resolution cell of the pair has grey tone 1. In Figures 3-c through 3-f we calculate all four distance 1 grey tone spatial dependence matrices.

If needed, the appropriate frequency normalization for the matrices are easily computed. When the relationship is nearest horizontal neighbor (d=1 and $\alpha=0^\circ$), there will be $2(N_x-1)$ neighboring resolution cell pair on each row and there are N_y rows providing a total of $2N_y(N_x-1)$ nearest horizontal neighbor pairs (see Figure 3). When the relationship is nearest right diagonal neighbor (d=1, $\alpha=45^\circ$) there will be $2(N_x-1)$ 45° neighboring resolution cell pairs for each row except the first, for which there are none, and there are N_y rows. This provides a total of $2(N_y-1)(N_x-1)$ nearest right diagonal neighbor pairs (see Figure 4). By symmetry there will be $2N_x(N_y-1)$ nearest vertical neighbor pairs and $2(N_x-1)(N_y-1)$ nearest left diagonal neighbor pairs.

Let us now consider how to use such spatial dependence information. We have suggested generating a homogeneity and unhomogeneity image from the original image on the basis of the grey tone dependence matrix. (The homogeneity image is an enhanced display of all

the homogeneous areas while the unhomogeneity image is an enhanced display of all the unhomogeneous areas.) At any resolution (m,n), the homogeneity image I_h has an integer valued grey tone 0 to 8 depending on how many of resolution cell (m,n)'s 8 nearest neighbors on the original image I have respective grey tones which are "sufficiently similar" to the grey tone at (m,n) on image I. Similarity of two grey tones i and j is determined on the basis of whether the grey tones occur next to each other sufficiently often; that is, if the element P(i,j) of the spatial dependence matrix is large enough. At any resolution cell (m,n), the unhomogeneity image I_u has a grey tone 0,1,2,3,4,5,6,7 or 8 depending on how many of resolution cell (m,n)'s 8 nearest neighbors on the original image I have respective grey tones which are "sufficiently dissimilar" to the grey tone at (m,n) on image I. Dissimilarity of two grey tones i and j is determined on the basis of whether the grey tones occur next to each other sufficiently rarely, that is, if the element P(i,j) of the spatial grey tone dependence matrix is small enough.

The idea of large enough or small enough implies a thresholding of the grey tone dependence matrix and depending on what level the threshold is set the resulting homogeneity and unhomogeneity images appear differently. Thus undesirable arbitrary thresholds must be introduced. Fortunately, it is possible to do away with thresholding. Instead of defining similarity as an all or nothing affair, we can define the similarity between grey tones i and j to be P(i,j), the frequency with which i and j co-occur next to each other, some function of P(i,j) such as $\log P(i,j)$ or perhaps even some function of i and j such as $\frac{1}{1+(i-j)^2}$. Dissimilarity between i and j can be measured by $(i-j)^2$.

Texture-context features are easily derived from the homogeneity or unhomogeneity image. For example, the greater the total homogeneous region area, then the darker the homogeneity image. Hence, the mean grey tone of the homogeneity image provides a measure of the "smoothness" of the original image. The grey tone variance of the homogeneity image provides a measure of how the homogeneous areas are spread out on the image. Low variance would indicate large area uniform homogeneity while high variance might indicate many small area homogeneous regions.

It can be shown that the computation of the average grey tone on the homogeneity or unhomogeneity image J can be done without having to have the image J generated. The average grey tone can be computed directly as a function of the spatial grey tone dependence matrices. In this paper we explore only those features which can be computed directly from the spatial dependence grey tone matrix and do not require the homogeneity or unhomogeneity image to be determined.

In the discussion which follows on the use of the spatial grey tone dependence matrices as texture context features for image data, we shall be concerned with forms such as

$$\sum_{a=1}^{N_g}\sum_{b=1}^{N_g}(a-b)^2 P(a,b)/{}^{\#}R$$, the angular second moment difference (ASMD);

$$\sum_{a=1}^{N_g}\sum_{b=1}^{N_g}\frac{1}{1+(a-b)^2}P(a,b)/{}^{\#}R$$, the angular second moment inverse difference (ASMID);

$$\sum_{a=1}^{N_g}\sum_{b=1}^{N_g}\left[\frac{P(a,b)}{{}^{\#}R}\right]^2$$, the angular second moment (ASM);

$$\frac{COV}{VAR}$$, the correlation between neighboring grey tones (COR);

Note: $^{\#}R$ is the number of neighboring resolution cells.

The ASM feature is the sum of the squared terms of the grey tone spatial dependence matrix normalized by the total number of possible adjacencies, $^{\#}R$, for the given angle. For each spatial dependence matrix, there is a corresponding ASM but there has been a great reduction of data because each ASM (as each ASMD and ASMID) is only a number not an array. The ASMD feature is the sum of the members of a grey tone spatial dependence matrix, each member multiplied by the squared difference of the grey tone values and normalized as before. The ASMID feature is the sum of the members of a grey tone spatial dependence matrix, each member divided by one plus squared grey tone difference. The correlation feature COR is actually the value of the two-dimensional autocorrelation function of the picture where the autocorrelation function is evaluated for a particular distance and angle lag.

Each of these features is a function of the angle and distance between what we consider to be neighboring resolution cells. We consider 4 angles, 0°, 45°, 90°, and 135° at distances of 1, 3, and 9 resolution cells. This provides an initial set of 48 features. The number of features is thus reduced by calculating the mean, range, and mean deviation of each type of feature at a given distance over the four angles. The features which are actually first considered by the decision rule are ASM, ASMID, ASMD, COR evaluated at distances of 1, 3, and 9 resolution cells with the average, range, and mean deviation for each feature and distance calculated over the four angles. This is a total of 36 features. Figure 5 illustrates the calculation of three representative features of the image of Figure 3a.

AUTOMATIC SCENE IDENTIFICATION

Automatic scene identification using the 36 texture context features presents a difficult problem because of the relative sparcity of the data: for each of 9 categories there are only 6 samples with each sample having a 36 dimensional feature vector. The difficulty is really twofold: (1) There are so few samples that it is difficult to learn anything about the patterns which are characteristic of the category, (2) The decision rule must contain a minimum of parameters so that the decision rule does not "memorize" the data. Hence the approach we take relies on the simplest type of data statistics: the minimum and maximum value each feature

can take on for measurements in a given category.

Figure 6 illustrates for each pair of categories which variable will separate them. Figure 6 shows that variable 4, ASMID at distance 1, has its average, range and mean deviation appearing a total of 56 times in separating categories. Of those categories which are not separated by the distance 1 ASMID features, COR at a distance 1 has its average, range and mean deviation appearing a total of 8 times in separating categories. Of those categories which are not separated by the distance 1 ASMID or COR features, ASM at distance 1 has its average, range and mean deviation appearing a total of 4 times in separating categories. Of those categories which are not separated by distance 1 ASMID, COR or ASM features, ASM at distance 3 has its average, range and mean deviation appearing a total of 1 time in separating categories. Hence, of the initial 36 features, we use only the following 12 features:

ASM	AVG	
ASM	RANGE	
ASM	DEV	
COR	AVG	DISTANCE 1
COR	RANGE	
COR	DEV	
ASMID	AVG	
ASMID	RANGE	
ASMID	DEV	
ASM	AVG	
ASM	RANGE	DISTANCE 3
ASM	DEV	

For automatic identification, we use a decision rule which is a maximum likelihood decision rule under the assumptions that the 12 feature variables are independent having uniform distributions. Under this assumption, the density function for the k^{th} category is

$$f(x_1,x_2,\ldots,x_{12}|k) = \prod_{n=1}^{12} \frac{1}{(a_{nk}-b_{nk})} \quad \text{for all}$$

$(x_1,x_2,\ldots,x_{12})$ such that

$$b_{nk} \le x_n \le a_{nk},\ n=1,2,\ldots,12,$$

where b_{nk} and a_{nk} define the minimum and maximum values of the uniform distribution on the n^{th} component.

Hence, a measurement $(x_1,x_2,\ldots,x_{12})$ is assigned to category k if and only if

(1) $b_{nk} \le x_n \le a_{nk}$, $n=1,2,\ldots 12$ and

(2) $$\prod_{n=1}^{12} \frac{1}{(a_{nk}-b_{nk})} \ge \prod_{n=1}^{12} \frac{1}{(a_{nj}-b_{nj})}$$

for all j such that $b_{nj} \le x_n \le a_{nj}$, $n=1,2,\ldots 12$.

If there exists no k such that $b_{nk} \le x_n \le a_{nk}$, $n=1,2,\ldots 12$, then $(x_1,x_2,\ldots x_{12})$ is assigned to category k if and only if

$$\sum_{n=1}^{12} \min\{|x_n-a_{nk}|, |x_n-b_{nk}|\}\ (a_{nk}-b_{nk}) \ge \sum_{n=1}^{12} \min\{|x_n-a_{nj}|, |x_n-b_{nj}|\}\ (a_{nj}-b_{nj}),$$

$j=1,2,\ldots,K.$

The minimum and maximum statistics a_{nk} and b_{nk} are estimated in the following way:

Let α_{nk} = the maximum n^{th} component for all measurements designated in k^{th} category;

β_{nk} = the minimum n^{th} component for all measurements designated in k^{th} category.

Assume that category k has M_k measurements, then

$$b_{nk} = \beta_{nk} - \frac{(\alpha_{nk}-\beta_{nk})}{M_k-1}$$

$$a_{nk} = \alpha_{nk} + \frac{(\alpha_{nk}-\beta_{nk})}{M_k-1}$$

Notice that a_{nk} is larger than the maximum by some fraction of the range and b_{nk} is smaller than the minimum by some fraction of the range. Hence, the range $a_{nk}-b_{nk}$ is larger than $\alpha_{nk}-\beta_{nk}$. Under the assumption that the variable has a uniform distribution, the expected value of $\alpha_{nk}-\beta_{nk}$ is $\frac{M_k-1}{M_k+1}$ · (true range) while the expected value of $a_{nk}-b_{nk}$ is the true range.

The identification experiment was done in two ways using the above decision rule. In the first case the entire set of 54 samples was used to train on, i.e. gather the statistics α_{nk}, β_{nk}, $n=1,2,\ldots 12$, $k=1,2,\ldots 9$, and then on the basis of the α_{nk}'s and β_{nk}'s calculated, each sample was assigned to a category. Figure 7 illustrates the contingency table of the resulting assignments. A total of 53 out of 54 samples were correctly identified. We shall have more to say about the interpretation of 53/54 in a moment.

In the second case, the identification experiment was repeated 54 times, each time using a different set of 53 samples to train on. The 54th sample was assigned to a category on the basis of the minimum maximum statistics gathered from the other 53 samples. Figure 8 illustrates the contingency table resulting from these assignments. A total of 38 out of 54 samples were correctly identified for a percentage of approximately 70%.

To help interpret these results a sequential decision algorithm in the form of a dichotomous key was tried. A dichotomous key successively splits a group of measurements in two based on whether a given component is greater than or less than some value. The dichotomous key itself is illustrated in Figure 9. It takes 13 decision points to perfectly separate the 54 measurements into their designated categories. If the 5 decision points, whose sole function is to correctly separate measurements

which were incorrectly assigned, are removed, then it takes 8 decisions to correctly assign 49/54 measurements. Under the assumption that the twelve variables are independent at each decision stage, and that the two category groups being split have the same uniform distribution, Figure 10 illustrates the contingency table resulting from these assignments. Under the assumption that the twelve variables are independent at each decision stage, and that the two category groups being split have the same uniform distribution, the probability of being able to achieve perfect separation of two categories in two decisions is less than 10^{-12}.

The automatic texture-context scene analysis experiment was compared with the identification which five photointerpreters were able to make with the same data set. The photointerpreters were given the original 9"x9" photographs and were allowed to use as much context information as they could in making the identification. These experiments yielded an average of 81% correct identification for the five photointerpreters.

DISCUSSION AND CONCLUSION

An image data set of 54 scenes consisting of 6 samples from each of the nine categories scrub, orchard, heavily wooded, urban, suburban, lake, swamp, marsh, and railroad yard was analyzed manually and automatically.

For the automatic analysis, a set of features for texture context was defined and on the basis of these features and a simple decision rule, an identification accuracy of 70% was achieved. This identification accuracy must be compared with the average 81% correct identification which five photointerpreters achieved with the same scenes, although the 81% correct identification is the accuracy achieved when they used the 9"x9" photograph to interpret from. The photograph is data of considerably higher resolution having much more context information on it than the small digitized 1/8"x1/8" area the automatic analysis had available.

Furthermore, the 70% correct identification arose in the case when the automatic technique trained on 53 samples and assigned an identification to the 54th sample and repeated the experiment 54 times. This means that for each experiment, there was one category which had 5 samples instead of 6 samples. For this category, there is a probability of 1/3 that for each feature the missing sample had minimum or maximum value over all samples for the category. Hence there is a high probability that the missing sample provided significant information which is not available in the sample without it.

Looking at the situation another way, 100% correct identification was achieved by the optimal dichotomous key which required 13 decision points. The probability that such good identification could happen by chance is very small. In fact, the number of 2 celled partitions which the simple hyperplanes used could generate for N samples in a d-dimensional space is only d(N-1) and this number should be compared to $2^{N-1}-1$, the total number of non-trivial distinct 2 celled partitions possible. In our case d=12, N=54 and the ratio

$$\frac{d(N-1)}{2^{N-1}-1} = \frac{12\times 53}{2^{53}-1} \leq \frac{2^{10}}{2^{53}} = 2^{-43}$$

Hence our ability to perform the category separation with such a small chance of available partitions is significant.

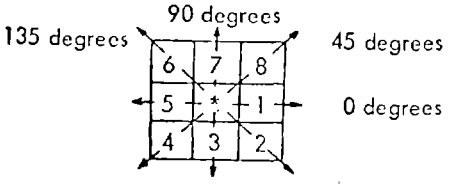

Figure 1. Resolution cells nos. 1 and 5 are the 0-degree (horizontal) nearest neighbors to resolution cell '*', resolution cells nos. 2 and 6 are the 135-degree nearest neighbors, resolution cells 3 and 7 are the 90-degree nearest nearest neighbors, and resolution cells 4 and 8 are the 45-degree nearest neighbors to '*'. (Note that this information is purely spatial, and has nothing to do with grey tone values.)

(1,1)	(1,2)	(1,3)	(1,4)
(2,1)	(2,2)	(2,3)	(2,4)
(3,1)	(3,2)	(3,3)	(3,4)
(4,1)	(4,2)	(4,3)	(4,4)

$L_y = \{1,2,3,4\}$

$L_x = \{1,2,3,4\}$

$$P_H = \{((k,l),(m,n)) \in (L_y \times L_x) \times (L_y \times L_x) \mid k-m = 0,\ |l-n| = 1\}$$

$$= \{((1,1),(1,2)), ((1,2),(1,1)), ((1,2),(1,3)), ((1,3),(1,2)), ((1,3),(1,4)), ((1,4),(1,3)), ((2,1),(2,2)), ((2,2),(2,1)), ((2,2),(2,3)), ((2,3),(2,2)), ((2,3),(2,4)), ((2,4),(2,3)), ((3,1),(3,2)), ((3,2),(3,1)), ((3,2),(3,3)), ((3,3),(3,2)), ((3,3),(3,4)), ((3,4),(3,3)), ((4,1),(4,2)), ((4,2),(4,1)), ((4,2),(4,3)), ((4,3),(4,2)), ((4,3),(4,4)), ((4,4),(4,3))\}$$

Figure 2 illustrates the set of all distance 1 horizontal neighboring resolution cells on a 4 by 4 image.

0	0	1	1
0	0	1	1
0	2	2	2
2	2	3	3

Figure 3-a.

		Grey Tone			
		0	1	2	3
Grey Tone	0	#(0,0)	#(0,1)	#(0,2)	#(0,3)
	1	#(1,0)	#(1,1)	#(1,2)	#(1,3)
	2	#(2,0)	#(2,1)	#(2,2)	#(2,3)
	3	#(3,0)	#(3,1)	#(3,2)	#(3,3)

Figure 3-b. This shows the general form of any grey tone spatial dependence matrix for an image with integer grey tone values 0 to 3. #(i,j) stands for number of times grey tones i and j have been neighbors.

0°

$$P_H = \begin{pmatrix} 4 & 2 & 1 & 0 \\ 2 & 4 & 0 & 0 \\ 1 & 0 & 6 & 1 \\ 0 & 0 & 1 & 2 \end{pmatrix}$$

Figure 3-c.

90°

$$P_V = \begin{pmatrix} 6 & 0 & 2 & 0 \\ 0 & 4 & 2 & 0 \\ 2 & 2 & 2 & 2 \\ 0 & 0 & 2 & 0 \end{pmatrix}$$

Figure 3-d.

135°

$$P_{LD} = \begin{pmatrix} 2 & 1 & 3 & 0 \\ 1 & 2 & 1 & 0 \\ 3 & 1 & 0 & 2 \\ 0 & 0 & 2 & 0 \end{pmatrix}$$

Figure 3-e.

45°

$$P_{RD} = \begin{pmatrix} 4 & 1 & 0 & 0 \\ 1 & 2 & 2 & 0 \\ 0 & 2 & 4 & 1 \\ 0 & 0 & 1 & 0 \end{pmatrix}$$

Figure 3-f.

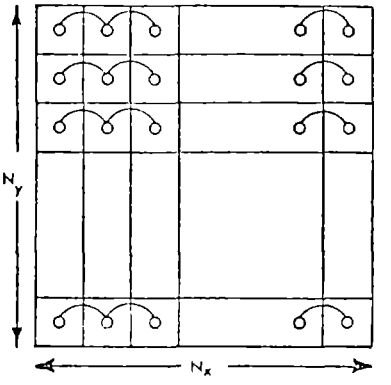

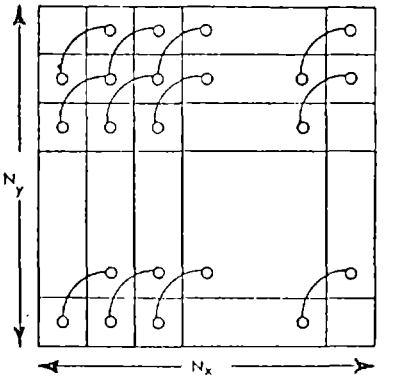

Figure 4 illustrates how the members of horizontal and right diagonal neighboring resolution cells are counted.

$$ASM\ (0^\circ) = \frac{1}{(24)^2}(4^2 + 2^2 + 1^2 + 0^2 + 2^2 + 4^2 + 0^2 + 0^2 + 1^2 + 0^2 + 6^2 + 1^2 + 0^2 + 0^2 + 1^2 + 2^2) = \frac{84}{(24)^2} = .14583$$

$$ASMD(90^\circ) = \frac{1}{24}(6\cdot0 + 0\cdot1 + 2\cdot4 + 0\cdot9 + 0\cdot1 + 4\cdot0 + 2\cdot1 + 0\cdot4 + 2\cdot4 + 2\cdot1 + 2\cdot0 + 2\cdot2 + 0\cdot9 + 0\cdot4 + 2\cdot1 + 0\cdot0) = 1.083$$

$$ASMID(135^\circ) = \frac{1}{18}\left(\frac{2}{1} + \frac{1}{2} + \frac{3}{5} + \frac{0}{10} + \frac{1}{2} + \frac{2}{1} + \frac{1}{2} + \frac{0}{5} + \frac{3}{5} + \frac{1}{2} + \frac{0}{1} + \frac{2}{2} + \frac{0}{10} + \frac{0}{5} + \frac{2}{2} + \frac{0}{1}\right) = .5111$$

$$COR(45^\circ) = \frac{COV(45^\circ)}{VAR(45^\circ)} = \frac{2.111 - 1.4983}{2.333 - 1.4983} = .734$$

where $COV(45^\circ) = \frac{1}{18}(0\cdot0\cdot4 + 0\cdot1\cdot1 + 0\cdot2\cdot0 + 0\cdot3\cdot0 + 1\cdot0\cdot1 + 1\cdot1\cdot2 + 1\cdot2\cdot2 + 1\cdot3\cdot0 + 2\cdot0\cdot0 + 2\cdot1\cdot2 + 2\cdot2\cdot4 + 2\cdot3\cdot1 + 3\cdot0\cdot0 + 3\cdot1\cdot0 + 3\cdot2\cdot1 + 3\cdot3\cdot0) - \frac{1}{(18)^2}(0\cdot5 + 1\cdot5 + 2\cdot7 + 3\cdot1)^2$

$$VAR(45^\circ) = \frac{1}{18}(0^2\cdot5 + 1^2\cdot5 + 2^2\cdot7 + 3^2\cdot1) - \frac{1}{(18)^2}(0\cdot5 + 1\cdot5 + 2\cdot7 + 3\cdot1)^2$$

Figure 5 illustrates the calculation of texture context features at distance 1 for the image of Figure 3a.

SCRU	ORCHR
AVG	1
DEV	7
AVG	9
AVG	12

SCRU	H WOO
AVG	3
AVG	7

SCRU	URBA
AVG	1
AVG	2
RANGE	4
DEV	4
AVG	4
AVG	5
DEV	7
AVG	8
AVG	9
RANGE	9
DEV	9
AVG	12

SCRU	SUBUR
AVG	1
RANGE	2
DEV	2
RANGE	3
DEV	3
RANGE	4
DEV	4
AVG	4
AVG	5
DEV	6
AVG	8
AVG	8
AVG	9
AVG	12

SCRU	LAK
RANGE	3
DEV	3
AVG	3
AVG	5
AVG	7
AVG	9

SCRU	MARS
DEV	2
RANGE	3
DEV	3
AVG	4
DEV	7

SCRU	SWAM
AVG	1
AVG	2
RANGE	2
DEV	2
RANGE	3
DEV	3
AVG	3
RANGE	4
DEV	4
AVG	4
AVG	5
DEV	6
AVG	6
AVG	7
AVG	8
AVG	9
AVG	10
AVG	12

SCRU	RAILY
AVG	1
RANGE	2
DEV	2
RANGE	3
DEV	3
RANGE	4
DEV	4
AVG	4
AVG	5
DEV	7
AVG	8
AVG	9
AVG	10
AVG	12

ORCHR	H WOO
AVG	1
AVG	2
AVG	5
RANGE	8
DEV	8
AVG	8
AVG	9

ORCHR	URBA
AVG	1

ORCHR	SUBUR
RANGE	2
DEV	2
DEV	3
RANGE	4
DEV	4
AVG	4
AVG	8

ORCHR	LAK
AVG	1
AVG	2
DEV	3
AVG	3
AVG	5
DEV	7
AVG	8
RANGE	8
DEV	8
AVG	9
AVG	12

ORCHR	MARS
RANGE	2
DEV	2
DEV	3
AVG	5
RANGE	6
DEV	6
AVG	9
AVG	12

ORCHR	SWAM
AVG	2
RANGE	2
DEV	2
RANGE	3
DEV	3
AVG	3
RANGE	4
DEV	4
AVG	4
AVG	5
DEV	6
DEV	8
AVG	8
AVG	9
AVG	12

H WOO	SUBUR
AVG	1
AVG	2
AVG	3
RANGE	4
DEV	4
AVG	5
RANGE	6
DEV	6
RANGE	8
DEV	8
AVG	8
AVG	9
AVG	12

H WOO	LAK
AVG	5
AVG	9

H WOO	MARS
AVG	4
AVG	8

H WOO	SWAM
AVG	1
AVG	2
RANGE	2
DEV	2
RANGE	3
DEV	3
AVG	3
RANGE	4
DEV	4
AVG	4
AVG	5
RANGE	5
DEV	5
AVG	6
AVG	6
RANGE	6
DEV	6
AVG	7
AVG	8
AVG	9
AVG	10
AVG	12

H WOO	URBA
AVG	1
AVG	2
AVG	3
RANGE	4
DEV	4
AVG	4
AVG	5
RANGE	6
DEV	6
RANGE	8
DEV	8
AVG	8
AVG	9
AVG	12

URBA	RAILY
RANGE	3

SUBUR	LAK
AVG	1
AVG	2
AVG	3
AVG	4
RANGE	4
DEV	4
AVG	5
RANGE	6
DEV	6
RANGE	7
DEV	7
AVG	8
AVG	9
AVG	12

SUBUR	MARS
AVG	1
RANGE	4
DEV	8
AVG	9

SUBUR	SWAM
AVG	2
RANGE	2
DEV	2
RANGE	3
DEV	3
AVG	3
AVG	4
AVG	6
AVG	7
RANGE	8
DEV	8
AVG	8
AVG	9
AVG	12

SUBUR	RAILY
AVG	4
AVG	5
RANGE	6
DEV	6
RANGE	7
DEV	7
AVG	8
AVG	9
AVG	12

LAK	SWAM
AVG	1
RANGE	2
DEV	2
RANGE	3
DEV	3
RANGE	4
DEV	4
AVG	4
AVG	5
RANGE	6
DEV	6
RANGE	8
DEV	8
AVG	8
AVG	9
AVG	12

LAK	RAILY
AVG	1
RANGE	2
AVG	3
RANGE	3
RANGE	4
DEV	4
AVG	4
AVG	5
DEV	6
RANGE	8
DEV	8
AVG	8
AVG	9
AVG	12

MARS	SWAM
RANGE	2
DEV	2
RANGE	3
DEV	3
AVG	4
AVG	6
AVG	8

MARS	RAILY
RANGE	4
DEV	4

SWAM	RAILY
AVG	2
AVG	3
AVG	4
RANGE	4
DEV	4
RANGE	5
DEV	5
AVG	6
AVG	7
AVG	8
RANGE	8
DEV	8

FEATURE	DISTANCE 1	3	9
ASM	1	5	9
ASMD	2	6	10
COR	3	7	11
ASMID	4	8	12

KEY TO VARIABLE NUMBERS

Figure 6a tabulates for each category pair which of the 36 feature variables can separate the category pair.

Figure 6b is a continuation of Figure 6a and tabulates for each category pair which of the 36 feature variables can separate the category pair.

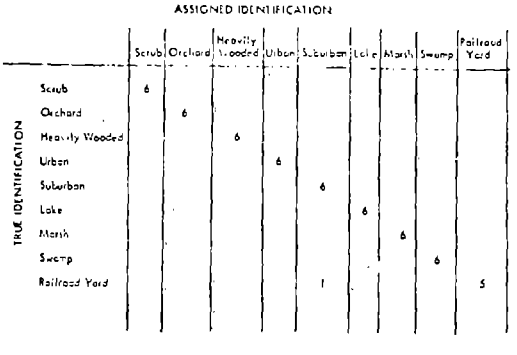

Figure 7 shows contingency table of true identification when statistics are gathered from the full 54 samples and the assignments are made on all the 54 samples.

ASSIGNED IDENTIFICATION

TRUE IDENTIFICATION	Scrub	Orchard	Heavily Wooded	Urban	Suburban	Lake	Marsh	Swamp	Railroad Yard
Scrub	4	1	1						
Orchard		4		1			1		
Heavily Wooded	1		4			1			
Urban				3	2		1		
Suburban				1	3		1		1
Lake			1			5			
Marsh				1		1	4		
Swamp								6	
Railroad Yard									5

Figure 8 shows contingency table of true identification versus assigned identification when the following experiment is repeated 54 times: statistics are gathered from 53 samples and an assignment is made on the 54th sample.

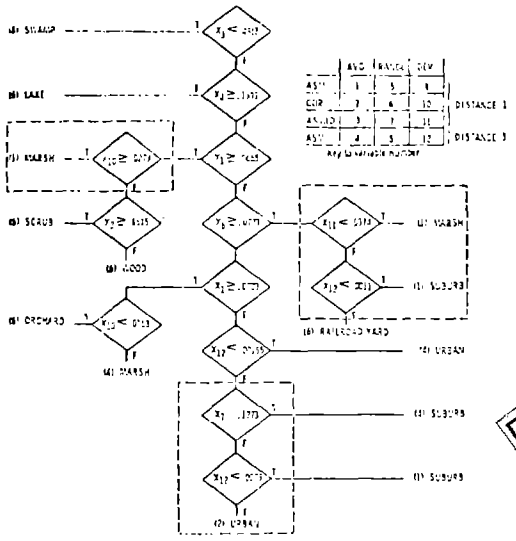

Figure 9 diagrams the Optimal Dichotomous Key (Sequential decision rule).

ASSIGNED IDENTIFICATION

TRUE IDENTIFICATION	Scrub	Orchard	Heavily Wooded	Urban	Suburban	Lake	Marsh	Swamp	Railroad Yard
Scrub	6								
Orchard		6							
Heavily Wooded			6						
Urban				4	2				
Suburban					5				1
Lake						6			
Marsh			1				4		1
Swamp								6	
Railroad Yard									6

Figure 10 shows contingency table of true identification versus assigned identification for the dichotomous key of 8 decision points. The total probability of correct identification is $\frac{49}{54}$ or 91%.

APPENDIX III

by

Robert M. Haralick
James D. Young
Dinesh K. Goel
K. Sam Shanmugam
Center for Research, Remote Sensing Laboratory
University of Kansas
Lawrence, Kansas

A COMPARATIVE STUDY OF DATA COMPRESSION TECHNIQUES FOR DIGITAL IMAGE TRANSMISSION

ABSTRACT

We investigate three methods of data compression for aerial image data: (1) Differential Pulse Code Modulation, (2) Principal Components, and (3) Hadamard Transform. We compare these methods in terms of data compression factor versus rms error. Our comparison indicates that the Principal Components method is uniformly better than the Hadamard Transform method. Furthermore, for compression ratios greater than 5, the Hadamard Transform and Principal Component technques are better than the Differential Pulse Code Modulation. It is only for scenes which are relatively unstructured and compressed at compression ratios of less than 5 that Differential Pulse Code Modulation performs better.

INTRODUCTION

Since there is a high positive correlation between the grey levels of spatially adjacent resolution cells on aerial imagery, the imagery contains a large amount of redundant information. Hence, image data is a good candidate for data compression which would, for example, permit more images to be stored per roll of tape or permit more images to be transmitted per unit time over a given communication channel. And, in fact, several image data compression techniques have been suggested and are in use to eliminate many of the digital bits representing redundant information (see the special issue on redundancy reduction, Proceedings of the IEEE, Vol. 55, 1967; Arguello, 1971; Wilkins and Wintzs' bibliography on data compression, 1971; Claire, et al., 1971). In this paper, we investigate three methods of data compression:

(1) Differential Pulse Code Modulation
(2) Principal Components
(3) Hadamard Transforms

In reviewing some of the picture coding techniques, W. F. Schreiber (1967) had indicated that it is very difficult to compare the different data compression techniques because of the great disparity in the subject matter, methods of evaluation and reproduction of output pictures. The approach used in this study provides an unified method of comparing different data compression techniques since we have used the same images, approximately the same data compression factors, and the same method for evaluation and reproduction of reconstructed images.

DIFFERENTIAL PULSE CODE MODULATION

The statistical relationship between nearby picture elements and the greater sensitivity of the eye to spatial and temporal grey tone differences to absolute grey tone values has led to suggestions for data compression using grey tone differences (Seyler, 1965). The most straight-forward technique is called Differential Pulse Code Modulation (DPCM). Here the data is compressed by transmitting the quantized difference between the correct grey tone at the transmitter and the last reconstructed spatially adjacent grey tone at the receiver (O'Neal, 1966). The data compression is accomplished in the quantizing step since the number of possible quantizer levels used to transmit the grey level differences between spatially adjacent resolution cells is smaller than the number of possible levels used to transmit the actual grey tones at each resolution cell. Because differential quantizing tends to preserve edge information, for any given number of bits per image element, it tends to produce better quality images than ordinary Pulse Code Modulation.

PRINCIPAL COMPONENTS

In the Principal Component method, the image is first split into a number of small mutually exclusive spatial regions and we shall consider the grey tones of these regions to be N-dimensional vectors sampled from source probability distribution. The image is then a collection of these vectors. In the principal component method, these N-dimensional vectors are projected onto some smaller K-dimensional subspace having maximal variance. In this way, the N components of the original vectors may be expressed in terms of K components, thereby achieving some data compression.

An optimal set of coordinates for the K-dimensional subspace is the set of K eigen vectors having largest eigenvalues of the covariance matrix of the sample of N-dimensional vectors. The principle on which this method is based, namely, the Karhunen-Loeve expansion, is well known (Watanabe, 1965). However, this technique has been used on a rather limited basis for image compression applications, even though it has been known to lead to very good comparison performances for analog data such as EKG (Andrews, et al., 1967) and multispectral scanner data (Ready, et al., 1971).

HADAMARD TRANSFORM

In the Hadamard Transform data compression technique, the image is split up into small spatial regions as in principal components. The lower sequencies of the Hadamard Transform of these regions are then transmitted. The image is reconstr-cted at the receiver using the same lower sequency functions. The method works

because the image data there is usually a high positive correlation between adjacent resolution cells and, therefore, the image tends to have a characteristic frequency spectrum with the low frequencies dominating the high frequencies. And although a Hadamard sequency is not the same as the frequency, their general behavior is often similar. Hence, in image data, the low sequencies tend to dominate the high sequencies. Data compression is achieved by use of only the few dominant sequency components. Pratt, et al., 1969, has used the Hadamard Transform for image data compression by transmitting the entire quantized Hadamard Transform of the image.

RESULTS

For comparison purposes a set of sixty-six digital images were processed using the three methods of data compression. These images were obtained by digitizing sections of aerial photographs containing a wide variety of scenes. Eleven scene categories, with six images for each type of scene, were processed. The scenes included both natural scenes such as wooded areas, lakes, and man-made scenes such as urban areas, suburban areas and railroad yards. The digitized images were of 64 x 64 size and the grey levels of individual cells had been quantized into 64 levels.

Using computer programs, the images were transmitted and the RMS errors between the original integer images and the corresponding reconstructed integer images were computed. For each type of scene, the average RMS error was calculated by averaging the rms errors of the six images of the scene. The original and reconstructed images were digitally printed out using 13 grey levels. These digital printouts provide the basis for visual comparison of the original and reconstructed images.

A comparison in terms of data compression factor versus rms error between the original image and the reconstructed compressed image indicate that Principal Components is uniformly better than Hadamard Transforms. Furthermore, for compression ratios greater than 5, Principal Components and Hadamard Transforms are better than Differential Pulse Code Modulation. It is only for relatively unstructured scenes compressed at compression ratios less than 5 that the Differential Pulse Code Modulation performs better. Plots of rms error vs data compression factor for four scene categories are shown in Figure 1.a-d.

Visual comparison of the images compressed by the three methods tend to support the following conclusions:

(1) Of the images compressed by the three procedures, the images compressed by the principal components procedure most resemble the original images.

(2) The images compressed by the Hadamard transform procedure are comparable to the images produced by the principal component procedure. However, these images have a "checkerboard" look.

(3) DPCM procedure tends to "blurr" the boundary lines in the images. At high data compression factors, the images compressed by the DPCM procedure bore very poor resemblance to the original.

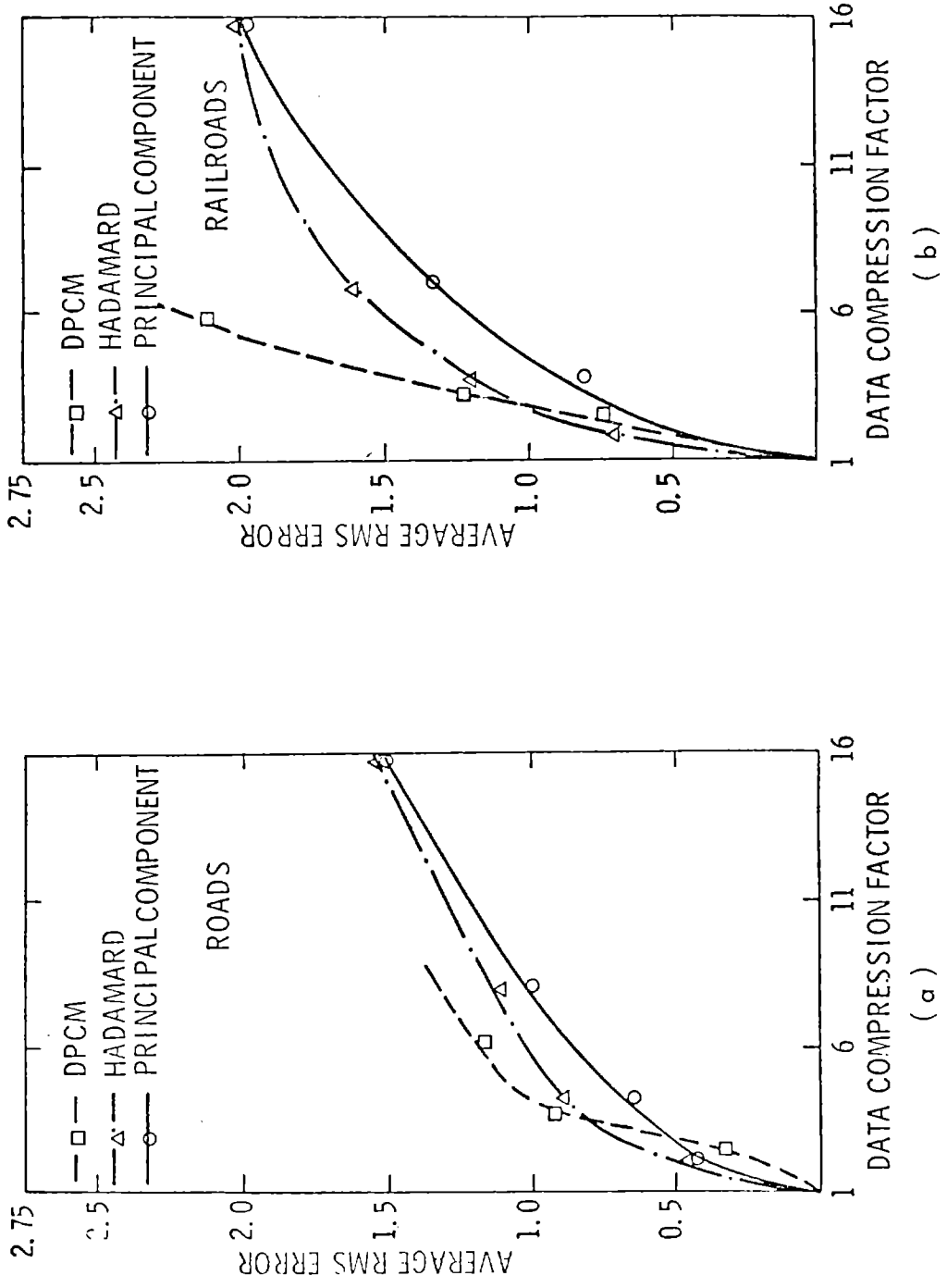

Figure 1. - Data Compression Factor vs. RMS Error

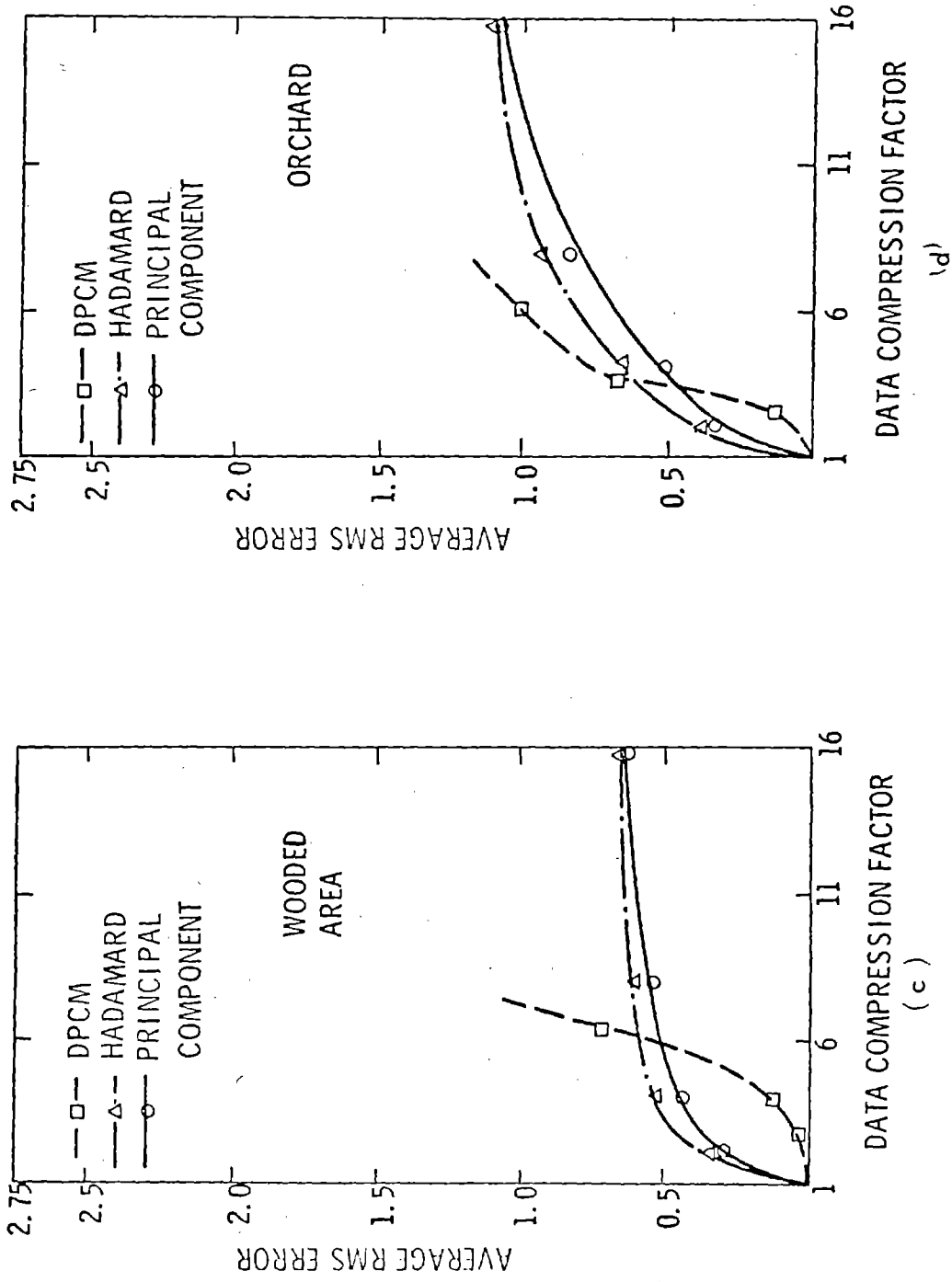

Figure 1. -Data Compression Factor vs. RMS Error

REFERENCES

1. Roger J. Arguello, "Encoding, Transmission and Decoding of Sampled Images," Proceedings of the Perkins-Elmer Symposium on Encoding Transmission and Decoding of Sampled Images, Perkins-Elmer Co., 1971.

2. Proceedings of the IEEE, Special Issue on Redundancy Reduction, vol. 55, pp. 253-401, March 1967.

3. A. J. Seyler, "Statistics of Television Frame Differences," Proceedings of the IEEE, vol. 53, pp. 2127-2128, December 1965.

4. J. B. O'Neal, "Predictive Quantizing for Transmission of TV Signals," Bell Sys. Tech. J., vol. 45, pp. 689-722, October 1966.

5. S. Watnabe, "Karhunen-Loeve Expansion and Factor Analysis," Tran. 4th Prague Conf. on Information Theory, 1965.

6. C. A. Andrews, J. M. Davies and G. R. Schwarz, "Adaptive Data Compression," Proceedings of the IEEE, vol. 55, pp. 267-277, March 1967.

7. William K. Pratt, Julius Kane, Harry C. Andrews, "Hadamard Transform Image Coding," Proceedings of the IEEE, vol. 57, pp. 58-68, January 1969.

8. J. B. O'Neal, "Data Modulation Quantizing Noise Analytical and Computer Simulation Results for Gaussian and Television Signals," Bell Sys. Tech. Journal, January 1966.

9. H. L. Vantries, "Detection, Estimation and Modulation," John Weily, New York, 1968.

10. K. W. Cattermole, "Principles of Pulse Code Modulation," American Elsevier Pub. Comp., New York, 1969.

11. R. M. Haralick and D. Anderson, "Texture Tone Study with Applications to Digitized Images," Technical Report No. 182-2, 1972, University of Kansas Center for Research, Inc., Lawrence, Kansas 66044.

12. W. F. Schreiber, "Picture Coding," Proceedings of the IEEE, vol. 55, pp. 320-330, March 1967.

13. H. C. Andrews, "Computer Techniques in Image Processing," Academic Press, 1970, New York.

14. L. C. Wilkins and Paul A. Wintz, "Bibliography on Data Compression, Picture Properties and Picture Coding," IEEE Trans. Inf. Theory, vol. IT-17, pp. 180-197, March 1971.

15. E. J. Claire, S. M. Forber, and R. R. Green, "Practical Techniques for Transform Data Compression/Image Coding," IEEE Trans. on Electromagnetic Compatibility, vol. EMC-13, pp. 1-5, Aug., 1971.

16. P. R. Ready, P. A. Wintz, S. J. Whitsitt and J. A. Landgrebe, "Effect of Compression and Random Noise on Multispectral Data, Proceedings of the Seventh International Symposium on Remote Sensing of Environment, pp. 1321-1342, University of Michigan, Ann Arbor, May, 1971.

17. D. A. Landgrebe, "The Development of Machine Technology Processing for Earth Resources Survey," Third Annual Earth Resources Program Review, NASA MSC Report # MSC 03742, December, 1970.

RADAR SIGNATURE AND SYSTEMS STUDIES AT KANSAS UNIVERSITY

by

Richard K. Moore, Director
Remote Sensing Laboratory
The University of Kansas
Lawrence, Kansas 66044

The radar signature and systems studies described here have concentrated in two areas: octave bandwidths radar spectrometry, using a truck-mounted system, and scatterometry using primarily the 13.3 GHz system on the NASA/MSC aircraft. In addition, the results of the experiments to date have been synthesized into a pair of representative designs for spacecraft radar systems—one for small spacecraft and one for large spacecraft.

Our activities in the use of radar images have been described by Haralick, McCauley and Morain, so this paper concentrates on the non-imaging systems, except in the final system design.

OCTAVE BANDWIDTH SPECTROMETRY

Responses over several octaves in the visible and infrared ranges of the spectrum have been measured for decades. In the microwave region of the spectrum, however, both active and passive systems have concentrated on single spot frequencies and measurements of continuous responses are new. We have reason to believe that the resonances that occur in nature in the microwave region will give rise to variations in response with frequency comparable in magnitude to those observed in the visible and infrared regions; but the work described here is to our knowledge the first extensive effort to determine such responses.

The University of Kansas radar spectrometer is mounted on a "cherry picker" truck that permits measurements from a height of about 12 meters. The system operates in the octave from 4 to 8 GHz, a wavelength range of 7.5 to 3.75 cm. This range was originally chosen because it was the highest frequency range for which octave bandwidth equipment is readily available. Because most of the imaging radar equipment operates at higher frequencies and because spectral responses over a wider bandwidth are desirable, the equipment is currently being extended to an upper-frequency limit of 18 GHz (1.67 cm).

The original octave bandwidth spectrometer was a pulse system that used bursts of energy 20 ns long (3 m resolution). The system was built that way so it could also be used to produce radar images in which panchromatic averaging was used. The value of the panchromatic averaging for images has now been demonstrated, and the system used in the summer of 1971 was modified from a pulse to an FM system to permit use at shorter ranges. The original pulse system would not allow vertical incidence measurements from the 12 m height, since the closest range that could be observed was about 24 m; the new system is useable at ranges as short as 5 m.

Figure 1 shows a block diagram of the system currently in use. The signal is obtained from a standard sweep oscillator and amplified to a level as high as 20 watts. The output of the amplifier is leveled with a feedback loop. The signal is transmitted through an appropriate circulator, but a sample of the signal is fed into a mixer where it is combined with the received signal. Because the transmitted signal has changed frequency during the time for the wave to travel from the antenna to the ground and back, the mixer observes two different frequencies: the one being transmitted and the one that was transmitted a short time before. The difference frequency for these experiments was set at 37 kHz; this difference frequency was amplified and filtered and the output observed on a voltmeter. Averaging was achieved by sweeping over a bandwidth of approximately 0.4 GHz for each measurement. The center frequency for the sweep was stepped between measurements.

Measurements were made during July of 1971 at more than 80 fields in the vicinity of Lawrence, Kansas. Different orientations were used relative to the rows of crops so that the effect of look direction could be established.

The system was calibrated by measuring the return from a metal sphere suspended by nylon string from the guy wire of a radio station. Because of some doubt regarding the accuracy of this calibration, the data presented have been normalized to the data observed for returns from cornfields since more cornfields were sampled than fields of any other crop.

Figure 2 shows the variation with angle at a frequency near the bottom of the band of the instrument. Since normalization is with regard to corn, corn shows no variation, whereas the other crops observed—soybeans, alfalfa and sorghum—do show an angular variation. This sort of curve is similar to that obtained by the usual single frequency scatterometer. Notice the difference between the shape of the curves for horizontal and vertical polarization.

Figure 3 shows similar curves at 5.8 GHz, and Figure 4 shows the result at 7.4 GHz near the top of the frequency band of the instrument. Variations in the angular behavior at the different frequencies are apparent. The data are still being examined for consistency and for interpretation of these variations.

Results like those shown in Figures 2, 3, and 4 could have been obtained with fixed frequency scatterometers, although in this case the broad bandwidth permitted better averages at each angle than would have been possible with narrow bandwidth systems. Figure 5 shows the variation across the band as a function of frequency—a type of presentation possible only with the octave bandwidth system. Again, note the difference between the shape of the curve for vertical and horizontal polarization, and note also that at this angle of incidence (30°) the sorghum is uniformly low but not too different from the corn for horizontal polarization, whereas alfalfa peaks somewhat below the middle of the frequency range but is lower on both sides and soybeans are low at low frequencies but higher at the high frequency end. The variations are not as pronounced for vertical polarization, but they are present there too.

Figure 6 shows similar results plotted for an incidence angle of 50°. Notice that at this incidence angle the trends are different and the variations for vertical polarization are considerably more striking than at the steeper incident angle.

These results are only samples; the data are still being analyzed. Measurements were made at angles from vertical incidence (0°) to 70°, and the angular curves could have been plotted for each of the frequencies shown as points on the spectral curve.

A major purpose of the broad spectrum measurements is to illustrate the potential for polypanchromatic radar systems, i.e., for radars that attain averaging of the phase interference effects by panchromatic transmission, but split up the panchromatic band into segments to achieve spectral signatures. Observation of the curve of Figures 5 and 6 shows that some differences do exist, but a more striking illustration is obtained by using the mean of each one-third octave to set the brightness of one of the three primary colors (red, green, and blue), and combining these colors to achieve a resultant color characteristic of the particular spectral response. Figure 7 shows the result obtained by such color combination at four different angles for soybeans. Note that for vertical polarization the colors are all about the same—red—although there is significant difference for each angle for horizontal polarization. The problem for vertical polarization is that all the soybean echoes peak at the low frequency end of the spectrum. To obtain a greater variability the spectral response was normalized relative to the average for all crops at a given angle, and the deviation from this average used to determine the color in each one-third octave band. Figure 8 shows what this does to the colors of Figure 7. Here not only have the colors for the horizontal polarization been changed, but there is some variation showing for vertical polarization. With the soybeans for the steeper incidence angles, however, the result is always white; that is, the variation across the band is small. Figures 9 and 10 show the similar result for 30° and 50° for all four crops. Clearly at either angle distinctions could be made between the crops on this basis if both polarizations are available, although at 30° horizontal polarization does not permit distinction between sorghum and soybeans, and vertical polarization between sorghum and alfalfa. At 50° with horizontal polarization, soybeans and alfalfa are the same, and with vertical polarization only alfalfa is different. Thus it appears that, in this part of the frequency range, both polarization and frequency are necessary to separate the crops; but the separation is quite adequate at each angle when both polarizations are used.

These results must be considered preliminary and further analysis may show that they are not completely consistent so that more data will have to be collected. Nevertheless we do believe that they show the potential of polypanchromatic systems and, indeed, final analysis of the data from July 1971 may verify the conclusions one can draw from these illustrations.

OCEANIC SCATTEROMETRY

A major effort has been expended over the last three years to evaluate fully the operating problems and capabilities of the 13.3 GHz scatterometer system flown on the MSC aircraft. Some of the reports issued dealing with analysis of the data and of the system itself are shown in Figure 11. Other reports have not been formally designated but have been provided to MSC in letter form or over the telephone, and still further analyses are being completed. We believe that the system can be considered reliable for measurement of the ratio of scattering coefficients at two angles for any given year, although differences exist from year to year because of changes in the antenna pattern caused by handling and more particularly by the change from the P3 aircraft for Missions 88 and 119 to the C130 aircraft for Mission 156. Data analysis techniques have been developed to compensate for these effects as much as possible.

Under a contract with the Naval Ordnance Laboratory, The University of Kansas has developed a scatterometer system of its own which has been flown this past year in a University aircraft. Figure 12 shows a photograph of the system mounted in the passenger compartment of the University aircraft. The two units on the left with handles visible are the scatterometer and its measuring instruments; the rest of the equipment shown has to do with the tape recorder which appears at the bottom of the illustration. This instrument has now flown both in the Arctic north of Alert and near Thule, and in Kansas, including the Garden City test site. Figure 13 shows representative data obtained from these missions. Further analysis of these data is continuing.

The major effort in recent years with the NASA/MSC scatterometer has been to collect and analyze oceanographic data. Because of possible variations in the calibration of the system, data have all been normalized to the scattering coefficient measured at 10°. This is a procedure that eliminates all effects of gain changes or changes in the calibration signal "constant." The analysis of the system shows that the calibration constant may in fact vary from mission to mission, although it should remain fixed during a particular mission.

Other potential error sources exist in the data reported here. A major source of error is knowledge of the windspeed itself. Even for the flights near the Argus Island tower, there is uncertainty about the windspeed, as described by Pierson and Moore in another paper in this meeting. Although the aircraft attitude is recorded when the ADAS is operating satisfactorily, error in this recording could cause use of the wrong gain value because of rapid fluctuations in the antenna pattern with depression angle. On some missions the ground speed measurement with the Doppler navigator on the aircraft appears to be inaccurate, and in fact some of the flight lines were made with estimates rather than with the Doppler measurement because of a failure of the Doppler system. Such an error in ground speed causes assignment of the scattering coefficient measured at a particular frequency to the wrong angle, which has the dual effect of showing it at the wrong angle and of causing use of the wrong antenna gain.

The effect of these potential error sources is believed to be random and to result in a scatter of points about the regression line. Nevertheless, the scatter is relatively small in terms of percentage of the wind speed or the measured scattering coefficient value. We are quite encouraged by the results.

Figure 14 shows the normalized scattering coefficient plotted versus the wind speed on a log-log plot for 35° incidence angle and the upwind direction. Note that the points for Mission 156 were raised 1.6 dB. The need for this is believed due to the change in the antenna pattern in moving the scatterometer from the P3 to the C130 aircraft. The dash-lines show the rms error about the regression line. The scattering coefficient varies approximately proportional to the 1.4 power of wind speed. There has been some discussion about the two points at 49 kts lying beneath the 1σ value. However, Figure 15 shows the same result for 25°, and the points for 49 kts at this angle lie almost exactly on the regression line. Thus we believe the 35° points may be partly in error due to some lack of knowledge of aircraft attitude and should not be construed as proving that some sort of "saturation" takes place.

Crosswind data are shown in Figure 16 for 35°. Here the 49 kt points lie above the regression line. Crosswind data for 25° are shown in Figure 17 where again the 49 kt points lie rather high. Notice that at 25° the wind speed variation for

both upwind and crosswind is significantly less than it is at 35°, and that for crosswind the variation is less than for upwind.

A similar analysis has been conducted of Naval Research Laboratory observations available to us, namely those from JOSS I in 1970 and from the North Atlantic mission conducted from Ireland in 1969. Figure 18 shows a sample of the kind of variation observed for the NRL data where the points from the two missions have been separately fitted to regression lines. The regression lines have somewhat different slopes, but nevertheless they both show a variation significantly greater than linear. In our analysis of the NRL data, we have used the same technique that was used with the MSC data; that is, these two regression lines have been brought together at 20 kts and all the points on the lower line have been moved up by the amount necessary to make the lines intersect at that point. When this new cluster of points has been plotted, the modified points have been used in the regression program to obtain a new composite regression line.

The results of these analyses of NRL data are summarized in Figure 19 where the exponent in a power law variation of scattering coefficient with wind speed is plotted. The downwind data appear somewhat more consistent than the upwind data, but in both cases the scattering coefficient variation with wind speed is at least linear. Notice that for horizontal polarization and larger incidence angles the variation of scattering coefficient with wind speed approaches a square law. This indicates that horizontal polarization is superior to vertical polarization for radar anemometry of the sea, but it must be balanced against the weaker signal return for the horizontal signals for moderate seas and the consequent increase in required power.

Since the radar data is to be applied to anemometry, we felt it appropriate to plot "anemometer calibration curves" for our own and NRL data for the different angles, directions, and polarizations. In this case, the wind speed is the dependent variable and the scattering coefficient is the independent variable. Figures 20, 21, 22 and 23 show the MSC data plotted this way for upwind and crosswind for 35° and 25° again with the 1σ error bars shown alongside the trendlines. A better anemometer has a more nearly horizontal calibration line because this means that a larger variation in scattering coefficient is required to indicate a small variation in wind speed. Similar plots have been made for the NRL data; two samples are shown in Figures 24 and 25 for 60° upwind with horizontal and vertical polarization. Clearly the horizontal polarization, since it is significantly less steep than the vertical polarization, will make an anemometer less sensitive to errors in the measurement of the scattering coefficient.

A significant difference was noted between the North Atlantic and Bermuda missions, both for the MSC and for the NRL data. With the NRL data, we see no solid instrumental reason to expect this variation, although one can easily rationalize it in terms of changes in the MSC antenna pattern. It may be that other factors will have to be taken into account in using radar for anemometry, for instance the air/sea temperature differences or differences in the surface tension in different parts of the ocean. Presumably the further experimentation being conducted using the S193 Skylab experiment can answer some of these questions much better than any aircraft program making measurements in different parts of the ocean on different years.

ICE SCATTEROMETRY

Although an aircraft scatterometer may have operational application over the Arctic ice, a spacecraft scatterometer or radiometer will have such a poor resolution that it can only be used for gross measurements in the polar regions (or anywhere else for that matter). Thus, one of the major purposes of the scatterometer over the ice, as well as over land, is to determine the sensitivity and dynamic range required for a radar imager. Since the imager will be able to operate with fine resolution from spacecraft altitudes, it definitely is the preferred sensor for the ice.

The data from Mission 126 have been analyzed with this in mind. Figure 26 shows the spread of the average scattering coefficient for nine different ice types as a function of angle of incidence. Figure 27 shows this converted into dynamic range requirements for the ice imager. Clearly an imager operating at steep angles of incidence required wide dynamic range from about -12 to +15 dB; whereas an imager whose closest angle of incidence is only about 35° can get by with a dynamic range of considerably less than 20 dB as shown, but must have a sensitivity at least of -14 dB. Analysis of these data along these lines is continuing.

AGRICULTURAL SCATTEROMETRY

Figure 28 summarizes the agricultural scatterometry program. Unfortunately we have not received any complete data sets from the missions flown in the summer of 1970 or 1971. Preliminary data were received from Mission 130, flown in 1970, as requested. These were used during the summer of 1971 to establish improved format specifications for processing the remainder of the scatterometer data. By a preliminary examination of one line, it was possible to specify the most efficient use of the computer time for agricultural scatterometry. Also specified was the need for the automatic data output plot to be scaled so that it could be directly overlaid on a photographic mosaic. The data processing sample length was specified and the angular resolution frequency band required was also specified.

The 400 MHz scatterometer data flown in 1970 over the Garden City test site have been received and are being analyzed. No results are available yet.

SATELLITE RADAR SYSTEM

The major goal of our program is specification of appropriate satellite radar systems and their applications. This paper closes with a discussion of two representative systems which might be flown on satellites. These systems are not to be considered as final specifications; they could be modified in many ways depending upon the constraints associated with the satellite.

Figure 29 shows the specifications for a radar for a small satellite capable of supplying 450 watts of power. With this much power the system could have a resolution as fine as 10 m with a swathwidth of 40 km. To achieve this large swathwidth, however, requires erecting an antenna on the small satellite with a length of the order of 6 to 10 m. Note that if the radar is only used 20% of the time, the average power over an orbit is only 90 watts. The system was selected to operate out to an incidence

angle of 60° for geologic purposes. A 30° incident angle appears quite adequate for agricultural purposes and many geologic purposes. With such an incident angle the power requirement could be reduced to 275 watts, which means that the average over an orbit is only 55 watts.

Such a system would, we assume, transmit raw video data to the ground via a wideband telemetry link. Processing would then take place on the ground. The power for the telemetry link is not included in the figure. Of course, a system with a poorer resolution could get by with significantly less power for both radar and telemetry.

Figure 30 shows a possible system for a large satellite such as a shuttle. Here a polypanchromatic system is postulated with first the power required with no averaging, then that with 200 MHz, and then with 400 MHz averaging. The 200 MHz averaging gives about 10 independent samples per cell due to panchromatic illumination and the 400 MHz gives about 20 per cell. Note that this 4-frequency system requires a total of 975 watts without averaging, but with 10 independent samples per cell the power requirement goes up by a factor of about 10. The frequencies were chosen somewhat arbitrarily because we still do not have adequate data over a wide range. However, 16 GHz appears about the highest reasonable frequency for a spacecraft imaging system both from the standpoint of available components and of atmospheric effects. The 10 GHz band is quite common and many data have been gathered at this frequency that indicate the value of radar. Our recent observations over the octave bandwidth indicate that the 4 and 8 GHz regions are also useful. All of these frequencies are near to frequencies that may be available for allocation for imaging radar systems.

As our analysis of the observations both with the imaging radars and the radar spectrometer and scatterometer continue, we hope to be able to refine these specifications. Nevertheless we believe if a radar system could be constructed for spacecraft use immediately, these specifications could serve as a reasonable guide.

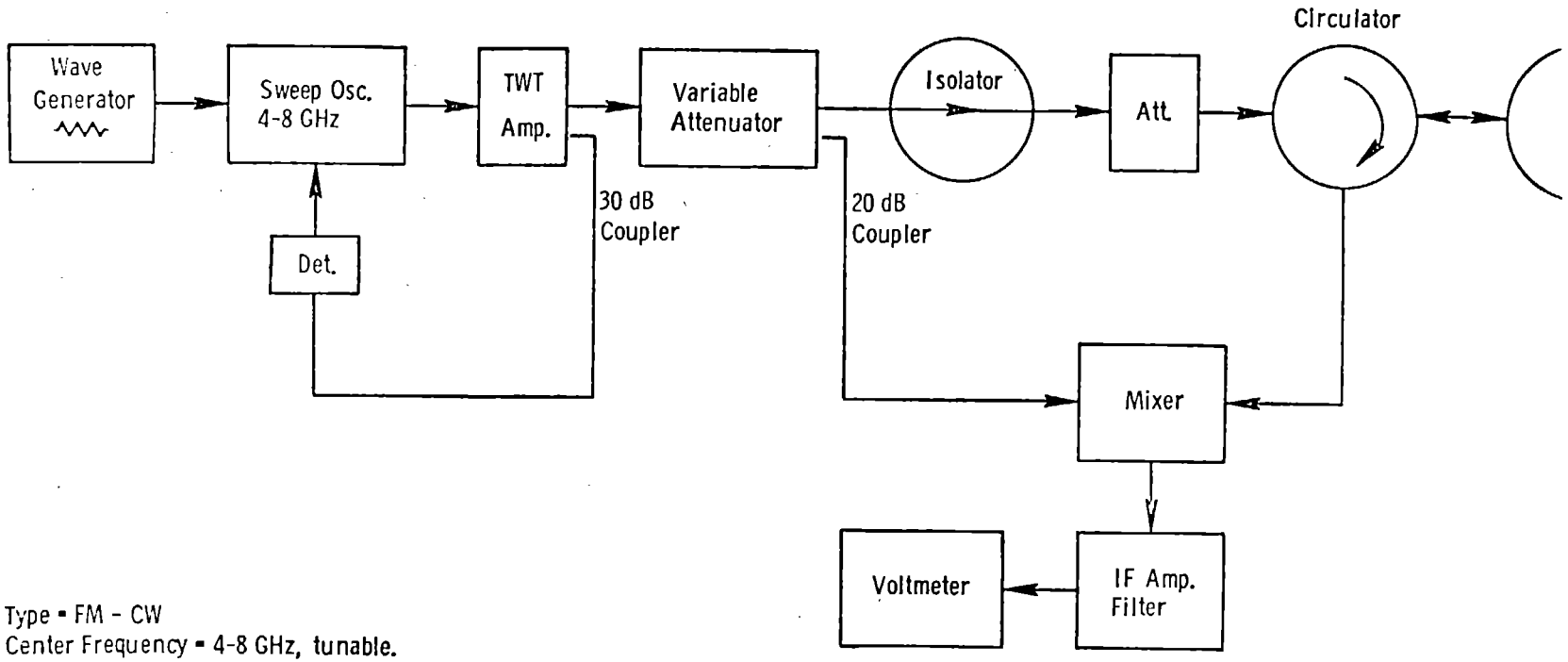

Type = FM - CW
Center Frequency = 4-8 GHz, tunable.
Modulation Bandwidth = 400 MHz
IF Frequency = 37 KHz
Antenna = 3' diameter dish

Figure 1. Block diagram of FM-CW Octave-Bandwidth Radar Spectrometer.

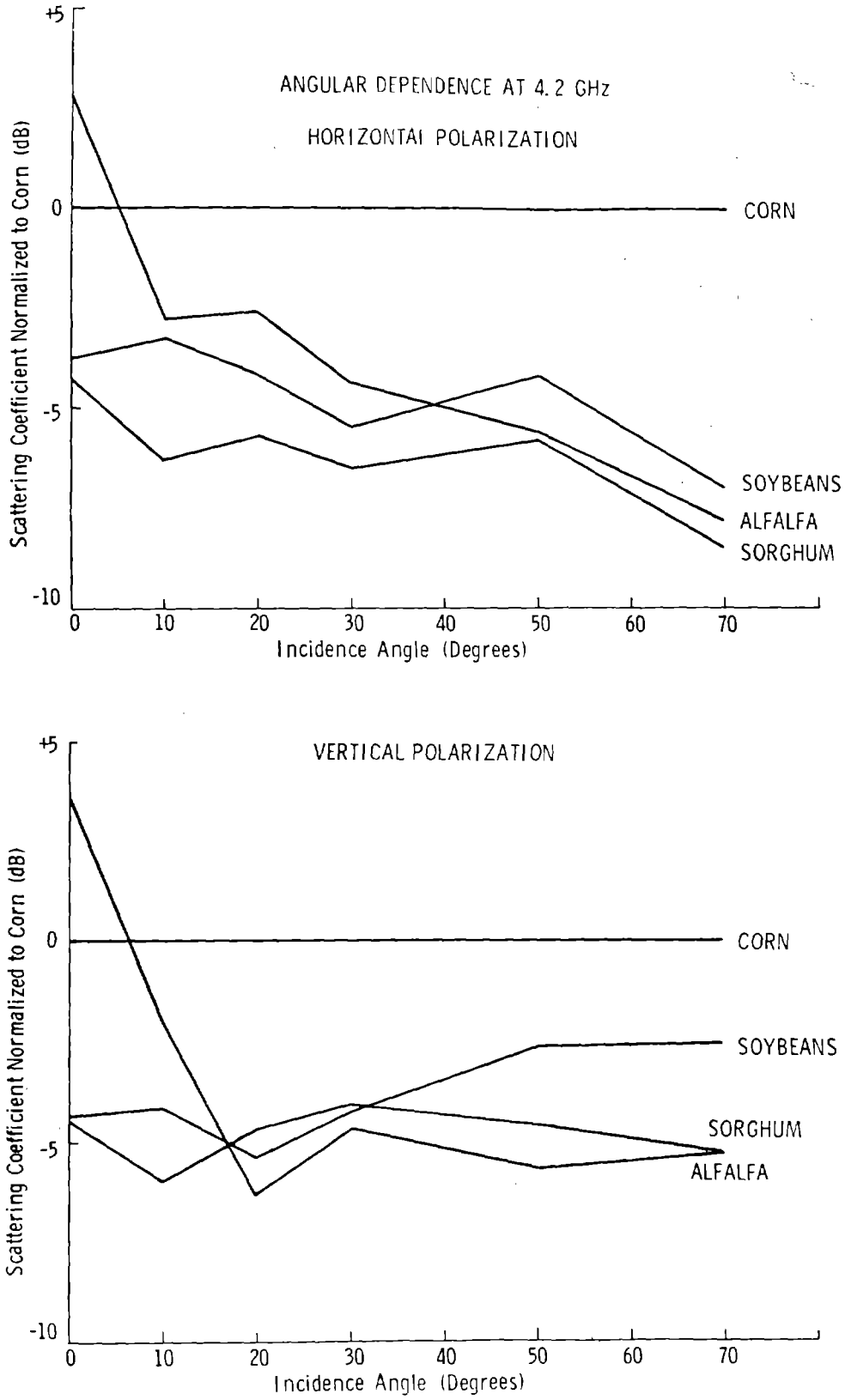

Figure 2. Example of single-frequency observations of radar backscatter, July 1971.

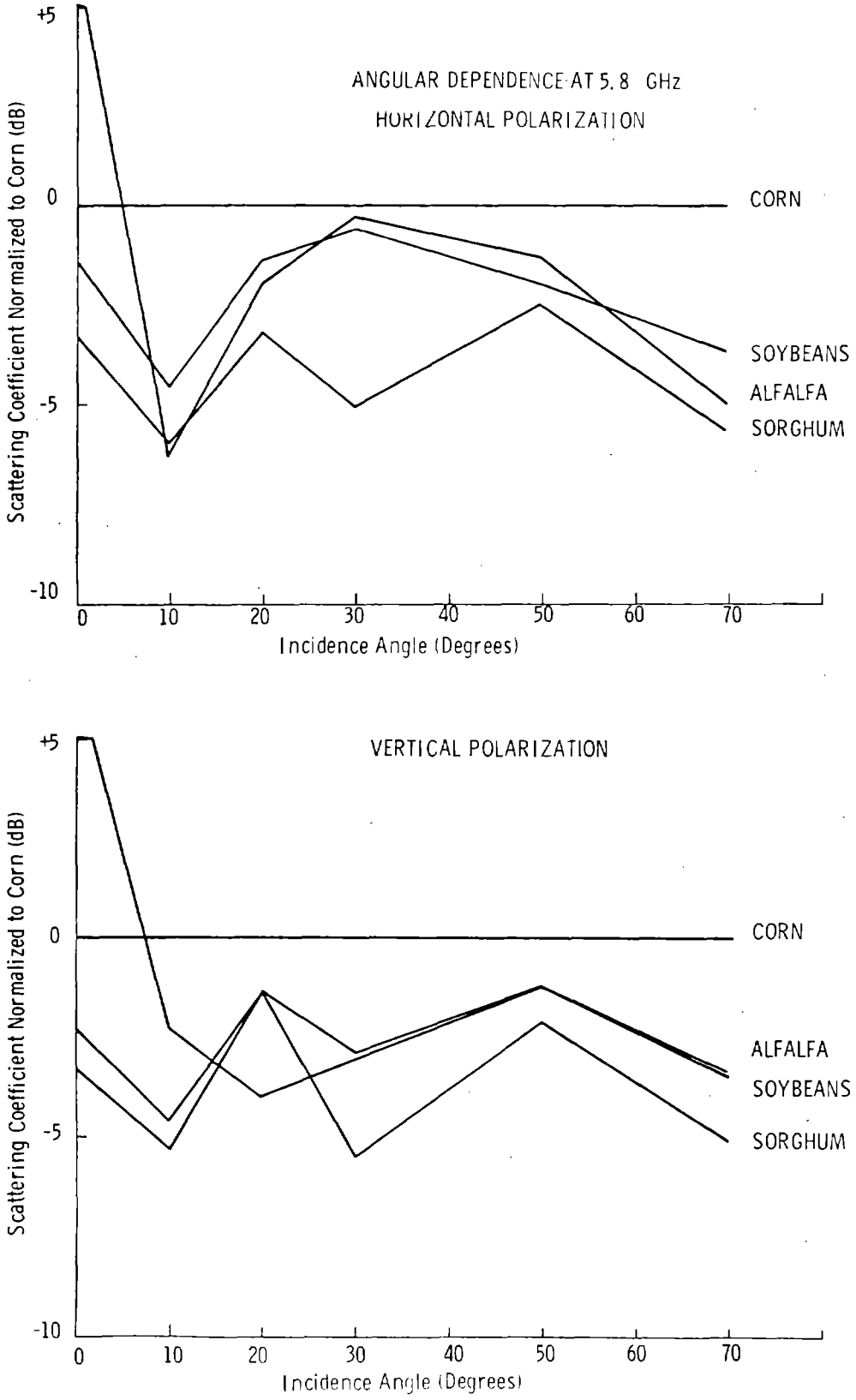

Figure 3. Example of single-frequency observations of radar backscatter, July 1971.

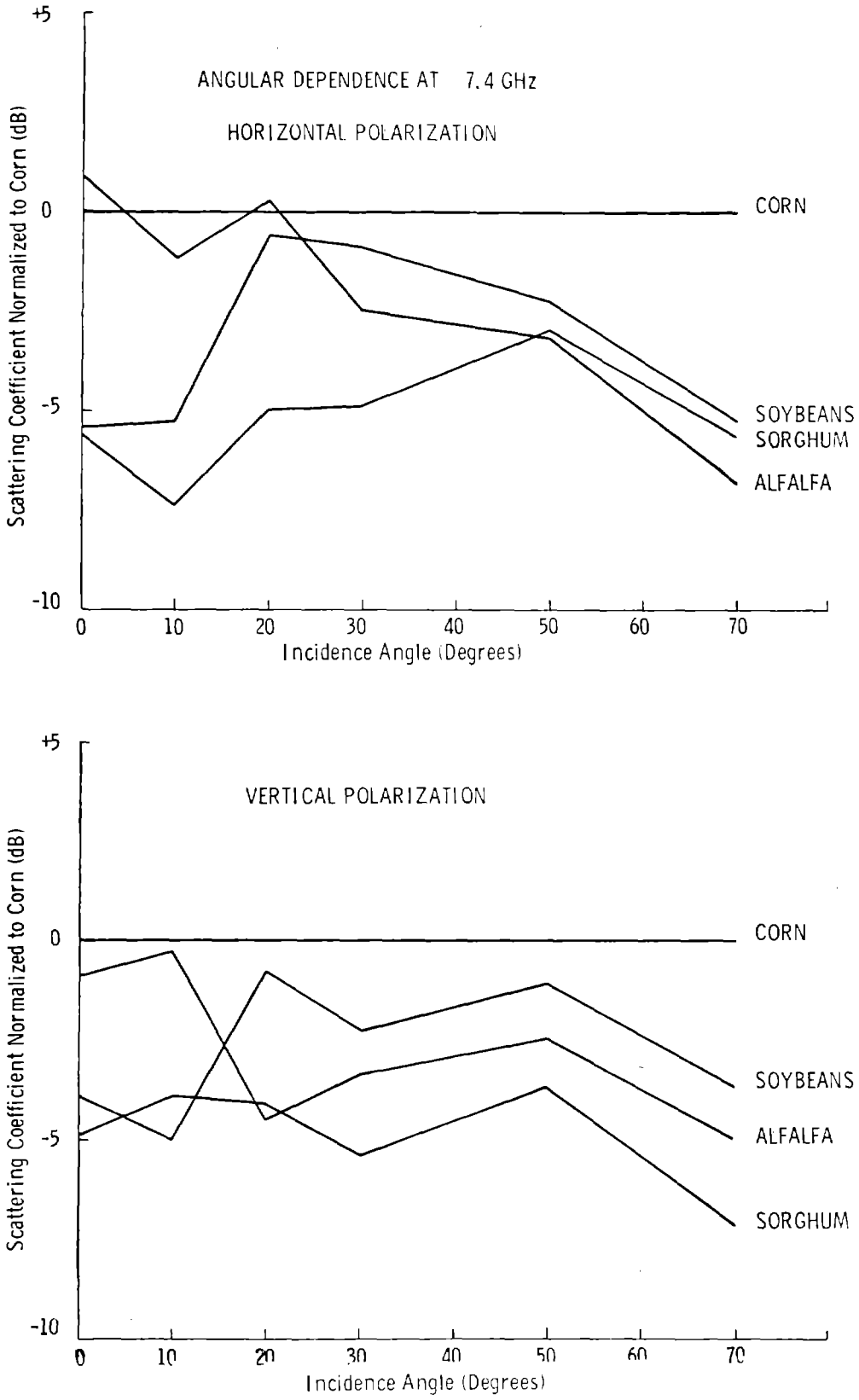

Figure 4. Example of single-frequency observations of radar backscatter, July 1971.

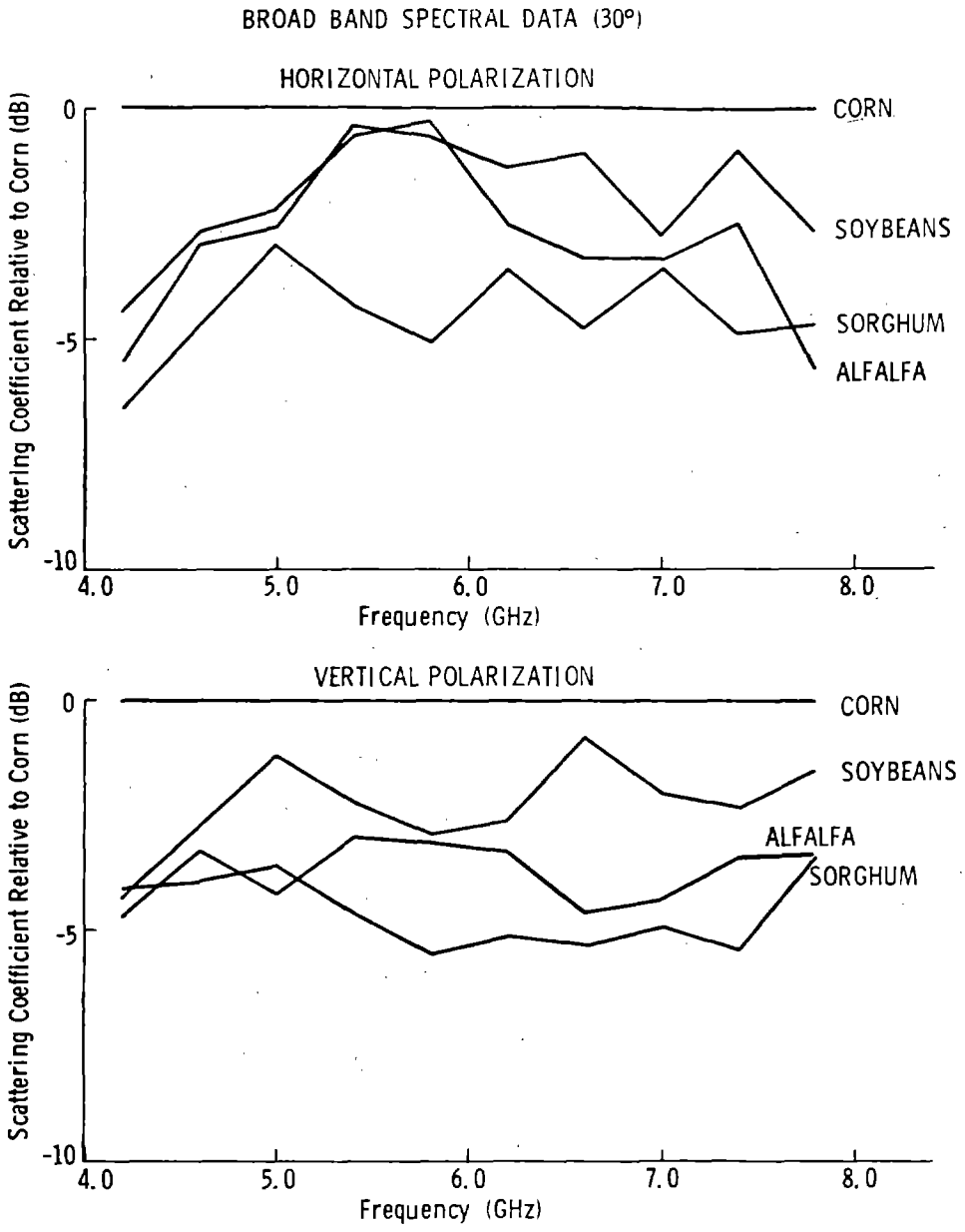

Figure 5. Example of radar spectral response, July 1971.

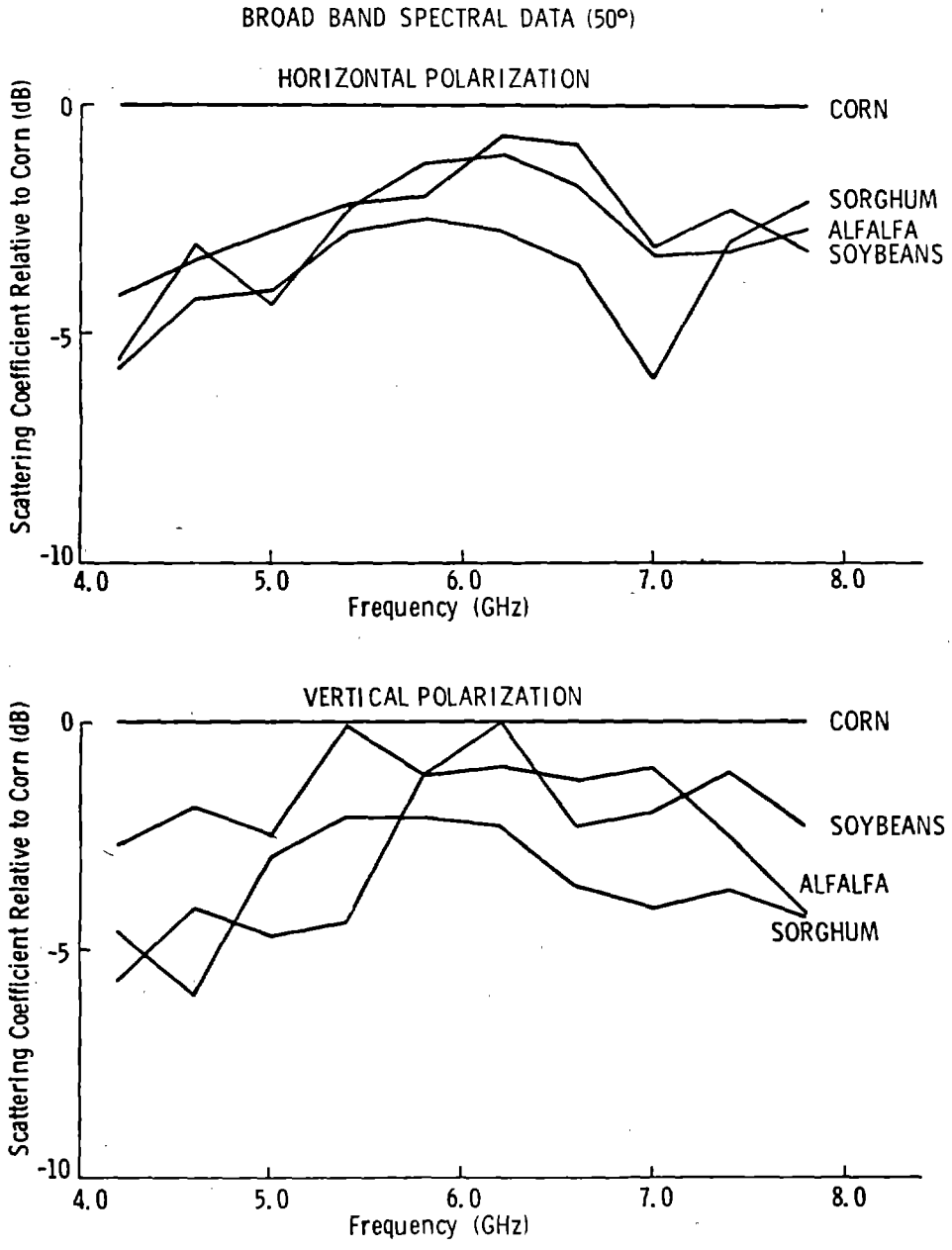

Figure 6. Example of radar spectral response, July 1971.

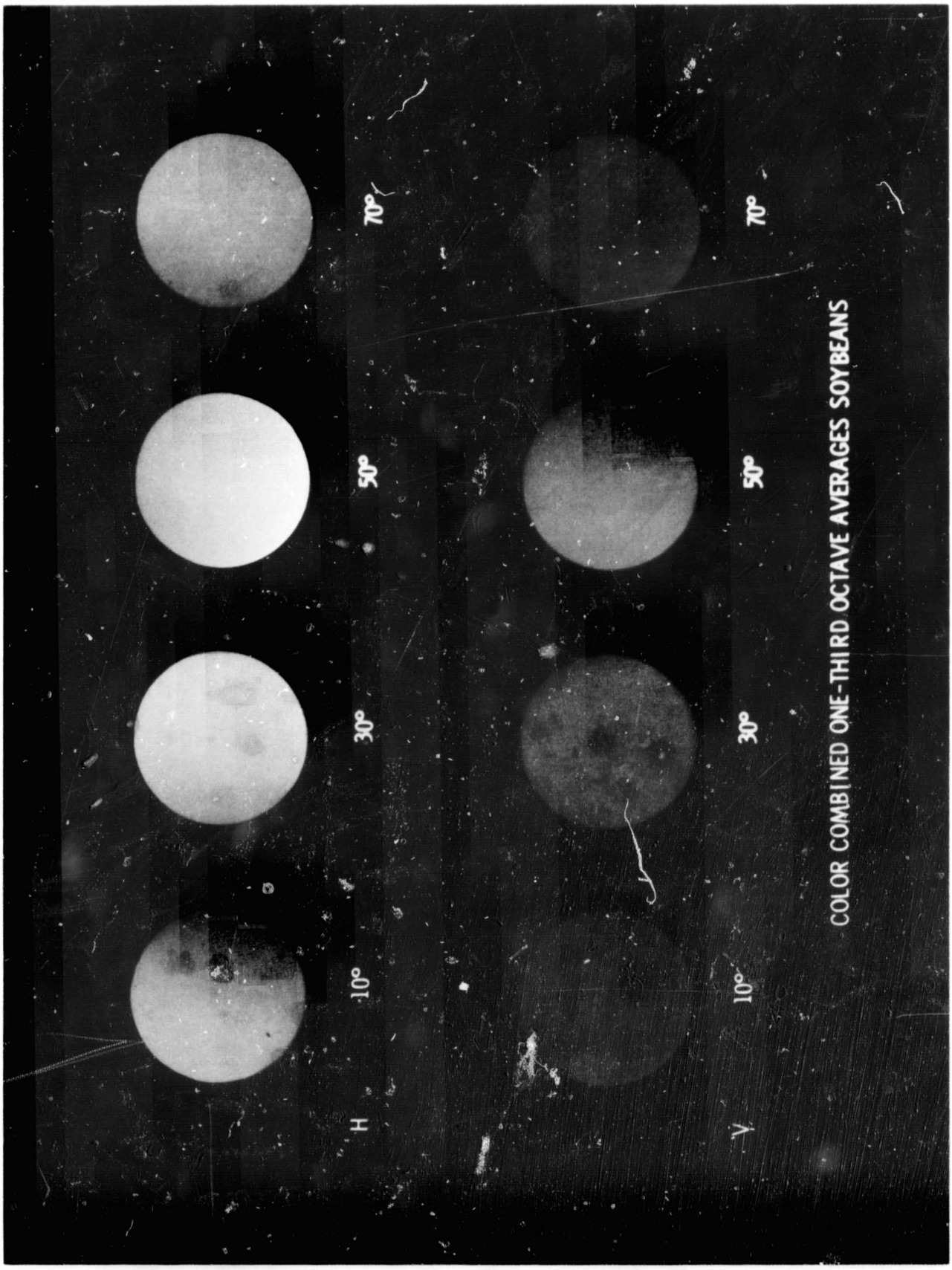
COLOR COMBINED ONE-THIRD OCTAVE AVERAGES SOYBEANS
H
V
10°
30°
50°
70°
10°
30°
50°
70°

Figure 7.

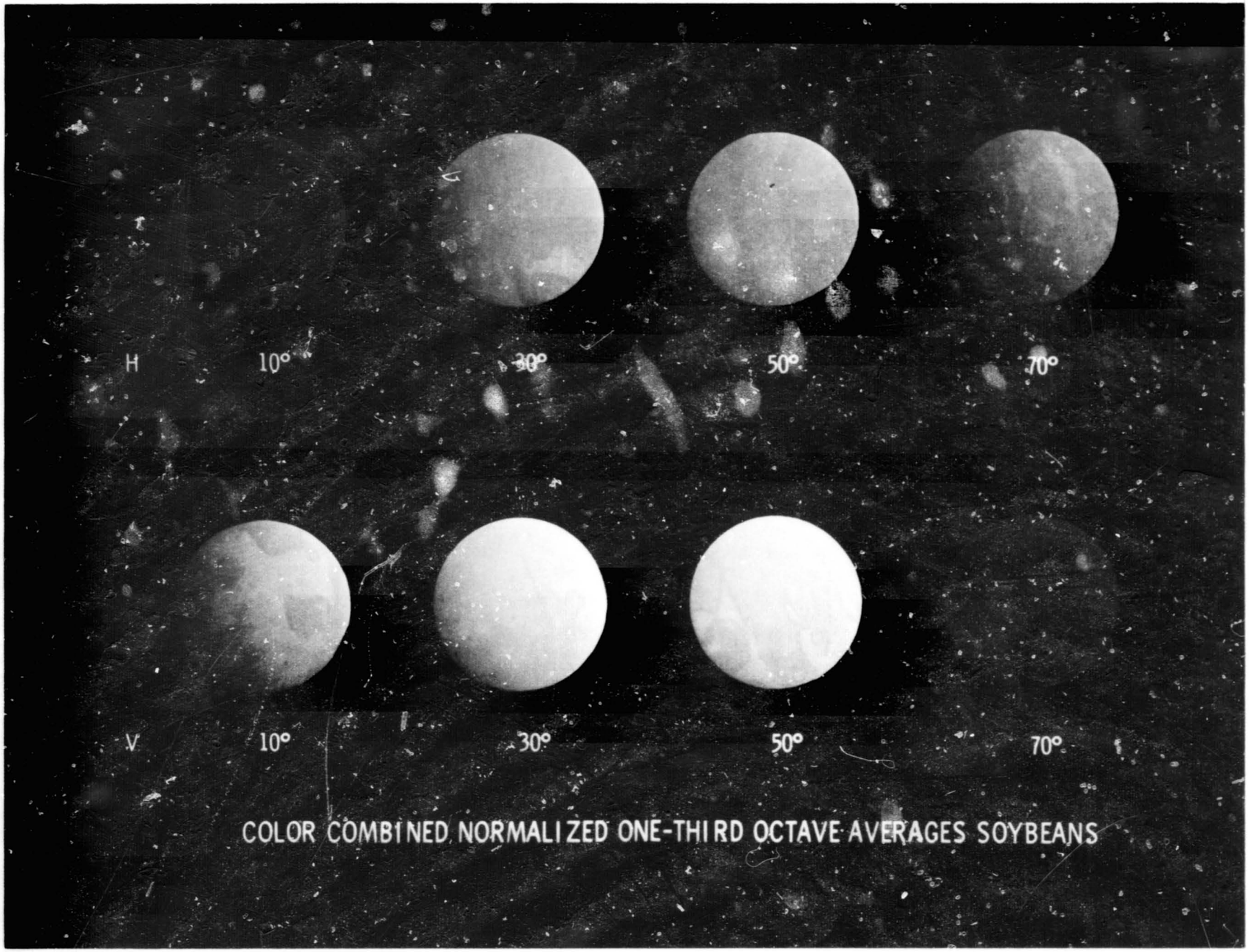
H
10°
30°
50°
70°
V
10°
30°
50°
70°
COLOR COMBINED NORMALIZED ONE-THIRD OCTAVE AVERAGES SOYBEANS

Figure 8.

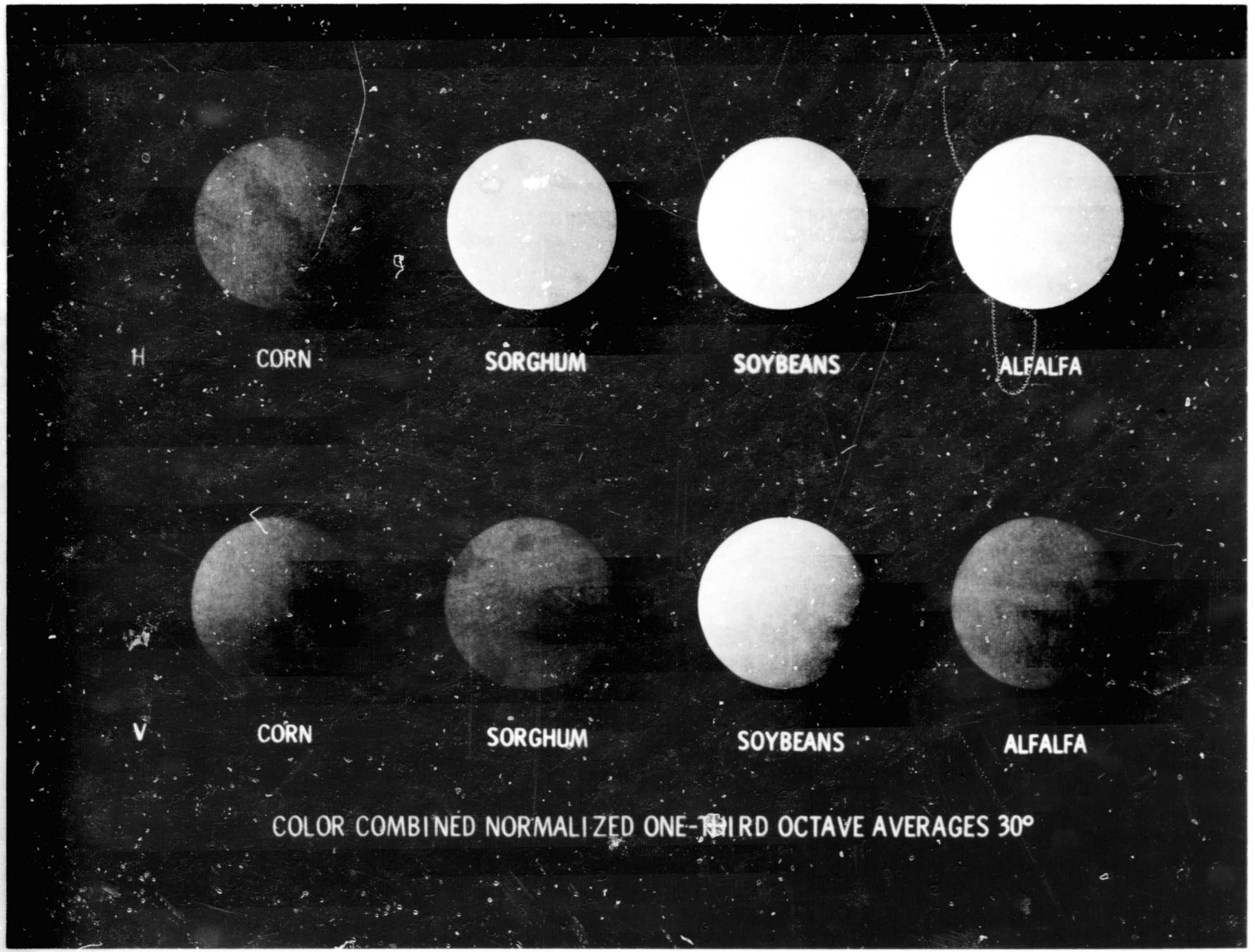
H
CORN
SORGHUM
SOYBEANS
ALFALFA
V
CORN
SORGHUM
SOYBEANS
ALFALFA
COLOR COMBINED NORMALIZED ONE-THIRD OCTAVE AVERAGES 30°

Figure 9.

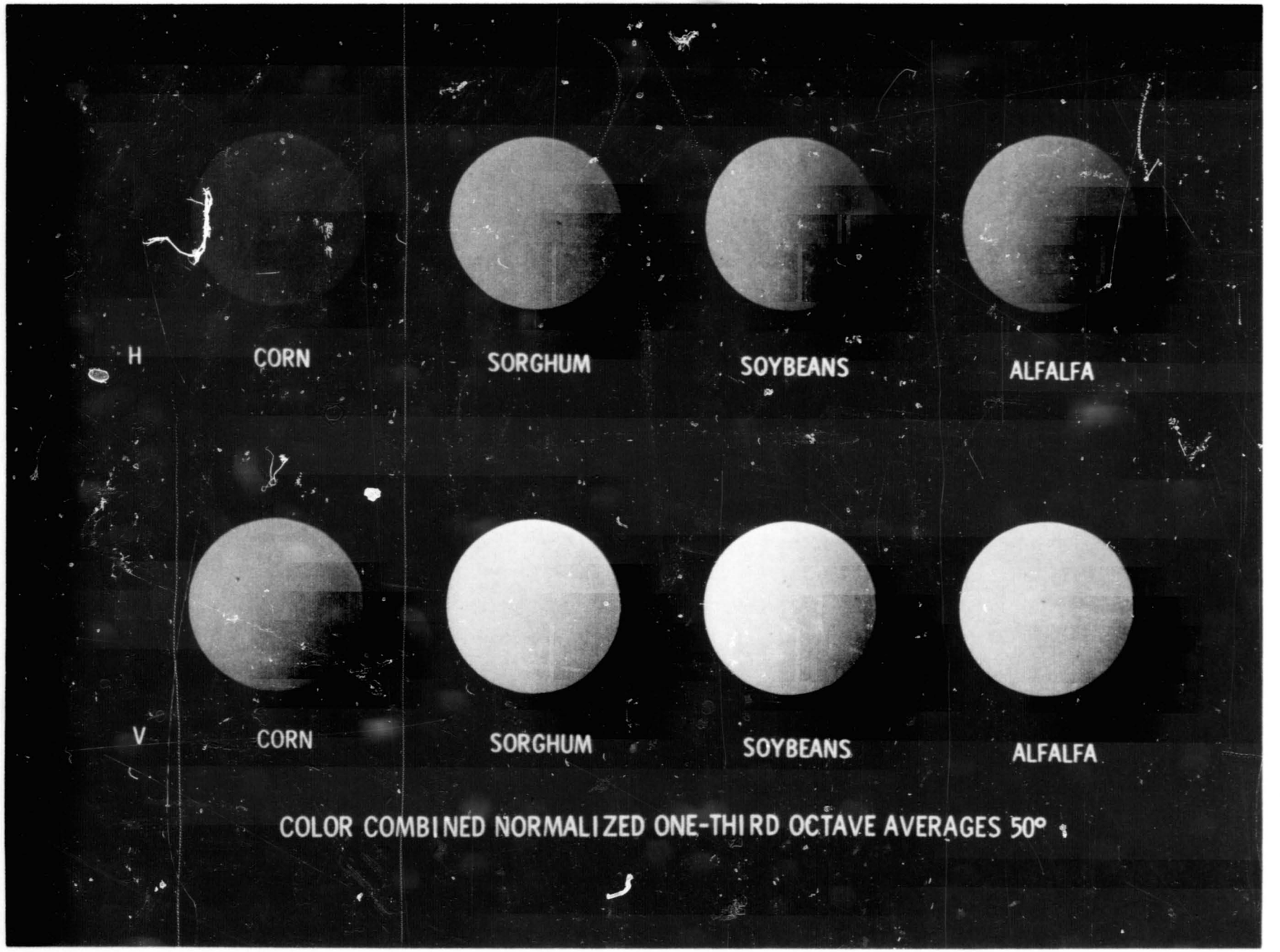
H
CORN
SORGHUM
SOYBEANS
ALFALFA
V
CORN
SORGHUM
SOYBEANS
ALFALFA
COLOR COMBINED NORMALIZED ONE-THIRD OCTAVE AVERAGES 50°

Figure 10.

13.3 GHz SCATTEROMETER SYSTEM ANALYSIS

"THE EFFECT OF AMPLIFIER SATURATION ON A DOPPLER SCATTEROMETER," TECHNICAL REPORT 118-17.

"POST-FLIGHT OPERATIONAL ANALYSIS OF THE NASA 13.3 GHz DUAL-POLARIZED RADAR SCATTEROMETER—NASA/MSC AIRCRAFT MISSION 102, SITE 76, GARDEN CITY, KANSAS, FLIGHT DATE: 3-4 SEPTEMBER 1969," TECHNICAL MEMORANDUM 118-18.

"AN ANALYSIS OF RF PHASE ERROR IN THE 13.3 GHz SCATTEROMETER," TECHNICAL MEMORANDUM 177-1.

"AN ANALYSIS OF METHODS FOR CALIBRATING THE 13.3 GHz SCATTEROMETER," TECHNICAL REPORT 177-1.

"SIGNAL ANALYSIS OF THE SINGLE-POLARIZED 13.3 GHz SCATTEROMETER," TECHNICAL REPORT 177-2.

"AN ANALYSIS OF THE EFFECTS OF AIRCRAFT DRIFT ANGLE ON REMOTE RADAR SENSORS," TECHNICAL REPORT 177-5.

"A NOTE ON THE ANTENNA BEAMWIDTH TERM USED IN THE SCATTEROMETER DATA REDUCTION PROGRAM," TECHNICAL MEMORANDUM 177-13.

Figure 11. Reports describing analysis of 13.3 GHz radar scatterometer system.

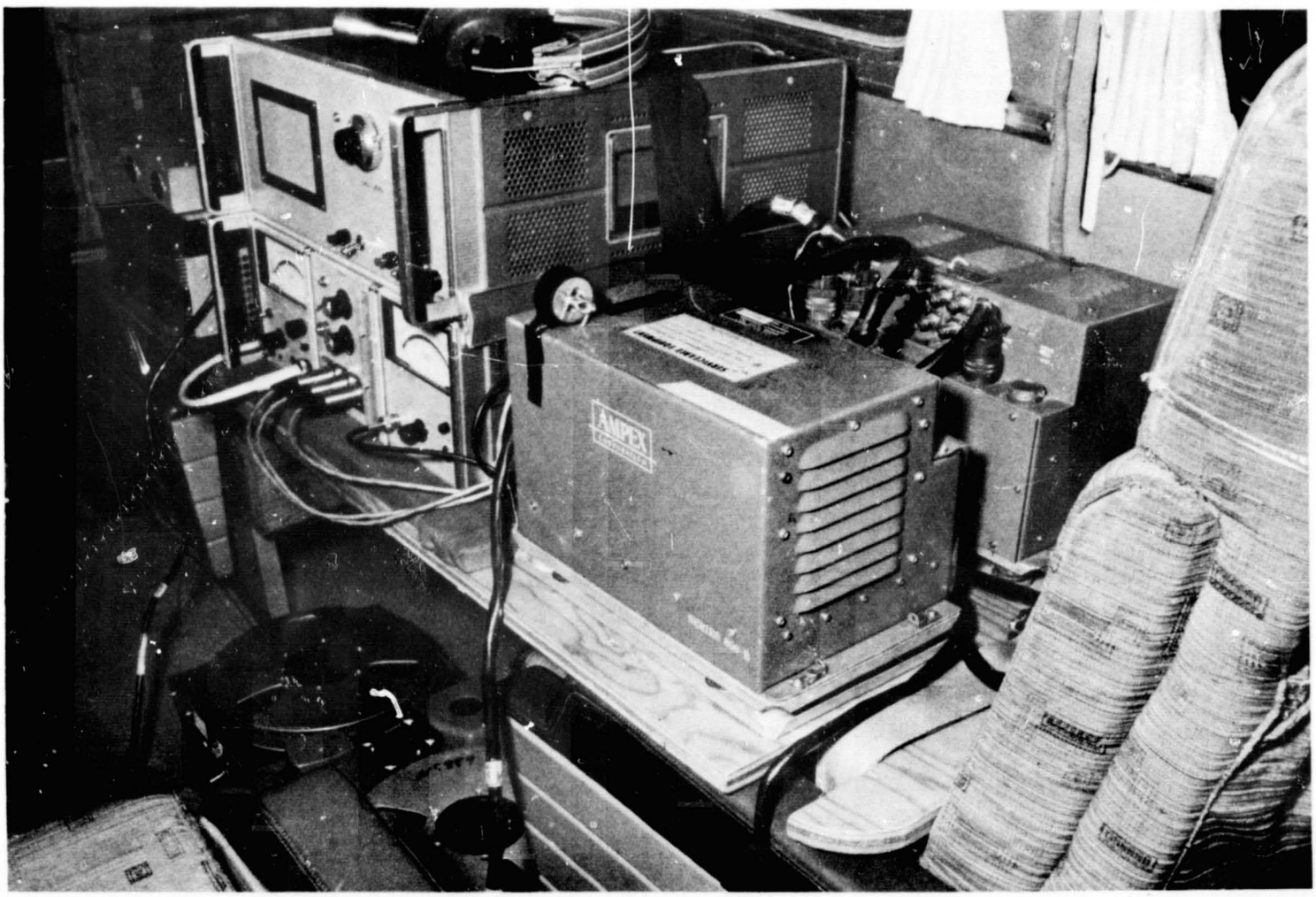

Figure 12. Kansas University 9.3 GHz radar scatterometer mounted in passenger compartment of C-45 aircraft. Scatterometer units beneath headphones; other units are parts of recorder.

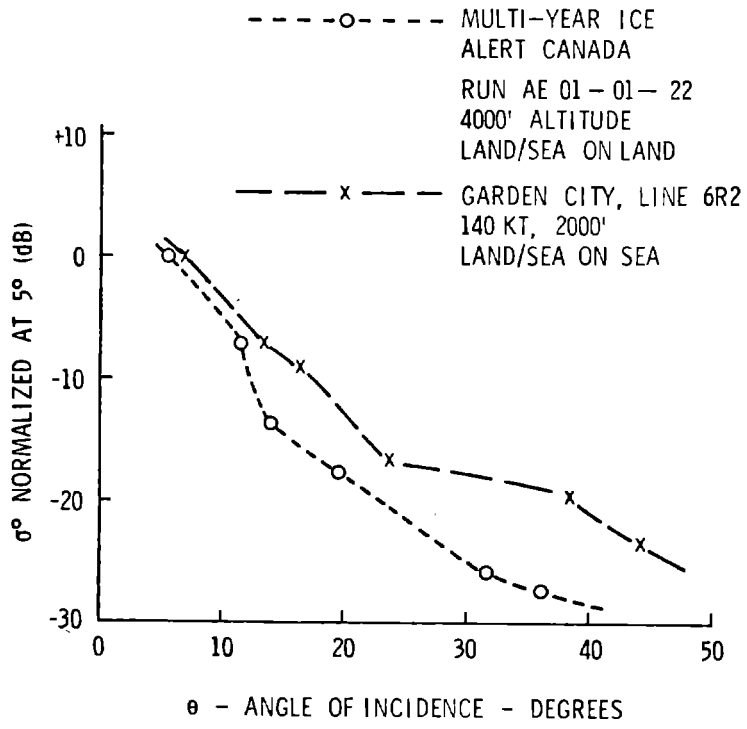

Figure 13. Kansas University 9.375 GHz scatterometer. Preliminary data.

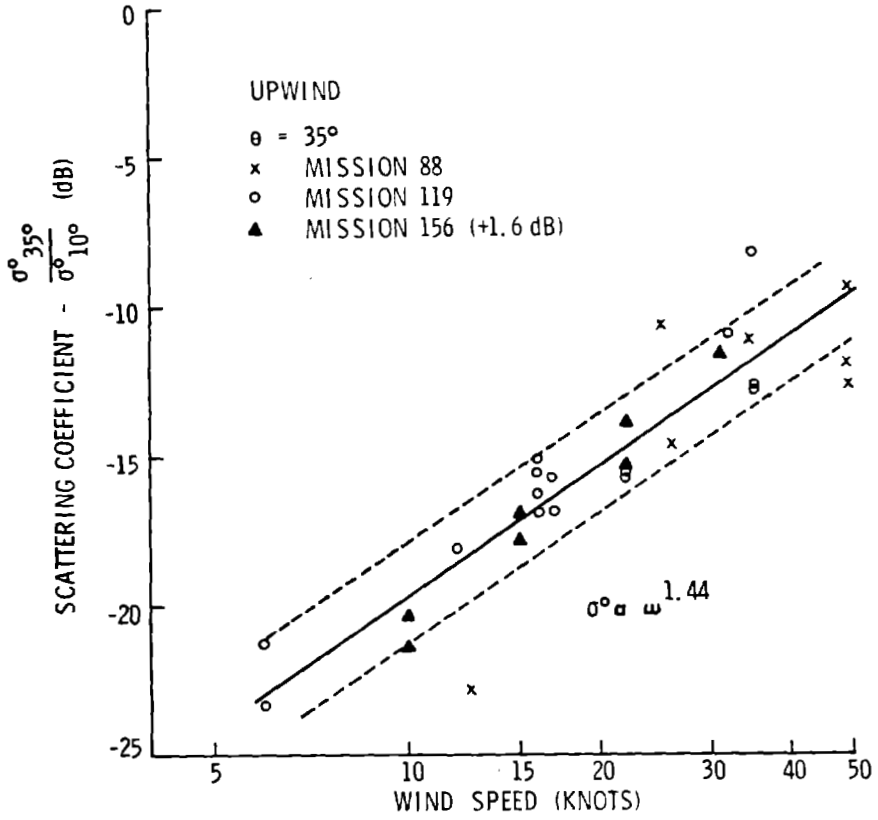

Figure 14. Oceanic scattering at 13.3 GHz 35° upwind.

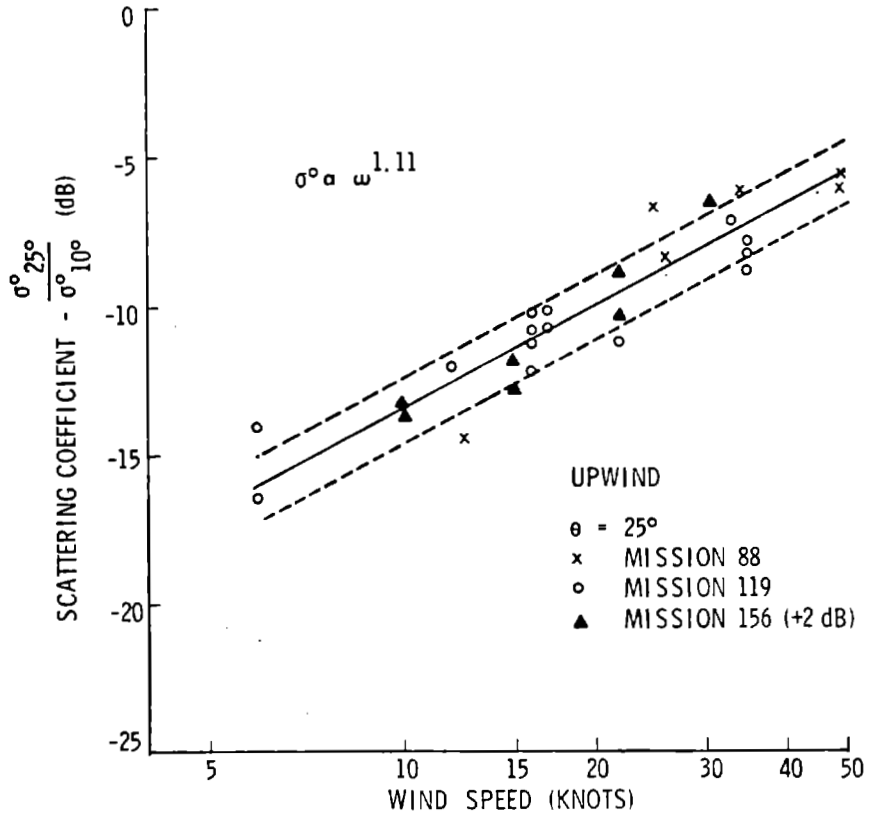

Figure 15. Oceanic scattering response at 13.3 GHz 25° upwind.

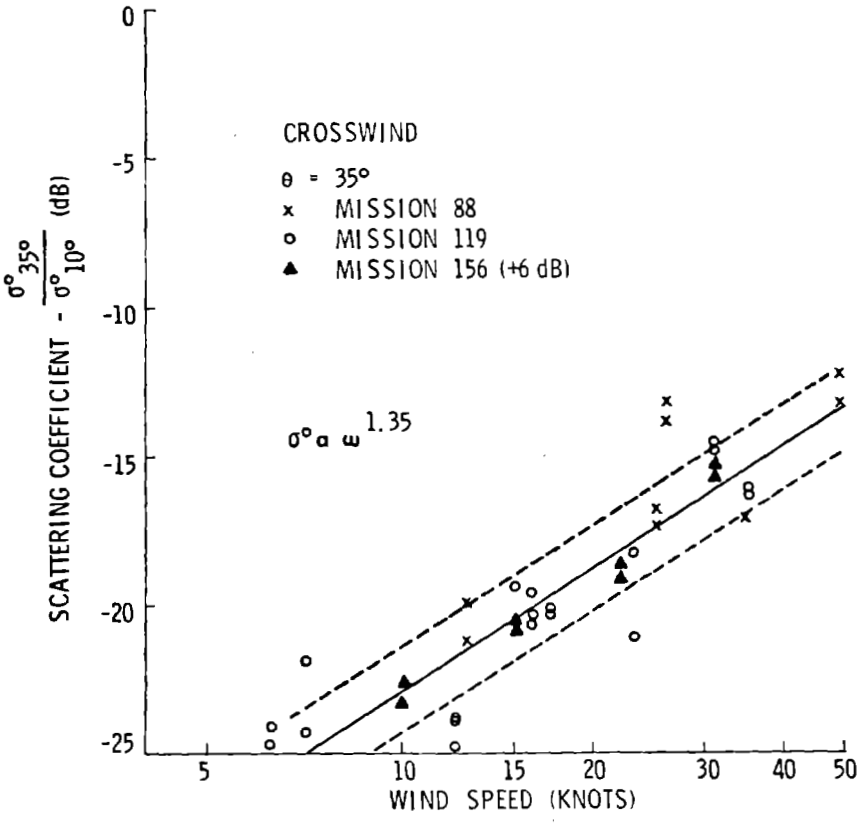

Figure 16. Oceanic scattering response at 13.3 GHz 35° crosswind.

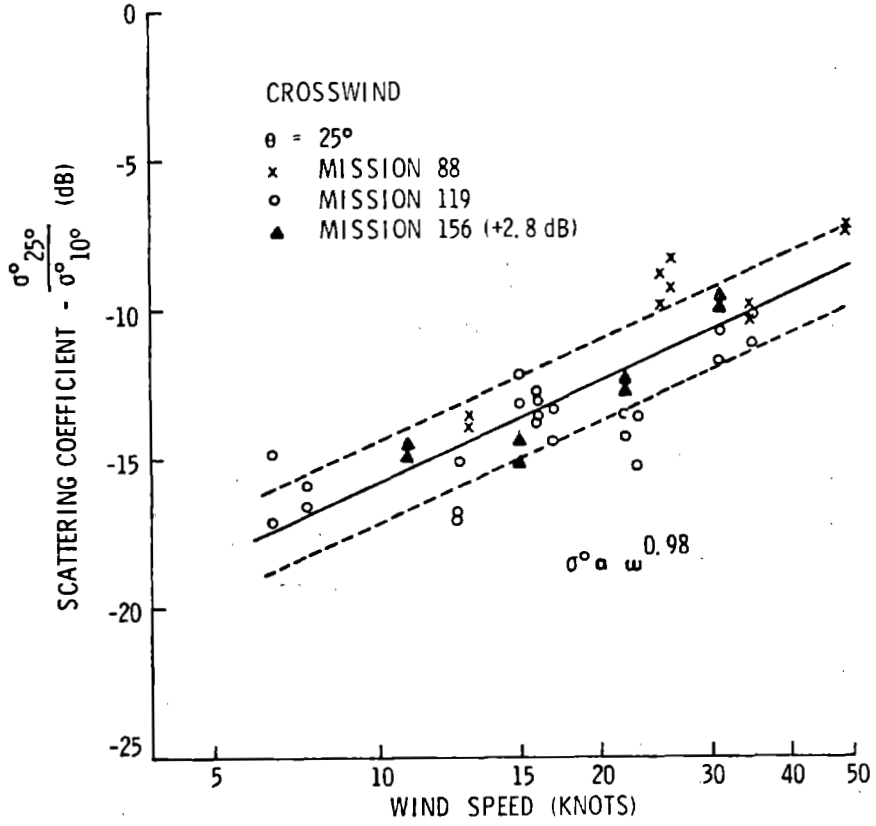

Figure 17. Oceanic scattering response at 13.3 GHz 25° crosswind.

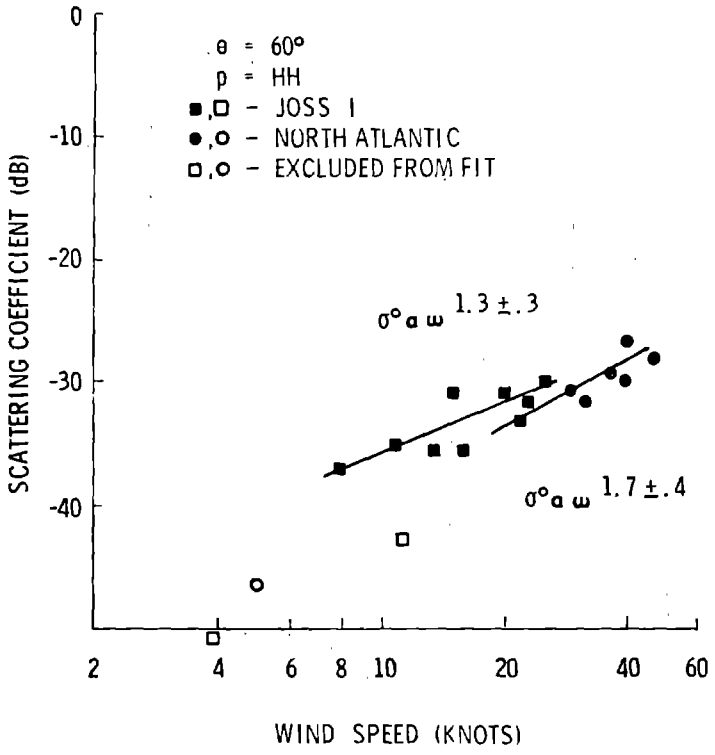

Figure 18. Oceanic scattering response at 8.9 GHz. NRL data showing separate regression lines for two missions.

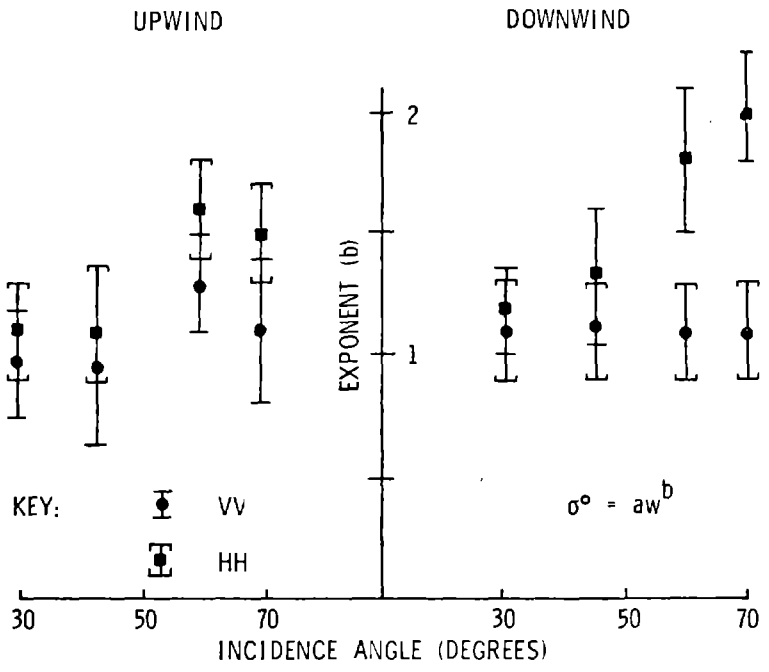

Figure 19. Power law character of NRL X-band data after adjustment.

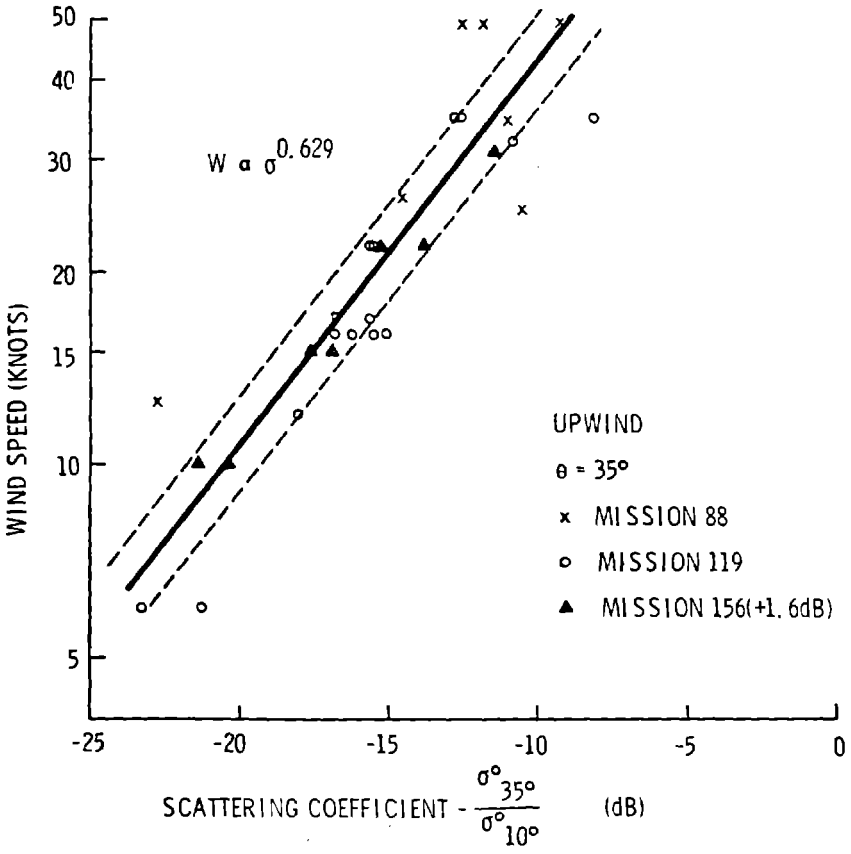

Figure 20. Anemometer calibration curve 13.3 GHz scatterometer 35° upwind.

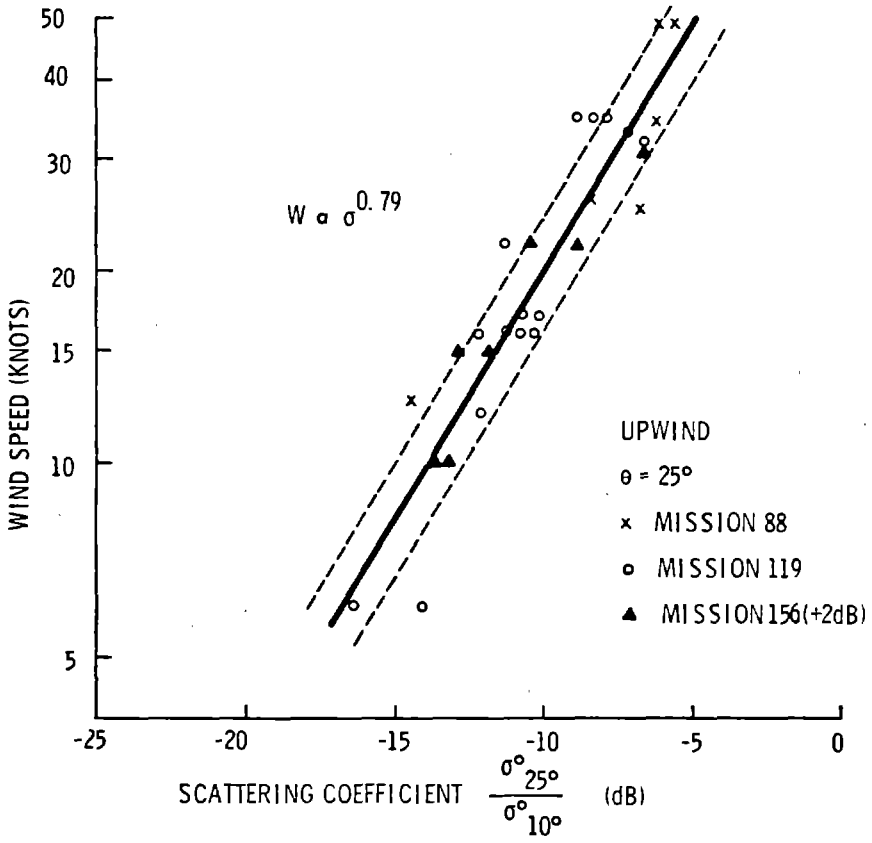

Figure 21. Anemometer calibration curve 13.3 GHz scatterometer 25° upwind.

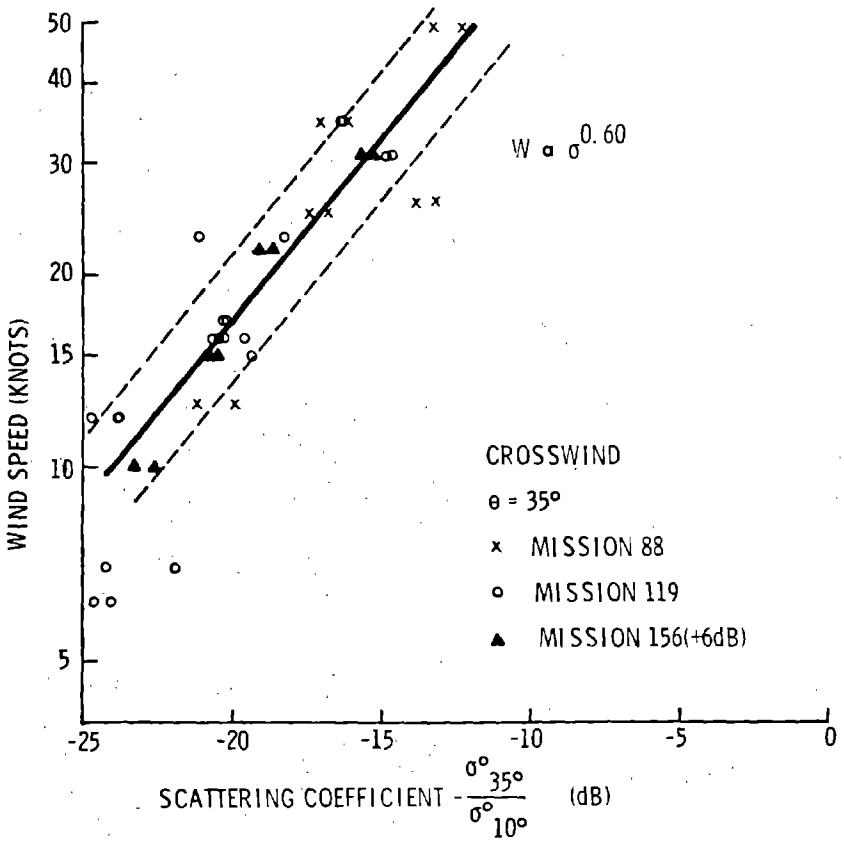

Figure 22. Anemometer calibration curve 13.3 GHz scatterometer 35° crosswind.

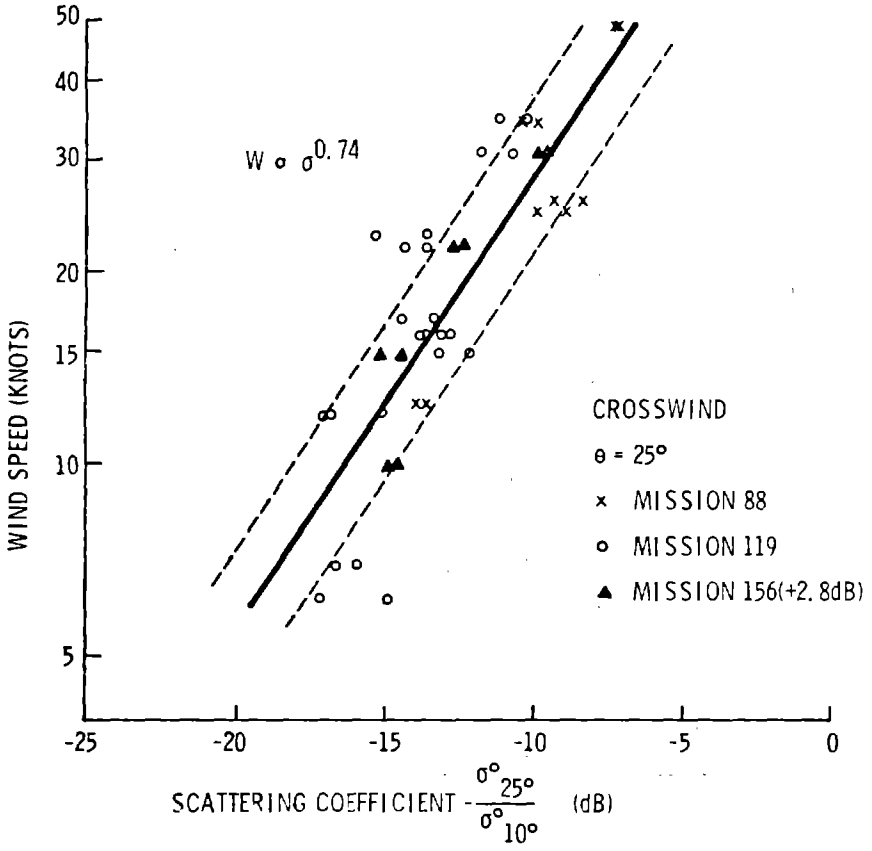

Figure 23. Anemometer calibration curve 13.3 GHz scatterometer 25° crosswind.

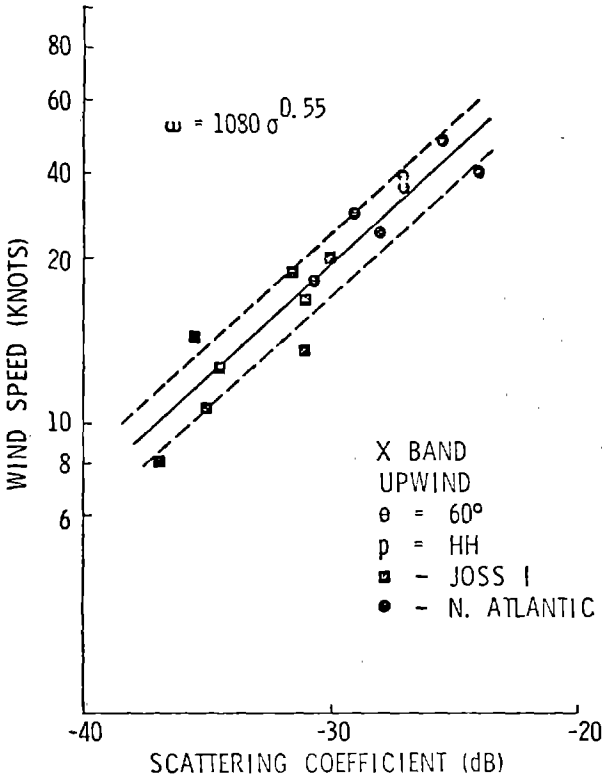

Figure 24. Wind speed as a function of scattering coefficient based on adjusted NRL data with standard deviation in wind estimate indicated.

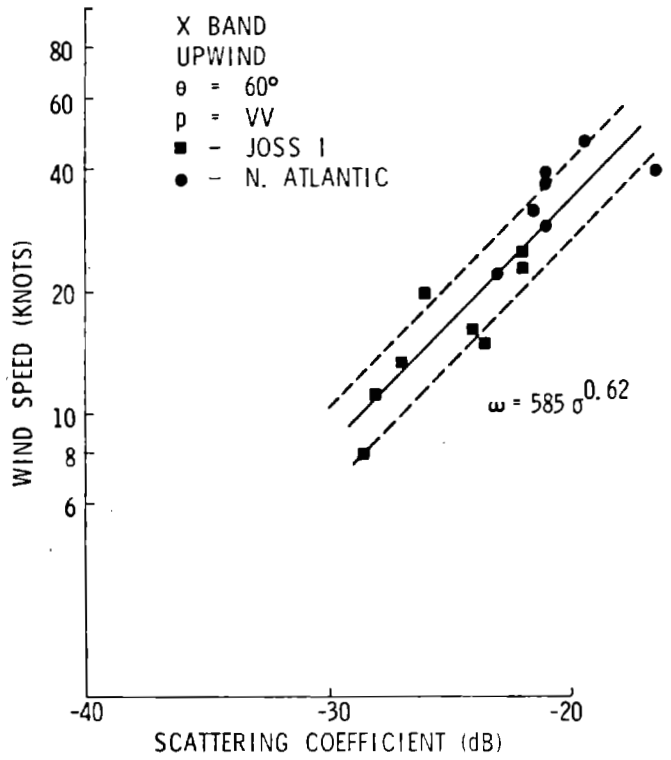

Figure 25. Wind speed as a function of scattering coefficient based on adjusted NRL data with standard deviation in wind estimate indicated.

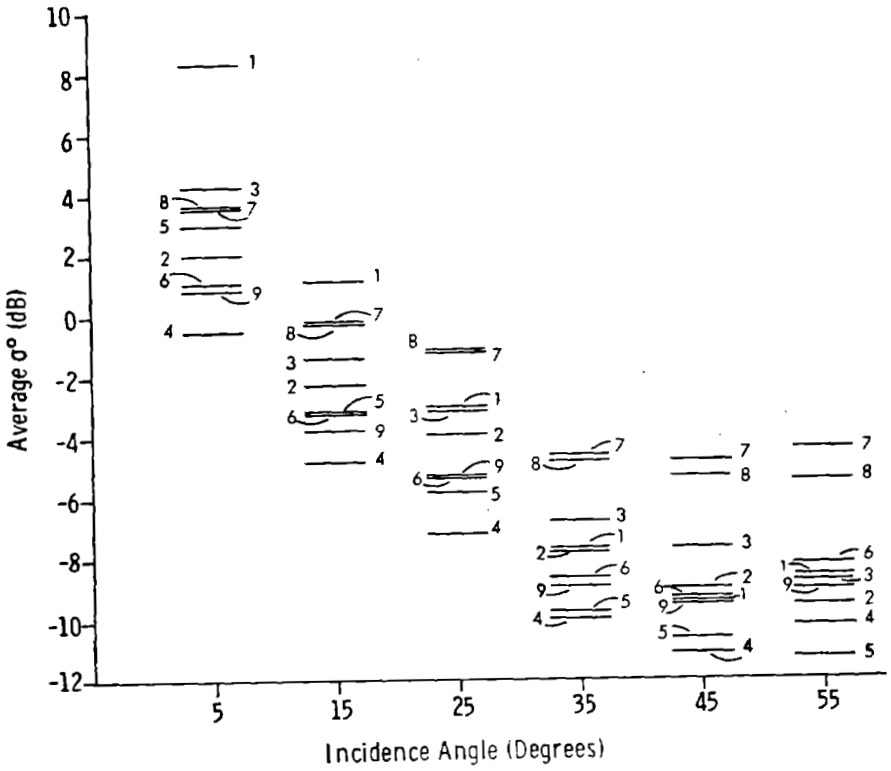

Figure 26. Spread of average σ° for nine ice-types versus angle.

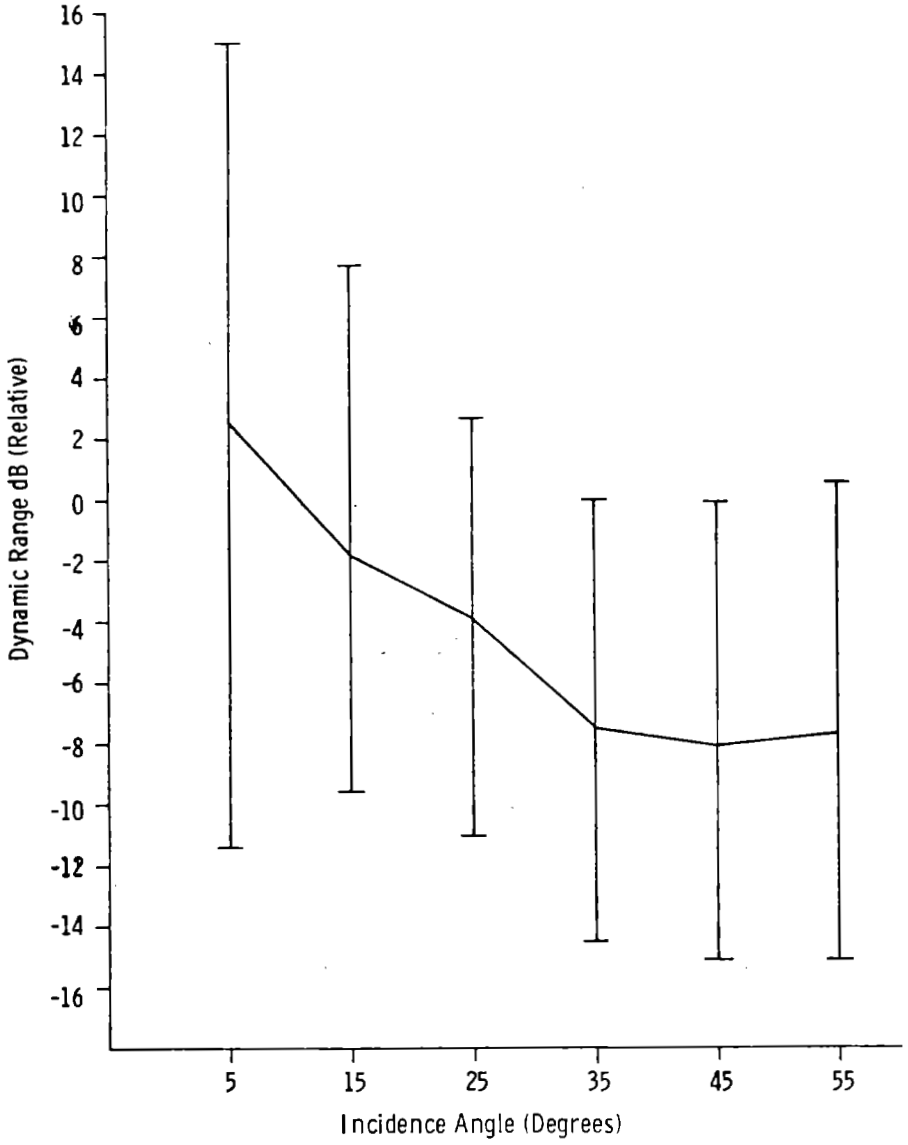

Figure 27. Dynamic range requirements for ice imager-radar.

AGRICULTURE SCATTEROMETRY PROGRAM

I. PRELIMINARY ANALYSIS OF MISSION 130 LINE OF 13.3 GHz DATA COMPLETED.

II. PROCESSING FORMAT SPECIFICATIONS COMPLETED FOR REMAINDER OF SCATTEROMETER DATA.
   1. SCALE OF DATA PLOT EQUAL TO PHOTOGRAPHIC SCALE.
   2. DATA PROCESSING SAMPLE LENGTH 0.3275 SECOND.
   3. ANGULAR RESOLUTION FREQUENCY BANDS SPECIFIED FOR +5°, THROUGH +60° WITH 5° INTERVALS.

III. ANALYSIS OF THE 400 MHz DATA FROM MISSIONS 130 AND 133 IN PROCESS.

IV. AWAITING 13.3 GHz DATA FROM MISSIONS 133, 153, 165, 168 AND THE REMAINDER OF LINES FROM MISSION 130.

Figure 28.

RESOLUTION: 10 m
SWATHWIDTH: 40 km
HEIGHT: 600 km
σ°: -25 dB
INCIDENCE ANGLE: 60°
SNR: 6 dB

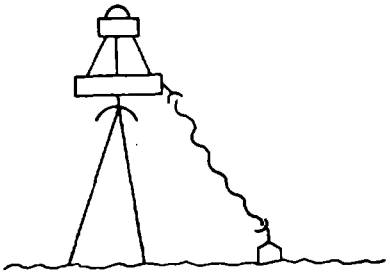

AVERAGE TRANSMITTED POWER: 125 W

POWER (INCLUDING SYSTEM & LOSSES) = 450 W

AVERAGE POWER FOR A 20% ORBITAL DUTY CYCLE: 90 W

30° INCIDENCE ANGLE GIVES A 8.4 dB SNR, ALLOWING 275 W AVERAGE POWER WITH ORBITAL AVERAGE OF 55 W.

Figure 29. Representative design for SLAR for small satellite. Poorer range resolution would allow lower power.

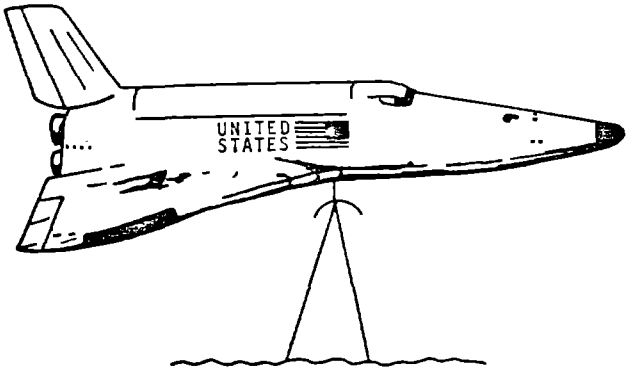

RESOLUTION: 10 m
SWATHWIDTH: 40 km
HEIGHT: 300 km
σ°: -25 dB
INCIDENCE ANGLE: 60°
SNR: 6 dB

FREQUENCY (GHz)	AVERAGE RADIATED POWER (W)	TRANSMITTER POWER (W)	POWER REQUIRED FOR WIDE-BAND AVERAGING (W) 200 MHz	400 MHz	SYSTEM POWER (W)
4	26	76	1020	2220	240
8	52	157	1870	3880	↓
10	64	192	2500	5200	
16	102	303	3980	8300	
		Σ 735	9350	19400	
POWER REQUIRED →		975	9590	19640	

Figure 30. Representative polychromatic/polypanchromatic radar system for large space craft.

N72-29340

SECTION 40

AN INTEGRATED STUDY OF EARTH RESOURCES IN THE STATE OF CALIFORNIA USING REMOTE SENSING TECHNIQUES*

by

Robert N. Colwell
Associate Director
Space Sciences Laboratory Berkeley
University of California

ABSTRACT

The urgent need to manage earth resources wisely generates, in turn, a need to inventory them accurately. As a prerequisite to intelligent management, the earth resource manager must know, for each component of the earth resource "complex", how much of it is located in each portion of the area which he seeks to manage, i.e., he must have an "integrated" inventory. During the past two years remote sensing scientists on 6 campuses of the University of California have been engaged in a NASA-funded project which seeks to make an integrated study of the entire resource complex for one of the three areas which have been selected by NASA as primary test sites for earth resource surveys, viz. the state of California. Many of the earth resource components in California, as in most other parts of the world, are dynamic rather than static. Therefore, it is necessary for these resources to be inventoried frequently and rapidly -- frequently so that resource trends can be followed -- rapidly so that resource management decisions can be made and implemented while the inventory data are still current. Our present studies, based largely on NASA-flown photography, are giving major emphasis to such considerations. These studies give particular consideration to the opportunities that will soon be afforded for satisfying these requirements through a combination of human and machine processing of ERTS-A data acquired (weather permitting) every 18 days. However, the wise management of earth resources in an area such as the state of California depends on far more than the mere acquiring of timely, accurate resource inventories. Even when given such information,

*Paper presented at the Fourth Annual Earth Resources Program Review, NASA Manned Spacecraft Center, Houston, Texas, on January 18, 1972.

the resource manager could easily make wrong decisions if he were to ignore certain important socio-economic factors. Alternately stated, human needs and emotions cannot be overlooked (particularly in these days of the environment "crusaders") as we seek better to manipulate earth resources, whether on a local, regional, national or global basis. As will be indicated in the present paper, due consideration is being given to each of the foregoing factors in this "integrated" study.

INTRODUCTION

Most university faculty members cherish the privilege of working on research projects which are of their own choosing. In the university atmosphere a research scientist usually is permitted and even encouraged to devise his own research program, obtaining financial support for it as necessary through his own vigorous efforts. In fact, a major factor governing his rate of promotion within the university is his "creativity" as evidenced by his ability to perform such tasks.

The antithesis of such a project might seem to be embodied in the NASA-funded "integrated" study, which is the subject of my paper. That study is being undertaken by more than 20 senior scientists and approximately 40 graduate and undergraduate students on 6 campuses of the University of California. Each scientist participating in the study (details of which are about to be described) has found it necessary to sacrifice some of the research autonomy to which he has grown accustomed, in order to improve the degree of integration that might be achieved, and hence the overall effectiveness of the study. In addition he has had to demonstrate an unusual amount of adaptability in the reporting of his research results since there frequently has been a need for his contribution to be integrated into the overall progress report in a way that did not recognize his individual contribution as clearly as it would have been in more conventional studies. In view of these facts I would be remiss, in my capacity as principal investigator for our integrated study, if I did not take this opportunity at the outset to commend these participating scientists, eminent experts as they are in their own right, for the very high degree of adaptability and cooperativeness which they have demonstrated.

It is my privilege today, speaking on behalf of the many competent individuals who have been participating in the project, to do the following: (1) describe briefly the rather untraditional way in which our project got started, (2) indicate the specific nature of the project, (3) describe some of our research accomplishments to

date, and (4) state what we hope to accomplish in the future.

ORIGIN OF THE INTEGRATED PROJECT

Early in 1969 the Director of NASA made a proposal somewhat along the following lines to the Director of the NASA-funded Space Sciences Laboratory of the University of California: "In addition to the research which your laboratory is already doing for NASA in such fields as planetary physics and systems analysis, it would seem desirable for you to consider doing work which is related to NASA's Earth Resources Survey Program".

These words of encouragement led to a series of planning sessions, most of which were participated in by faculty representatives from all of the major campuses of the University of California, together with one or two NASA representatives. The university scientists prepared various remote sensing proposals dealing with a large number of topics which ranged from the global monitoring of volcanic eruptions to the study of aerosols in the atmosphere. Among these was a proposal to conduct an integrated study of California's entire "resource complex" through remote sensing from aircraft and spacecraft.

Of these various proposals, only the latter led to funding by NASA, the first allocation of funds having been made in May, 1970. From the outset, half of these funds have been contributed by the NASA Earth Resources Survey Program and half by the NASA Office of University Affairs, but with a substantial amount of matching support by the University of California.

Since its inception this study has been given the rather cumbersome but aptly descriptive title: "An Integrated Study of Earth Resources in the State of California Using Remote Sensing Techniques". Reasons for selecting the state of California for the test site included the following:

1. It exhibits a great variety of earth resources, landforms and climatic factors.

2. Large amounts of remote sensing data and associated ground truth data already are available for many parts of California.

3. With respect to earth resource management, various social and environmental stresses already are being felt strongly, making California a model of things to come, both nationally and globally.

4. Many competent physical and social scientists now residing in California could be, and want to be, assigned to such integrated studies.

5. Appropriate NASA-funded facilities and associated administrative capabilities for the conduct of such studies already exist in California.

NATURE OF THE STUDY

It was recognized in our proposal to NASA that little would be accomplished under this integrated study if we attempted to investigate, at the outset, all components of California's entire earth resource complex, statewide. Ideally we would begin our study by investigating some phase of this complex which was both discrete and limited, but which nevertheless required a consideration of both the resource interrelationships and the attitudes of the people in a very sizable part of the state. Given these constraints and ambitions we tentatively selected the "California Water Project" as the focal point for this initial phase of our study. The word "tentatively" is used advisedly because it was recognized that resource managers and administrators, particularly within the Administrative Branch of the state of California, would need to be consulted in order to determine (1) whether such a study would meet with their favor or disfavor and (2) whether, in the event that we were authorized and funded to conduct such a study, mutually beneficial working relationships with resource managers in the Administrative Branch might be developed.

Initially there were some serious reservations expressed by personnel in the California Resources Agency, and elsewhere in the Administrative Branch, as to the advisability of our conducting those aspects of our study that related specifically to the California Water Project. They pointed out that most of the decisions that were required both in conceiving and in developing the California Water Project already had been made long before our study was proposed. We were well aware of this fact and had been regarding it as a major strength rather than a weakness in our proposed study, since our objective was not to provide a "critique" of either the concept that resulted in authorization of the California Water Project or the steps being taken to implement it. Instead, we were hoping to be able to use in our proposed study the valuable experiences gained and ground truth data acquired by those who had been working for many years on the California Water Project. We recognized that it would be prohibitively costly and time consuming for us to attempt to acquire this same kind of "input" independently. However it was our belief, as

expressed in our proposal, that this situation enhanced the usefulness of the state of California as a "calibration" test site, and of the California Water Project as a "calibration" project, so that our research findings could be applied, by extrapolation, to other parts of the world that were less developed than California yet highly analogous to it in terms of characteristics of the total resource complex. By the time these discussions had been concluded, an amicable relationship with the Administrative Branch had been developed and this fact was made known to the appropriate NASA authorities at the time when final consideration was being given to our proposal.

During the period in which we have been conducting this NASA-funded study, we have given numerous briefings to the appropriate individuals in the California Administrative Branch. In recent months this procedure has been responsible, in part, for the development of complementary rather than competitive ERTS-A and SKYLAB proposals by the Administrative Branch and the University of California, respectively. Evidence of the success that has thus been achieved, despite the fact that initially there were many formidable diplomatic difficulties, can be found in the following quotes from a letter to NASA from California's Lt. Governor Reinecke, dated April 13, 1971, the purpose of which was to comment upon the University's ERTS-SKYLAB proposal as viewed by the Administrative Branch: "On behalf of the State of California, I wish to take this opportunity to strongly endorse this proposal . . . Mr. Norman B. Livermore, Secretary-Resource Agency, and Mr. Earl Coke, Secretary-Agriculture and Services Agency, who represent the largest segments of state government utilizing this data, and who have contributed guidance and impetus to the proposed program, will provide further leadership and assistance as required".

The emphasis already given in this paper to matters of "protocol" is a highly purposeful one. For herein may lie the greatest determinant of future successes for the entire NASA-sponsored Earth Resources Survey Program. The skeptics are finally becoming convinced that meaningful resource surveys and related information of a highly detailed nature can be acquired primarily by means of remote sensing from aircraft and spacecraft. Therefore, many of them are becoming quite sensitive about the kinds of surveys that should be permitted. To ignore this fact in future studies conducted under the NASA Earth Resources Survey Program may be to ensure at the outset the ultimate failure of such studies. So important is this development, in the view of the present writer, that it will be referred to again in a concluding section of his paper, but with reference there primarily to its international implications.

FRAMEWORK WITHIN WHICH TO VIEW THE STUDY

A key word in the title of this study, which serves to differentiate it from other earth resource survey studies that have been funded to date by NASA, is the word "integrated". According to the dictionary, the term "integrate" means "to form into a whole; to unite with something else; or to incorporate into a larger unit". In order to appreciate how such a concept might best apply to the individual and collective efforts under this multi-campus project, let us consider the desires of two groups that are certain to be interested in this project and its findings.

On the one hand, there are those already referred to who need to make major policy decisions with respect to the earth resources in a particular geographic area and then to develop management plans that will permit those decisions to be implemented in an efficient manner.

On the other hand, there are data acquisition and data processing specialists who are interested in knowing (a) what package of remote sensing devices (and the associated aircraft and spacecraft for transporting these devices) might best be used to collect meaningful earth resource data on a global basis, and (b) what techniques and equipment should be used in extracting useful information from the acquired data.

The interest of both groups in having research done in the state of California results primarily from the fact that the findings made there by a competent group of scientists might be applied, with only slight modification, to vast parts of the globe which are, to varying degrees, analogous to the state of California in terms of the complex of earth resources exhibited and earth resource management decisions to be made.

The links of a chain which might serve to tie these two groups together are indicated in the diagram in Figure 1. Areas of research emphasis of the different campuses responsive to these different links are illustrated in Figure 2.

An additional way in which to view the links by means of which remote sensing techniques can be used to satisfy the informational requirements of various resource management groups appears in Figure 3. It is to be emphasized that our initial efforts, as suggested by the central portion of this diagram, have dealt with one resource -- the water resource -- and furthermore have been quite specific in dealing almost entirely with one example of that resource and the management problems associated with it, viz. the California Water Project. Even

within this limited context, however, we are making a sizable effort to achieve "integration" in our study from three standpoints, data acquisition, data analysis and data use as indicated in the three paragraphs which follow.

From the data acquisition standpoint this study seeks to integrate: (1) data acquired from sensors operating in several wavelength bands (the Multispectral or Multiband concept); (2) data acquired from sensors operating at several different times (the Temporal or Multidate concept); (3) data acquired from two or more stations in the same flight path (the Parallax or Multistation concept; (4) data acquired using both like- and cross-polarization sensors (the Multipolarization concept); (5) data acquired from two or more nearly identical images (the "improved signal-to-noise" or Multi-image Correlation concept); and (6) data acquired from space, air and ground (the Multi-stage concept).

From the data analysis standpoint this study seeks to integrate: (1) analyses contributed by analysts from several disciplines (the Multi-disciplinary concept); (2) analyses made possible through the making of various optical and electronic image enhancements (the Multi-enhancement concept); and (3) analyses made possible through proper interaction between humans and machines (the "Human" vs. "Automatic" or Multiple Data Processing concept).

From the information use standpoint this study seeks to integrate: (1) information about all components of the total resource "complex" and the inter-relations of these components (the Multi-resource concept); (2) information needed in producing several kinds of earth resource products from the same piece of property (the Multi-use concept); (3) information needed by several types of earth resource managers and consumers (the Multi-user concept); (4) information displayed in various formats (thematic maps, 3-D models, annotated photo mosaics, tables, graphs, etc.) to better satisfy the various multi-use and multi-user requirements and preferences (the Multi-display concept); and (5) information about inter-relations among earth resource components and the uses of these components in one geographic area vs. another (the Multi-association concept).

While this "multi" concept could be still further enlarged upon, perhaps it already has been overdone in the preceding paragraphs. Nevertheless, at the very heart of our integrated study is the central theme implied above and expressed as follows: The providing of useful information about earth resources through the use of remote sensing techniques is, at best, a difficult task. In fact it becomes an almost futile task if only one image of the area of interest is given in the completely unenhanced form, to one analyst, and he uses only

one approach in attempting to extract useful information from it that might be of use to only one of the host of potential beneficiaries of such information. In contrast with this limited approach, each of the "multi" concepts just expressed may add a small amount to his ability to improve the usefulness of resource information that he is attempting to provide. Furthermore, the overall usefulness of the final product may be improved far more than might be suggested merely by summing up the improvements made possible through employing these various "multi" concepts, as appropriate. Hence, at some point in the process a threshold is crossed, to the left of which the information acquired by remote sensing is virtually worthless and to the right of which it becomes progressively more useful, even to the point of becoming the most useful combination of tools and techniques available to those interested in achieving the wisest possible management of this globe's critically limited complex of earth resources.

NATURE OF THE CALIFORNIA WATER PROJECT

Because of the initial emphasis being placed in our study on the California Water Project, it is deemed appropriate to provide here a brief historical review and synopsis of that project.

The California Water Project is the first major water resource development under the California Water Plan. The masterplan was published by the Department of Water Resources (Bulletin 3) and approved by the State Legislature in 1959. It is the outgrowth of studies in the 1950's of the ultimate potential use of the land and water resources of the state as per Bulletins 1 and 2 of the DWR.

The State Water Project (see Figure 4) will deliver 4,320,000 acre feet of water annually to Central and Southern California. The major supply of water comes from the Feather River and is impounded by the Oroville Dam for subsequent release through the Sacramento River and the Delta pool to pumps on the south side of the Delta. Water is pump lifted to the South Bay Aqueduct and the California Aqueduct (244 feet).

The California Aqueduct, which will deliver the water to Southern California, carries the flow to the joint federal-state utility, San Luis Reservoir, the second major storage reservoir of the Project. Deliveries are made from the San Luis Reservoir to the federal Central Valley Project in the California Aqueduct for delivery to the southern San Joaquin Valley and Southern California. At the south end of the Central Valley, Project water is pump lifted nearly two thousand feet through the Tehachapi Mountains. South of the Tehachapi's the system

divides into a West Branch for delivery to the MWD and a number of smaller contractors, and an East Branch for delivery to Antelope Valley-Mojave Desert water agencies and the balance of the MWD commitments. The terminal reservoirs for the project are Castaic in the East and Lake Perris in the southeast. The Project is the largest single water resource development undertaken in the United States. In addition to the transfer of 4,230,000 acre feet annually through 684 miles of aqueducts it provides a storage capacity of nearly 7 million acre feet. The project facilities will generate 5.3 million kilo-watt hours of electricity annually and consume 13.4 million kilo-watt hours annually at full development.

A number of essential features of the California Water Project are still in various stages of study and litigation. Future water supplies to augment the California Aqueduct and the Delta Pool may be needed before the project can operate at full capacity. A Peripheral Canal around the Delta has been proposed to protect the ecology of the San Francisco Bay and Delta areas as well as to provide for an adequate flow of fresh water. The Central Valley Master Drain to prevent soil salts from accumulating is still in abeyance until agreement is reached on repayment of its cost.

In total, the State Water Project is over 95% completed or under construction. As of late 1969 it was operational to northern Kern County. The tunnels through the Tehachapi Mountains are completed and most of the construction on the pumping plants has been completed, with the result that the first water from this project was delivered to Southern California in October, 1971. The aqueducts of both the West and East Branches of the system are under construction as well as the four major reservoirs, Pyramid Lake, Castaic Lake, Silverwood Lake and Lake Perris. The delivery of water to Los Angeles County is soon to be followed by delivery of water to both San Bernardino and Riverside Counties.

Water deliveries from Castaic Lake will be made to three water contractors. The principal user, Metropolitan Water District of Southern California, will receive more than 1.4 million acre feet per year from that facility after 1990. Water delivery at the Devil Canyon Powerplant near San Bernardino will include service to all the San Bernardino-Riverside area. When the terminus reservoir, Lake Perris, is completed, it will serve this area as well as the extensive water market which includes San Diego and Orange Counties. Water delivery from the Perris Reservoir is expected in the early months of 1973.

Financing for the State Water Project has been a problem area almost from its inception. At the time of its authorization in 1960

the cost was estimated at 1.75 billion dollars. Today the conservative costs estimates of the DWR amount to 2.8 billion dollars, while more liberal estimates project a cost of 4.0 billion dollars. Project customers will repay those amounts allocated to water supply, hydroelectric power and agricultural waste disposal amounting to 90%. The remaining 10% will be repaid by federal flood control funds and state tideland oil and gas revenues.

The California Water Project is only one of a number of large inputs into the Southern Coastal Hydrographic Unit. The local safe yield supplies and the imported water from Owens Valley and the Colorado River exceed the projected import of Project waters. The problems associated with water resources and water importation are numerous. The Project will alleviate such situations as sporadic water runoff, maldistribution of water supply, ground water overdraft and the intrusion of sea water. On the other hand, it raises and contributes to still other problems such as inadequate drainage, disputed water rights, water pricing policies of agencies such as the MWD and the general efficacy of water redistribution and the efficiency of water use.

UNIVERSITY PARTICIPANTS AND THEIR FIELDS OF STUDY

Figure 4 shows the locations of study areas for certain of the participants in this 6-campus project. A seventh campus (San Diego) also is shown because of the probability of participation by scientists from that campus and from others whose research activities on our integrated project are of such a nature that they are not logically directed toward any one of the study areas shown in Figure 5.

A summary of the co-investigators on the various campuses and of the specific phases with which they are concerned is as follows:

1. Definition of earth resource policy and management problems in California

   C. West Churchman and Alexander Mood
   (Berkeley and Irvine campuses)

2. Definition of the information requirements of hydrologic resource managers

   Robert Burgy and David Storm (Davis campus)

3. Measurement of hydrologic resource parameters through remote sensing in the Feather River headwaters area

   Gene Thorley, et al (Berkeley campus)

4. Studies of river meanders

   Gerald Schubert and Richard Lingenfelter
   (Los Angeles campus)

5. Assessment of the impact of the California Water Project, the westside of the San Joaquin Valley

   John Estes, et al (Santa Barbara campus)

6. Assessment of the impact of the California Water Project, southern California

   Leonard Bowden, et al (Riverside campus)

7. Digital handling and processing of remote sensing data

   Vidal Algazi and Dave Sakrison
   (Davis and Berkeley campuses)

8. Investigation of atmospheric effects in image transfer

   Kinsell Coulson and Robert Wolraven (Davis campus)

The above listing of the various phases of our integrated study serves to indicate its unusually great breadth as compared with other studies that have been funded to date under the NASA Earth Resources Survey Program. Because of this breadth it has been necessary to give a considerable amount of thought to the question of how one might best report, in a brief paper such as this, the most significant results of our integrated study. As recently as 6 or 8 years ago the most effective report on such a project probably would have been one in which great emphasis was placed on the inclusion of highly colorful infrared Ektachrome photos of various portions of our test site, together with the inclusion of suitable annotations and captions indicating their usefulness in resource inventory. At that time most of the present participants in the nationwide NASA Earth Resources Survey Program had seen few, if any, infrared Ektachrome photos, even though others in the program have been working on such photography for nearly 30 years. The situation has changed dramatically in the last few years, however, to the point where most of us probably are weary of seeing the other fellow's latest infrared Ektachrome photos,

however enthusiastic we may be about our own! *

Similarly, any such report, if given as recently as two or three years ago, might appropriately have placed its major emphasis on quantitative expressions of the extent to which certain important earth resource features can be identified on various kinds of imagery taken from aircraft and spacecraft. At that time there was a crying need for such quantitative information -- a fact that was vigorously pointed out by the NASA convenors of one of our annual reviews. This situation, likewise, has been dramatically rectified in the interim to the point that many of our present-day reports to NASA seem to be literally clogged with confessions about our "errors of omission", "errors of commission" and "probable levels of significance".

Many apsects of our 6-campus integrated study have, indeed, entailed the use of beautiful infrared Ektachrome photos. Furthermore, some of our findings are, indeed, highly significant to umpteen places and several degrees of confidence, if not overconfidence. These facts will be apparent to anyone who reads our periodic reports. However, there are other aspects of this study which would seem to merit even greater emphasis now that the concept of inventorying earth resources by remote sensing has come of age. These are aspects resulting from the attention which is being given in our integrated study to certain broad questions which pertain, not to resource inventory, but to resource management. Such questions are arising at this particular time in relation to the Earth Resources Survey Program primarily because of the following reason: The studies which many investigators, nationwide, have been conducting under that program are at last convincing the skeptics that it soon will indeed be possible to make meaningful earth resource surveys primarily by remote sensing from aircraft and spacecraft. Now that they are beginning to take us seriously, they also are beginning to raise some hard questions about the impact which such surveys may have, directly or indirectly, upon man and his environment.

But first let us provide a brief summary of some of our findings to date relative to the inventory of relevant components of the resource complex with which the California Water Project is concerned. Consistent with our previous description of this project we will report findings separately for the "source", "central" and "sink" areas.

---

*In this regard a fellow scientist said recently, "Sometimes I think the whole world must be turning red".

REMOTE SENSING ACTIVITIES AND ACCOMPLISHMENTS IN THE SOURCE AREA FOR THE CALIFORNIA WATER PROJECT

The headwaters of the Feather River, principal source of water for the California Water Project, includes the NASA Bucks Lake Forestry Test Site. Under sponsorship of the NASA Earth Resources Survey Program, that test site had already been under study by University of California scientists for approximately 5 years before the start of the present integrated study. During this prior period, emphasis had been placed on determining the extent to which various kinds of earth resources (timber, forage, soils and water, as well as geologic and recreational resources) could be inventoried through the use of modern remote sensing techniques. Consequently, much was known at the start of the present study that was at least indirectly related to the problem of determining the volume of surface and subsurface flow of water by means of remote sensing. This is true because the volume of water which a watershed will yield during any given season obviously depends not only on the nature, amount and distribution of precipitation during that season, but also on the geologic, soil and vegetation characteristics of each portion of the watershed. Furthermore, since the remote sensing imagery used in these earlier studies had been flown to various specifications in terms of spectral regions, time of day, season of year and flight altitude, much also had been learned about the optimum specifications for remote sensing imagery used in estimating certain of the parameters which are known to affect water yield.

Our present studies in the source area are building on the base which was established by this previous work. Specifically, our investigators who presently are working in the Feather River Watershed area are concentrating on: (1) defining the parameters which are both pertinent to a determination of water yeild and discernible through the use of remote sensing techniques; (2) determining the accuracy with which the parameters can be measured and mapped using remote sensing data flown to various specifications; and (3) relating the water yield predictions thus made to actual water yield; both for the entire Feather River drainage and for various components of it.

In performing this work our investigators are being given an excellent opportunity to demonstrate the validity of one of the most important concepts on which the NASA Earth Resources Survey Program is based. This is the 2-stage concept of (1) initially making the earth resource survey studies on a relatively small but highly representative "calibration area", in this case the Bucks Lake Forestry Test Site of approximately 100 square miles, for which ground truth

is accurately known. (In so doing the investigators determine the optimum remote sensing specifications and data analysis techniques for the type of earth resource survey that eventually is to be made operational.); and (2) then making at least a semi-operational evaluation of these findings on a very large "extended area", in this case the entire Feather River Watershed of approximately 3,600 square miles. Ordinarily the establishment of "ground truth" for so vast an extended area would be a formidable task in itself. In this investigation, however, the ultimate measure is the volume of water, in any given period of time, which is yielded by the entire watershed. Fortunately for purposes of our study, water from the entire Feather River Watershed is impounded in the Oroville Reservoir, where an accurate measurement of the volume of water that is present at any given time can easily be made. Thus a suitable check is readily obtainable on the accuracy of the overall estimate, for any specified period of time, as made by remote sensing. Similarly, since there is a dam and associated reservoir at the lower end of each of several sub-units of this drainage system, an accuracy check also is available for these sub-units. Consequently, if large errors of estimate based on remote sensing are found in certain of these sub-units, but not in others, an opportunity is afforded for making more detailed studies of conditions in these areas in order to determine the exact cause of the errors and thus to devise means of minimizing them in future studies. Authorities who control the volume of water that is impounded at any given time behind Oroville Dam (the largest earth-filled dam in the world, and more than 700 feet high) have told us that they greatly need more accurate information about the volume of run-off that can be expected from the Feather River Watershed during various specified periods of time. In the absence of accurate information, they must incorporate a very large safety factor in deciding upon the volume of "draw-down" which they must effect at Oroville Reservoir, particularly just before heavy spring run-off from the vast Feather River Watershed. Without such a safety factor there would be no way of preventing disastrous floods in the event that the rate and amount of spring run-off greatly exceeded expectations; but through use of such a sizable safety factor, in most years large amounts of water must be discharged from the reservoir and allowed to flow out to sea, even though that water could have been used to great advantage during the summer months.

None of the foregoing is meant to imply that haphazard techniques are currently being used by those who control the flow of water from the Feather River Watershed. To the contrary they are using some of the most suitable techniques currently available, while readily agreeing that there is a great need for more suitable techniques of the type that we are seeking to devise through our remote sensing research.

An important aspect of the research which our investigators are conducting in the Feather River Watershed Area seeks to develop means for better monitoring the rate of snow accumulation in the late fall and winter and of snow melt in the spring and early summer. Prior to the start of our present integrated study we had made only a few preliminary attempts to do this with the aid of remote sensing data acquired at suitable time intervals. Consequently we are in the process of improving our capability in this regard using photography flown at 18-day intervals by NASA's U-2 aircraft. At the same time we are converting our previously-developed classification schemes for the mapping of vegetation, soils and other components of the earth resource complex into schemes which will be more indicative of water yield. Details as to our accomplishments to date in these various respects will be found in our forthcoming progress report to NASA which is scheduled for completion in May, 1972.

REMOTE SENSING ACTIVITIES AND ACCOMPLISHMENTS IN THE CENTRAL AREA OF THE CALIFORNIA WATER PROJECT

A major part of our interest in this Central area (consisting mainly of the West Side of the San Joaquin Valley) is in using remote sensing techniques to monitor an agricultural region in its initial stages of development. As stated by Senger (1972), who is one of the participants in our integrated study: "This initial phase is important because it is a time of experimentation. Different segments of the local community often will devise a variety of approaches for developing the land. The results of these efforts may eventually produce a defined pattern to the landscape that will serve as a basis for labelling the area as a distinctive agricultural region or an extension of one already existing." Consequently, if this area develops into a distinctive type of agricultural region, our study could make a contribution to investigations that seek to explain the evolution of an area and the processes that help to determine its outcome.

As early as 1957 agricultural cropland had expanded about as far as it could within the West Side of the San Joaquin Valley until such time as water could be transported to the area for use in irrigation. Of the 1,350,000 acre feet per year of water which will be delivered to this area by the California Water Project, the overwhelming majority of it will be used for agricultural purposes. At the present time farmers in the area are attempting to discover what kinds of crops can be grown at a reasonable cost under existing environmental conditions, are readily marketable, and can show a

good profit. Up to the present time there has been very little specific plant breeding for this environment and farmers are obliged to experiment mainly with crops which were developed for adaptation to other areas. Yet cropping is about the only alternative to the present widely practicied grazing of the area. For example, the area is quite isolated from population centers of California so it is not realistic to consider the development of an industrial park. Because of the marginal value of the land for crop production (prior to the importation of water from the California Water Project) no sense of urgency had been inspired to conduct more than general surveys of the soils, geology, vegetation and climate of the area. Consequently the avilability of water from the California Aqueduct has come at a time when no one could say for sure whether the area is suitable for irrigated agricultural development. Hence we see here a case in which technology (the construction of the Aqueduct and the subsequent influx of water) has occurred before the local populous was ready for it. Hence farmers are now having to learn about their local environment while at the same time having to grow crops that will enable them to stay in business. In addition, various irrigation systems are still being experimented with, and the whole landscape conveys the appearance on remote sensing imagery of being in an "experimental" state, which indeed it is. There are very large areas, now used only for grazing, which are available for more intensive agricultural development, but not likely to be developed until the end of this experimental period.

In a somewhat broader context, Spencer and Horvath (1963) have stated that there are six major factors influencing the development and the cultural processes of a landscape. They are psychological, agronomic, political, historical, technologic and economic. It is believed, from the studies which we have conducted to date in this area, that a final decision as to whether or not to develop irrigated agriculture can be attributed primarily to a combination of economic and psychologic processes. Farmers do not want to leave the area, but can they afford to stay? Water is being made available to them at a cost ranging from $8.00 per acre foot for subsidized federal water to $15.00 per acre foot for unsubsidized state water. While this may still leave some margin for profit, the farmers are in an unfavorable competitive position with those only a short distance to the east (on the East Side of the San Joaquin Valley) who pay only $2 to $3 per acre foot for water.

The first few sets of U-2 photographs that are being flown of this area by NASA at 18-day intervals have now been made available for our use. By means of this photography and appropriate field checking we will be able to continue our monitoring of both the short term and long term changes that are occurring in this area,

particularly with respect to land use. While so doing we will be able to develop photo interpretation keys which will facilitate land use mapping in areas similar to this one on simulated space photography.

REMOTE SENSING ACTIVITIES AND ACCOMPLISHMENTS IN THE SINK AREA OF THE CALIFORNIA WATER PROJECT

Studies to date in this area have been largely confined to two specific regions: (1) the Perris Valley surrounding the future Lake Perris; and (2) the Sheep Creek Fan-Mirage Basin area of the Mojave Desert. Progress in studying remote sensing imagery in only the first of these two areas will be reported here, as being representative of the types of investigation being conducted by those scientists on the Riverside Campus of the University of California who are participating in this integrated study.

To date studies by that group in the Perris Valley Area have taken three approaches: (1) a land use survey has been made in a sample study area using both ground observations and interpretation of high altitude color infrared photography; (2) a survey has been made, partly through the use of questionnaires, to determine the attitudes of residents relative to the proposed changes to be made in the area because of the California Water Project; and (3) estimates have been made of the potential population changes and land value changes likely to occur in various portions of the area. These latter studies have been carried out using conductive sheet analog models. Future simulations will add greater realism to the models and should provide valuable insights to social, economic, and land-use planning problems within the area of interest.

At the time of this writing, our land use survey in the Perris Valley area has been confined to a sample area of one census tract which is located centrally to Perris Valley and adjacent to the future Lake Perris. The photography which our group initially studied of this area consisted of high altitude (1:50,000 and 1:100,000 scale) color infrared metric imagery flown in May, 1970. Additional photography recently has been obtained at frequent intervals by the NASA U-2 aircraft. Consequently, an inventory of the remainder of the area, and a monitoring of changes throughout the entire area currently are being undertaken through use of this photography.

Recently, it has been found that land developers in this area

have established a number of locations for the promotion of present agricultural land for non-agricultural purposes and at non-agricultural prices. This activity appears to be directly related to future potential uses of this land for recreational and other purposes as a result of the construciton of Lake Perris. It appears from our studies that land developers and speculators play a significant role in determining the future land use in this area, including immediate changes in the regions land use patterns and activities. Consequently, in additon to the completion by the Riverside group of a survey of present land use in the Perris Valley area, the group is also attempting to assess the role and activities of land developers in the area and the direction and rate of change in land use for various portions of the area.

As detailed in our periodic progress reports, similar studies are being undertaken by the Riverside scientists in other parts of the so-called "sink" area of the California Water Project.

OTHER ACCOMPLISHMENTS TO DATE UNDER THIS INTEGRATED STUDY

The social sciences group which is participating in this study is using a systems analysis approach which seeks to optimize 3 types of models: (1) the data-collection and information-extraction model, from the viewpoint of those engaged in earth resource inventory; (2) the decision-making model, from the viewpoint of those engaged in earth resource management; and (3) the ultimate beneficiary model, from the viewpoint of members of the public who may benefit or be harmed by such decisions.

Part of this work is fitted closely to that of other investigators and is being applied to the geographic areas within which the previously-described studies are being made. Additional aspects of the work take cognizance of the fact that what is done with one kind of resource in one part of the state has broad implications with respect to other components of the resource complex within that area and also in other parts of the state. Consequently, a somewhat broader approach both geographically and disciplinary-wise is being taken by the Social Sciences group.

As with previously-described phases of our integrated study, the interested reader is referred to our periodic progress reports for additional details with respect to the very broad scope of activities currently being undertaken by the Social Sciences group.

A LOOK TO THE FUTURE FOR THIS INTEGRATED STUDY

Briefly stated, the direction of our activities in the immediate future under this integrated study will be along three general lines, all of which will be oriented toward maximizing our ability to make meaningful interpretations of ERTS-A data which we anticipate will soon be acquired of vast portions of the state of California: (1) continuation of studies on the California Water Project in the "source", "central" and "sink" areas along lines indicated in earlier sections of this report. (It is planned that these future studies also will include investigations of the Sacramento River Delta area); (2) initiation of studies in the coastal zone of California, within which 80 percent of California's total population is reportedly localized and for which resource monitoring, beyond that presently being accomplished, is vitally needed; and (3) continuation of studies by the Social Sciences group, particularly with reference to the third of its three "models", the "user" model. In addition, it is probable that our proposed work involving the making of regional agricultural surveys will be initiated, using San Joaquin County, California as the focus for that study.

The providing of further details relative to our proposed future activities would not be fruitful at this time and might even be considered presumptuous until the exact scope and level of funding for our integrated study are more clearly defined in conferences soon to be held with our NASA monitors.

CONCLUSION

As I look for some highly relevant note to sound in ending this presentation, I can do no better than to echo the sentiments of NASA's Dr. Wernher von Braun, which were expressed by him several years ago when the overall space program in general, and the Earth Resource Survey Program in particular, had come under rather severe criticism. Paraphrased, here are the comments, as well as I can remember them, which Dr. von Braun made to several of us on that occasion: Critics of the NASA program are bemoaning the fact that so much of this country's scientific talent, and in so many different disciplines, is being diverted into a single effort -- the space program. These critics imply that much more could be accomplished that would be of potential benefit to mankind if each such scientist were left to pursue a research program of his own choosing.

Dr. von Braun said that he viewed the matter quite differently: What these scientists from so many disciplines have needed for years is a large, peace-oriented focal point for these many talents so that the result of their efforts would be something far greater than might be expected from the sum of their individual contributions. He pointed out that NASA's Space Program in general, and its Earth Resources Survey Program in particular, provided the best opportunity to date for mounting such a worthy integrated effort.

Having been deeply involved in such an integrated effort through the project which I have just described, I find myself in complete agreement with Dr. von Braun's observation.

LITERATURE CITED

Senger, Lester E. "Irrigated Agricultural Developments of the Southern West Side of the San Joaquin Valley with Special Reference to Major Oil Company Holdings." Ph.D. Thesis, Department of Geography, University of California at Los Angeles. 181 pp; illus. February, 1972.

Space Sciences Laboratory, University of California. "An Integrated Study of Earth Resources in the State of California Using Remote Sensing Techniques." First Annual Progress Report. May 1, 1971.

Spencer, J. E. and Ronald J. Horvath. "How Does an Agricultural Region Originate?". Annals of the Association of American Geographers. Vol. 53, No. 1, pp 74-92. March, 1963.

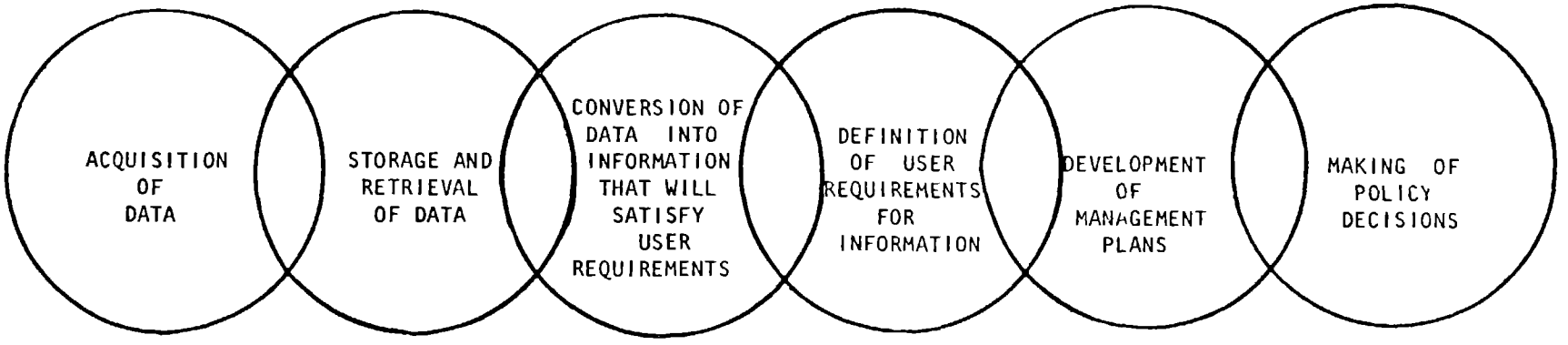

Specify spectral and spatial resolution characteristics of sensors, atmospheric constraints, target illumination and weight, power and volume requirements of the sensors. Specify performance characteristics of vehicles needed to transport sensors, including speed, attitude control, service ceiling, stay time and ability to satisfy weight, power and volume requirements of the sensor package.	Specify the "model" or "models" that will best facilitate the storage of data and its retrieval periodically by those who are to convert the data into information that will satisfy specific requirements of the various users.	Establish the "signature" for each type of earth resource feature that is to be identified, as a function of its spectral, spatial, goniometric and temporal characteristics. By proper use of humans and ADP machines, provide an "in-place" delineation, area-by-area, of each type of earth resource, including vegetation type, soil type, water quantity and quality, topography, culture, and multi-resource interrelationships.	Precisely define the kinds of earth resource information needed by those who must develop and implement management plans and policy decisions; also define the speed with which these types of information must be provided following acquisition of remote sensing data, and the frequency with which these kinds of resource information are likely to be needed by the various users.	Determine, for example, how best to manage the watershed with a view to multiple use management; also how and where to store water and to develop and distribute hydroelectric power from it. Also, how best to transport water to farmlands, urban areas and other places of water consumption.	Determine, for example, whether to encourage or discourage (1) the growth of a megalopolis in a particular area, (2) the intensification of agriculture in a second area, etc.

Figure 1. LINKS BY MEANS OF WHICH REMOTE SENSING TECHNIQUES CAN BE USED TO SATISFY THE INFORMATION REQUIREMENTS OF VARIOUS RESOURCE MANAGEMENT GROUPS

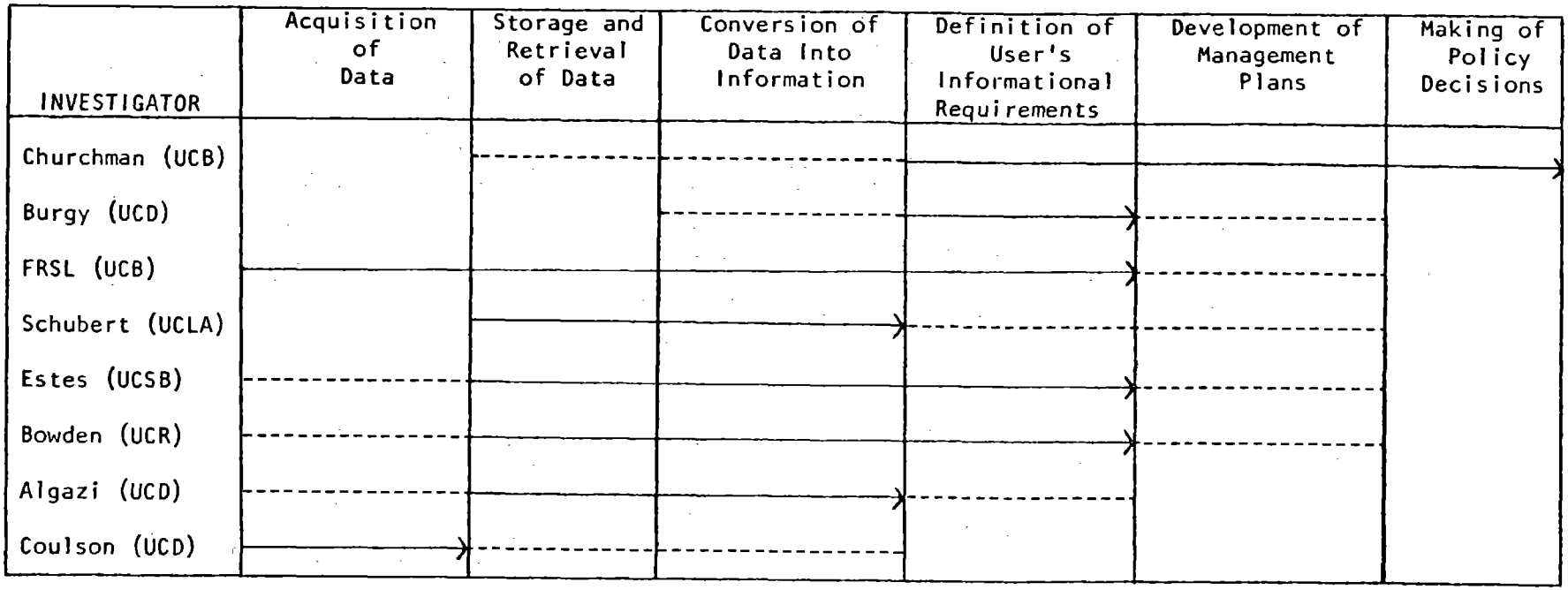

——————— = primary emphasis by the investigator

- = secondary emphasis by the investigator

Figure 2. AREAS OF RESEARCH EMPHASIS OF THE VARIOUS PARTICIPANTS IN THIS INTEGRATED STUDY OF EARTH RESOURCES

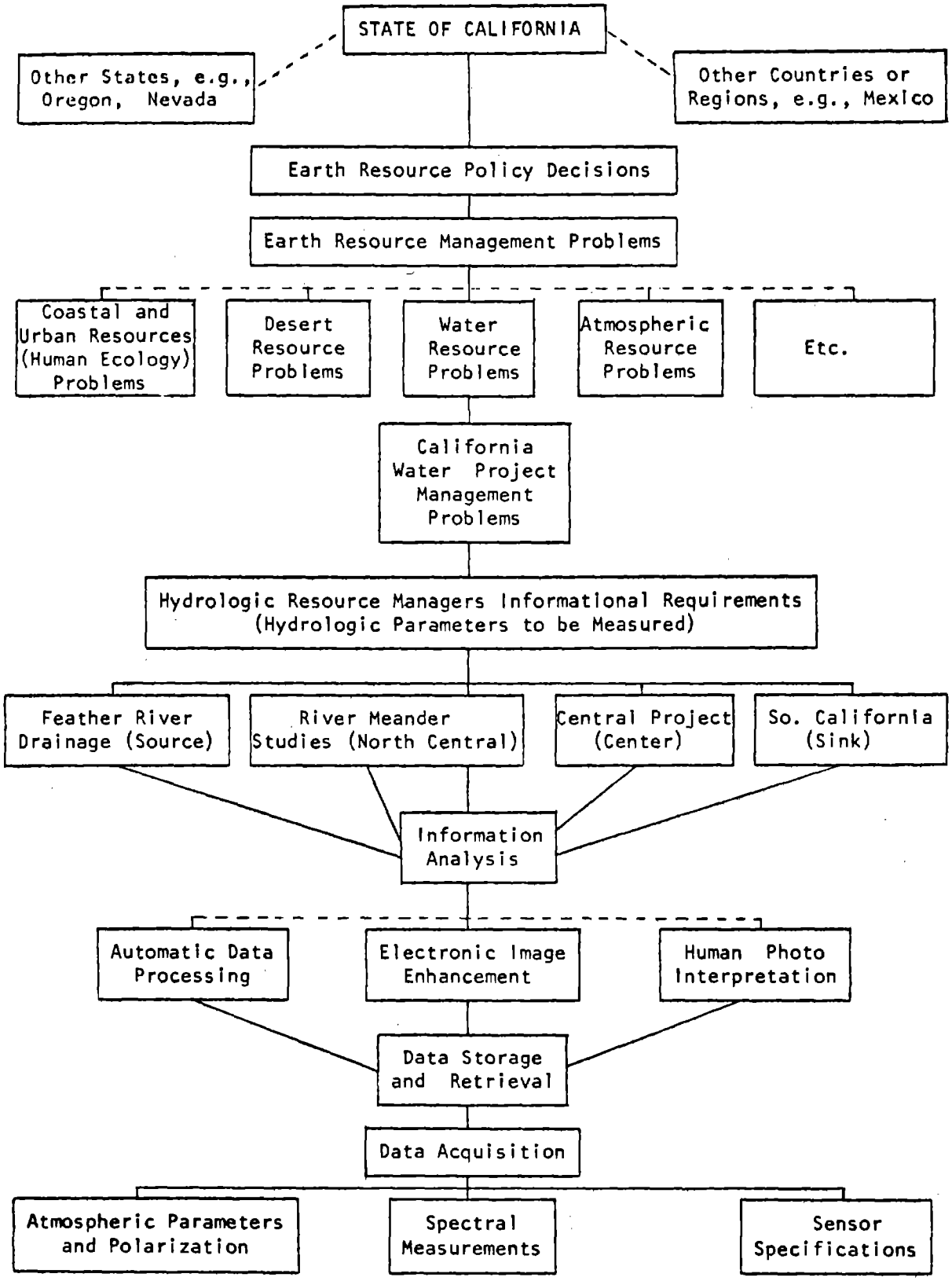

Figure 3. DIAGRAM ILLUSTRATING THE STRUCTURE OF THE INTEGRATED PROJECT AND ITS RELATION TO OTHER CRITICAL RESOURCE PROBLEMS IN CALIFORNIA

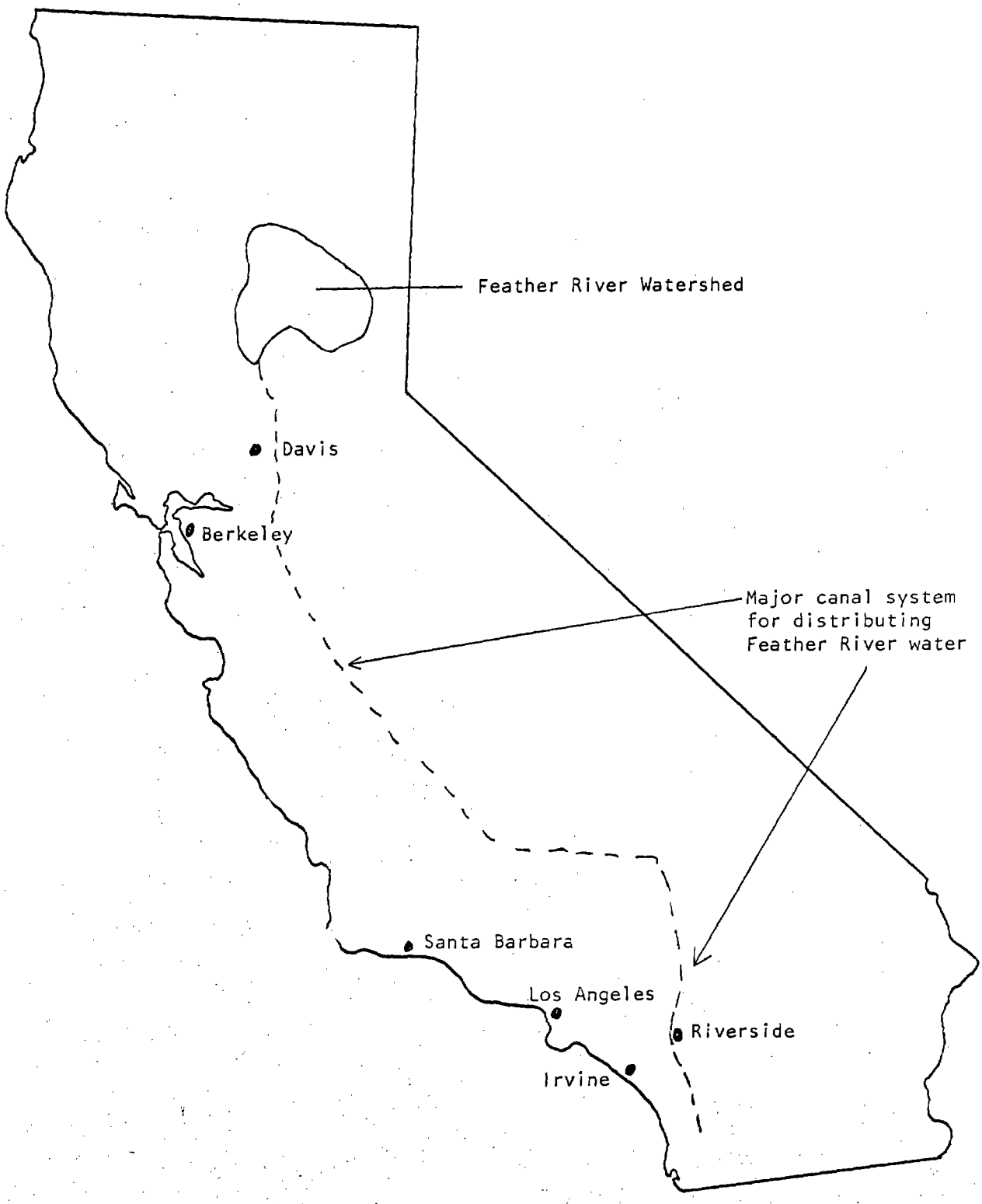

Figure 4. Location of participating campuses that are involved in the Integrated Study and their relation to the California Water Project.

N72-29341

SECTION 41

REMOTE SENSING OF SOILS, LAND FORMS, AND LAND USE IN THE NORTHERN GREAT PLAINS IN PREPARATION FOR ERTS APPLICATIONS[1]

by

C. J. Frazee, F. C. Westin, J. Gropper and V. I. Myers[2]
Remote Sensing Institute and
Plant Science Department
South Dakota State University
Brookings, South Dakota

INTRODUCTION

Information about soil limitations is necessary to determine the capability and suitability of an area for different land uses. The various types of soil limitations, according to the Soil Conservation Service (SCS, 1961), are erosion, wetness, soil rooting zone and climate. This information is normally derived from interpretation of detailed soil surveys. The primary sources of soil surveys are the USDA Soil Conservation Service and the cooperative soil survey which is composed of agencies, both state and federal, who compile and use soil survey information for land use planning. Following are two examples illustrating the use of information about soil limitations for land use decisions. A detailed soil survey is the first requirement of a farm conservation plan by the Soil Conservation Service. Based upon the soil survey, the capability of each piece of land is planned for a particular land use. One of the first items the Bureau of Reclamation needs for the proposed irrigation plan of an area is a detailed land classification indicating the suitability of the land for irrigation. Examples such as the above can be cited for practically any agency involved in land use planning.

---

[1]Approved for publication by the Director of the South Dakota Agr. Exp. Sta. as ~~Journal Series No.~~ 1070. RSI-72-02. Work performed under NASA contract NGL 42-003-007 under the direction of the Earth Observations Office and the Office of University Affairs. Presented at the Fourth Annual Earth Observations Program Review, Jan. 17-21, 1972. Manned Spacecraft Center, Houston, Texas.

[2]Assistant Professor and Professor, Plant Science Department; Research Assistant and Director, Remote Sensing Institute, South Dakota State University, Brookings, S. D. 57006, respectively.

With present techniques this type of information will not be available for all of the United States until the 1990's. For instance, South Dakota has current soil surveys for slightly less than one-third of the 65 counties. Using present techniques soil scientists are not producing this needed information as fast as it is being demanded. More detailed and accurate information is essential for the more intensive land uses of the future. Hopefully, remote sensing is a tool that can help satisfy this problem. However, considerable research will be necessary to determine the exact role of remote sensing for providing soil limitation data.

The long range objective of this research is to establish principles for recognizing and mapping soil limitations using remote sensing techniques. The present concept for using remote sensing to collect data about soil limitations encompasses using multispectral and temporal data from spacecraft and aircraft. The satellite imagery will be interpreted by standard techniques of photo interpretation for delineation of general soil areas. The aircraft imagery will be used to identify and map the component parts of the general soil areas.

With this concept in mind the objectives for the study in 1971 were:

1. To determine proper timing and wave lengths for identifying and mapping soil limitations.

2. To establish rangeland test sites for determining the usefulness of ERTS imagery.

The first objective relates to studying a proposed irrigation project of an area of fairly intensive agriculture where detailed information about soil limitations is needed. With the present predicted resolution of ERTS imagery, this level of information is not expected to be obtained from the use of ERTS data. The second objective relates directly to potential ERTS applications. The type of soils data needed for rangeland areas is more general and ERTS type imagery should be able to provide a major part of this information.

LOCATION AND DESCRIPTION OF STUDY AREAS

OAHE

The study area established in 1969 (Frazee et al., 1970, 1971) includes soils and land uses typical of the proposed Oahe irrigation project and the adjacent glacial drift area (Figure 1). This area was selected for remote sensing research because of the large amount of

ground truth data available. The South Dakota Agricultural Experiment Station in cooperation with the Soil Conservation Service has conducted a detailed soil survey of the area (Westin et al., 1954). The Bureau of Reclamation furnished detailed land classification maps of the portion of the flight line that lies in the proposed Oahe project. A unique advantage of studying this area is the opportunity of using remote sensing to follow the development of an irrigation project from initial land classification to actual water use and the eventual effects of irrigation on land use.

The Oahe project encompasses most of the Lake Dakota Plain (Flint, 1955), the site of a glacial lake late in the Wisconsinan glacial period. The surface of the Lake Dakota Plain is extremely flat, except where shallow stream channels occur, ranging in elevation from 1295 to 1310 feet above sea level. The soil parent materials are laminated lacustrine silt and clay deposits varying in thickness from 3 to 35 feet (Westin, 1970). The climatic environment is cool-temperate with irregular and usually deficient rainfall.

The flight line may be separated into two broad physiographic units, the Lake Dakota Plain and the Williams Loamy Plain (Frazee et al., 1971). The soils vary from friable silt loams with no limitations other than climate to soils with dense subsurface horizons (claypans) close to the surface which are not suited for irrigation.

The primary soil limitations are:

1. erosion of convex upland slopes
2. wetness in depressional or alluvial areas
3. soil rooting zone limitations
    a. claypans of varying density and thickness occurring at varying depths from the surface
    b. stoniness
    c. slowly permeable substratum

Additional information about the study area may be found in Westin et al., 1954 and Westin, 1970.

BENNETT COUNTY

Bennett County lies in the Missouri Plateau subdivision of the Great Plains physiographic province which is covered by Tertiary sediments (Fenneman, 1938). This area was selected because of the large amount of ground truth available (Collins, 1959, 1960; Chamberlin and Radeke, 1971). The county is part of the Pine Ridge Indian Reservation with about 300,000 out of the 761,000 acres managed by the Bureau of Indian Affairs. The major land uses are ranching (75%)

and winter wheat farming (23%).

The climate of Bennett County is semiarid and continental with large variations in seasonal temperatures and precipitation. Approximately three-fourths of the county is covered with native mid- to short-range grasses. The soil parent material consists primarily of silty to sandy sediments with associated alluvium.

The major soil limitations are:

1. erosion of sloping upland soils
2. wetness of depressional or alluvial areas
3. soil rooting zone limitations
   a. claypans of varying depths and thickness
   b. shallow depth to gravel
   c. shallow sandy and silty soils
   d. shallow depth to bedrock

Additional information about Bennett County and the study area may be found in Chamberlin and Radeke, 1971, and Collins, 1959, 1960.

EXPERIMENTAL METHODS AND PROCEDURES

Flights by the Remote Sensing Institute aircraft were conducted along the Oahe flight line during the 1970 crop growing season for the purpose of collecting photographic imagery within the ERTS wave length bands for studying soil limitations (Figure 1, Table I). NASA aircraft flights (RB-57 and C-130) were requested but none were obtained. Ground truth information on the various land use and soil conditions was recorded at the time of overflight. The film transparencies from these flights were evaluated for image quality (American Society of Photogrammetry, 1960) and prints were made of selected areas for laboratory and field study. Camera, film and filter data for imagery studied in detail are listed in Table I.

To help interpretation of the film transparencies listed in Table I, a density slicing system (Figure 2) which color encoded the various film density levels (Spatial Data Datacolor 703-32)[3] was used by experienced soil surveyors in order to identify and map soil limitations. The resultant color encoded representation was photographed and an enlarged print was made for field checking.

---

[3]Trade name is included only for benefit of reader and does not imply endorsement or preferential treatment.

The density slicing system analyzes the variation in tone of transparencies and displays the color encoded density levels on a color television screen. The system has the following components identified in Figure 2:

1. light box to illuminate the film transparencies
2. precision monochromatic television camera
3. electronic color analyzer which separates the shades of gray and color codes the signal for each gray level into as many as 32 levels
4. color television monitor for displaying either the color analysis or an image from the original transparency
5. electronic planimeter that measures the percent area of each color encoded density level
6. control keyboard

A standard step wedge may be used to calibrate the color levels to optical densities. Spectral filters may be used on the television camera to enhance the data received from the three spectral sensitive layers of color films.

The Bennett County flight line (Figure 1) was established in 1970 to study remote sensing of soil limitations in rangeland areas in preparation for ERTS applications. Camera, film, and filter data for imagery collected for the study area are listed in Table I. The major effort during this reporting period consisted of locating areas to be used as test sites for research using ERTS data and interpreting the imagery collected for features expected to be identifiable on ERTS imagery. Thematic maps were produced using aerial photo analysis for land use and drainage patterns. These will be used as ground truth for studying the potential of ERTS data for detecting soil limitations, identifying landforms, and determining land use.

RESULTS AND DISCUSSION

TEMPORAL ANALYSIS

Description of Photographs

Color infrared and black and white photographs taken on six different dates during the 1970 growing season were studied to evaluate the usefulness of seasonal information for mapping soil limitations (Table I). Two aspects were considered, the best time to obtain the photographic information and the value of using information from more than one time to study soil limitations. Several fields of the major crops grown in the Oahe area were studied. One 32 hectare field showing representative seasonal changes of the spring grains, which are

the major crops of the area, will be discussed and illustrated (Figure 1).

Four different situations were observed for the six flight dates available for study (Figure 3). The ground features on the photographs from the May, June and July dates were all different whereas the ones from the August, September and November dates were similar but different from the above times.

A more or less random pattern of different tones is shown on the May image (Figure 3). The field was planted to spring wheat, which was 5-10 cm high. The resulting pattern is produced primarily by the soil surface. The lightest tones are severely eroded areas whereas the darkest tones are areas with wetness limitations (Frazee et al., 1970). This same pattern would be expected if the field were fallowed or unplanted. However, the effect of the wheat crop is to change the density or color value of the tones of the surface features. Therefore although the photographic pattern of this field and a fallow field may be the same, in order to map the soil limitations of these fields different signatures would be necessary.

By June 25 the wheat had grown to full height, 80 cm, and was weedy (Figure 3). The soil surface pattern of the May image is almost completely masked. The pattern consists of varying levels of infrared reflectance with distinct circular light spots which are weeds. Some of the severely eroded areas can be identified.

On July 21 the spring wheat was 80 cm high, 90% mature, and weedy. The photographic pattern is due almost entirely to differences in the vegetation. Very few distinct differences in reflectance are noted (Figure 3). A few areas with wetness limitation are evident (Figure 3).

The August 12, September 10 and November 5 photographs were taken after the spring wheat was harvested. A stubble 15 cm high with weeds masked the soil surface and is responsible for the photographic pattern. Of these data, only the November photographs are illustrated (Figure 3).

DENSITY SLICING ANALYSIS

The Spatial Data System (Figure 2) was used to enhance the photographic density differences present for the different dates. The color encoded May and June images represent primarily soil and vegetation modified soil features, while the July and November images show some cultivation or cultural effects.

The color encoded representation of the May image is best for

obtaining information about soil limitations. The severely eroded areas are shown in yellow, the areas with slight to moderate erosion hazard are green, the red color portrays the normal soils, and the wet areas are blue on the May image (Figure 4). This color encoded representation was field checked and was found to correlate with the soil limitations actually present (Frazee et al., 1971).

The density slicing analysis of the June image is somewhat different (Figure 4). Although most of the severely eroded areas are color encoded yellow, the other soil limitations are not represented. The spring wheat has masked the soil surface except for the severely eroded areas and the resulting vegetative cover does not reflect or show the other soil limitations present. This is the major problem of using vegetation as an indicator of soil limitations in cultivated areas. The crop grown is normally selected to minimize the effects of soil limitations or is not affected every year.

The primary feature shown on the color encoded July image is a somewhat rectangular area in the middle of the field (Figure 4). This feature is interpreted to be the result of the farmer's cultural or cultivation practices.

A similar feature is illustrated on the November image (Figure 4). However, the location of the area is different.

On the basis of this analysis, the May 26 image was best for identifying and mapping soil limitations. The reason being that the soil surface pattern was most apparent at that time. Therefore, the optimum time for obtaining imagery to study soil limitations in the study area is when the soil surface pattern can be sensed or photographed. In the Oahe area this is May. The percent of fields along the flight line for which soil limitations could be adequately mapped using this criteria (observable soil surface patterns) for the various times studied is: May 26, 59%; July 21, 20%; August 13, 18%; September 10, 18%; and November 5, 21%. These results suggest that to map soil limitations of the study area by remote sensing techniques, imagery from more than one time or year will be required.

COMPARISON OF DENSITY SLICING ANALYSIS WITH SOIL SURVEY

The density slicing analysis of the best seasonal image for detecting soil limitations was compared with the existing soil survey map of this field (Westin et al., 1954) to analyze the value of density for mapping soil limitations (Figures 5 and 6). The soil map shows two mapping units which differ in slope and composition (Figure 6). The No. 67 mapping unit is Williams-Bowbells loams, undulating (3-5% slope). The No. 23 mapping unit is Bowbells-Williams loams, nearly level (0-2% slope). At first glance the density slicing analysis bears

little resemblance to the soil map (Figure 6). There is a higher percentage of yellow and green color encoded areas in upper left of the image. These colors are associated with the soils occurring on more sloping areas. The color encoded representation shows the complex of four soils better than the original soil map. The density slicing analysis was checked in the field and correlates with the soils found in this field (Figure 5).

Additional and more accurate information about the boundaries delineating areas of similar soil limitations is obtainable from the density slicing analysis than from the existing soil map. There are two major reasons for this. First, the density slicing system is extremely fast and efficient at measuring film density and grouping areas of the same densities. This allows for many more observations than a human could feasibly make in a reasonable length of time. The other reason is related to the quality of the photograph which the soil scientist used to make the soil survey (Figure 7). The photograph was a standard ASCS photograph taken with panchromatic film with minus blue filter in August, 1939. The soil surface was covered almost completely by a crop and very little information could be derived from photograph by the soil scientist to make inferences about the soils present in this field (Figure 7). This is the problem of using standard ASCS photographs for mapping soils. ASCS photographs are taken primarily to locate and measure cropped field boundaries for compliance with government farm programs. The ASCS photographs are normally taken in mid-summer, which, as shown in the previous analysis (Figures 3 and 4), is not the optimum time for obtaining photographs for soil surveys in cultivated areas. The most important immediate use of remote sensing for soil surveys would be to provide the soil surveyor with an image or photograph taken specifically for soil survey.

FILM QUALITY

The film transparencies obtained from the 70 mm Hasselblad cameras using black and white films filtered for the green and red portions of the spectrum and black and white infrared film were evaluated for the film quality characteristics of tone contrast and sharpness, (American Society of Photogrammetry, 1960) (Table I). The purpose was to evaluate imagery collected in similar wavebands as will be used in RBV television cameras on the ERTS satellite for observing soil patterns. From this simple analysis, the RBV camera filtered for the red portion of the spectrum appears most useful for studying soil (Table II). The soil patterns were nearly always observed easiest on the Plus-X or Tri-X film filtered for the red portion of the spectrum because of greater tone contrast and image sharpness.

BENNETT COUNTY

The mosiac of the Bennett County flight line is shown in Figure 8. The primary features are the sandy rangelands, southern part of south half of flight line, cultivated areas in the middle of the flight line, and the silty and loamy rangelands on the north half of the flight line (Figure 8). This flight line was established to collect data for testing the usefulness of the ERTS satellite for studying soil limitations.

Drainage pattern and land use have been interpreted for the flight line. A representative area of the flight line will be used to illustrate the nature of the test data.

The drainage pattern of the northern half of the flight line correlates with land use boundaries (Figures 9 and 10). The areas suitable for cultivation are not dissected by drainageways or have very few drainageways. The density of the drainage pattern has some correlation with slope (Figure 9).

The land use boundaries were determined primarily by observing the presence of regular patterns or field boundaries (Figure 10). Of the land use categories, rangeland and cropland appear to be easily separated, but the cropland and hayland areas are hard to distinguish from each other.

SUMMARY

Research to determine the optimum time or season for obtaining imagery to identify and map soil limitations was conducted in the proposed Oahe irrigation project area in South Dakota. The optimum time for securing photographs or imagery is when the soil surface patterns are most apparent. For cultivated areas similar to the study area, May is the optimum time. The fields are cultivated or the planted crop has not yet masked the soil surface features. Soil limitations in 59 percent of the field of the flight line could be mapped using the above criteria. The remaining fields cannot be mapped because the vegetation or growing crops did not express features related to soil differences. This suggests that imagery from more than one year is necessary to map completely the soil limitations of Oahe area by remote sensing techniques. Imagery from the other times studied is not suitable for identifying and mapping soil limitations because the vegetative cover masked the soil surface and did not reflect the soil differences.

The density slicing analysis of the May image provided additional and more accurate information than did the existing soil map. The soil boundaries were more accurately located. The use of a density

analysis system for an operational soil survey has not been tested, but is obviously dependent upon securing excellent photographs for interpretation. The colors or densities of photographs will have to be corrected for sun angle effects, vignetting effects, and processing to have maximum effectiveness for mapping soil limitations.

Rangeland sites were established in Bennett County, South Dakota to determine the usefulness of ERTS imagery. Imagery from these areas was interpreted for land use and drainage patterns.

LITERATURE CITED

1. American Society of Photogrammetry. 1960. Manual of Photographic Interpretation.

2. Chamberlin, E. and R. E. Radeke. 1971. Soil Survey of Bennett County, South Dakota. USDA Soil Conservation Service.

3. Collins, S. G. 1959. Geology of the Martin quadrangle. S. Dak. Geo. Survey map and text.

4. Collins, S. G. 1960. Geology of the Patricia quadrangle. S. Dak. Geo. Survey map and text.

5. Fennemann, N. M. 1938. Physiography of Eastern United States. McGraw-Hill, New York.

6. Flint, R. F. 1955. Pleistocene Geology of Eastern South Dakota. U. S. Geol. Survey Prof. Paper 174.

7. Frazee, C. J., R. D. Heil, and F. C. Westin. 1970. Remote Sensing for detection of soil limitations in agricultural areas. In Third Annual Earth Resources Program Review. MSC-03742(NASA). Vol. II: Agricultural/Forestry and Sensor Studies, Sec. 25, NASA Manned Spacecraft Center, Houston, Texas, Dec. 1-3.

8. Frazee, C. J., R. D. Heil, and F. C. Westin. 1971. Remote Sensing for detection of soil limitations in agricultural areas. RSI 71-3. Remote Sensing Institute, South Dakota State Univ., Jan., 1971.

9. Soil Conservation Service. 1961. Land Capability Classification. Agriculture Handbook No. 210, USDA.

10. Westin, F. C., G. J. Buntley, W. C. Moldenhauer, and F. E. Schubeck. 1954. Soil Survey of Spink County, South Dakota. S. Dak. Agr. Exp. Sta. Bul. 439.

11. Westin, F. C. 1970. Genesis of the soils of Lake Dakota Plain in Spink County, South Dakota. S. Dak. Agr. Exp. Sta. Tech. Bul. 37.

TABLE I. CAMERA, FILM AND FILTER DATA FOR STUDY AREAS

January 1, 1970 - December 31, 1970

Mission	Date	Altitude AGL Ft.	Time of day-hrs.	Sensor	Film type	Filter	Wavelength μ	Roll or tape No.
				Oahe Study Area				
104	5-26-70	14,000	14:56-15:19	*Hass.70mm camera A	8403 Tri-X	58	.465-.620	70-144
				Hass.70mm camera B	8403 Tri-X	25A	.580-.710	70-145
				Hass.70mm camera C	8443 EK-IR	15G/30M	.510-.900	70-146
				Hass.70mm camera D	2448 EK-MS	HF3+4	.375-.710	70-147
				K-17 9x9in camera	8443 EK-IR	15G/30M	.510-.900	70-157
112	6-25-70	14,500	12:48-13:11	Hass.70mm camera A	8403 Tri-X	58	.465-.620	70-191
				Hass.70mm camera B	8403 Tri-X	25A	.580-.710	70-192
				Hass.70mm camera C	8443 EK-IR	15G/30M	.510-.900	70-193
				Hass.70mm camera D	2424 BW-IR	89B	.680-.900	70-194

*Hasselblad 500 EL

TABLE I. CONTINUED

Mission	Date	Altitude AGL Ft.	Time of day-hrs.	Sensor	Film type	Filter	Wavelength μ	Roll or tape No.
121	7-21-70	14,500	15:45-16:17	Hass.70mm camera A	8403 Tri-X	58	.465-.620	70-224
				Hass.70mm camera B	8403 Tri-X	25A	.580-.710	70-225
				Hass.70mm camera C	8443 EK-IR	15G/30M	.510-.900	70-226
				Hass.70mm camera D	2424 BW-IR	89B	.680-.900	70-227
				Thermal Scanner			4.5-5.5	5847
140	8-13-70	14,000	12:07-12:35	Hass.70mm camera A	2402 Plus-X	58	.470-.610	70-263
				Hass.70mm camera B	2402 Plus-X	25A	.590-.710	70-264
				Hass.70mm camera C	8443 EK-IR	15G/30M	.510-.900	70-265
				Hass.70mm camera D	2424 BW-IR	89B	.680-.900	70-266

TABLE I. CONTINUED

Mission	Date	Altitude AGL Ft.	Time of day-hrs.	Sensor	Film type	Filter	Wavelength μ	Roll or tape No.
				Thermal Scanner			4.5-5.5	5858
157	9-10-70	14,500	11:51-12:04	Hass.70mm camera A	2402 Plus-X	58	.470-.610	70-316
				Hass.70mm camera B	2402 Plus-X	25A	.590-.710	70-317
				Hass.70mm camera C	8443 EK-IR	15G/30M	.510-.900	70-318
				Hass.70mm camera D	2424 BW-IR	89B	.680-.900	70-319
				Thermal Scanner			4.5-5.5	5923

TABLE I. CONTINUED

Mission	Date	Altitude AGL Ft.	Time of day-hrs.	Sensor	Film type	Filter	Wavelength μ	Roll or tape No.
171	11-5-70	13,500	11:25-12:06	Hass.70mm camera A	2402 Plus-X	58	.470-.610	70-368
				Hass.70mm camera B	2402 Plus-X	25A	.590-.710	70-369
				Hass.70mm camera C	2443 EK-IR	15G/30M	.510-.900	70-370
				Hass.70mm camera D	2424 BW-IR	89B	.680-.900	70-371
				Thermal Scanner			4.5-5.5	5910

TABLE I. CONTINUED

Mission	Date	Altitude AGL Ft.	Time of day-hrs.	Sensor	Film type	Filter	Wavelength μ	Roll or tape No.
				Bennett County Study Area				
166	10-15-70	12,000	12:15-13:03	Hass.70mm camera A	2402 Plus-X	58	.470-.610	70-347
				Hass.70mm camera B	2402 Plus-X	25A	.590-.710	70-348
				Hass.70mm camera C	2443 EK-IR	15G/30M	.510-.900	70-350
				Hass.70mm camera C	2424 BW-IR	89B	.680-.900	70-349
				Thermal Scanner			4.5-5.5	5895

TABLE II. FILM QUALITY ANALYSIS OF OAHE STUDY AREA
January 1, 1970 - December 31, 1970

Mission	Date	Film No.	Filter No.	Tone	Sharpness	Film Characteristics
112	6-25-70	70-191	58	2	2	all imagery suitable for
		70-192	25A	1	1	interpretation
		70-194	89B	3	3	
121	7-21-70	70-224	58	3	3	all imagery suitable for
		70-225	25A	1	1	interpretation
		70-227	89B	2	2	
140	8-13-70	70-263	58	3	3	all imagery suitable for
		70-264	25A	1	1	interpretation
		70-266	89B	2	2	
157	9-10-70	70-316	58	3	3	all imagery suitable for
		70-317	25A	1	1	interpretation
		70-319	89B	2	2	
171	11-5-70	70-364	58	3	3	all imagery suitable for
		70-365	25A	1	1	interpretation
		70-367	89B	2	2	

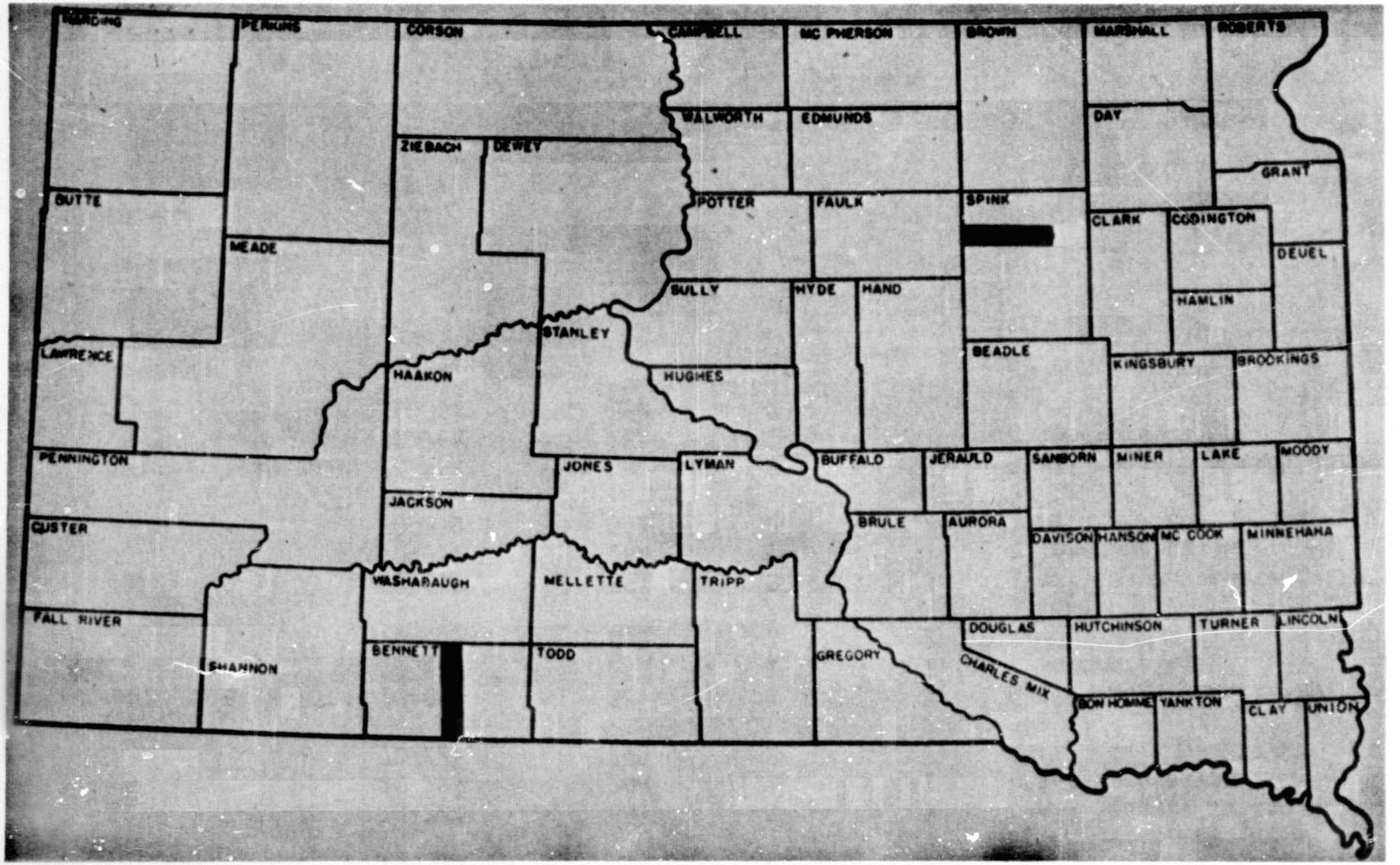

Figure 1.- Oahe and Bennett County Study Area.

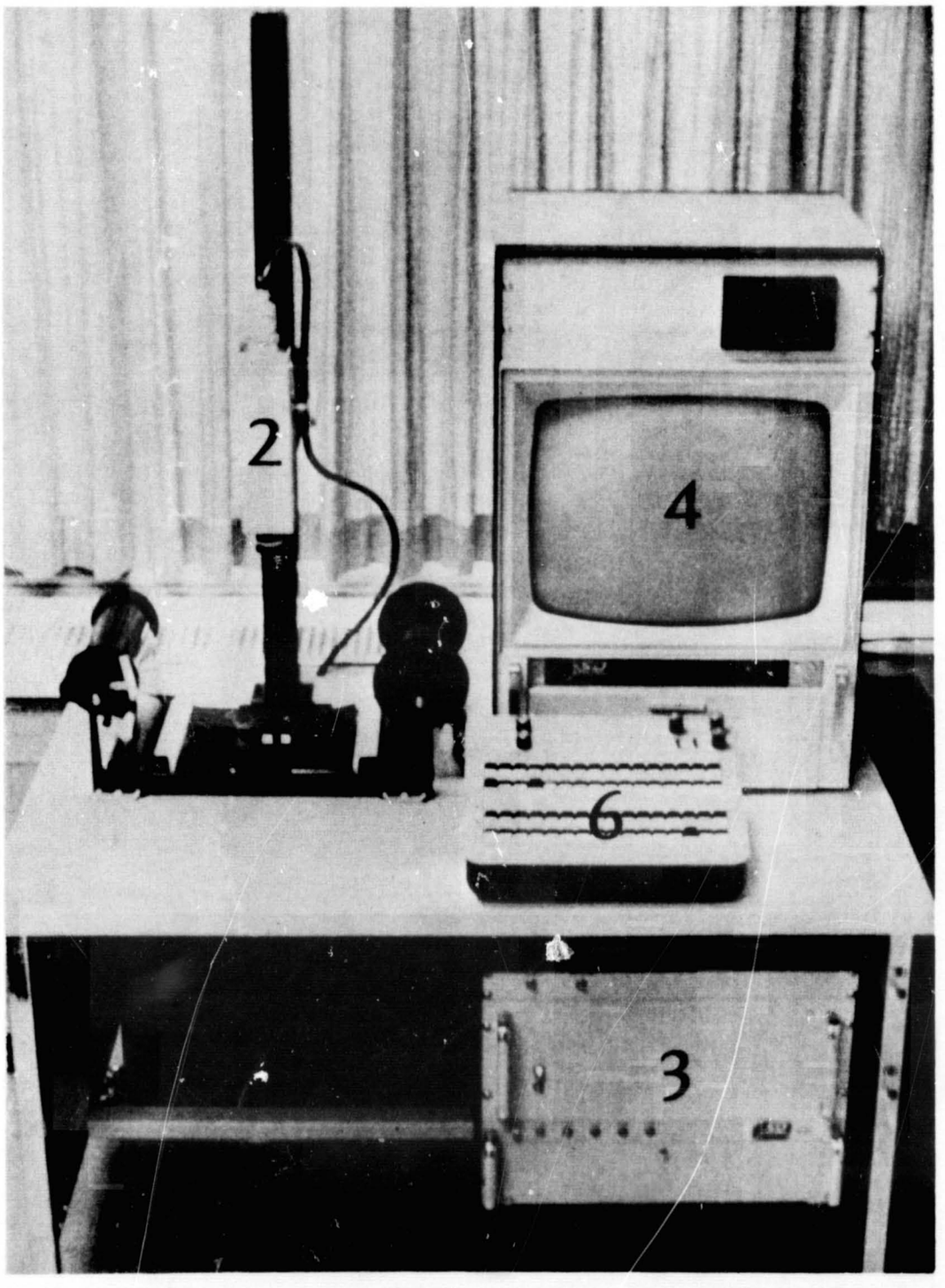

Figure 2.- Spatial Data Datacolor 703-32 density slicing system.

May 26

June 25

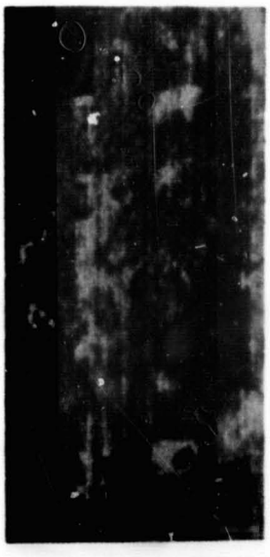

July 21

November 5

Figure 3.- Color infrared photographs of 1970 time analysis. T118N, R65W, Sec. 3, NE 1/4. Crop is spring wheat. Scale = 1:12,675.

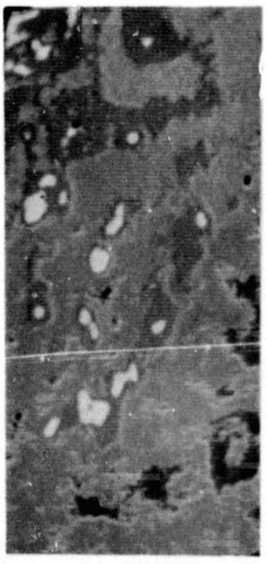

May 26

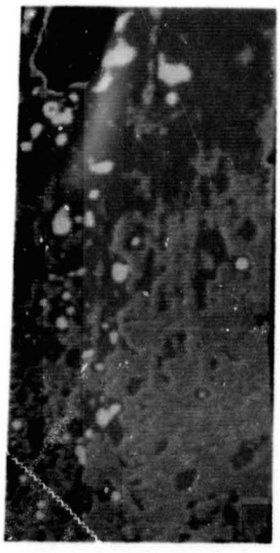

June 25

July 21

November 5

Figure 4.- Color encoded representation of Figure 3.

Color infrared
imagery May, 1970

Density slicing analysis

Figure 5.- Density slicing analysis of best seasonal image of 1970 for detecting soil limitations. T118N, R65W, Sec. 3, NE 1/4. Scale = 1:6,330.

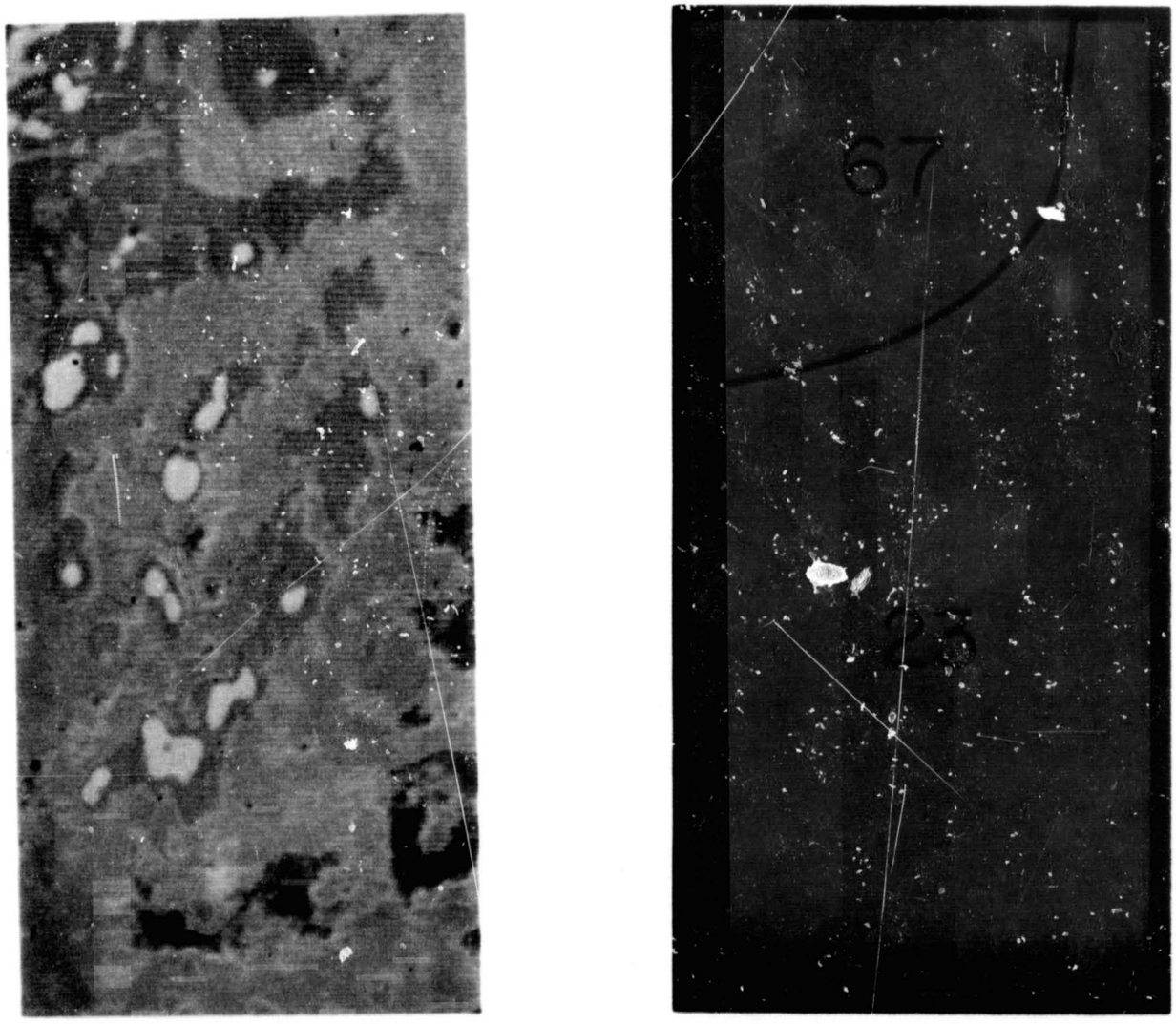

Density slicing analysis

Existing soil map

Figure 6.- Comparison of density slicing analysis with existing soil survey map. T118N, R65W, Sec. 3, NE 1/4. Scale = 1:6,330.

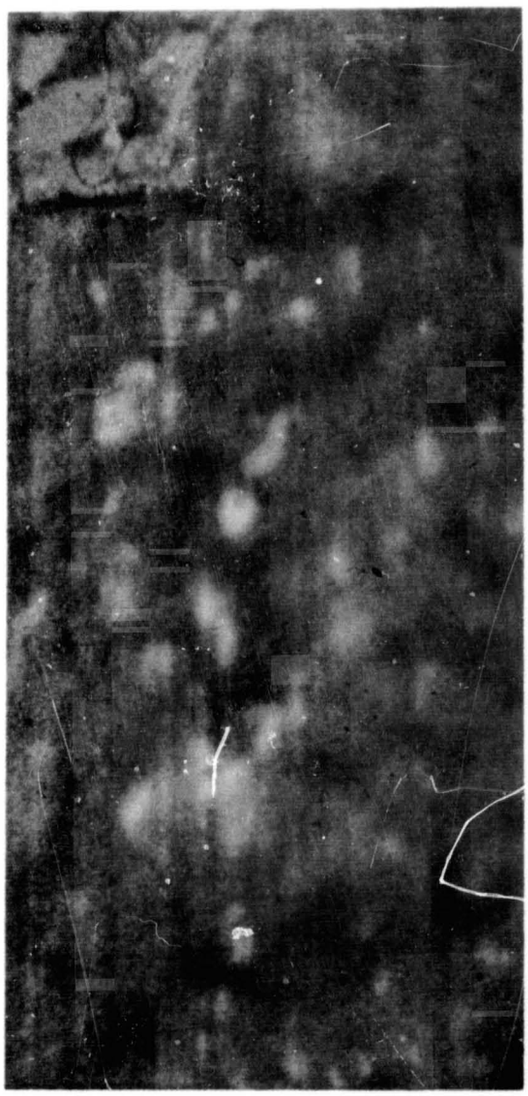

Color infrared
imagery May, 1970

Panchromatic film
August, 1939

Figure 7.- Comparison of remote sensing photograph with photograph used by soil scientists for soil survey. T118N, R65W, Sec. 3, NE 1/4. Scale = 1:6,330.

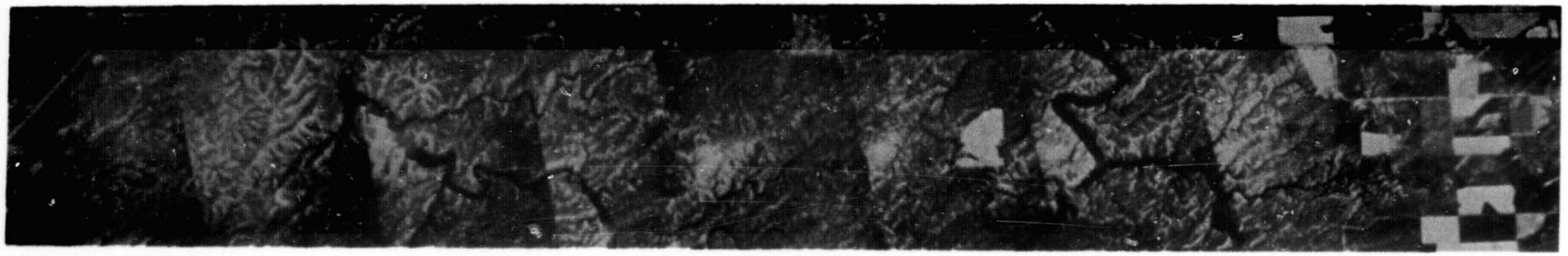

North half

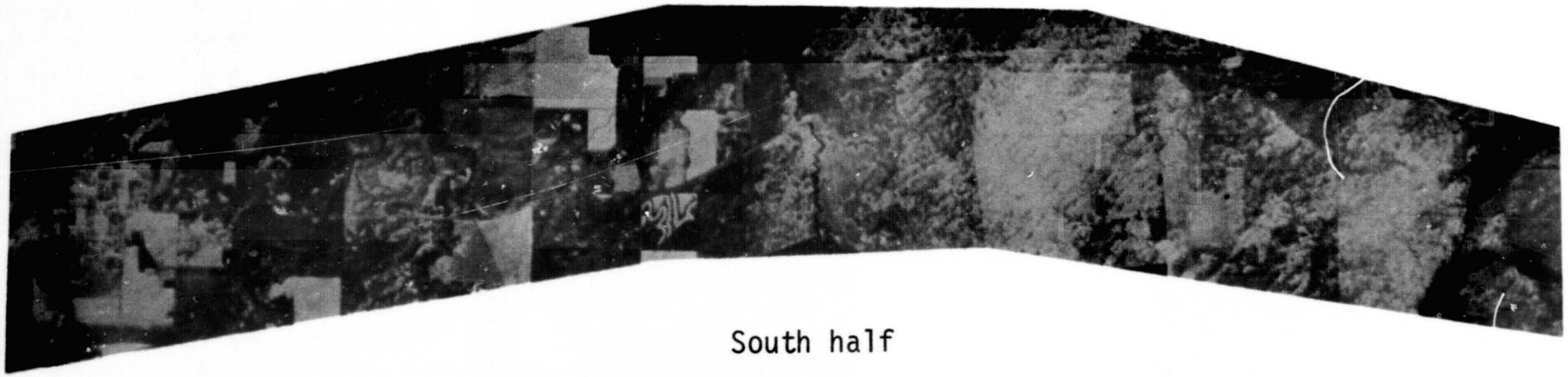

South half

Figure 8.- Bennett County flight line mosaics. Plus-X film with 25A filter. June, 1971. Scale = 1:125,000.

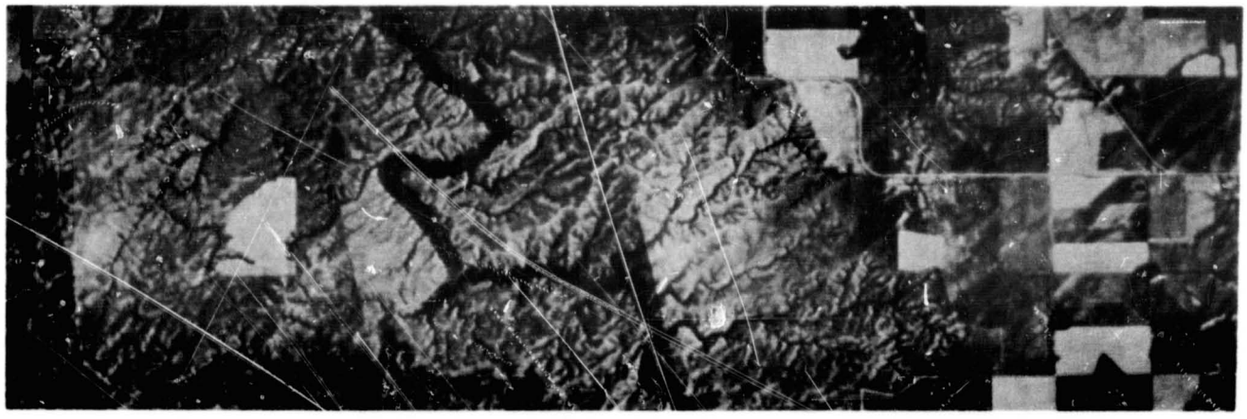

Plus-X film with 25A filter, June, 1971

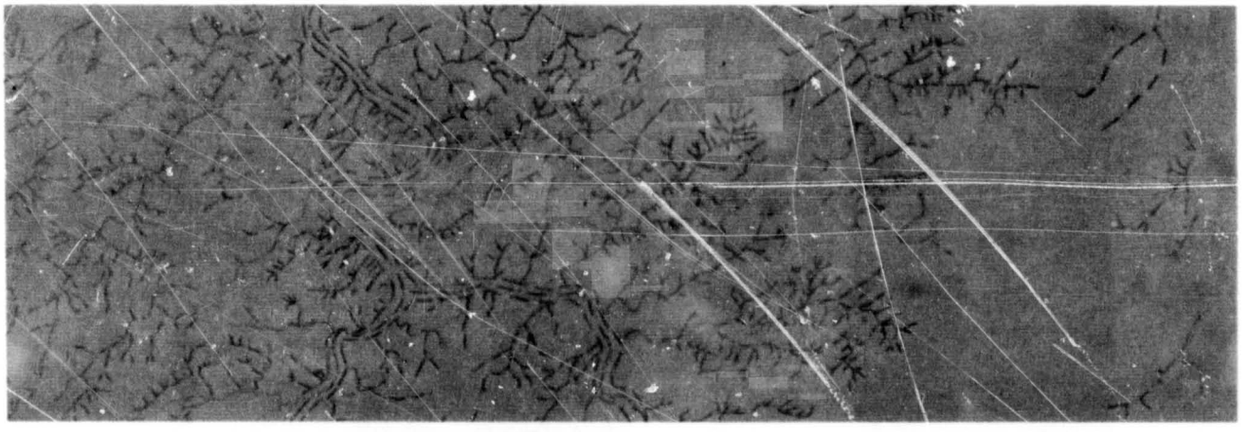

Drainage pattern

Figure 9.- Drainage analysis of a representative area of the northern half of the Bennett County flight line. Scale = 62,500

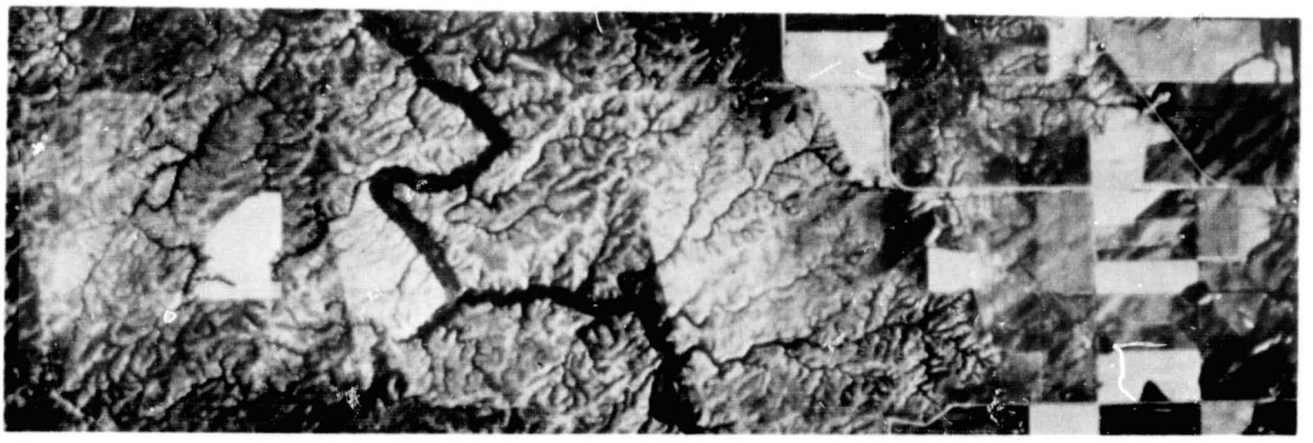

Plus-X film with 25A filter, June, 1971

Land use

Figure 10.- Land use analysis of a representative area of the northern half of the Bennett County flight line. Scale = 62,500. Yellow = cropland, Green = hayland, Brown = range or pasture.

SECTION 42

N72-29342

PATTERN RECOGNITION

SYSTEM AND PROCEDURES

Gerald D. Nelson
Remote Sensing Institute and
Electrical Engineering Department

and

David V. Serreyn
Remote Sensing Institute
Brookings, South Dakota

INTRODUCTION

The objectives of the pattern recognition tasks are to develop (a) a man-machine interactive data processing system and (b) procedures to determine effective features as a function of time for crops and soils.

This paper reports on the progress made toward achieving these objectives. The specific projects done and currently in progress are considered necessary to aid in the specification of data processing and classification techniques.

To assume that the data or features are multivariate Gaussian is sometimes unreliable. Therefore, in computer simulation studies when pseudo-random number generators are used to generate the feature vectors with specified statistical parameters, a criteria to judge the probability of the data being from the specified probability density function is required. The Kolmogorov-Smirnov test is used to determine if the pseudo-random number generator produced Gaussian data.

Another problem area is to determine the advantages and disadvantages of transforming the measurements. Experimental work by Nalepka (1) has shown the advantage of the ratio technique.*

In this paper the ratio transformation is considered. However, the effect of noise is implied to be additive. The case of multiplicative noise should also be pursued.

The selection of quantizer parameters for a two-class recognition problem under the criteria of minimizing the probability of error is also discussed.

Contextual data (2) has been used to show decreased probability of error in classification experiments. A study to evaluate the conditions necessary to provide this decreased probability of error is in progress. The purpose and method of the study is discussed.

---

*In the abstract of this paper (Nelson and Serreyn) an incorrect statement was made by Nelson concerning the work on the ratio technique reported by Nalepka. Instead of the ratio transformation always yielding poorer classification results than the original data the classification results are always better.

The man-machine interactive data processing system is referred to at the Remote Sensing Institute as the Signal Analysis and Dissemination Equipment, SADE. This system is described and plans for its use indicated.

The work on transformations of Gaussian variates (3) was done by John E. Boyd, previously a graduate student in the Electrical Engineering Department at South Dakota State University.

The remainder of the reported work was done at the Remote Sensing Institute at South Dakota State University in Brookings, South Dakota. The work was performed under grant number NGL 42-003-007 which is supported by the Office of University Affairs and the Earth Observations Office of NASA.

MULTIVARIATE GAUSSIAN ASSUMPTION

A very common assumption made by investigators is that the features used to represent the pattern classes are multivariate Gaussian. To validate the Gaussian assumption is not a trivial task. Papoulis (4) discusses the bivariate Gaussian case. If the joint probability density function is bivariate Gaussian it is also true that the marginal probability density functions are also Gaussian. However, if the marginal probability density functions are Gaussian the joint probability density function is not necessarily bivariate Gaussian.

To study by computer simulation methods the effectiveness of contextual data requires the use of a pseudo-random number generator. The generation of Gaussian random variates can be conveniently done by the use of the IBM subroutines GAUSS and RANDU. RANDU generates a uniform random number between zero and one by a power residue method. GAUSS requires twelve uniform random numbers to generate one Gaussian random variate. The central limit theorem is used with the number of uniform random numbers set at twelve instead of approaching infinity in order to make the procedure feasible.

Another method of generating Gaussian random variates is known as the Muller method (5). The equations which relate T, Y, U and V are

$$T = \sqrt{-2\ln U} \quad \cos(2\pi V)$$

$$Y = \sqrt{-2\ln U} \quad \sin(2\pi V)$$

The validity of the computer simulation study depends on the probability density function (pdf) of the data produced by the random number generators. To test the pdf's the Kolmogorov-Smirnov test

(K-S test) (6) was used on RANDU, GAUSS and the Muller produced pseudo-random numbers. The results of the K-S test as a function of the number of samples are presented in Table I.

The results of the K-S test indicate that except in several cases the pseudo-random numbers have less than 90 percent chance of being from either uniform or Gaussian pdf's.

GAUSS uses the output of RANDU and the Muller method uses the output of RANDU twice, with different seeds as listed in Table I. The means and variances for RANDU are very good estimates of the specified population means and variances. The results of the K-S test indicate that before the computer simulation experiment is performed the pseudo-random number generator should be evaluated by this test.

TRANSFORMATIONS OF GAUSSIAN VARIATES

In this two-class problem the features selected are denoted X_1 and X_2. For class one these features are uncorrelated, and each is Gaussianly distributed with mean zero and variance one. For class two these features are correlated, and each is Gaussianly distributed with mean zero and variance one. Therefore class one and two are overlapping bivariate Gaussian probability density functions. The contours of these two overlapping probability density functions are shown in Figure 1.

To classify the data based on the features X_1 and X_2 the Bayes classifier was derived and the decision boundaries determined. Figure 2 represents the three sigma contours of the class one and two bivariate Gaussian probability density functions. The decision boundaries are shown as hyperbolas. The alpha and beta errors are .216 and .053 respectively with a total error of 0.1345.

It can be shown (4) that Z, the ratio of two Gaussian variates, $X_1/X_2=Z$ has an univariate Cauchy probability density function. The pdf of X_1 and X_2 is

$$f(X_1,X_2)= \frac{1}{2\pi\,\sigma_1\sigma_2\sqrt{1-r^2}} \exp\left[\frac{-1}{2(1-r^2)}\left(\frac{X_1^2}{\sigma_1^2} - \frac{2rX_1X_2}{\sigma_1\sigma_2} + \frac{X_2^2}{\sigma_2^2}\right)\right]$$

For class one the correlation coefficient r is zero and for class two is .98.

The Cauchy pdf of Z is

$$f(Z) = \frac{\sqrt{1-r^2}}{\pi[\sigma_2^2(Z-r\frac{\sigma_1}{\sigma_2})^2 + \sigma_1^2(1-r^2)]} \quad \sigma_1\sigma_2$$

The classification process is now based on the feature Z which is the ratio X_1/X_2. The probability of error is of prime interest. The Bayes classifier for Cauchy data was derived and the results determined. The alpha and beta errors are .347 and .130, respectively. See Figure 3. The total probability of error is .2385. Therefore, under the assumption of this problem it is obvious that taking the ratio is not useful to decrease the probability of error. In fact the probability of error has increased 10.4 percent from 13.45 percent to 23.85 percent.

QUANTIZATION

The effects of using quantized data on classification error was investigated for a two-class problem involving a single feature or attribute. The results of this study are summarized here and given in a Technical Interim Report (7).

A quantizer is best described by its transfer characteristic. The transfer characteristics for an even and odd equi-interval quantizer are shown in Figures 4 and 5 respectively. The input to the quantizer consists of data whose distribution is assumed to be normal. The effect of the quantizer is to assign a specific value to any of the data that falls in a given range. The value for r, the quantization interval, is constant for a given quantizer but varies with the number of levels.

The output of the quantizer consists of NQ values where NQ is the number of quantize levels. Each of these NQ values is weighted by the area under the normal curve within the input range as given by the transfer characteristic. For the multi-sample problem, the pdf (probability density function) is multinomial. This is due to the fact that the output consists of NQ levels. If only two levels are present, then the sampled data is distributed binomially.

For the one sample case, the pdf for the data is the output pdf of the quantizer. The probability of error is given by

$$P(E) = q_1\alpha + q_2\beta$$

where q_1 and q_2 are probabilities of occurrence for each of the two classes. At the output of the quantizer, the probability of error is a summation given by

$$P_q(E) = (q_1/2)\sum_{k=N+1}^{NQ} [\text{erf}\{u_{k+1}+s)/\sqrt{2\sigma}\} - \text{erf}\{(u_k+s)/\sqrt{2\sigma}\}]$$

$$+ (q_2/2)\sum_{k=1}^{N} [\text{erf}\{(u_{k+1}+s-\mu)/\sqrt{2\sigma}\} - \text{erf}\{(u_k+s-\mu)/\sqrt{2\sigma}\}].$$

for the normal case. This reduces to

$$P_q(E) = (q_1/2)[1-\text{erf}\{(u_{N+1}+s)/\sqrt{2\sigma}\}]$$

$$+ (q_2/2)\ 1+\text{erf}\{(u_{N+1}+s-\mu)/\sqrt{2\sigma}\}].$$

In the above equations s is a shift factor, u_{N+1} is the location of the $(N+1)^{th}$ input location. The decision boundary is at the N^{th} impulse. The probability of error is graphed in Figure 6 for various values of N. The entire graph for each value of N is not given. The location of equal probability of error are drawn in. The X locates the minimums.

To find the location of the minimums involves taking the derivative setting to zero and solving for the variable in question, namely r. Solving for r yields

$$r = \{(2\sigma^2/\mu)\ln(q_1/q_2) + \mu-2s\}/(2N-NQ).$$

This value of r gives the minimum probability of error. In fact, this value makes the probability of error equal to that of the continuous case. In Figure 7, the probability of error is graph for two values of r. One case is the derived while the other involves an r that minimizes the mean-square-error between input and output derived by Max (8).

As the number of samples increases before a decision is made, the probability of error decreases in the continuous case. The same is true of error for the multi-sample case is shown in Figure 8 for a two and three level quantizer as well as continuous. Ones does get more probability of error in the quantized case. However, the

differences in error may be acceptable if one is concerned with the accuracy of the measurement and the cost of obtaining such accuracy.

CONTEXTUAL DATA

The data that occurs adjacent to the cell of the image to be classified provides additional information to be combined with the data of the cell. This additional data is known as the contextual data, and the information added is contextual information. The contextual data is added to the decision rule of the classifier by the following product of sums of probability density functions (2).

$$\prod_{i=1}^{4} \sum_{\theta_{k_i}} p(X_{k_i}|\theta_{k_i})\, p(\theta_{k_i}|\theta_k)$$

where

$p(X_{k_i}|\theta_{k_i})$ is the conditional pdf of the measurement vector X_{k_i} given the cells identity, θ_{k_i}.

$p(\theta_{k_i}|\theta_k)$ is the conditional pdf of the occurrence of the θ_{k_i} class given the k^{th} cell identity, and

k_i's are the nearest neighbors to the k^{th} cell.

The complete decision rule is to

$$\text{Minimize} \sum_{\theta_k} L(\theta_k,a)\; p(X_k|\theta_k)G(\theta_k) \prod_{i=1}^{4} \sum_{\theta_{k_i}} p(X_{k_i}|\theta_{k_i})p(\theta_{k_i}|\theta_k)$$

The terms are:

θ_k is the k^{th}class.

X_k is the optical density measurement of the k^{th}class.

a is $(a_1,a_2,- - - a_n)$.

a_k is the decision that the k^{th} class is present.

$L(\theta_k,a)$ is the loss associated with making a decision.

The assumptions are that contextual relationships between non-adjacent cells are negligible which can be stated as

$$p(X_b|\theta_c,X_i,\theta_i) = p(X_b|X_i,\theta_i)$$

for all i and cells b and c are nonadjacent. The appearance x_k of a class θ_k is a function only of θ_k, and if θ_k is known neither the nature nor the appearance of any other class provides additional information about X_k. This can be stated as

$$p(X_k|\theta_k,X_i,\theta_i) = p(X_k|\theta_k).$$

For a special case of a temporal signal on line scan data this contextual rule can be more easily interpreted and the effect of the contextual data illustrated if a two-class problem is discussed. The next equation specifies the mathematical operations necessary to make a decision.

$$\frac{p(X_k|\theta_1)}{p(X_k|\theta_2)} > KM \quad \text{decide } \theta_1$$

$$\leq KM \quad \text{decide } \theta_2$$

where

$$K = \frac{G(\theta_2)L(\theta_2,a)}{G(\theta_1)L(\theta_2,a)},$$

and

$$M = \frac{[p(X_{k_1}|\theta_1)p_{12}+p(X_{k_1}|\theta_2)p_{22}][p(X_{k_2}|\theta_1)p_{12}+p(X_{k_2}|\theta_2)p_{22}]}{[p(X_{k_1}|\theta_1)p_{11}+p(X_{k_1}|\theta_2)p_{21}][p(X_{k_2}|\theta_1)p_{11}+p(X_{k_2}|\theta_2)p_{21}]}$$

The notation p_{ij} is used for the a priori probabilities $p(\theta_i|\theta_j)$.

If contextual data is not used the decision rule reduces to

$$\frac{p(X_k|\theta_1)}{p(X_k|\theta_2)} > K$$

or M is assumed to be unity.

To determine the value of M only the measurements in the nearest neighbor cells and the a priori probabilities of occurrence of each class as represented by p_{ij} for all i and j are required. The measurement in cell k provides the needed data to evaluate the left hand side of the decision rule. Since the right hand side, the product of K and M varies one can think of contextual data as providing a decision boundary which varies as a function of the measured data.

A computer simulation is nearly completed which will provide a comparison of the probability of error if (a) contextual data are not used and (b) contextual data are used, as well as these comparisons for more than one measurement per cell.

The similarity of this simulation to data to be extracted from imagery should be noted. The cells correspond to data windows whose width will vary according to field size. The use of the nearest neighbor cells can be easily extended to be used by obtaining the data from the preceeding and succeeding scan lines in the respective cells.

The necessity of having line scan data and a procedure to edit the ground truth data into the system so that it can be used effectively is imperative.

To use this technique on imagery, requires knowledge of at least the soils type and/or crop type for all fields within the training set.

Only the two class case has been discussed, but generalization to more classes has been done (2).

SIGNAL ANALYSIS AND DISSEMINATION EQUIPMENT

INTRODUCTION

This section discusses the Remote Sensing Institute's Signal

Analysis and Dissemination Equipment (SADE).

This equipment was designed as a state-of-the-art data analysis system for a medium cost with highly flexible modular design. The maximum resolution of any individual module is not as great as may be achieved at a higher cost. However, the integration of each segment with a medium high resolution has produced a system of outstanding capabilities. The SADE system includes the following features:

high resolution, high quality digitization of black and white and color film transparencies,

35mm, 70mm, 9½ inch single frame or roll films may be accommodated,

multiple frames may be registered with respect to one another conveniently and accurately,

registration of images can be accomplished off-line without interaction with the computer,

analog magnetic tape data can be digitized for computer analysis from one to six channels,

a refresh memory is provided for the display of processed data on the video monitor and for multiple frame registration,

refresh memory is expandable for storage of high frame resolution imaged data and larger display formats,

memory format is Pax II picture processing language (9) oriented for processing within the computer,

processed digital data may be converted to hard copy using a line printer,

control of the system's components in communication with the computer is provided via teletype and system control panel.

SYSTEM CONFIGURATION

The system is configured in five major units:

1. The Spatial Data camera, level slicing, and color display monitor;

2. The image digitizer utilizing an image dissector tube;

3. The data control and conversion unit which contains elements for high speed memory, analog tape conversion and control functions,

4. The Lockheed 417 seven track analog tape recorder, and

5. The Daedalus Film Printer.

SYSTEM FUNCTIONS

The SADE system will provide the following system functions:

Visual display of digitized film data,

Digitized image data transmitted to the computer,

Analog tape data digitized and transmitted to the computer,

Processed image data transmitted to the display monitor through the refresh memory for visual interpretation,

Processed digital data to the Daedalus Printer for 70mm film output,

Registration of images via the digitizer and display monitor, and

System control.

MODES OF OPERATION

The SADE system can be operated in the image data and analog tape data digitization modes. The image can be digitized and displayed on the color monitor, and the digitized data transmitted to the computer memory. A second image can be digitized and through mechanical manipulation be registered by observation of the color display which displays both the first and second images simultaneously through use of the raster interlaced system. After registration the digitized data which represents the second image is transmitted to the computer memory. Likewise, maps may be made, digitized and stored in the computer memory and the image overlayed on the map on the display.

The image can be quantized according to the optimal quantizer derived in this paper and the resulting color encoded image displayed on the monitor. This is one method of classifying the image according to optical density which has been shown to be useful by Frazee (10).

Classification of the data if multiple features are used will be done by K-class, Bayes or contextual data classifier algorithms. The classification results will be color encoded and displayed on the monitor.

The digitized image can also be transmitted to the Daedalus printer for 70mm hard copy.

The analog tape digitization mode of operation provides the capability to digitize from one to six channels of multi-spectral data stored on analog magnetic tape. The data can be displayed one channel at a time on the display. The data can be digitized 6 channels at a time and transmitted to the computer for storage in digital form. Possible inputs to the analog tape conversion unit includes thermal scanner data, multispectral scanner data up to 6 channels and weather satellite image data.

ANTICIPATED USES OF THE SADE SYSTEM

The SADE system was designed as a flexible research tool for data processing and data classification which can be expanded. The SADE system can also be expanded to provide information dissemination capabilities. These information dissemination capabilities include television broadcasts, special systems and output copy. The dissemination system chosen will depend upon the specific application and output form desired by the user. Although the SADE system is designed as a research tool, it is also anticipated that analysis completed in the research phases will be implemented in an operational system for individual users. Thus, a state agency interested in surface water could use, on an operational basis, information from the ERTS-A satellite in their daily decision-making processes.

CONCLUDING REMARKS

The objectives of the pattern recognition tasks are to develop (a) a man-machine interactive data processing system and (b) procedures to determine effective features as a function of time for crops and soils.

The initial objective of developing an interactive system will be almost complete at the end of April with the installation of SADE (Signal Analysis and Dissemination Equipment). Classification programs already developed such as K CLASS, Bayes and contextual data will be utilized with SADE. Boundary detection algorithms which are being worked on will also be utilized. In order to speed up processing, a variable quantizer with parameters which are specified by the operator, has also been implemented.

The study of transformation of variables (features), especially those experimental studies which can be completed with the SADE system, will be done. The multivariate Gaussian assumption will either be justified and/or nonparametric techniques will be applied to imagery data. The secondary objective of determining effective features for crops and soils will not be achieved until the SADE system is operational.

BIBLIOGRAPHY

(1) R. F. Nalepka, "Investigation of Multispectral Discrimination Techniques", Infrared and Optics Laboratory, Willow Run Laboratories, Institute of Science and Technology, Contract #12-14-100-9548(20), January, 1970.

(2) J. R. Welch and K. G. Salter, "A Context Algorithm for Pattern Recognition and Image Interpretation", IEEE Transactions on Systems, Man and Cybernetics, Vol. S MC-1, pp24-30, January, 1971.

(3) J. E. Boyd, "Classification Error of Gaussian and Transformed Gaussian Variates", Master of Science Thesis, Department of Electrical Engineering, South Dakota State University, Brookings, South Dakota, 1971.

(4) A. Papoulis, Probability, Random Variables and Stochastic Processes, New York, McGraw Hill Book Company, 1965.

(5) G. M. Dilliard, "Generating Random Numbers Having Probability Distributions Occuring in Signal Detection Problems", IEEE Transactions on Information Theory, Vol. IT-13, No. 4, pp 616-617, October, 1967.

(6) B. W. Lindgren, Statistical Theory, New York, Macmillan, 1962.

(7) D. V. Serreyn and G. D. Nelson, "Classification Error Using Quantized Data", Remote Sensing Institute, South Dakota State University, Brookings, South Dakota; Interim Technical Report RSI-71-21, November, 1971.

(8) J. Max, "Quantization for Minimum Distortion", IRE Transactions on Information Theory, Vol. IT-16, No. 1, pp 7-12, March, 1960.

(9) E. G. Johnson, "The Pax II Picture Processing System" from Picture Processing and Psychopictories edited by B. S. Lipkin and A. Rozenfeld, Academic Press: New York, 1970, pp. 427-512.

(10) C. J. Frazee, R. D. Heil, and F. C. Westin, "Remote Sensing for Detection of Soil Limitations in Agricultural Areas", Annual Report, Remote Sensing Institute, South Dakota State University, Brookings, South Dakota, June, 1970.

TABLE I K-S Test Results

PROBABILITY THAT DATA HAS SPECIFIED PDF

Number of Samples	RANDU seed 98765	RANDU seed 12345	GAUSS 12345	MULLER 98765 and 12345
100	35.7	43.3	11.1	64.6
200	46.4	88.4	50.0	92.5
300	81.9	98.8	47.1	88.7
400	88.4	77.3	44.9	77.2
500	99.6	28.0	48.6	90.7
600	15.7	10.4		
700	10.3	24.8		
800	6.0	36.1		
900	15.8	29.7		

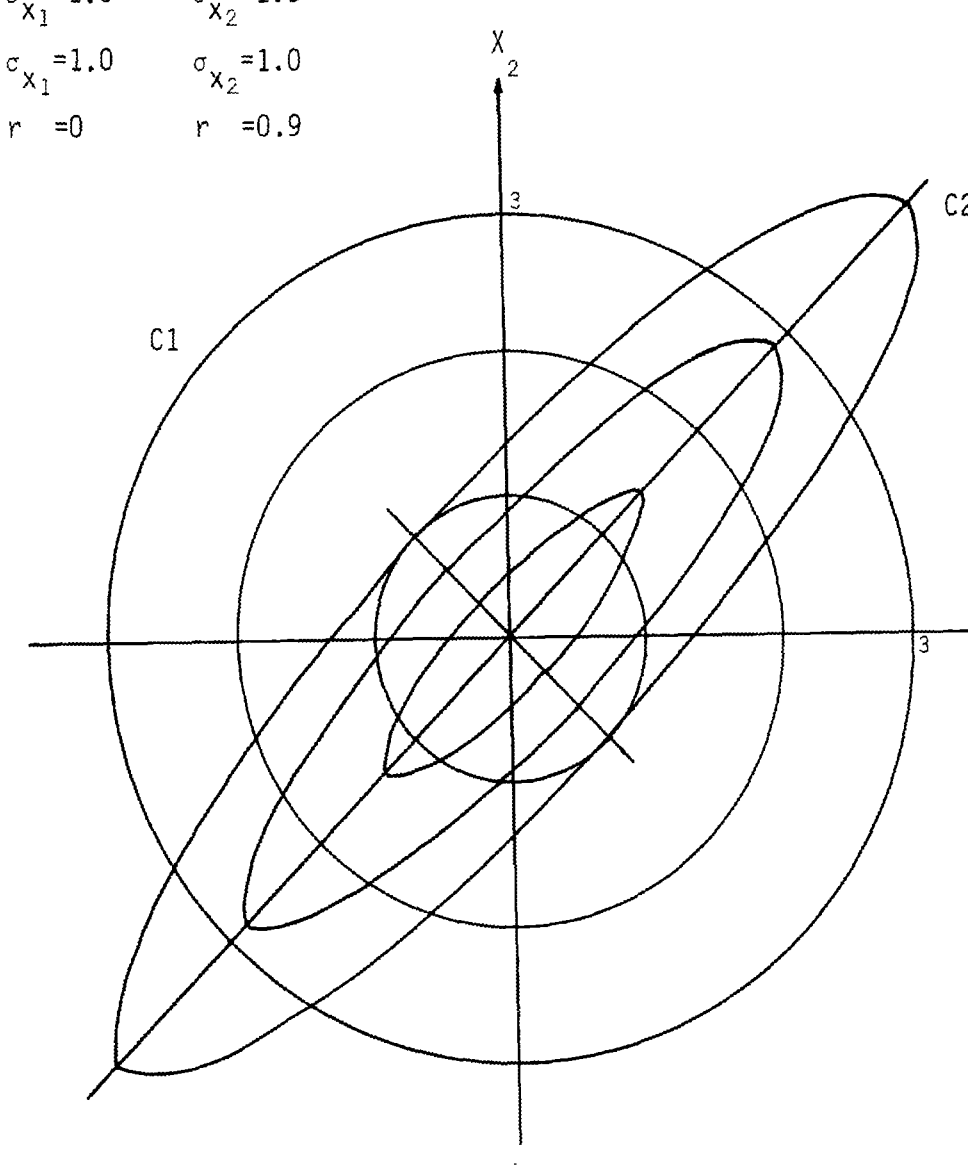

Figure 1.- Contours of two overlapping bivariate Gaussian probab
density functions.

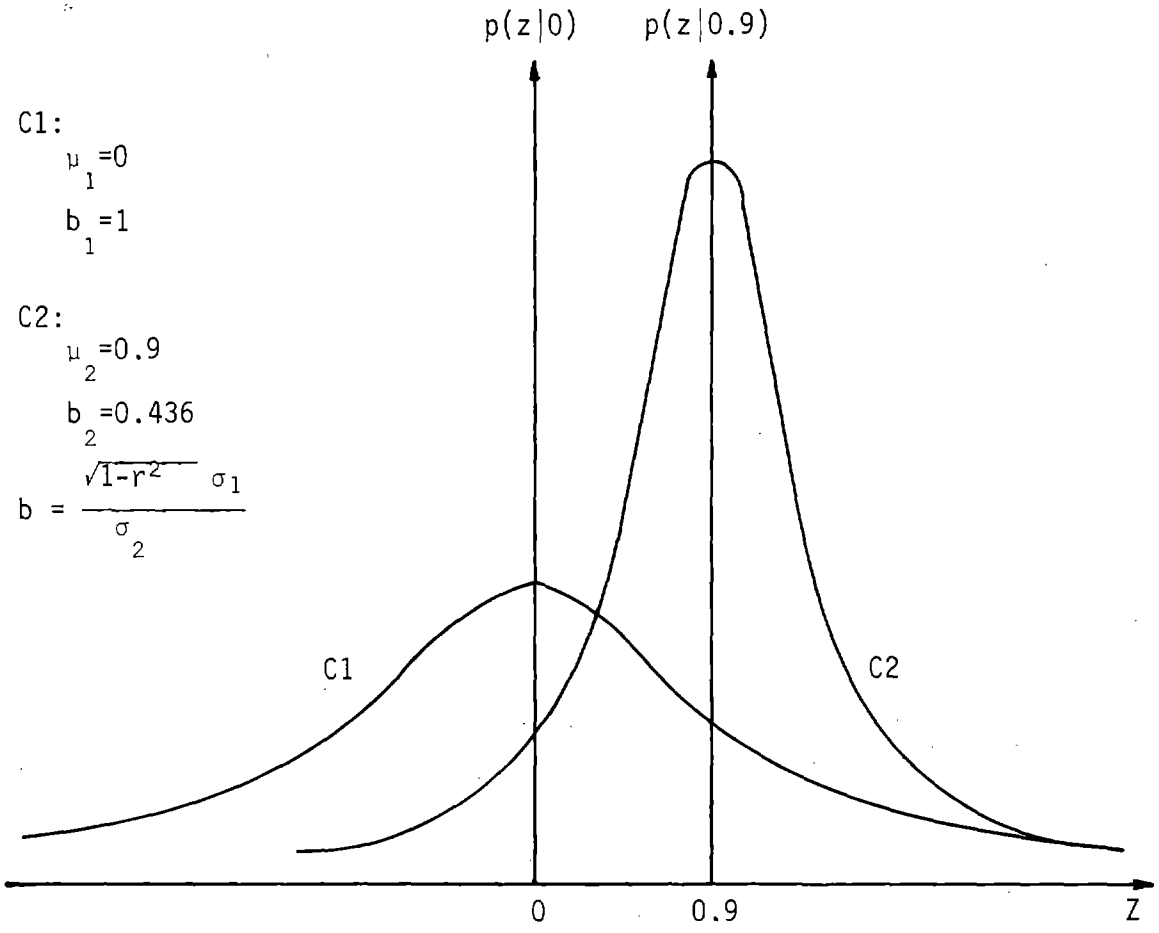

Figure 2.- Two overlapping univariate Cauchy probability density functions.

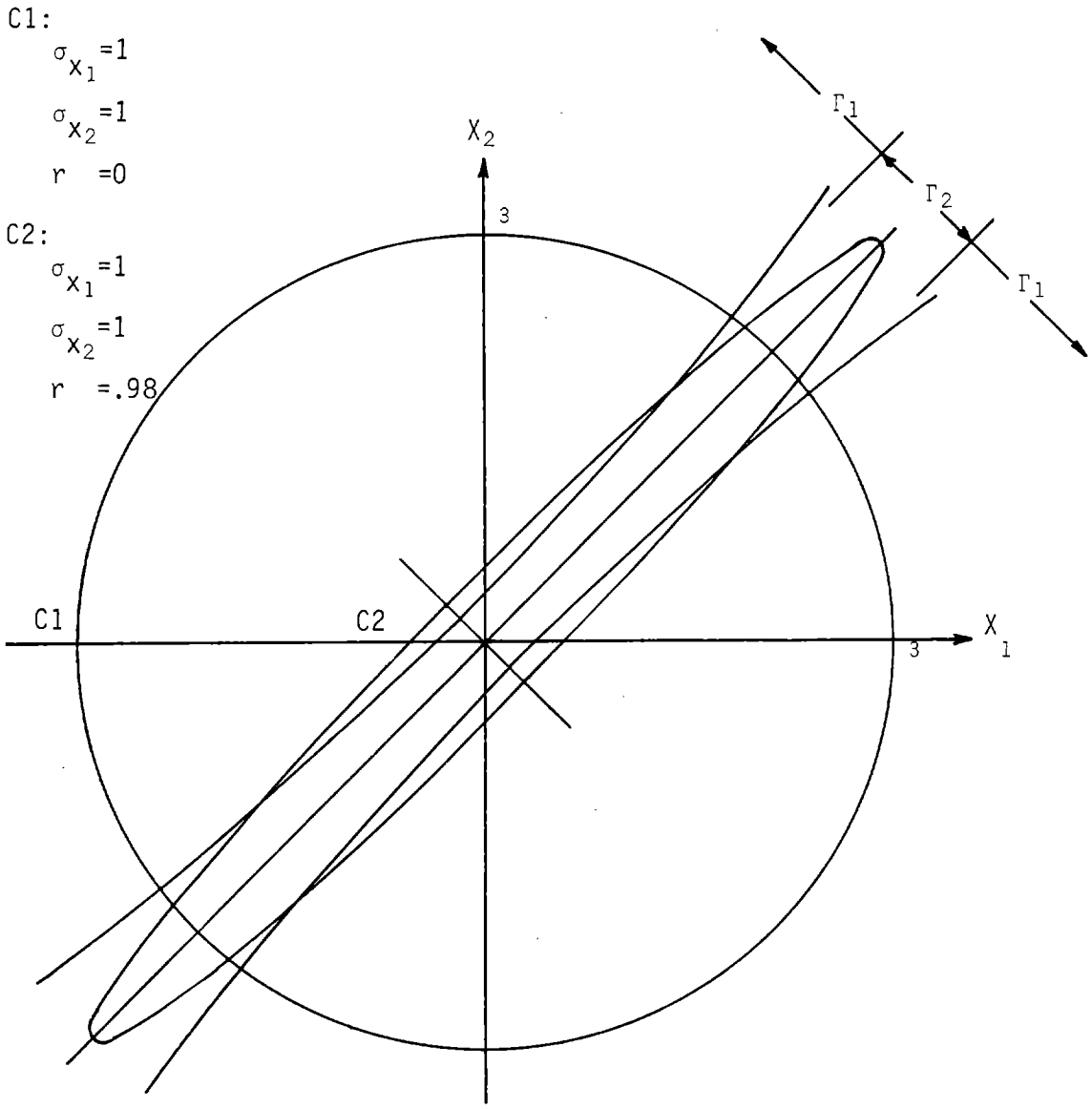

Figure 3.- Decision boundary for Bayes' classification of two bivariate Gaussian distributions, r=0.98.

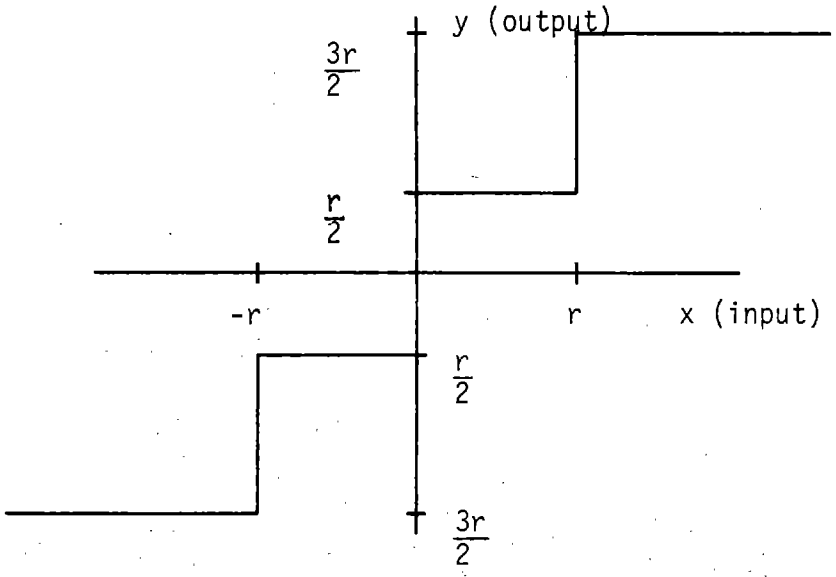

Figure 4.- Transfer characteristic for equiinterval quantizer with an even number of levels (four).

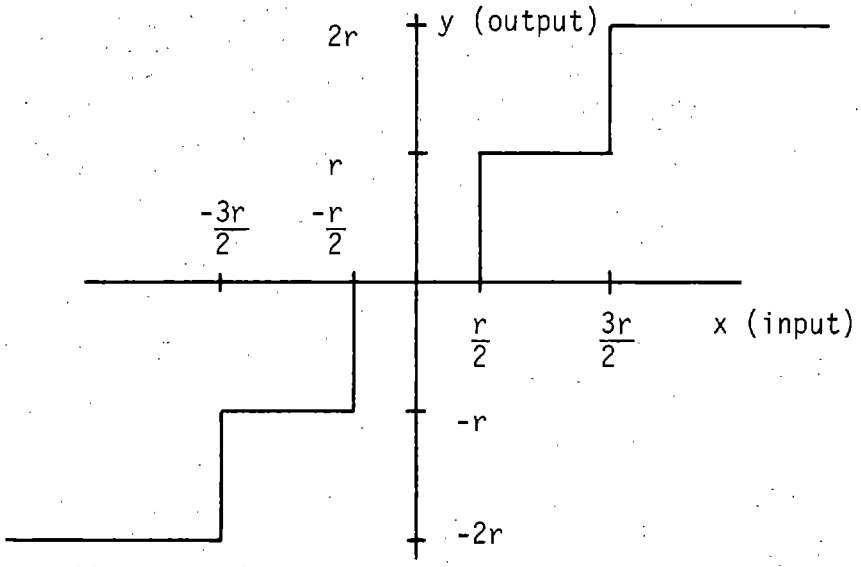

Figure 5.- Transfer characteristic for equiinterval quantizer with an odd number of levels (five).

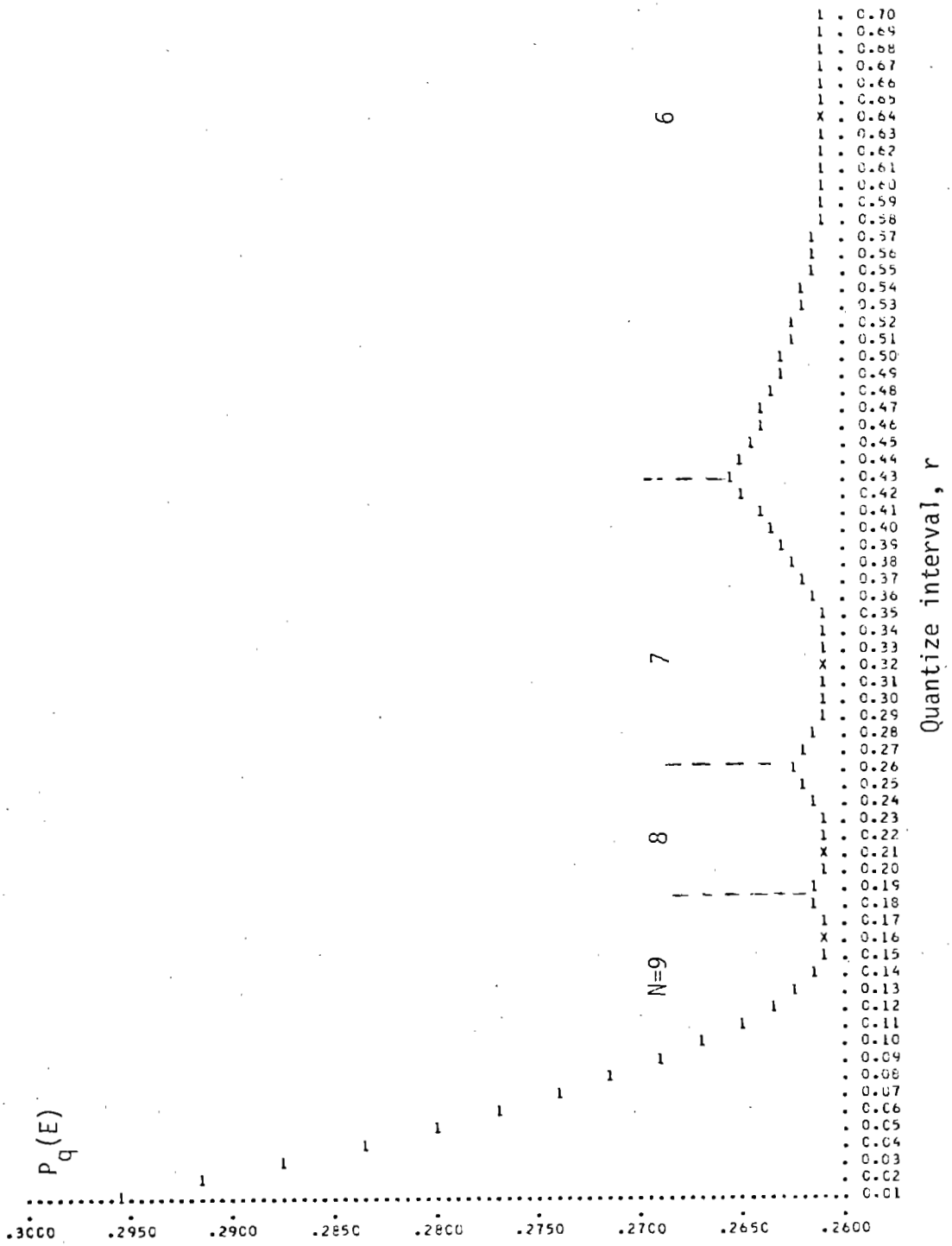

Figure 6.- Probability of error for different decision boundaries for varying quantization interval with a ten level quantizer.

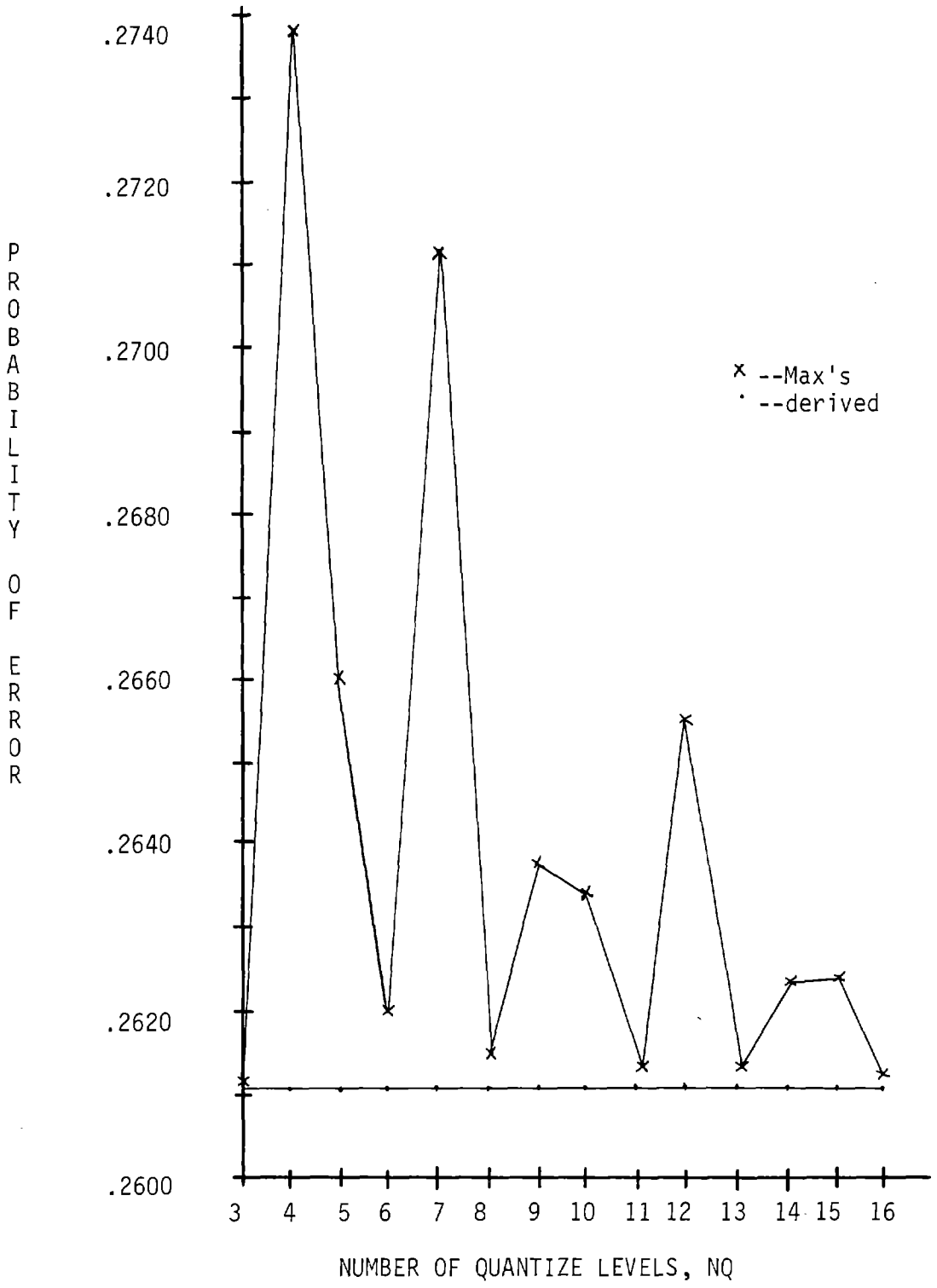

Figure 7.- Probability of error utilizing Max's interval and the derived interval.

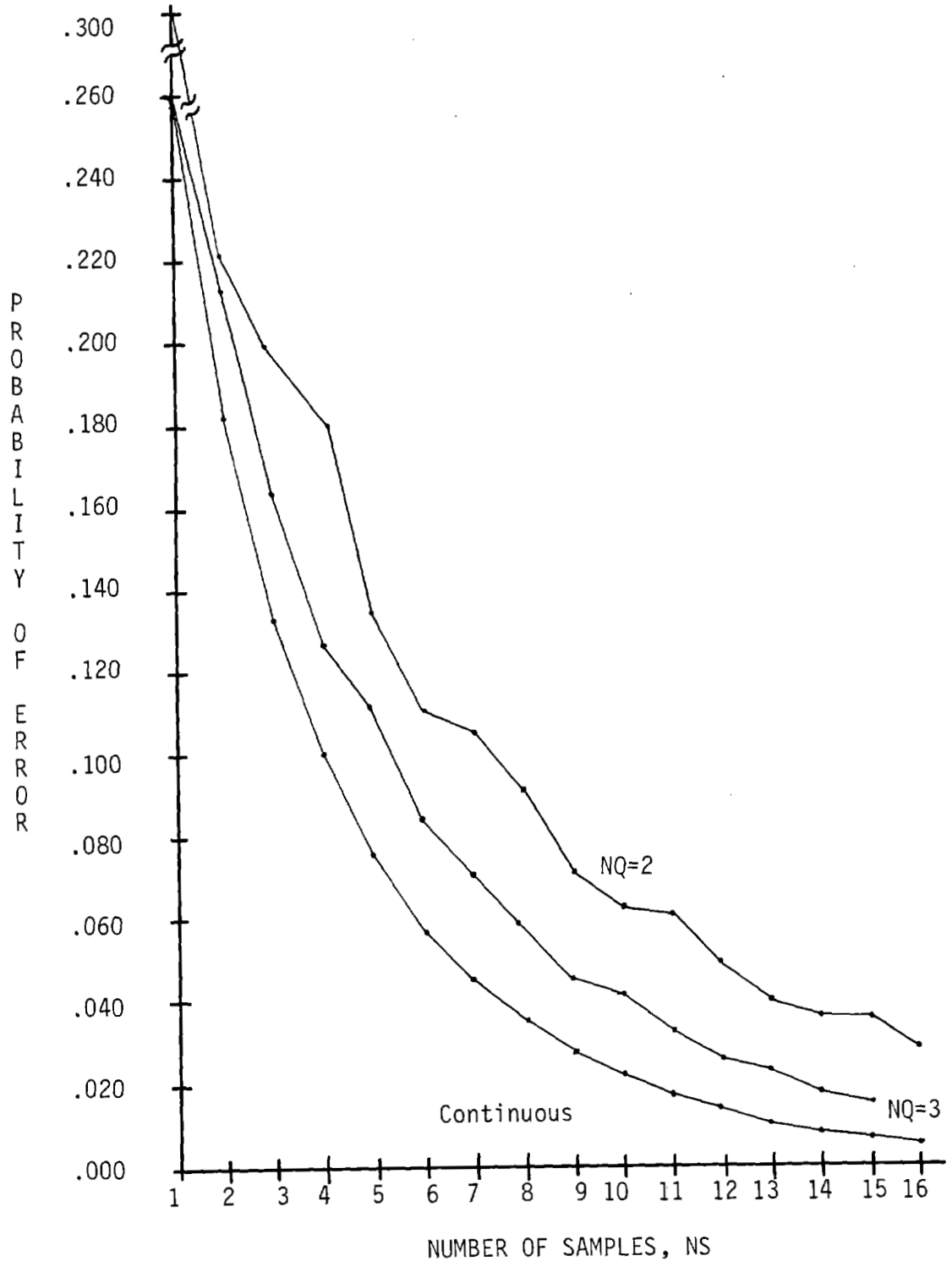

Figure 8.- Probability of error as a function of samples for Max's quantized data and continuous data.

SECTION 43

BONANZA PROJECT - 1971

by

Keenan Lee
Geology Department
Colorado School of Mines
Golden, Colorado

INTRODUCTION

This paper presents a review of the activities of the Colorado School of Mines on the Bonanza Project. Activities prior to 1971 are included in this review only in a general way; activities during 1971 are discussed in detail.

The Bonanza Project is a joint effort of the Colorado School of Mines (CSM) and the Martin Marietta Corporation (MMC). CSM brings to this effort faculty and graduate students with recognized ability in the geological sciences, while MMC has demonstrated competence in aerospace technology. This combined capability then, working together with the same data from different approaches, attempts to maximize the extraction of geologic information from remote sensor data.

The Bonanza Project began in 1969 with a grant from the Office of University Affairs (OUA). Since that time, support has come jointly from both OUA and the Earth Resources Survey Program Office, under NASA Grant NGL 06-001-015. Dr. Arch Park is technical monitor of this grant.

The objectives of the Bonanza Project are twofold: (1) to develop an educational program of graduate study in geologic remote sensing, and (2) to conduct research on the applications of remote sensing to the mineral industry.

EDUCATIONAL PROGRAM

COURSES OFFERED

Faculty working under this grant have developed three graduate courses in geologic remote sensing:

Introduction to Remote Sensing

Geologic Applications of Remote Sensing

Seminar in Geologic Remote Sensing

The first course in this series, Introduction to Remote Sensing, deals with the theory of active and passive remote sensing systems, using the energy path concept in the ultraviolet through radar portions of the electromagnetic spectrum. Students are introduced to remote sensing instruments and the interpretation of representative data. Geologic applications are briefly surveyed.

To date, this course has been offered four times, twice as part of the CSM Continuing Education Program, which made the class available to practicing scientists and engineers in the Denver metropolitan area. Combined enrollment has totalled 46 students, including undergraduates, graduate students and professional scientists and engineers.

The second course, Geologic Applications of Remote Sensing, stresses the application of remote sensing to geologic and mineral resource investigations. The course includes detailed study of remote sensing techniques, with field and laboratory experiments and experience in data reduction, analysis and interpretation. Case studies of demonstrated applications are presented, and potential uses are examined. Students conduct excercises in mission planning and selection of optimum sensor systems for specific geologic targets. This course is currently being taught for the second time. Combined enrollment totals 15 graduate students.

The third course of the series, Seminar in Geologic Remote Sensing, consists of group discussions and individual student presentations on current literature and research. Enrollment in the seminar to date has totalled 13 graduate students.

GRADUATE STUDENT SUPPORT

The Bonanza Project has supported the research of seven students working toward advanced degrees. One M.S. program has been completed, one is in progress, and four Ph.D. programs are in progress.

RESEARCH PROGRAM

DATA COLLECTION

All data used in this project were acquired by NASA aircraft, either for the Bonanza Project directly, or for other investigators. Those missions flown over the Bonanza Test Site (Site 185) include all or parts of Missions 101, 105, 153, 168, and 184. Data have been collected from each of the three current MSC aircraft, the P3A, C130 and RB57.

Photographic coverage is shown in Figure 1, which is a composite of all missions to date. The quality of this photography ranges from poor to excellent, being generally good.

Non-photographic data coverage is shown in Figure 2. SLAR imagery, acquired over relatively large areas for regional geologic studies, has generally been of poor quality. Fair to excellent thermal infrared imagery, both day and night, was flown over selected smaller areas, mostly for local structural information. Line data, including infrared spectrometry, multifrequency microwave radiometry and radar scatterometry, were acquired, but have yielded little geologic information.

DATA HANDLING

Photo interpretation techniques (and associated imagery interpretation techniques) have been the main analysis techniques used. This emphasis upon the human interpreter (as opposed to automatic pattern recognition techniques) evolves from three considerations:

1) Background of researchers. With one exception, all CSM personnel are geologists, and are consequently experienced in the extraction of geologic information from aerial photographs;

2) Quality of data received. To date, the best data received from NASA aircraft missions have been color and color infrared photographs. Other very useful data have included multiband photography and thermal scanner imagery,

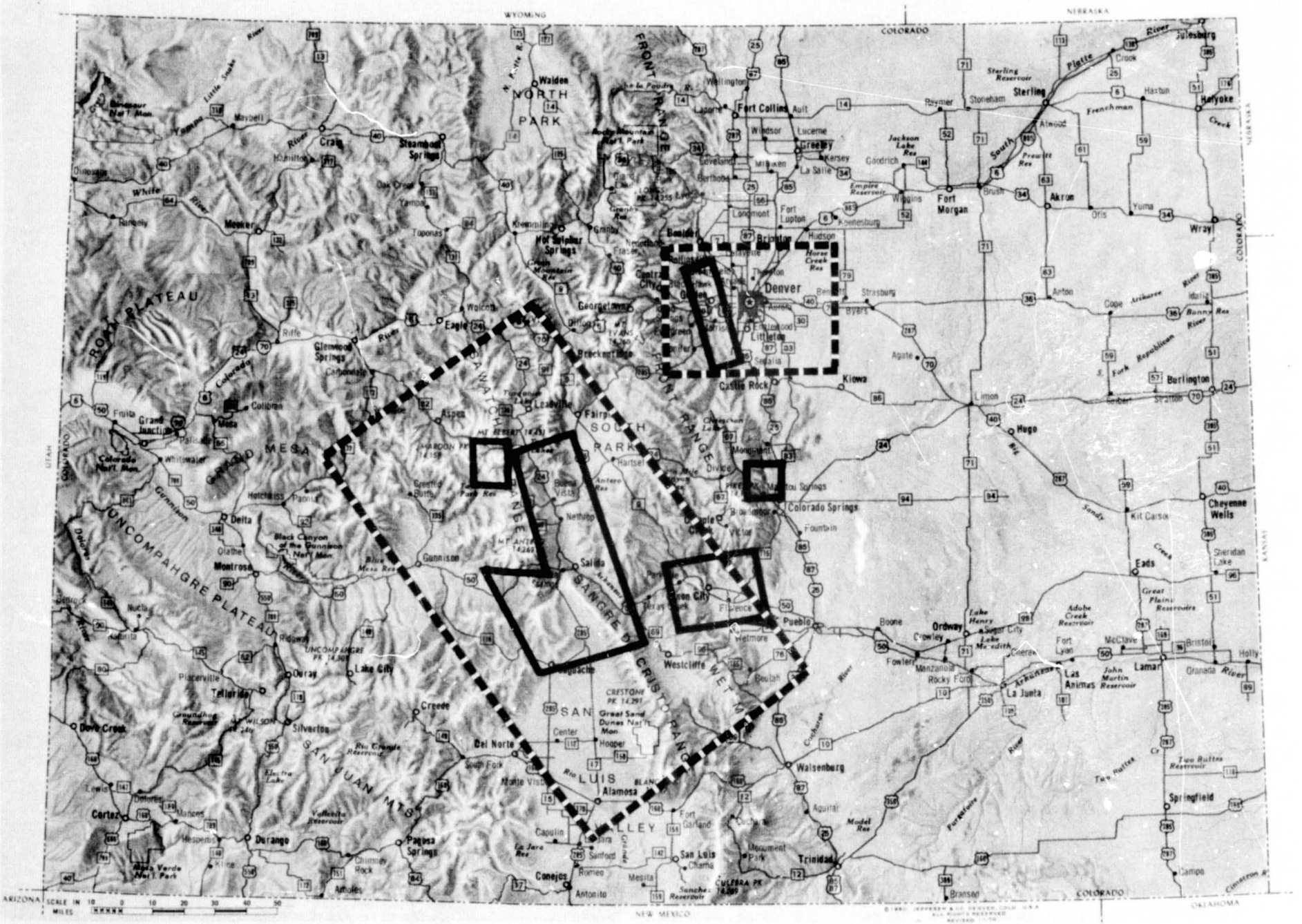

Figure 1.- Photographic coverage by NASA aircraft. Areas within dashed line are covered by small-scale (>1:100,000) photography, within solid lines the photography is large scale (<1:30,000).

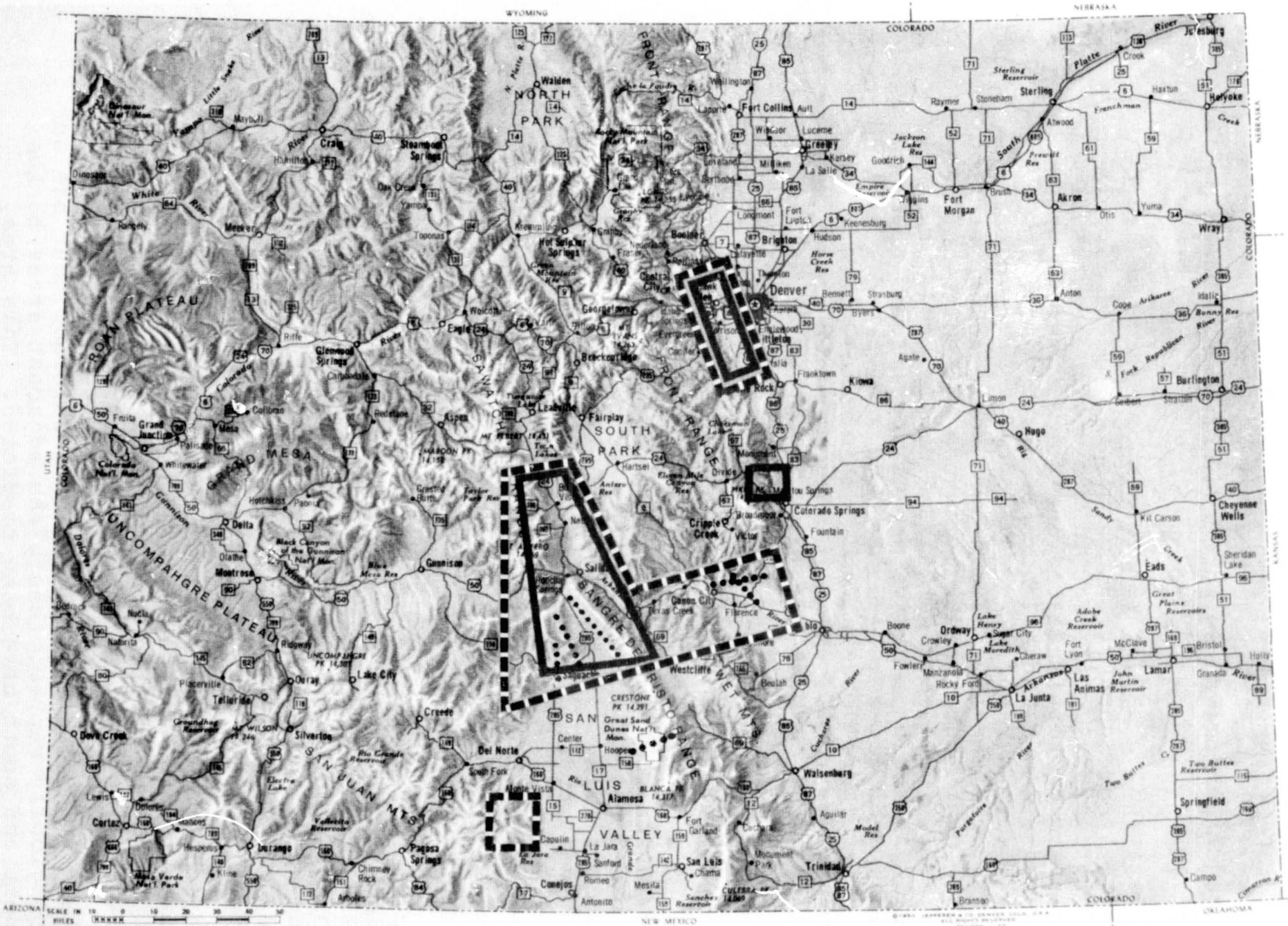
WYOMING
COLORADO
NEBRASKA
UTAH
ARIZONA
NEW MEXICO
OKLAHOMA
NORTH PARK
SOUTH PARK
SAN LUIS VALLEY
FRONT RANGE
SAWATCH
PARK RANGE
SANGRE DE CRISTO
SAN JUAN MTS
UNCOMPAHGRE PLATEAU
GRAND MESA
ROAN PLATEAU
Denver
Colorado Springs
Fort Collins
Boulder
Greeley
Pueblo
Walden
Steamboat Springs
Craig
Meeker
Rifle
Glenwood Springs
Eagle
Aspen
Leadville
Fairplay
Buena Vista
Salida
Canon City
Cripple Creek
Victor
Westcliffe
Alamosa
Monte Vista
Del Norte
Creede
Lake City
Ouray
Telluride
Silverton
Durango
Cortez
Dolores
Pagosa Springs
Grand Junction
Fruita
Delta
Montrose
Gunnison
Crested Butte
Hotchkiss
Paonia
Meeker
Yampa
Hayden
Craig
Dinosaur
Maybell
Loveland
Berthoud
Longmont
Brighton
Fort Lupton
Greeley
Evans
Windsor
Wellington
Laporte
Fort Collins
Aurt
Raymer
Stoneham
Sterling
Atwood
Haxtun
Holyoke
Julesburg
Crook
Platte River
Sterling Reservoir
Jackson Lake Res
Empire Reservoir
Prewitt Res
South Platte River
Frenchman Creek
Akron
Otis
Yuma
Wray
Burlington
Stratton
Cope
Arikaree River
Republican River
Bonny Res
Idalia
Anton
Byers
Strasburg
Bennett
Hudson
Keenesburg
Fort Morgan
Brush
Horse Creek Res
Arapahoe
Douglas
Elbert
Lincoln
Kiowa
Limon
Hugo
Agate
Franktown
Parker
Castle Rock
Monument
Palmer Lake
Woodland Park
Cascade
Colorado Springs
Fountain
Ellicott
Calhan
Kit Carson
Cheyenne Wells
Sheridan Lake
Eads
Great Plains Reservoirs
Adobe Creek Reservoir
Lake Henry
Lake Meredith
Sugar City
Crowley
Ordway
Boone
Fowler
Manzanola
Rocky Ford
Cheraw
Fort Lyon
McClave
Bristol
Holly
Granada
Lamar
John Martin Reservoir
Las Animas
La Junta
Arkansas River
Two Buttes Reservoir
Springfield
Campo
Branson
Trinidad
Walsenburg
Aguilar
Model Res
Purgatoire River
Cucharas River
Huerfano River
Apishapa
Pueblo
Florence
Canon City
Texas Creek
Penrose
Beulah
Rye
Colorado City
Great Sand Dunes Nat'l Mon.
Center
Hooper
Mosca
Sanford
La Jara
Capulin
Romeo
Antonito
Conejos
Mesita
San Luis
Chama
Fort Garland
Blanca Pk 14,317
Crestone Pk 14,291
Culebra Pk 14,069
Sangre de Cristo Wet Mts
Arkansas River
Rio Grande
Rio Grande Reservoir
Electra Lake
Valle Vista Reservoir
Groundhog Recreation
Mt Wilson Pk 14,246
Uncompahgre Pk 14,309
Dove Creek
Lewis
Mancos
Hesperus
Kline
Chimney Rock
Arboles
Alpine Verde Nat'l Park
Mesa Verde Nat'l Park
Black Canyon of the Gunnison Nat'l Mon.
Colorado Nat'l Mon.
Dinosaur Nat'l Mon.
Gunnison River
Colorado River
Dolores River
Gunnison River
White River
Yampa River
Little Snake River
Roaring Fork River
Eagle River
Blue Mesa Res
Morrow Pk 14,159
Taylor Park Res
Antero Res
Eleven Mile Canyon Res
Chaffee Mountain Park
Arkansas River
Sangre de Cristo Wet Mts
Mt Massive 14,421
Mt Elbert 14,431
Mt Sherman 14,036
Mt Evans 14,264
Mt Bierstadt 14,060
Mt Blue Sky 14,271
Mt Audubon 13,223
Mt Meeker 13,911
Longs Pk 14,255
Pikes Pk 14,110
Spanish Peaks 13,626
Greenhorn Mt 12,347
Wet Mountain Valley
Huerfano River
Cucharas River
Purgatoire River
Two Buttes Reservoir
Model Res
Sanchez Reservoir
Valle Vista Reservoir
Electra Lake
Rio Grande Reservoir
Taylor Park Res
Antero Res
Eleven Mile Canyon Res
Horse Creek Res
Jackson Lake Res
Empire Reservoir
Prewitt Res
Sterling Reservoir
Lake Henry
Lake Meredith
Adobe Creek Reservoir
John Martin Reservoir
Great Plains Reservoirs
Two Buttes Reservoir

while line data received so far have not been of good quality; and

3) Anticipated use of remote sensor data. The techniques being researched at CSM should be suitable for the average professional geologist in his work, and thus preclude reliance on sophisticated analytical instruments available only in research laboratories.

Despite the emphasis placed upon photo interpretation techniques, other data handling methods are being investigated as well, including optical and digital image enhancement, multiband color additive projection, video image processing, and computer reduction and analysis of infrared spectrometry. More detailed accounts of these interpretation techniques are discussed in the companion paper in these Proceedings by James Muhm.

GEOLOGIC APPLICATIONS

The rationale for using remote sensing for geology, as for any other discipline, is predicated on what are, by now, familiar arguments. Specifically, the remotely sensed data must provide either:

(a) new information not obtainable by other means, or

(b) a reduction in time (cost) necessary to obtain information.

New geologic information derives mainly from the synoptic view afforded by remote sensors. This "forest for the trees" situation has been used most advantageously in structural geology studies, where discontinuous surface elements are found to define a single geologic structure. Many such examples have been demonstrated, most dramatically by space photography.

The reduction in time necessary to obtain geologic information is also a recognized advantage of remote sensing, although it has not been demonstrated as well. The following example will give some indication of time-saving capability.

Figure 3 shows an area in Central Colorado that has not been geologically mapped, though the adjacent areas to the north, west and south have benn completed. This area,

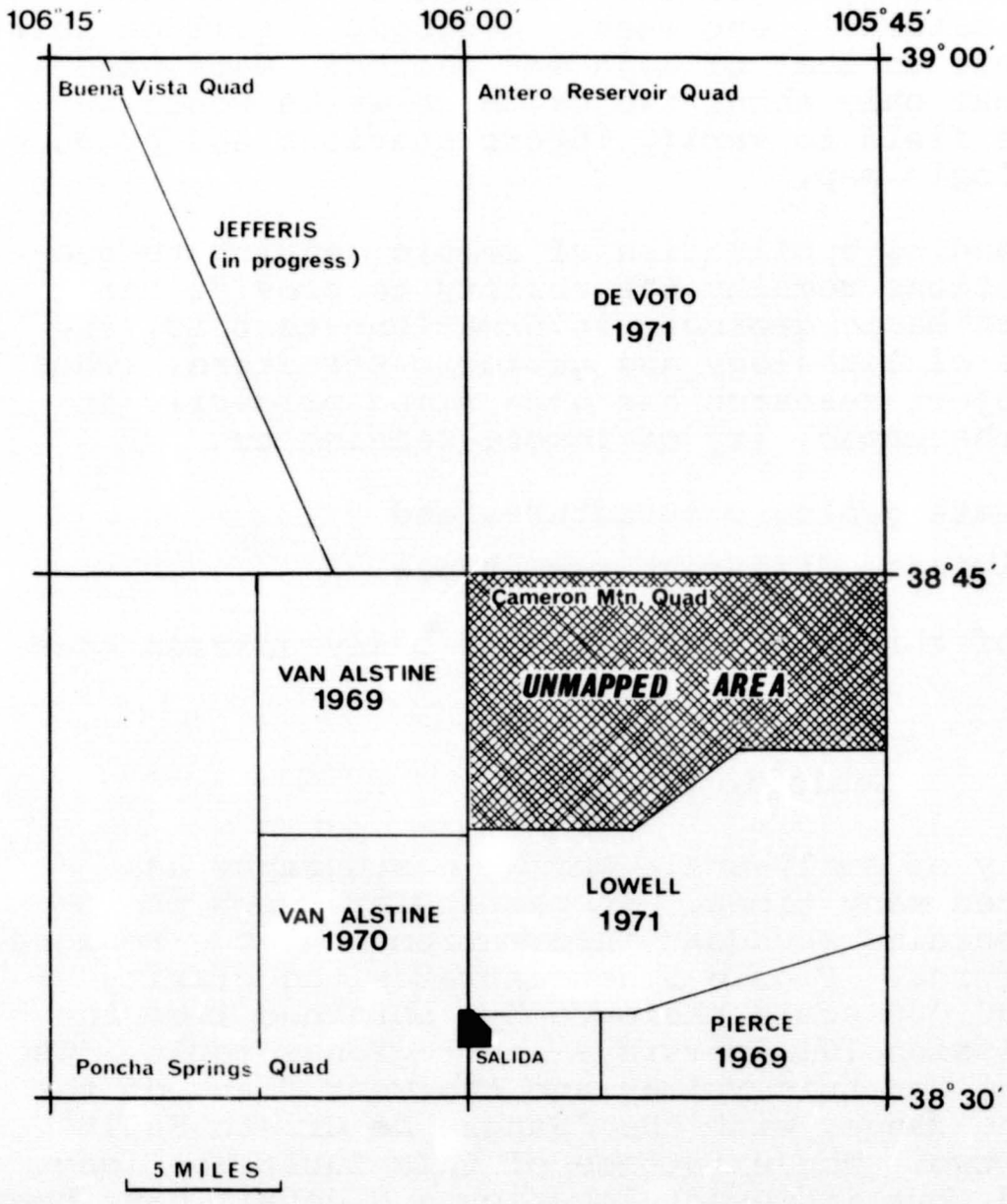

Figure 3.- Index of geologic field mapping north of Salida, Colo.

comprising about two 7½' topographic quadrangles, is typical of an area that would be assigned to a M.S. candidate for a Master's thesis, which would entail at least a full summer of field mapping. Figure 4 is a photo-geologic map produced by interpretation of NASA photography, including color, color infrared and low sun angle photography (LSAP). This study was completed by a graduate student on the Bonanza Project in approximately one week. Geologic detail of this map is comparable to that of adjacent geologic maps, and it is estimated that only about two or three weeks would be required in the field to verify interpretations and produce a finished geologic map.

The outstanding application of remote sensing to geologic investigations remains the ability to provide the interpreter with basic geologic information--that is, the surface aspects of lithology and geologic structure. Thus the Bonanza Project research has been aimed primarily at investigating the capability of remote sensing to

(1) delineate geologic structure, and

(2) discriminate different rock types.

The remainder of this paper will specifically address these two topics.

Geologic Structure

The utility of small-scale aerial photography has been demonstrated many times. In particular, such photography often contains abundant information on large regional geologic structures. Figure 5 demonstrates the clarity with which 1:100,000 scale photography, obtained from the NASA RB57 on Mission 101, portrays one regional fault. The photo covers the San Luis Valley and the west flank of the Sangre de Cristo Range, with the "Sangre de Cristo Fault" separating the two. The existance of this fault has long been postulated, but its exact location and detail have been poorly understood and the only age which could be ascribed to the fault was post-Oligocene. The synoptic view afforded by this photography allows the interpreter to join together discontinuous lineaments to synthesize one continuous fault zone, and the photos clearly show recent movement along some segments. This color IR photo has a slight advantage over regular color photography because portions of the fault line trace are marked by linear stands of aspen, which are enhanced somewhat by the IR sensitivity of this film.

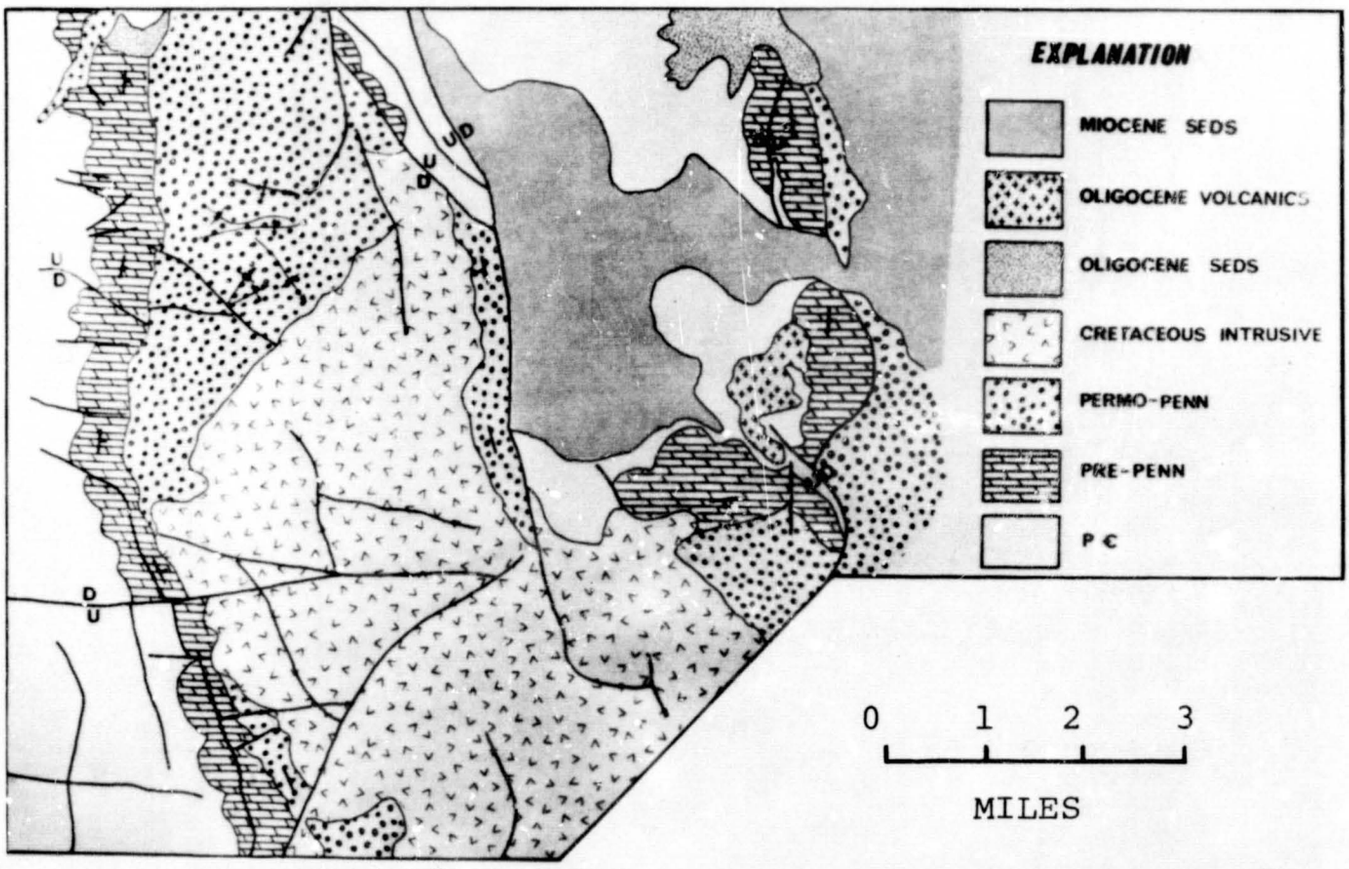

Figure 4.- Photo-geologic map of area shown in Fig.3. Information interpreted from color, color infrared and low sun-angle photography.

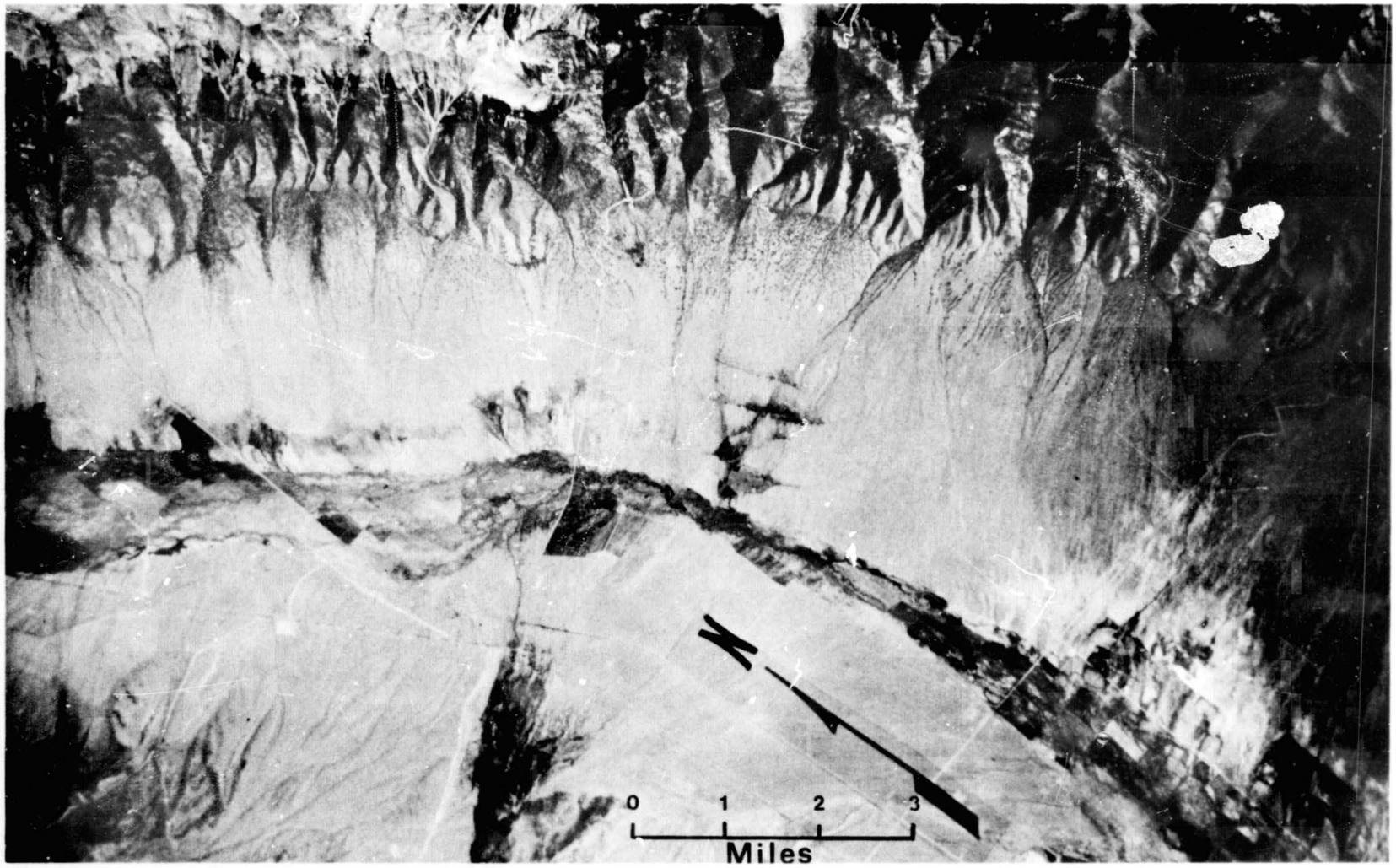

Figure 5.- Reproduction of color infrared photo over Sangre de Cristo Mtns. and San Luis Valley. SO-117 film with 500 nm filter.

Although fault control along the base of the range is obvious across the photo, indications of fairly recent movement along the fault can be seen only in the northern part. To the immediate south of the photo, similar indications of recent displacement are also seen, but the southern half of Figure 5 lacks these features. In an attempt to locate evidence of recent faulting in this anomalous area, thermal IR scanner imagery was flown by the NASA P3A on Mission 105. Interpretation of the IR imagery also failed to detect recent faulting along the base of the range in this area, but the imagery did reveal a series of en echelon fault scarplets trending away from the mountain front (Fig. 6). Clearly then, recent stress release has occurred all along the range, but in this one area the faulting trended away from the range rather than along the base. These faults displace alluvial fans of probable late Wisconsin age, and as such are probably less than 10,000 years old. The demonstration of this style of faulting here is significant, in that it lends credence to the growing argument that the modern San Luis Valley is tectonically part of the Basin and Range province, rather than the typical Laramide Rocky Mountains.

Figure 7 is low sun-angle photography (LSAP) along the Front Range of Colorado, flown at optimum time to enhance subtle topographic variations. Geologic structure is enhanced where structure is the dominant control on topography, as is the case with these hogbacks (in areas of non-structural control of topography, such as the upper part of Fig. 7, this photography is useful for geomorphic studies). The LSAP shown in Figure 8 portrays some large faults that were not previously known, even though this area had already been mapped by conventional techniques, and permits the extension of faults previously mapped. Black and white IR film (Type 2424) was used with a Wratten 25 filter for this photography, because (1) the 600-900 nm bandpass allows better "penetration" of early morning haze, and (2) the topography is better enhanced by the strong black shadow areas that result from the lack of sensitivity to short wavelength light.

In an attempt to evaluate more quantitatively the benefit of remote sensing for obtaining geologic structural information, two small studies were conducted. In the first, interpretations of conventional aerial photos were compared with interpretations of NASA data from Mission 105 (Fig. 9 shows each of the resulting maps). The dramatic increase in structural detail is obvious, but it should be pointed out

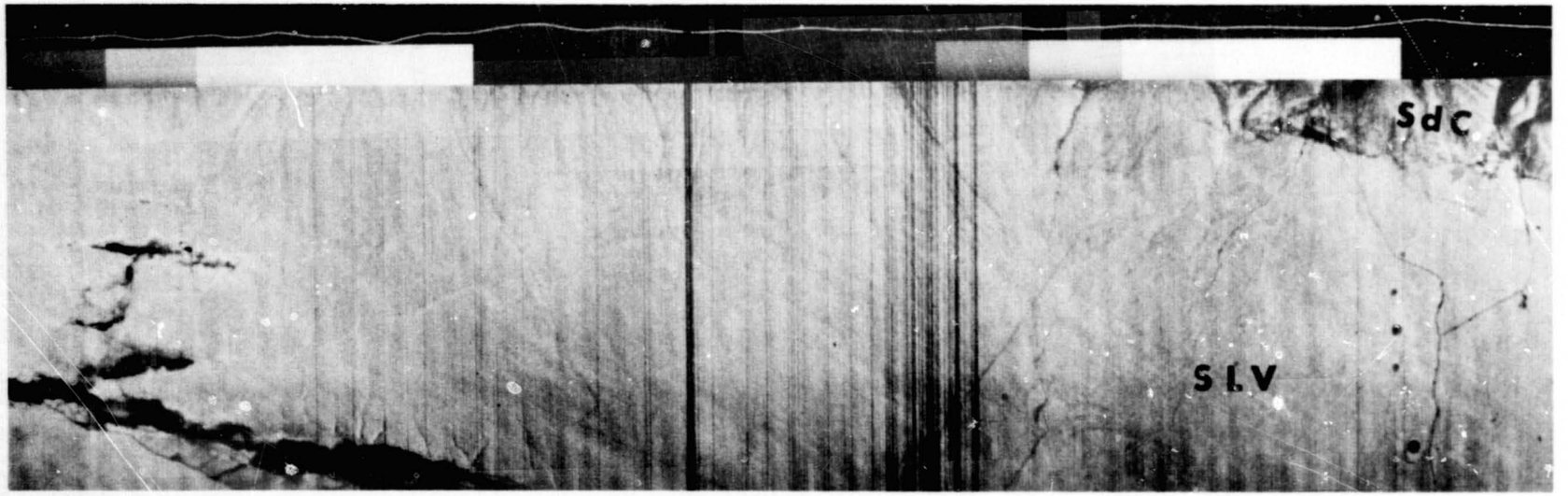

(a) RS-14 imagery, 8-14 μm, flown 2 Oct 69 at 1308 MDT. Dark features at left appear in center of photo, Fig. 5. SdC, Sangre de Cristo Mtns.; SLV, San Luis Valley.

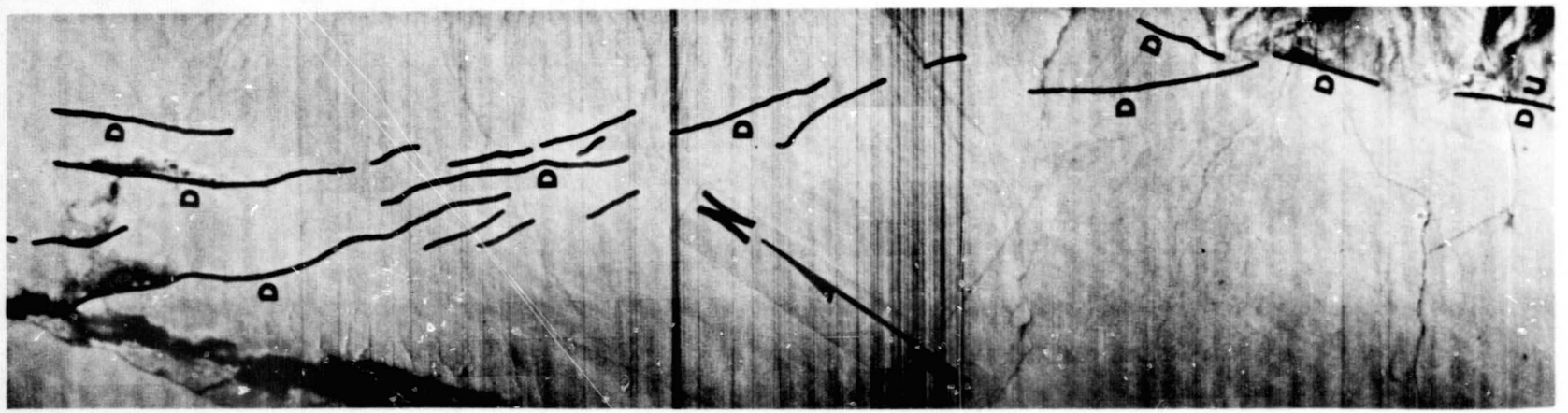

(b) Imagery same as above, with fault annotations (D on downthrown side).

Figure 6.- Recent faults on daytime thermal imagery, Mission 105.

Figure 7.- Low sun-angle photo along Front Range at Morrison, Colorado. Type 2424 film with W25 filter. Sun angle 12°.

Figure 8.- Low sun-angle photograph near Salida, Colo. Type 2424 film with W25 filter. Sun angle 20°. (p€, Precambrian; LP, lower Paleozoic sedimentary rocks; PP, Permo-Penn sedimentary rocks; Tdu, Dry Union Fm; Qf, fan.)

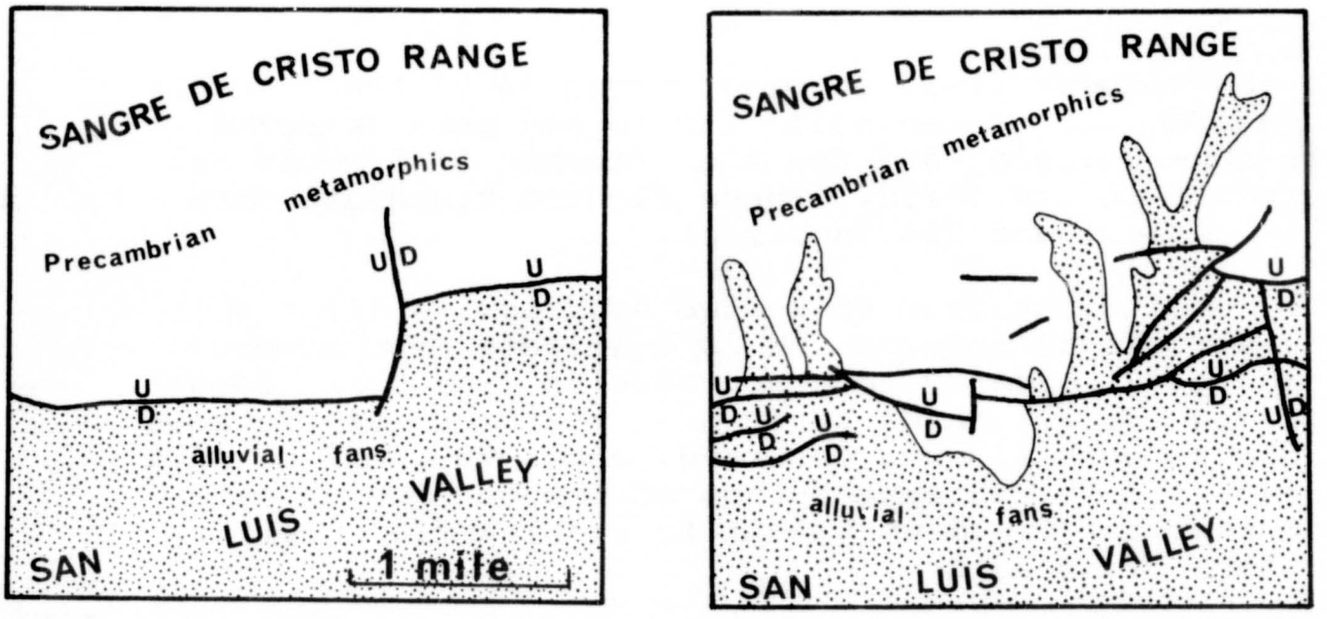

A. Structural interpretation from Forest Service B/W photos, 1954. (1: 20,000)

B. Structural interpretation from MX 105 color photos (1: 16,000).

Figure 9.- Comparison of photo-geologic maps from different types of photos.

that not only is more detail available (16 faults vs. 2 faults), but the information is more accurate, since the original interpretation was later proved erroneous. In this and nearby areas, interpretation of NASA photos delineated 26 faults. Subsequent field checking showed 8 of these to be definite faults (all of the major ones), 13 to be geologic discontinuities of some sort (not determinable in the field--either faults or fractures), and 5 were non-geologic phenomena (fencelines, trails, etc.). Thus, roughly 80% of the photo lineaments proved to have geologic significance and 20% were erroneous.

In a somewhat similar study in the Bonanza Mining District, Mission 105 data were interpreted for structural information in a complex volcanic area. These data included color and color IR photography and RS-14 thermal infrared imagery. The resulting interpretation map contained 63

faults. Subsequent field mapping proved 44 of these to be faults (again, all of the major faults had been detected), 14 to be non-geologic, and the significance of 5 could not be determined in the field. These figures translate into about 75% correct and 25% incorrect.

The conclusions from these two studies are (1) new geologic structural information is available from remote sensing data (2) greater accuracy results from using remote sensing data (3) all major structural features were detected, (4) of all structural data obtained, about 75% were correctly identified, and (5) interpretation of remote sensing data will not supplant field work, but it enables field work to be done more efficiently.

ROCK DISCRIMINATION

The ability to discriminate different rock types on remote sensor photography and imagery has so far proved to be one of our most difficult tasks, yet one which is patently fundamental to any geologic application. The obvious choice of sensors for this task, high quality color photography, has, of course, yielded the best results to date, and most likely will continue to do so. There is no need to burden the reader with yet another example of color vs. black and white photography, since the advantages of the former have been amply demonstrated. That is not to say, however, that color photography is the best tool available in all cases, and we are pursuing other techniques as well.

Although multiband photography has been used and interpreted in our work for some time now, it has only been in the past year that research has been directed toward fundamental rock reflectance studies and machine-assisted data interpretation. Geologists from CSM and atmospheric scientists from MMC have been working together in the field in an attempt to overcome problems of surface irradiance fluctuations due to atmospheric variables, and thus to obtain basic reflectance spectra of rocks on the outcrop. Figure 10 shows representative spectra, in this case for three different formations that are difficult or impossible to discriminate on black and white or color photography. Quaternary gravels (Qg) normally are impossible to distinguish from Pierre Shale (Kp), and the Niobrara Formation shales (Kn) are difficult to separate from the other two. A simple, but effective, film/filter combination which records beyond 620 nm has the capability of discriminating

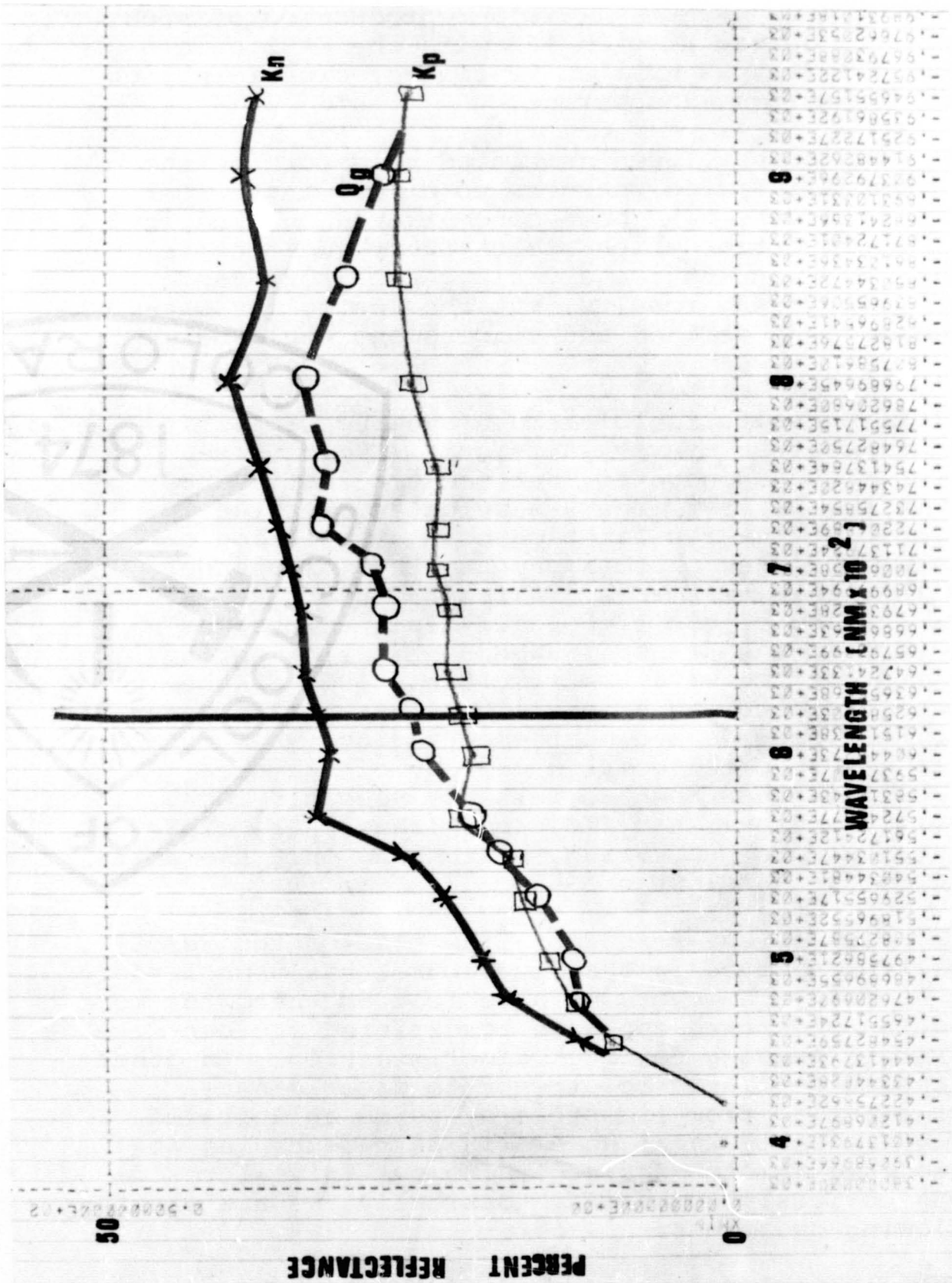

Figure 10.- Reflectance spectra of three geologic formations; Kn, Niobrara Fm. shale; Kp, Pierre Shale; Qg, Quaternary gravels.

the three rock types. Figure 11 is a reproduction of such a photo, acquired during Mission 168 with the KA62 camera and Type 2424 film with a Wratten 92 filter; discrimination of the three formations is apparent.

Similar studies have been initiated to determine the ability of thermal infrared scanners to discriminate rock types. Efforts to date have been concentrated on studying the basic rock properties which affect their radiometric temperatures. Mission 168 imagery along the Front Range has provided encouraging results, but the instrument capability remains to be defined and conclusions would be premature.

Quantitative evaluation of remote sensing capability for rock discrimination is very difficult. Conclusive studies have not been conducted, but one small study may prove informative. A test area was selected near the Bonanza Mining District for lithologic interpretation of color and color infrared photography and thermal scanner imagery. Within this test area, 78 fault-bounded areas were interpreted, and one of six lithologic designations was assigned to each of the areas. Subsequent field mapping provided ground control with the result that 62% of the areas had been assigned the proper lithology and 38% were incorrect. These figures are most encouraging, when consideration is given to the complex geology of the area; all of the rocks in question are Tertiary volcanic rocks, consisting of lava flows, ash flows and laharic breccias, and all are rather drab appearing, exhibiting only the most subtle differences in color.

To date, most of our research, like most of the remote sensing research reported in the literature, has been largely deductive. Recently, however, we have felt the need for more emphasis upon an inductive approach to defining the capability of remote sensing for rock discrimination. In other words, is it even realistic to attempt to discriminate granite, for example, from limestone by using an infrared scanner? Fundamentally then, we are in part returning to Step 1 of geologic remote sensing, where our initial residence time was obviously too brief. Basically, we are examining the following questions:

(1) What physical and chemical differences exist between different rocks?

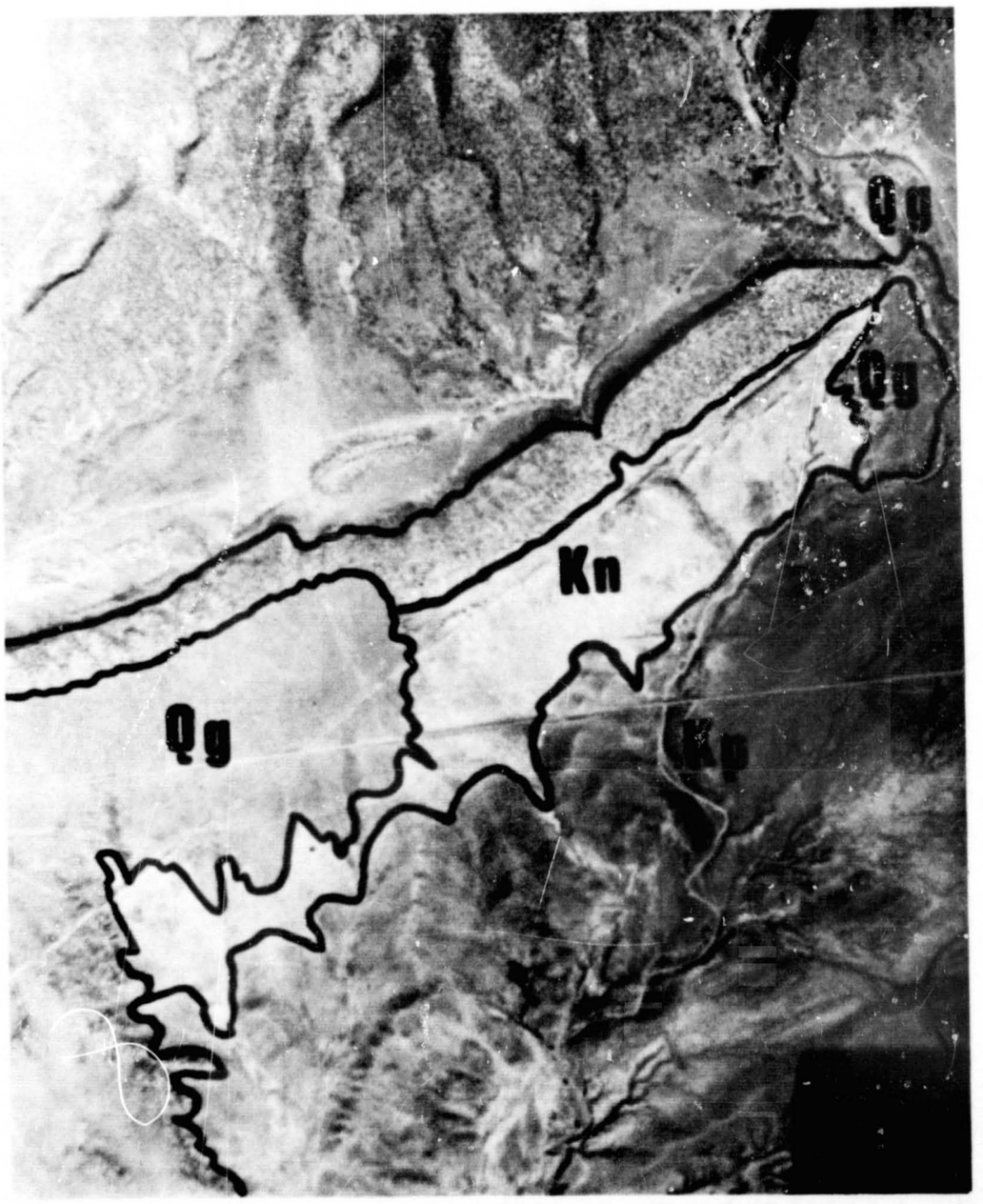

Figure 11.- One frame from KA62 multiband camera cluster. Type 2424 film with W92 filter (effective passband 620-900 nm). Kn, Niobrara Fm. shale; Kp, Pierre Shale; Qg, Quaternary gravels. Compare with Fig. 10.

(2) Which of these properties provide sufficient contrast to distinguish the rocks?

(3) Which of these properties are capable of being remotely sensed? And then logically,

(4) How can we best use remote sensors to do the job?

Our initial approach has been to examine these questions in terms of specifics, rather than generalities. Consequently, we have defined an area of study (test site, if you will) along the Front Range for this purpose, an area which includes at least 18 different geologic formations. The following procedure evolved:

A. List basic properties: All rock properties were listed. Any basic rock parameter which could be described or measured was included in the list, regardless of any other consideration. 31 parameters were listed.

B. Formation/Property Matrix: A matrix was formed in which all of the parameters from A could be listed for each of the 18 formations. Each of the spaces in this 18 x 31 matrix were then filled in (where possible) with qualitative descriptors (Table 1 is only a portion of this matrix).

Table 1

ROCK PROPERTY - FORMATION MATRIX

Formation / Property	MORRISON FORMATION	DAKOTA SANDSTONE	FT. HAYS LIMESTONE
LITHOLOGY	Shale	Qtz. ss	Limestone
GRAIN SIZE	v. fine	med	v. fine
ALBEDO	low	mod	high
COLOR	green	tan	tan
DENSITY	low	mod	high

C. Select promising parameters: Examination of the matrix focused attention upon those parameters which qualitatively showed promise of having the most contrast between adjacent formations.

D. Quantification: Attempts were made to quantify those parameters selected in C. Emphasis was placed upon methods easy to employ in the field without specialized equipment; for example, color measurements were made using GSA Rock Color Charts, and "albedo" (visible reflectance) was measured with common light meters and standard reflectance cards. An example of the resulting quantitative matrix is included in Table 2.

Table 2

ROCK PROPERTY - FORMATION MATRIX			
FORMATION / PROPERTY	MORRISON FORMATION	DAKOTA SANDSTONE	FT. HAYS LIMESTONE
GRAIN SIZE (ϕ)	5	2	5
ALBEDO	30%	43%	59%
COLOR	5G 6/1	10YR 7/6	10YR 8/2
TEMP, ^{o}C 2200 HRS	-6.1	-3.2	+1.4

E. Select useful parameters: Based upon the quantitative values determined in D, the parameters found consistently most useful for discrimination were defined. For the formations in the area of study, the four most useful parameters are listed in Table 3.

Table 3

MOST USEFUL GEOLOGIC CHARACTERISTICS
• 31 PARAMETERS INVESTIGATED • 10 PARAMETERS PROBABLY USEFUL • 4 PARAMETERS MOST USEFUL 1. TOPOGRAPHIC LANDFORM 2. COLOR 3. ALBEDO 4. SURFACE TEMPERATURE

F. Define contrasts required: An attempt was made to define those contrasts between parameters which are capable of being remotely sensed. The approach here was empirical--that is, rather than simply checking manufacturers' instrument specifications (which generally apply to laboratory, or at least optimum conditions), studies were conducted on typical NASA aircraft-acquired data to estimate what contrasts have actually been detected. Some of these estimates are listed in Table 4.

Table 4

EMPIRICAL DETERMINATION OF SENSOR DISCRIMINATION CAPABILITY	
PAN FILM	15-20% albedo contrast
COLOR FILM	Hue - 2.0 Value - 1.2 Chroma - 0.8
THERMAL SCANNER	~1°C

G. Select remote sensor(s): The next logical step then was to cross-correlate the matrices of parameter contrast and sensor capability in order to select the optimum remote sensor(s) which offered the greatest probability of success in discriminating the rocks.

Six different investigators followed the above procedures, each one working independently with different geologic formations within the test site. Their conclusions are shown in Table 5. It should be stressed that these recommendations apply to these specific formations in this specific test site. There is ample bias in this initial study to preclude extrapolation into other areas; nonetheless, the results are informative.

Table 5

RECOMMENDED SENSORS				
Investigator	Best Single Sensor			2 Sensor Package
	1	2	3	
D. Orr	C	CIR	B/W	C + θIR
D. Knepper	C	CIR	B/W	C + CIR
G. Raines	C	CIR	θIR	C + CIR
L. Jefferis	C	CIR	θIR	C + θIR
D. Wychgram	CIR	C	MB	CIR+θIR
D. Bruns	CIR	θIR	B/W	CIR+θIR
CONSENSUS	C	CIR	B/W	C + θIR

C=color photography, CIR=color infrared photography, B/W=black and white photography, MB=multiband photography, θIR= thermal infrared imagery.

N72-29344

SECTION 44

A COACTIVE INTERDISCIPLINARY RESEARCH PROGRAM WITH NASA

by

John W. Rouse, Jr.
Remote Sensing Center
Texas A&M University
College Station, Texas

ABSTRACT

The Applications area of the Texas A&M University Remote Sensing Program consists of a series of coactive projects with NASA/MSC personnel. The close working relationships developed between the Texas A&M University applications specialists has proven this to be an economic and efficient approach leading to pertinent research results. The success of this program is well illustrated by the Virus-Host Model Study and the Houston Ship Channel Water Quality Studies which were initiated during the last year. In each case, the Remote Sensing Center has served to complement and enhance the research capability within the Manned Spacecraft Center.

In addition to the Applications study area, the Texas A&M University program includes coordinated projects in Sensors and Data Analysis. Under the sensors area, an extensive experimental study of microwave radiometry for soil moisture determination established the effect of soil moisture on the measured brightness temperature for several different soil types. The Data Analysis area included a project which ERTS-A and Skylab data were simulated using aircraft multispectral scanner measurements at two altitudes. This effort resulted in development of a library of computer programs which provides an operational capability in classification analysis of multispectral data.

The level in diversity of the overall program has led to the formation of several formal laboratory groups, each headed by experienced professionals. These groups represent a wide range of disciplines selected to directly support the NASA/MSC HATS and related activity.

INTRODUCTION

The Remote Sensing Center at Texas A&M University is a consortium of four colleges: Agriculture, Engineering, Geosciences and Science.

We are an integral part of the University research program and consequently we are able to employ almost the full range of research facilities available on our campus; including equipment, laboratories, ships, aircraft, and agricultural experiment stations. More importantly, the Center is structured to enable it to effectively employ the outstanding faculty of the participating colleges, who are especially strong in application research.

The main structure of the Center which serves to coordinate all remote sensing research at TAMU, consists of eight working groups (figure 1). The sustaining University program provides the foundation for this organization and the selection of these particular groups was dictated for the most part by the objectives of our NASA Grant program. However, most of these groups have additional contract support.

The NASA Grant program consists of a balance between techniques and applications (figure 2). Although we still have a strong interest in microwave sensors, the more recent activity in development of computer softward for multispectral analysis and in applications research are now being stressed under the NASA sponsorship.

PROJECTS

Under the Sensors area, we are investigating a new idea which is based upon the behavior of the depolarized electromagnetic backscatter (figure 3). The theoretical work, presented at the URSI meetings at UCLA this fall, indicates that near surface volumetric properties dominate the depolarized component. A vivid illustration is shown in this radar image of the Pisgah Crater area (figure 4) in which the volume scatter properties of the lava flow provide a sharp contrast in the depolarized image which is not evident in the like-polarized image.

In the analytical model describing these effects it can be seen (figure 5) that whereas the like-polarized term is very sensitive to the dielectric constant of the terrain, the cross-term is relative insensitive. However, in the next graph (figure 6), it is seen that the volume reflection coefficient greatly effects this depolarized component, but does not appreciatively alter the like-term. These characteristics have been verified in independent experiments, and we are presently developing a laser sensor to utilize this effect in measuring water turbidity and surface pollutants. We are also preparing to assemble a radar system to utilize the effect.

Our work on radar return from Arctic ice using NASA/MSC data from Mission 47 and 126 has led to development of a model which predicts the backscatter from a variety of ice types with a reasonable degree of

reliability (figure 7). Recent work with Mission 126 data has supported earlier findings using Mission 47 data (figure 8) and confirms the ice type identification potential.

The data indicates that the dielectric constant of relatively new ice is an agreement with the waveguide measurements of CRREL, but that the effective dielectric constant of multi-year ice is much higher than predicted (figure 9). This indicates the need for reexamination of the physical sea ice model.

A project which has received special emphasis under the NASA program during the last year is the study of microwave radiometry for soil moisture determination (figure 10). Like most of our Sensor studies, an analytical model is used as a reference system for the investigation. Verification of the model required information about the source, measurements under highly controlled conditions, and finally airborne data.

Soil samples were collected at each of seven sites in Texas (figure 11) for waveguide measurements of their complex dielectric constant (figure 12). The sites were selected in support of our Skylab proposal for use of the microwave data. The dielectric constant data showed that in general sandy soils were more sensitive to moisture variations than clay soils (figure 13). In addition it was found that the absorption process in clay soils is such that the dielectric constant change with the length of time after moisture was applied (figure 14). Also wet clay soils were very sensitive to compaction, whereas, sandy soils were relative insensitive to absorption or compaction. A detailed knowledge of the characteristics of the soils is important in analysis of microwave emission from terrain because the contribution of the normal sky temperature term is low-much lower than for water measurements, for example.

The airborne measurements obtained by NASA/Goddard indicated in soil moisture dependence of approximately 1.5°K/1% soil moisture which is in excellent agreement with both the analytical model and the ground-based tower measurements (figure 15). However, the variance of the data was such that the results indicates that the present system capability for measurement of soil moisture using airborne microwave radiometers is no better than 10-15% soil moisture, that is, we believe that considerably more work is needed before radiometry can be shown to be a practical sensor for soil moisture delineation.

The Data Analysis group activities (figure 16) are devoted to developing a capability within the Center for effective use of the computer in statistical data analysis.

The products of this effort include what we call production programs (figure 17) that especially facilitate reduction of microwave

C.7

data. These programs permit the automatic reduction of a large volume of data, for example an entire line of radar scatterometry data, to a form which is compatible with our standard analysis techniques.

We have also developed the software for multispectral analysis using each of several statistical methods (figure 18).

The strong point of this activity is the excellent computer facility at TAMU which is located in the same building as the Remote Sensing Center. As you can see (figure 19), the machine has an expanded capability, but more important is the low cost and unusually good availability of the equipment. The average turnaround time on jobs is just 15 minutes, which is exceptional for a university-owned facility. The computer is supported by a large staff which is part of a $2M/yr. data processing center facility.

Within the last year the Center has acquired three new staff members whose activities are devoted to remote sensing applications. This has caused a pronounced shift in our research emphasis which we feel will increase the relavency of our products. In November we cooperated with NASA/MSC in an experiment on the Houston Ship Channel (figure 20). Airborne multispectral data were obtained using the University of Michigan aircraft. This work is part of an effort to provide our state's responsible agency with new methods of monitoring and regulating effluents. Under the new Texas laws governing pollution, the task of monitoring the state's inland water resources and coastal regions has expanded. The Texas Water Quality Board is looking to remote sensing for assistance in their programs.

Finally, I want to introduce you to one of the most exciting practical applications of remote sensing data that we have been involved in. A private land developer in Houston recently approached us for assistance in assessing the best way to utilize the natural vegetation and soils distribution on a land area scheduled for development (figure 21). The impact of urban development upon virgin lands has generally been severe and some effort was needed to minimize destruction and if possible to capitalize on the existing terrain to reduce development costs and maintain the aesthetic value of the land. This project has only just begun, but we have established several test plots on the site and have acquired aerial photography of some sections. We are hopeful that NASA will designate the area as a HATS test site and assist us with the data acquisition and analysis.

C.7

CONCLUSION

The Texas A&M program is a rapidly expanding effort which is greatly assisted by the excellent cooperation received from the NASA/MSC personnel. We believe that this coactive effort will prove to be an important part of the overall NASA/MSC involvement in remote sensing applications research.

The following paper by Dr. Robert Toler details another of the Remote Sensing Center's project which typifies the type of coactive interdisciplinary research which we are establishing with the Manned Spacecraft Center.

RSC LABORATORIES

- ELECTRO-OPTICAL SYSTEMS

  DR. W. T. MAYO, JR.

- MICROWAVE & INFRARED SYSTEMS

  DR. J. W. ROUSE, JR.

- DATA ANALYSIS

  J. A. SCHELL

- ENVIRONMENTAL MONITORING

  DR. W. P. JAMES

RSC LABORATORIES

- SPACE OCEANOGRAPHY

  DR. G. L. HUEBNER, JR.

- VEGETATION SYSTEMS

  DR. R. H. HAAS

- PLANT PROTECTION

  DR. R. W. TOLER

- SOIL-WATER SYSTEMS

  DR. C. H. M. VAN BAVEL

NASA GRANT PROGRAM

I. SENSORS

ACTIVE MICROWAVE, PASSIVE MICROWAVE

INFRARED, LASER

II. DATA ANALYSIS

MULTISPECTRAL, MICROWAVE

III. APPLICATIONS

WATER QUALITY, PLANT DISEASES (VIRUS)

RANGELAND, AG STATION SURVEY

NEAR-SURFACE VOLUME SENSOR
(LASAR AND RADAR)

APPLICATIONS: WATER TURBIDITY, OIL SPILLS, TERRAIN COMPOSITION AND MOISTURE

SENSOR CONCEPT IS BASED UPON DEVELOPMENT BY ROUSE (1971) WHICH DESCRIBES DEPENDENCE OF BACKSCATTER ON SUBSURFACE VOLUME SCATTER CHARACTERISTICS.

C
D
HH
HV
Pisgah Crater Area, California
0
5 Miles
N
B
A

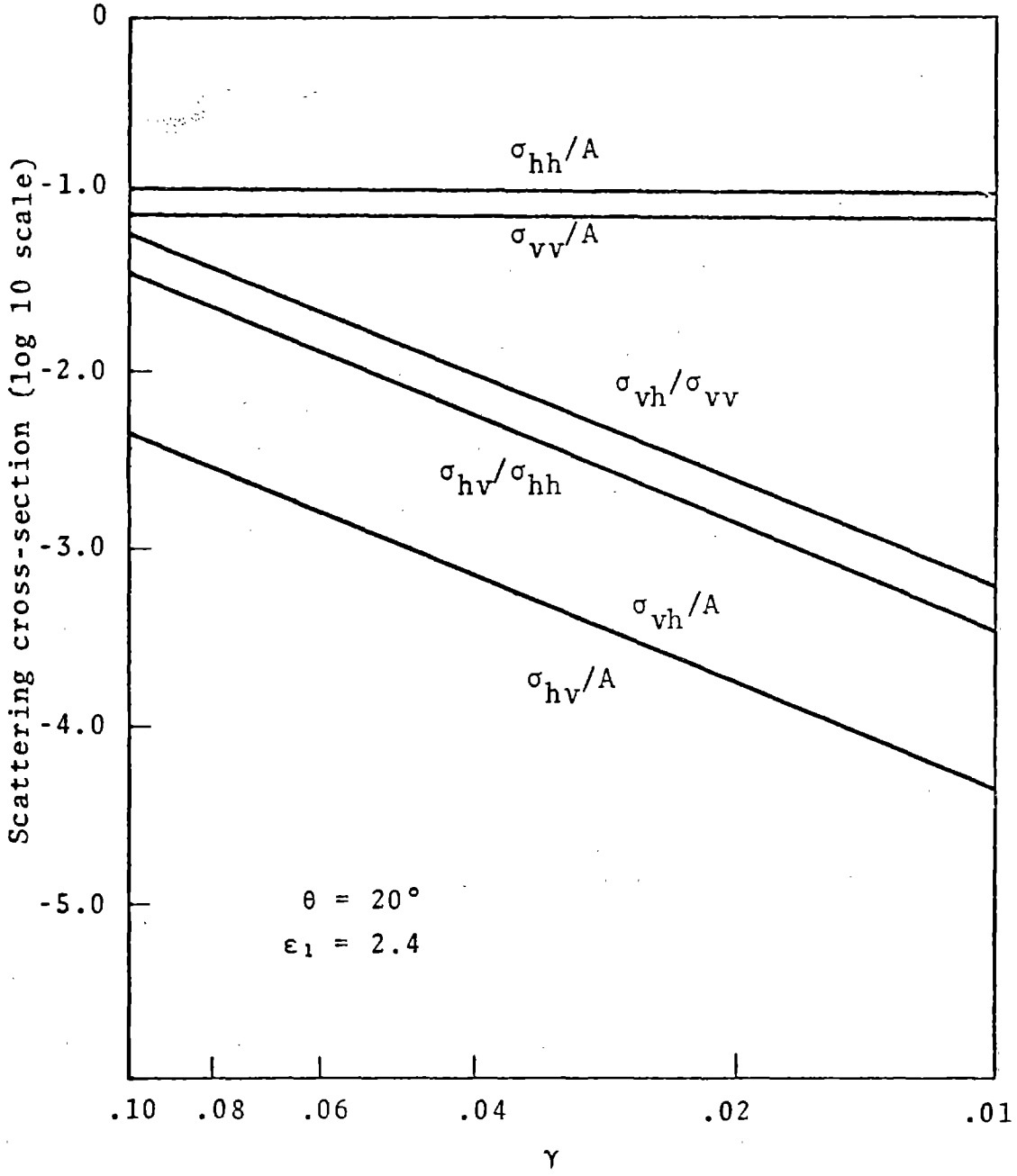
0
-1.0
-2.0
-3.0
-4.0
-5.0
Scattering cross-section (log 10 scale)
σ_{hh}/A
σ_{vv}/A
σ_{vh}/σ_{vv}
σ_{hv}/σ_{hh}
σ_{vh}/A
σ_{hv}/A
$\theta = 20°$
$\varepsilon_1 = 2.4$
.10
.08
.06
.04
.02
.01
γ

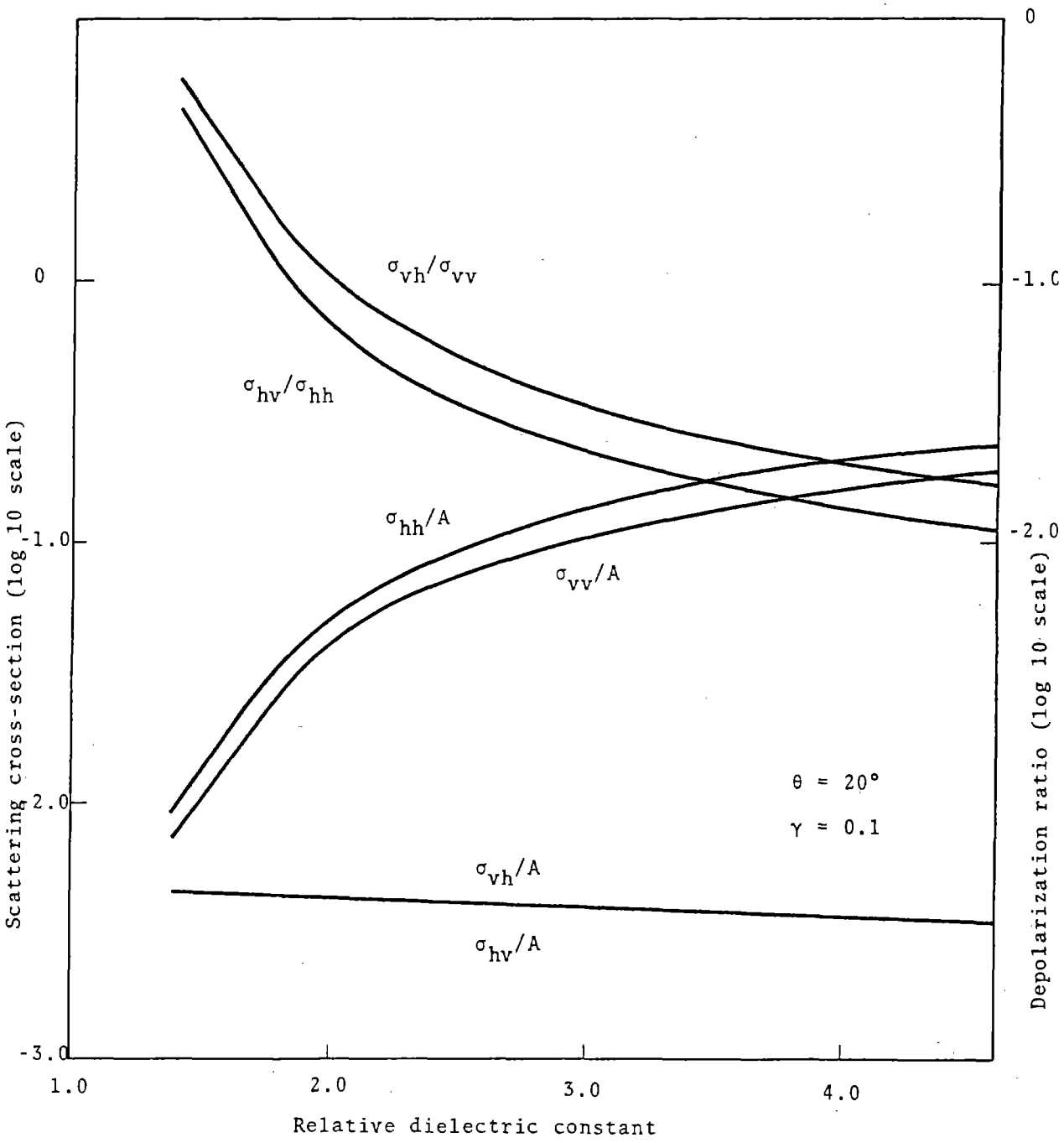
0
-1.0
-2.0
0
-1.0
-2.0
-3.0
σ_{vh}/σ_{vv}
σ_{hv}/σ_{hh}
σ_{hh}/A
σ_{vv}/A
σ_{vh}/A
σ_{hv}/A
θ = 20°
γ = 0.1
1.0
2.0
3.0
4.0
Relative dielectric constant
Scattering cross-section (log 10 scale)
Depolarization ratio (log 10 scale)

RADAR BACKSCATTER - ARCTIC ICE

DEVELOPMENT OF BACKSCATTER MODEL AND VERIFICATION OF MODEL USING MISSIONS 47 AND 126 13.3GHz RADAR DATA.

MODEL INDICATES THAT SURFACE ROUGHNESS FACTOR DECREASES AND EFFECTIVE DIELECTRIC CONSTANT INCREASES WITH AGING OF ICE. CHANGES ARE 10:1 DURING FIRST YEAR AFTER FORMATION.

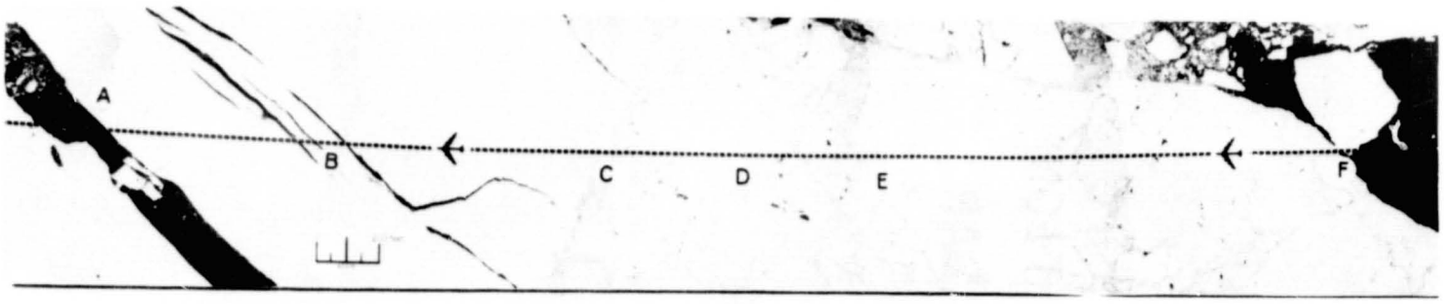

Air Photo Mosaic: Arctic Ice, Off Shore of Barrow, Alaska, 12 May 1967, line 91

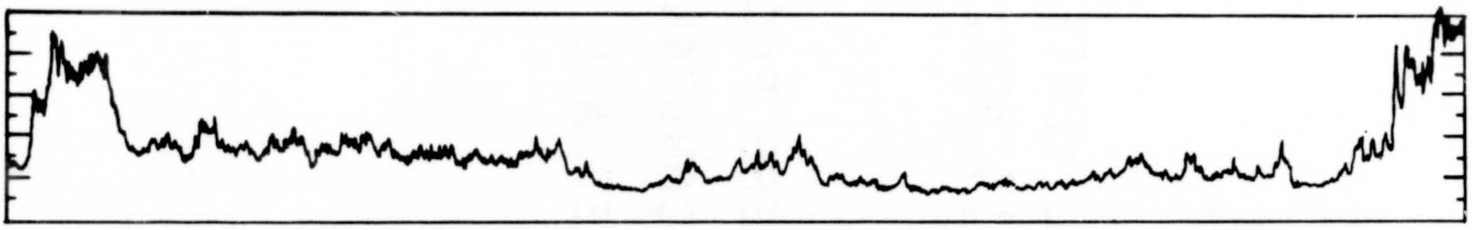

Radar Return at 2.5° Incidence Angle

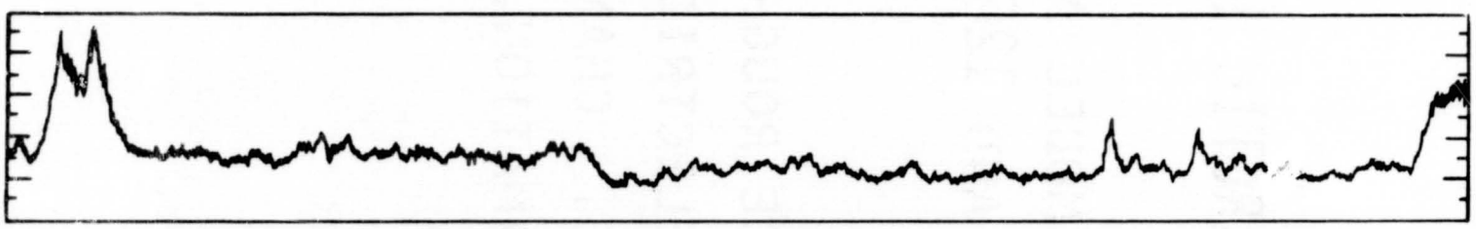

Radar Return at 6.7° Incidence Angle

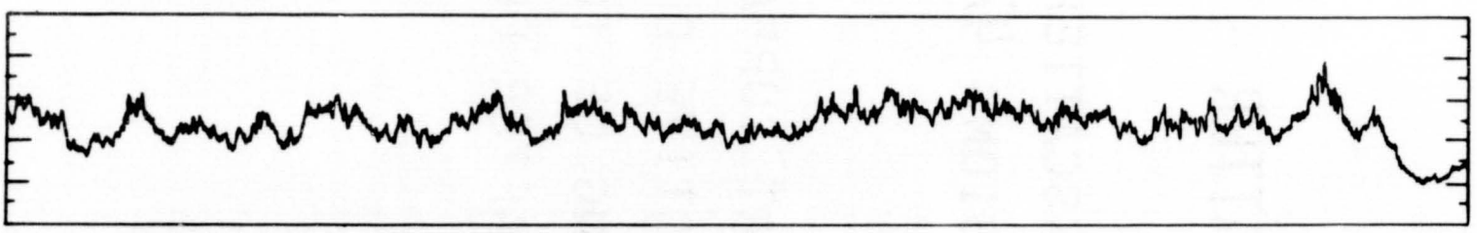

Radar Return at 25.0° Incidence Angle

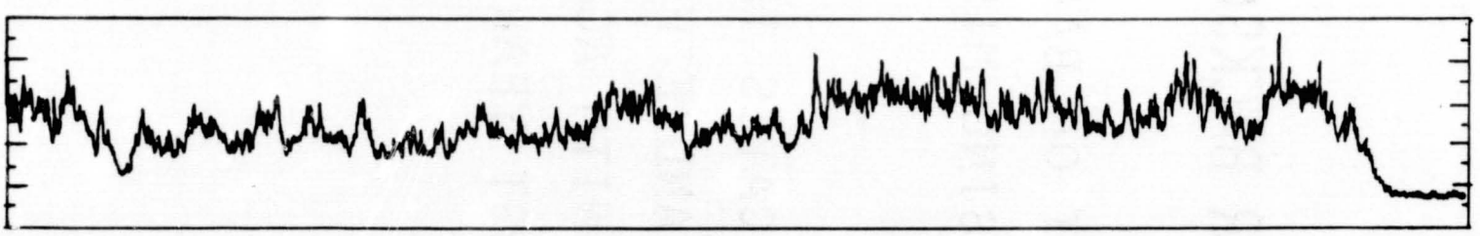

Radar Return at 52.1° Incidence Angle

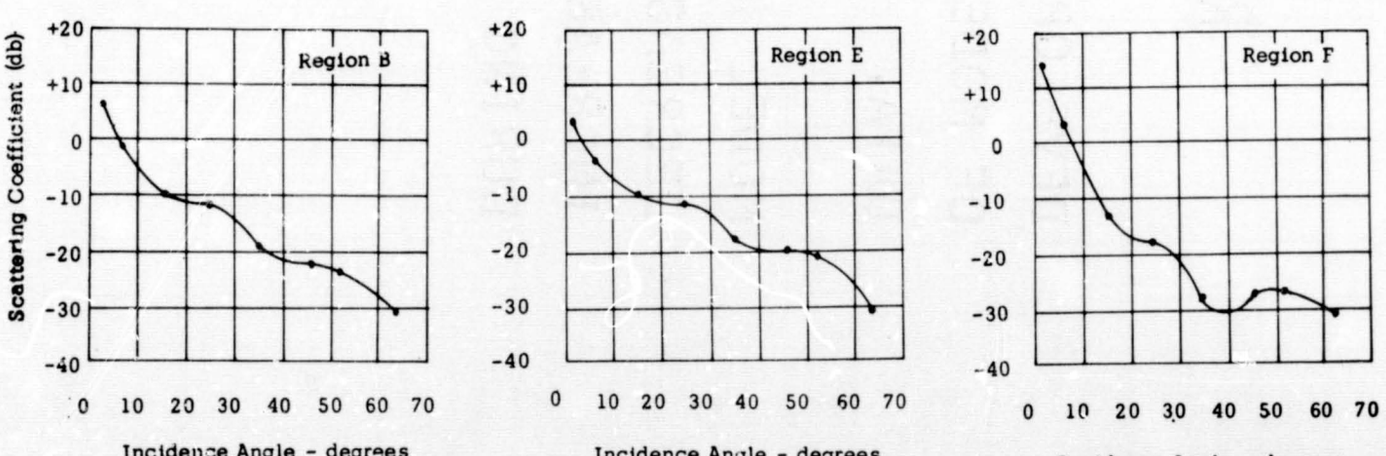

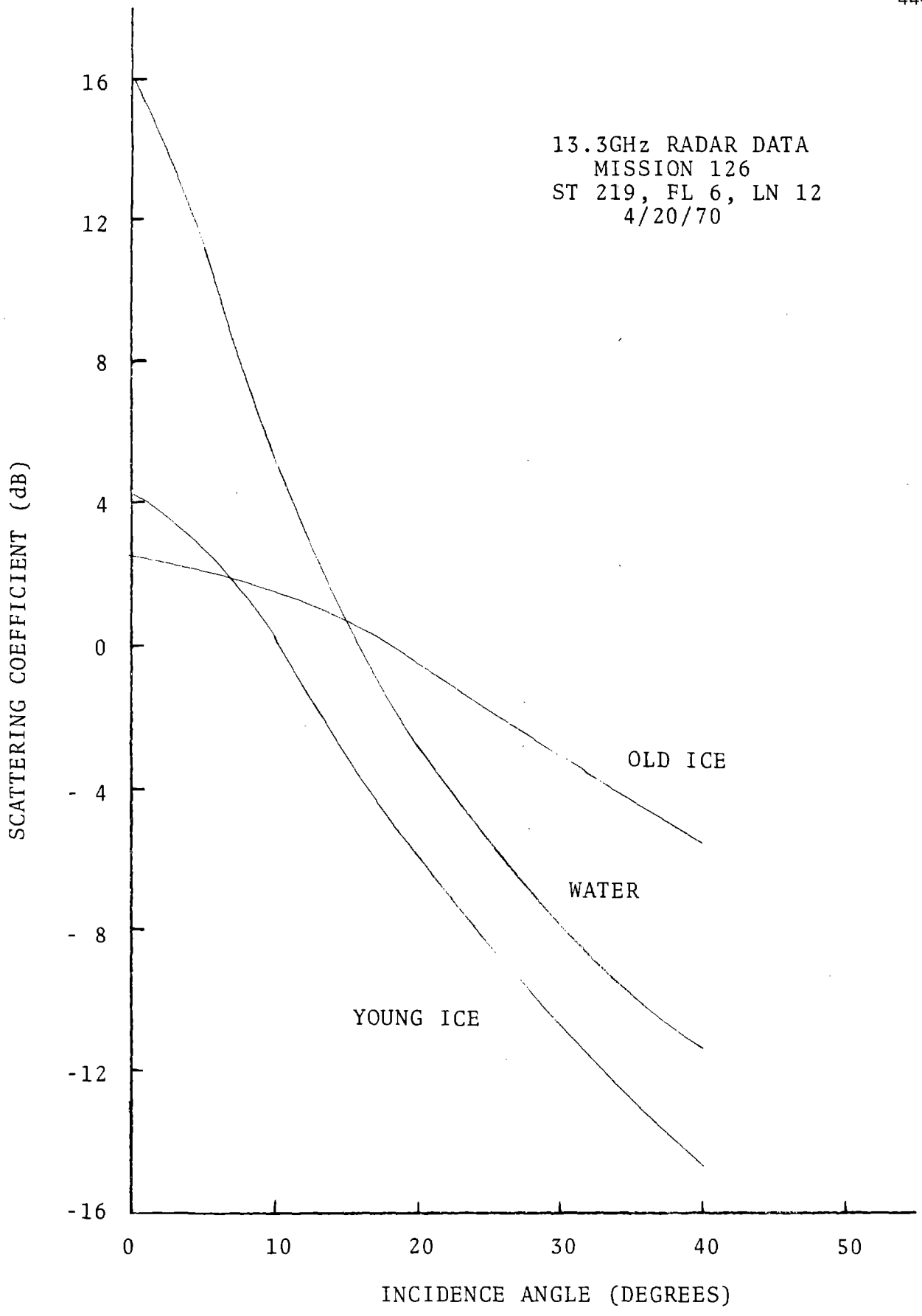
13.3GHz RADAR DATA
MISSION 126
ST 219, FL 6, LN 12
4/20/70
OLD ICE
WATER
YOUNG ICE
SCATTERING COEFFICIENT (dB)
16
12
8
4
0
- 4
- 8
-12
-16
0
10
20
30
40
50
INCIDENCE ANGLE (DEGREES)

SOIL MOISTURE DETERMINATION

- DEVELOPMENT OF ANALYTICAL MODEL BASED UPON PEAKE MODEL
- WAVEGUIDE MEASUREMENTS OF COMPLEX DIELECTRIC CONSTANT OF TEXAS SOILS
- TOWER-MOUNTED RADIOMETER MEASUREMENTS OF SOIL SAMPLES UNDER CONTROLLED CONDITIONS
- AIRBORNE MULTI-FREQUENCY RADIOMETER MEASUREMENTS OF DOCUMENTED SITES (WESLACO)

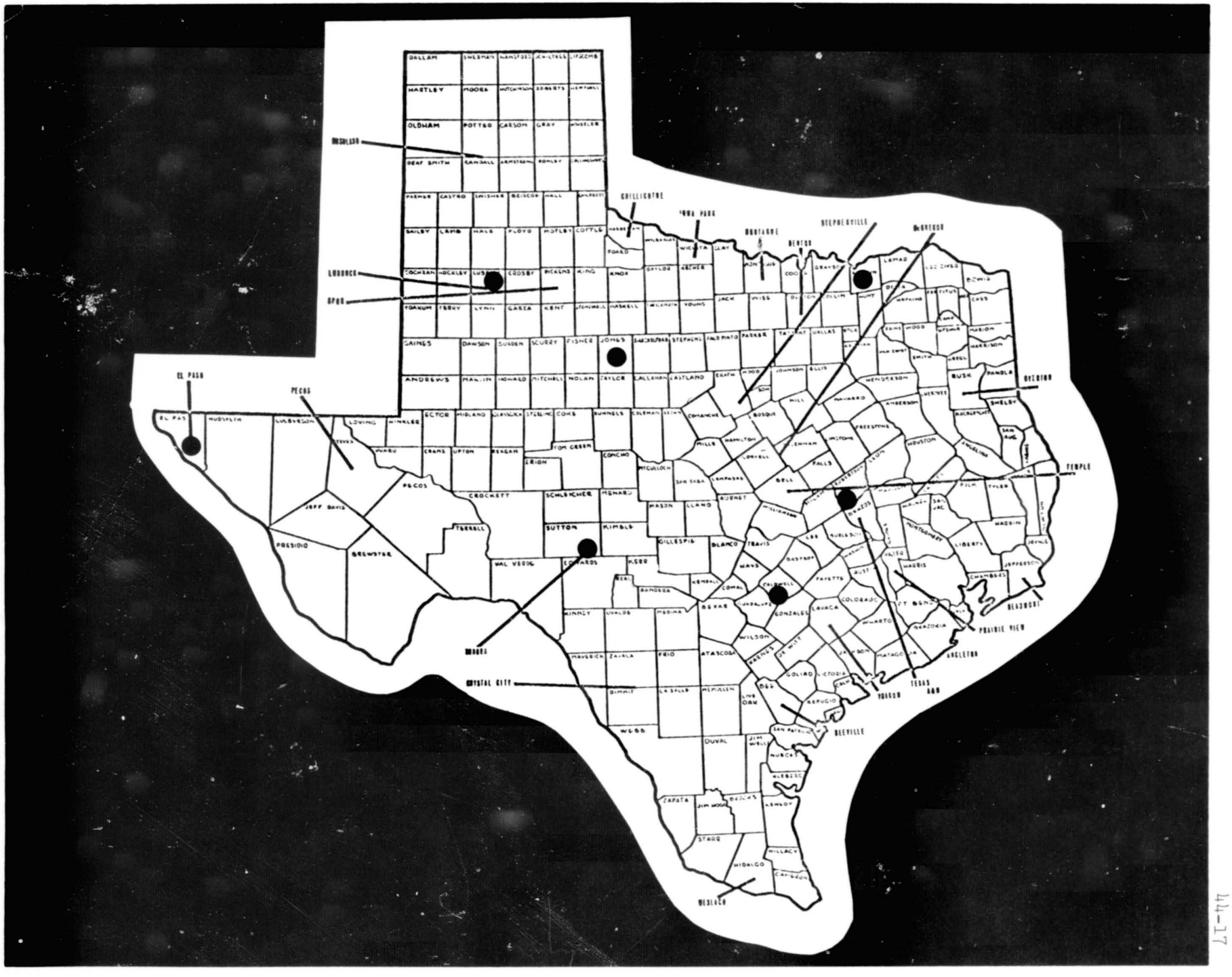
DALLAM
SHERMAN
HANSFORD
OCHILTREE
LIPSCOMB
HARTLEY
MOORE
HUTCHINSON
ROBERTS
HEMPHILL
OLDHAM
POTTER
CARSON
GRAY
WHEELER
DEAF SMITH
RANDALL
ARMSTRONG
DONLEY
COLLINGSWORTH
PARMER
CASTRO
SWISHER
BRISCOE
HALL
CHILDRESS
BAILEY
LAMB
HALE
FLOYD
MOTLEY
COTTLE
FOARD
HARDEMAN
WILBARGER
WICHITA
CLAY
MONTAGUE
COOKE
GRAYSON
LAMAR
RED RIVER
BOWIE
CROSBY
DICKENS
KING
KNOX
BAYLOR
ARCHER
YOAKUM
TERRY
LYNN
GARZA
KENT
STONEWALL
HASKELL
THROCKMORTON
YOUNG
JACK
WISE
DENTON
COLLIN
HUNT
FANNIN
GAINES
DAWSON
BORDEN
SCURRY
FISHER
JONES
SHACKELFORD
STEPHENS
PALO PINTO
PARKER
TARRANT
DALLAS
ANDREWS
MARTIN
HOWARD
MITCHELL
NOLAN
TAYLOR
CALLAHAN
EASTLAND
ERATH
HOOD
JOHNSON
ELLIS
HENDERSON
RUSK
PANOLA
UPSHUR
MARION
HARRISON
EL PASO
HUDSPETH
CULBERSON
LOVING
WINKLER
ECTOR
MIDLAND
GLASSCOCK
STERLING
COKE
RUNNELS
COLEMAN
BROWN
COMANCHE
BOSQUE
HILL
NAVARRO
ANDERSON
SHELBY
WARD
CRANE
UPTON
REAGAN
IRION
TOM GREEN
CONCHO
MCCULLOCH
SAN SABA
LAMPASAS
MILLS
HAMILTON
CORYELL
FALLS
LIMESTONE
FREESTONE
LEON
HOUSTON
TRINITY
ANGELINA
TEMPLE
BELL
WILLIAMSON
MILAM
ROBERTSON
BRAZOS
GRIMES
WALLER
HARRIS
MONTGOMERY
SAN JAC
MADISON
LIBERTY
JEFFERSON
CHAMBERS
BEAUMONT
PRAIRIE VIEW
TEXAS A&M
HOUSTON
PECOS
CROCKETT
SCHLEICHER
MENARD
MASON
LLANO
BURNET
JEFF DAVIS
TERRELL
PRESIDIO
BREWSTER
SUTTON
KIMBLE
GILLESPIE
BLANCO
TRAVIS
LEE
BURLESON
WASHINGTON
AUSTIN
WALLER
VAL VERDE
EDWARDS
REAL
KERR
BANDERA
KENDALL
COMAL
CALDWELL
FAYETTE
COLORADO
LAVACA
MATAGORDA
BRAZORIA
GALVESTON
KINNEY
UVALDE
MEDINA
BEXAR
GUADALUPE
GONZALES
WILSON
KARNES
DE WITT
JACKSON
MAVERICK
ZAVALA
FRIO
ATASCOSA
GOLIAD
VICTORIA
CALHOUN
CRYSTAL CITY
DIMMIT
LA SALLE
MCMULLEN
LIVE OAK
REFUGIO
ARANSAS
CORPUS CHRISTI
NUECES
WEBB
DUVAL
JIM WELLS
SAN PATRICIO
BEEVILLE
KLEBERG
ZAPATA
JIM HOGG
BROOKS
KENEDY
STARR
HIDALGO
WILLACY
CAMERON
BROWNSVILLE

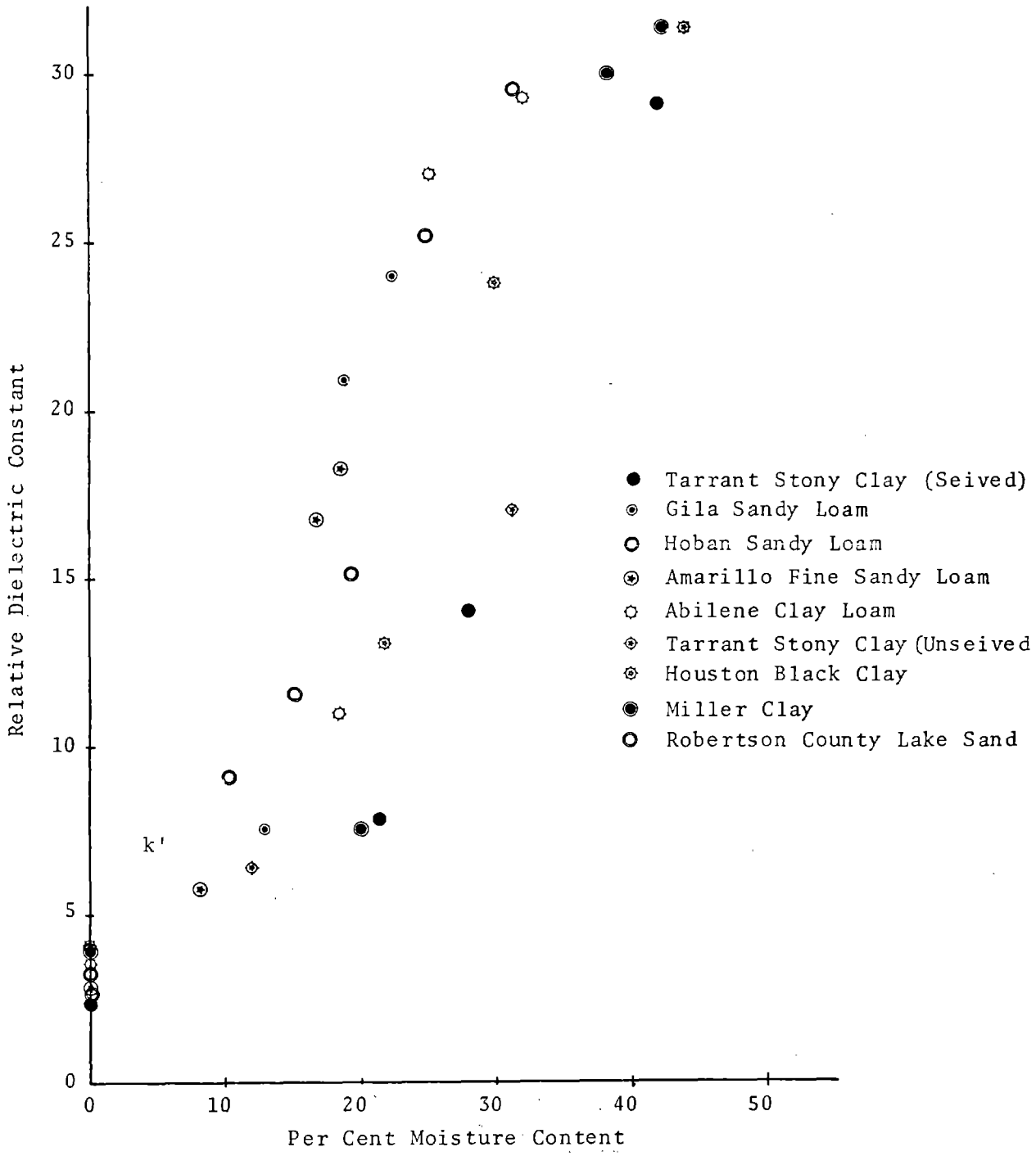
Relative Dielectric Constant
30
25
20
15
10
5
0
k'
0
10
20
30
40
50
Per Cent Moisture Content
Tarrant Stony Clay (Seived)
Gila Sandy Loam
Hoban Sandy Loam
Amarillo Fine Sandy Loam
Abilene Clay Loam
Tarrant Stony Clay (Unseived
Houston Black Clay
Miller Clay
Robertson County Lake Sand

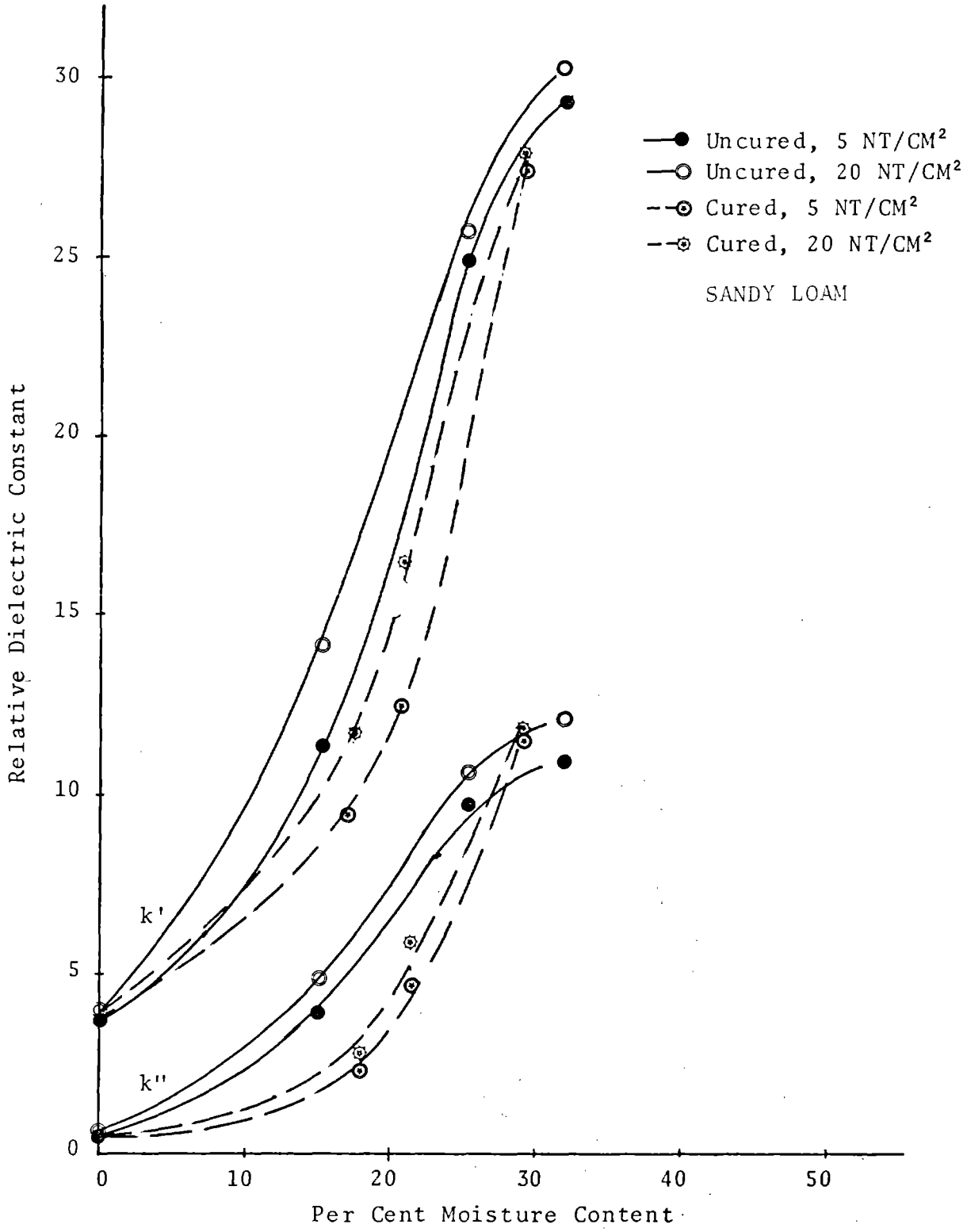
Uncured, 5 NT/CM²
Uncured, 20 NT/CM²
Cured, 5 NT/CM²
Cured, 20 NT/CM²
SANDY LOAM
Relative Dielectric Constant
Per Cent Moisture Content
k'
k''
0
5
10
15
20
25
30
0
10
20
30
40
50

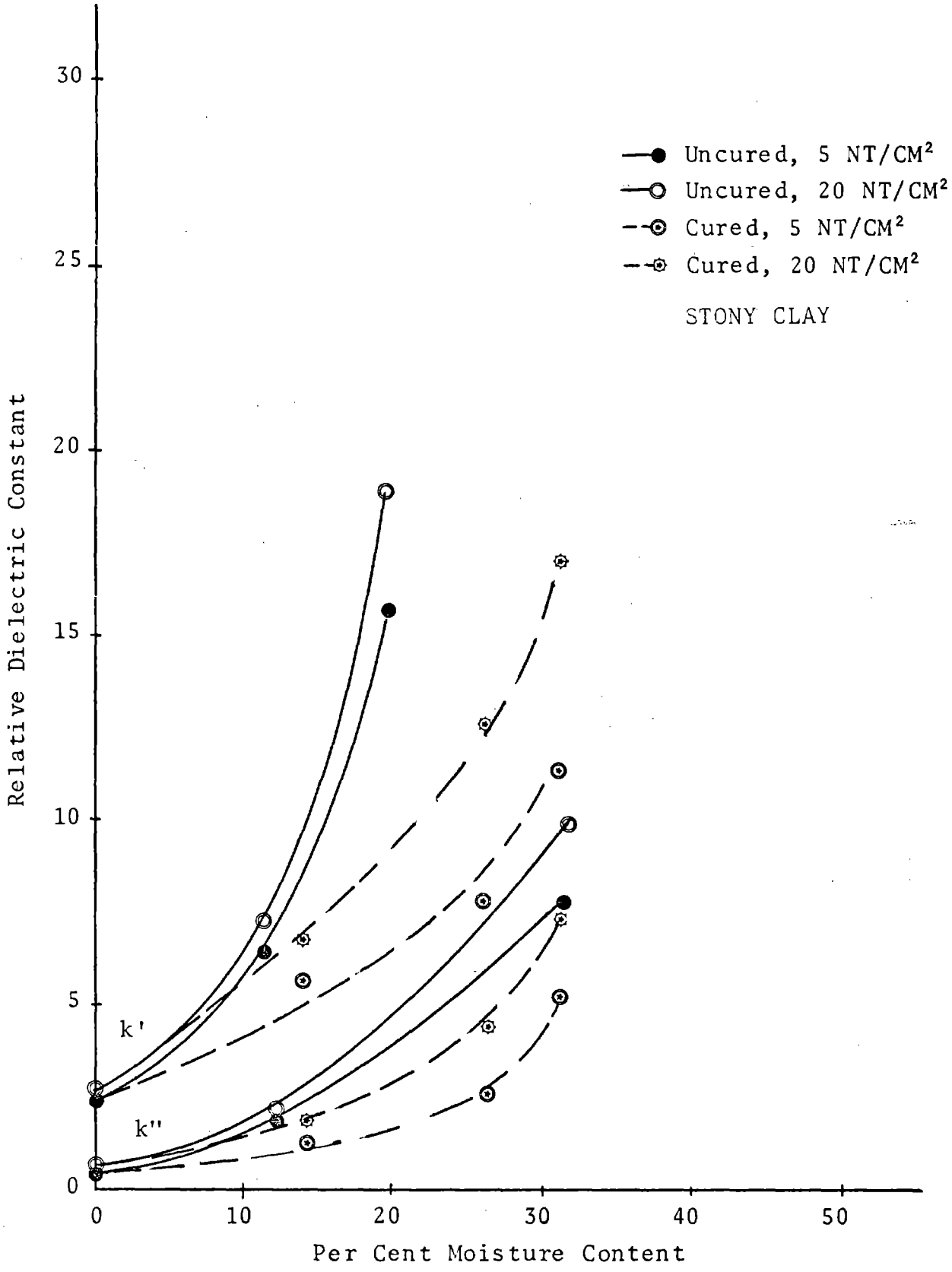
Uncured, 5 NT/CM²
Uncured, 20 NT/CM²
Cured, 5 NT/CM²
Cured, 20 NT/CM²
STONY CLAY
Relative Dielectric Constant
Per Cent Moisture Content
k'
k''
0
5
10
15
20
25
30
0
10
20
30
40
50

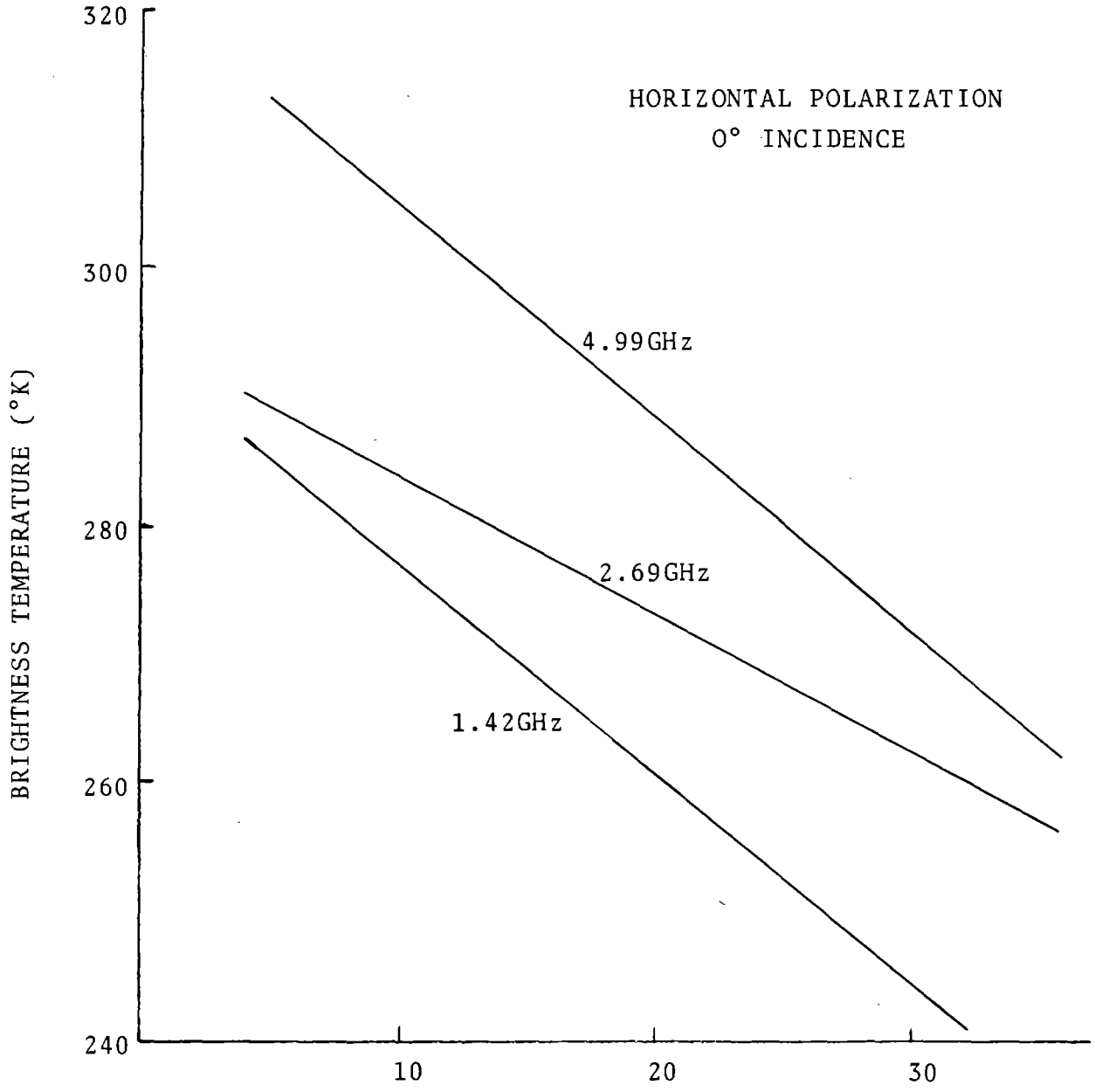
320
300
280
260
240
BRIGHTNESS TEMPERATURE (°K)
HORIZONTAL POLARIZATION
0° INCIDENCE
4.99GHz
2.69GHz
1.42GHz
10
20
30
PERCENT MOISTURE (DRY WEIGHT)
NASA/GSFC DATA
WESLACO 1971

DATA ANALYSIS LABORATORY OBJECTIVES

- PROVIDE STATE-OF-THE-ART ANALYSIS OF MULTI-SENSOR DATA
- IMPLEMENT AND DEVELOP COMPUTER SOFTWARE
- INVESTIGATE THE EFFICIENT UTILIZATION OF THE TOTAL DATA SYSTEM

ARCTIC ICE ANALYSIS

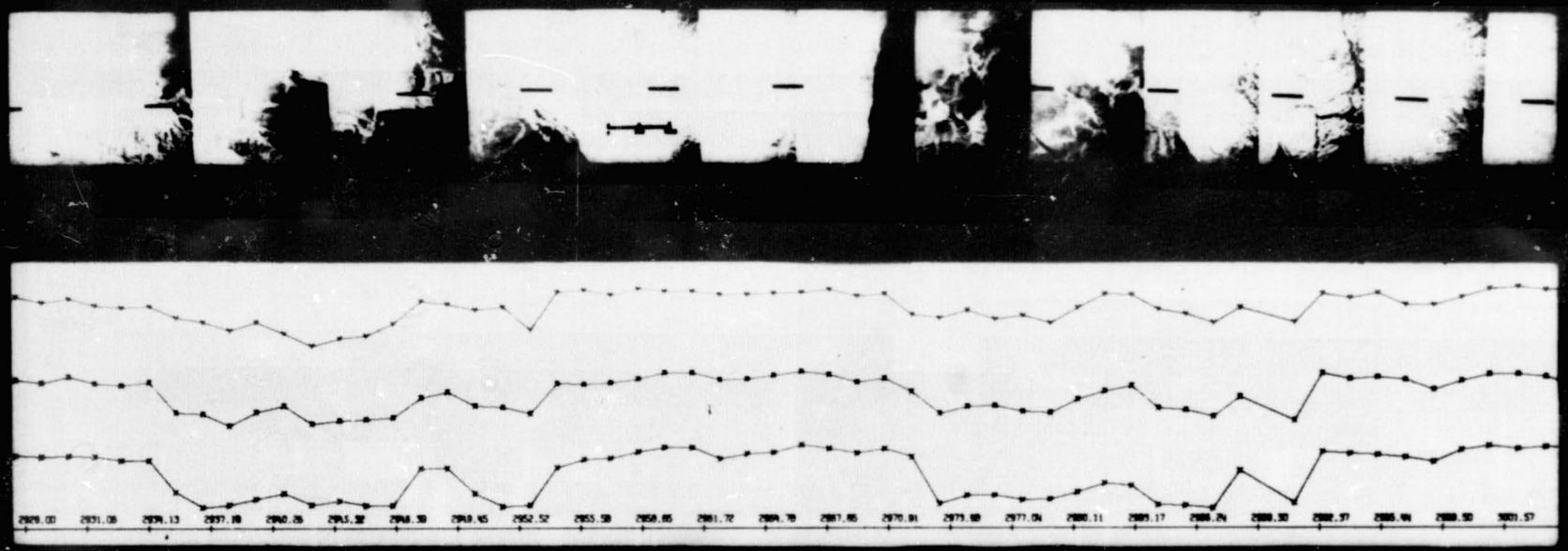

MISSION

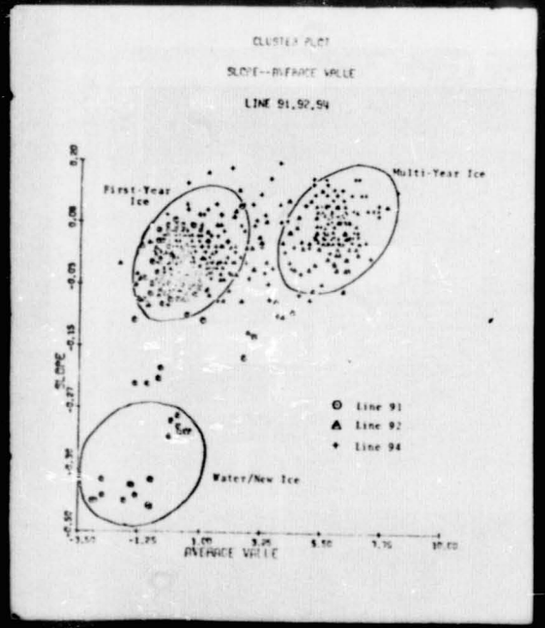

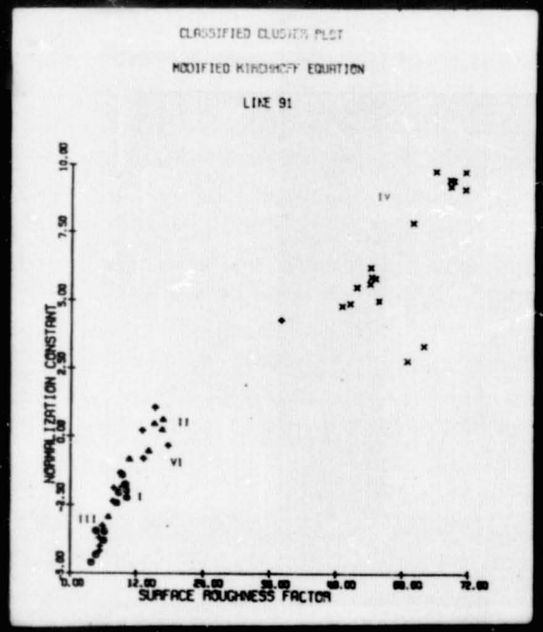

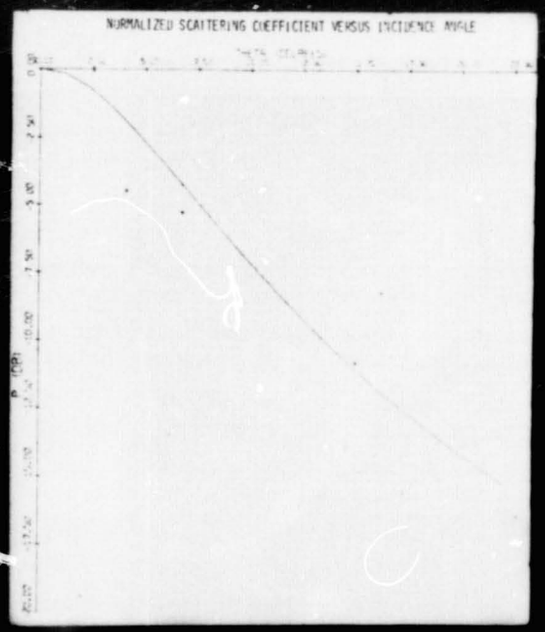

MISSION

MULTISPECTRAL SCANNER

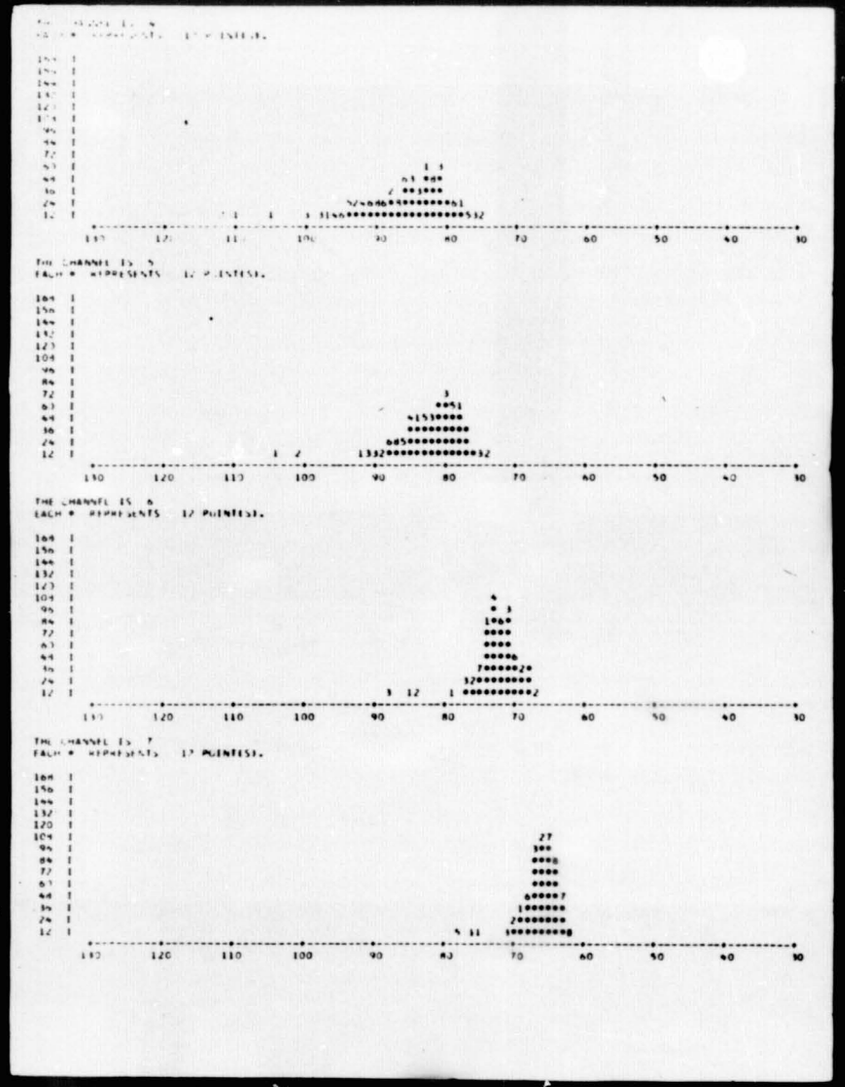

WESLACO 5166

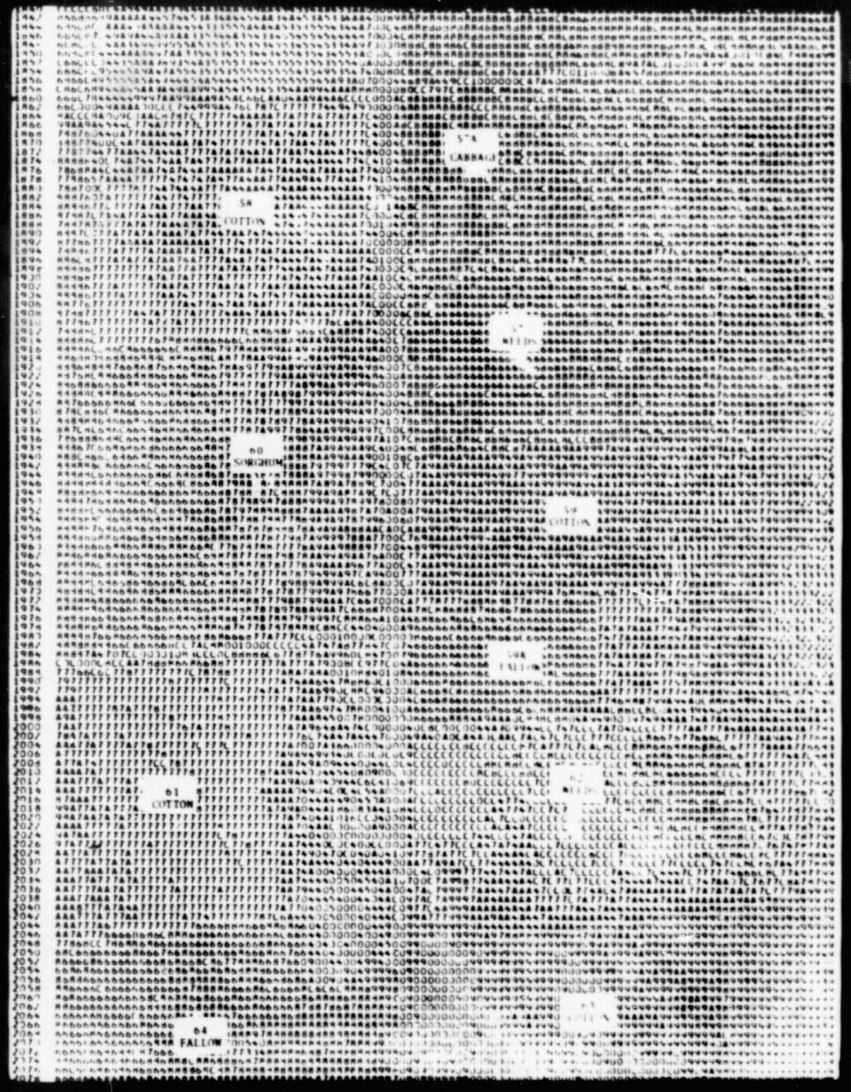

CLASSIFICATION ANALYSIS

IBM 360/65 DIGITAL COMPUTER

- UNIVERSITY OWNED TO PROVIDE LOW COST, EFFICIENT OPERATION WITH A FULL RANGE OF COMPUTER CAPABILITY AND USER SERVICE.

- 6 MILLION BITS CORE STORAGE
- DISC STORAGE
- MAGNETIC TAPE (MULTIPLE TRACK, DENSITY)
- MULTIPLE COMPILER/UTILITIES
- CORE RESIDENT WATFIV (SOFTWARE DEVELOPMENT)
- MVT OPERATING SYSTEM (OPERATIONAL COST/TURNAROUND

- RAPID TURNAROUND (TYPICALLY 15 MINUTES)
- USER COST $375/CPU HOUR

WATER POLLUTION
RESEARCH
TEXAS A&M UNIVERSITY
CIVIL ENGINEERING DEPARTMENT

HOUSTON SHIP CHANNEL WATER QUALITY STUDY

COOPERATIVE STUDY WITH NASA/MSC, TAMU CIVIL ENGINEERING DEPARTMENT AND TEXAS WATER QUALITY BOARD.

OBJECTIVE: ESTABLISH FEASIBILITY AND PROCEDURE FOR IMPLEMENTING REMOTE SENSING TECHNIQUES INTO OPERATIONAL MONITORING ACTIVITIES OF THE TEXAS WATER QUALITY BOARD.

HUD CITY PROJECT

(GEORGE MITCHELL ASSOC. DEVELOPMENT)

PLAN FOR TOTAL CITY (POP. 100,000) ON 17,500 ACRE SITE NORTH OF HOUSTON - 20 YR. DEVELOPMENT PLAN TO INCLUDE INDUSTRIAL, RESIDENTIAL, COMMERCIAL, EDUCATIONAL, AND RECREATIONAL FACILITIES.

OBJECTIVE: TO UTILIZE REMOTE SENSOR DATA TO MINIMIZE IMPACT OF MAJOR URBAN DEVELOPMENT ON THE ENVIRONMENT AND TO CAPITALIZE UPON THE CHARACTERISTICS OF THE NATURAL TERRAIN.

Real Estate Map

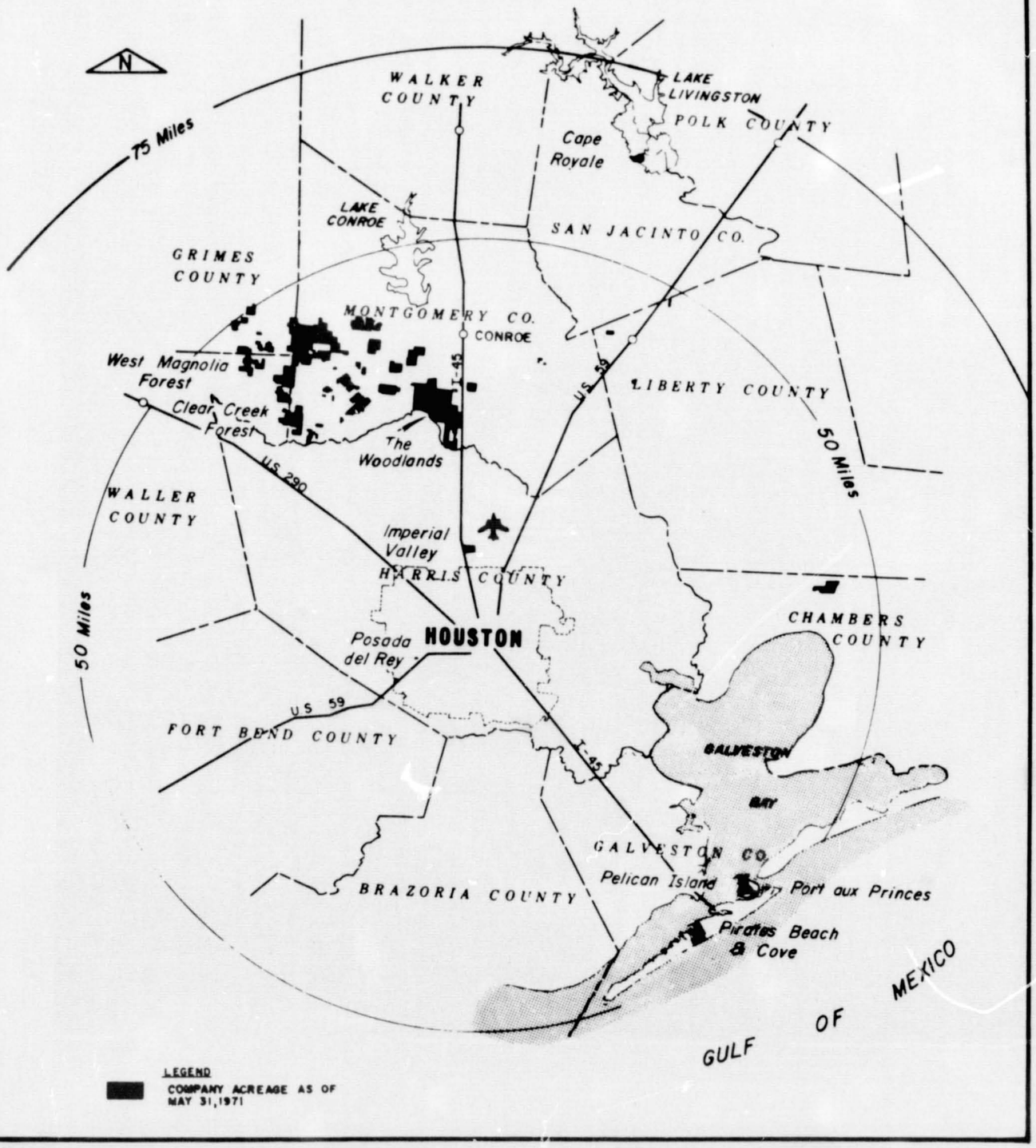

SECTION 45

SPECTRAL REFLECTANCE MEASUREMENTS OF A VIRUS HOST MODEL

by

Robert W. Toler, Associate Professor
Department of Plant Sciences
Remote Sensing Center
Texas A&M University
College Station, Texas 77843

N. K. Shankar, Staff Engineer
Lockheed Electronics Co.
Houston, Texas

INTRODUCTION

Insects, weeds, and diseases are hazards to crop production and must be managed. Plant protection is designed for reduction of these crop pests, in order to provide our society with food, fiber, oils and ornamentals while preserving a wholesome environment. Plant diseases are caused by bacteria, fungi, nematodes, phanerogams (parasitic seed plants), mycoplasma, and viruses; viruses incite diseases that limit production of the major food crops of the world. The plant viruses and mycoplasma in most host translocate to the growing point of the plant. Viruses are obligate parasites and multiply only in living cells. A few examples are: Maize Dwarf Mosaic Virus which causes losses in corn, sorghum, and millet; Wheat Streak Mosaic Virus reduces production of wheat, oats, and barley; Barley Yellow Dwarf Virus invades barley, wheat, and oats; Sugarcane Mosaic Virus lowers yield of sugarcane, sorghum, and corn; Tungro or Yellow Orange Leaf Virus is one of the most serious diseases of rice in Asia today and Hoja Blanca Virus attacks rice here in the western hemisphere; and Coconut Lethal Yellowing has destroyed coconut plantings in Jamaica and Florida. Disease management programs to be used effectively in intergrated systems for controlling all pests on a crop will require new disease survey techniques.

This research was a cooperative effort of the Department of Plant Sciences College of Agriculture, Remote Sensing Center, Texas A&M University, College Station, Texas (supported by NASA Grant NsG 239-62) and NASA/MSC/EOD, Applied Physics Branch, Houston, Texas. Valuable assistance was provided by Dr. Forrest Hall,

physicist, Applied Physics Branch NASA/MSC/EOD, Houston; Mr. E. H. Krauss, supervisor, and Mr. Jack Hartman, photoscientist, Lockheed Electronics, Inc., Houston Aerospace Systems Division Photo-optical Science Section NASA/MSC/Houston; and Mr. William Odle, Graduate Assistant, Department of Plant Sciences, Texas A&M University, College Station, Texas.

Virus-host Model

St. Augustinegrass (Stenotaphrum secundatum), the host of St. Augustine Decline, was selected as a disease model to study spectral reflectance properties in order to differentiate healthy from infected grass by remote sensing techniques. In this disease-host combination the host was selected because it is 1) a monocot, 2) produces turf, 3) perennial in nature, 4) vegetatively propagated, 5) genetically stable, 6) adapted to the test site environment, 7) the disease reaction is a typical mosaic, and 8) susceptible to mechanical transmission. The incubation period of the disease is 21-30 days transmitted mechanically, and has a limited host range that includes crabgrass, millet, and St. Augustinegrass.

The experiment discussed here is the multispectral tone signatures of the St. Augustine Decline diseased and healthy targets. Two objectives were: 1) to predict theoretical tone values of healthy and infected St. Augustinegrass on various film/filter/polarization combinations, using spectrometric measurements of light reflectance, film sensitivity data, and filter transmittance curves; 2) to measure the correlation between theoretical tone values and actual tone values as obtained by densitometric analysis of photo negatives. From this information multispectral tone signatures of the healthy and infected St. Augustinegrass can be determined, and optimum film/filter combinations to be used in multispectral photography can be selected.

PROCEDURE

Plant material for laboratory and field studies employed both mechanically inoculated and naturally infected grass showing varying levels of disease development. The split plot technique was used in our field trials with the healthy controls and St. Augustine Decline diseased grass. The plot size was 8 x 8 ft. replicated 12 times (Figure 1). Mechanical inoculations were made in the greenhouse using 600 mesh carborundum and phosphate buffer pH 7.5, .01 M. Inoculum was diseased leaf tissue and buffer at a 1:1 ratio by

weight, ground in a mortar with 1 percent carborundum. Data acquisition included: 1) measuring the spectral reflectance of samples in the laboratory, using the Cary-14 RI spectrophotometer, 2) measuring the spectral reflectance of field plots, using field instruments such as the EG&G spectroradiometer, 3) photographing laboratory samples and field plots, using multiband photographic sensors with various film/filter/polarization combinations, and 4) performing polarization measurements in the laboratory, using a modified Cary-14 RI spectrogoniophotometer.

Cary-14 RI Laboratory Data Acquisition

The model - 14 RI spectrophotometer was employed for automatic recording of spectra in the wavelength region of 2,250 Å to 30,000 Å with good resolving power and high photometric accuracy. Interchangeable light sources for the instrument are a hydrogen lamp, a tungsten lamp for the visible region, and a tungsten lamp for the near-infrared region.

Samples of St. Augustinegrass plants were inoculated with virus at various intervals. These plants were kept under controlled greenhouse conditions at Texas A&M University. Grass blades from these plants were cut to size to be placed in the sample cup of the reflectometer. Various orientations of the grass blades in the sample cup were used to measure the diffuse spectral reflection function in the wavelength region of 350 to 900 nm. Similar measurements were made on the healthy grass samples. The effects of background on the samples were also explored (Figure 2).

Spectral reflectance curves obtained from Cary-14 are shown in Figures 3 and 4.

Multiband Photography

An array of four Nikon-F cameras was mounted on a specially made frame (Figure 5). This frame was then mounted on a tropod stand. Each camera was boresighted on the target. Field irradiance shutter speed calibration and spectral transmission of each lens/filter combination were performed. Three film/filter combinations were selected. Wratten filters 47B, 58, and 25, in combination with black and white plus-X type film, were used in taking spectral multiband photographs of healthy and infected St. Augustinegrass plants, in daylight at various sun angles and in photoflood light under indoor

lighting conditions. Black and white IR, color IR, and Ektrachrome color photographs were also made. Very good correlation between Cary-14 data and photographic density was observed. The results are shown in Figures 6 and 7.

The Nikon camera array was used in the multiband photography of control plots and field work. A cherry picker crane was used to hoist the equipment 35 to 45 ft. above the ground.

Polarization Spectral Reflectance Measurements

The polarization spectral reflectance of grass samples was measured using a modified Cary-14 RI spectrophotometer with a Cary model 50-400-000 gonioreflectometer. The instrument was modified to accept an externally mounted RCA C31034D GaInAs photomultiplier tube and FET-preamp. The Cary gonioreflectometer employs a 25-cm diameter integrating sphere with a tiltable sample holder in the center of the sphere. The sphere is illuminated with undispersed light from a 1,000-W quartz-iodine lamp. A 5-cm quartz lens mounted in the bottom of the sphere projects the image of the lamp filament on the underside of the sample holder. The measurements of the vertical and horizontal polarization components of the reflected light was accomplished by positioning two 3-cm aperture Glan-Thompson prisms in the two sample cell holders located in the sample cell compartment. The reflectance data, 0 percent, 10 percent maximum, and 100 percent of the two components, were recorded on punched paper tape, using the Datex model CU-702-0 data logger. Polarization spectra of healthy and infected grass samples were measured and recorded on the paper tape. This tape was fed into a time-sharing terminal of an XDS Sigma 7 computer. The data was edited, translated, normalized, and reduced to give average reflectance and percent polarization. Polarization values from +100 percent to -100 percent were plotted on an X-Y recorder (Figure 5). Individual perpendicular and parallel polarization components and average values were also plotted. Polarizing filters in conjunction with spectral bandpass filters were used on the Nikon camera systems to record multispectral photographic data.

Spectroradiometer Measurements

The model 580/585 EG&G spectroradiometer system, consisting of a 580-11A indicator unit, a 580-20A series detector head, 585-30 series beam input optics, 585-11 monochromator housings with proper gratings

of the 580-20 series, and other accessories, was used for measuring the spectral reflectance power of healthy and infected St. Augustinegrass plots in the field. The input optical unit mounted along with the monochromator unit and detector head, on a tripod mount, was pointed toward the target. Monochromator slits were adjusted to the calibrated settings. Current output of the detector for each wavelength setting was monitored on the indicator unit and recorded. Prefilters were used to eliminate the high-order interference. A standard white reference target was placed in front of the sensing unit, and spectral reflectance values were measured at the same lighting conditions. The ratios of currents of sample grass to white reference at all wavelengths were calculated. One sample of such experimental data is presented in Figure 8. The hemispherical flux input received at the ground level was measured using an ISCO radiometer. These data were used to apply corrections to EG&G data.

RESULTS AND DISCUSSION

Spectral reflectance data from the Cary-14 RI spectrophotometer showed spectral differences between healthy and diseased plants. Ten to 15 percent differences were found in the 450 to 480 nm (blue) region, the 550 to 560 nm (yellow green) region, and the 670 to 680 nm (red) region. Variations in the dominant peak wavelength were observed. These differences were also observed in the field data taken with the EG&G spectroraiometer. Polarization measurements indicated major spectral differences between healthy and infected plants; as much as 34 percent difference in reflectance in the 450 to 480 nm region and 40 percent difference in the 670 to 680 nm region. Very little difference was observed in the 540 to 550 nm region.

Qualitative measurements from photographs of plants in the blue and red regions with polarization show that light reflected from healthy plants is more strongly polarized than that from diseased plants. Photographs taken through the blue Wratten 47 filter in conjunction with a polarizer show an excellent differentiation. A large photographic difference also appears in the red region (filter 25 and polarizer combination). Much smaller differences were noted in the 540 to 550 nm region. Although the intensity in the near-IR region (750 to 1,200 nm) is much higher than the visible region of the spectrum, differences in the healthy and diseased plants' reflectance were quite small. A maximum of 10 percent difference was observed in the spectra obtained with the

Cary-14 RI spectrophotometer. Near-IR photographs taken with color IR and black and white IR films showed relatively small tone change between the healthy and infected grass plots.

Black and white negatives of the control plots taken with red, green, and blue filters plus polarizers were analyzed using color density contouring and slicing techniques. A multiband TV display unit manufactured by the IIS Corporation was used for this purpose. The results are shown in Figures 9 and 10. Ratioing densities of the green region to the red region, and the green region to the blue region were attempted using the IIS Corporation imaging system. The results are shown in Figures 11 and 12. There seems to be good correlation between the laboratory results and field data. The healthy grass consistently exhibited a darker image on the negative compared to the diseased grass.

An analysis of results using absolute reflected energy levels will be made in the future work schedule. Modeling for aircraft operation is also contemplated in this schedule. With time progression data acquisition, effective previsual analysis prediction will be attempted.

In conclusion, a technique has been developed to detect the characteristic spectral signature of healthy and infected St. Augustinegrass. It is possible to predict the coverage of the infected area provided ground truth coverage shows positive St. Augustinegrass turf. Positive identification of healthy and diseased grass is attempted, but no attempt has been made to isolate the virus symptoms from any other symptoms or effects.

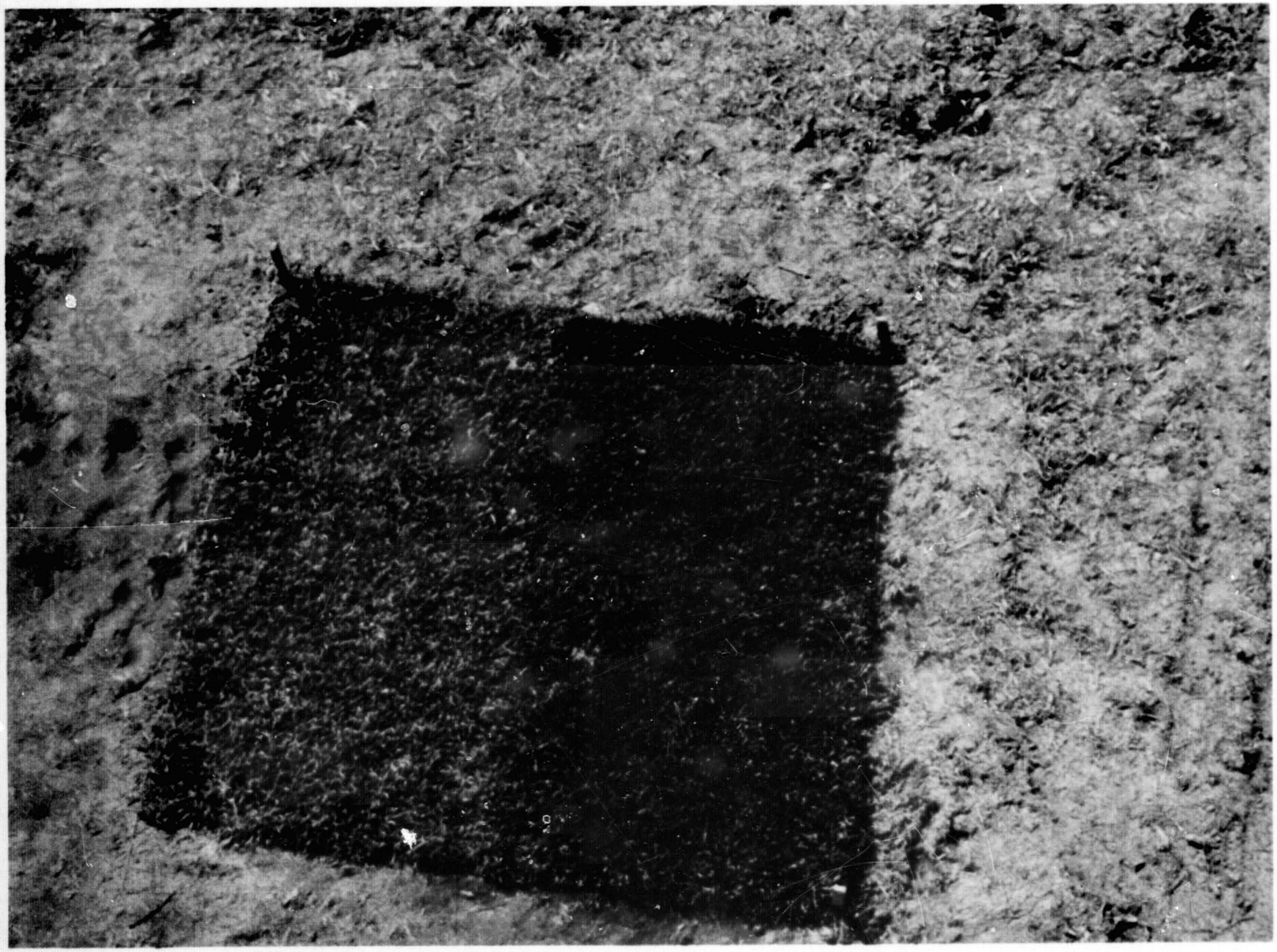

Figure 1. Field plot 8 x 8 ft. split 4 x 8 ft. healthy grass and 4 x 8 ft. St. Augustine Decline diseased grass.

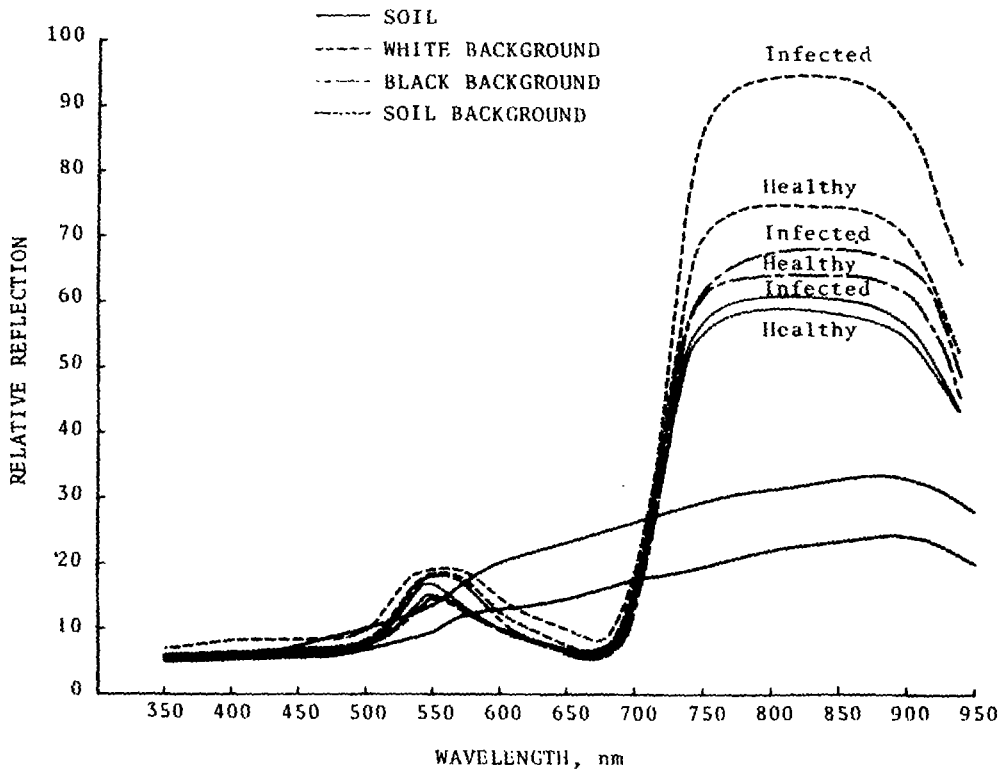
SOIL
WHITE BACKGROUND
BLACK BACKGROUND
SOIL BACKGROUND
Infected
Healthy
Infected
Healthy
Infected
Healthy
RELATIVE REFLECTION
100
90
80
70
60
50
40
30
20
10
0
350
400
450
500
550
600
650
700
750
800
850
900
950
WAVELENGTH, nm

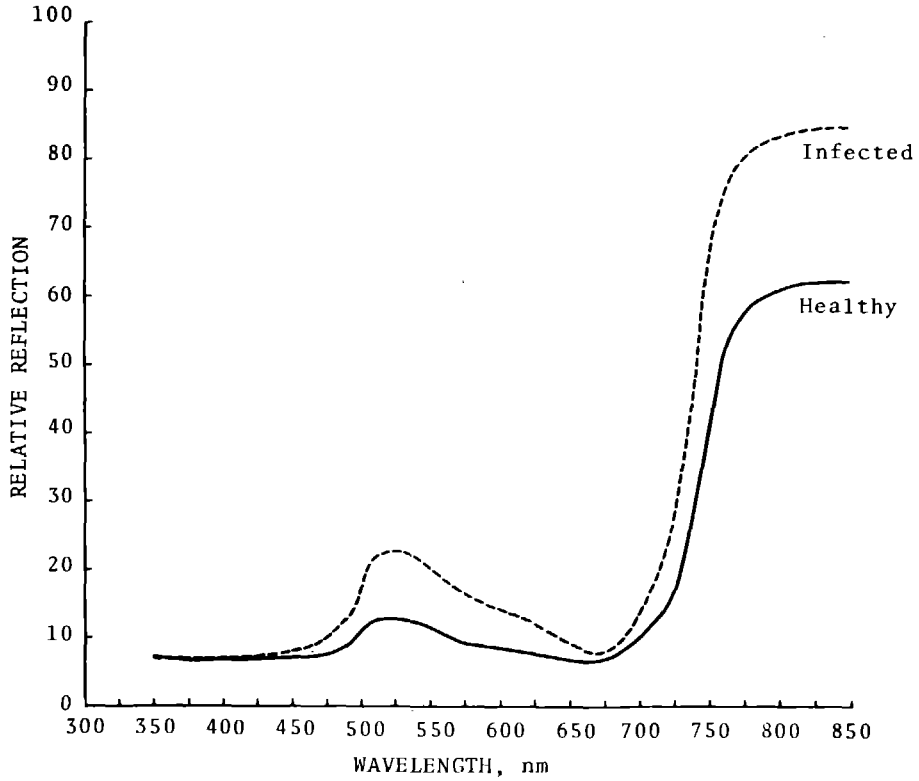

Figure 3. Cary-14 RI spectrophotometer results: reflectance spectra of healthy and infected St. Augustinegrass samples.

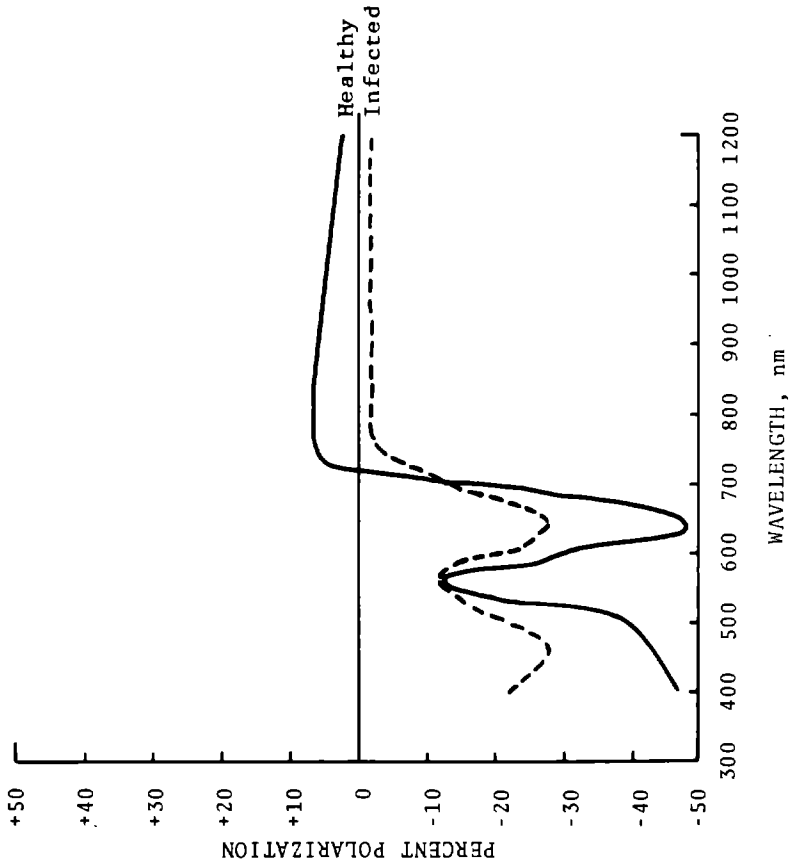

Figure 4. Cary-14 RI spectrophotometer results: polarization reflectance spectra of healthy and infected St. Augustinegrass samples.

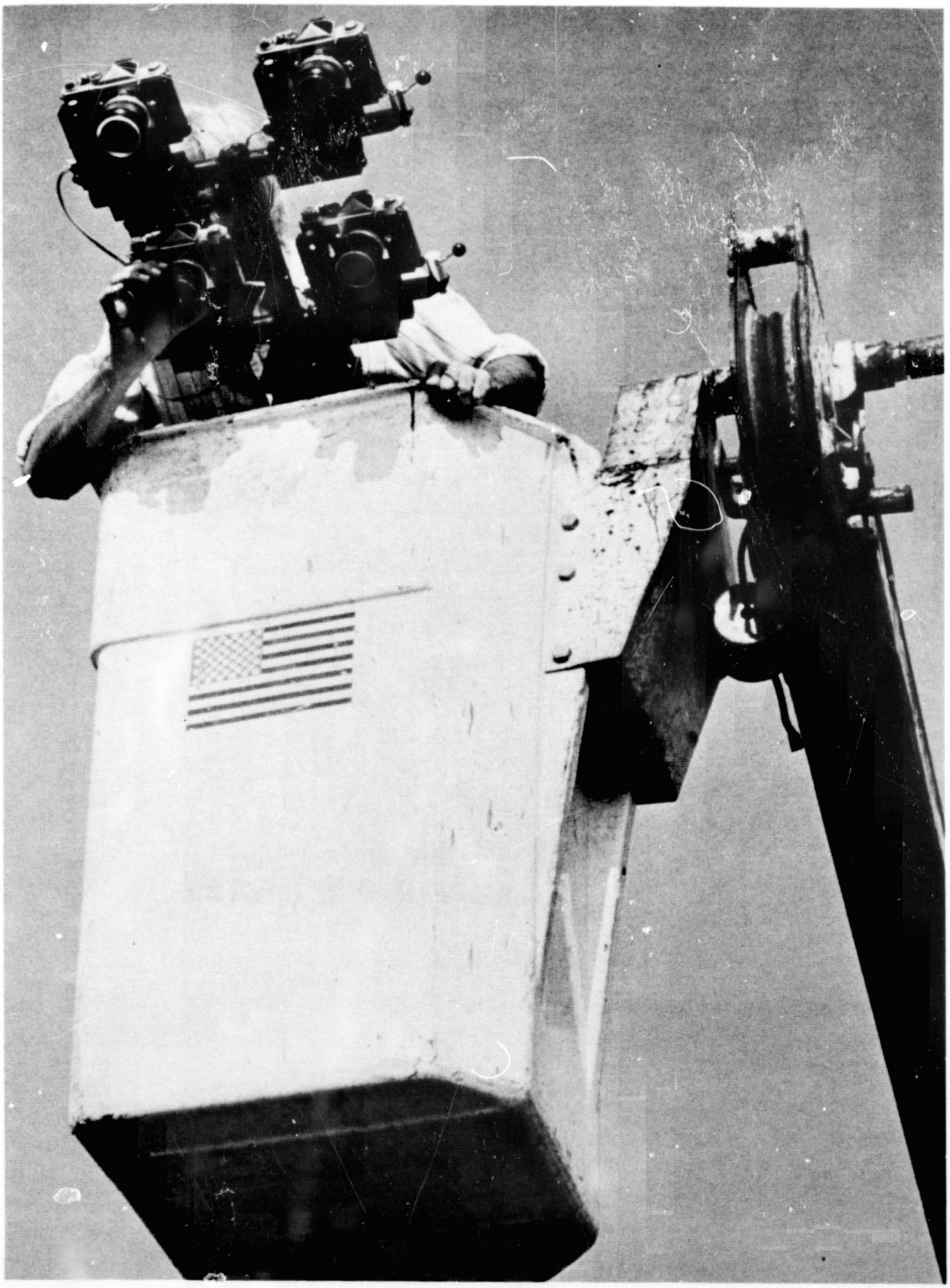

Figure 5. Nikon camera four-band system on the cherry picker crane.

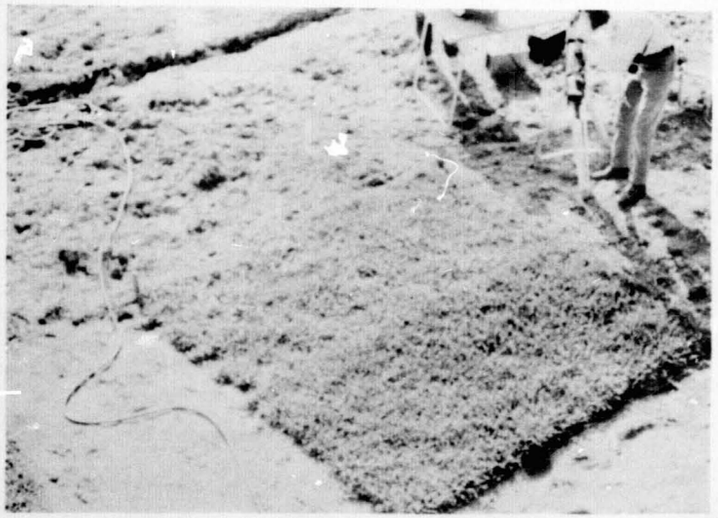

Wratten 25 (red)

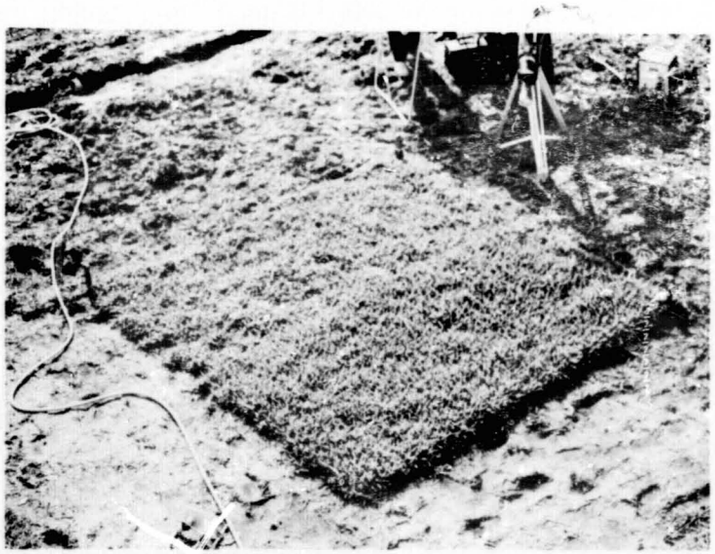

Wratten 58 (green)

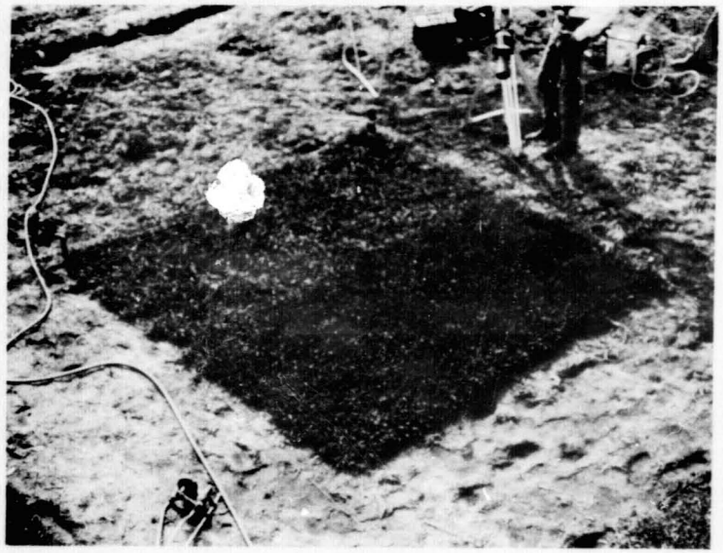

Wratten 47B (blue)

Figure 6. Field plot photographed through Wratten 25, Wratten 58, and Wratten 47B filters.

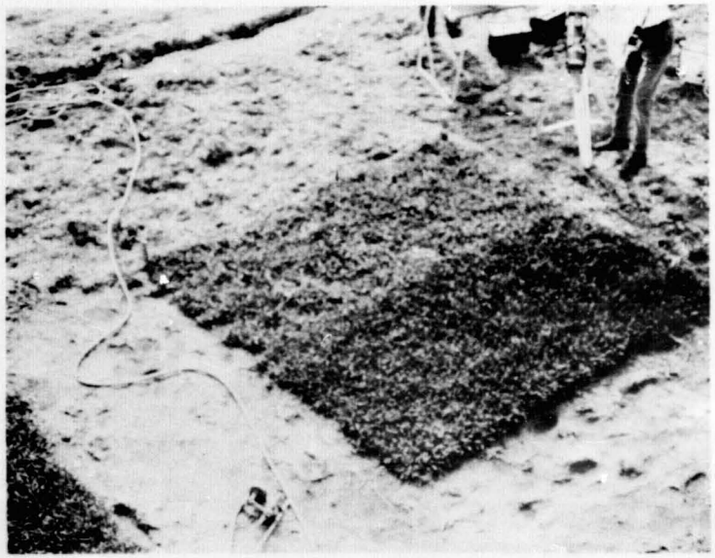

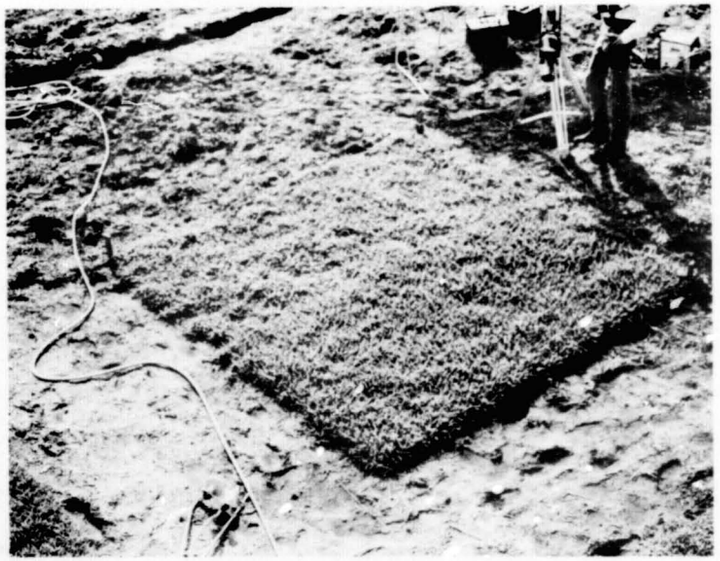

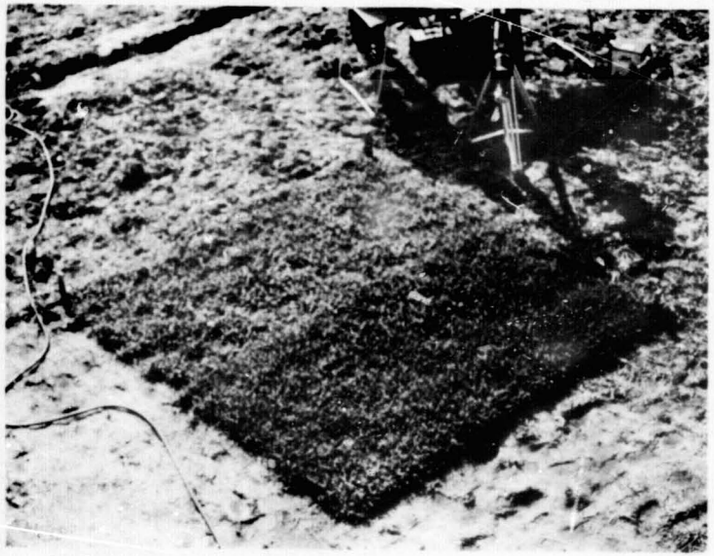

Figure 7. Field plot photographed through Wratten 25 and polarizer, Wratten 58 and polarizer, and Wratten 57B and polarizer.

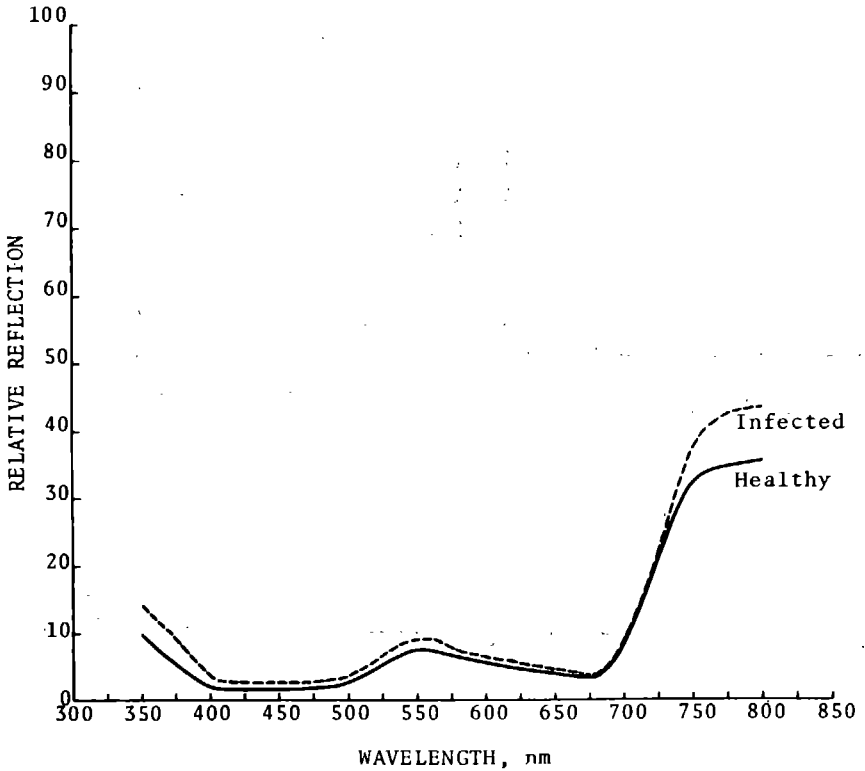

Figure 8. EG&G field measurement results: reflectance spectra of healthy and infected St. Augustinegrass samples.

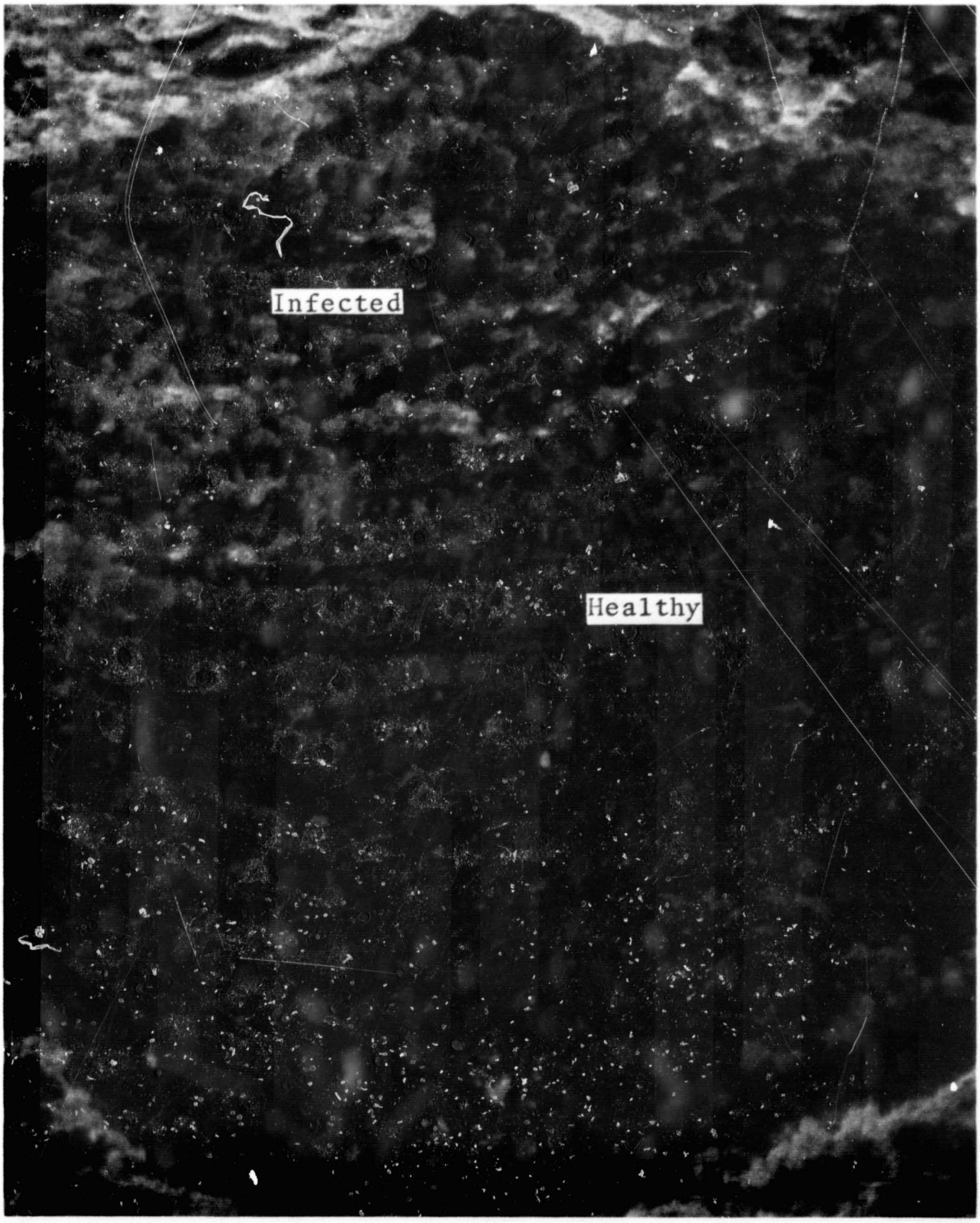

Figure 9. Color density photo of I^2S system photograph of the projection screen. (Red filter and polarizer)

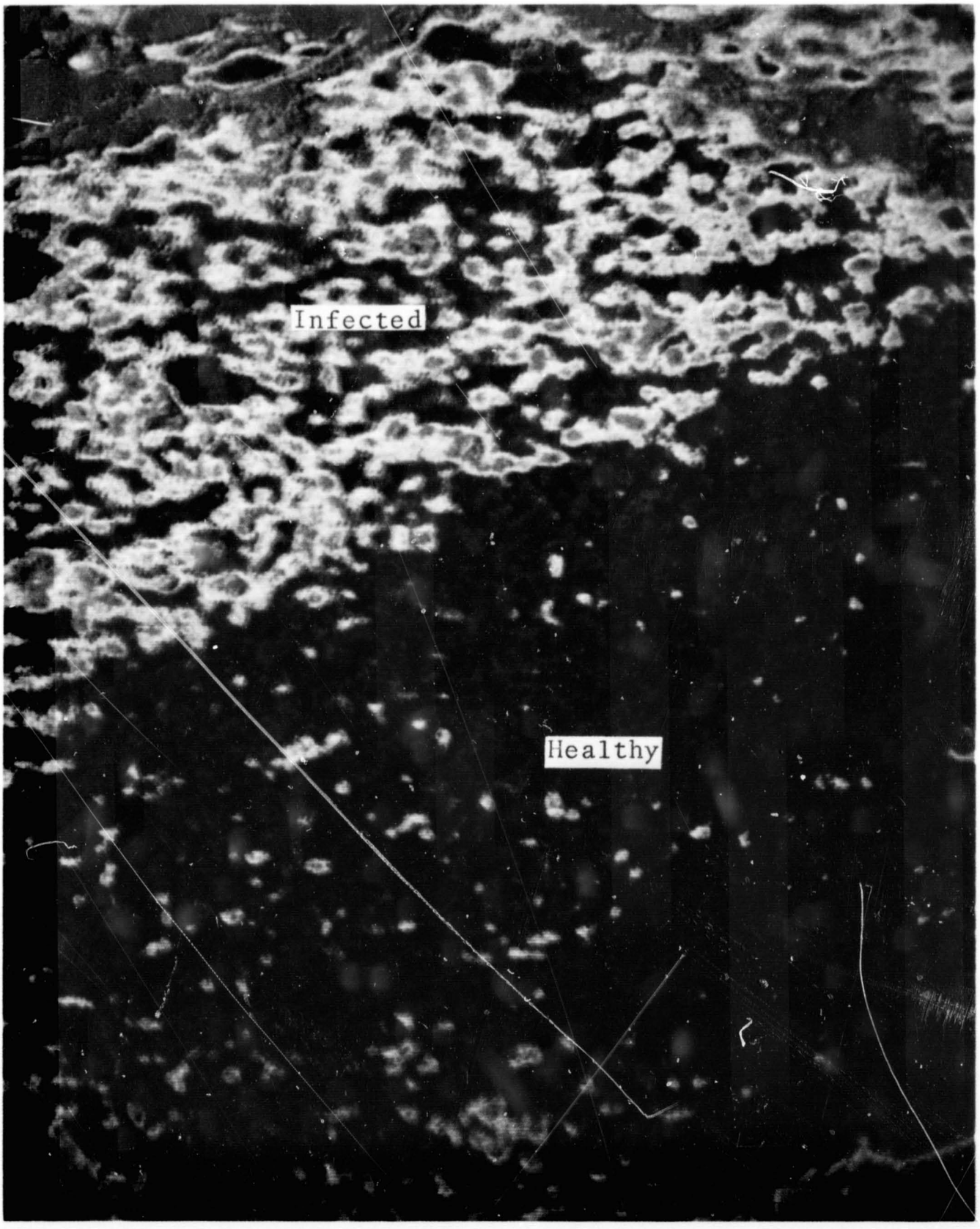

Figure 10. Color density photo of I^2S system photograph of the projection screen (blue filter and polarizer) (concluded).

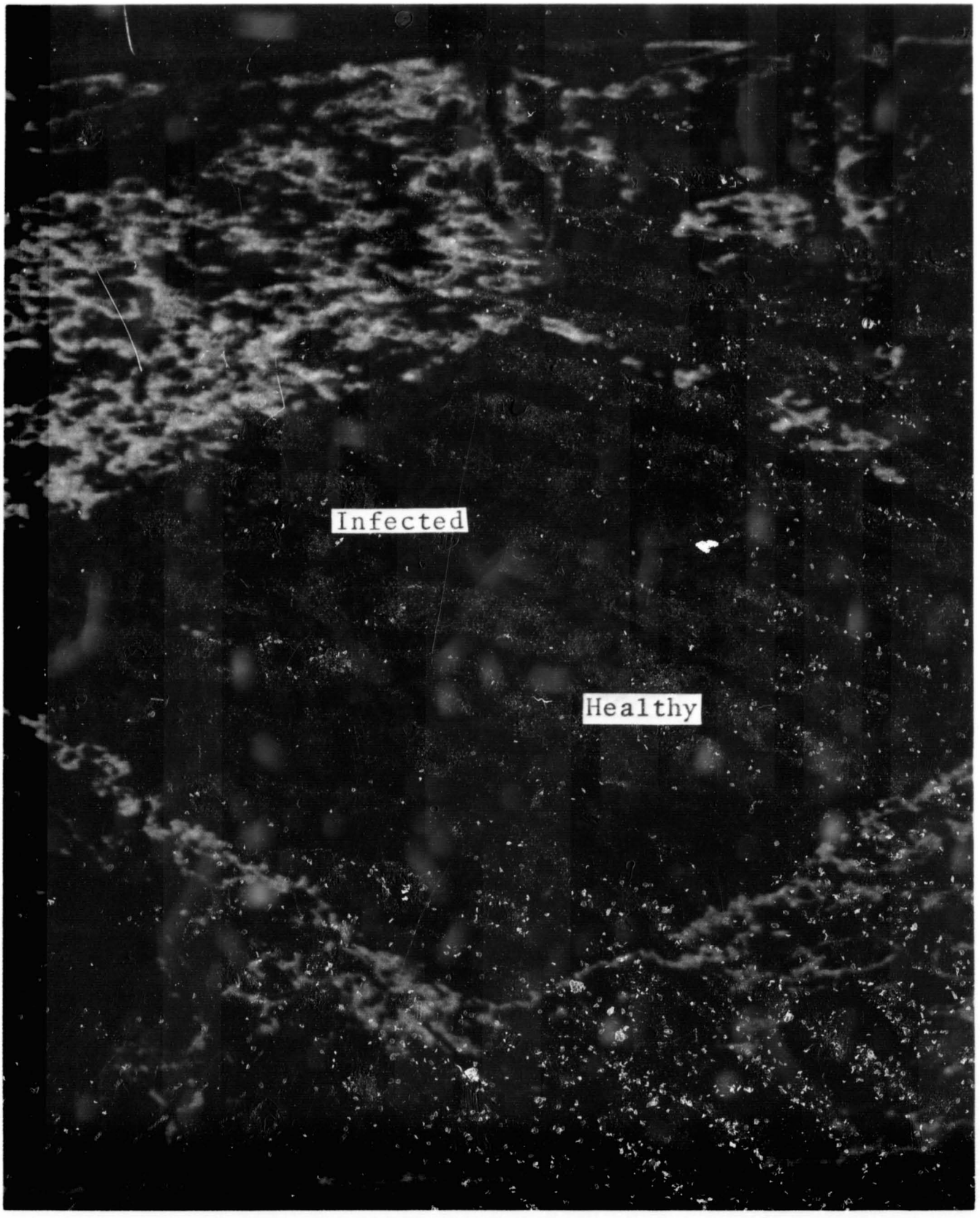

Figure 11. Density discrimination between healthy and infected grass. (Ratio of green density to red density)

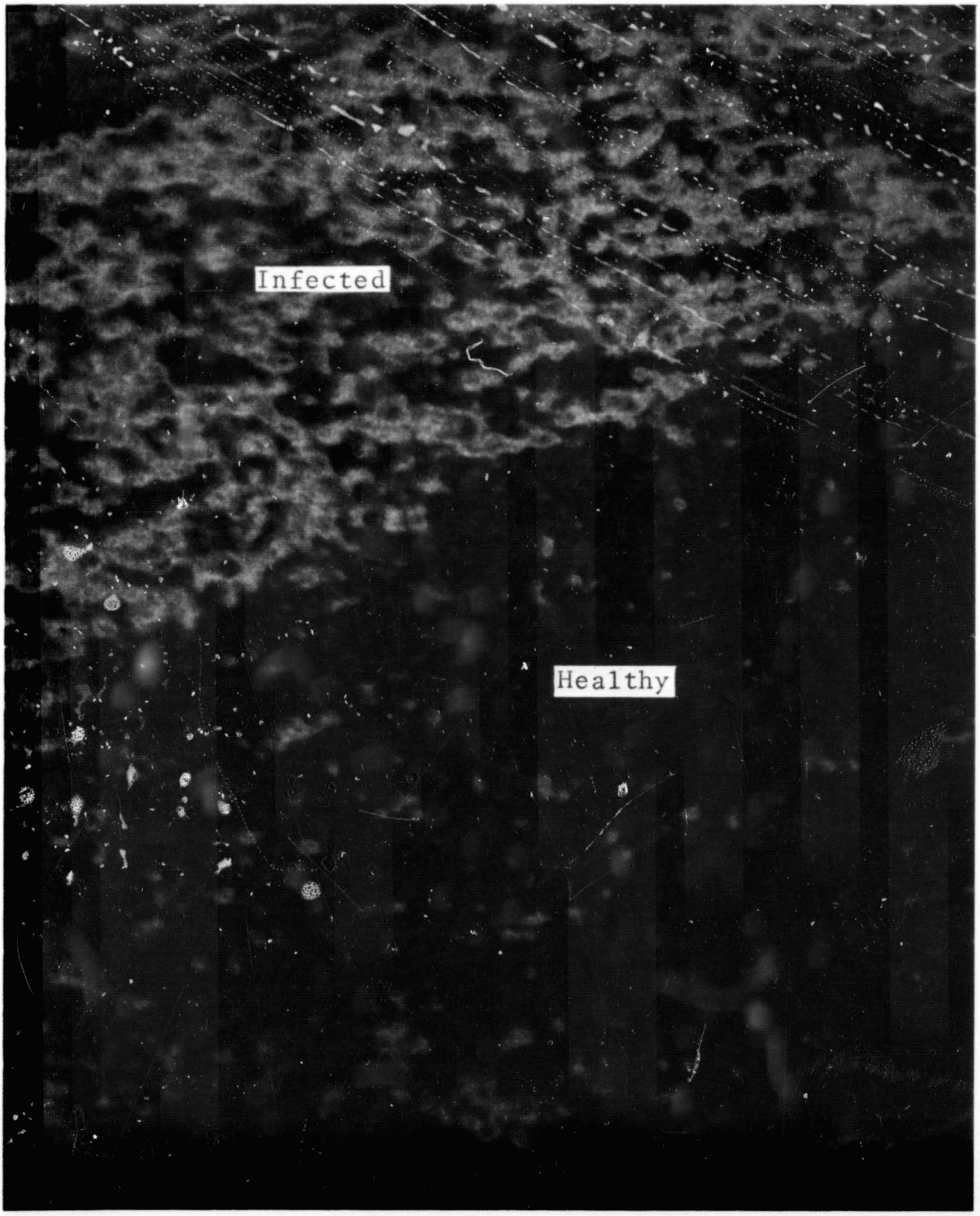

Figure 12. Density discrimination between healthy and infected grass (ratio of green density to blue density) (concluded).

SECTION 46

APPLICATION OF REMOTE SENSING TO WATER RESOURCES PROBLEMS

by

James L. Clapp
Remote Sensing Program
Institute for Environmental Studies
The University of Wisconsin
Madison, Wisconsin

INTRODUCTION

BACKGROUND

This paper is a report on research done under a NASA Grant to the University of Wisconsin for Multidisciplinary Research in Space Science and Engineering (NGL 50-002-127) during 1970-71. This research was focused upon the problem of developing remote sensing methods for the detection and monitoring of pollutants in water. It was specifically directed towards the investigation of the application of remote sensing to: (1) Water Quality Monitoring; (2) Detection of Mixing Zone; and (3) Surface Parameters of Large Water Bodies.

It was the intent of this program to achieve the most effective application of funds and personnel available for remote sensing research. This was accomplished by: (1) applying the major thrust of the research effort toward critical problems faced by State and Federal agencies charged with water quality planning and protection; (2) coordinating data acquisition operations on as broad a base as possible in order to make maximum use of the data acquired; (3) involving the appropriate State and Federal agencies with the research effort in order that existing ground truth could be utilized and that positive research results could be made operational in a minimum time; and (4) coordinating information and data dissemination in order that all investigators were kept abreast of developments in related areas.

RELATIONSHIP TO OTHER PROJECTS AND AGENCIES

Since environmental ground truth is so complex and remote sensing data acquisition is costly, it was imperative that related research efforts be coordinated in order to derive maximum benefits from funds

and personnel. Therefore, the work done under the remote sensing project funded by NASA's Office of University Affairs was coordinated with related environmental projects. This interdisciplinary approach proved most successful in all phases of the project.

Wisconsin Department of Natural Resources

The Wisconsin Department of Natural Resources is directly concerned with all three areas of interest covered in this investigation. In the case of the Mixing Zone Study, this agency has funded a portion of the research not directly concerned with remote sensing, the development of the mathematical model. In the case of the Water Quality Study, the Department of Natural Resources has cooperated in the definition of the problem and, within the limits imposed by it's own operational requirements, provided ground truth support as requested through the program leader by the principal investigator.

Marine Studies Center

The Marine Studies Center is funded by the National Science Foundation through the University of Wisconsin Sea Grant Program. The Surface Parameters of Large Water Bodies portion of this research was conducted in conjunction with this program. The NASA funds have been used to provide the remote sensing data acquisition and analysis while the Marine Studies Center funds and equipment were used to provide the required ground truth measurements.

National Center for Atmospheric Research

A portion of the aviation support for the Remote Sensing Program has been provided by the National Center for Atmospheric Research. They have provided overflight support in the thermal and photographic region.

International Biological Program

The Lake Wingra Study, as part of the International Biological Program, funded by the National Science Foundation, has as its goal the development of a computer simulation model for complex lake basin ecosystems. As such, a great quantity of ground truth is generated by conventional ground based measurements. The acquisition of the ground truth information was primarily funded by the Lake Wingra Program. NASA funds were used to supplement these measurements, obtain the required remote sensing data, and provided for the analysis of the remote sensing data as they applied to lake ecosystem modeling.

Institute for Environmental Studies

In January of 1970 the Institute for Environmental Studies (IES) was administratively restructured and staffed to provide improved leadership and impetus to the University of Wisconsin's research and teaching efforts in the environmental studies area. IES provides leadership in interdisciplinary environmental research by initiating new and coordinating existing research programs. Thus, IES has provided the administrative organization for the Remote Sensing Program.

The multidisciplinary nature of the Remote Sensing Program can easily be ascertained from the preceding organizational overview. The complex nature of environmental ground truth and the high cost of acquiring and analyzing remote sensing data require that a coordinated interdisciplinary effort be made to insure that each data gathering flight and supporting ground truth acquisition be utilized to the fullest. Furthermore, inasmuch as information gained in one portion of the research is likely to have significant influence upon other efforts, a coordinated organization is essential. Principal investigators from each sub-project are represented on the remote sensing steering committee which serves as the coordination and information distribution element of the program. At the present time the Remote Sensing Program employs some fifteen faculty members and approximately forty students from twelve different departments and/or programs.

WATER RESOURCES PROBLEMS

Because remote sensing techniques offer the capability of covering large areas in a real time scale they can be applied directly to the characterization and monitoring of environmental pollutants -- especially those entering a body of water. Although all water related remote sensing research carried on at the University of Wisconsin can be classified under the heading of applications of remote sensing to "water resource problems" the direction of each individual research project can be best delineated if they are explained separately.

WATER QUALITY RESEARCH*

During the period 1965-1967, Remote Sensing research at the University

*Dr. James P. Scherz, Principal Investigator, Department of Civil and Environmental Engineering and Institute of Environmental Studies.

of Wisconsin in conjunction with the State Department of Natural Resources concluded that reflectance characteristics of water are caused by suspended particulate matter and that these characteristics vary, depending upon the effluent and the receiving water. Work done at Wisconsin under the NASA Multidisciplinary Grant, during the period 1967-1971, concluded that the reflectance characteristics of a pollutant can be positively correlated to suspended solids and that theoretically the solids content can be determined by Remote Sensing technology. Since the solids content and other water quality parameters are at times positively correlated, it may be possible to determine pollutant load in general from the concentrations of solids -- provided the characteristics of an effluent from a particular plant are known.

The present research work and that conducted during the summer and fall of 1971 is directed towards the establishment of a statistical correlation between remote sensing responses and actual water conditions. From the use of spectrophotometers and ground sampling in conjunction with aerial photography, it has been established that in the photographic part of the energy spectrum, the remote sensing response is primarily correlated with the solids in the water (see Figure 1). There is an important depth penetration consideration that must also be considered in that different wavelengths of energy penetrate to different depths into the water. The research work during the summer of 1971 dealt with: (a) establishing a reliable correlation between remote sensing images (reflectance) and the concentration of solids in outfalls from several industrial plants on the Wisconsin River (see Figure 2), and (b) investigating the depth penetration characteristics of color and color infrared film in relation to lakes, rivers, and industrial pollution outfalls. The results of the above research should bridge the gap between aerial remote sensing images and the actual ground conditions on matters relating to water quality; or in other words, the results should determine what is being sensed on the remote sensing images in regard to water quality.

Suspended Solids

The amount of reflectance is directly correlated with the amount of suspended solids but it has been concluded that the laboratory analysis of such wastes at best leaves much to be desired because of the bottom reflection effects of the laboratory sample tube. Actual correlation of suspended solids with images on aerial photographs must be made in the field rather than in the lab, and proper allowance must also be made for bottom effects.

Bottom Effects

There is always some reflectance coming from the bottom of the

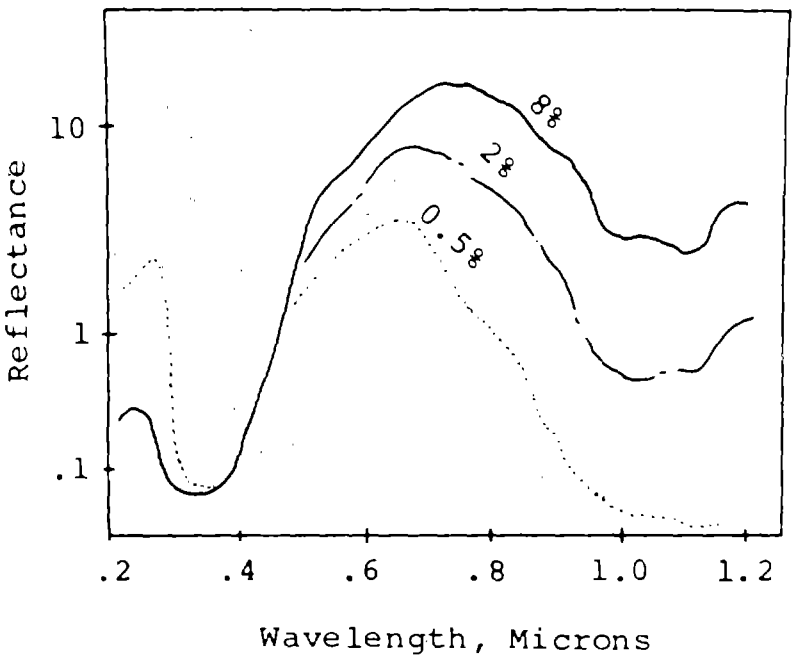

Figure 1.- Change in reflectance of sulfite liquor from Nekoosa, Wisconsin, as a function of concentration of solids.

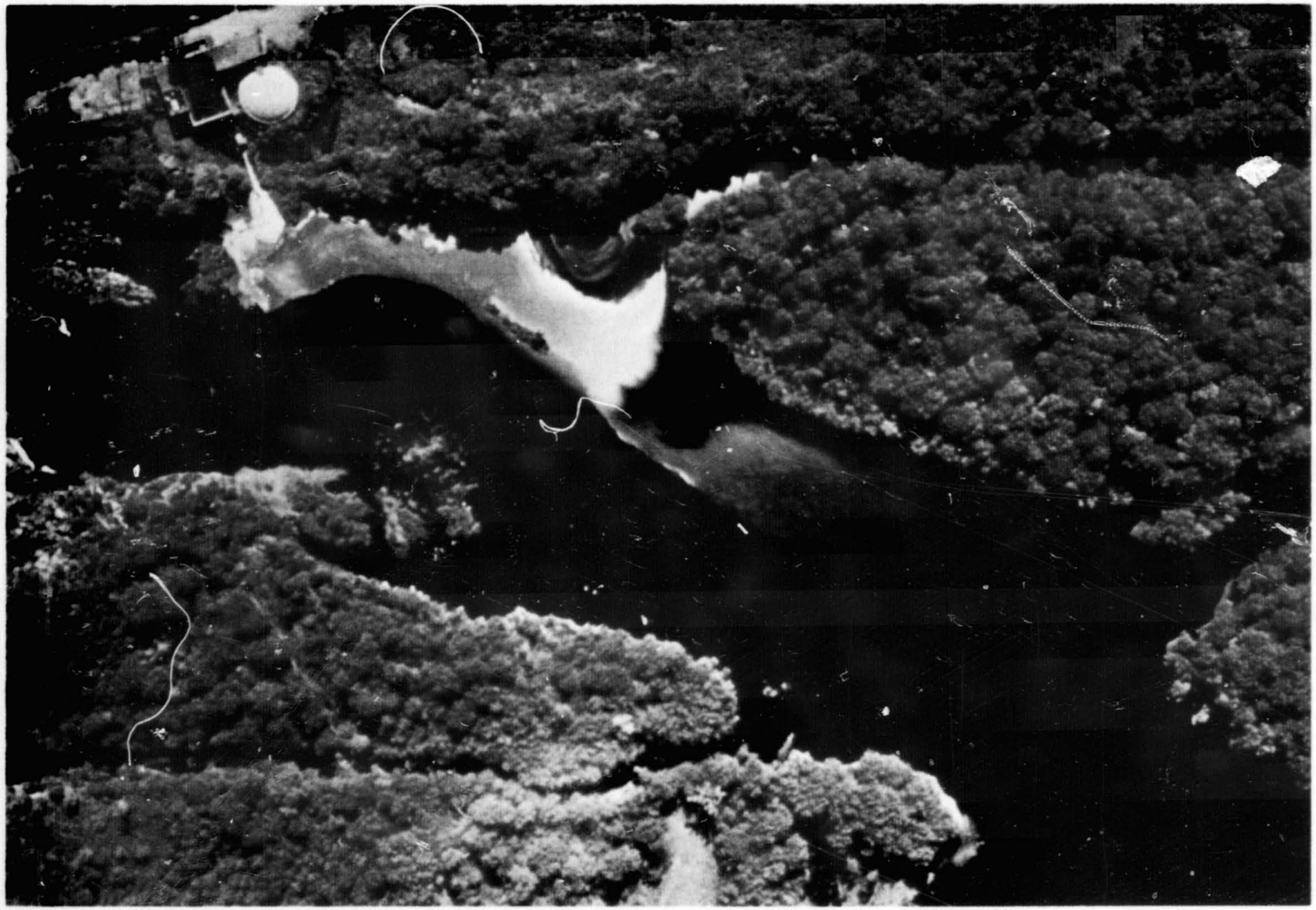

Figure 2.- IR Aerial photograph of paper mill waste entering Wisconsin River near Mosinee, Wisconsin.

sample tube that can make it impossible to exactly extrapolate the laboratory data to predict what will show up on the image without taking into account the bottom effects of both the sample tube and the water site itself. Not enough is now known about these bottom effects to accurately make the correlation between laboratory and the field. Additional work must be done hand in hand between field investigators and laboratory researchers in order to understand these bottom effects and how to deal with them.

Results to date however have shown that one can cancel out the bottom effects by picking the correct part of the spectrum either with filters before taking the photo or by proper choice of wavelengths when working with the microdensitometer-spectrophotometer apparatus during analysis of the color and color IR film. To date it can be concluded that the UV wavelengths reflect only from the surface of the water without penetration and that the IR is absorbed by the water and shows no depth effects and that the blue-green wavelengths penetrate and show the unwanted bottom effects. It appears that by selecting the proper wavelengths one can handle the bottom effect problem and that an understanding of bottom effects is absolutely necessary if one is to look at only the desired water being monitored.

1971 SUMMER RESEARCH

The summer efforts for 1971 consisted of massive correlation efforts between ground truth and simultaneous flights with color and color IR microfilm at four sites on twelve separate days. Ground sampling has been conducted for turbidity, solids, light penetration and color of the industrial waste. The samples have been analyzed at the Institute of Paper Chemistry at Appleton, Wisconsin, and at the Civil Engineering Sanitary Laboratory at the University of Wisconsin, Madison. Several Industrial and Municipal sewage sources on the Fox and Wisconsin Rivers have been photographed and sampled during the summer in order to obtain enough data to get a statistical correlation between the actual pollution and the remote sensing imagery. Primary emphasis was placed on correlation of suspended solids and the density of the image as obtained in relation to that of a standard styrafoam reflectance panel. Secondary emphasis was on seeing to what extent the suspended solids is a real measure of water pollution as indicated by conventional pollution parameters. Figure 3 indicates (in preliminary analysis at .610 microns) a definite correlation between the imagery and suspended solids. This would indicate, in fact, that the suspended solids can be determined from a photograph. Further analysis is in progress to determine the reliability and accuracy of this correlation.

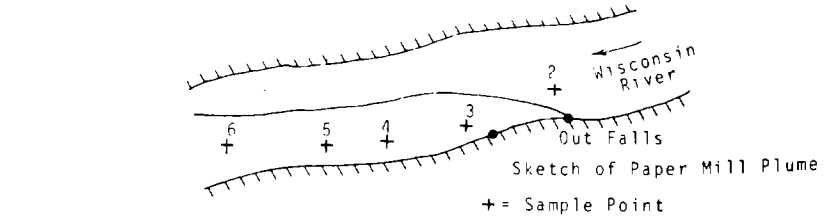

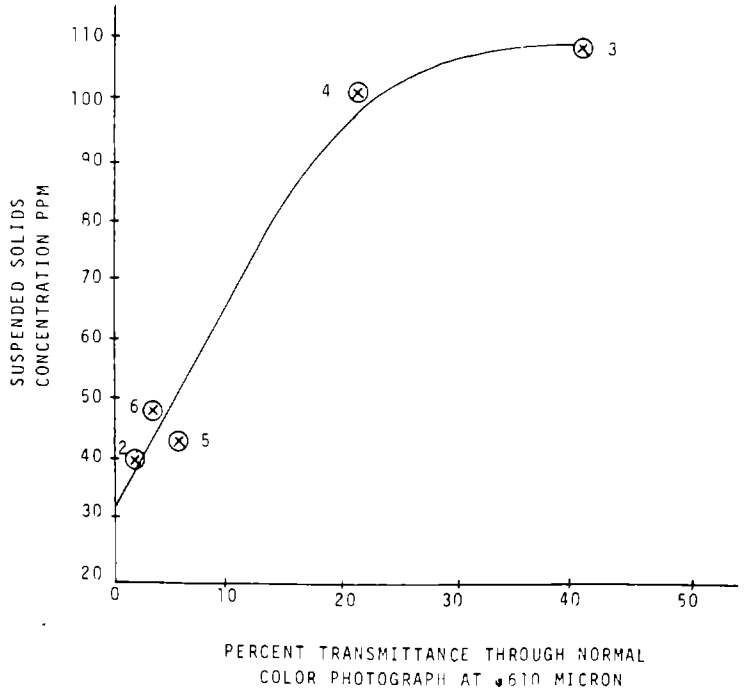

Figure 3.- Graph of suspended solids vs. percent transmittance showing correlation between imagery and suspended solids.

APPLICATION TO MIXING ZONE MONITORING*

The mixing zone is defined as that part of the water region in which pollutants, if they are introduced, are transported and dispersed to concentrations obtainable by total mixing. The mixing zone is a dynamic region, changing continuously in size and shape in response to effluent and water body conditions. The dilution process within the mixing zone is a two-stage process, as shown on the Schematic Diagram (Figure 4). The central objective of our project is the study of the mechanisms of transport and dilution in the mixing zone and the development of a relationship for the extent of the mixing zone as a function of effluent, outfall and water body characteristics. This relationship may be used: (1) in the establishment of definite and rational water quality guidelines; (2) in the development of a sampling and regulation program by governmental agencies; and (3) in the design and location of outfalls by industries and municipalities. In order to accomplish this goal, an integrated program of mathematical and laboratory modelling and field testing is being carried out.

The study now involves the correlation of physical characteristics of pollution as measured on the ground (suspended solids, total solids, dissolved solids, temperature and color) with remotely sensed measurements as reflectance (using film densitometer), emitted radiation (using a PRT-5) and thermal scanning. A related problem is the determination of a 3-dim. picture (basically vertical structure) from such (primarily) surface (2-dim.) indicators. If such correlations can be developed, it will be possible to use remote sensing techniques, together with the established ground techniques, for quantitative measurement of the temporal and spatial presence, character, and concentrations of pollutants in surface waters. In this way the ground and aerial work is complementary and thus permits more effective and accurate monitoring, discovery and characterization.

Field Research

Figure 5 is a graphic representation of the mixing zone characteristics at the Weston Power Plant near Rothschild on 26 August 1970. The high rate of flow on this date (1800 CFS) caused the plume to hug the shore for a long distance. Accompanying strong winds induced strong vertical mixing which in turn caused a slower lateral mixing. On this particular date a good correlation between the boundary of the mixing zone as determined by the aerial photographs and ground sampling is evident. Different flow conditions however may cause a variation in

*Drs. John A. Hoopes and James R. Villemonte, Co-Principal Investigators, Department of Civil and Environmental Engineering.

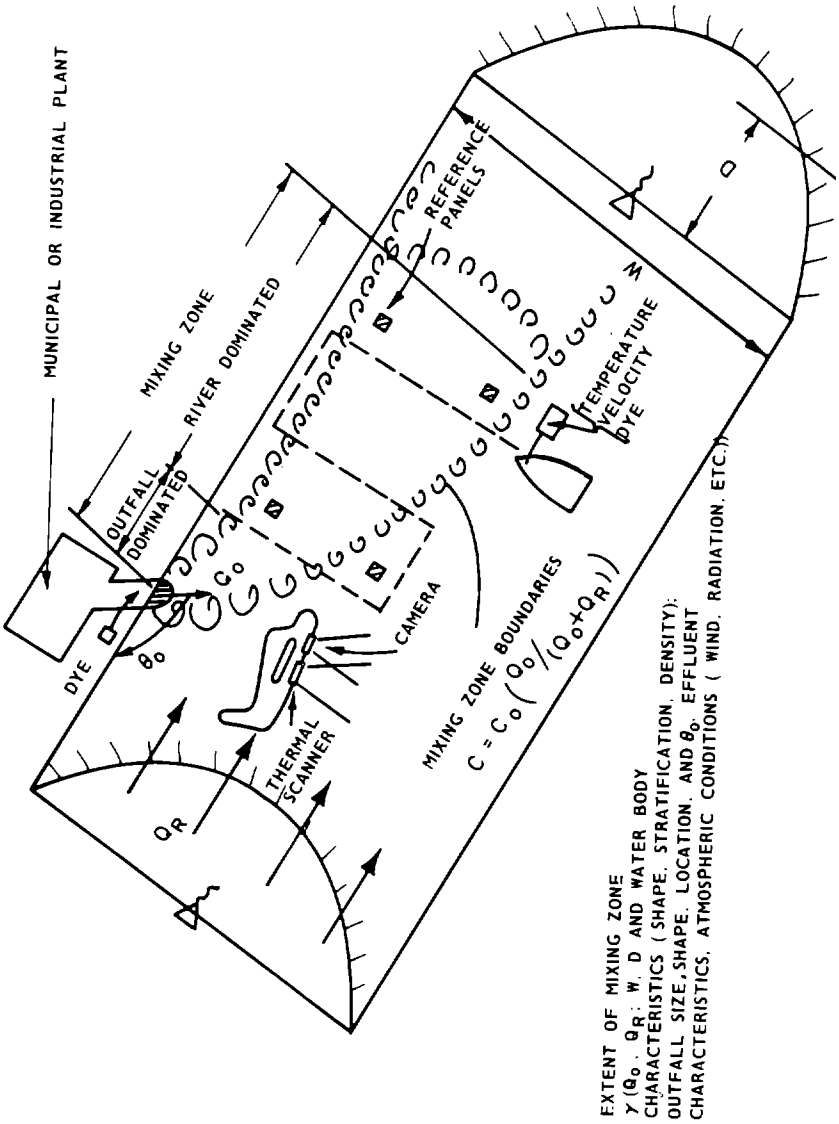

Figure 4.- Schematic diagram of mixing zone parameters.

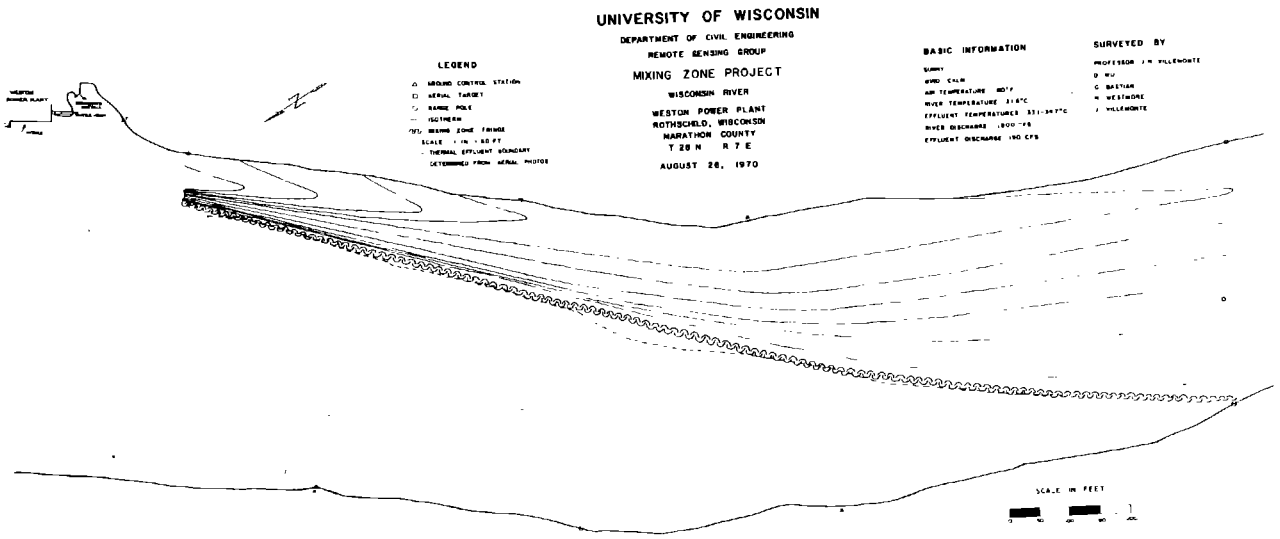

Figure 5.- Graphic representation of mixing zone characteristics of Weston power plant on 26 August 1970.

this correlation. Recent thermal imagery of this location has been linearized and processed for enhancing water temperature variations. Analysis of this imagery is currently in progress.

LEGAL ASPECTS OF WATER POLLUTION DETECTION THROUGH REMOTE SENSING*

One obvious domestic use for remote sensing devices is as an aid in water pollution detection. For the past two and a half years the University of Wisconsin's Remote Sensing Program of the Institute for Environmental Studies has been conducting research on the remote sensing of water pollution. As part of this study, aerial surveillance of a number of industrial firms heavily polluting Wisconsin's rivers has been undertaken, frequently supplemented with ground samples.

Standing alone, however, such efforts are largely self-contained. They do not lead to the abatement of pollution nor do they constitute proof, in a strict legal sense, of pollution. It was because of this aspect of the Remote Sensing Program that Professor Scherz of the Civil Engineering School suggested that remote sensing evidence be tested in a court of law.

Through the cooperation of the United States Attorney for the Western District of Wisconsin and the Department of Natural Resources remote sensing data was used in the spring of 1971 in an actual criminal case against a creamery polluting a major tributary of the Wisconsin River (United States vs. Wisconsin Dairies Cooperative, 71 Cr. 56, W.D. Wisc.; filed 14 April 1971). Since the case ended with a plea of nolo contendere, an admission of guilt for the purposes of the case, the data gathered was not actually used in court. Other cases, however, are currently being developed. It is expected that they will result in remote sensed data being used in a disputed case so that its reliability will be judicially established.

REFLECTANCE AND TRANSMITTANCE CHARACTERISTICS OF SELECTED GREEN AND BLUE-GREEN UNIALGAE*

The two-fold purpose of these sets of experiments was to evaluate

*Dr. Frank M. Tuerkheimer, Principal Investigator, Visiting Associate Professor of Law.

**Drs. William C. Boyle and Lorne C. Gramms, Co-Principal Investigators, Department of Civil and Environmental Engineering.

the feasibility of using the reflectance and transmittance characteristics of unialgae to differentiate between green and blue-green algae and to formulate eutrophication indices from the derived data. Two types of green algae, Selenastrum and Chlorella, and two types of blue-green algae, Microcystis and Anabaena, were evaluated in this study. The reflectance and transmission characteristics of these algae were recorded between .375 and .8 microns.

Experimental Design and Results

A two-level, four factor factorial design for each of the four algal cultures was performed. The dependent variables were transmittance and reflectance properties of the suspensions. Independent variables for each unialgal suspension included algal concentration, suspension depth, SiO_2 concentration, and the length of the experimental chamber.

The results of our experiments can be summarized by considering four general areas: (1) algal species differentiation, (2) algal concentration estimation, (3) effects of particulate interference, and (4) effects of phosphorous deficiency on the reflectance measurements.

Algal Species Differentiation Figure 6 shows the reflectance spectra of the four types of algae. As can be seen in the diagram, the green algae have a characteristic absorption at .650 microns, while the blue-green algae do not. From this we have been able to find a method of differentiating between the two types of algae by measuring the ratio of the reflected light at .650 microns to the intensity at .625 microns. We have been able to conclude that the ratio is greater than one for the blue-green and less than one for the green algae.

In order to assess the possibility of determining algal suspension concentrations using certain wavelengths or ratios of wavelengths, two of the algae, Selenastrum and Anabaena, were studied in detail at different algal concentrations.

Algal Concentration Estimation Figure 7 depicts curves of the reflectance spectra of the algal Selenastrum for four different concentrations. Investigations of the reflectances indicate that for Selenastrum the reflectance at .550 microns was approximately halved for each doubling of the concentration of the algae. The results for Anabaena showed a similar but not identical relationship.

Effects of Particulate Interference In order to study the effects of turbidity of the water on the reflectance spectra of these algal, an amount of fine sand was added to the experimental mixtures. The curves in Figure 8 represent the reflectance spectra of Anabaena at

different concentrations with and without the SiO_2 added. The results were somewhat discouraging. It was found that for low concentrations of the algal (4 mg/l) the reflected signal decreased with the addition of SiO_2, but the converse was found for the higher concentration. The reflected signal was greater with the addition of the SiO_2 for the 8 mg/l concentration of the Anabaena. Thus, the effect of turbidity could cause false reflectance measurements.

Even though the SiO_2 changed the reflectance and transmittance properties, it did not change the characteristic ratio of the intensities between the green and blue-green algal. Thus we can still qualitatively distinguish between the two types of algal independent of turbidity.

Effects of Phosphorous Deficiency The removal of phosphorous from the growth media had a pronounced effect on the spectral reflectance properties of the experimental algal cultures. The graphs in Figure 9 depict the results of this experiment. In general the limited phosphorous media resulted in increased intensity of the reflectance spectra.

AQUATIC MACROPHYTES AS EUTROPHICATION INDICATORS*

Aquatic macrophytes as well as algae can be used as eutrophication indicators. Eutrophication of the Madison area lakes is primarily due to the infusion of nutrients from many varied sources including agricultural runoff and storm sewer drainage.

Background

Lake Wingra, which is situated within the Madison city limits, is the site of several intensive ecosystem studies as part of the International Biological Program (IBP). The primary productivity of the aquatic macrophytes is one component of this systems study which is being analyzed by biomass sampling and net photosynthesis studies. The possibilities of using remote sensing techniques to save time and effort in the biomass studies are of particular interest to investigators in the remote sensing program and in the biological systems study. These possibilities are being examined at the present time by comparing the collected ground data and aerial photographs taken during the past summer. This joint effort has been fruitful in increasing the efficiency of future production estimates, in providing data not readily available from more traditional methods, and in providing for the ultimate modeling of this aquatic ecosystem.

*Dr. Michael S. Adams, Principal Investigator, Department of Botany.

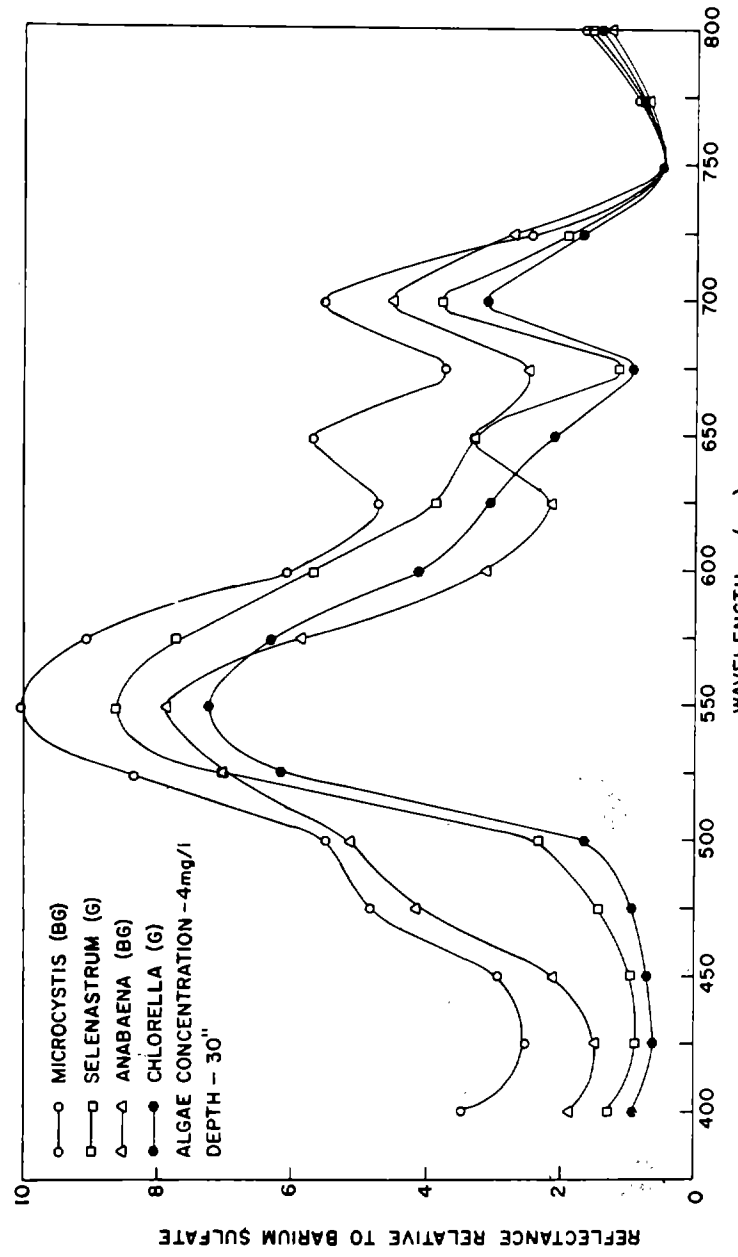

Figure 6.- Reflectance spectra of two green and two blue green algae.

C.8

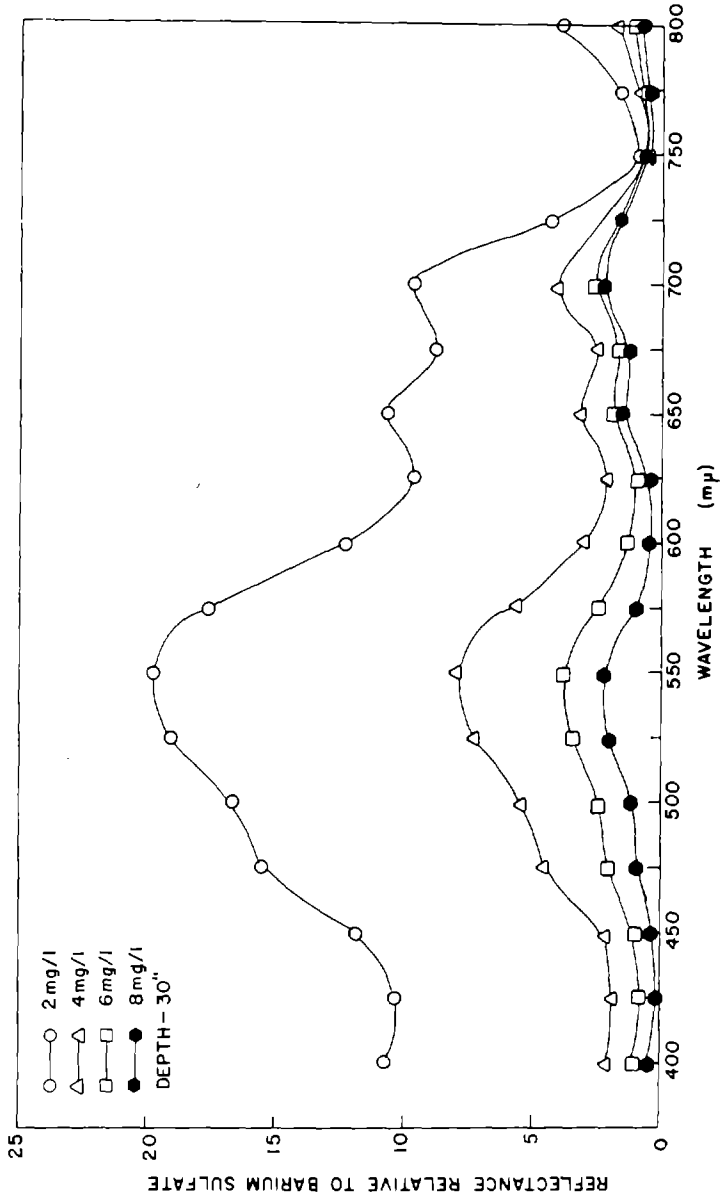

Figure 7.- Reflectance spectra of algal Selenastrum.

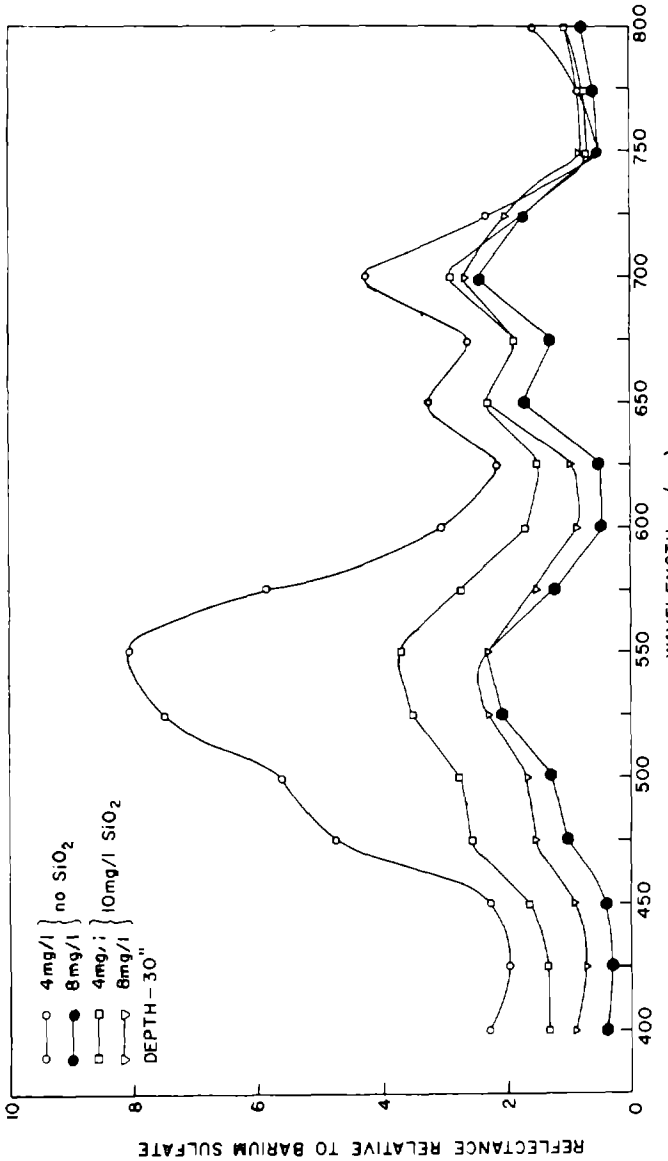

Figure 8.- Reflectance spectra of algal Anabena.

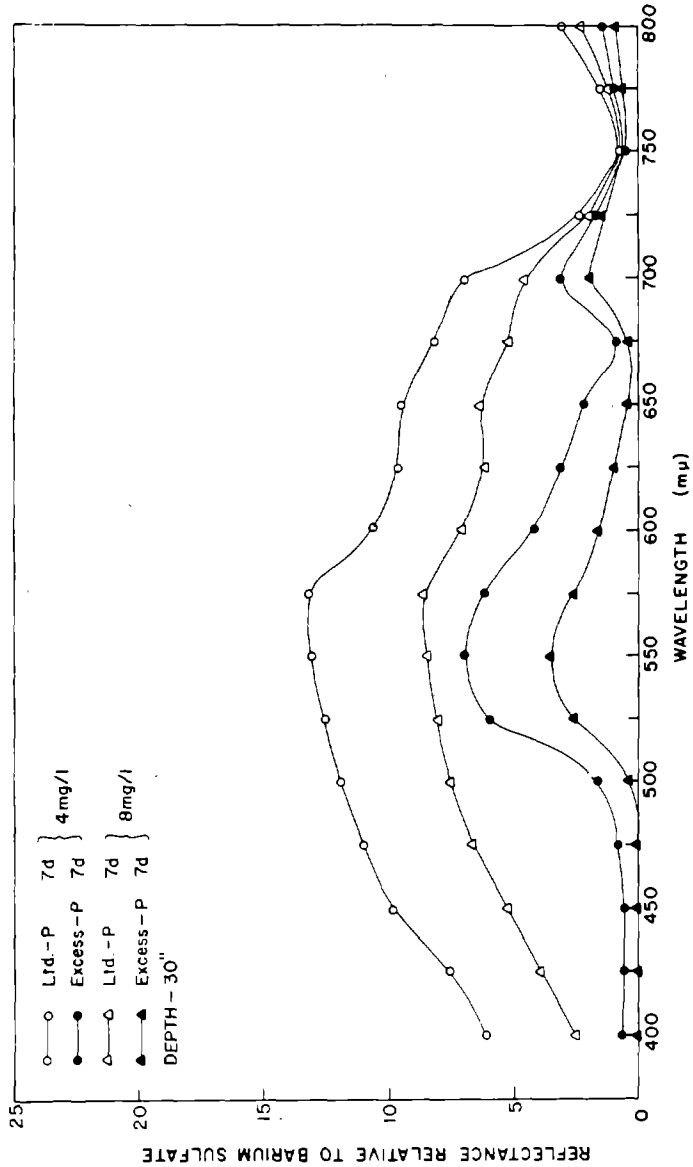

Figure 9.- Increased intensity of reflectance spectra in limited phosphorous media.

Figure 10.- IR Aerial photograph of west end of L. Wingra taken in August, 1971.

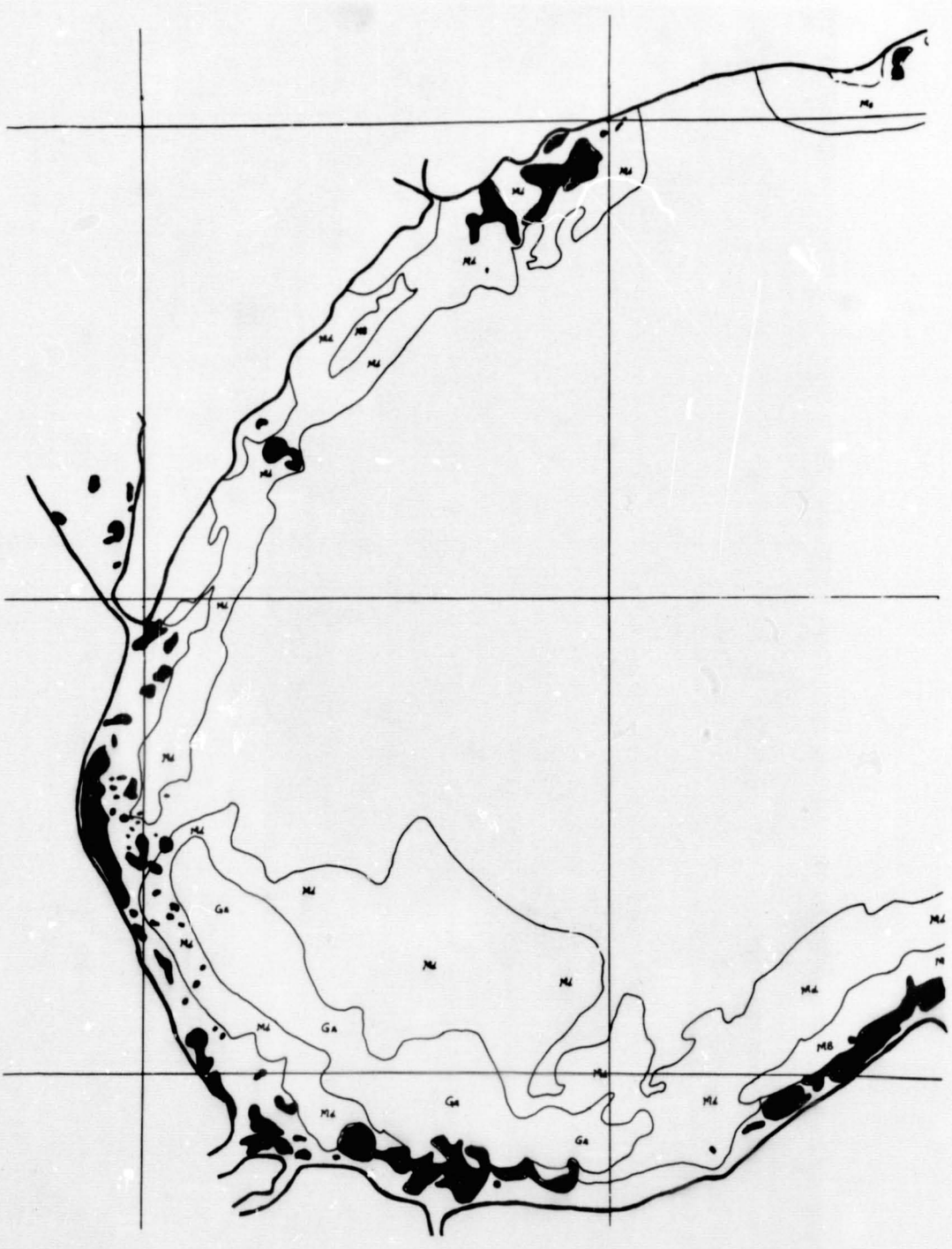

Figure 11.- Community map of a portion of west end of Lake Wingra. Md= myriophylum, GA= green algae overgrowth, MB= marl.

Applications of Remote Sensing

The color and infrared slides taken during the summer of 1971 have revealed several valuable uses for remote sensing of the lake and suggest further research. Color IR photographs are valuable in determining the physiological state of aquatic plants. The encrustment of plant leaves with carbonates, the senescense of plant tissue and the life cycle stages are easily discernible.

The appearance of the Myriophyllum spicatum L. communities is very pronounced in the aerial photographs. Figure 10 is a color IR aerial photo of the west end of Lake Wingra taken in August of 1971. With the aid of vertical photographs taken this season, the various communities have been mapped. A portion of the August map showing Myriophyllum and water lily communities with mat of green algae is shown as Figure 11. Information from the analysis of these maps can be used to make biomass and productivity estimates when used in conjunction with other biological data. The aerial photographs will also be correlated with the annual cycle of plant growth and community development. The infrared film is particularly effective in differentiating the marl bottom from vegetation. Marl is calcium carbonate which is precipitated out in hard water lakes. In regular color film the marl appears green but appears white in color infrared, thereby distinguishing it from vegetation. During the growing season the Myriophyllum becomes progressively encrusted with diatoms as well as calcium carbonate. In the infrared photographs the weed beds appear lighter due to this, and thus the accumulations can be monitored. Thermal imagery shows some application to the macrophyte study and is currently undergoing analysis.

The major effort of this past summer has been to correlate the biomass measurements taken last year with the vertical photographs, using both mapping techniques and intensive ground sampling. Remote sensing techniques are definitely applicable to the study of aquatic macrophytes and future work will be undertaken to further correlate imagery data with lake eutrophic state.

SURFACE PARAMETERS OF LARGE BODIES OF WATER*

The application of Remote Sensing to the measurement of the Surface Parameters of large water bodies is a multidisciplinary effort supported by the National Aeronautics and Space Administration program and the University of Wisconsin Sea Grant Program in conjunction with the University of Wisconsin Marine Studies Center. During the past year the

*Drs. Theodore Green III and Robert A. Ragotzkie, Co-Principal Investigators, Marine Studies Center.

direction of this project has been toward data acquisition during the summer and preliminary analyses of this data during the past fall.

The two geographical areas studied this past year were the Southern Lake Superior coast along the Keweenaw Peninsula and the Western Coastal Zone of Lake Michigan with special emphasis placed upon a nuclear power plant near Manitowoc, Wisconsin (Figure 12). Thermal scanner data were acquired at 5 other power plants along the coast in conjunction with the Wisconsin Department of Natural Resources.

Lake Superior-Keweenaw Current Study

The Keweenaw Current is the dominant feature of the water circulation in Lake Superior. This current is analagous to the Gulf Stream in the Atlantic Ocean; although it varies considerably in strength, it is strongest in the latter part of July and early August. From this study we hope to generate a better understanding of the mixing processes of near shore currents in large bodies of water. This project provides a unique opportunity to develop methodology to study a major current of varying magnitude with an emphasis upon the coastal waters mixing into the lake. A thorough understanding of this mixing process is imperative for making reasoned decisions regarding the future location and design of waste product outfalls, including those of a thermal nature. To preserve the purity of our coastal waters, it is important that waste products dumped into lakes and oceans are speedily diluted to a safe concentration.

Experiment and Results.- In the past this current has been studied using airborne radiometric methods. In our experiments this past summer we have used a thermal line scanner to map the current temperature and extent, and photogrammetric techniques to precisely measure the surface velocity structure near Eagle Harbor, Michigan. Figure 13 is a graphic representation of these results. To measure the velocity, drift cards were distributed in the water in lines perpendicular to the coast. These were photographed from an aircraft using a precision aerial mapping camera approximately every 8 minutes for several hours. The measured photo coordinates were entered into a computer and the actual ground coordinates as a function of time were then calculated for the drift cards using photogrammetric modeling techniques. The velocity structure of the current was then calculated.

The simultaneous radiometric and thermal line scanning used to map temperature distributions and the extent of the Keweenaw Current provide a measurement of relevant small scale parameters which are not available by other means and are vital to the investigation of the dynamic structure of lake currents.

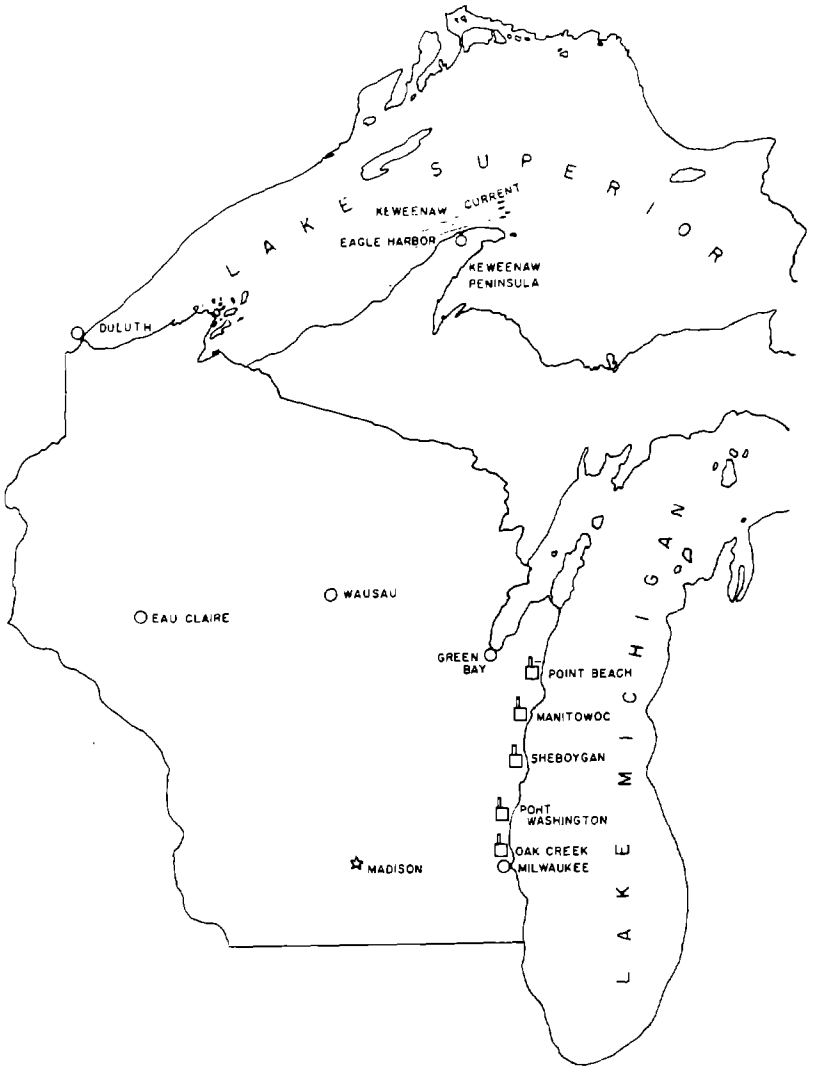

Figure 12.- Map of Wisconsin showing relative position of power plants.

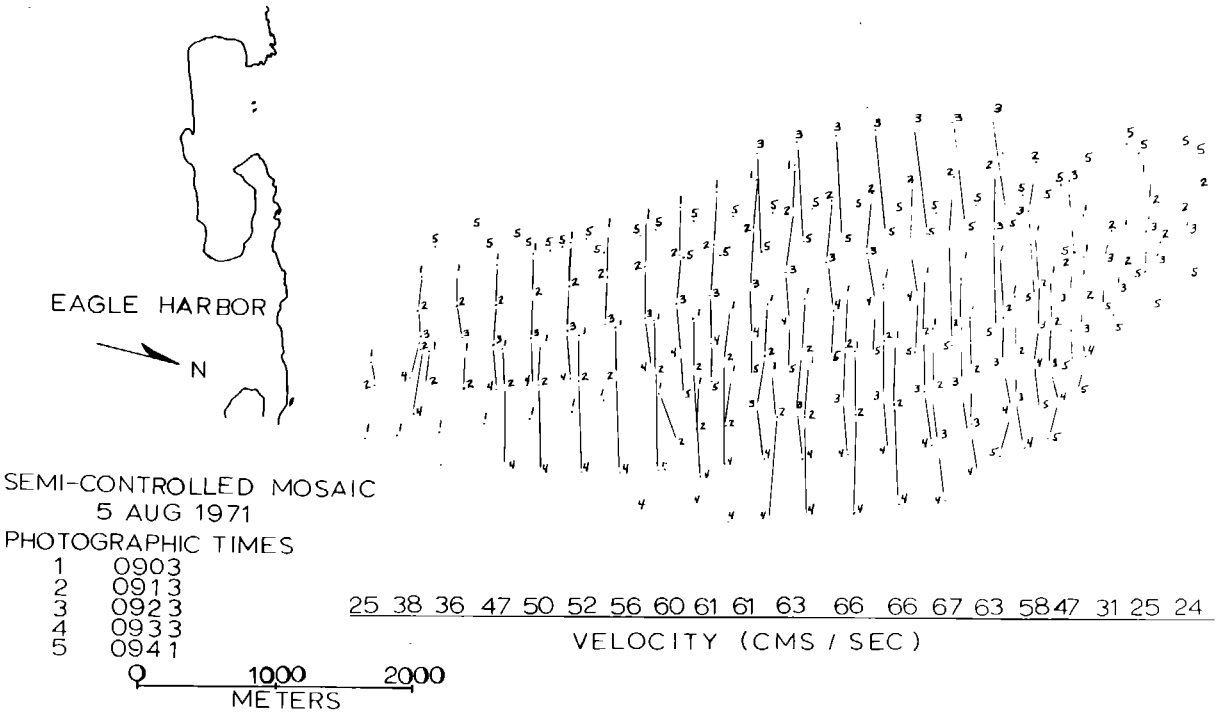

Figure 13.- Semi-controlled mosaic of current velocity structure off Eagle Harbor.

LAKE MICHIGAN COASTAL ZONE*

Thermal line scanner imagery of a portion of the Western Coastal zone of Lake Michigan was acquired in September 1971 on four consecutive days. We were mainly interested in the nearshore circulation and the surface details of the thermal discharges of power plants into the lake.

A prominent feature of the thermal imagery of the coastal zone is the relatively sharp demarcation between the cold nearshore water and the warmer offshore water (see Figure 14). From supporting color and color IR photography of the coast (flown by a NASA RB 57 at 60,000 feet), we suspect that there is not only a sharp thermal gradient but also a sharp discontinuity in the concentrations of suspended solids in the offshore waters as illustrated in Figure 15. Concurrent wind data suggest that these contrasts are due to upwelling, and that the scanner may be used to investigate coastal upwelling in lakes. Figure 16 depicts the thermal imagery of a portion of the coast for the three successive days. Further experiments are planned this spring and summer to closely monitor the changes in thermal structure. We plan to measure this coastal thermal structure every few hours to determine the time scale of the upwelling and its sensitivity to the wind speed and direction.

Thermal imagery of the power plant discharges along the western coast of Lake Michigan was obtained during the same experiment. Emphasis was placed on studying the Point Beach Nuclear Power Plant plume in detail. This plant is located on Lake Michigan approximately five miles north of Two Rivers, Wisconsin, and produces 500 megawatts of power while operating at half capacity. A total of 350,000 gallons of heated water is discharged each minute into the lake near shore. We attempted to measure both the thermal and velocity structures of this plume.

Using precise analytical photogrammetric techniques, the positions of many drogues at various times set for different depths were calculated. Figure 17 shows the results of analyzing one of the several experimental runs over this plume.

Figure 18 shows a thermal line scanner image of the Point Beach Power Plant thermal plume. To us, the most interesting features of this thermal picture are the thermal fronts moving concentrically outward from the outfall in a wave-like fashion. Since we have thermal pictures of the plume every five minutes, we can follow each of the fronts as it moves outward. From this (neglecting turbulent mixing) we may estimate the velocity structure of the plume.

---

*Drs. Theodore Green III, Robert A. Ragotzkie, and Paul R. Wolf, Co-Principal Investigators, Marine Studies Center and Dept. of Civil and Environmental Engineering.

Figure 14.- Print of thermal imagery showing sharp demarcation between cold nearshore and warmer offshore water on western coast of L. Michigan.

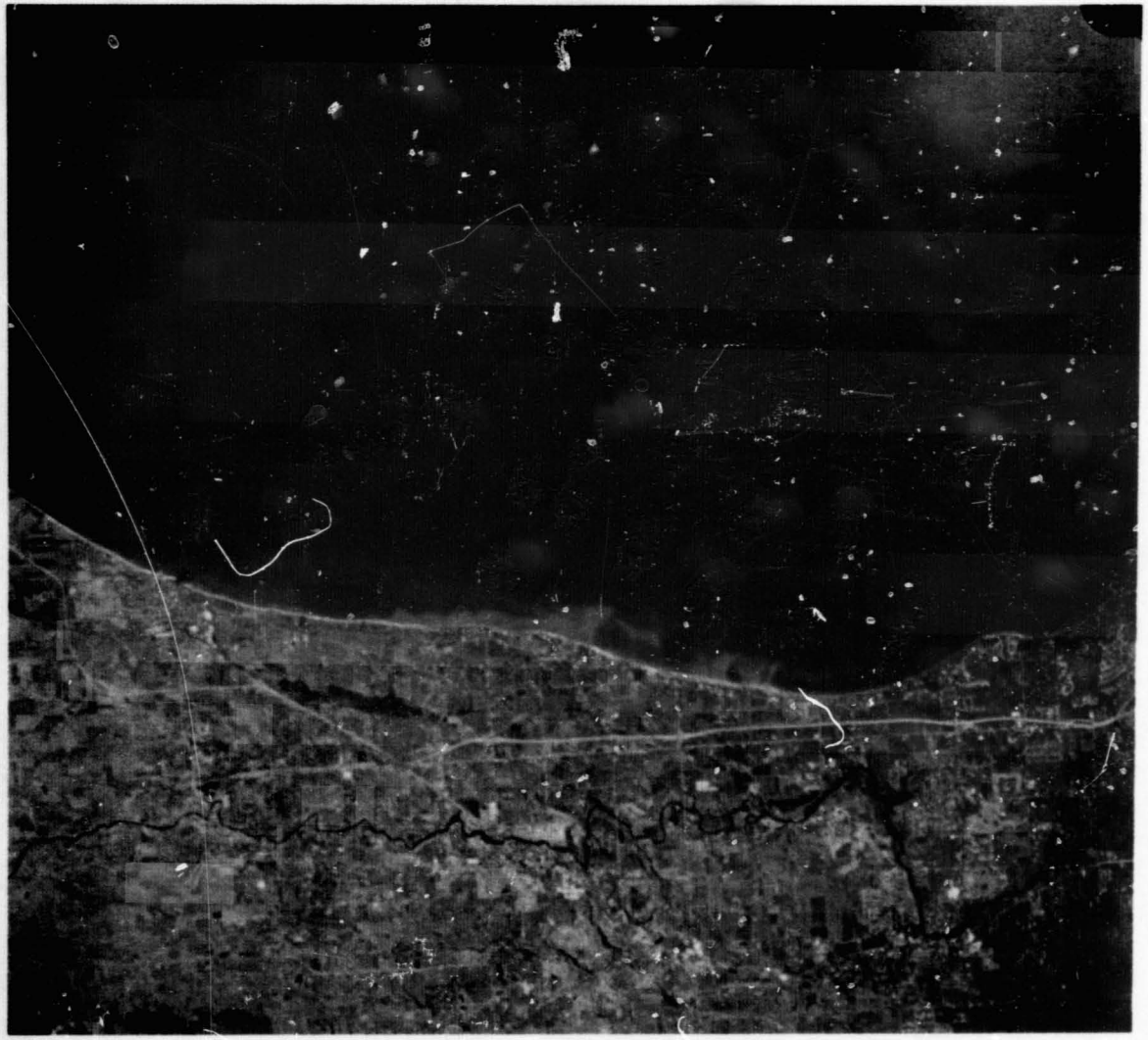

Figure 15.- High altitude photograph showing discontinuity in concentration of suspended solids.

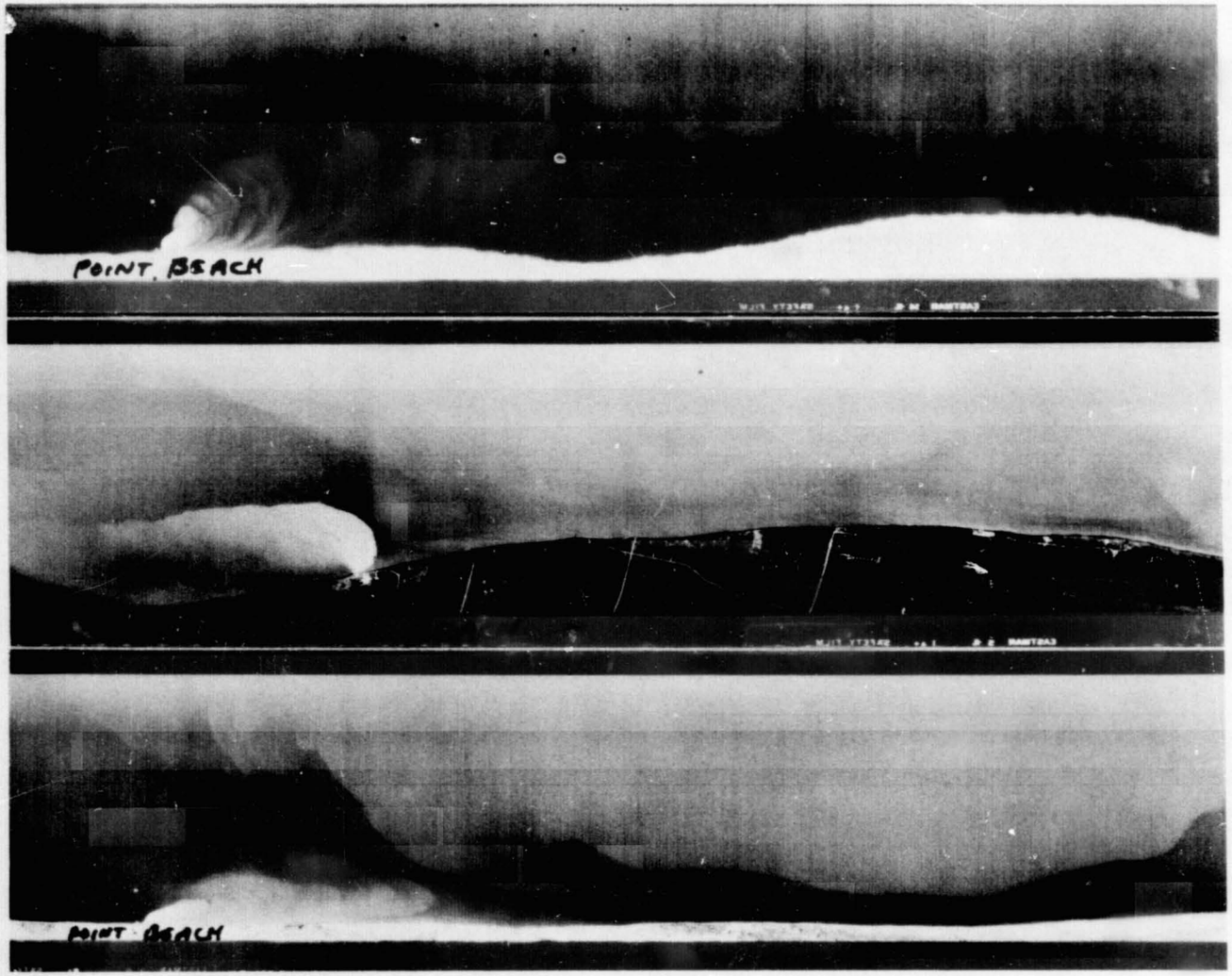

Figure 16.- Thermal imagery of Point Beach plume on three successive days.

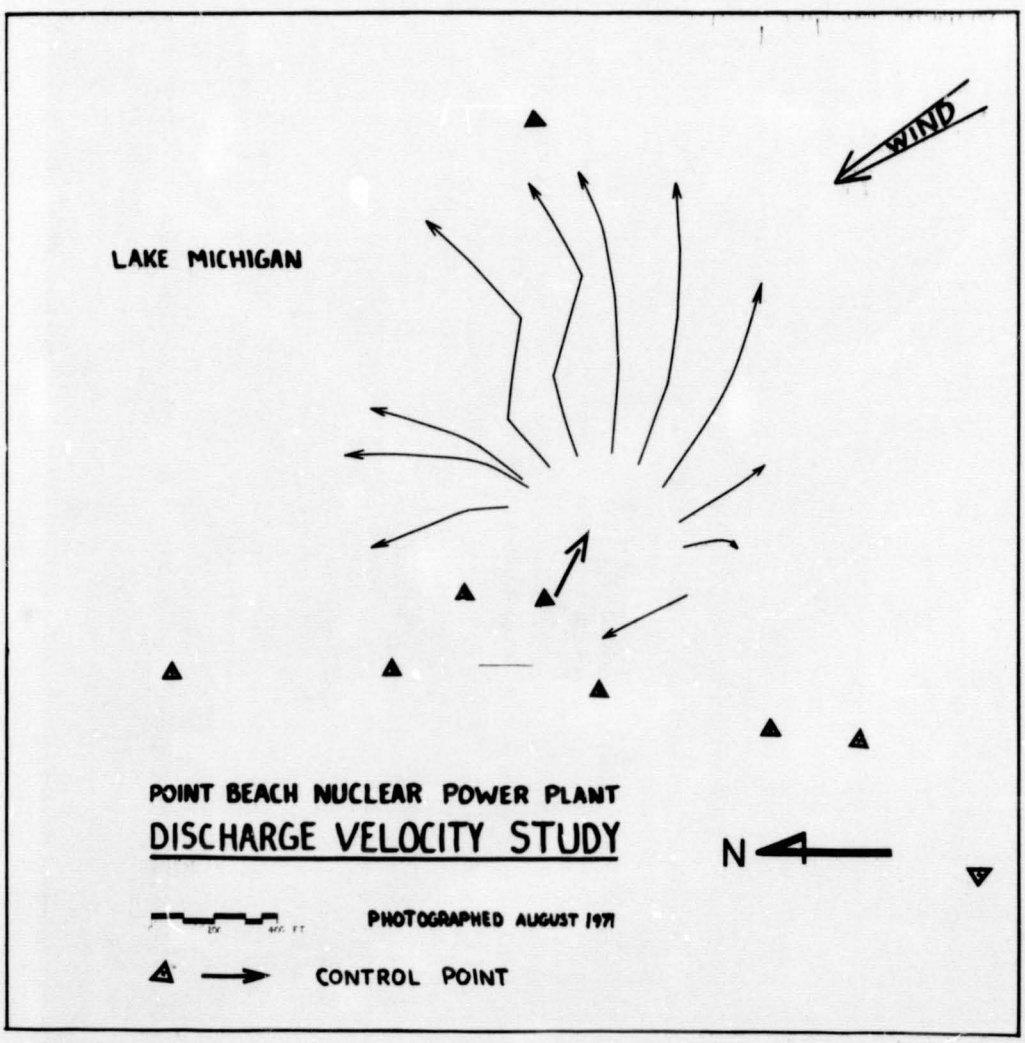

Figure 17.- Graphic representation of drogue positions over time.

Figure 18.- Thermal line scanner image of Point Beach nuclear power plant plume.

Figure 19 shows a schematic of the plume velocity structure. This is a preliminary analysis based upon tracings of successive thermal fronts from projections of the thermal imagery. Digitized information from this thermal imagery has been analyzed and Figure 20 illustrates the temperature contours of this plume at the same time as the velocity structure shown in Figure 19.

Figure 21 shows the same plume, but was flown at 5000 feet. Wave-like thermal fronts extend several miles south of the plant but are by no means unique to the Point Beach power plant. Figure 22 shows a similar structure at the power plant near Sheboygan, Wisconsin. We have reason to suspect that these thermal fronts are not just surface phenomena. Figure 23 depicts a recording of the temperature at a fixed point in the middle of the Point Beach plume at a depth of 6 feet. The periodic variation of 2 to 3°C may indicate the passage of a thermal front. Plans are now underway to erect a permanent platform in the plume with the capability of recording the temperature at many depths as well as the velocity of the current.

ADDITIONAL RELATED RESEARCH

APPLICATION OF REMOTE SENSING TO HYDROGEOLOGY*

In continuation of our research on the application of remote sensing in the evaluation of shallow ground water flow systems, two landfill sites in the city of Madison, Wisconsin, were overflown with a Daedalus thermal scanner and PRT-5 (8-14μ) at altitudes between 1600-1800 feet. Simultaneously with the thermal flights, ground truth information was gathered and the data obtained are now being correlated with the imagery obtained by the thermal sensor. An analysis is being made of such masking effects as: vegetation and color of soils; depth to the water table; topography; diurnal soil temperature variations; heat conduction originated by the decomposition of the refuse. Extensive ground water flow system evaluations, both physical and chemical, had already been accomplished at these two sites using conventional ground based techniques.

Our research so far has led to the conclusion that remote sensed thermal imagery (8-14μ) can be a valuable tool in rapid reconnaissance of ground water discharge into surface water bodies. In particular, the color separation processing of original analog data from magnetic tape corresponding to thermal levels has shown itself to be especially useful. Despite the abundance of masking effects, principally vegetation,

*Dr. David A. Stephenson, Principal Investigator, Associate Professor of Geology and Geophysics, Chairman - Water Resources Management Program.

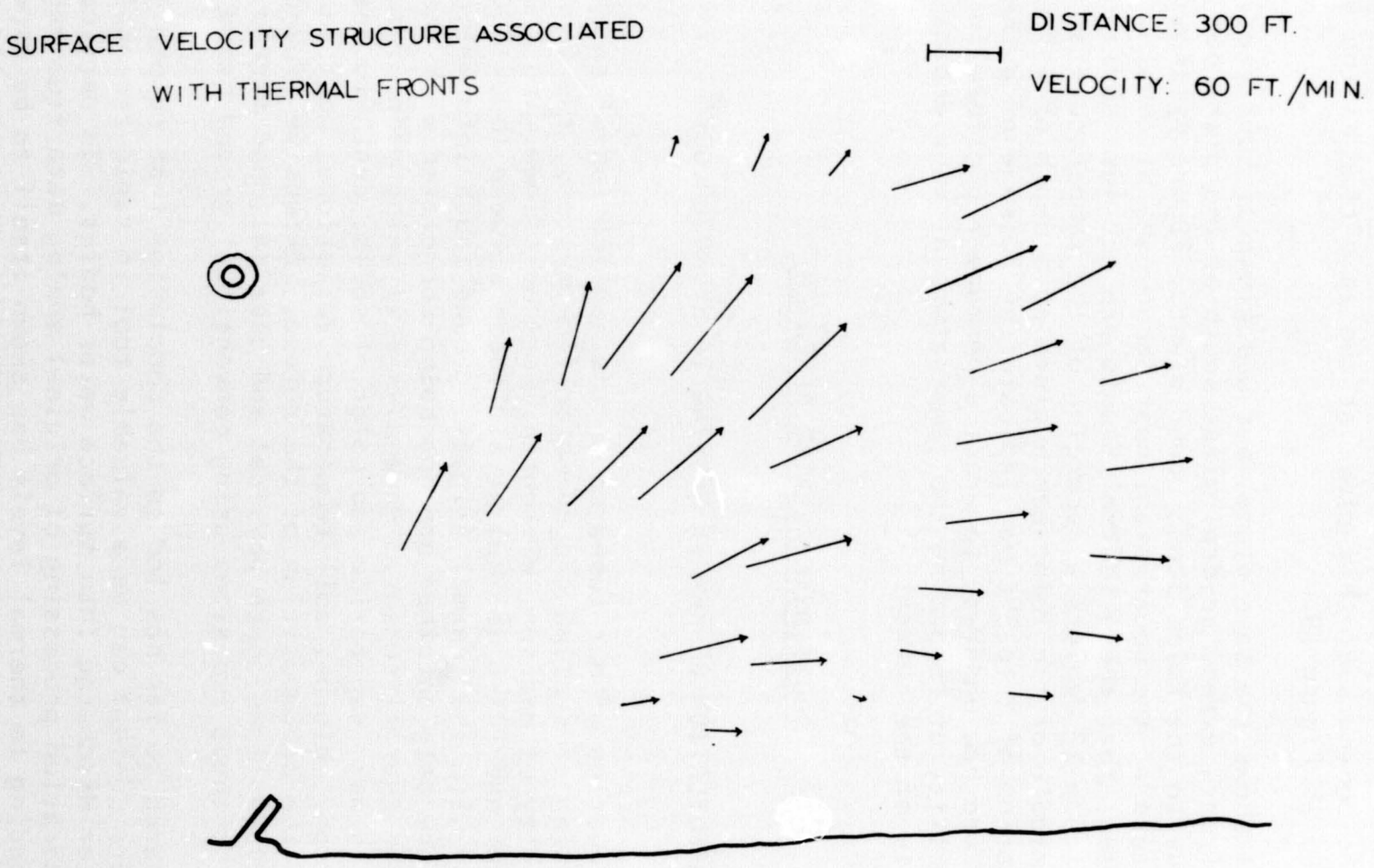

Figure 19.- Schematic diagram of Point Beach plume velocity structure.

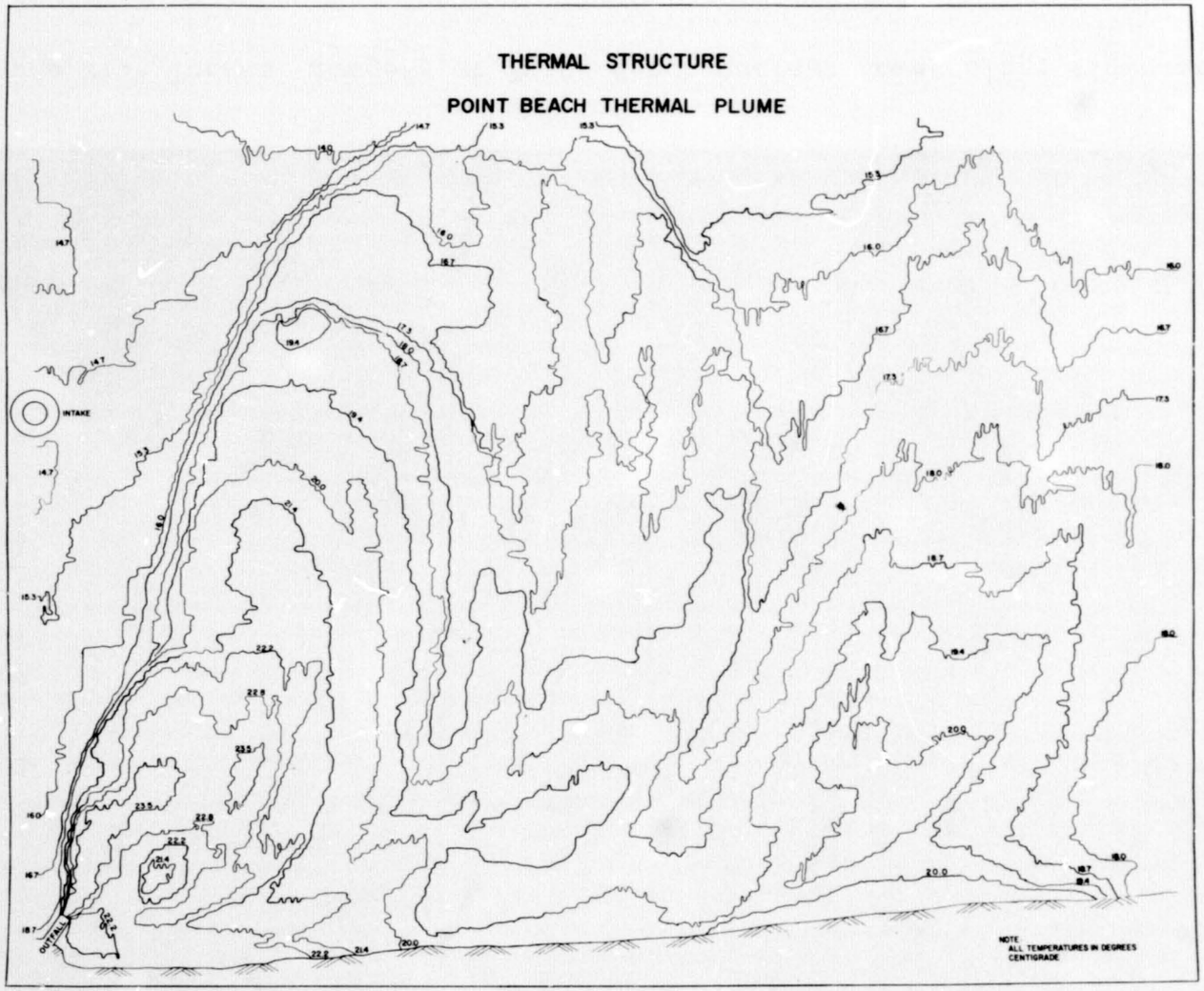

Figure 20.- Temperature contours simultaneous with velocity structure shown in Figure 19.

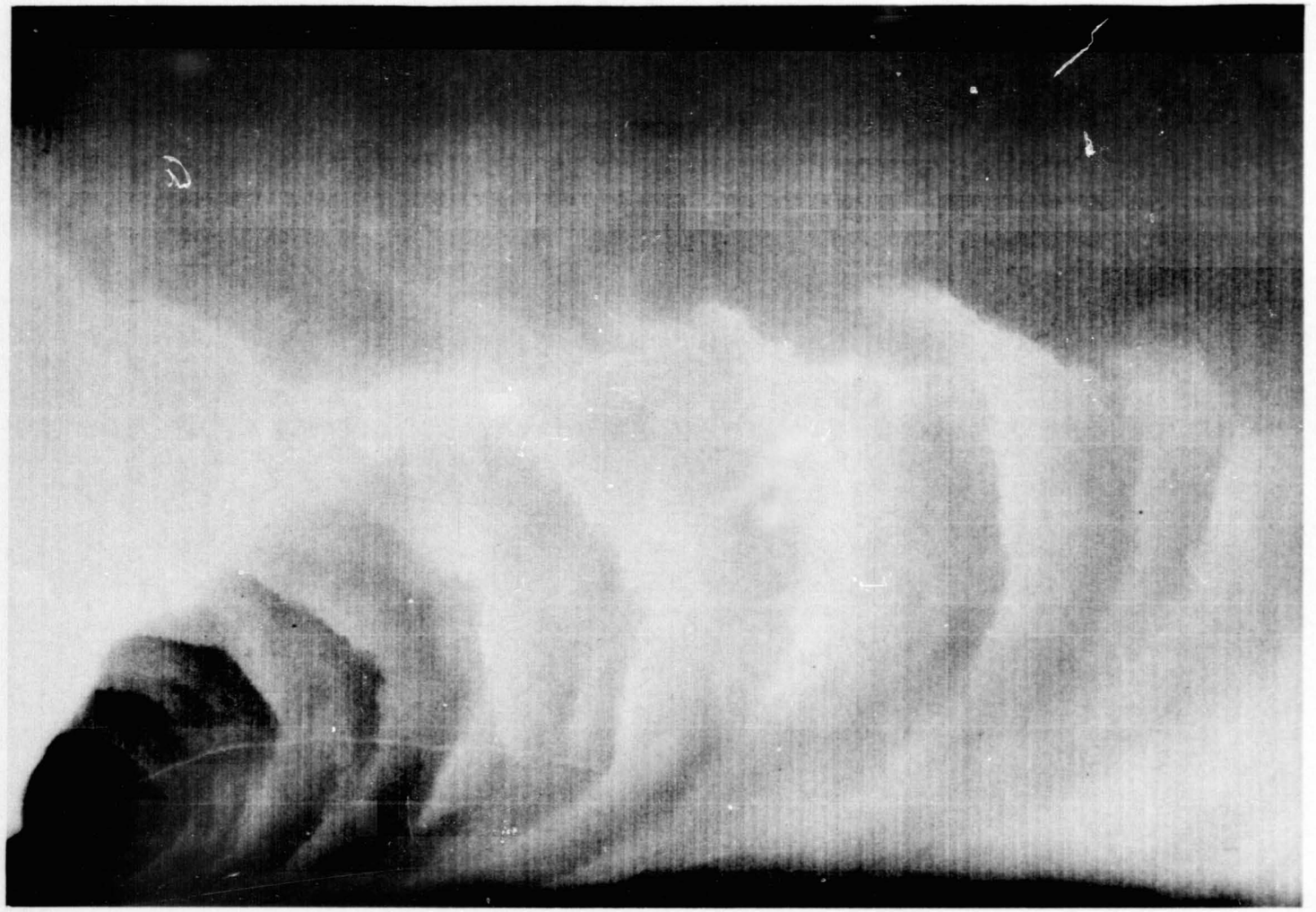

Figure 21.- Thermal imagery of Point Beach nuclear power plant flown at 5000 feet.

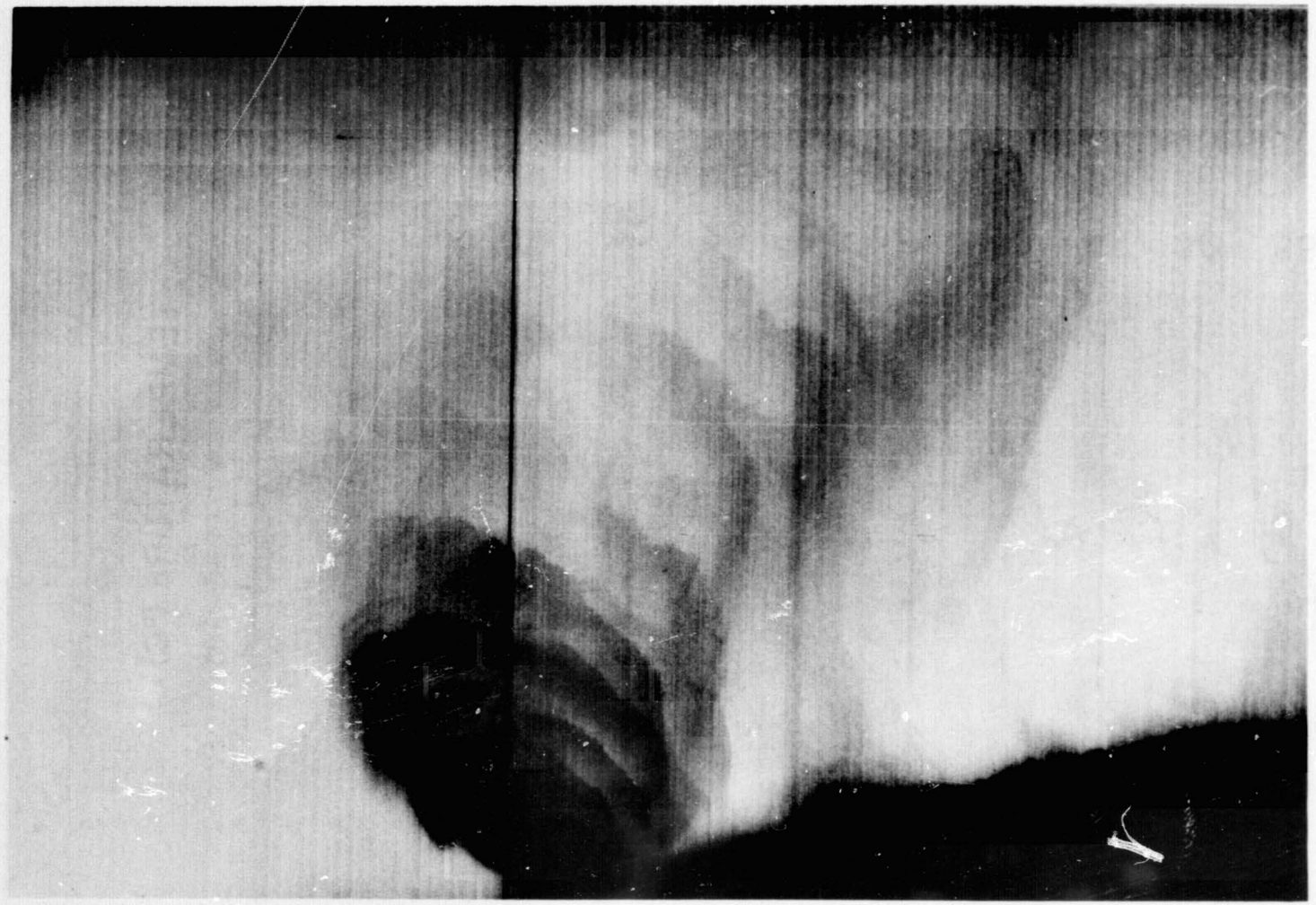

Figure 22.- Thermal imagery of power plant near Sheboygan, Wisconsin.

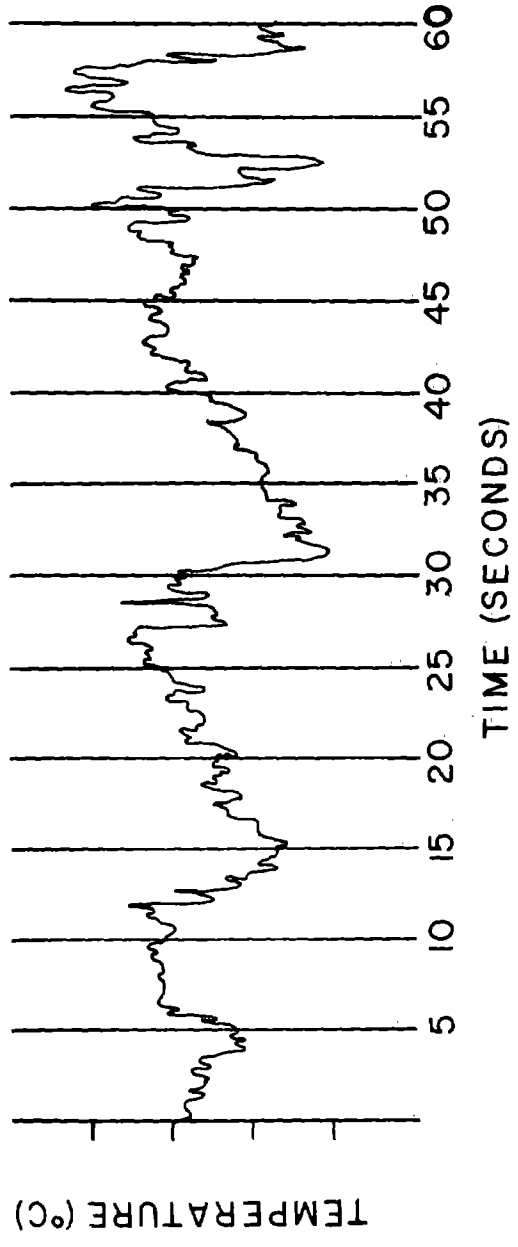

Figure 23.- Recording of temperature at a fixed point in middle of Point Beach plume at a depth of 6 feet.

springs discharging into Wingra Creek, which borders the Olin Avenue landfill site, were detected in the "color separated" imagery. The "normal black and white thermal image" fails to reveal to the naked eye these springs. They could only be detected with the time-consuming use of a scanning densitometer.

Whether thermal sensors (8-14μ) can help in locating ground water discharge zones will depend principally on the type or absence of vegetative cover, and on the time of the year. From the point of view of reducing the masking effects of vegetation, early spring, or whenever the spring thaw occurs, seems to be the best period of the year. The reduction in vegetative cover effects will probably compensate for the fact that the contrast between surface and ground water temperatures is smaller than in the summer or winter.

The possibility that the remote sensors investigated -- thermal IR, color and infrared color film -- can be used for the evaluation of different quality ground water discharges into surface water bodies is very small. In the two landfill sites studied, the water that infiltrates into the refuse and is later discharged into adjacent surface water bodies is too diluted to be detectable by present available remote sensors; in fact, it is even difficult to detect using conventional ground based instruments. The possibility that the water that infiltrates into the refuse becomes warmer and would therefore be detectable when discharged into a surface water body seems to be rather limited, since much of the heat conducted by the ground water along its "flow line" has probably been dissipated by the time it is discharged into a surface water body.

DETERMINATION OF OIL FILM THICKNESSES

USING REMOTE SENSING TECHNIQUES*

The purpose of the study was to determine the feasibility of measuring the depth of an oil slick by employing Remote Sensing techniques. A constraint imposed was: that the materials and equipment used be easily obtainable, inexpensive and fairly simple to use. Because of this constraint the photographic portion, 0.375 microns to 0.800 microns, of the electromagnetic spectrum was chosen for use in the study. A three camera bank was utilized so that simultaneous photographs could be made with the three film and filter combinations selected for study. Agfachrome CT-18, no filter; Kodak Ektachrome-X, exposed through a polarizing filter turned to maximum polarization; and

*Dr. James P. Scherz, Principal Investigator, Department of Civil and Environmental Engineering and Institute for Environmental Studies.

Kodak Infrared Aero Film, Type 8443, exposed through a #15 Wratten filter, were the combinations chosen.

Photographs were taken on a bright, clear day and on a cloudy, overcast day to see what affect these conditions would have on the final results and to also see if the procedure had an all weather capability. A hoop was floated on the surface of Lake Monona in Madison and filled with varying amounts of oil. Each successive depth of oil was then photographed using the three camera bank. The hoop was used as the reflectance standard against which reflectance values for the increasing depths of oil were compared. This gave a percent reflectance value which could be plotted against wavelength for each different depth of oil. The percent reflectance readings were obtained by analyzing the transparencies developed from the three films. The equipment utilized was a Gamma Scanning Microdensitometer Assembly Model 700-10-80 and a Gamma Scientific Model 2020 Spectrophotometer. It was hoped that a correlation between percent reflectance and oil depth could be found that would enable an interpreter to accurately estimate the depth of an oil slick.

Analysis of the transparencies obtained showed, that for the oil used, Mobil Oil, 20W, and accurate estimation of a slick's depth can be made. The two film and filter combination will enable an investigator to secure reliable results no matter what the sky conditions are at the site of the spill. Generally, on a bright day, Agfachrome CT-18 films, no filter, will prove the most useful for detecting and delineating the slick visually. Ektachrome-X film, exposed through a polarizing filter did not yield meaningful results. Kodak Infrared Aero Film, Type 8443, will provide the best correlation between reflectance readings and oil depths during the machine analysis of the transparencies. On a cloudy day, all three films will sharply delineate the extent of the spill visually. The infrared film will again be the best film for providing the correlation between percent reflectance and the depth of the oil spill during machine analysis. The agfachrome film can provide a check on the depth of thin oil films. The Ektachrome-X proved to be of little value.

USE OF REMOTE SENSING TO IDENTIFY HYDROLOGICALLY ACTIVE SOURCE AREAS*

Hydrology, by the most accepted definition, is a discipline dealing with the origin, properties, movement and distribution of water on and beneath the surface of the earth. Application of remote sensing tech-

*Dr. Dale D. Huff, Principal Investigator, Department of Civil and Environmental Engineering.

niques to hydrology should therefore be a process by which characteristics of objects connected with the origin, properties, movement and distribution of water on and beneath the surface of the earth are obtained without physically touching them.

A review of the available literature indicates that infrared photography and thermal imagery have been used fairly extensively in ground water explorations and water quality studies. At the present time, however, there has been little or no effort made to determine parameters of the hydrological cycle using remote sensing techniques.

In the recent past a new idea called the "source area concept" has been added to the study of runoff hydrology. Proposed by Hewlett in 1961 as a better way to interpret and explain storm and base flows from forested watersheds, this concept has now gained some headway through the efforts of many engineers and hydrologists in applying it to local situations. While outlining this concept as it is known today, this research is analyzing the possibility of using remote sensing techniques for locating such source areas.

Successful identification of these hydrologically "active" areas by means of remote sensing techniques will not only help in developing a more accurate "runoff generation model" but will also have numerous uses in the following fields of studies: (1) Water quality; (2) Water and land management; and (3) Erosion and soil conservation.

CONCLUSIONS

Based upon the results of the past years' research effort by the University of Wisconsin's Remote Sensing Program, the following conclusions were reached concerning the applications of remote sensing to water resources problems.

1. Remote sensing methods provide the most practical method of obtaining data for many water resources problems.
2. Effective use of remote sensing research funds can be achieved by cooperative efforts with other environmental research efforts and agencies.
3. The multi-disciplinary approach is essential to the effective application of remote sensing to water resource problems.
4. There is a correlation between the amount of suspended solids in an effluent discharged into a water body and reflected energy. However, bottom effects may mask the signal if not properly accounted for.
5. Remote sensing provides for more effective and accurate monitoring, discovery and characterization of the mixing zone of effluent discharged into a receiving water body.
6. It is possible to differentiate between blue and blue-green algae

by comparing the ratios of reflected light at 0.650 microns and 0.6250 microns.

7. The reflectance at 0.550 microns is approximately halved for each doubling of algae Selenastrum and Anabaena concentration. However, this effect is masked by turbidity.
8. Multiband photography provides for rapid mapping of aquatic macrophytes.
9. Simultaneous radiometric, photogrammetric, and thermal line scanning can be used to provide measurement of relevant parameters which are not available by other means and are vital to the investigation of the dynamic structure of lake currents.
10. The velocity structure of some thermal plumes may be obtained from sequential thermal imagery by tracing the propagation of thermal fronts in the plume.
11. It is unlikely that photography or thermal IR can be used to evaluate the quality of ground water discharges into surface water bodies.
12. Kodak Infrared Aero Film, Type 3443 can be used to obtain accurate estimates of oil slick depth for Mobil Oil, 20W.

SECTION 47

DIFFERENTIATING ELEMENTS OF THE SOIL-VEGETATION COMPLEX*

by

M.F. Baumgardner and Staff
Laboratory for Applications of Remote Sensing (LARS)
Purdue University
West Lafayette, Indiana

One of the most exciting prospects in the application of remote sensing technology is that of identifying, characterizing, measuring, and mapping different elements of the soil-vegetation complex. Important elements in this complex include soil properties, plant species, and the conditions of both soils and plants.

One of the problems in the use of remote sensing to study the soil-vegetation complex is the quantification and precise location of ground observation data such that it can be correlated with multispectral data acquired from aerospace platforms. A technique which has been found to be very effective in relating precisely these two sources of data involves the gridding and sampling of an area to be studied such that the exact location where soil or plant samples are obtained can be related precisely to a known address on a magnetic tape containing multispectral scanner data of the area. Once this has been accomplished, analytical data (ground observations) of each soil or plant sample from a specific grid point can be examined and related to quantitative multispectral data from an airborne scanner corresponding to the appropriate address or location on the magnetic tape.

For the past two years this approach has been used at Purdue University to determine if a correlation exists between the multispectral characteristics of a resolution element or scene and various physico-chemical parameters within the soil-vegetation complex of that scene. These techniques were used in a study of soils and crops in a 60-hectare field in Tippecanoe County, Indiana (Figure 1). This area known as Soil Test Area 6 (STA 6), is made up of soils formed under tall prairie grass vegetation. A comparison of the photograph (Figure 1a) with the soils map (Figure 1b) shows a close similarity of soils patterns.

---

*In this paper, results from a number of studies are summarized; researchers are identified in the Acknowledgment section.

One of the soil parameters that correlated well with spectral response was organic matter content. The correlation coefficient between organic matter content and multispectral response for data from approximately 200 grid points was 0.70. Grid points with known organic matter contents were used as the training set for computer-implemented analysis of the multispectral data and for the generation of a spectral map of four levels or organic matter content (Figure 2)

Although the correlations between multispectral response and both extractable soil phosphorus and exchangeable soil potassium were low, distinct soil or spectral patterns, representing different levels of soil P and soil K, were produced when analytical values from the grid points were used as training sets to produce computer-implemented maps of soil phosphorus and soil potassium (Figure 3).

In 1970 the northern third of STA 6 was planted in corn and the southern two thirds in soybeans. Corn and soybean leaf samples were obtained at specific grid points in August, 1970, the day on which multispectral data were obtained by the University of Michigan aircraft scanner. Grid points where plant nutrient (N,P,K) contents were known were used as the training sets for computer-implemented analysis and mapping of plant nitrogen, plant phosphorus, and plant potassium (Figure 4). Spectral data were used to produce maps delineating three levels of N for corn and three levels of N for soybeans (Figure 4A); three levels of P for corn and three levels of P for soybeans (Figure 4B); and three levels of K for corn and two for soybeans (Figure 4C).

Although statistical analysis did not produce a high correlation between spectral data and plant content of N, P, and K, definite spectral patterns were produced. Before valid conclusions can be drawn from an experiment with dynamic systems, such as plant nutritional status, the experiment must be conducted over a number of years and under a variety of geographical, climatic, and environmental conditions. Plant nutritional and spectral response studies are continuing at LARS.

If it becomes possible to use remote sensing to characterize crop conditions through the growing season, crop yield prediction capabilities may be improved. A preliminary yield study was conducted in STA 6. Yield samples were obtained at specific grid points. Spectral data relating to different yield levels at the grid points were used as the training set for computer-implemented analysis and production of the corn yield map (Figure 5A) and the soybean yield map (Figure 5B). These results are preliminary and were conducted in a very limited area. Such studies must be conducted through several growing seasons and under a variety of conditions before it can conclusively be stated that yields can be related to multispectral response.

These studies opened up a number of very interesting problems. One of these relates to the mechanism or technique of gridding. How is a precise grid point located in the scanner data? Is this important? In the first attempt to match the analytical ground data from the array of grid points with spectral data from an array of addresses on the magnetic tape, the geometric distortion inherent in the scanner was not considered. In a second correlation analysis, geometric corrections were made which gave a much more precise matching of ground data points and addresses on the magnetic tape. Great improvements were achieved in the correlation coefficient values, in one case an improvement in r^2 from 0.38 to 0.72 in a study of the correlation between soil organic matter content and spectral response.

Another important question which has been considered is: What is the best array of spectral channels (or wavelengths) for measuring or mapping a particular surface feature? In response to this question a study was conducted to determine the best portion of the reflective spectrum for delineating different levels of soil organic matter by remote sensing techniques. Multispectral scanner data obtained in May 1969 and May 1970 over three soil test areas (STA 4, 5 and 6) were used in this study. Each of the soil test areas was gridded, and organic matter content was determined for the surface soil sample taken at each of the 500 grid points. The best channel (or wavelength band) or best array of channels of spectral data for estimating organic matter content was selected by two computer programs. One method is based on the stepwise regression principle; the other is a LARS- developed program for channel selection based on divergence (1). Data from thirteen spectral channels in the visible and reflective infrared regions of the electromagnetic spectrum were used (Table 1).

Based on previous experience in channel selection, channels 5, 7, 8, and 10 were chosen for a special study. Various combinations of these four channels have a significant effect on the correlation of reflectance with soil organic matter content (Table 2).

Horvath and Baumgardner (2) concluded from this study that:

1. There is a high correlation between soil reflectance and soil organic matter.

2. Selection and number of multispectral channels used had a profound influence on this correlation.

3. The best combination of three channels gave superior correlations over those of the best two channels.

4. In some cases four channels gave superior correlations over those of the best three channels; five or more channels seldom improve r^2 values over those obtained with three or four best channels.

5. There is no single best array of spectral channels for computer-implemented mapping of soil organic matter under a wide variety of conditions and locations.

A question closely related to that of channel selection is: What is the optimum size of training sets in order to obtain the best correlation between multispectral response and a particular parameter of an earth surface feature. In this case soil organic matter content was selected as the parameter to be used. For the limited area and conditions under which this study was conducted, it was found that increasing the size of the training set (the number of scanner resolution elements around each field grid point to be used to train the computer) up to an optimal size improved the correlation between reflectance and organic matter content (Table 3).

Roth and Baumgardner (3) concluded from this study that:

1. Training set size significantly affected correlation between soil reflectance and organic matter content.

2. Training sets used for computer-implemented analysis of multispectral data should consist of at least 36 scanner resolution elements for best correlation with soil analysis data.

One of the very promising applications of the techniques presented in this paper is in the inventorying and mapping of the soils resources of the world. Scientists at LARS are working with the Soil Conservation Service in Indiana to evaluate various remote sensing techniques as an aid in classification and mapping of soils. Recently spectral classifications of soils have been made from multispectral scanner data obtained in May 1971 over flightline 212 in Montgomery County, Indiana. The objective of this research is to find that combination of training data, training set size, array of spectral channels and other techniques which will produce the most meaningful and useful spectral classification or map of surface soils. It is the goal of the soil scientists at LARS to be able to put into the hands of the soil surveyor spectral maps which will greatly accelerate and improve the accuracy of soil surveying and mapping.

In the Montgomery County study fourteen spectral classes of soils were mapped by computer (Figures 6 and 7). In Figure 6 data from all

twelve available reflective channels were used in the spectral classification. The classification results in Figure 7 were obtained with the analysis of data from the four best channels as selected by the divergence method (1). In this study it was found that the classification results are greatly affected by the method which is used to select the spectral classes. Where total reflective data were used as a basis for spectral class selection, the classification results gave indistinct class boundaries and much more complex spectral patterns (Figure 6A and 7A) than were achieved where only visible reflectance (Figures 6B and 7B) and only reflective infrared (Figures 6C and 7C) were used for spectral class selection.

Although fourteen spectral classes would seldom be meaningful and useful in delineating soil types in so small an area, this research provides a basis for better spectral classification. Further study is needed to assist in combining classes and select boundaries between spectral classes to generate a more usable product.

Scientists at Pennsylvania State University and Purdue University are cooperating in a project funded by the U.S. Department of Transportation (4). This project involves the analysis and interpretation of multispectral scanner data from a 47-mile flightline in southeastern Pennsylvania (Figure 8). Scanner data were obtained in May 1969 at a time of maximum bare soil exposure. Seven segments, each 3 to 5 miles in length and containing primarily one parent material were designated for study. Parent materials along the flightline include limestone, shale, sandstone, conglomerate, and perhaps others. To date, four of these segments have been studied in detail using pattern recognition techniques. Results indicate that parent materials can be mapped in the individual segments. Spectral mapping of surface soils has been done in the limestone area. Many of the soil features and patterns are easily seen in an aerial photograph (Figure 9). The patterns in the spectral map delineating three classes of soils and one class of green vegetation compare very well with the field survey map (Figure 10).

Plans for the Earth Resources Technology Satellite (ERTS) Experiment have captured the imagination and interest of people around the world. For many months investigators at LARS have been preparing and training for receiving, analyzing and interpreting earth resources data to be obtained from ERTS. Digitized data from the multichannel photography taken on March 12, 1969, as a part of the S065 Experiment of Apollo 9 have been used to simulate ERTS data. Digitization and analysis techniques have been described by Anuta and MacDonald (5).

One of the important agricultural regions in the U.S. which was photographed in the S065 Experiment is the Southern Great Plains Region

around Lubbock, Texas (Figure 11). A general soils map of Crosby County, Texas, which occupies 911 square miles in the center of the Apollo 9 photograph, clearly illustrates the differences between the High Plains and the Rolling Plains (Figure 12). The White River and its many small tributaries are clearly seen in the eastern and southeastern portions of the map of Crosby County.

Without any ground identification of surface features other than those provided in a Soil Survey Report of Crosby County (6), a spectral analysis and classification were made of Crosby County, using the digitized 3-channel (2 visible, 1 infrared) photographic data (Figure 13). Many surface features are easily identifiable and separable with this spectral data. These include towns, highly reflective dry riverbeds, bodies of surface water, irregular spectral patterns associated with rangelands, and regular patterns associated with cultivated agricultural areas. Within the cultivated region many levels of spectral response are separable and mappable by pattern recognition techniques. Those fields having very high reflectance in the visible spectrum may be covered with residue from the previous crop of grain sorghum. Fields having very low reflectance may be wet, freshly plowed, or be covered with winter wheat. There also seem to be many fields with neither high nor low relative reflectance. The reflecting surfaces of such fields may contain cotton or grain sorghum residues which have been incorporated and mixed into the surface soil to varying degrees by different tillage operations.

The White River Reservoir, which serves as the muncipal water supply for Crosbyton, Texas, is located in the southeastern corner of Crosby County (Figure 14). The reservoir, the dry river channels, the random patterns of the surrounding rangelands, and the ordered shapes of the cultivated fields are easily discernible.

It is a simple operation to instruct the computer to print or map only those features of interest (Figure 15). This technique can delete superfluous data from the scene and can allow the investigator to observe and display only the desired data.

Remote sensing techniques hold great promise for man in differentiating elements of the soil-vegetation complex. There is much that man does not understand about the relationships between the many physical-chemical parameters and the energy which is radiating from the soil-vegetation complex. The results which have been presented in this paper give rise to great optimism in the search for better understanding and definitions of those relationships. And with this understanding will come the technology and capability to apply remote sensing and automatic data processing techniques to a better use of earth resources and the preservation and maintenance of the quality environment.

It is with great anticipation that scientists around the world look forward to receiving, analyzing, interpreting, and evaluating earth resources data from the ERTS and Skylab Experiments.

ACKNOWLEDGMENT

The research summarized herein was supported by NASA under Grant NGL 15-005-112. Grateful appreciation is expressed to NASA for this support. The various individual studies were carried out by Drs. A. H. Al-Abbas, Jan E. Cipra, Stevan J. Kristof, Charles B. Roth, Terry R. West, of the LARS staff and Mr. Emil Horvath, Purdue undergraduate student.

REFERENCES

1. Swain, P.H., T.V. Robertson and A.G. Wacker, 1971. Comparison of the divergence and B-distance in feature selection. LARS Information Note 020871.

2. Horvath, E.E. and M.F. Baumgardner, 1971. Multispectral remote sensing of soils, II. Optimum spectral wavelength for computer-implemented mapping of soil organic matter. Agronomy Abstracts, p. 99.

3. Roth, C.B. and M.F. Baumgardner, 1971. Multispectral remote sensing of soils, I. Optimum training set size for computer-implemented mapping of soil organic matter. Agronomy Abstracts, p. 105.

4. West, T.R., 1972. Engineering soils mapping from multispectral imagery using automatic classification techniques. Paper presented at 51st Annual Meeting of Highway Research Board.

5. Anuta, P.E. and R.B. MacDonald, 1971. Crop surveys from multiband satellite photography using digital techniques. Remote Sensing of Environment 2: 53-67.

6. Soil Survey, 1966. Crosby County, Texas. Soil Conservation Service, U.S. Department of Agriculture.

Table 1. Summary of Spectral Channel Selection

Conditions:
1. Data for 1969 and 1970
2. Data for 3 soil test areas
3. Channel selection made by 2 methods
4. Best 1, 2, and 3 channels selected

Channel No.	Wavelength (in μm)	Color	No. of Times Selected as Best Channel (12 possibilities)	No. of times selected among 1, 2, or 3 Best Channel (72 possibilities)
1	.40-.44	Violet	1	4
2	.46-.48	Blue	0	0
3	.50-.52	Blue-green	0	3
4	.52-.55	Green	1	1
5	.55-.58	Yellow	0	3
6	.58-.62	Orange	2	3
7	.62-.66	Red	2	12
8	.66-.72	Dark red	0	5
9	.72-.80	Reflective IR	1	4
10	.80-1.00	Reflective IR	3	9
11	1.00-1.40	Reflective IR	0	7
12	1.50-1.80	Reflective IR	0	5
13	2.00-2.60	Reflective IR	2	16

Table 2. Effect of spectral channels selected or the correlation of reflectance with soil organic matter

Channel Combinations	r^2 values
5,7,8,10	.69
5,7	.68
5,8	.60
7,10	.45
8,10	.45
7	.44
5	.38

Table 3. The effect of training set size on the correlation between soil reflectance and soil organic matter content (Channels 5 & 7)

Number of Resolution Elements	r^2 values
1	.52
4	.59
16	.64
36	.68
144	.69
722	.70

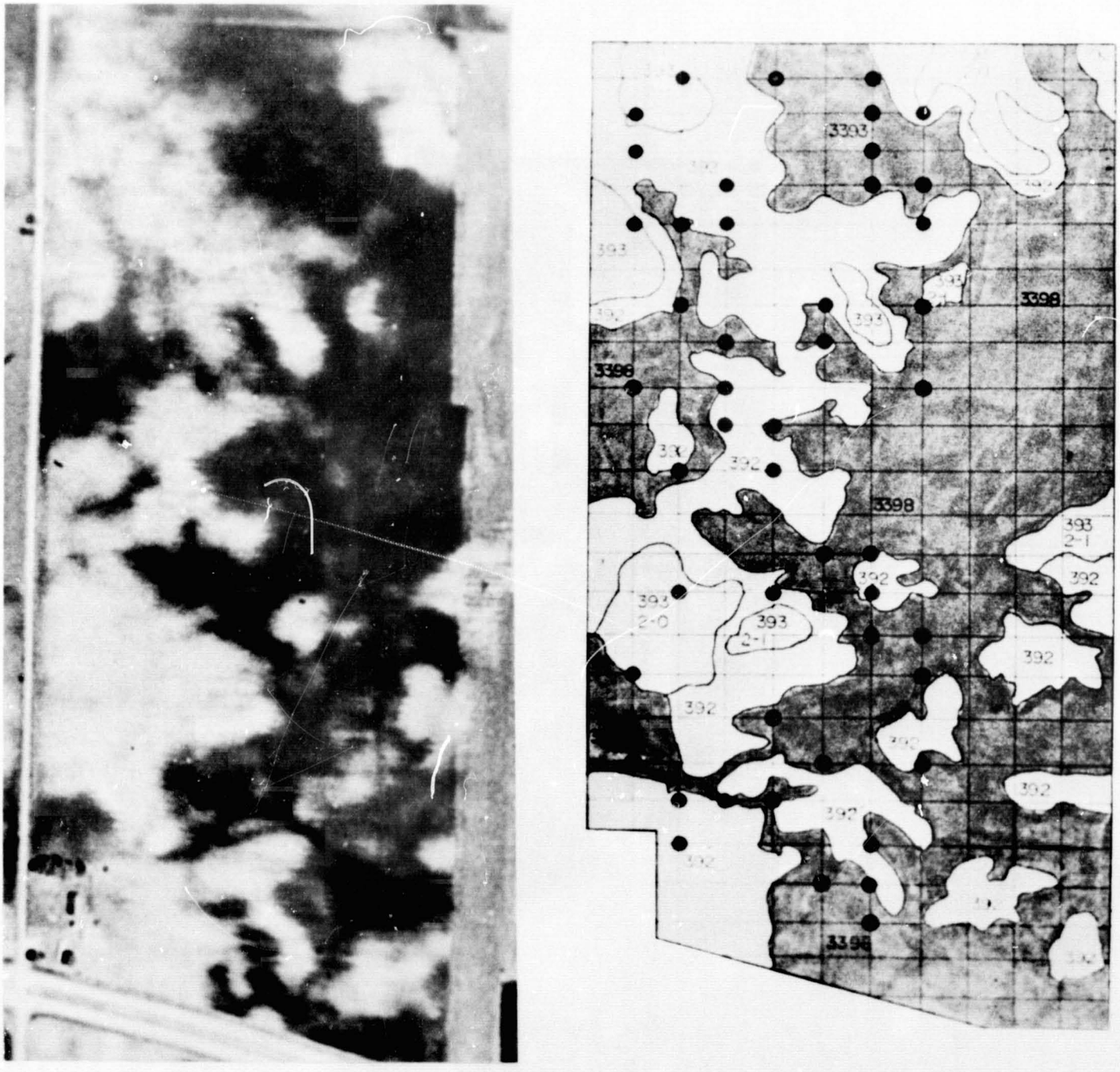

a. Aerial Photograph

b. Soils map

Figure 1. Soil Test Area 6 in Tippecanoe County, Indiana.

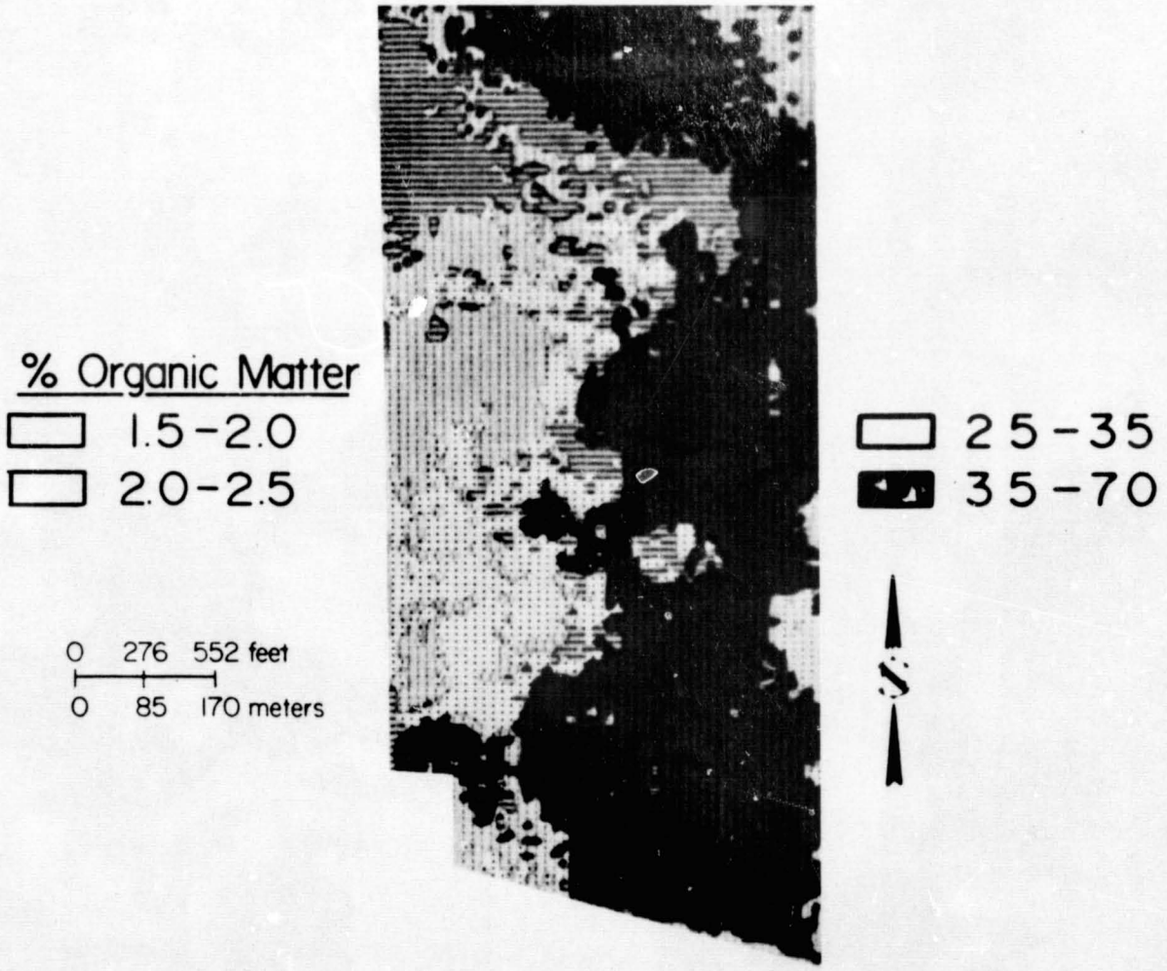

Figure 2. Organic matter content of surface soils, STA 6, July 1970

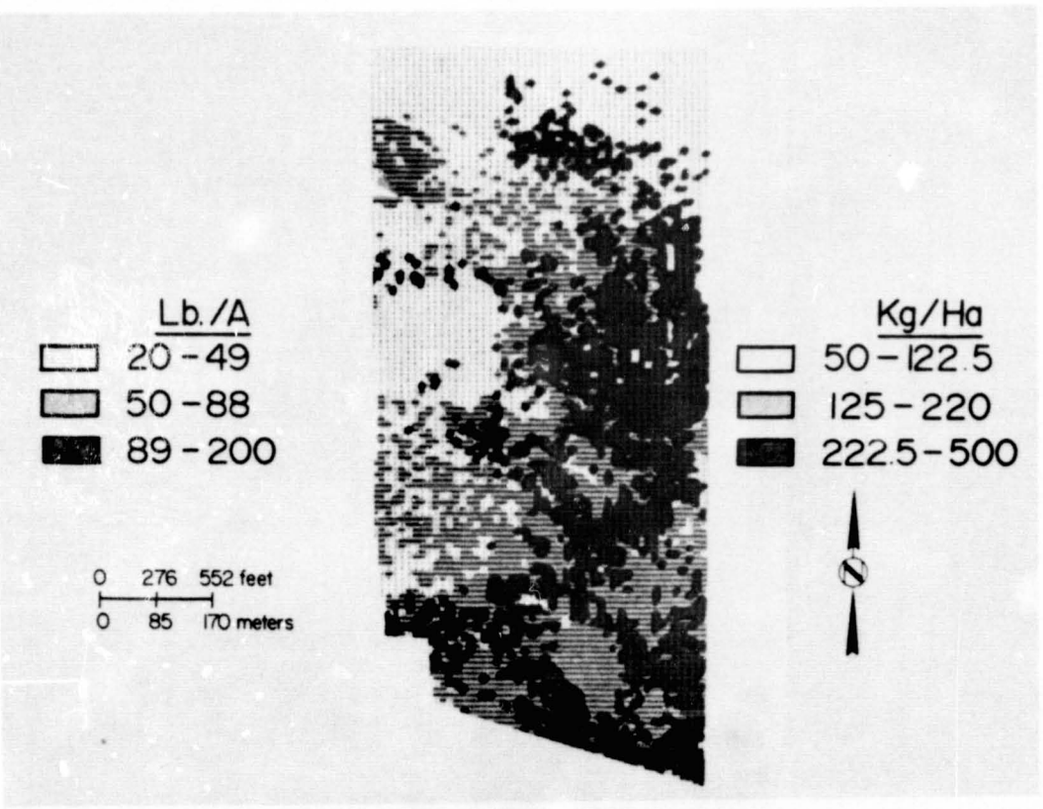

a. Extractable P

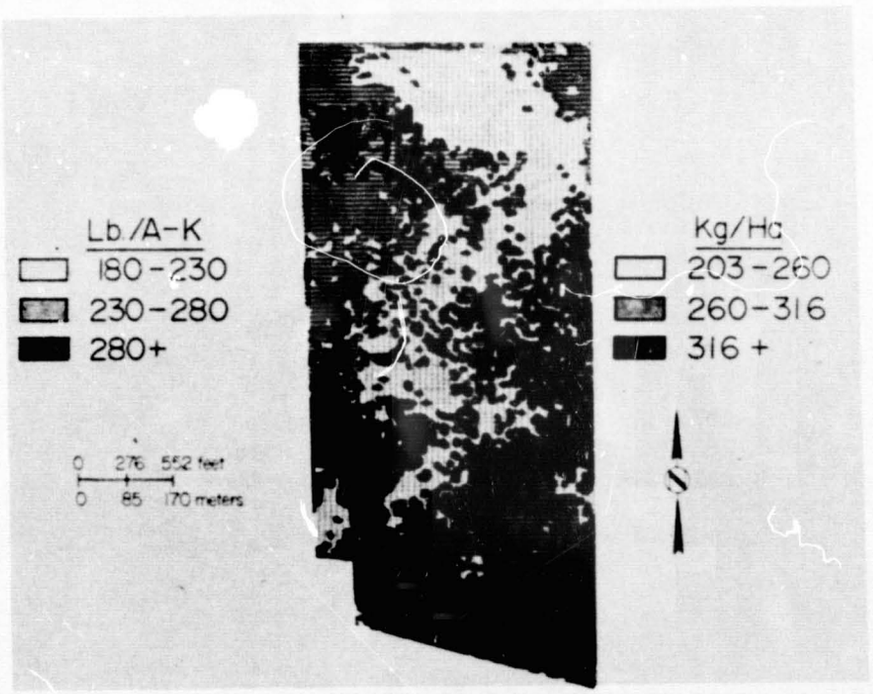

b. Exchangeable K

Figure 3. Computer map of extractable soil phosphorus and exchangeable soil potassium, STA 6, July, 1970

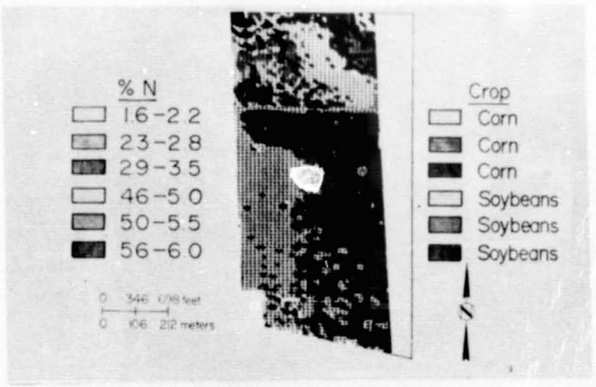

a. Plant N

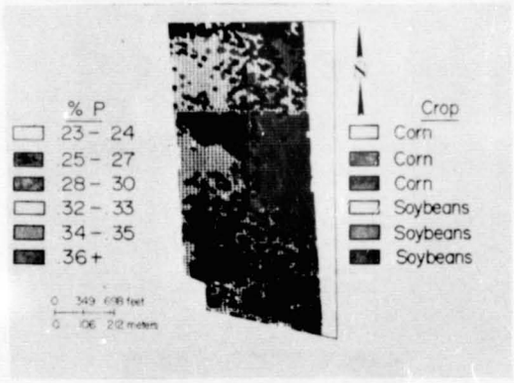

b. Plant P

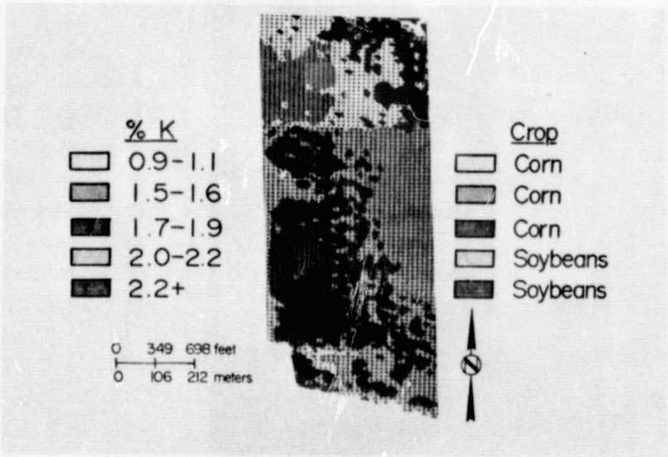

c. Plant K

Figure 4. Sepctral maps representing different levels of plant nitrogen, phosphorous, and potassium, STA 6, August 1970

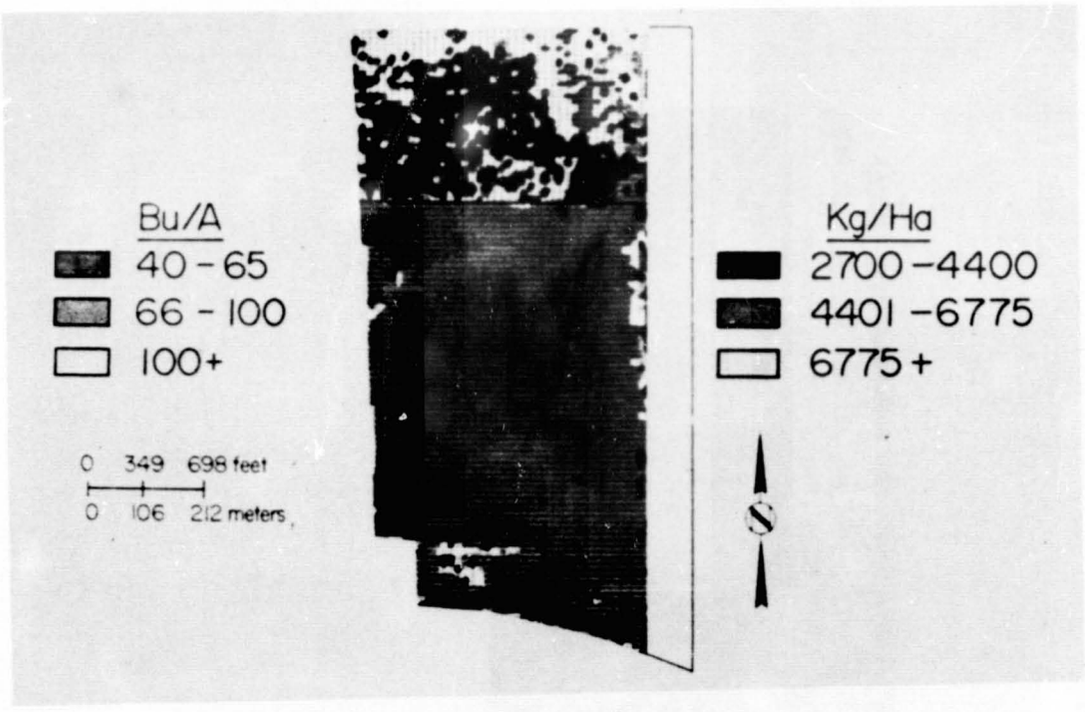

a. Corn yield
(upper one-third of field)

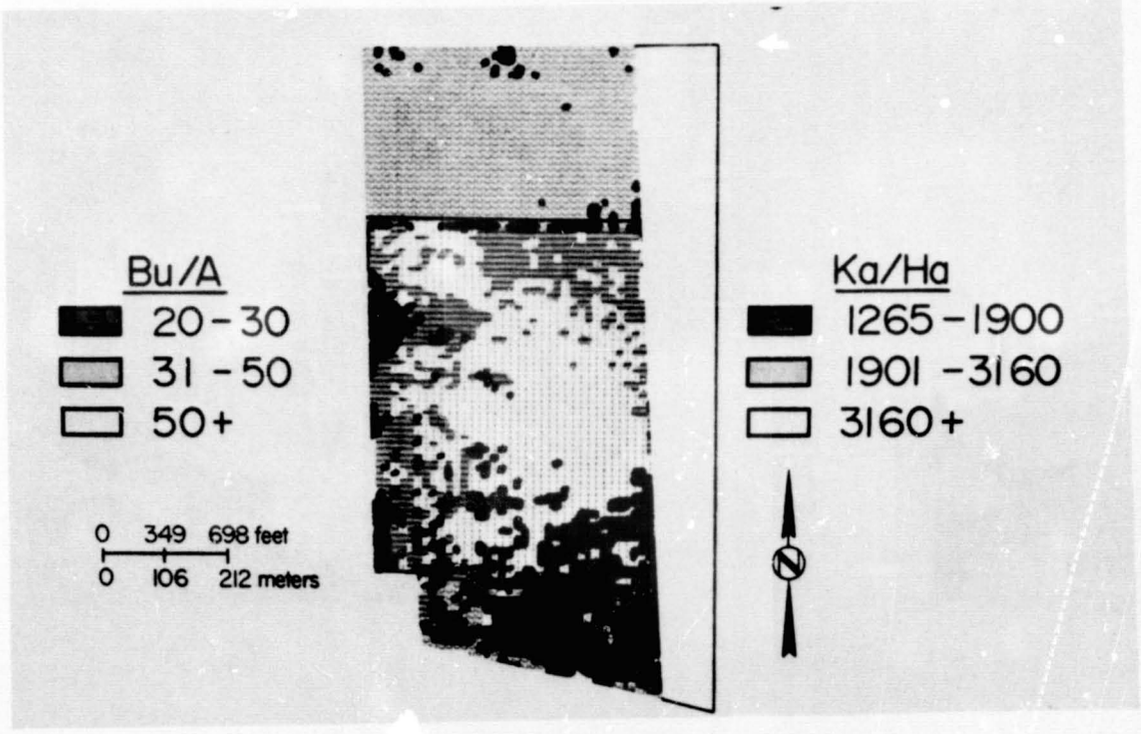

b. Soybean Yield
(lower two-thirds of field)

Figure 5. Computer maps relating crop yield to spectral response.
STA 6, August 1970

(a)

(b)

(c)

Figure 6. Fourteen spectral classes of soils in selected fields from flightline 212, Montgomery County, Indiana, 12-channel (0.4-1.8 μm) classification

Reflectance data used to select classes:
(a) Total (b) Visible (c) Infrared

(a)

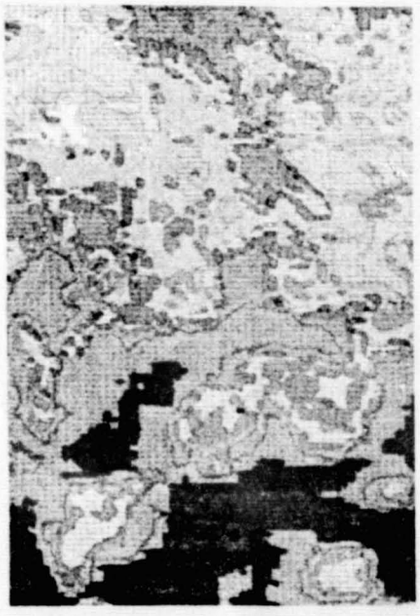

(b)

(c)

Figure 7. Fourteen spectral classes of soils in selected fields from flightline 212, Montgomery County, Indiana, 4-channel classification

Reflectance data used to select classes:
(a) Total (b) Visible (c) Infrared

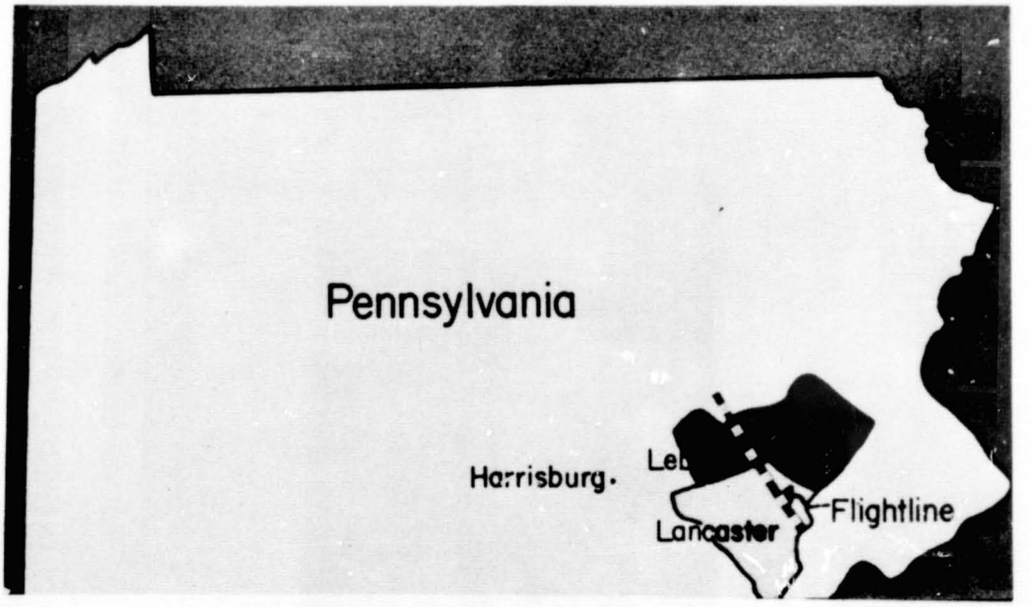

Figure 8. Pennsylvania test site

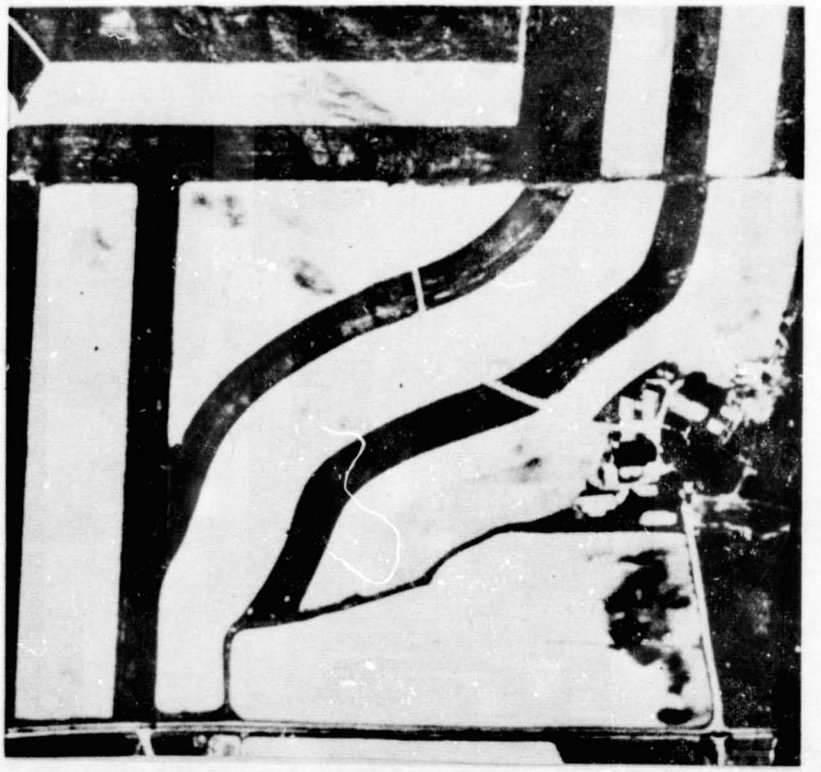

Figure 9. Aerial photograph of test field in Lancaster County, Pennsylvania

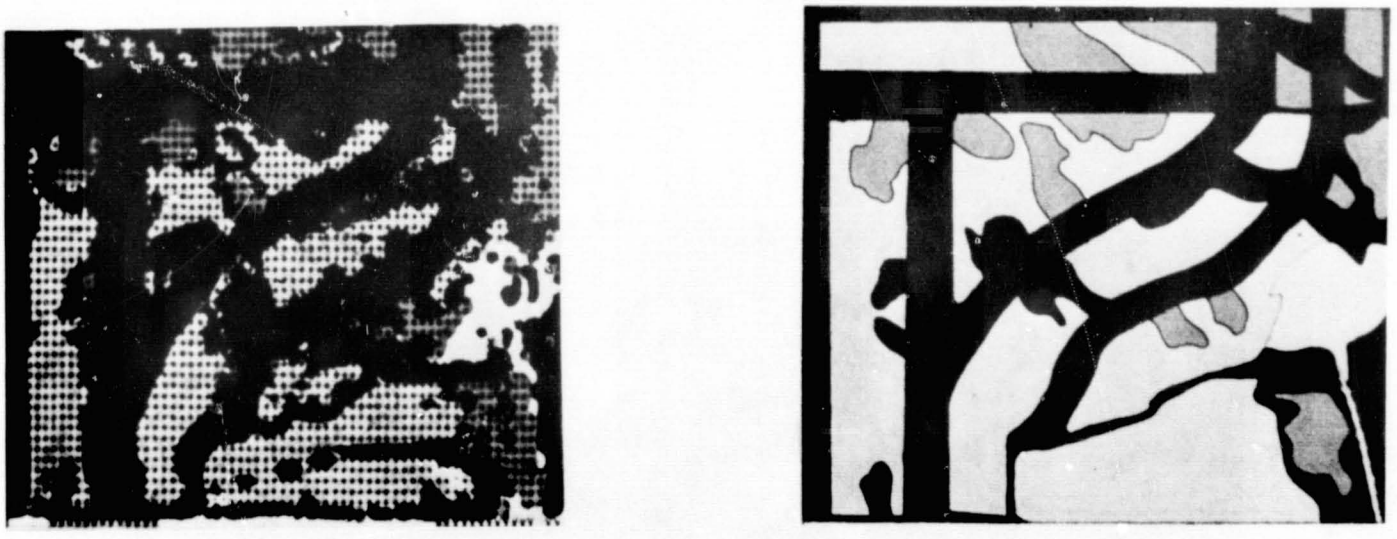

(a) (b)

Figure 10. Spectral mapping of limestone soils Lancaster County, Pennsylvania

(a) Multispectral Computer Map (b) Field Survey Map

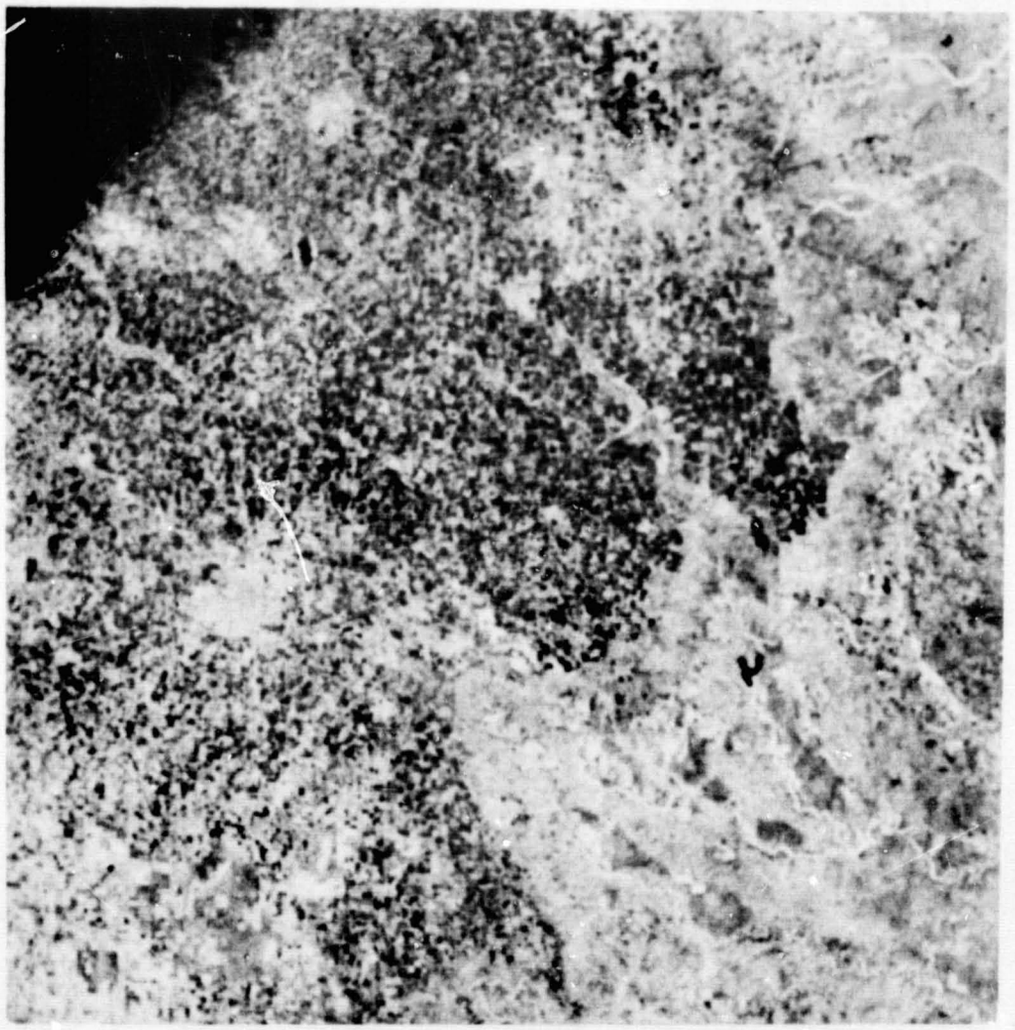

Figure 11. Apollo 9 photograph of the Lubbock, Texas, region (NASA frame 3808)

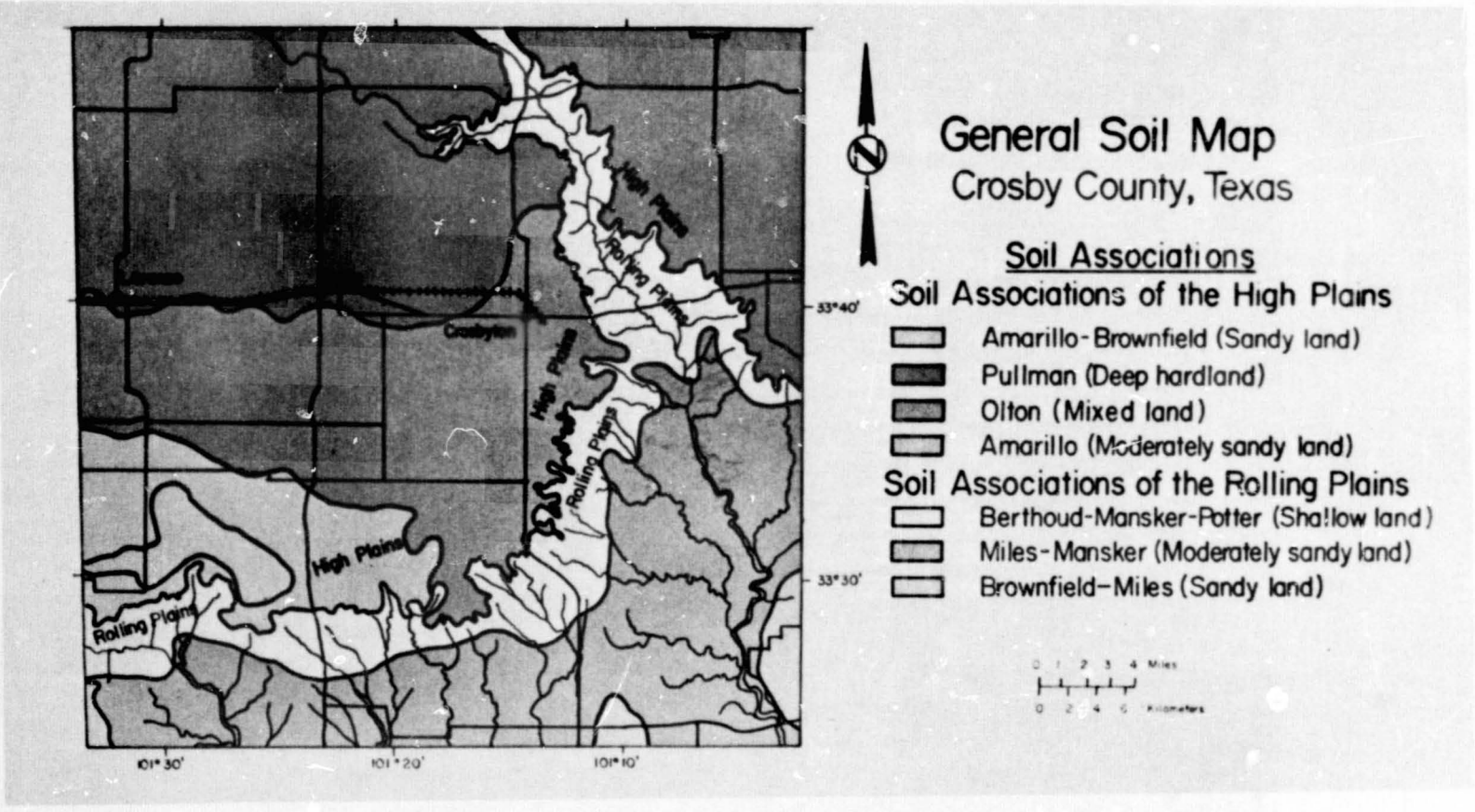

Figure 12. General soils map of Crosby County, Texas.

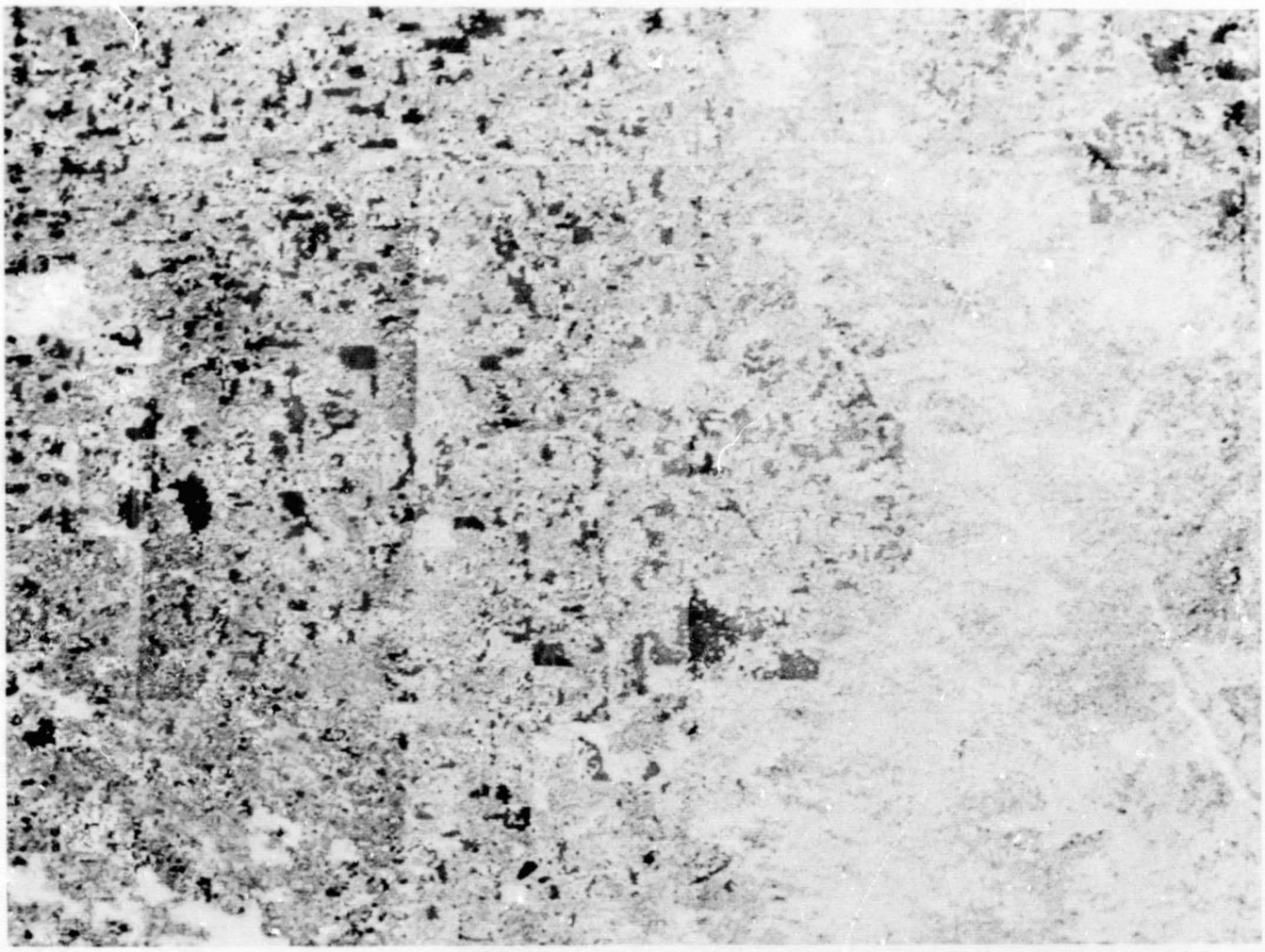

Figure 13. Spectral classification of east central portion of Crosby County, Texas; data from Apollo 9, March 12, 1969

Figure 14. Computer map of spectral classes of surface features around White River Reservior. Crosby County, Texas. Data from Apollo 9, March 1969

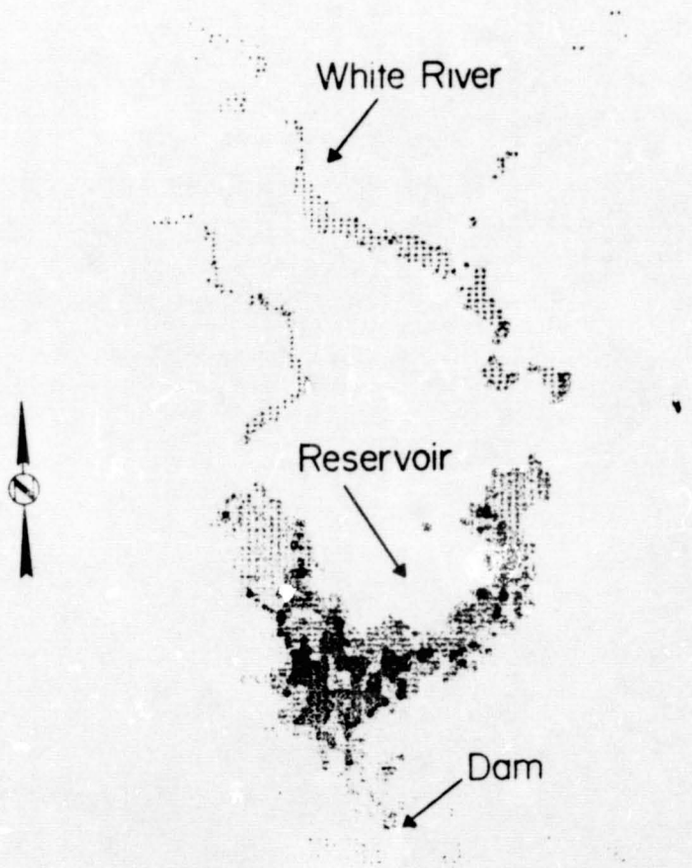

Figure 15. Computer map of the White River and Reservoir in Crosby County, Texas. Data from Apollo 9, March 1969

SECTION 48

LAND UTILIZATION AND WATER RESOURCE INVENTORIES OVER EXTENDED TEST SITES*

by

Roger M. Hoffer and Staff
Laboratory for Applications of Remote Sensing
Purdue University
West Lafayette, Indiana

INTRODUCTION

During the past decade, many actual and potential applications for remote sensing technology have been determined. This past year has seen a tremendous amount of interest generated in the application of remote sensing to problems related to land-use. A key element in applying remote sensing to land-use studies involves accurate identification of basic and vegetative cover types. In work with automatic data processing (ADP) techniques it is found that as information requirements become more specific, the analysis task becomes more complex. In dealing with many problems involving automatic mapping of vegetative cover types conditions, one finds that an analysis sequence similar to that shown in Figure 1 must be pursued. As is indicated, there are many possible categories of basic cover types, and within the "vegetation" category there are many potential subgroups. Once a particular species has been identified, there are many interrelated factors affecting the potential yield of that crop. Of course, the crop yield is of considerable importance to a large number of "users", but since yield cannot be measured directly from remote distances, the factors related to yield and condition of the crop must be determined.

Much of the LARS research effort this past year was devoted to the Corn Blight Watch Experiment, discussed in the January 17th session of this review. As is indicated in Figure 1-C, Southern Corn Leaf Blight is only one of many different kinds of diseases or other stress factors which can affect vegetative conditions. This first figure

---

*In this paper, results from a number of studies are summarized; researchers are identified in the Acknowledgement section.

indicates the degree of difficulty of some of the problems encountered in the corn blight analysis sequence, thereby giving some insight into the real significance of being able to reliably identify the corn at various stages of development as well as identifying blight levels within the corn.

In addition to the work on the corn blight this year, several other analysis tests were completed which resulted in significant findings. These aspects of our work will be discussed as follows:

1. Field spectral measurements of soil conditions.
2. Analysis of extended test site data. This discussion involves three different sets of data analysis sequences.
3. Urban land-use analysis, for studying water runoff potentials.
4. Thermal data quality study, as an expansion of our water resources studies involving temperature calibration techniques.

FIELD SPECTRAL MEASUREMENTS OF SOIL CONDITIONS

In order to accurately interpret remote sensor data, an adequate understanding of energy-matter interactions is mandatory. Use of a field spectroradiometer for detailed studies of selected situations in a natural environment offers one of the best ways for developing a better understanding of many of these complex energy-matter interactions. One study completed this past year involved work with several soil conditions using an Exotech Field Spectroradiometer. (The paper by Dr. LeRoy Silva describes this instrument.) Since the instrument is capable of measuring incoming irradiance as well as the radiance from the soil of interest, the resultant data could be reduced to percent reflectance measurements. Although the instrument is capable of obtaining data throughout the optical portion of the spectrum and data were actually collected throughout the 0.4-16 micrometer wavelengths, limitations in our software for handling the recorded data forced the restriction of reduction and analysis of the visible wavelengths.

Figure 2-A shows the spectral reflectance in the visible portion of the spectrum for three different soil types. One sees that there is a much wider variation in the reflectance characteristics for these different soil types than normally is found for different species of green vegetation. In this illustration, only spectra for dry soil conditions are shown. Figure 2-B indicates the dry versus wet reflectance for two soil types, and one sees some very marked differences, with the dry soil conditions having much higher reflectances than the wet soil conditions. However, it is not always easy to separate dry from wet soil moisture conditions when different soil types are involved.

Figure 2-C shows a very high reflectance for dry Fincastle soil but a reflectance for the wet Fincastle that is very similar to the reflectance for dry Dana soils. Nevertheless, much work has indicated that it ought to be possible to use the thermal and microwave portions of the spectrum to considerable advantage in separating wet and dry soil conditions, even among the many different soil types of concern.

Not only do variations in soil moisture cause distinctive differences in percent reflectance for the same soil type, but variations in the surface condition, such as crusting, will cause very distinct differences in percent reflectance. Figure 2-D shows the reflectance for a soil sample in which the action of the rain had crusted, or smoothed out the soil surface, causing a relatively high reflectance. After the crust was broken, the surface soil condition was still dry, but a much lower reflectance was measured at all wavelengths in the visible region.

From these few examples, one sees that several natural causes of large variations in spectral response can be encountered. A field instrument such as the Exotech spectroradiometer has many advantages such as a fast scan rate; use under natural illumination conditions; and the collection of data from approximately the same instantaneous field of view, as well as look angle, as the scanner in the aircraft. Future studies with this instrument should enable significant progress to be achieved in determining the optimum times during the growing season for flight missions to be scheduled, studying spectral characteristics of various vegetative and soil conditions throughout the optical wavelength region, species differentiation as a function of temporal changes, and other energy-matter interactions.

ANALYSIS OF EXTENDED TEST SITE DATA

In studying results from several of our computerized analyses of multispectral scanner data collected over fairly large geographical areas, it became apparent that several possible causes of spectral variability must always be considered. Some of the major causes of such variability which are particularly noticeable in analysis of vegetative ground cover and which are of primary concern to the user of this data are:

- .Percentage of Vegetative Cover
- .Spectral Response of Vegetation
- .Spectral Response of Soil Background
- .Illumination, Crop and/or Sensor Geometry, and Instrumentation Variables

Some of these variables are a function of the vegetation and soils while others are not. In our work in the Biogeophysical Research Program, we are particularly interested in the spectral characteristics of the vegetation and soils, but we find that illumination, geometry, and instrumentation factors affect the scanner data in ways that frequently make it difficult to separate and identify which factors are affecting the spectral characteristics of vegetative ground cover. Therefore, one must consider all possible factors which could affect spectral characteristics of scanner data, in order to properly and accurately interpret this type of data.

One of the major questions that frequently arises is: How well can one extrapolate from small sets of training sample data obtained in one geographic location to an automated classification of large geographic areas? Certainly, if we are ever going to utilize these techniques on an operational basis, we must know the limitations and capabilities for extrapolating small data sets to large areas. In looking to the future and preparing for ERTS and SKYLAB, considerable effort this year was devoted to further examination of natural and other causes of spectral variability, and how this influences our capability to extrapolate to large geographic areas.

CLASSIFICATION OF A 42,000-ACRE AREA

The first study over extended test sites to be reported upon involved data collection in a north-south flightline in Central Indiana. These data were collected in late April (spring-time) from an altitude of 3200 feet by the University of Michigan multispectral scanner system. We have previously reported on our capability to reliably identify basic cover types (Hoffer, 1968). In further analysis of this data, we utilized less than 1% of the total area as a training set. All of the training data came from one small area near the northern part of the flightline. After classification, 256 test areas were selected at random, accounting for several thousand data points in each cover type category, and the computer classifications were tabulated for all data points in these test areas. The results indicated accuracy of over 97% for the automated classification of the basic cover types. However, we did notice a slight decrease in accuracy as the area being classified became more distant from the area where the training samples had been obtained. Samples from the northern and from the southern portions of the flightline were then selected and compared. Figure 3 shows the results of this comparison for three different wavelength bands. The cross hatched areas indicate data from northern portions of the flightline and solid blocks indicate data from the southern portion

of the flightline. The length of the bar indicates the mean spectral response, plus or minus one standard deviation. Therefore, a longer bar will indicate more variability, whereas the bars of shorter length indicate relatively small amounts of spectral variability within that particular wavelength band and cover type. As can be observed, there is little difference in spectral response between the northern and the southern portions of the flightline for the bare soil areas. Water showed a distinctly higher response in the southern portion of the flightline than in the water in the northern portion of the flightline in the visible wavelengths but, as expected, there is little difference in radiance in the reflective infrared portion of the spectrum. The low response in the reflective IR for water is attributed to the high absorption characteristics of water in these wavelengths, while the differences in response between the northern and southern portions of the flightline in the visible wavelengths is ascribed to different sediment loads between the North and South Fork of the White River, where the data was obtained. We had anticipated that vegetation in the southern portion of the flightline would have a higher response than the vegetation in the northern portion of the flightline. This was the case in the blue portion of the visible wavelengths, but in the reflective infrared, just the opposite situation occurred. It is believed that this was because the data collected in the northern portion of the flightline largely consisted of dense winter wheat stands and forested areas that were mostly in the low-lying bottom-lands along the streams. These forested bottom-lands consisted of cottonwood and sycamore trees which had leafed out earlier than the upland forest cover that predominated in the southern portion of the flightline. Thus, just because data came from a more northerly area, it is not safe to assume that the vegetation as a whole will be leafed out more in more southerly areas on any particular date during the spring.

In summary, we believe that the variability observed in this set of data was caused primarily by the natural spectral differences in the materials involved.

EAST-WEST FLIGHTLINE EXTENDING OVER A 133-MILE AREA

Since the basic cover type mapping in the first analysis had indicated some slight changes in spectral response but since these changes did not seriously affect the classification results, the next logical step seemed to be to conduct a more complicated analysis involving identification of a particular crop species over a large geographic area. To limit some of the north-south geographic variation which had been observed in the first analysis, and which can be severe in large geographic areas, flightlines were laid out in an east-west direction to sample a 40-county area in Indiana and Illinois, as shown

in Figure 4-A. To limit the total amount of data collected, only segments from a 133-mile flightline were recorded. The length of each of these segments and the distance between the segments is indicated in Figure 4-B.

The multispectral scanner data for this experiment were obtained by the University of Michigan aircraft on July 1, 1970. However, the analysis of these data had not been completed in time for the 3rd Annual Earth Resources Program Review, so are reported this year. As an indication of the difficulties sometimes encountered in conducting this type of experiment, the following comments are included. Initially, it was planned that the following conditions were to have been met as nearly as possible:

(1) Wheat would be at a mature stage of development. It was assumed that approximately uniform conditions of maturity would exist along an east-west flightline and that therefore the wheat would have a similar spectral response throughout the data.

(2) All data would be obtained from a 5000-foot altitude during a single flight sequence to minimize differences in atmospheric attenuation and electronic drift in the data.

(3) Ground observations of cover types (species and crop condition) would be obtained for Flightline 25 in Indiana. Aerial photography taken at the same time as the scanner data would then be used to extrapolate cover type identification from FL 25 to the other flightlines to the west.

(4) The classifier would be trained with data from FL 25 and this training set would be used to classify data from the entire sequence of flightlines covering a geographic area of more than 130 miles from the eastern-most end of FL 25 to the western-most end of FL 43.

The actual conditions at the time of the flight failed to meet the desired ones in several ways. This caused a number of changes in the data analysis plans and affected some of the results and conclusions.

Since flight missions through NASA must be set up several months in advance because of aircraft scheduling requirements, we had requested the flight for the last week in June because past experience had indicated that in Indiana this would be the optimum time for mature wheat. Normally, harvesting does not start until the early part of July. However, in 1970 the crop conditions were on the early side of "normal," and the flight was conducted during the latter portion of the scheduled time period (July 1). This combination resulted in data in which some of the wheat in Indiana was being harvested or had been harvested at the time of flight. In Illinois, the growing conditions appeared to be about one week ahead of those in Indiana, and much of the wheat had been harvested. Some fields, believed to be wheat

stubble, already had an undergrowth of weeds, giving these fields a spectral response somewhat like that of hay fields. Since both standing wheat and wheat stubble were present, we were required to train the classifier portion of the computer programs on both mature wheat and wheat stubble of varying age and condition.

At the time data was being collected, scattered cumulus cloud cover developed over the eastern portions of the flightline area, thereby forcing the FL 25 data to be collected from 3,500 feet altitude and with variable cloud shadow effects on the ground, whereas the other four flightlines of data had been collected from 5000 feet altitude under mostly clear, sunny conditions. This change in data collection caused the use of FL 40 (on the Indiana-Illinois border) for a training area, with FL 25 being used only as a test area to check effects of altitude change and cloud shadows.

The use of aerial photos in lieu of ground observations on some of the flightlines did not prove to be as reliable for accurate identification of cover types as had been anticipated. This was due to variable illumination conditions in parts of the flightline at the time the photography was obtained, poor quality and resolution in the black and white photography, and completely unusable results for the color infrared photos. The variability of ground cover conditions added to the difficulty.

The procedures used in the experiment were therefore modified to optimize utilization of the actual data collected. This resulted in the following set of objectives being defined:

(1) Reaffirm previous work at LARS showing the capability for identifying wheat vs. everything else. Test and training samples to be obtained from FL 40.

(2) Determine capability for identifying wheat (or wheat stubble) over an extended test site area, using training samples from one geographic area to classify a completely different area. In this case, the training samples from FL 40 would be used to classify data from FL 41, 42, and 43. Test samples from all four flightlines would be obtained to quantitatively check classification results.

(3) Determine the capability for classifying FL 25 data using training samples from FL 40, recognizing the fact that FL 25 data were collected from 3500 feet altitude under somewhat cloudy conditions, as opposed to 5000 feet altitude and mostly clear conditions for the FL 40 data.

(4) Determine variability of incoming solar radiation at the aircraft location over the entire 130-mile flightline area, and utilize data handling techniques developed by LARS to calibrate the spectral reflectance data as a function of the sun sensor signal.

(5) Determine utility of sun sensor calibration techniques for increasing accuracy of automatic classification of cover type, if significant variability is found in sun sensor signal in Step 4 above.
(6) Determine major sources of variation in spectral response of cover types, the severity of such variations as it affects automatic classification techniques, and whether such variations can or cannot be corrected with various calibration and data analysis procedures.

Results

Initial analysis efforts showed that calibration of the data only for electronic drift was not adequate to allow accurate classification over the entire area. The ability to classify automatically wheat vs. everything else was demonstrated again (LARS, 1970) using training and test samples from FL 40. However, the classification of the other flightlines was only partially successful. There were many misclassifications present (primarily as wheat in areas that were not wheat), and a light threshold applied to the training data tended to cause most of the test area data to be thresholded.

The sun sensor signal for the entire flightline was examined and found to show significant changes in solar illumination (Figure 5). Generally, a moderate upward shift was found as the aircraft moved along the flightline. In some cases, distinct changes could be seen between the end of one flightline and the beginning of the next, and in FL 40 there were rapid, marked changes in illumination, even though the area was only six miles long and was flown in approximately three minutes.

The LARSYSAA multispectral scanner analysis program system contains a data calibration function in which the user may select the type of calibration to be applied, dependent upon his knowledge of any problems existing in the data (Phillips, 1969). The usual calibration is one which corrects for low frequency drift in the data collection or data processing system. If illumination changes are known to exist in the data run, an additional calibration may be made to change the data to a constant level in each data line. This will force data amplification to a fixed level in an attempt to correct for illumination changes as they are detected by the sun sensor.

Illumination usually will change as the aircraft moves through differing atmospheric conditions, and the sun sensor provides a measure of these changes as they are detected at the aircraft. Illumination at the aircraft may not change at the same time or at the same rate as

illumination at the ground target. An example is the situation in which the aircraft enters a cloud shadow and the sun sensor shows an abrupt change while the target may continue to be in full sunlight. The reverse will occur when the target is in shadow and the aircraft remains in full sunlight. These types of situations do not allow use of the sun sensor calibration, because such calibration under those circumstances would cause even larger differences in amplitude of the data. However, in the 40-county test site, the sun sensor pulse indicated a gradual increase in illumination. Thus, a two-point calibration for both drift and amplification could be effectively used, and was applied to this data.

In Figure 5, the abrupt change in Flightline 40 was due to an electronic gain change, or manual change in amplification of the signals. This gain change occurred in all the middle infrared channels (1.0-1.4, 1.5-1.8 and 2.0-2.6 μm), and caused distinctive changes in the gray scale printouts of the data at that point. The sun sensor calibration procedure adjusted effects of this gain change.

The results of the classifications with data calibrated for both drift and the sun sensor signal showed encouraging improvements in accuracy. On FL 40, the training data had an overall classification accuracy of 99% (98.5% correct classification for wheat, using 662 data points, and 99.9% correct classification for all other crops or cover types, using 3,104 data points). The test sample accuracy showed somewhat variable results from flightline to flightline, as shown in Table I. This is thought to be due to the natural variation in condition or degree of maturity of the cover types. Classification accuracy was very high in FL 43, approximately 80 miles distant from the area where training samples had been selected.

As a check on the effects of calibration on classification accuracy, two additional classifications were made. The first used the same channels that had been selected from the two-point calibration data but used data that had been calibrated only for electronic drift. The last classification used the best five channels, again using the data calibrated only for drift. In the latter case, the feature selection algorithm indicated a different set of 5 channels than had been used in the previous classification. The spectral bands were 0.55-0.58, 0.66-0.72, 0.80-1.00, 1.00-1.40, and 1.50-1.80 micrometers.

The test field percentages are given in Tables I, II, and III for the three classifications. For ease in comparison, Figure 6 shows the classification accuracy of the wheat test fields. The two-point calibration is consistently the best classification, with the two classifications having only drift calibration being about equal. The last classification, using the best five combinations of wavelength bands, was slightly more sensitive to accurate wheat classification

than the other classification using data calibrated only for drift, but was still much less accurate than the classification using data having two-point calibration. All three classifications had similar high test field accuracies in FL 40 where the training statistics had been obtained.

One additional test was made, using data from FL 25, the east-west line across Tippecanoe County, Indiana. These data were collected on the same flight as the data for FL 40-43, but FL 25 was flown at a lower altitude (3500 feet above terrain), and about 20 minutes later. Scattered cumulus clouds were present over this area. The line begins about 21 miles east of the FL 40 end point. The FL 25 data were classified using the training statistics obtained from FL 40 and the two-point calibration. A set of 17 wheat fields and 4 large areas of other cover were selected as test fields. Wheat fields were classified with 90.5% accuracy, but the other fields were only 30.6% correctly classified, indicating that many points were misclassified into the wheat category or thresholded. Vegetative conditions along this flightline were quite different than in the training area, as indicated by the fact that the wheat harvest was less than half finished on this flightline, in contrast to having been nearly completed in many areas in the Illinois flightlines. However, it is believed that the variable cloud conditions at the time these data were collected caused more error in these classification results than either the difference in altitude or the differences in vegetative cover conditions.

The conclusions from this experiment included the following:

(1) The capability for accurately identifying wheat using ADP techniques was shown to be high over relatively small areas (about 9 square miles).
(2) When training samples from one area were utilized to classify data from other geographic areas, classification accuracies tended to be rather poor unless a two-point calibration (which corrected for both electronic drift and variations in solar illumination) was utilized. The test field results indicated that without the two-point calibration, there was a general decrease in accuracy as classification was attempted for areas further and further from the training site.
(3) Proper calibration allowed recognition accuracies of 91% to be obtained for test areas 80 miles away from the training sample location.
(4) In general, the two-point calibration (drift and illumination) should be utilized in all data analysis involving large geographic areas.

C.9

(5) The calibration procedures utilized appeared to satisfactorily adjust for manual changes in the gain setting, although further analysis along this line is recommended.
(6) Use of the sun sensor to calibrate the scanner data proved unsatisfactory under conditions of scattered cumulus clouds, since the shadow conditions on the ground were quite variable and differences in illumination at the airplane and on the ground below the airplane did not coincide.
(7) Even though conditions of the ground cover were striking and more pronounced along the east-west flightline area than had been anticipated, adequate training of the classifier (involving selection of representative samples of data from the various conditions and stages of maturity), allowed reasonably accurate automatic classification results to be obtained from an area extending more than 90 miles from east to west.

It is strongly recommended that additional studies of natural variability over large geographic test sites be conducted for many cover types and species. It is anticipated that ERTS and SKYLAB data will offer many excellent opportunities for this type of endeavor.

ACREAGE ESTIMATES FOR A 504-SQUARE-MILE AREA

The third study to be reported involving automatic classification results over extended test sites concerned an attempt to convert automatic classification results to acreage estimates of various cover types, and to compare these acreage estimates to existing figures published by the Crops and Livestock Reports of the Statistical Reporting Service, U.S. Department of Agriculture, and the Census of Agriculture, U.S. Department of Commerce (Johnson, 1971).

In this study, five flightlines in Tippecanoe County, Indiana were analyzed. Tippecanoe County is an area of 504 square miles, or 322,560 acres, and the scanner data were collected by aircraft from an altitude of 5000 feet; a scanner swath width of 1.11 miles was utilized, resulting in an area of 82,072 acres being overflown. Therefore, 25.75% of the total area in Tippecanoe County was included in the sample. Each resolution element digitized and analyzed represented an area equivalent to approximately 1600 square feet (the resolution element immediately below the airplane represents a much smaller area than one off to the side of the flightline because of the geometry of multispectral scanners.) The data for each of the five flightlines was classified into cover types designated as:

.corn
.soybeans
.forages
.trees
.bare soil
.water

The "forages" category represents hay, pasture, wheat stubble and oat stubble. Table IV indicates the number of RSU's in each of the cover types in the test areas, the number of RSU's correctly classified in each cover type (by flightline), and the percentage correct classification for each cover type in the test areas. The accuracy of the training categories was even better than the test classification, as anticipated. Training field accuracies are not given here as they do not really represent the overall accuracy of automatic classification for the flightline. Figure 7 shows the classification results for each of the flightlines involved. This bar graph represents the material in Table IV, but in more understandable form, and with the water, soil, and tree classes combined as "other," since they represent relatively small numbers of data points. In this case, the height of the bar indicates the total number of points considered in testing the classification results. The number of points correctly classified are then indicated by the lower portion of the bar, the number incorrectly classified by the upper portion of the bar, and the percentage correct classification is also shown at the top of the individual bars. In comparing the height of the bar with the number of data points involved, (shown on the ordinate), one sees that there may be as much acreage planted in soybeans as in corn for an individual flightline. In other flightlines, there will be twice as much corn as soybeans present. This indicates that our techniques for sampling need to be carefully developed, and that an accurate sample of cover types is mandatory in order to obtain accurate acreage estimates for large geographic areas. Figure 8 shows the combination for all five flightlines. Again the height of the bar shows the number of data points involved in testing the accuracy of the classification. An actual percentage correct classification for the test areas for each of the four major cover type groups considered is shown at the top of the bar. Figure 9 shows the overall results for the sample area in terms of the percent correct classification. In this figure, the number of data points involved in determining the percent classification for each of the cover types is indicated on the bar. The classification accuracy for the "water," "soil," and "trees" categories (previously grouped together as "other") is also shown.

Since it appeared that the accuracy of the classification was reasonably high, the next step was to convert each resolution element in the scanner data to an acreage figure. Table V shows the number of data points in each cover type class for the entire area overflown. For this data, an average of 27.2 resolution elements in the scanner

data was used to represent one acre of cover type. This figure was then expanded to the entire 322,560 acres for the county, and an acreage estimate for each of the cover types of interest for the entire county was obtained. Figure 10 shows the results obtained. The percentage of the total area in the county estimated to be in the different cover types is also indicated. As can be seen, the computer acreage calculations resulted in an estimate of 323,850 acres for the total area in the county, whereas the actual area is 322,560 acres. Considering the fact that geometric correction had not been made on the data and that an average figure was used to represent the resolution elements for all look angles of scanner data, it is felt that this difference is well within the accuracy of the techniques utilized, and is therefore negligible.

The estimated acreage for the different cover types obtained by computer classification were then compared with the Census of Agriculture reports and the Crops and Livestock reports. In some cases, the different cover types could not be directly compared because the officially published figures did not contain any data for certain cover types which were used in our computer classification. As shown in Figure 11, there is a fairly wide variation in even the published estimates of acreage for some of the cover types. For example, the published reports indicate a variation for corn of from 82,510 to 76,900 acres. Therefore, we feel that our remote sensing estimate of 84,210 acres of corn in the county is well within reason, and compares favorably with the accuracy of current techniques for estimating acreage.

These results are particularly significant, in that this may be the first time that acreage estimates have been obtained from multispectral scanner data and that these estimates have then been compared to published figures for different cover types over a reasonably large geographic area. At least two factors appear to be required in order to obtain acreage estimates with scanner data which are reasonably close to actual acreage estimates for the area. First, the sample covered by the scanner data must be large enough to be representative of the area. Minimal sample size and number of samples required for any particular area would, of course, be a function of the variability of the materials within the area. A great deal of additional work needs to be done in sampling techniques for remote sensing purposes. The second requirement for accurate acreage estimates of an area would be that sufficiently accurate classification results must be obtained. Again, additional work remains to be done in order to define what a "sufficiently" accurate classification really involves.

URBAN LAND-USE ANALYSIS

Land-use is changing every year in many parts of the world and our nation. Such land-use changes often involve large geographic areas. The greatest portion of these changes in the United States during recent years has occurred when agricultural and forest lands are converted to housing, industry, highways, public buildings and parks. The effects associated with these changes are numerous and far-reaching. We feel that remote multispectral sensing has a potential for obtaining valuable data to use in land-use analysis and planning future developments. The capability for satellites to obtain remote sensing data over large geographic areas and at regular time intervals should offer a great deal of potential information to adequately plan for the early development of the landscape of our nation.

In a pilot project this past year, a typical small subdivision located near Lafayette, Indiana over which scanner data has been obtained, was analyzed. Automatic data processing techniques were utilized to determine the amount of the area in this urban development which was under hard surface cover and that which was under permeable cover types. Figure 12-A shows a black and white version of a color infrared photo of the area analyzed. Figure 12-B depicts the automatic computer classification of the areas identified as either trees, shrubs, or grass. Comparison between Figures 12-A and 12-B indicates a high degree of accuracy for the computer classification results. Figure 12-C shows the areas identified by the computer as man-made and hard surface areas. These have been subdivided into either "roof" or "streets and driveways." In some cases, the classification for roof surfaces is somewhat inaccurate due to shadow effects. However, the total hard surface area classification appears to be fairly accurate.

The classification accuracy of this analysis was tested using two different photointerpretation techniques. The first involved the use of a very fine dot grid count of the area. The second procedure was to planimeter the hard surface areas. Figure 12-D shows the comparison between the percentage of the area shown in Figure 12-A as determined by dot grid techniques, and the computer classification results. Thus, the computer indicated that 8% of the area was covered by roof surfaces, the photointerpretation dot grid estimate indicated 8.2% coverage by roof surfaces, etc. In total, the computer estimate indicated that 24.4% of this area was covered by hard surface whereas the dot grid analysis indicated 21.5% of the area had a hard surface cover.

We believe that the results of these types of analyses could be a value in planning for culverts and other runoff design specifications

in urbanized watershed areas. For example, a one-inch rain in a one-hour time period for an area such as this, where about 20-25% of the area is under impermeable cover, would call for a different runoff design than an area where 50% of the watershed is under hard surface cover.

This was the laboratory's first attempt to quantify an urban land-use scene. The results show promise for the role of remote sensing in the rapid identification and mapping of present and changing patterns in land-use. The rapid changes taking place in this country and the increasing pressure on our land resources indicate that these techniques will prove most valuable for the management and development of our land resources in the years ahead.

WATER QUALITY STUDIES

The water quality studies to be reported upon are an extension of water resource studies involving temperature calibration techniques of multispectral scanner data. The University of Michigan multispectral scanner has hot and cold plates mounted within the field of view of the thermal infrared channels. These calibration plates can be used to obtain calibrated data, in order to remotely measure true radiometric temperatures, providing the emissivity of the objects being scanned is approximately $\varepsilon = 1.0$. The previous work at LARS has shown that these calibration techniques can be used with a high degree of accuracy for obtaining temperature maps of water bodies. Measurements made of the water temperature from boats on the river at the time the scanner was flown over confirm that the accuracy of temperature measurements obtained from scanner calibration is usually with .2-.4°C of the temperature obtained for the same area from the scanner data.

In studying the correlation between temperature measurements made on the river and the temperature obtained from calibrated scanner data, we noticed that the scanner data seemed to be quite variable as one viewed the entire water body. Further investigation appeared to indicate that the variation observed was not due to normal variations in temperature of the water surface, but rather was due to noise in the scanner data. In an attempt to reduce the amount of noise in the scanner data, a sequence of line averaging and weighted line averaging studies were carried out. One must remember that in utilizing data from line scanner systems from altitudes of 2000 feet, only every 8th scan line is required for contiguous scanner coverage. Thus in our digitization process, seven of the eight scan lines normally were not being utilized. By digitizing all eight scan lines and averaging all eight scan lines, or four out of the eight, or three out of the eight, etc., we found that the amount of noise in the data could be substantially reduced. Figure 13 shows a single column line of data taken along the line of flight; the top of

this graph shows results of a single scan line, the bottom graph shows the results where eight scan lines were averaged together and displayed as single scan lines of data. The reduction in the amount of variability in the scanner data, due to use of the line averaging technique is quite apparent in this figure. Figure 14 shows the results of such line averaging applied to an entire segment of the flightline, and displayed in a map format. On the left is the scanner printout of calibrated thermal data in the 8 to 13.5 μm portion of the spectrum. The Wabash River is flowing from north to south, and the Tippecanoe River enters the Wabash from the west (left). From the calibration levels indicated for the data, it can be easily observed that the Tippecanoe River is cooler than the Wabash River into which it flows. Just above the junction of these two rivers there appears to be quite a great deal of variability in the temperature of the river as indicated by the scattering of points representing different temperature levels. The results of averaging eight scan lines and displaying them as a single scan line are shown on the right. In this case one sees that there is a much smaller amount of temperature variation in the data displayed. The results of averaging four scan lines and then not using the intervening four scan lines of data obtained at this altitude showed very similar results to those displayed in this figure. Thus, it appears that a considerable increase in data quality can be obtained through some of these preprocessing techniques. In addition, corrections for scanner look angle, sun angle, etc. must frequently still be applied. Additional work remains to be done to determine the effect of such line averaging techniques on the quality of the data for agricultural vegetation and soil analysis problems.

SUMMARY AND GENERAL CONCLUSIONS

The work this past year has indicated more clearly than ever before that when dealing with natural vegetative soil and hydrologic features, the natural variability of these materials is significant. However, as indicated in Figure 15, there are several other factors besides the natural geographic variation of the materials which can cause distinct and significant variation in the signals being recorded. We are looking forward with great anticipation to working with data from ERTS and SKYLAB, since data collected in these experiments will be obtained over a large geographic area and in an extremely short time period (as compared to the time required to collect the flightline data using an aircraft system), and also the satellite data will involve a much smaller scan angle. The ERTS and SKYLAB data should therefore allow some of the causes of spectral variability such as illumination conditions, instrumentation drift and adjustments, and atmospheric conditions (which change over time), to be minimized. This will allow us to better

understand the regional variation and spectral response of the vegetation, water, and soils, with which the Biogeophysical Group at LARS is particularly concerned.

Conclusions of the projects this past year involve several additional aspects, which can be summarized as follows:

1.) Basic cover types can be automatically mapped with a high degree of accuracy in spite of the natural variability of the material.
2.) Calibration of scanner data allows significant improvement in the accuracy of classification of crop species when extrapolating from one geographic area to another many miles away.
3.) Calibration and preprocessing techniques significantly improve many aspects of data quality. However, these techniques must be applied to the multispectral scanner data with caution, for they could cause more harm than help in the automatic classification of any particular set of data. For example, under conditions of variable cloud cover, sun sensor calibration proved quite unsatisfactory. In general, however, it would appear that drift and illumination calibration will generally be required for aircraft data collected over large geographic areas.
4.) Variations in ground cover conditions often are much more pronounced than anticipated. However, adequate training of the classifier, involving selection of samples to represent the total range of crop conditions and stages of maturity, did allow satisfactory classification of the data. Studies involving adaptive classification techniques must be developed and tested.
5.) Preliminary work on aerial estimates of acreage of major crop species and various other cover types for areas in excess of 300,000 acres indicated a high degree of accuracy, and offers good promise for improving current techniques for such acreage estimates. It is significant that these results were obtained with scanner data that had not been geometrically corrected. This technique also appears to offer another method of evaluating the accuracy of classification results, provided the area sampled is large enough, and that the existing acreage figures from other sources are reasonably accurate.

It is believed that these results concerning a developing capability to accurately identify and map various agriculture cover types and obtain accurate acreage estimates (as were indicated in Figure 18) are among the major milestones that have been achieved in automatic data analysis research to date.

ACKNOWLEDGEMENT

Appreciation is expressed to the Airphoto Interpretation and Photogrammetry Laboratory, School of Civil Engineering, Purdue University for use of the Highway 37 scanner and photographic data.

All aircraft scanner data and the 40-county photographic data used were collected by the Institute of Science and Technology, University of Michigan.

The research summarized herein was supported by NASA under Grant NGL 15-005-112. Grateful appreciation is expressed to NASA for this support.

The various individual studies were carried out by Dr. Jan Cipra, Research Agronomist at LARS; Mr. Eric Stoner, graduate student; Mr. Forrest Goodrick, Research Forester at LARS; Mr. Gary Johnson, graduate student; Dr. Christian Johannsen, Assistant Professor of Agronomy; Mr. Phillip LeBlanc, graduate student; Mr. Luis Bartolucci, graduate student; as well as the author.

REFERENCES

1. Hoffer, R.M. 1968. Biophysical Research at LARS-PURDUE. Earth Resources Aircraft Program Status Review, NASA Manned Spacecraft Center, Houston, Texas. Volume II, pp. 31-1 to 31-28.

2. Hoffer, R.M. and F.E. Goodrick. 1970. Geographic Considerations in Automatic Cover Type Identification. Proceeding of Indiana Academy of Science. (In press)

3. Johnson, Gary E. 1971. Land-Use Evaluation Via Remote Multispectral Sensing Techniques. Unpublished Ph.D. Thesis, Department of Geography and Geology, Indiana State University, Terre Haute, Indiana.

4. Laboratory for Agricultural Remote Sensing. 1970. Remote Multispectral Sensing in Agriculture; Volume No. 4, (Annual Report). Research Bulletin No. 844, Agricultural Experiment Station, Purdue University, Lafayette, Indiana. 112 p.

5. Phillips, Terry L. 1969. Calibration of Scanner Data for Operation Processing Programs at LARS. Information Note 071069, Laboratory for Applications of Remote Sensing, Purdue University, Lafayette, Indiana. 7 p.

TABLE I. CLASSIFICATION ACCURACY FOR TEST FIELDS IN AN EAST-WEST 133-MILE FLIGHTLINE, USING DRIFT AND GAIN CALIBRATION

Spectral bands: Best 5 bands when using 2-point calibration--0.50-0.52, 0.55-0.58, 0.66-0.72, 1.00-1.40, and 1.50-1.80.

Calibration: 2-point (drift and gain)

	Percent Correct Recognition			No. Test Fields	No. Data Points Used to Calculate Percentage Accuracy
Flightline	Overall	Wheat	Other Cover Types	Wheat/Other	Wheat/Other
40	96	92	96	10/10	519/2749
41	77	78	77	13/21	874/1430
42	82	79	84	8/13	802/1202
43	96	96	96	3/12	301/6322

Overall accuracy for all four flightlines = 91.2%; average accuracy for four flightlines = 87.8%.

TABLE II. CLASSIFICATION ACCURACY FOR TEST FIELDS;
BEST 5 WAVELENGTH BANDS WHEN USING DRIFT CALIBRATION ONLY

Spectral bands: Best combination of 5--0.55-0.58, 0.66-0.72, 0.80-1.00, 1.00-1.40, 1.50-1.80.
Calibration: Drift only

	Percent Correct Recognition*		
Flightline	Overall	Wheat	Other Cover Types
40	94	89	95
41	74	68	76
42	65	74	59
43	81	66	82

*Number of test fields and data points used to calculate percentage accuracy of classification results are identical to those shown in Table I.

TABLE III. CLASSIFICATION ACCURACY FOR TEST FIELDS; DRIFT CALIBRATION ONLY

Spectral bands: Same bands utilized as for classification (shown in Table II) using 2-point calibration--0.50-0.52, 0.55-0.58, 0.66-0.72, 1.00-1.40, 1.50-1.80.
Calibration: Drift

	Percent Correct Recognition*		
Flightline	Overall	Wheat	Other Cover Types
40	93	92	93
41	50	71	41
42	49	77	30
43	70	71	71

*Number of test fields and data points used to calculate percentage accuracy of classification results are identical to those shown in Table II.

TABLE IV. CLASSIFICATION ACCURACY FOR TEST FIELDS IN FIVE FLIGHTLINES IN TIPPECANOE COUNTY, INDIANA

Flightline	Cover Type					
	Corn	Soybeans	Forages	Water	Soil	Trees
21	4388/4144*	4169/4115	6700/6420	212/212	1037/933	168/154
22	8376/8218	3770/3512	5627/5440	310/310	611/560	540/537
23	11494/10081	6201/5551	8245/7922	658/657	132/124	606/602
24	8643/8004	3800/3176	8178/7989	166/164	344/249	385/384
25	6521/6236	4266/4008	6814/6678	237/237	713/600	591/590
Totals	39422/36683	22206/20362	35564/34449	1583/1580	2837/2466	2290/2267
Percentage Classification Accuracy-93.1% (by cover type)		91.7%	96.9%	99.8%	86.9%	99.0%

*Number of R.S.U.'s Present in Test Fields for Each Cover Type/Number R.S.U.'s Correctly Classified Into Each Cover Type.

TABLE V. COMPUTER CLASSIFICATION RESULTS FOR THE ENTIRE AREA OVERFLOWN (83,072 ACRES)

Flightline	Total Data Points	Cover Type						
		Corn	Soybeans	Forages	Water	Soil	Trees	Cultural and Other
21	446,810	102,428	101,361	167,786	1292	4350	24,168	45,428
22	391,118	127,859	65,469	131,461	1371	3992	25,190	35,776
23	495,388	111,996	72,302	219,567	5087	4508	38,728	43,200
24	449,690	122,604	84,904	130,823	1390	4306	64,268	41,395
25	505,232	125,440	73,890	230,762	2019	6801	29,328	36,992
Totals	2,288,238	590,327	397,926	880,399	11,159	23,957	181,679	202,791
Percentage	100.0%	25.8%	17.4%	38.5%	0.5%	1.0%	7.9%	8.9%

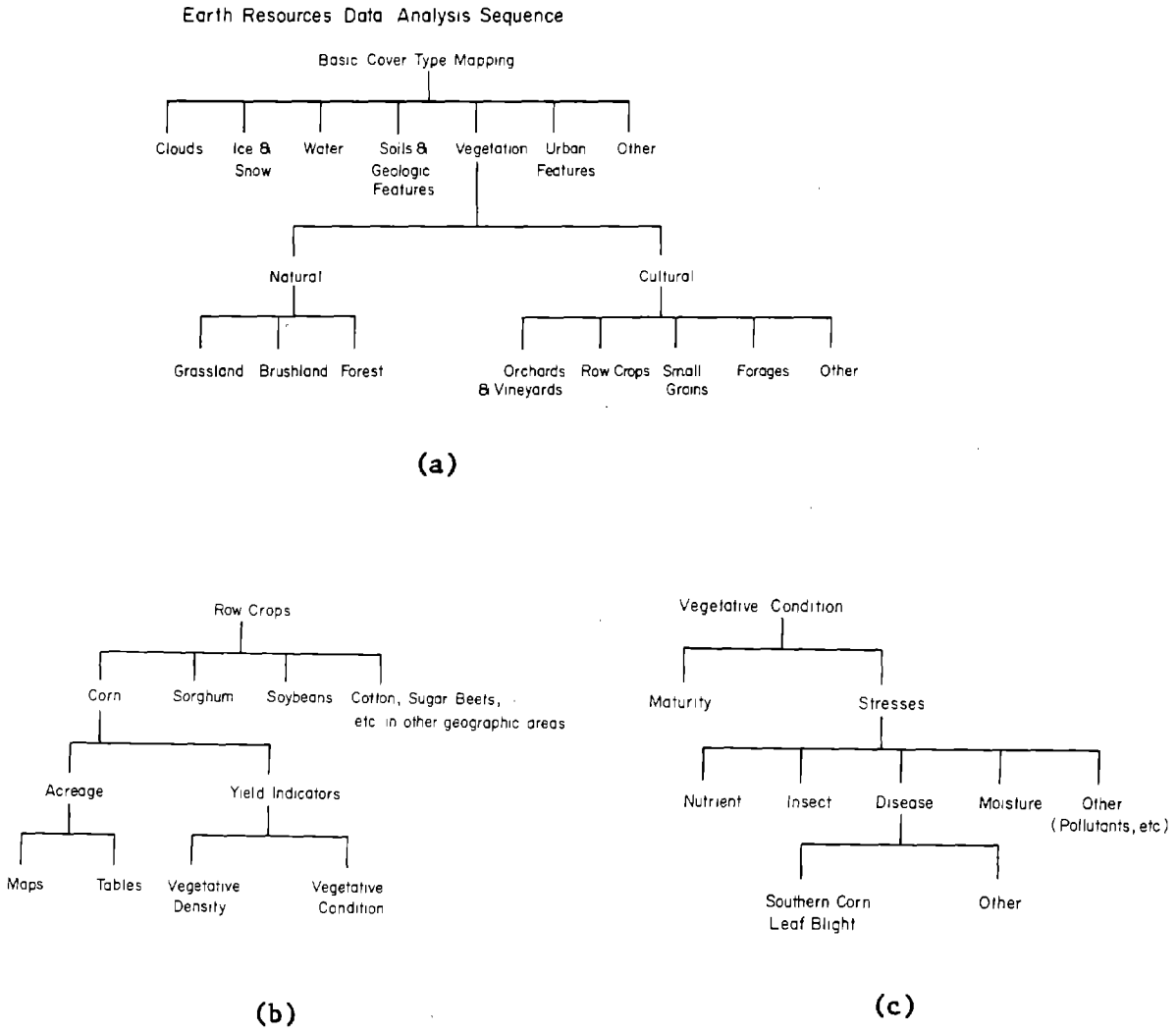

Figure 1. Data analysis sequence in automatic identification and mapping of various earth resources and their condition. Figure 1-a shows the basic cover types that could be mapped and one possible subdivision for the vegetative category. The acreage and yield factors are of primary concern for each species of concern, as pointed out in 1-b. The complex interactions of many stress factors, all of which may influence spectral response of the vegetation being sensed, are indicated in 1-c.

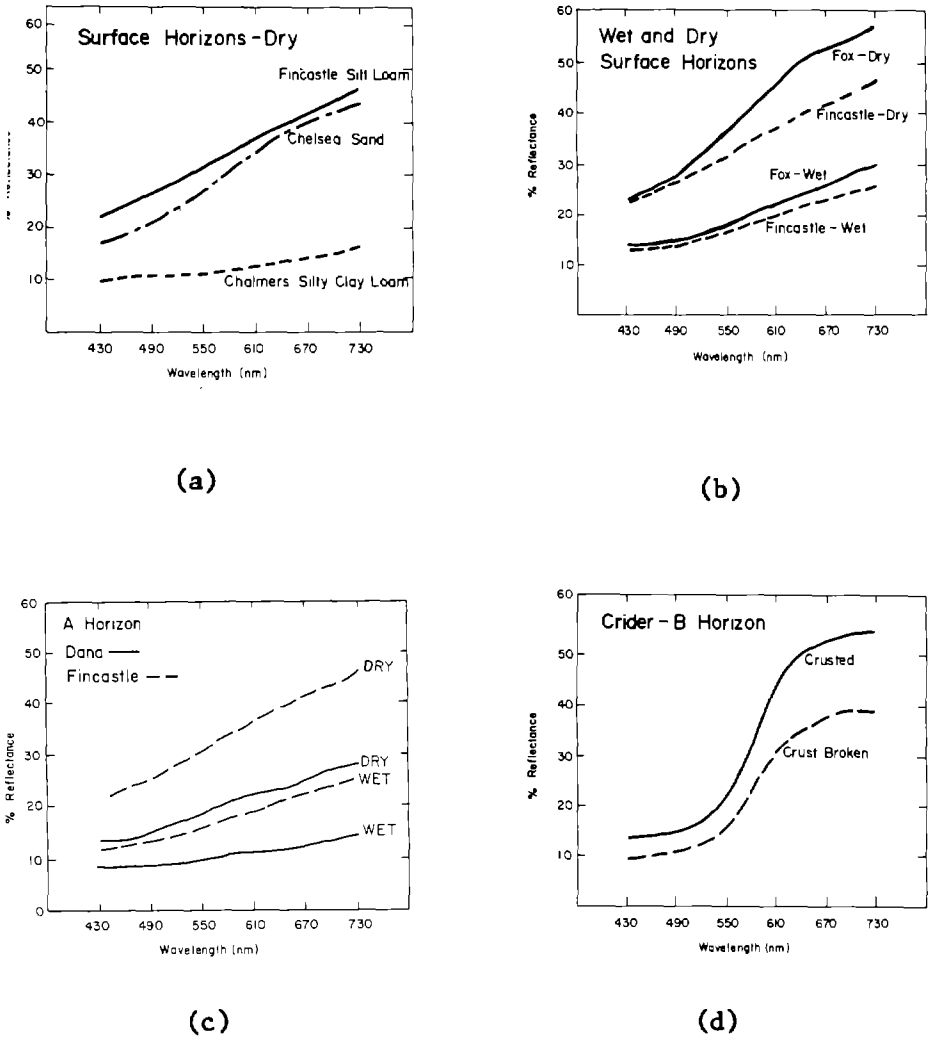

Figure 2. Spectral reflectance of various soil conditions. These data were obtained in situ under conditions of natural illumination. Figure 2-a shows reflectance of three soil types in a dry condition, while 2-b shows marked differences in reflectance between wet and dry soils for two soil types. Figure 2-c indicates that the reflectance for some soil types in a dry condition is very similar to the reflectance of other soils that are wet. The surface condition of a dry soil can cause significant differences in spectral reflectance, as shown in 2-d.

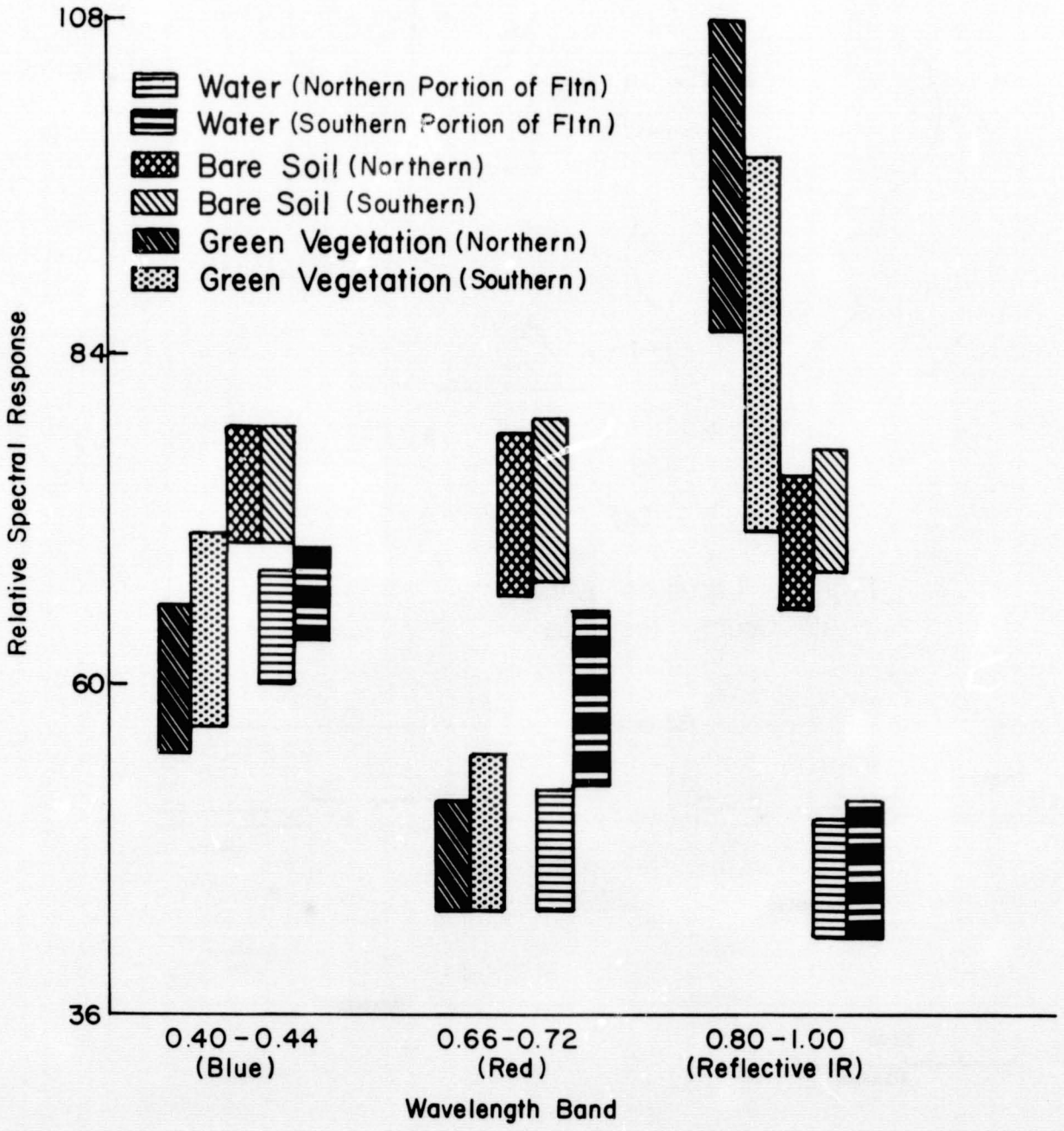

Figure 3. Spectral variabilitv of basic cover types along a North-South flightline. Data from areas about 60 miles apart are shown for three wavelength bands. The bars represent mean spectral response ±1σ. Distinct differences exist for the water and the vegetation response between the two locations sampled.

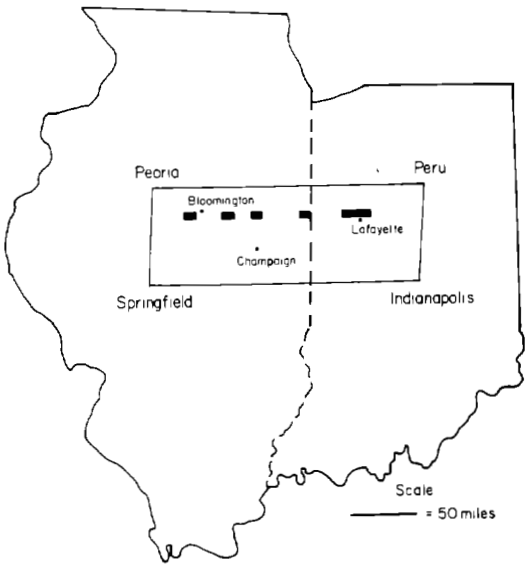

(a)

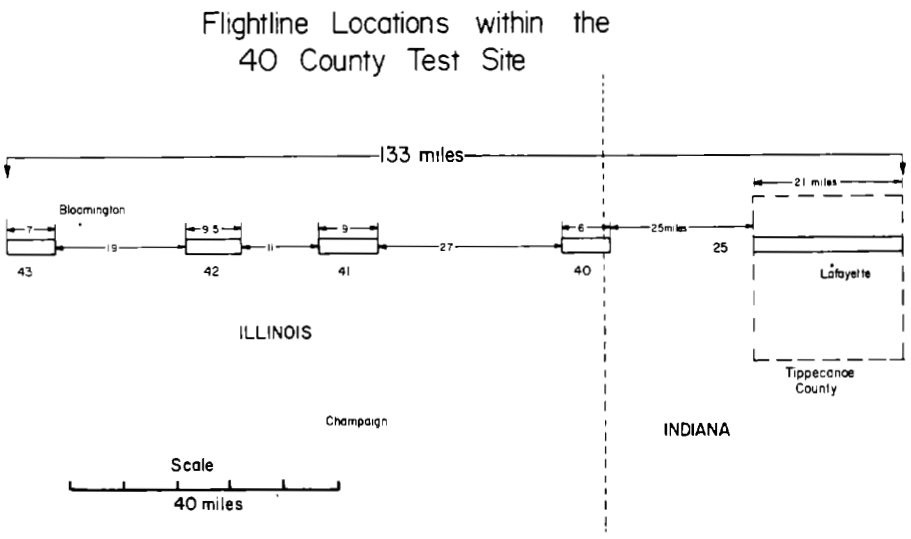

(b)

Figure 4. The 40-County test area showing the general location of the flightlines is shown in 4-a. The length of the flightline segments and distances between segments is shown in 4-b.

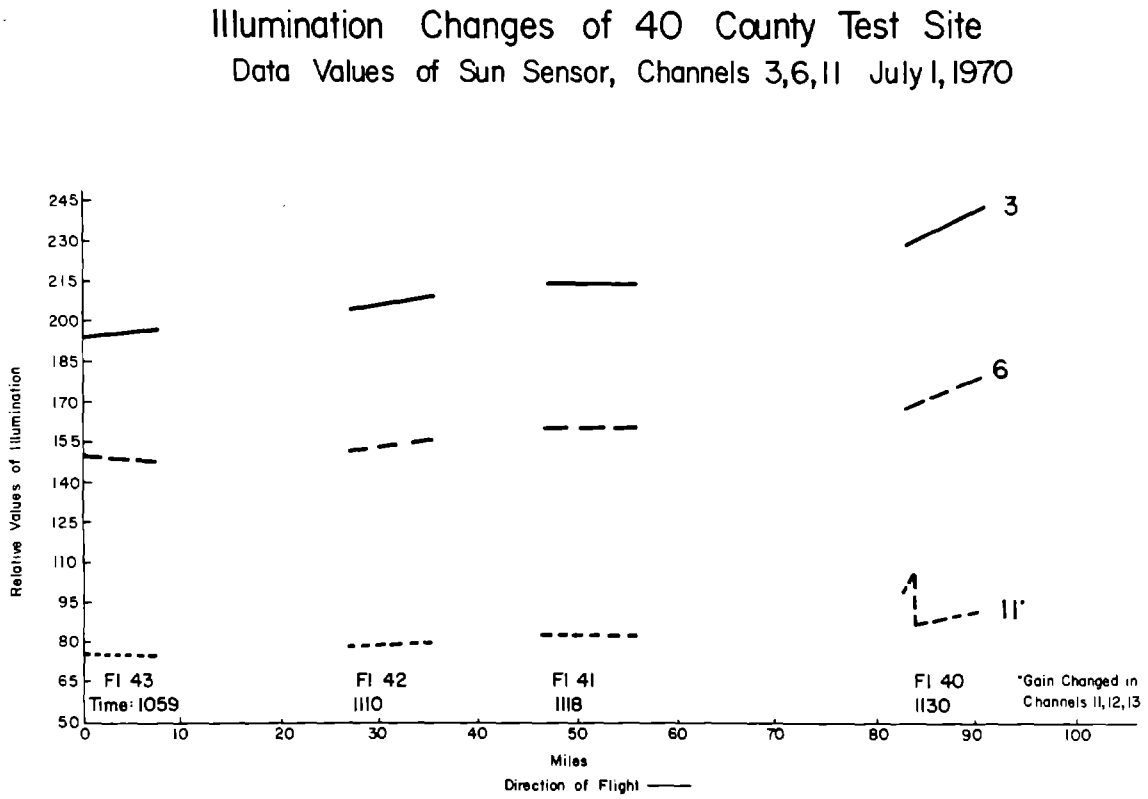

Figure 5. Sun sensor signals in three wavelength bands, along E-W flightline. Time of data collection is also shown, and indicates a general upward shift in illumination levels from west to east as the data were being collected. A distinct change in gain setting is indicated in the Channel 11 data in F.L. 40. These changes were corrected in the calibration procedures.

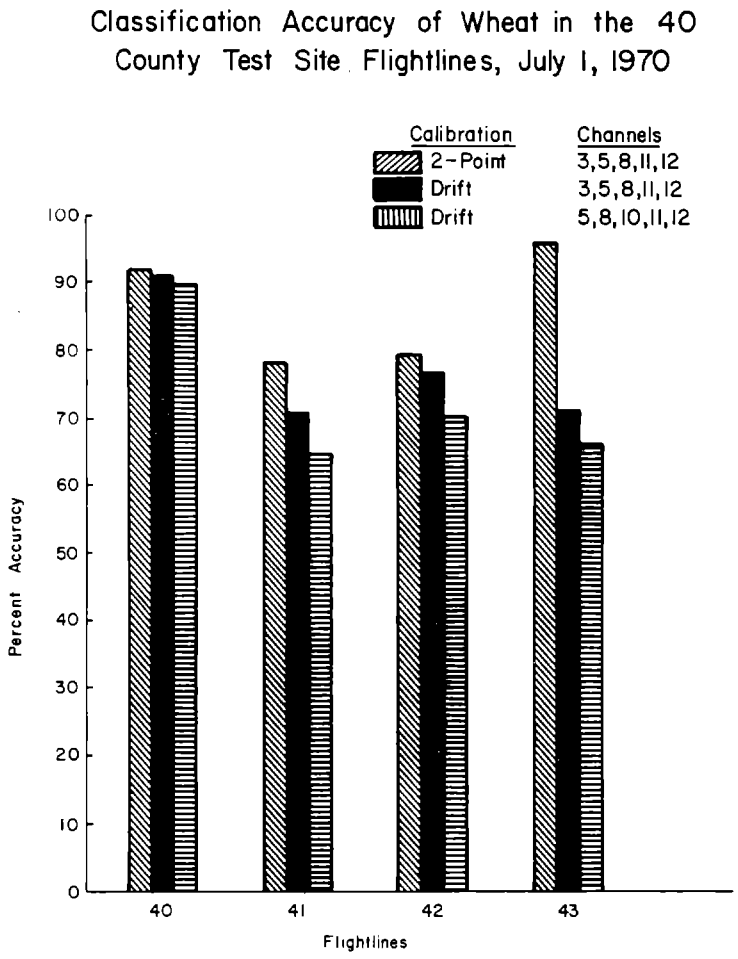

Figure 6. Classification accuracy for wheat test fields in each of the flightline areas. Only F.L. 40 was used for selection of training samples. The 2-point calibration (drift and sun sensor) appears to give much more accurate classification results than drift calibration only. Note that F.L. 40 (where the training samples were selected), is approximately 80 miles from F.L. 43.

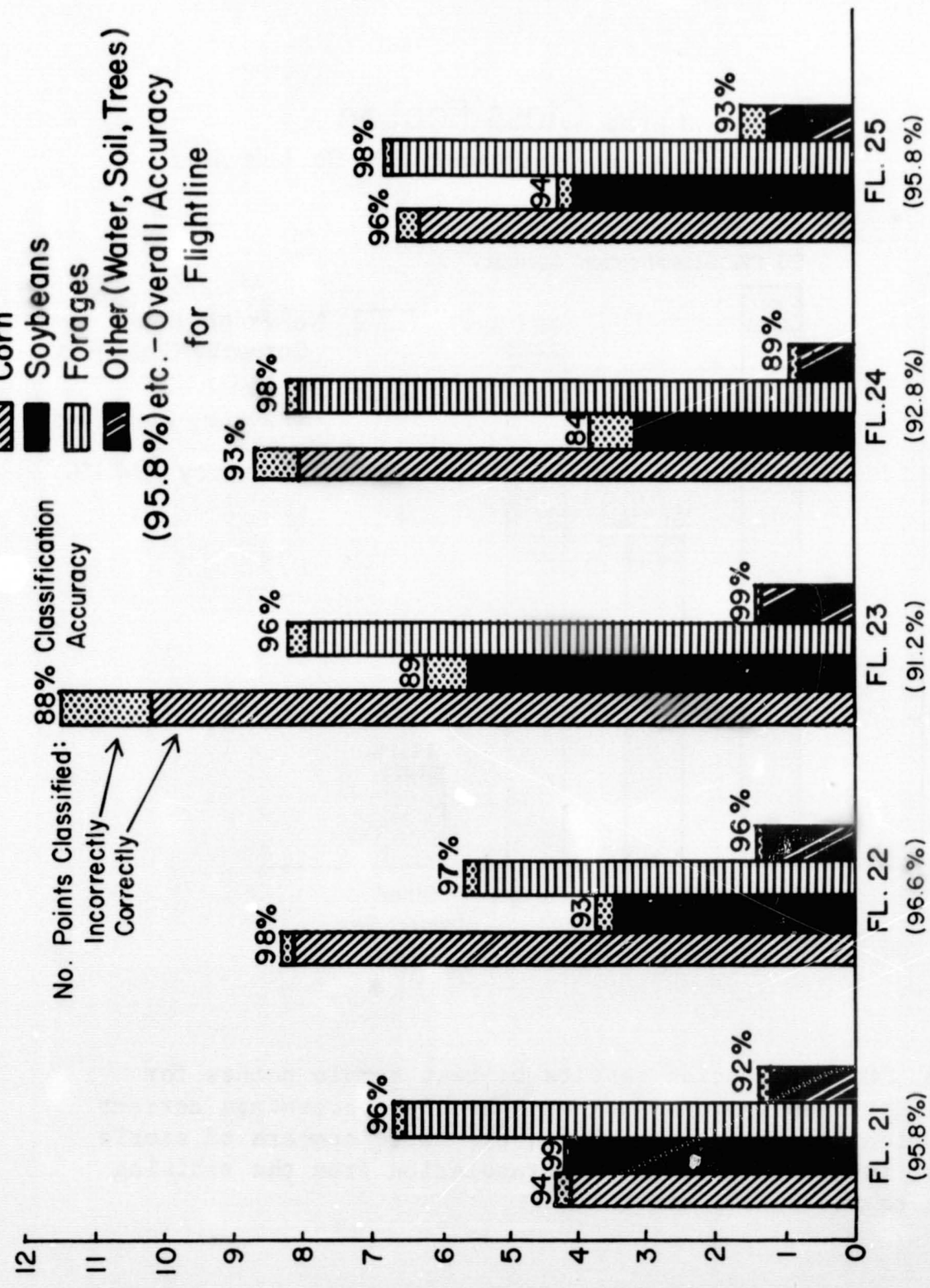

Figure 7. Classification results of test fields in each of the five flightlines. Note that a large number of individual sample points were utilized in determining percentage accuracy.

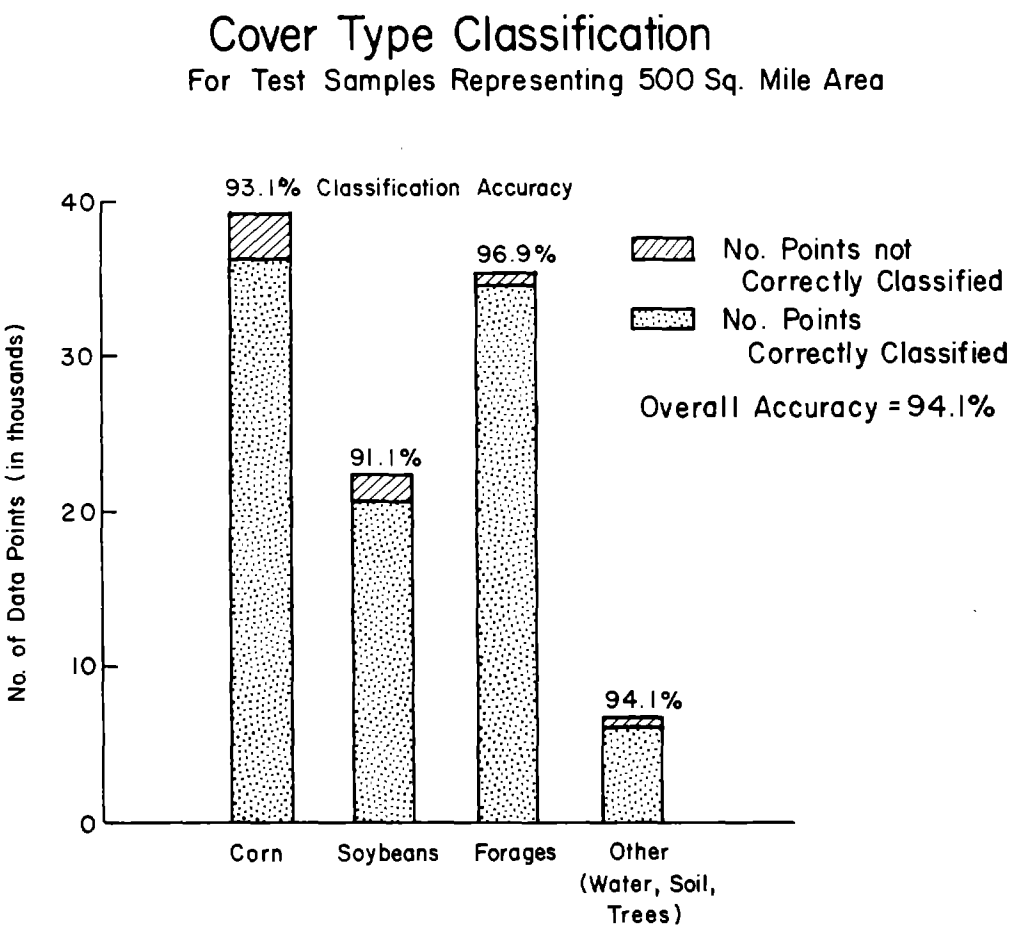

Figure 8. Classification results of test sample points for all flightlines in combination. The high percentage correct classification shown, along with the large numbers of sample points, indicates very good extrapolation from the training fields to the entire area.

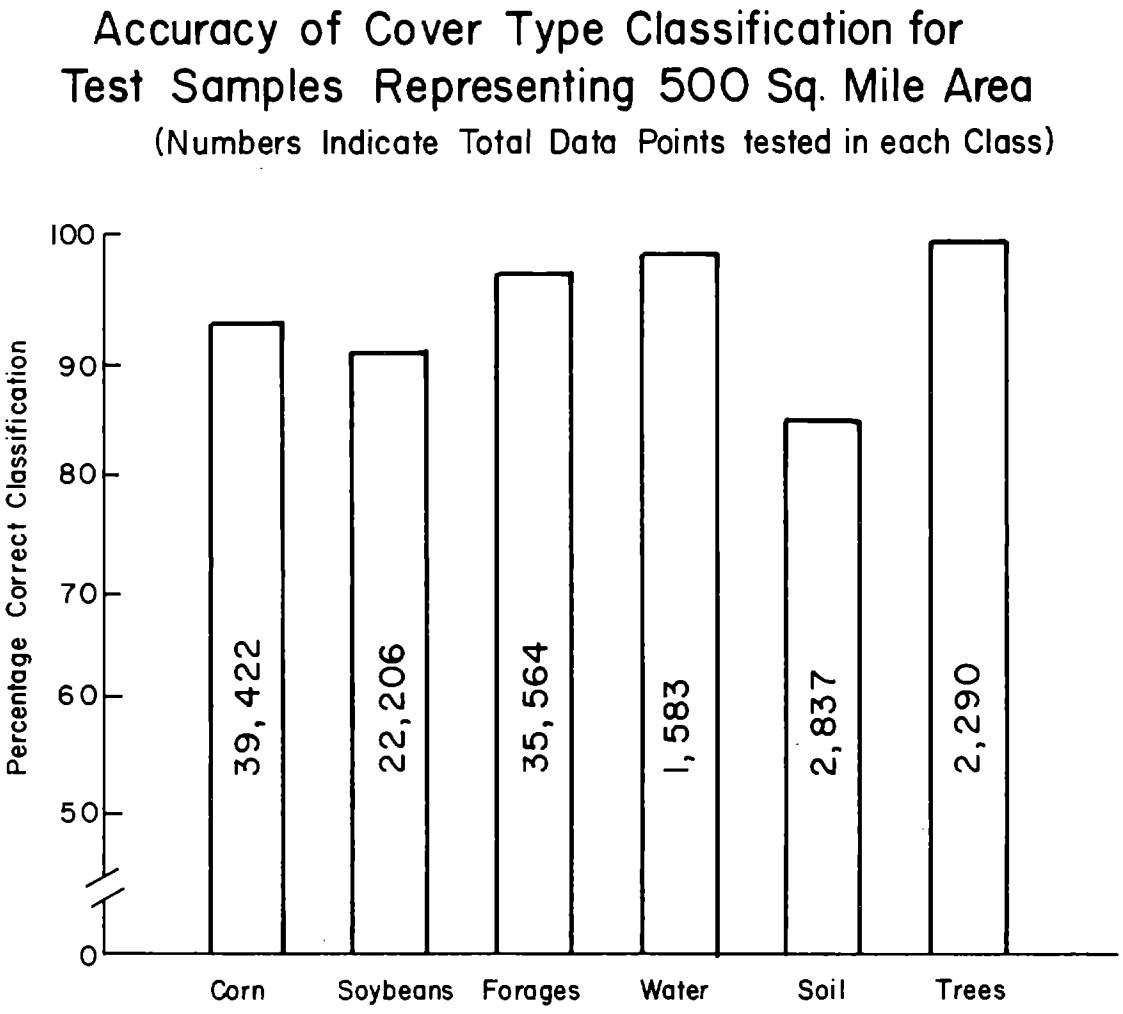

Figure 9. Accuracy of classification of test samples. The accuracy and number of data points involved are indicated. The individual classes of water, soil and trees (previously combined as "other") are also shown.

ADP Results of Acreage Estimates
(Actual Area = 322,560 Acres)

Cover Type	Computer Classification Acreage Estimate*	Percentage of Total Area
Corn	84,210	26.0
Soybeans	56,760	17.5
Forages (Hay, Pasture, Stubble)	123,020	38.0
Woods	25,940	8.0
Urban & Other (Roads, Water, Misc.)	33,920	10.5
Total =	323,850 Acres	100%

*An Estimated 83,072 Acres Were Scanned

Figure 10. Acreage estimates of major cover types in Tippecanoe County, based upon computer classification of the various cover types. The cover types have been combined to facilitate comparison with published figures of acreage estimates.

Comparison of Acreage Estimates for a 322,560 Acre Area

Cover Type	Computer Classification of MSS Data	Census of Agriculture	Crops and Livestock Report
Corn	84,210	82,510	76,900
Soybeans	56,760	60,470	56,900
Forages	123,020	109,860	———
Woods	25,940	21,210	———
Urban & Other	33,920	———	———
Total =	323,850 Acres		

Figure 11. Comparison of acreage estimates based upon automatic classification of multispectral scanner data to published estimates of various cover types for Tippecanoe County. Note that estimates by different agencies have a moderate amount of variation, and that the estimates obtained by remote sensing techniques are relatively close to the other estimates.

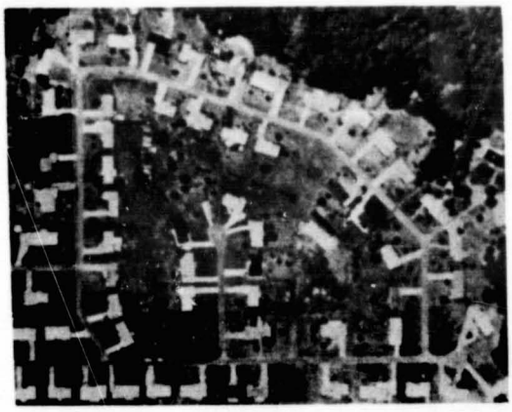

(a)

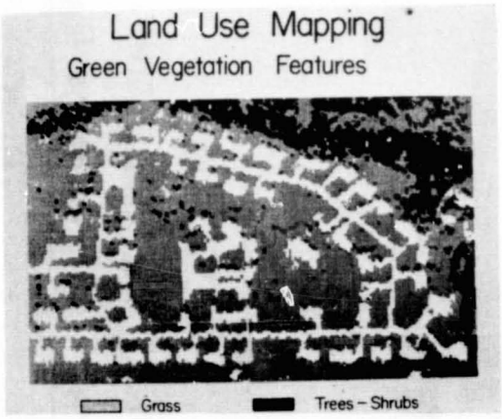

(b)

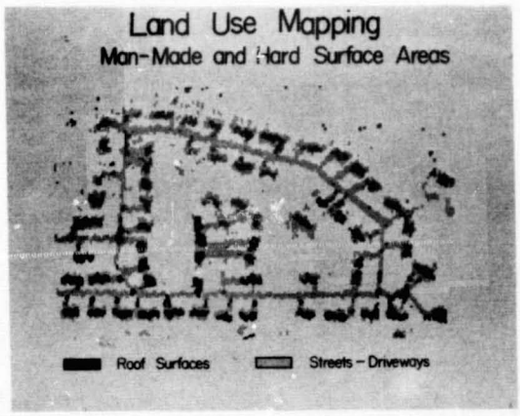

(c)

COMPARISON OF RESULTS

Material	Computer Classification	Estimate
Roof	8.0	8.2
Asphalt	10.1	7.6
Concrete	6.3	5.7
Trees	15.2	18.6
Grass	60.1	59.9

(d)

Figure 12. (a) Black and white reproduction of a color infrared photo of subdivision study area. (b) Computer printout of classification results showing only areas classified as tree & shrubs or as grass. (c) Printout of areas classified as man-made and hard surface area. (d) Percentage of total area classified into the various cover types by computer compared to area percentages estimated by a very fine dot grid and using an aerial photo.

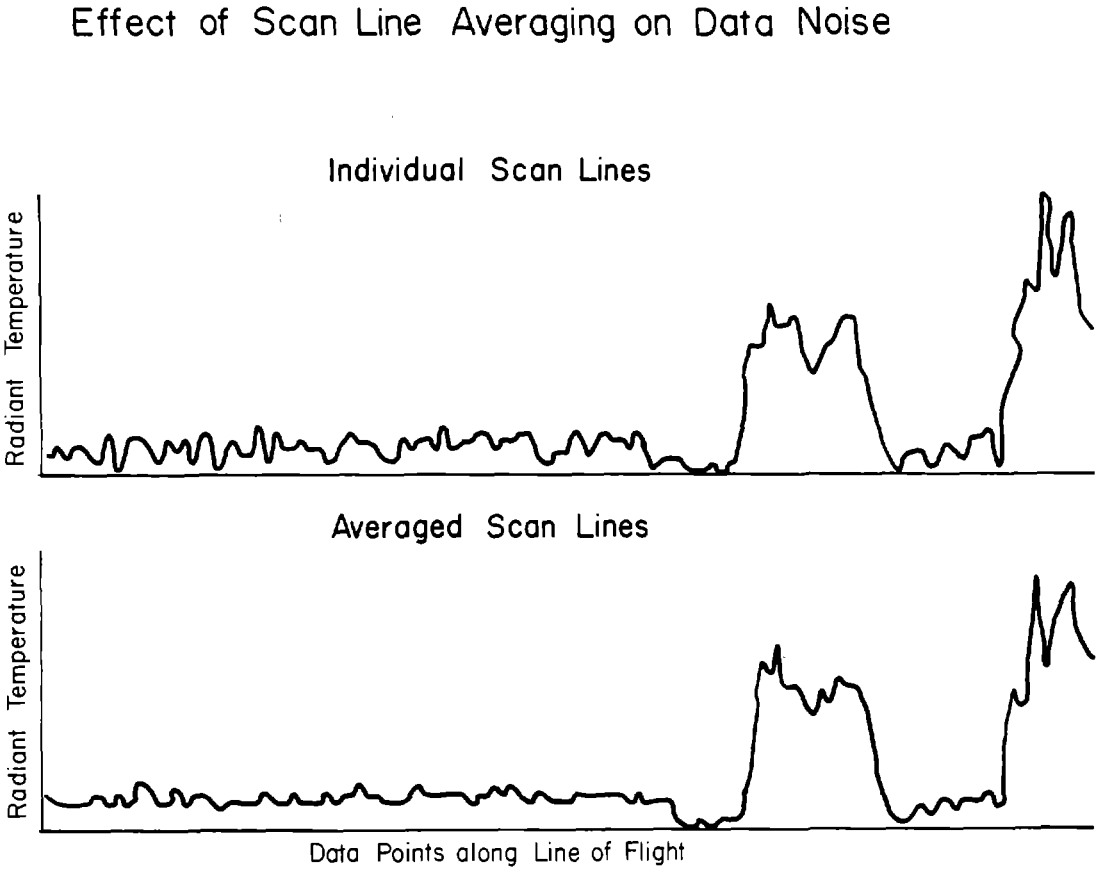

Figure 13. Effects of scan line averaging on data noise. Data on top shows data points along the line of flight for a single column of data, using non-averaged scan lines. Bottom data shows averaged scan lines. The reduction in the amount of noise in the data is evident.

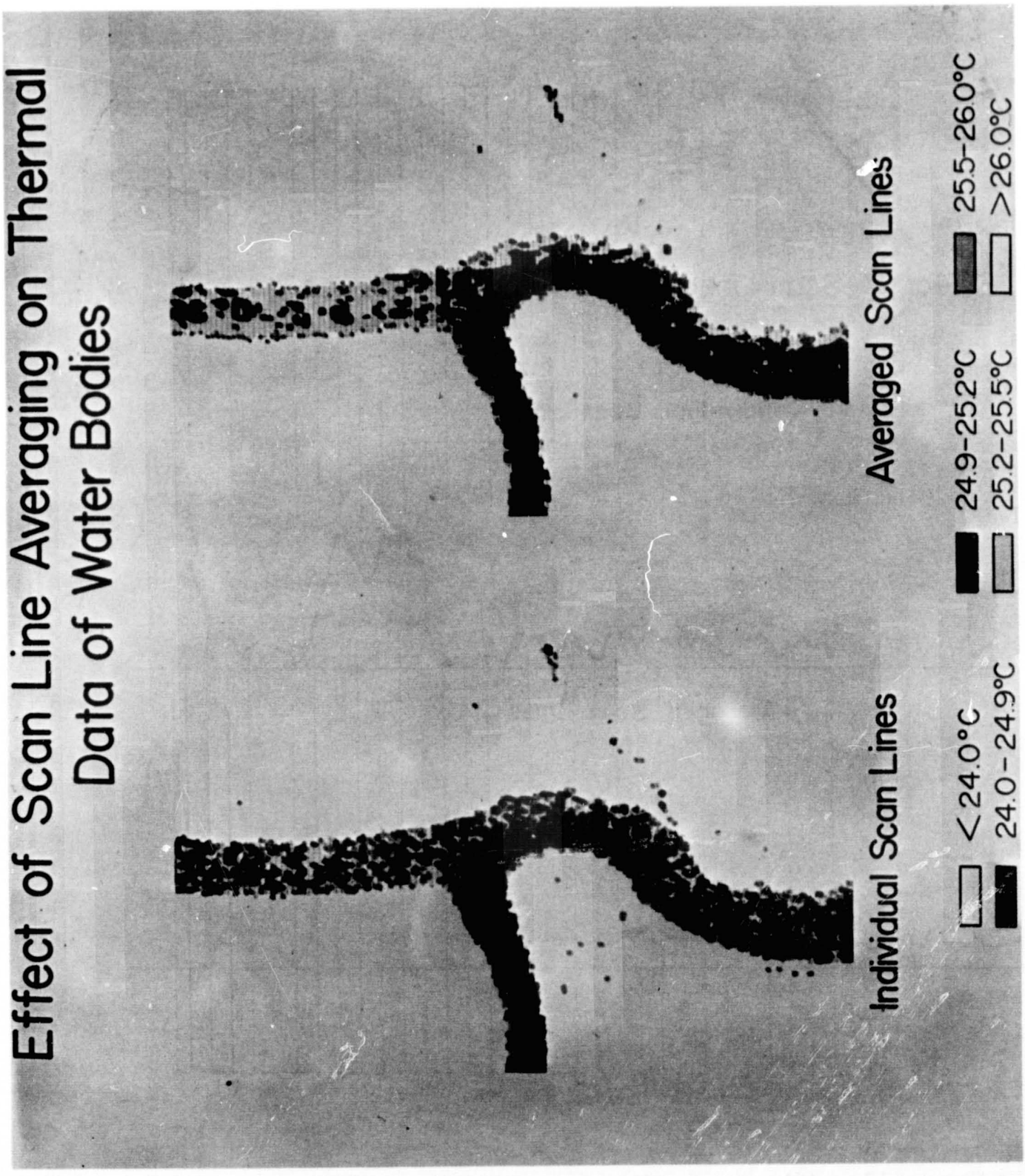

Figure 14. Computer printout of thermal data calibrated to indicate true radiometric temperature, and comparing individual scan lines and averaged scan lines of data. Note the more distinct "speckled" pattern in the individual scan line data, particularly in the portion of the Wabash River above the point where the Tippecanoe River comes in from the left (west).

Causes of Spectral Variability

- Natural, Geographic Variation of the Materials
- Illumination Conditions
- Atmospheric Conditions
- Instrumentation Drift and Adjustments
- Data System Imperfections

Figure 15. Major causes of spectral variability. Satellite data from ERTS and SKYLAB should allow some of these factors to be minimized (as compared to aircraft data collection techniques) thereby allowing a better understanding of the natural geographic variations of the vegetation, soils, water, and other earth resources materials of concern.

SECTION 49 N72-29349 49-1

MEASUREMENTS PROGRAM IN REMOTE SENSING AT PURDUE UNIVERSITY *

by

LeRoy F. Silva and Staff
Laboratory for Applications of Remote Sensing (LARS)
Purdue University
West Lafayette, Indiana

INTRODUCTION

The measurements program at LARS/Purdue has been concerned with five basic research areas during 1971. These areas are (1) the influence of haze layers upon remotely sensed surface properties, (2) electrical methods of soil moisture measurement, (3) thermographic studies of vegetation under nutritional stress, (4) improved field spectroradiometry, and (5) biological spectrophotometry.

All of these projects have risen out of problems generated from the overall laboratory mission. The emphasis in this paper is on instrumentation and techniques; whereas, related data and results on specific projects will be reported elsewhere. Each of the subject areas will be discussed individually.

INFLUENCE OF HAZE LAYERS ON REMOTELY SENSED SURFACE PROPERTIES

During the analysis of data gathered for the 1971 Corn Blight Watch Experiment a number of unexpected features were observed. One of particular interest was the appearance of bright and dark sides along the flightline of the aircraft. An example is shown in Figure 1, taken at 10:28 a.m. EST on June 30, 1971, over southern Indiana. The plane was headed south (top of figure) with surface illumination from the east (left) and ahead of the plane. Relative darkness on the left and bright-

---

* In this paper, results from a number of studies are summarized; researchers are identified in the acknowledgment section.

ness on the right is evident in the data as it appeared when displayed in digitized grey levels.

A check of the pilot's log revealed that visibility was estimated to be only 6 miles while hazy conditions were noted below the aircraft. The possibility that the presence of hazy layers may have contributed to the anomalous effects in the data prompted the computation of scattering angles for this flight. These are shown in Figure 2. The scattering angle varies from near side-scattering on the left (east) side of the flightline to near back-scattering on the right (west) side. Since the scattering properties of the aerosols which compose haze layers generally undergo marked variations over this range of scattering angles (Deirmendjian, 1969), an attempt to compute the expected variation of reflected intensities across the flightline was made. It was first necessary to assign physical parameters to the haze. As a first case, the size distribution of Deirmendjian's haze L (Deirmendjian, 1969) was selected as being typical of a continental-type aerosol distribution. His tabulations of the elements of the scattering matrix for a water haze L allowed the computation of the scattering phase function for the scattering angle interval of interest. This function, shown in Figure 3, for a wavelength of 0.45 micrometers undergoes a minimum near 120° from which it rises to a relative maximum at 165° with a secondary minimum between this point and the maximum value for 180° backscatter.

Combination of the computed scattering angles of Figure 2 with the phase function in Figure 3 allowed an estimate to be made of the variation in reflected intensity across the flightline. The result for a wavelength of 0.45 micrometers is presented in Figure 4 as the predicted curve. Lowest values occur along the left (east) side of the flightline. These correspond to minimum values of the scattering phase function near 120°. As scattering angles increase moving to the right (west) intensity increases reaching a peak for 165° scattering angle. Beyond this point the reflected intensity decreases toward the right-hand side of the flightline.

In order to obtain a measure of the agreement between these calculations and the observed intensities, the latter were averaged column-by-column for the total length of the flightline. The resultant values, computed for the 0.46 - 0.49 spectral interval, are shown as the observed curve in Figure 4. The agreement between the two curves is excellent for the left-hand side of the flightline, but differences as large as 30 percent occur near the right-hand side. At the present time, no satisfactory explanation exists for this discrepancy.

Although the agreement for this case between theory and observations is far from perfect, the results are sufficiently encouraging to warrant further study. At the present time, a model of atmospheric attenuation (Elterman, 1970) is being adapted for application to problems of this nature. The Elterman model consists of tabulations of attenuation coefficients at various wavelengths from 0.27 to 4.00 micrometers for several altitudes from the surface to 50 kilometers. The attenuation coefficients account for Rayleigh scattering, ozone, and aerosol extinction in the atmosphere. The manner in which the presence of a haze layer might be included in such a standard model is shown in Figure 5. In addition to reducing the radiation which reaches the surface and is reflected to the aircraft, the haze layer contributes a component through multiple internal scattering. As a result of the combination of these two factors, the spectral nature of the radiation received at the aircraft can be modified. It is hoped that it will eventually be possible to represent the haze layer by parameters such as an effective transmissivity and reflectivity. In this way it will be possible to improve the identification of surface properties from multispectral remote sensed data.

ELECTRICAL METHODS OF SOIL MOISTURE MEASUREMENT

Work on the electrical properties of soil has gone on for several decades. The electrical properties of soils are of interest for two basic reasons.

1. Can field soil moisture measurements be made more easily using some electrical technique?

2. Is it possible to extend the results of electrical measurements to remote sensing soil moisture measurement techniques?

The work of Blanchard[3] and of Rousch[4] concerning the measurement of soil moisture using microwave techniques has been reported elsewhere in these proceedings. Earlier, Davis et al[5] produced a study of the radar scattering characteristics of soils as a function of moisture content.

Purdue researchers decided to study the variation of soil permittivity; that is, a capacitance measurement versus moisture. This decision was made after an extensive literature study indicated that soil salt content strongly influenced results of techniques which depended upon conductivity measurements. The basic sample holder used is a coaxial structure in which laboratory prepared soil samples were inserted. The samples were prepared by mixing a particular soil type with ice in a

cold room and then packing the mixture into the soil sample holder. The sample holder is hermetically sealed so that the moisture content of this system remains stable after the sample holder is loaded. The sample is allowed to rise to room temperature at which time the capacitance (and conductance) of the sample holder and its contents is measured on a standard impedance bridge.

In Figure 6, the capacitance of a sample holder containing a particular soil type at a fixed percentage of moisture is measured as a function of frequency. In principle the capacitance of the sample should be frequency independent. But the presence of salts in the soil sample create free ions which form a polarization layer near the outside surface of the coaxial sample holder. This produces an effective resistance capacitance combination that appears in a series with the actual capacitance resistance combination of the soil sample itself. The capacitance of the soil sample is actually frequency independent; whereas, the capacitance of the polarization layer depends upon frequency due to ion inertia effects. In Figure 6 a theoretical curve based on a simple two-element lump capacitive model is also shown. On the same set of axes, some experimental data for a particular soil sample is also plotted. The difference between the two curves can be explained due to the simplicity of the lumped model. As more elements are inserted and the approximation to the actual distributed capacitance case is approached, one would expect experimental and calculated results to come closer together. Such modeling attempts are currently in progress.

In Figure 7a the relationship between capacitance and soil moisture for a particular soil type is plotted. Some scatter in the data is observed. However, no attempt was made during the preparation of these data to control the compaction and curing time of the sample. Curing time is defined as the period between the time the sample is loaded and the time the sample is measured. One would expect that if these two parameters were controlled that less scatter in the data would result. The important result to be derived from Figure 7 is that a definite well-defined trend does exist between soil capacitance and soil moisture. There is promise that a simple field probe based upon the principle discussed here could be developed that would simplify soil moisture measurements. The problem of extending these results to microwave measurements is considerably more involved and the question of whether a closed form solution exists to the analytical problem that is involved has yet to be determined.

THERMOGRAPHIC STUDIES OF NUTRITIONALLY STRESSED VEGETATION

A Barnes Model T-4 scanning radiometer has been used to study corn plants and leaves under several conditions of nutritional stress. Corn plants grown in a hydroponic green house experiment with controlled nutritional deficiencies were examined in a variety of environments to ascertain leaf-thermal variation. The thermogram of a sulfur deficient corn plant is shown in Figure 8. The sulfur deficient corn plant is in the left-hand portion of the figure, whereas a control healthy corn plant is in the right-hand portion of the figure. The object in the middle of the slide is a blackbody reference. The ambient temperature of this experiment was 24°C. However, the surface located immediately behind both plants was at a temperature of 16.5°C. The nutritionally stressed plant was approximately 1°C cooler than the control plant. This fact would have been difficult to ascertain with a conventional radiometer because of the thermal-spatial variations on the nutritionally stressed plant. Because of the fourth power variation of radiation with respect to temperature the warmer portions of the nutritionally stressed plant dominate the radiation of the whole plant and tend to obscure the actual thermal condition of the plant. The use of the scanning radiometer enables one to finely delineate the temperature profile of a plant when compared to a healthy controlled plant. One observes that the control plant exhibits a relatively uniform thermal-spatial variation. In Figure 9 a similar experiment involving a nitrogen deficient plant is shown. The nitrogen deficient plant exhibits approximately a 2°C cooler temperature again with a 16.5°C background reference surface and a 23°C ambient temperature. In both Figures 8 and 9 the scan time to develop the thermogram was six minutes.

In Figure 10 a thermogram of control and nutritionally stressed corn leaves is shown. From left to right the leaves are: control, three sulfur deficient leaves, a control leaf, three nitrogen deficient leaves, and another control leaf. The scan time used to develop the thermogram was 4 1/2 seconds. A styrofoam surface was used as the background for the corn leaves. A warm surface of approximately 35°C (a heating anemostat) was located near the experiment. The ambient temperature was approximately 23°C. The sulfur deficient leaves are approximately 1°C warmer; whereas, the nitrogen deficient leaves are approximately 2°C warmer than the control leaves.

The preliminary conclusion is that nutritionally stressed plants are not always hotter than a control plant, but apparently are influenced more strongly by environment. It is, therefore, possible for nutritionally stressed plants to be cooler than healthy plants in a similar environment if a cold surface is located nearby. It appears from this

experiment that nutritionally stressed plants are not as well able to control their temperature as a healthy plant in the same environmental situation. Controlled field experiments are being designed to see if this effect can be observed in a natural environment.

AN IMPROVED FIELD SPECTRORADIOMETER

Previously[6] it has been shown that it is essential to have rapid spectral scan capabilities in field spectroradiometric measurement situations. For example, in Figures 11 and 12 data taken with an SG-4 Perkin Elmer Spectroradiometer is shown. In Figure 6 it is seen that during the spectral scan period solar conditions changed which compromised the data that were being observed. To further illustrate the problems of spectral scan time, the same spectrometer was set at a particular wavelength and pointed at a corn plant. The spectrometer was located in an aerial lift system. The wobbles in the data taken at the fixed wavelength are not due to detector noise but are due to the wind disturbing the geometry of the corn plant. These effects are in addition to the appearance and disappearance of the sun due to cloud cover. Therefore, the requirement that relatively rapid spectral scans be available in field spectroradiometers was made evident.

A field spectroradiometer built to specifications developed by the USDA facility at Weslaco, Texas, Stanford University, and Purdue University was built by Exotech, Inc. of Gaithersburg, Maryland. This instrument, designated the Model 20B, has been described in detail at the Michigan Symposium of 1971.[7] In summary, the instrument featured refractive fore-optics and covered the wavelength range from .4 to .5μm and 2.8 to 15μm. Four detectors with Joule-Thompson cooling, circular variable filter wheel spectrum scanning, 1 to 30 second adjustable spectral scans and adjustable field of view from 3/4 to 15° were features of this instrument. Figure 13 shows this instrument under field trial.

Based upon field experience with this instrument, another instrument, designated the Model 20C, has been specified and built by Exotech, Inc. for LARS/Purdue. This instrument features a reflective fore-optic system (Newtonian telescopes), a field calibration system, and an in-line sighting system. In addition, several electronic improvements and an electrical view angle adjustment feature have been included.

A general view of the short wavelength head (.4μm to 2.5μm) along with its control console is shown in Figure 14. The control console is normally located in an instrument van and the operator can control scan speed, detector gain, field of view, and the viewing port inside the instrument van; the look angle and focus are controlled by an operator

located at the instrument head. A close-up of the instrument head is shown in Figure 15. The vertical tube contains a ceramic plate that approximates a Lambertian receiver so that the solar irradiance can be spectrally monitored almost simultaneously with the target radiance. The detectors are sensitive to either the solar irradiance or the target radiance, depending upon a position of a mirror within the instrument that is controlled by the operator. The view angle adjustment of the instrument is shown in Figure 16, whereas the features of the Newtonian telescope fore-optical system are illustrated in Figure 17.

The internal structure of the chopper module is shown in Figure 18. The chopper wheel, visible in the middle of the chopper module, is arranged so that each of the two detectors in the instrument head are alternately exposed to the incoming radiation and a blackbody reference located within the instrument. The circular variable filter wheels are joined together by a timing belt and are located between the detectors and a set of relay optics which focus the impinging radiation on the appropriate detector. The low noise pre-amplifiers are located in close proximity to the detectors and a carefully designed grounding system is used to minimize noise pick-up. Hall-Effect motors are used to avoid brush arcing effects. The Joule-Thompson cooling assembly is illustrated in Figure 19. Joule-Thompson coolers are used in preference to conventional liquid nitrogen cooled dewars so as to permit a wide range of instrument head operating angles. Some typical data that has been reported elsewhere[6] is shown in Figure 20.

The data from the instrument is recorded on a seven-channel analog tape recorder which is then subsequently digitized in the laboratory's analog to digital conversion system. A software system has been developed which enables the user to present the data in calibrated form in a variety of formats.

A BIOLOGICAL SPECTROPHOTOMETER

A new spectrophotometer, shown in Figure 21, designed expressly to obtain data on intact biological samples, has been recently developed. The radiation, which interacts with the specimen and is subsequently measured, is influenced by the absorption, distribution of the absorbing substances, light scattering, and geometry of the specimen. In order to quantify these factors, the primary design criterion was to develop a monochromator having high power output consistant with good quality spectra. High incident power contributes to improved spatial resolution and geometrical measurements of the radiation reflected or transmitted by the specimen as well as permitting greater freedom in the selection of the detectors.

The instrument source is a quartz iodine lamp. The lamp filament is at the focal point of the first or collimating mirror and replaces the entrance slit of a conventional monochromator design as shown in Figure 22. The lamp is water cooled and baffled in such a way that the light that enters the monochromator is restricted to that which is actually used by the optics of the system.

The primary dispersion element is a 5" x 6" defraction grading blazed at 600 nm. A linear variable-wavelength filter for order sorting and reducing stray light is located at the exit slit, and the movement of the filter is synchronized with the grading rotation. A reference cell is used to monitor the output of the monochromator.

Assemblies for measuring bi-directional reflectance and large area reflectance are shown in Figures 23 and 24. Typical data obtained from the bi-directional reflectance is shown in Figure 25 following procedures outlined by Breece and Holmes.[8]

The DC measurement system is available where the output of the detector is fed directly to an operational amplifier. Either linear or logarithmic output can be used. This system is very easy to operate and provides a means of radiation measurement for any source such as flourescence where light chopping cannot be accomplished easily. The chopped light system is also incorporated in the instrument in conjunction with a commercial lock-in amplifier and provides a lower noise equivalent power than the DC system.

Data are recorded on an XY recorder or may be recorded in digital form or subsequent digital processing. For normal use the data requires corrections for spectral response and wavelength. And the system is set up so that these corrections are subsequently made by a computer.

The performance summary of the system follows.

monochromator output power: (1000 watt lamp), 700nm, 10^{-2} watts
band pass: 10nm
wavelength range: 350 to 1200nm
scanning speed: .03nm/sec to 30nm/sec
detector noise equivalent power: 530nm
photomultiplier: 10^{-15} watts
recording-analog, XY recorder: 8 1/2" x 11"
digital paper tape, direct computer interface, record interval 10nm

The transmittance assembly capable of measuring the transmittance of fixed specimens is also included in the basic instrument structure. Transmittance spectra of specimens as thick as a grapefruit can be easily obtained on this instrument. A large reflectance assembly was designed

to provide a means for obtaining an area integrated reflectance measurement. Detector geometry can be modified to suit the experimental requirements. The bi-directional assembly was used to obtain reflectance data as a function of angle of incidence and angle of detection. The coordination of this instrument with the field spectroradiometer described in the previous section enables the researcher to develop a complete laboratory-field experimental design on many natural systems.

ACKNOWLEDGMENTS

The work described in this report represents the work of many investigators. They are as follows:

1. Influence of Haze Layers on Remotely Sensed Surface Properties
   Prof. Gerald Jurica, Mr. William Murray

2. Electrical Methods of Soil Moisture Measurement
   Prof. Floyd V. Schultz, Mr. James Zalusky

3. Thermographic Studies of Vegetation Under Nutritional Stress
   Dr. Hasan Al-Abbas, Prof. LeRoy F. Silva, Mr. Frederick L. Phillips

4. Improved Field Spectroradiometry
   Mr. Barrett Robinson, Mr. Robert Haselby, Prof. LeRoy F. Silva

5. Biological Spectrophotometry
   Dr. Gerald Birth

The work described in this paper was supported by NASA under contract #15-005-112.

REFERENCES

(1) Deirmendjian, D., 1969. Electromagnetic Scattering on Spherical Polydispersions. New York, American Elsevier Publishing Co., 290 pp.

(2) Elterman, L., 1970. Vertical-Attenuation Model with Eight Surface Meteorological Ranges 2 to 13 Kilometers. Air Force Cambridge Research Laboratories, Environmental Research Papers No. 318, Bedford, Mass., 56pp.

(3) Blanchard, B., 1972. Measurements from Aircraft to Characterize Watersheds, 4th Annual Earth Resources Program Review: NASA, Houston, Tex. Jan. 17-21, 1972.

(4) Rouse, J. A Coactive Interdisciplinary Research Program with NASA, 4th Annual Earth Resources Program Review: NASA, Houston, Tex. Jan. 17-21, 1972.

(5) Davis, B.R., J.R. Lundien, and A.N. Williamson, Jr., Feasibility Study of the Use of Radar to Detect Surface and Ground Water, Technical Report No. 3-727, U.S. Army Engineer Waterways Experiment Station, Corps of Engineers, Vicksburg, Mississippi, April, 1966.

(6) Remote Multispectral Sensing in Agriculture, Laboratory for Agricultural Remote Sensing, Volume 2 (Annual Report), p. 55, July, 1967.

(7) Silva, L., R. Hoffer, and J. Cipra, Extended Wavelength Field Spectroradiometry, Proceedings of the Seventh International Symposium on Remote Sensing of Environment, Volume II, P. 1509, May, 1971.

(8) Breece, H., III, and R. Holmes, Bidirectional Scattering Characteristics of Healthy Green Soybean and Corn Leaves in vivo, Applied Optics, Volume 12, p. 119, January, 1971.

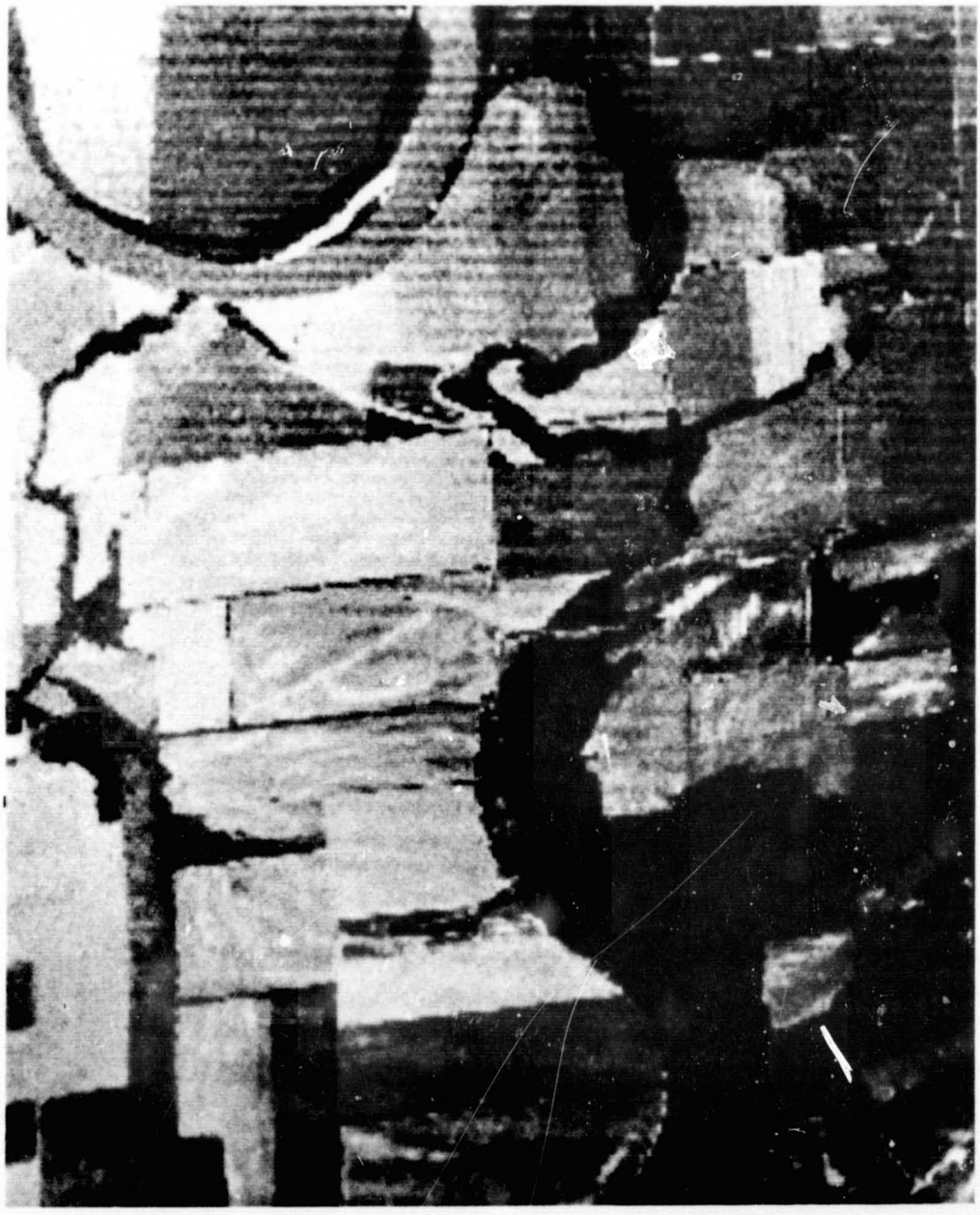

Figure 1. Data in 0.46-0.49 micrometers channel taken from June 30, 1971, flight over Pike County, Indiana (Segment 225)

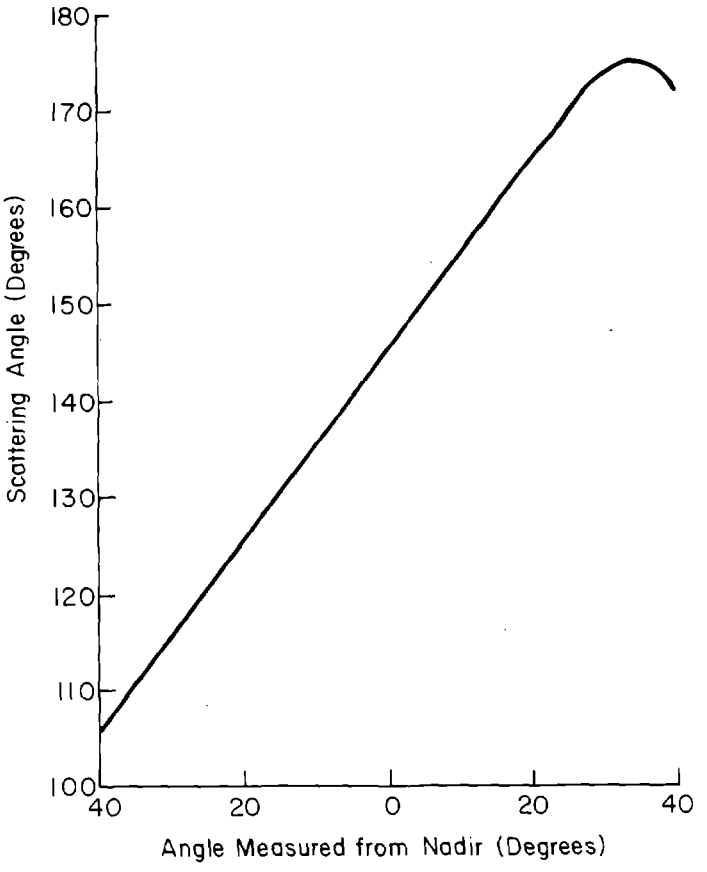

Figure 2. Scattering angles computed for June 30, 1971, flight over Segment 225.

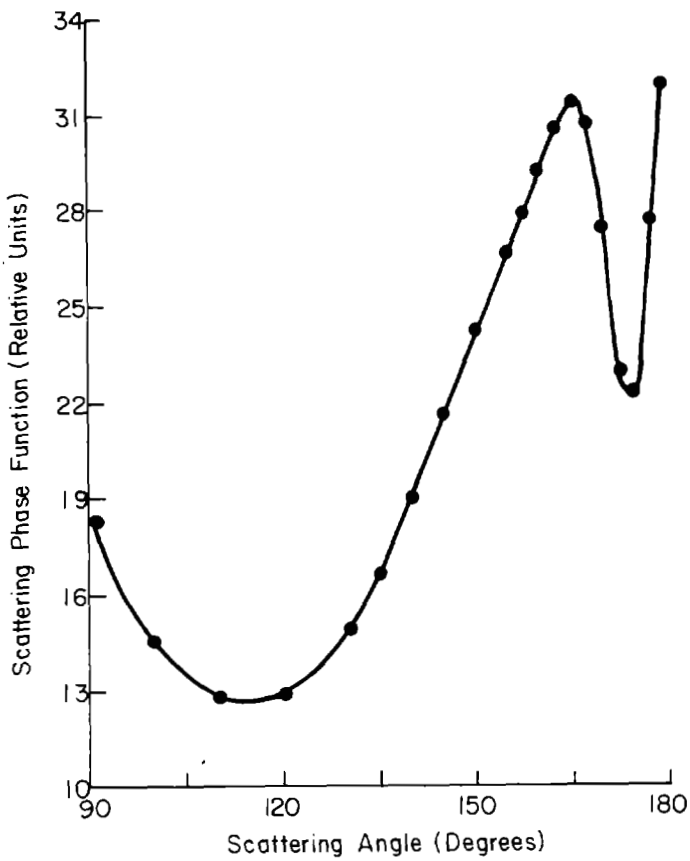

Figure 3. Scattering phase function at 0.45 micrometers as a function of scattering angle for a continental haze layer (after Deirmendjian, 1969).

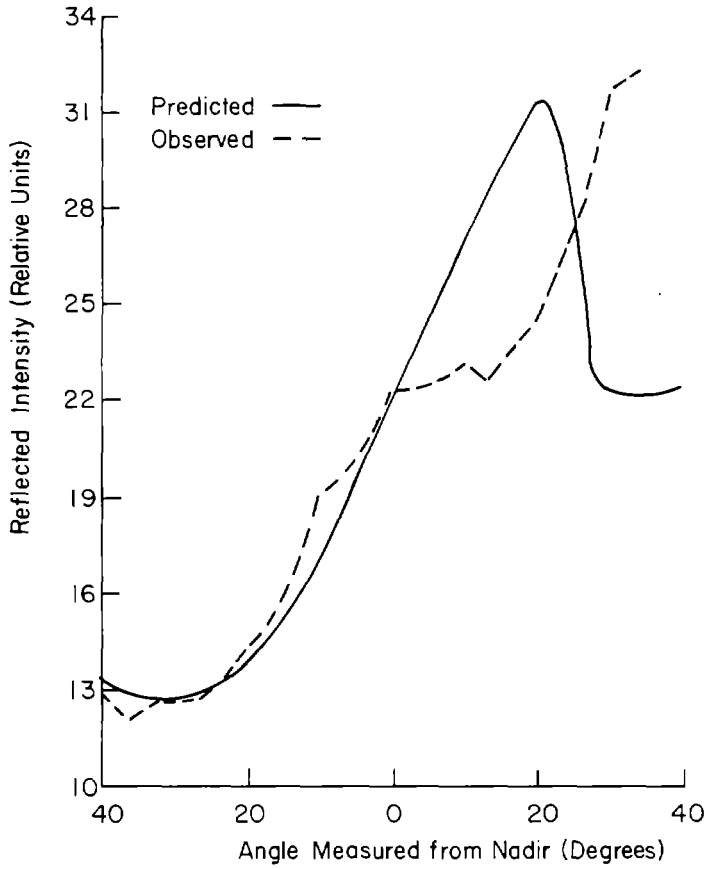

Figure 4. Comparison between predicted reflected intensity at 0.45 micrometers and observed values for 0.46-0.49 micrometers averaged for the length of the June 30, 1971, flight over Segment 225.

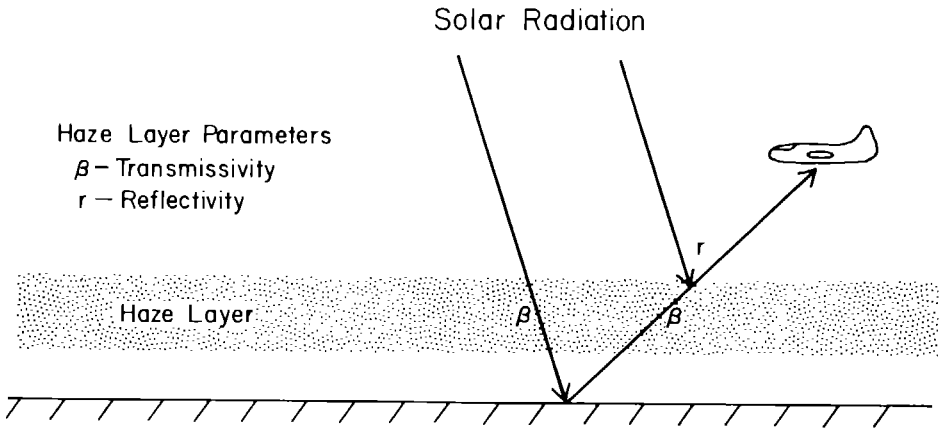

Figure 5. A schematic representation of the influence of a haze layer upon surface-reflected radiation measured from an aircraft.

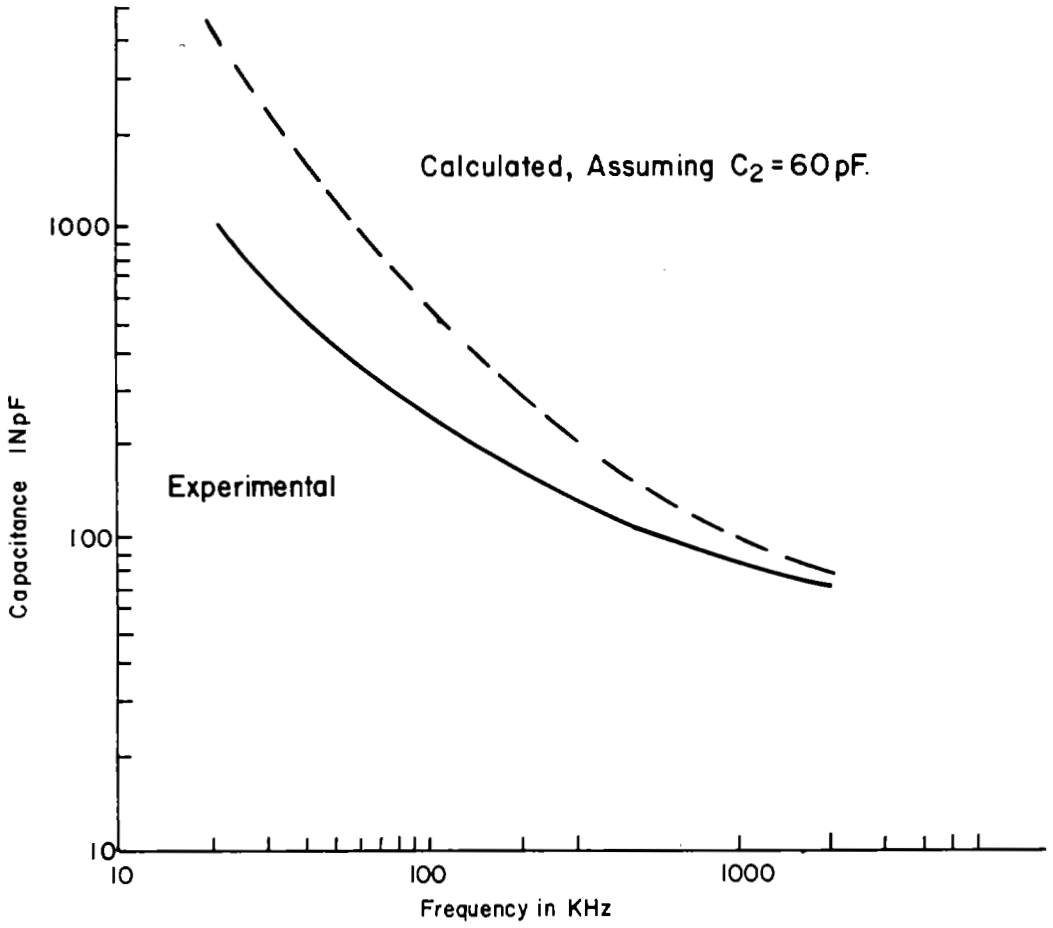

Figure 6. Capacitance of a coaxial sample holder loaded with Crider clay (42.8% moisture) as a function of frequency. Empty holder capacitance assumed to be 60pF.

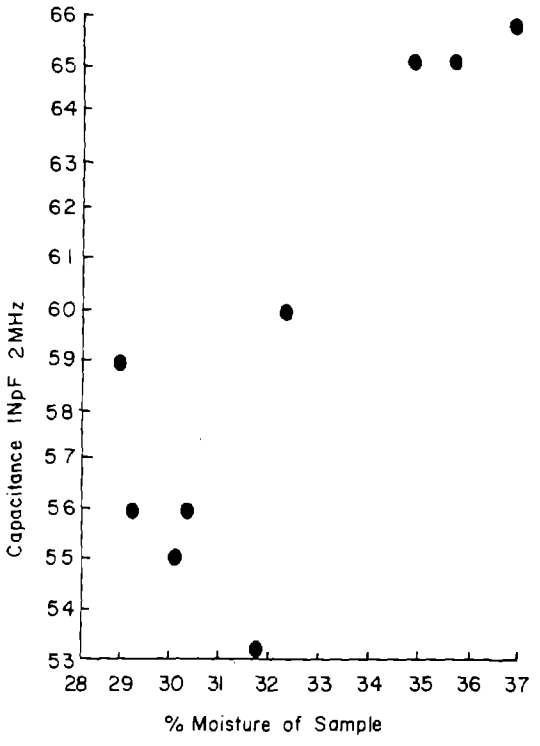

Figure 7. Capacitance of a coaxial sample holder loaded with Crider clay as a function of moisture content. Measurement frequency, 2MHz.

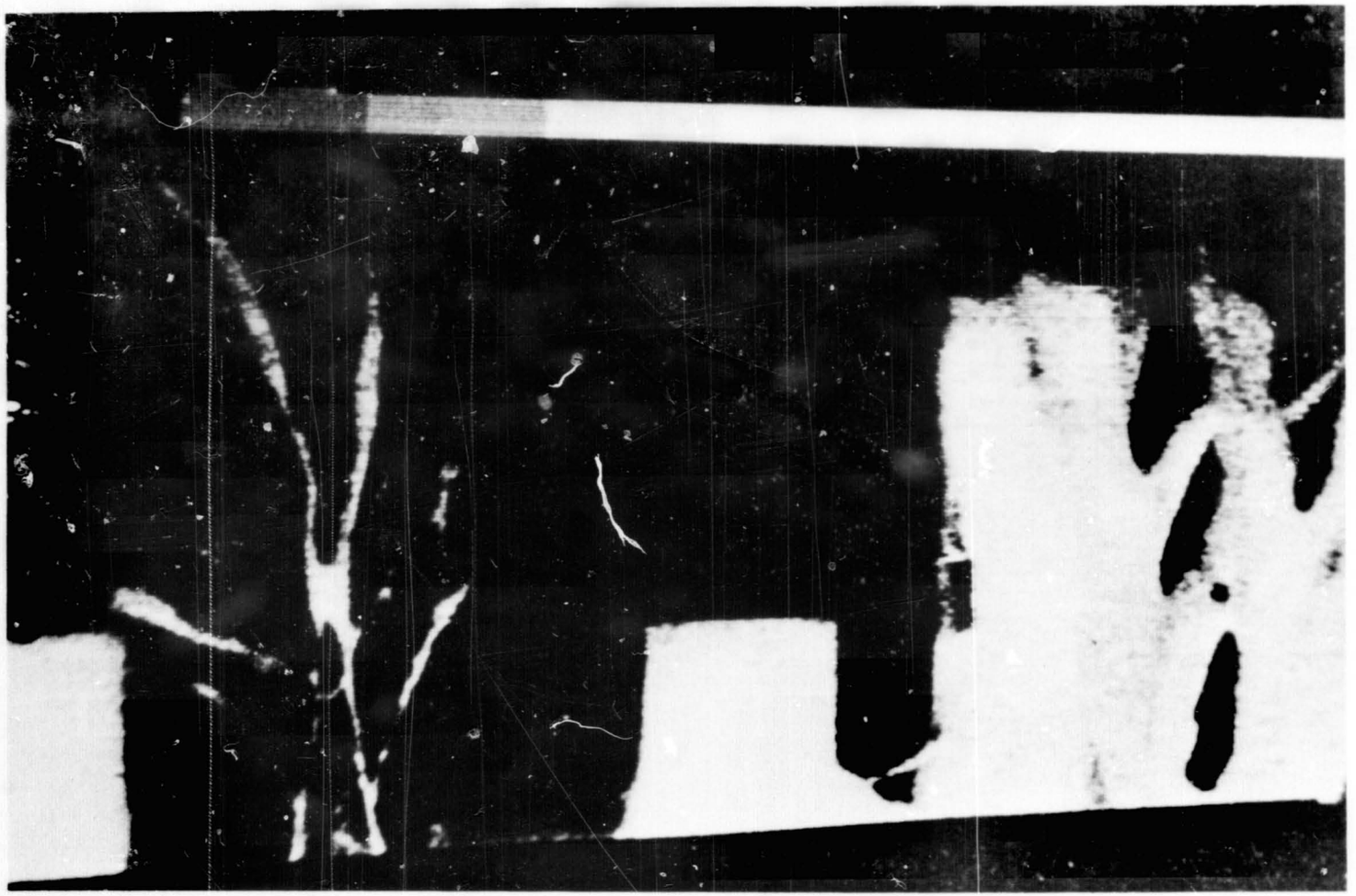

Figure 8. Thermogram of a sulfur deficient corn plant (on the left) as compared to a healthy corn plant (on the right). Ambient temperature is 24°C. A background behind the plants is at 16.5°C. The nutritionally stressed plant is approximately 1°C cooler than the healthy plant. Scan time: 6 minutes.

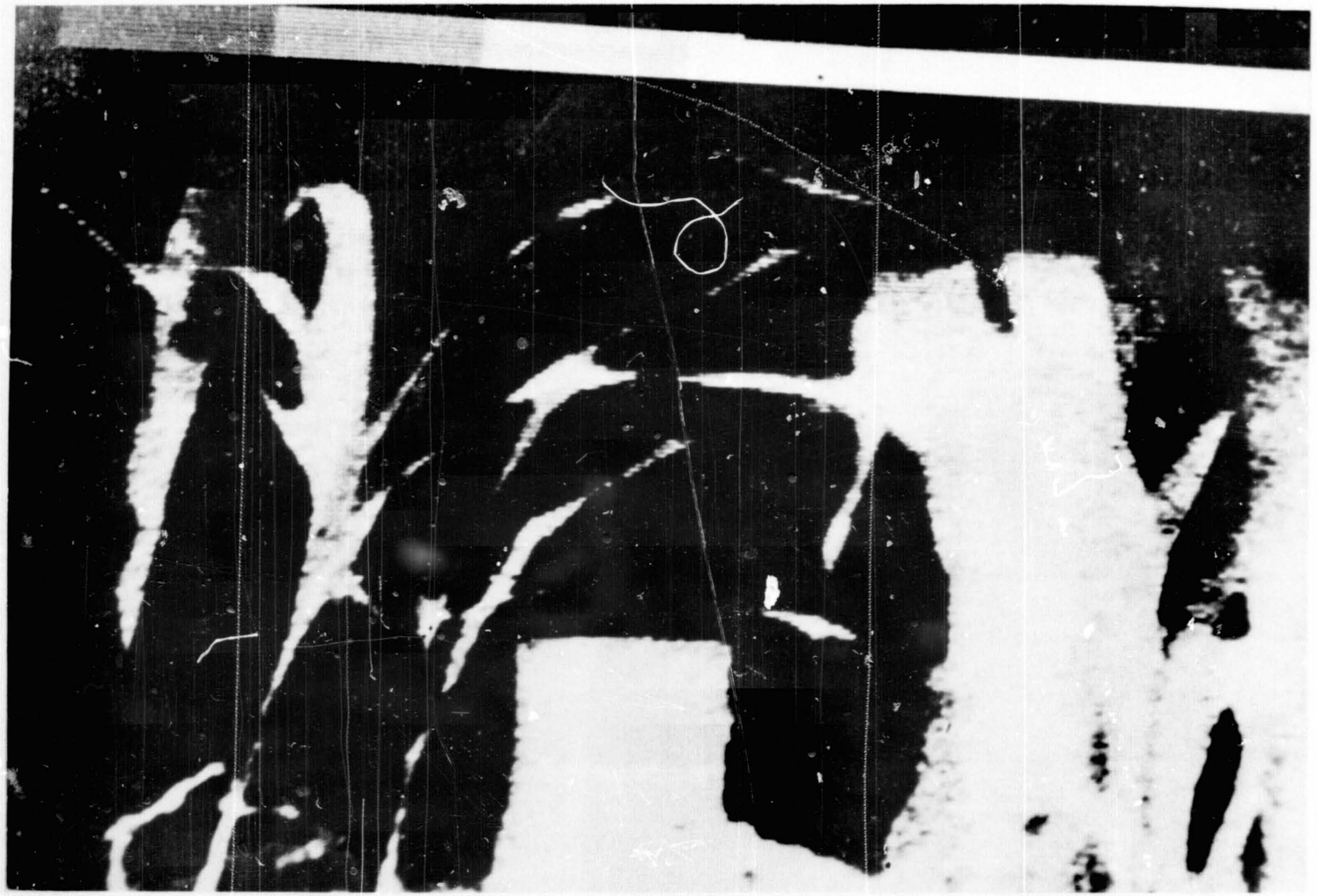

Figure 9. Thermogram of a nitrogen deficient corn plant (on the left) as compared to a healthy corn plant (on the right). Ambient temperature is 24°C. A background behind the plants is at 16.5°C. The nutritionally stressed plant is approximately 2°C cooler than the healthy plant. Scan time: 6 minutes.

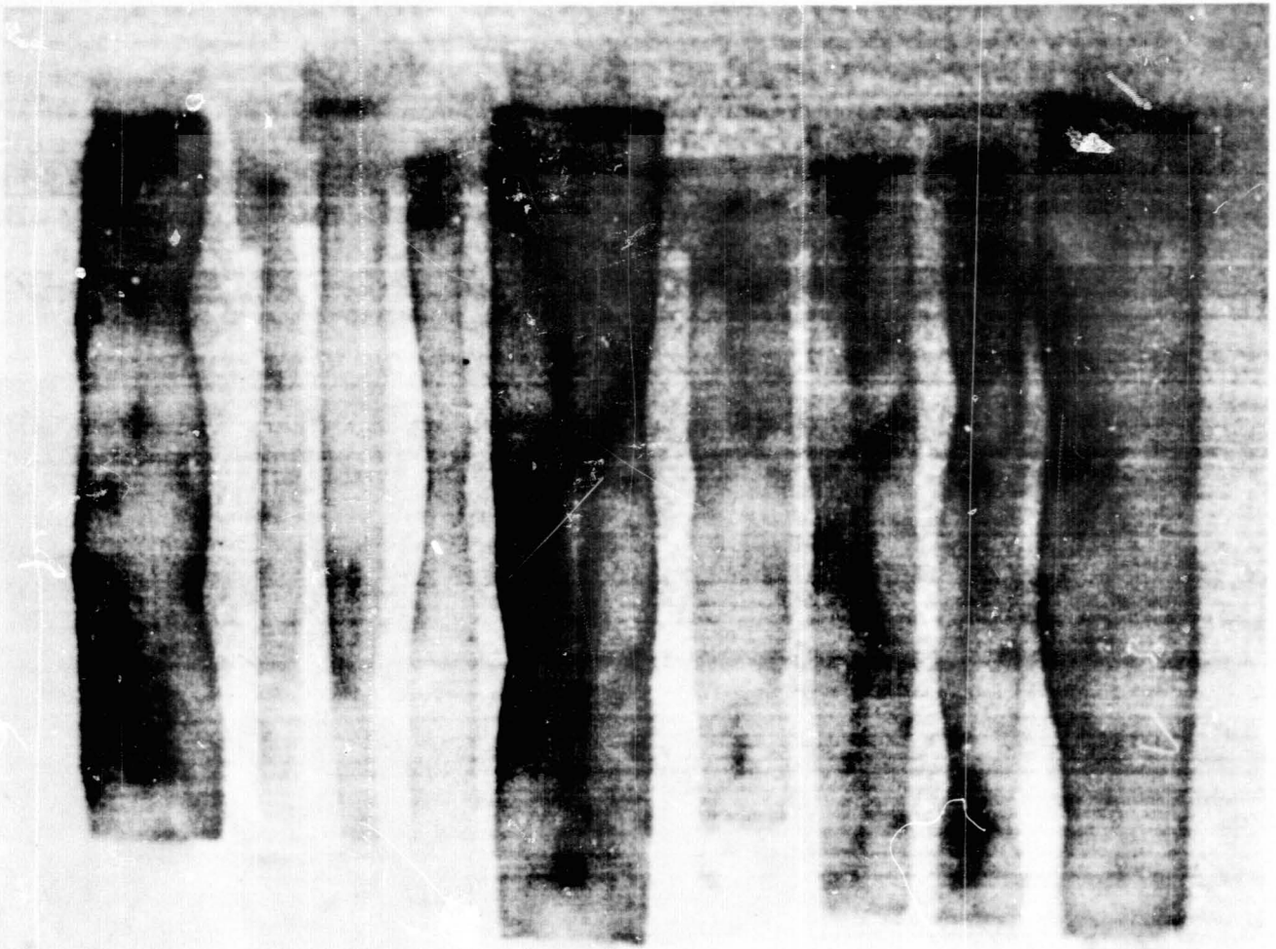

Figure 10. A thermogram of healthy and nutritionally stressed corn leaves. From left to right: healthy, three sulfur deficient, healthy, three nitrogen deficient, healthy, styrofoam background. Ambient temperature is 23°C but a 35°C surface is located nearby. The sulfur deficient leaves are approximately 1°C warmer and the nitrogen deficient leaves are approximately 2°C warmer than the healthy leaves.

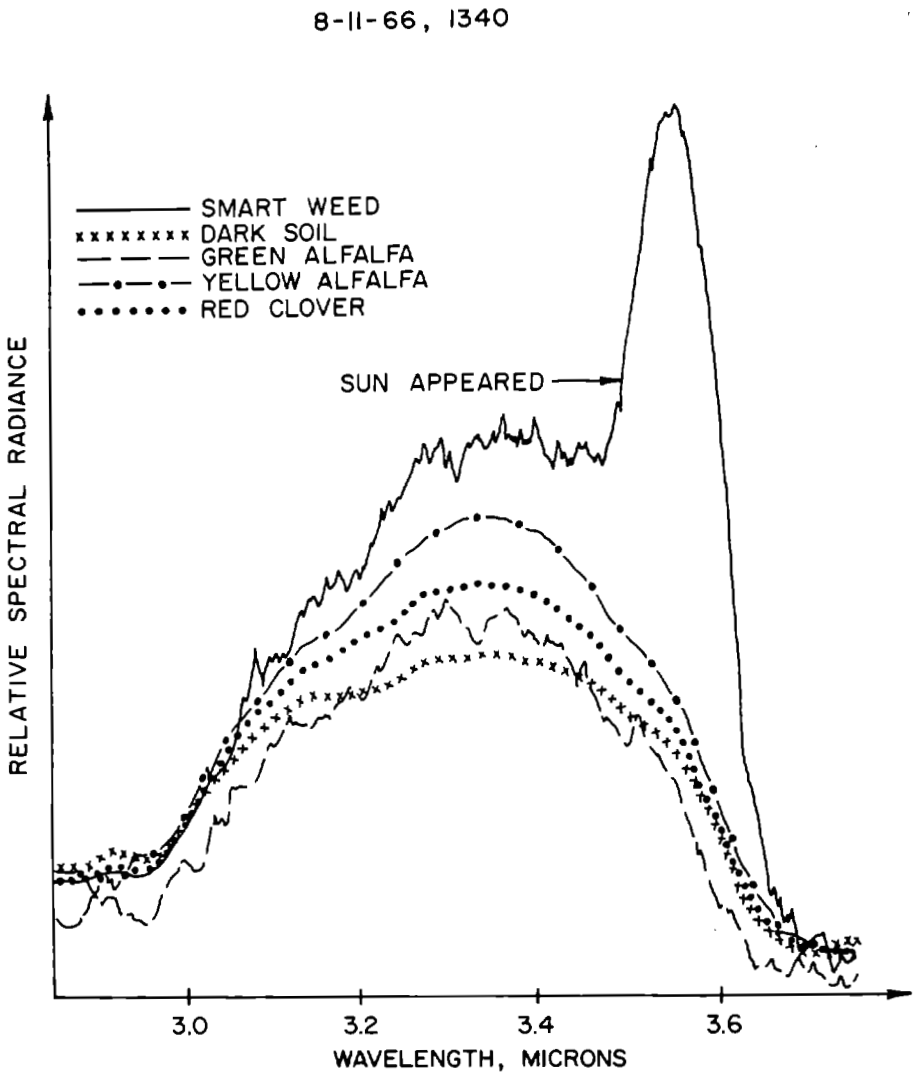

Figure 11. Spectral data taken with a Perkin-Elmer SG-4 spectroradiometer on a variety of cover types. The relatively long spectral scan time of the instrument permits environmental changes to compromise the data.

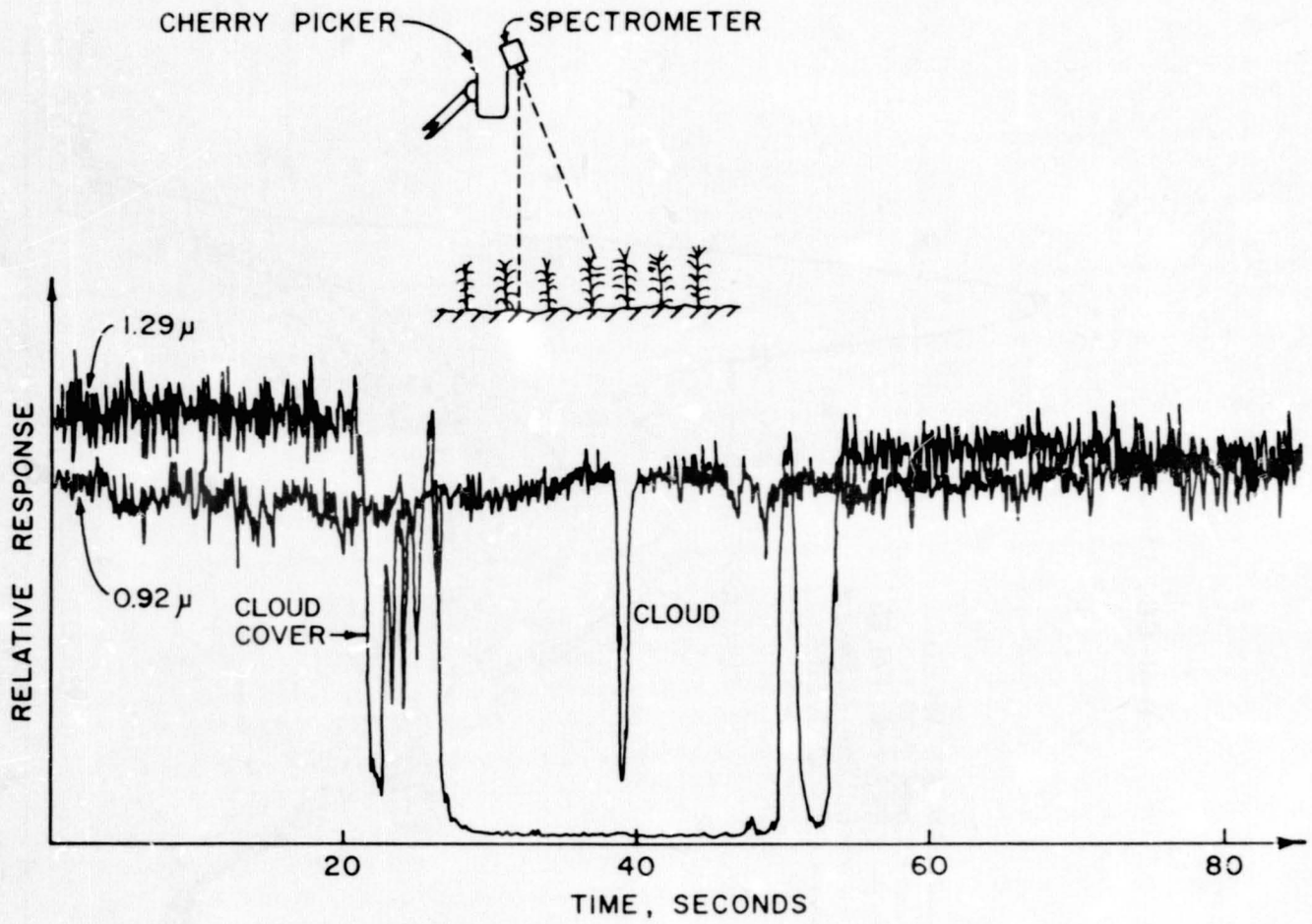

Figure 12. Radiometric data obtained by stopping the Perkin-Elmer SG-4 spectroradiometer at two fixed wavelength positions. The "noise" in the data is due to plant motion, not detector noise.

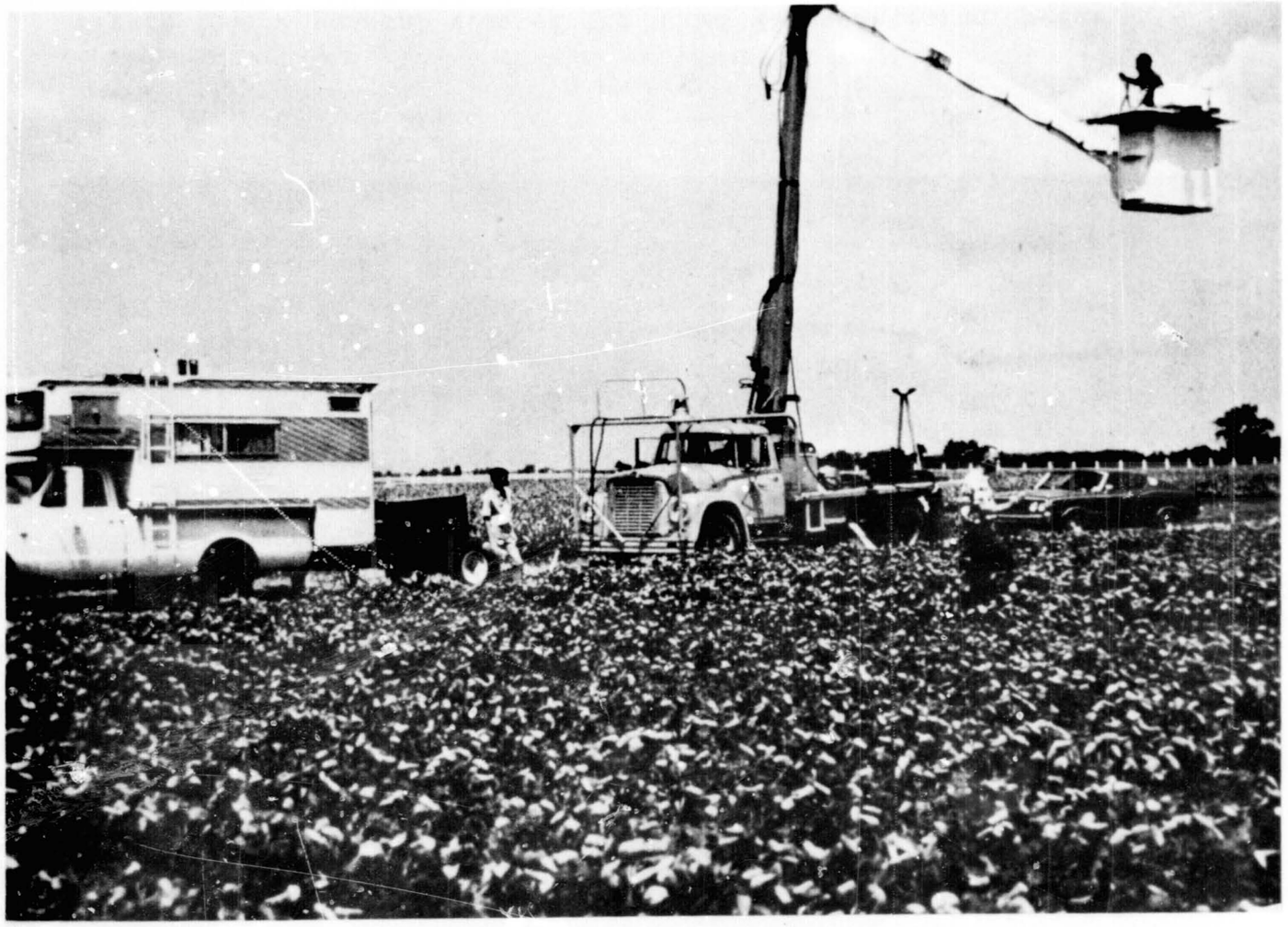

Figure 13. The Exotech Model 20B spectroradiometer undergoing field trials.

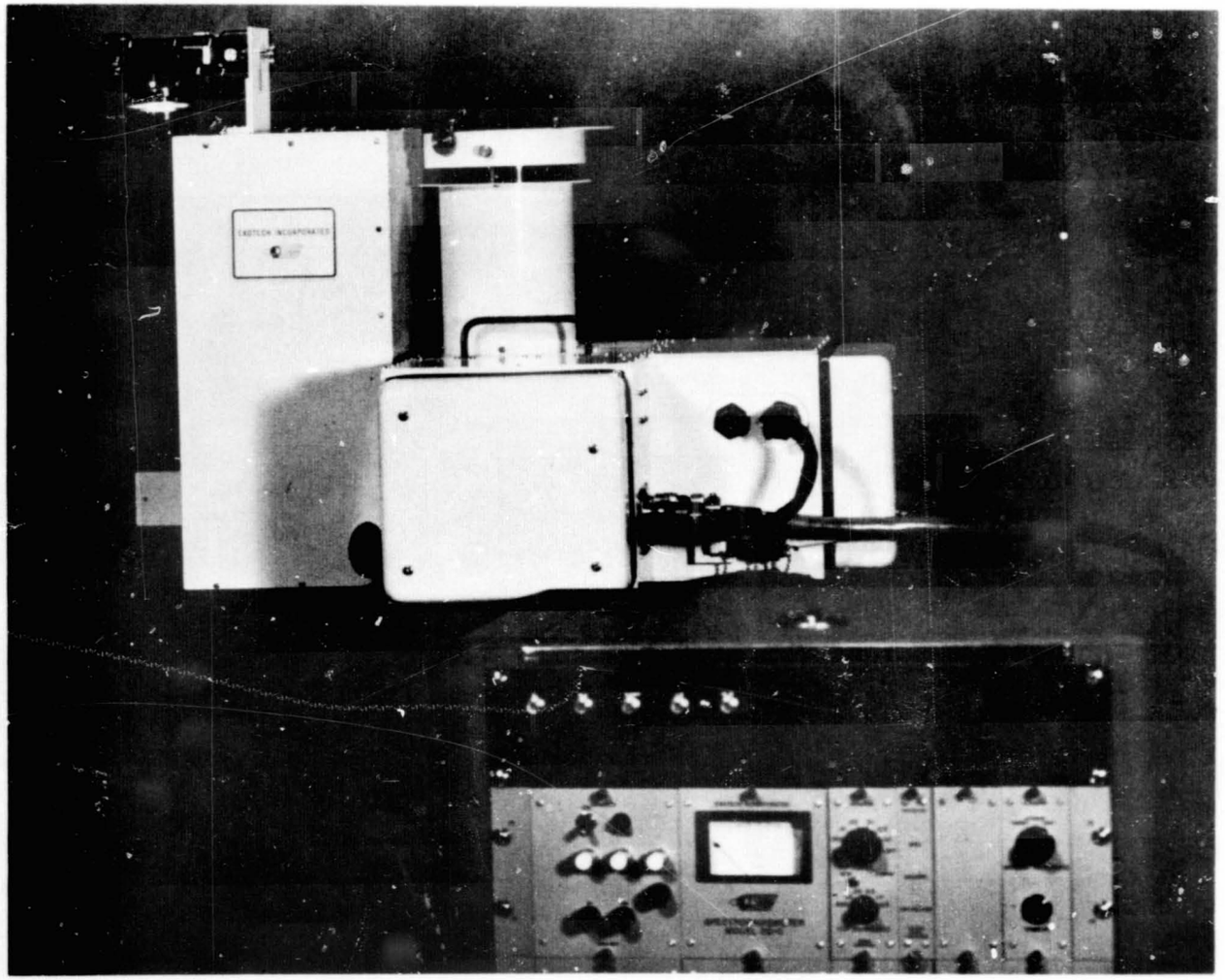

Figure 14. A general view of the Model 20C spectroradiometer short wavelength unit showing the control panel.

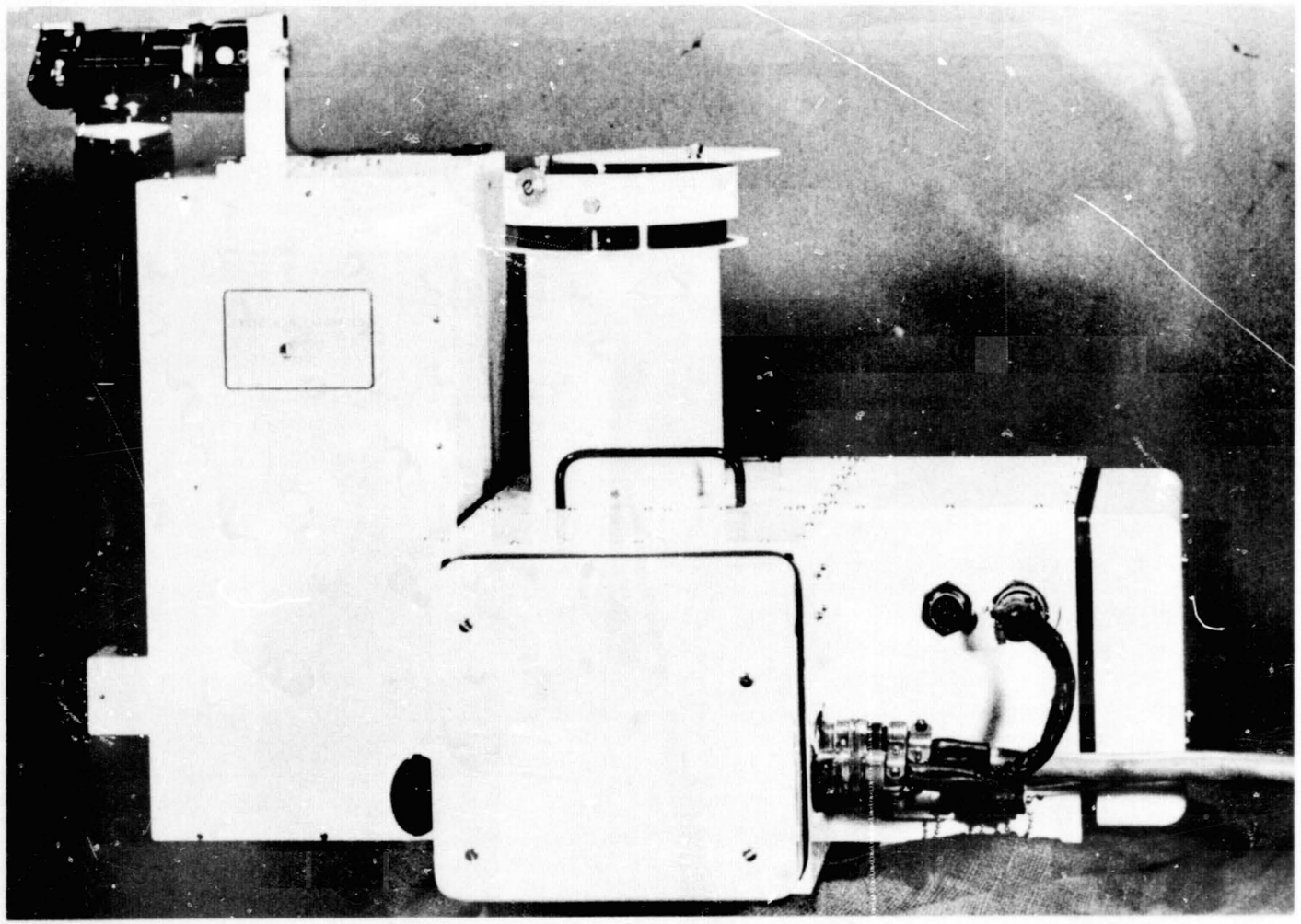

Figure 15. A close-up view of the Model 20C short wavelength head. The vertical tube is the solar irradiance input port.

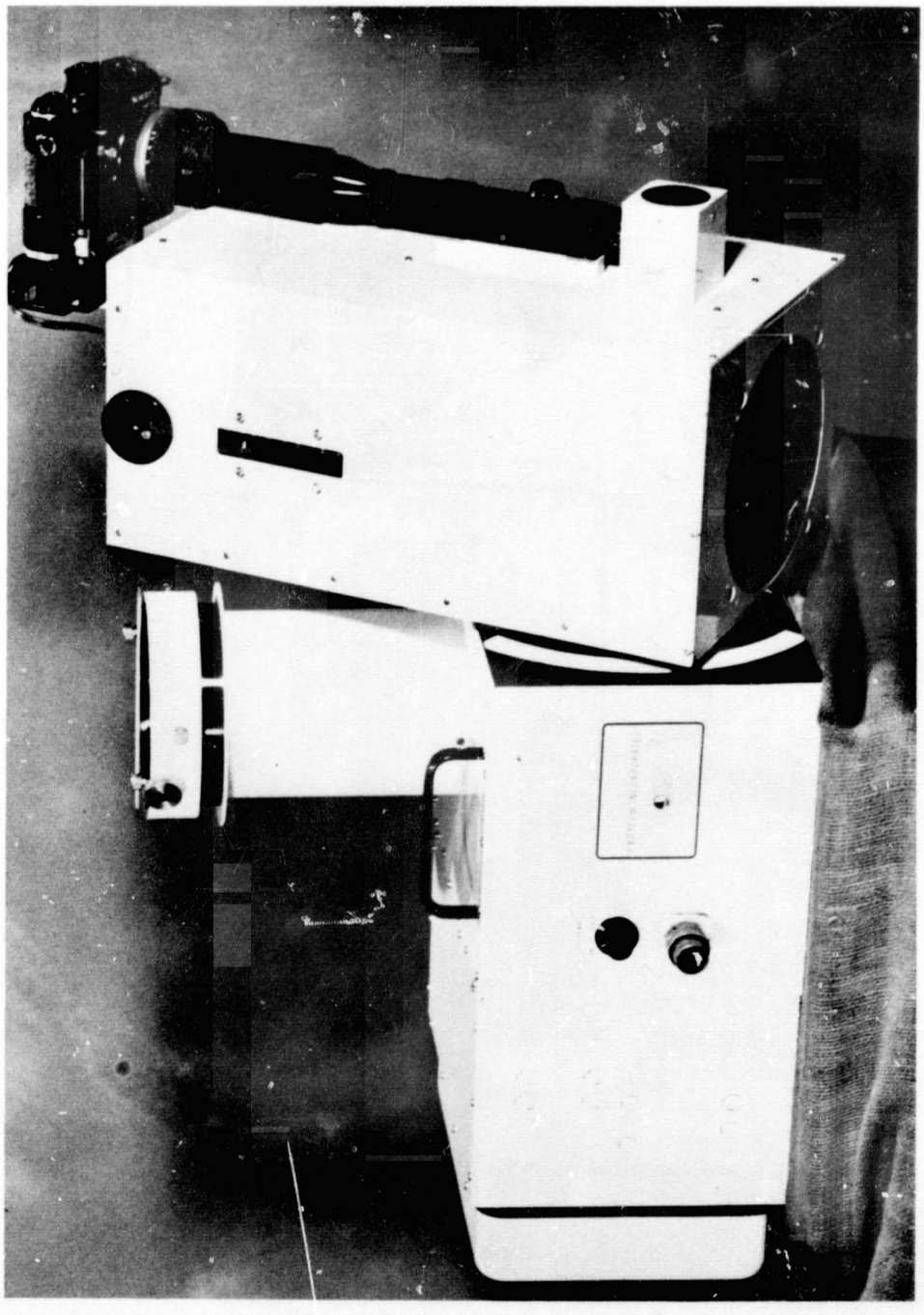

Figure 16. The view angle adjustment feature of the Model 20C spectroradiometer.

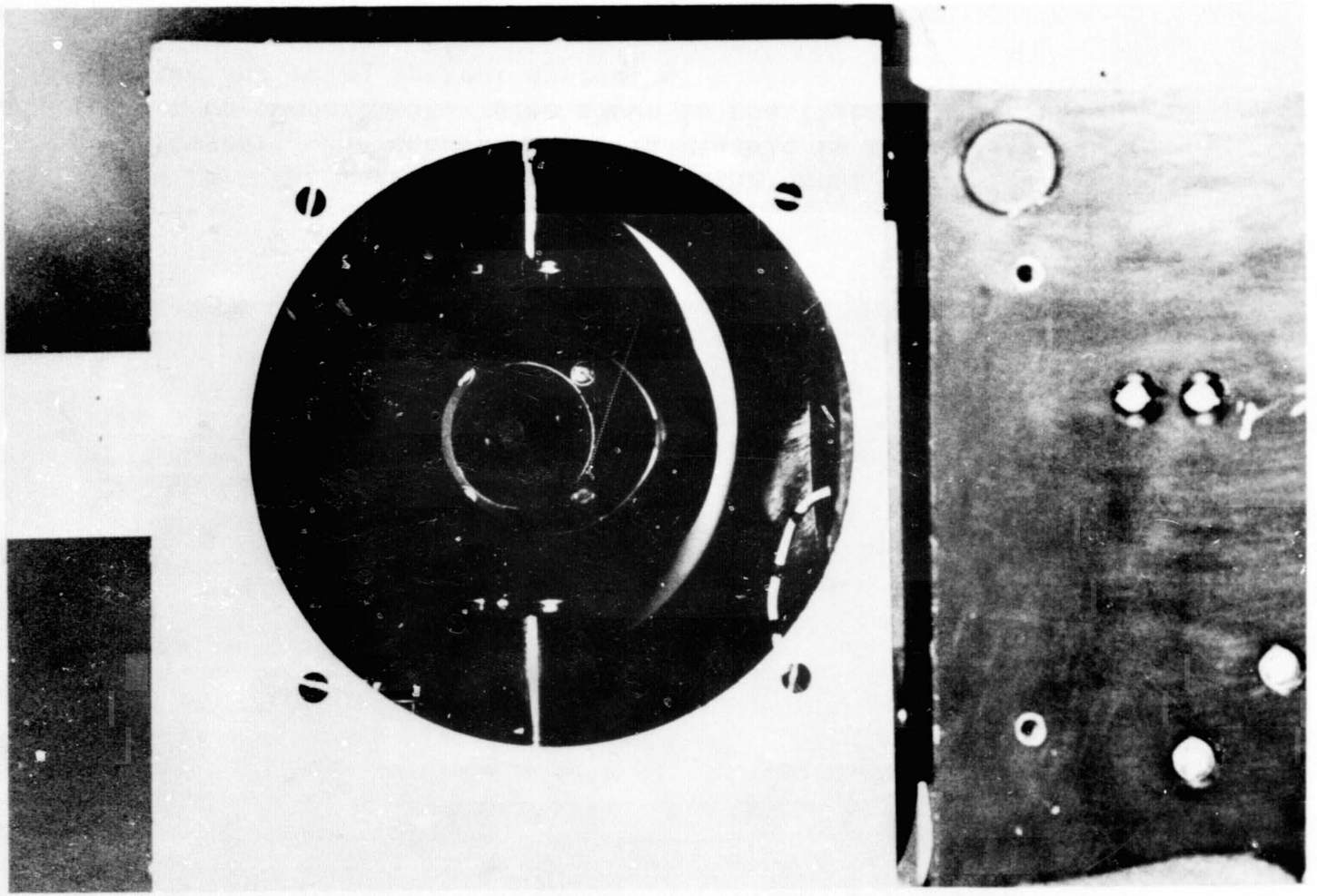

Figure 17. A view into the Newtonian fore-optical telescope of the Model 20C.

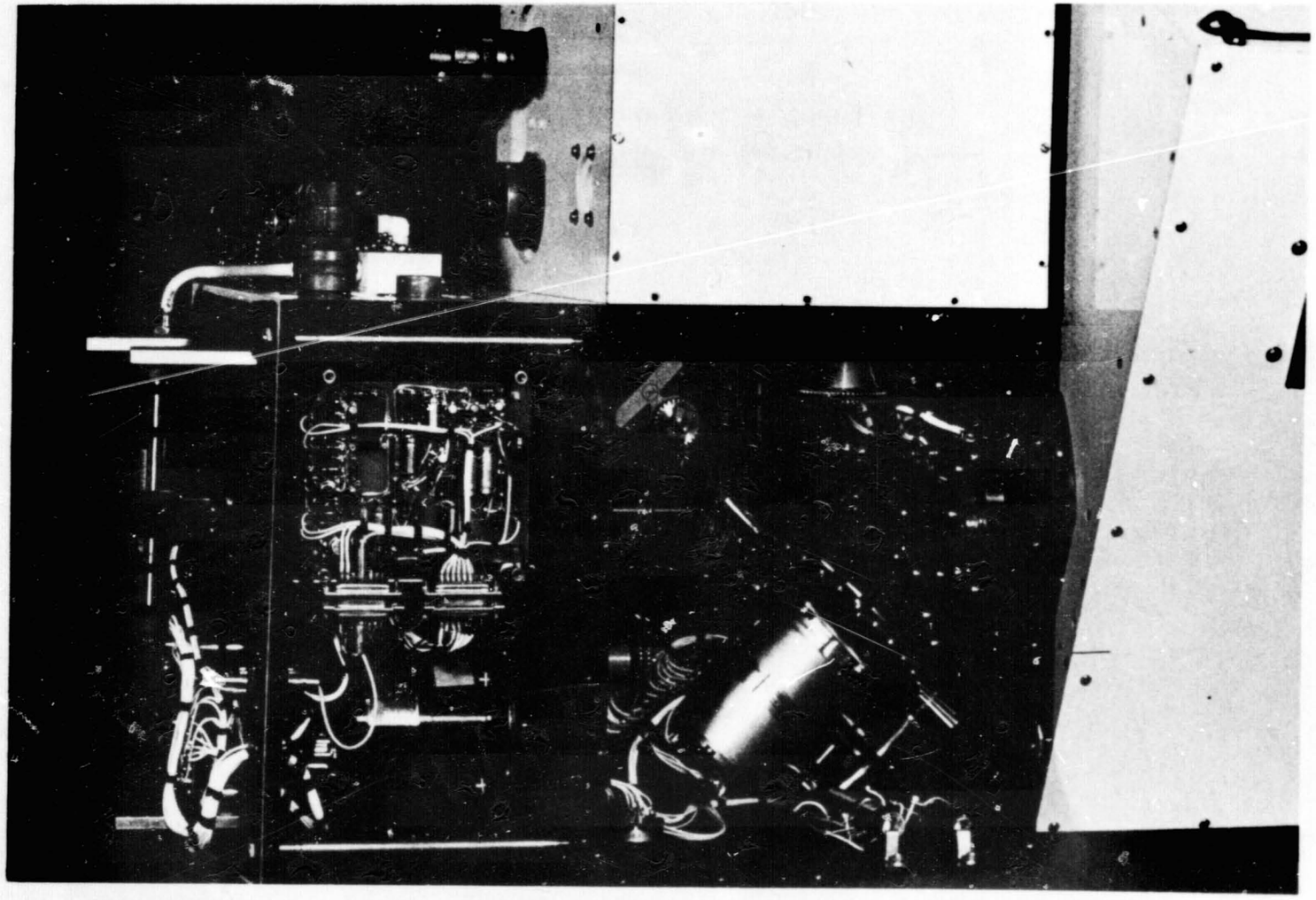

Figure 18. The internal structure of the Model 20C spectroradiometer. The chopper wheel is visible in the middle of the main compartment. Also shown is the filter wheel drive system and relay optical system.

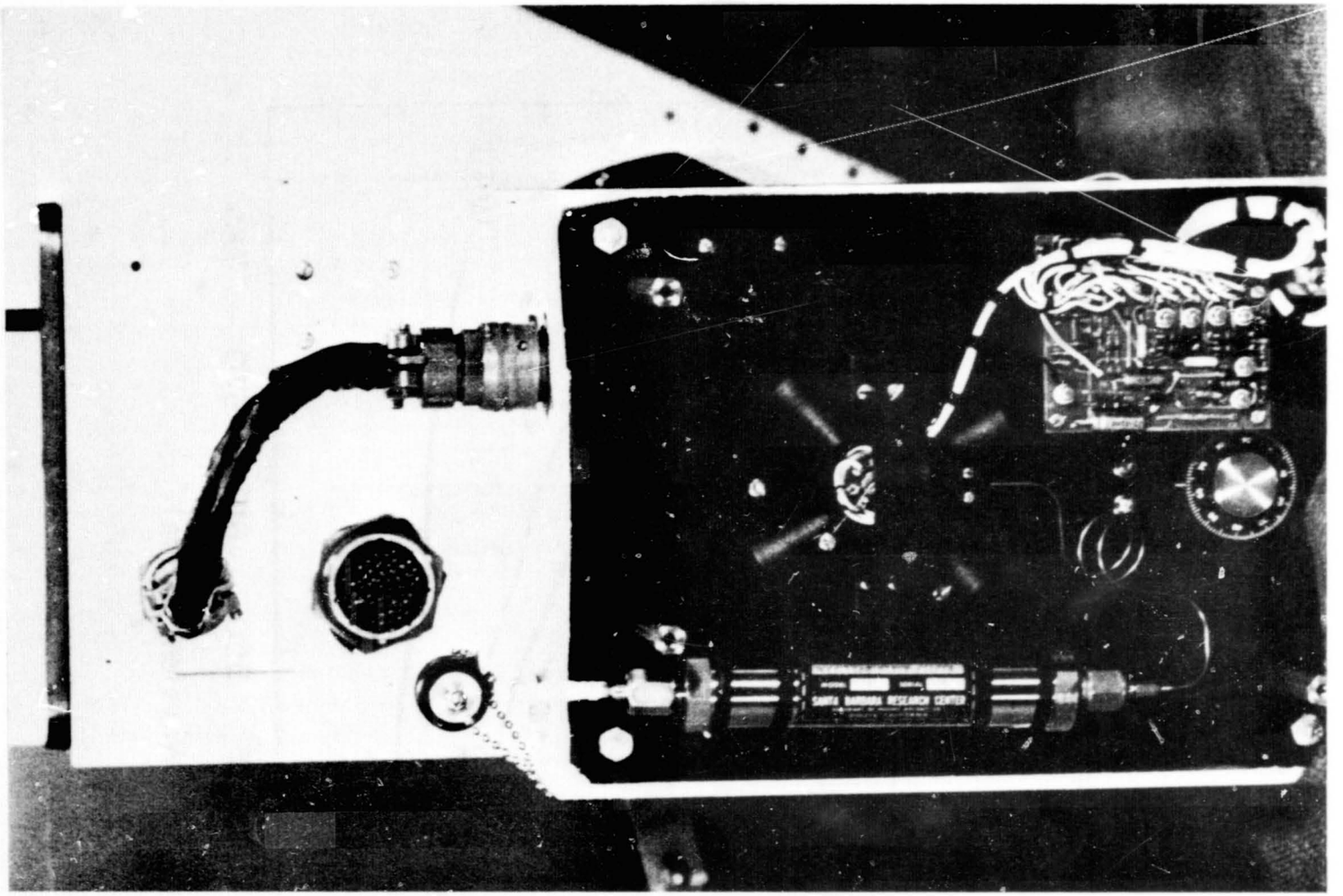

Figure 19. A view of the Joule-Thompson cooling system on the lead-sulfide detector of the Model 20C.

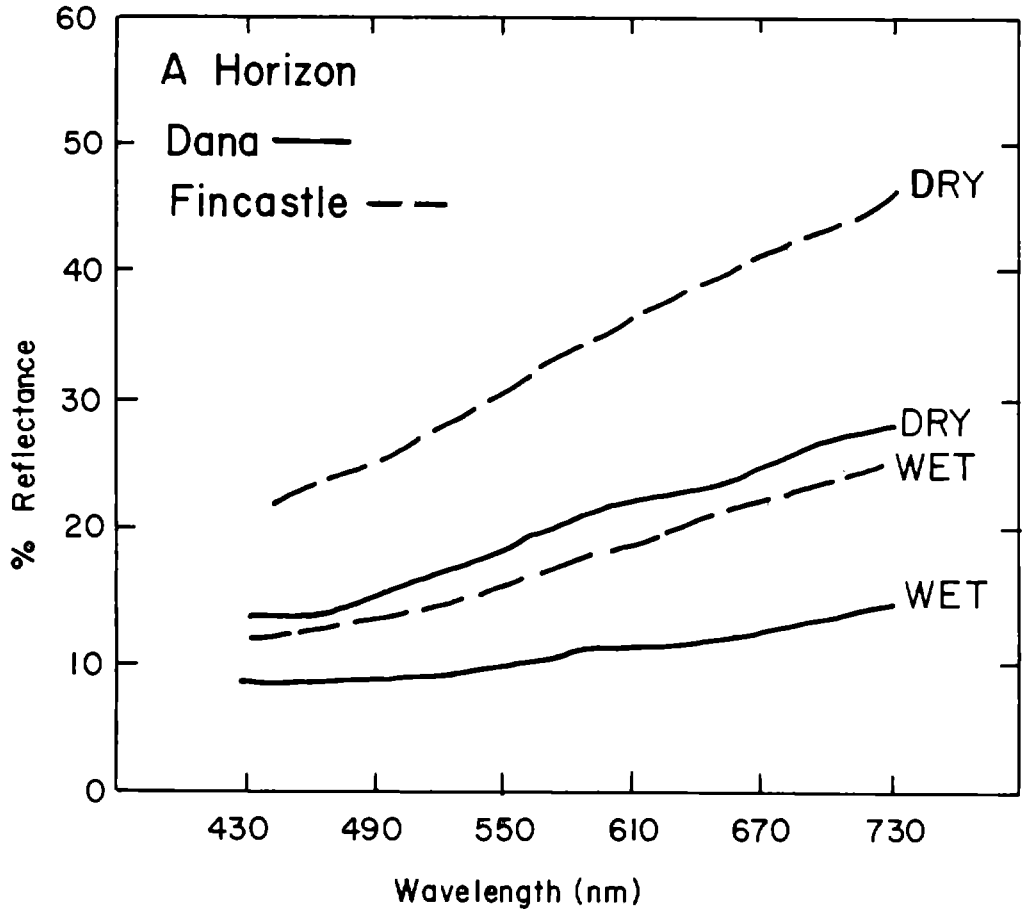

Figure 20. Soil spectral reflectance field, data obtained on the Model 20B spectroradiometer. The data were reduced manually.

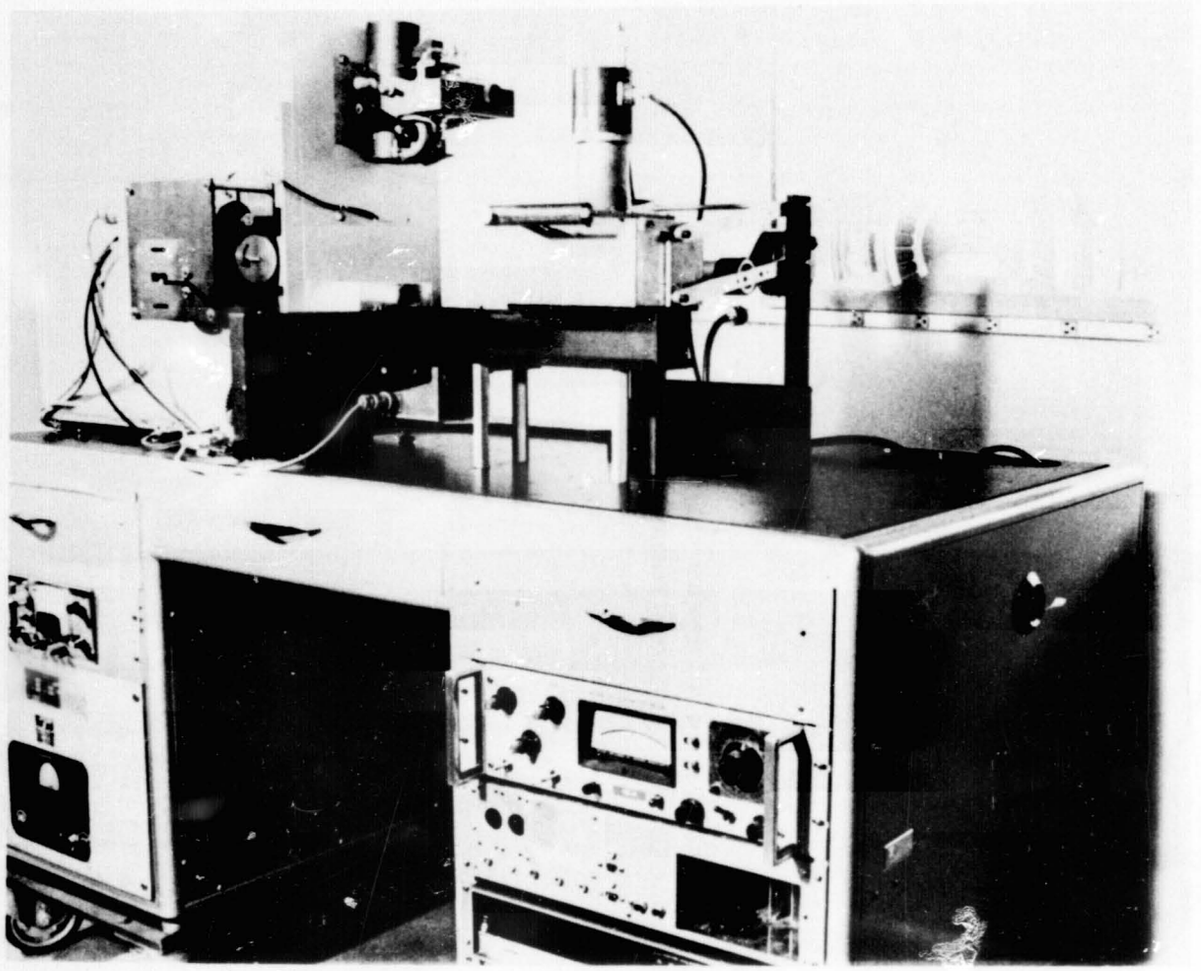

Figure 21. A general view of a large sample high-power, biological spectrophotometer.

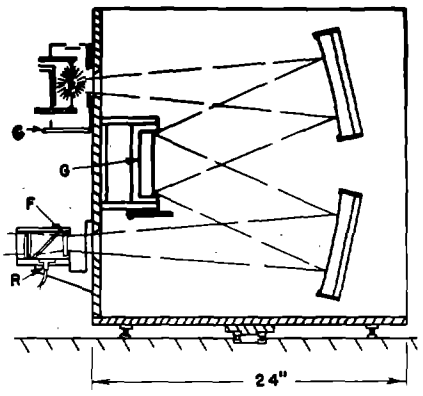

Figure 22. A schematic diagram of the biological spectrophotometer monochromator assembly.

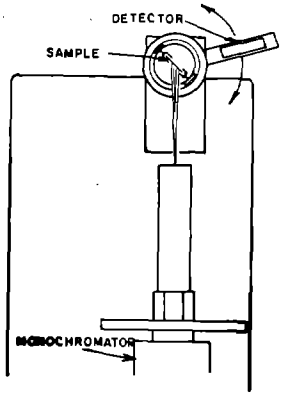

Figure 23. The bi-direction reflectance attachment for the spectrophotometer.

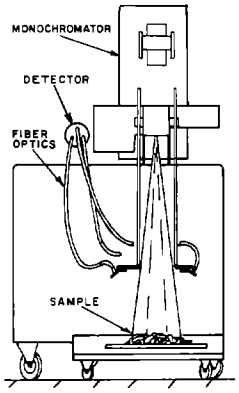

Figure 24. The large area reflectance attachment for the spectrophotometer.

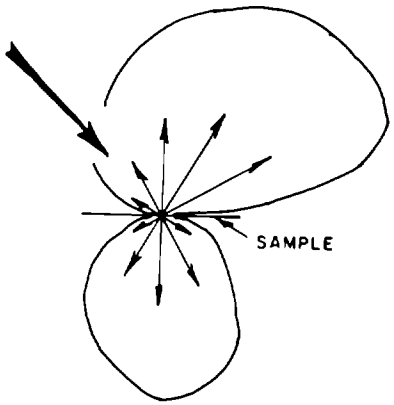

Figure 25. Typical bi-directional reflectance data for natural specimens.

SECTION 50

N72-29350

DATA PROCESSING I: ADVANCEMENTS IN MACHINE ANALYSIS OF MULTISPECTRAL DATA

by

Philip H. Swain and Staff
Laboratory for Applications of Remote Sensing
Purdue University
West Lafayette, Indiana

INTRODUCTION

Research in multispectral data processing at LARS/Purdue is directed at supporting a substantial level of applications research as well as advancing the technology of remote sensing data processing. During the past year significant progress has been made in both respects. Almost the entire multispectral data analysis process, from data editing to results evaluation, has been impacted, and the new level of technology has been vigorously tested by the data analysis operations associated with the 1971 Corn Blight Watch Experiment.[1]

The following discussion of these advancements is organized to follow generally the steps utilized in the multispectral data analysis procedure. In terms of Figure 1, we begin with the data display process used to accomplish data editing and proceed clockwise through clustering, statistics computation, etc. In the interest of brevity, each result will be treated here in a general way and references given to available sources where a more detailed treatment may be found.

DATA EDITING FACILITY

The special-purpose digital display system delivered to LARS/Purdue late in 1970 [1] represents a tremendous potential for facilitating the man/data interface. During 1971 the first software for utilizing this system became operational and was made available to LARSYS users [2]. With this software, the user can display a television-quality image of digitized multispectral data and, by means of a light pen and keyboard, accurately specify areas in the data to receive special attention

[1]The 1971 Corn Blight Watch Experiment is described elsewhere in these proceedings.

(Figure 2). Two advantages of this mode of man/data interface over the familiar gray-scale line-printer output (Figure 3) are the higher quality of the image available to the researcher and the ease and accuracy with which features in the data can be located and designated to the computer by means of the light pen. These features greatly improve both the speed and accuracy with which the data analysis can be executed.

Data editing represents only one of many potential uses of the digital display hardware. Examples of other applications to be studied include on-line display and evaluation of analysis results and implementation of a highly interactive data analysis capability.

One feels compelled to note at this point, however, that line-printer output still represents a proven and acceptable means for displaying both data and analysis results. But as technological advances bring down the cost of video-type displays and step up the speed of digital data transmission, digital display systems suitable for image data -- now available only on a limited basis as research tools -- will become increasingly attractive as a standard means of interfacing man with such data.

CLUSTER ANALYSIS

Multispectral cluster analysis (sometimes referred to in the literature as unsupervised classification) has been under study for some years as a means for data compression and similarity analysis. A clustering technique has been developed at LARS/Purdue, for use in conjunction with supervised classification, as an aid in class definition and training sample selection. A computer program [3] prints point-by-point maps of the clustering results (Figure 4), indicating the relative homogeneity of the analyzed areas; this information assists in the process of selecting training samples for characterizing the different spectral classes in the data. Also provided is a quantitative analysis of the separability of the clusters in the multivariate measurement ("feature") space.

The clustering technique described above processes data points in the measurement space. Another promising approach, currently under investigation and discussed further in a later section of this paper, is the clustering of sample statistics in parameter space.

FEATURE SELECTION

A feature selection criterion has been developed [4] which eliminates the considerable level of human interaction with the

computational processing heretofore required for the selection of data channels preferred for classification. The basic problem faced in connection with feature selection is finding a means for estimating error probabilities (or probabilities of correct classification) accurately since for multivariate problems it is generally not feasible to calculate these probabilities directly even in the relatively simple case in which Gaussian distribution of the data within classes is assumed. The problem of finding an estimator of probability of correct classification in the multiclass and multivariate case is unsolved. What is commonly done in practice is to estimate the probabilities associated with all pairs of classes and take an average or weighted average of the pairwise probabilities as an estimate of the overall probability of correct classification [5]. To do this effectively, however, requires availability of a function, based on the statistical separability of pairs of classes, which behaves like the probability of correctly discriminating between the classes.

Divergence is a monotonic function of statistical separability of two classes which has been used in this manner. However, this separability measure has the disadvantage that it increases without bound as separability increases, whereas probability of correct classification saturates at 100 percent (see Figure 5). This difficulty has been circumvented by writing the feature selection program to allow the user to specify a limiting value (MAX) which artificially saturates the separability measure. To do this properly, however, the user must learn to judge for a given type of problem what constitutes an appropriate saturation value.

In an effort to remove this latter shortcoming, alternative separability measures have been investigated. In particular, a separability measure referred to here as Bhattacharyya distance, or B-distance, has been found to have the sort of behavior sought and indeed to provide a much more reliable feature selection criterion than divergence [4]. This further suggested a transformation of divergence which closely approximates the feature selection properties of the B-distance but requires far less computation. The transformed divergence has been implemented at LARS/Purdue as the standard feature selection criterion.

POINT CLASSIFICATION

The next step in the procedure for multispectral data analysis, the multivariate classification method, has not been altered, but some newly completed research has reconfirmed the wisdom (from a practical viewpoint) of selecting the Gaussian maximum-likelihood approach for analysis of real-world multispectral data. This approach [6] assumes that the class-conditional distributions of the data in all classes to be recognized can be adequately represented by multivariate Gaussian distributions, or, in any case, by the union of a small number of such distributions. Although

pattern classifiers based on this approach have been applied successfully at various remote sensing facilities involved with machine analysis, some important questions regarding this choice of approach have remained open: How much improvement in classification accuracy could be obtained by using a nonparametric classification method which requires no a priori assumptions regarding the data distributions? How much would classification accuracy degrade if the classifier were of the computationally faster and simpler linear variety?

An experimental investigation yielding a considerable volume of results [3] has demonstrated that, for agricultural remote sensing data, very general nonparametric models can be expected to produce only marginally better results than the Gaussian classifier. In general the improvement is not sufficient to warrant the substantial increase in computational resources required (time, machine memory). On the other hand, another study [7] suggests that the extra cost of the Gaussian classifier by comparison with linear classifiers is generally well justified. The linear classifiers investigated have shown markedly poorer ability to generalize from training fields to data not used for training the classifier.

SAMPLE CLUSTERING AND SAMPLE CLASSIFICATION

The term "perfield classification" has been used in the literature to refer to the classification of an entire agricultural field based on all data drawn from that field. This approach takes advantage of the spatial context of the data, the fact that local regions tend to be composed of members of the same class (the same "population," in statistical terminology), by using the combined information in a number of observations to infer the classification of the aggregate. To divorce this concept from the agricultural frame of reference, "sample classification" is defined as the classification of any aggregate of data points assumed to be from the same population. It is often the case that decisions concerning the aggregate can be made faster and more reliably than decisions concerning the data points taken individually.[1]

As intensive study of this approach [3] has been completed in which both sample clustering and sample classification were investigated. The results of this study are too extensive, both in number and in scope, to receive adequate treatment here. Following are some highlights.

---

[1]The greatest benefits in this respect generally accrue when the aggregation is performed before the decision process is applied (eg. by finding a parametric characterization of the aggregate) rather than after (eg., poll-taking after classification).

For agricultural remote sensing data, the accuracy of sample classification is relatively insensitive to whether parametric or nonparametric methods are used to estimate probability distributions. As noted earlier in this paper the potential improvement in accuracy obtainable using nonparametric methods is too small to justify the considerable increase in computation time and complexity.

Although many measures of statistical separability are available for use in sample classification, the experimental results using agricultural data were relatively insensitive to the choice of separability measure used. However, a separability measure known as the Jeffries-Matusita distance does have some theoretical as well as practical advantages worth exploiting:

1. Its behavior as a function of dimensionality resembles that of probability of correct classification (in the parametric case).
2. It is a metric over a large space of distribution functions.
3. It is among the simplest separability functions to compute.

Sample clustering, achieved by first computing a parametric characterization of the samples and then applying cluster analysis to the statistical parameters (Figure 6), appears to offer several advantages over the more conventional point-by-point clustering. In experiments with agricultural remote sensing data, sample clustering has exhibited a distinct tendency to produce more appropriate class/subclass structures leading to better classification accuracy for both point and sample classification. In addition, a dramatic time saving is achieved for cluster processing because of the considerable degree of data reduction accomplished by representing a large number of data points by relatively few statistical parameters.

STATISTICAL DESIGN AND ANALYSIS

Finally, the effective utilization of large quantities of remote sensing data demands the development of statistical models which can be used for specifying data collection and data analysis schemes and for evaluating the results produced by such schemes. The 1971 Corn Blight Watch Experiment and forward-looking considerations related to the ERTS and SKYLAB satellites have particularly highlighted this need. Conventional models developed for ground data collection alone are simply not adequate.

A recent study [8] has formulated a three-stage sampling model for remote sensing and used the model to evaluate the precision of crop acreage estimates and to determine the effects of the number of flightlines, number of segments within flightlines, and the subsampling density within segments on the precision of these estimates. While this work has

has perhaps raised as many important questions as it has answered, it represents the initiation of a significant effort to determine systematically the cost-benefit relationships associated with the remote sensing technology and to utilize these relationships both in guiding and evaluating its application.

ACKNOWLEDGEMENT

The research summarized herein was supported by NASA under Grant NGL 15-005-112. Grateful appreciation is expressed to NASA for this support. The various individual studies were carried out by LARS staff members G. Santner, K. Hunt, Dr. L. Eisgruber; graduate students T. Robertson, A. Wacker, P. Scheffer; and the author.

REFERENCES

1. IBM 4507 Digital Image Display System, IBM Federal Systems Division, Gaithersburg, Maryland, October 1970.

2. FIELDSEL: LARS Data Editing Program, LARS Program Abstract No. 255, Laboratory for Applications of Remote Sensing, West Lafayette, Indiana. 47906.

3. Wacker, A.G., "The Minimum Distance Approach to Classification," Technical Report Number TR-EE71-37, School of Electrical Engineering, Purdue University, Lafayette, Indiana 47906, October 1971. Also LARS Information Note 100771, Laboratory for Applications of Remote Sensing, West Lafayette, Indiana 47906, October 1971.

4. Swain, P.H., T.V. Robertson, A.G. Wacker, "Comparison of the Divergence and B-Distance in Feature Selection," LARS Information Note 020871, Laboratory for Applications of Remote Sensing, West Lafayette, Indiana 47906, February 1971.

5. Fu, K.S., P.J. Min, "On Feature Selection in Multiclass Pattern Recognition," Technical Report Number TR-EE68-17, School of Electrical Engineering, Purdue University, Lafayette, Indiana 47906, July 1968.

6. Landgrebe, D.A., P.J. Min, P.H. Swain, K.S. Fu, "The Application of Pattern Recognition to a Remote Sensing Problem," Proceedings of the Seventh Symposium on Adaptive Processes, UCLA, Los Angeles, California, December 1968.

7. Robertson, T.V., "Some Experimental Results for Linear Classifiers Applied to Agricultural Remote Sensing Data," LARS Information Note 020972, Laboratory for Applications of Remote Sensing, West Lafayette, Indiana 47906 (in preparation).

8. Eisgruber, L.M., "The Effect of Subsampling Ratios on Precision of Estimates from Remote Sensing," LARS Information Note 021072, Laboratory for Applications of Remote Sensing, West Lafayette, Indiana 47906 (in preparation).

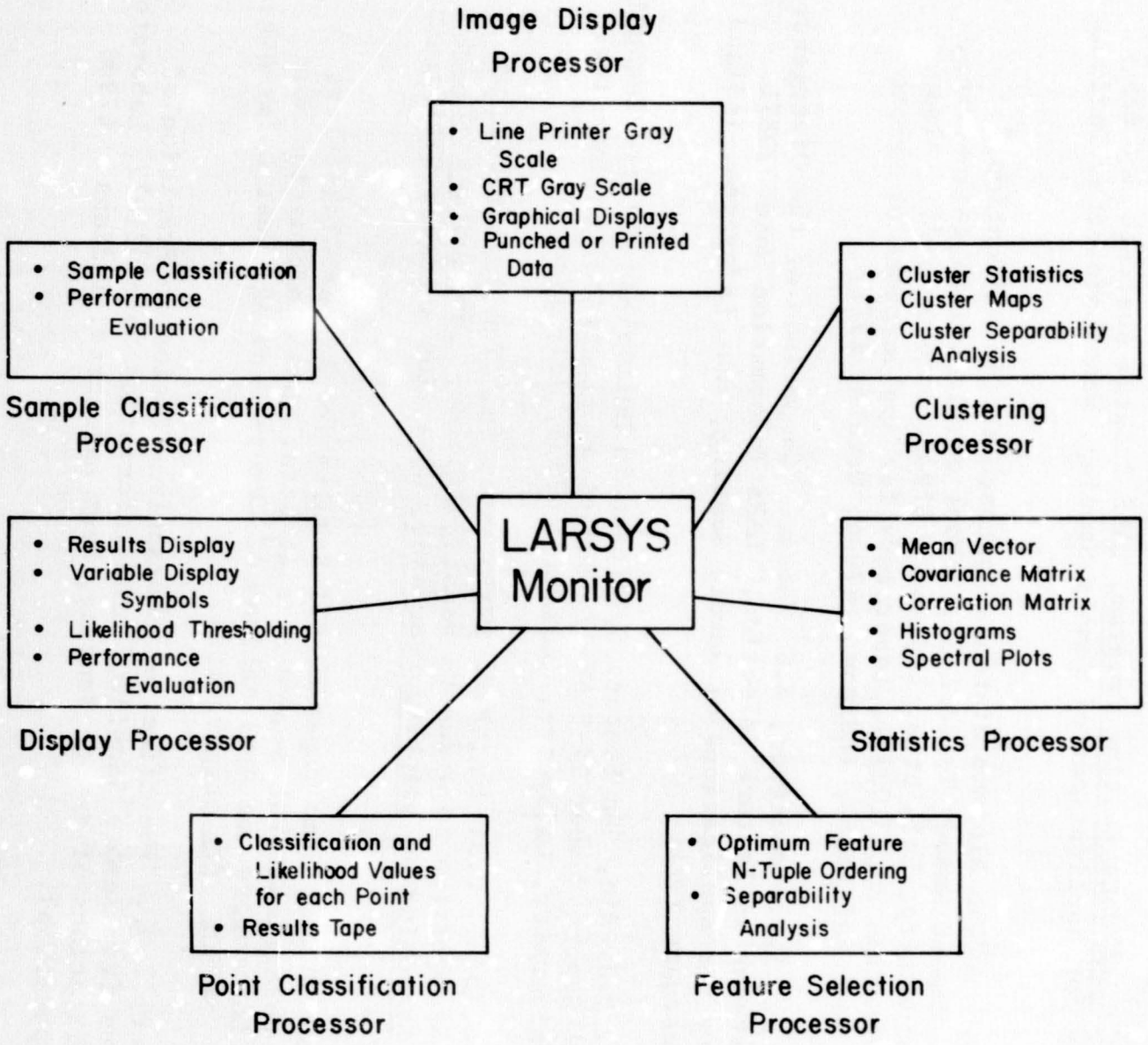

Figure 1. LARSYS: a software system for the analysis of multispectral remote sensing data.

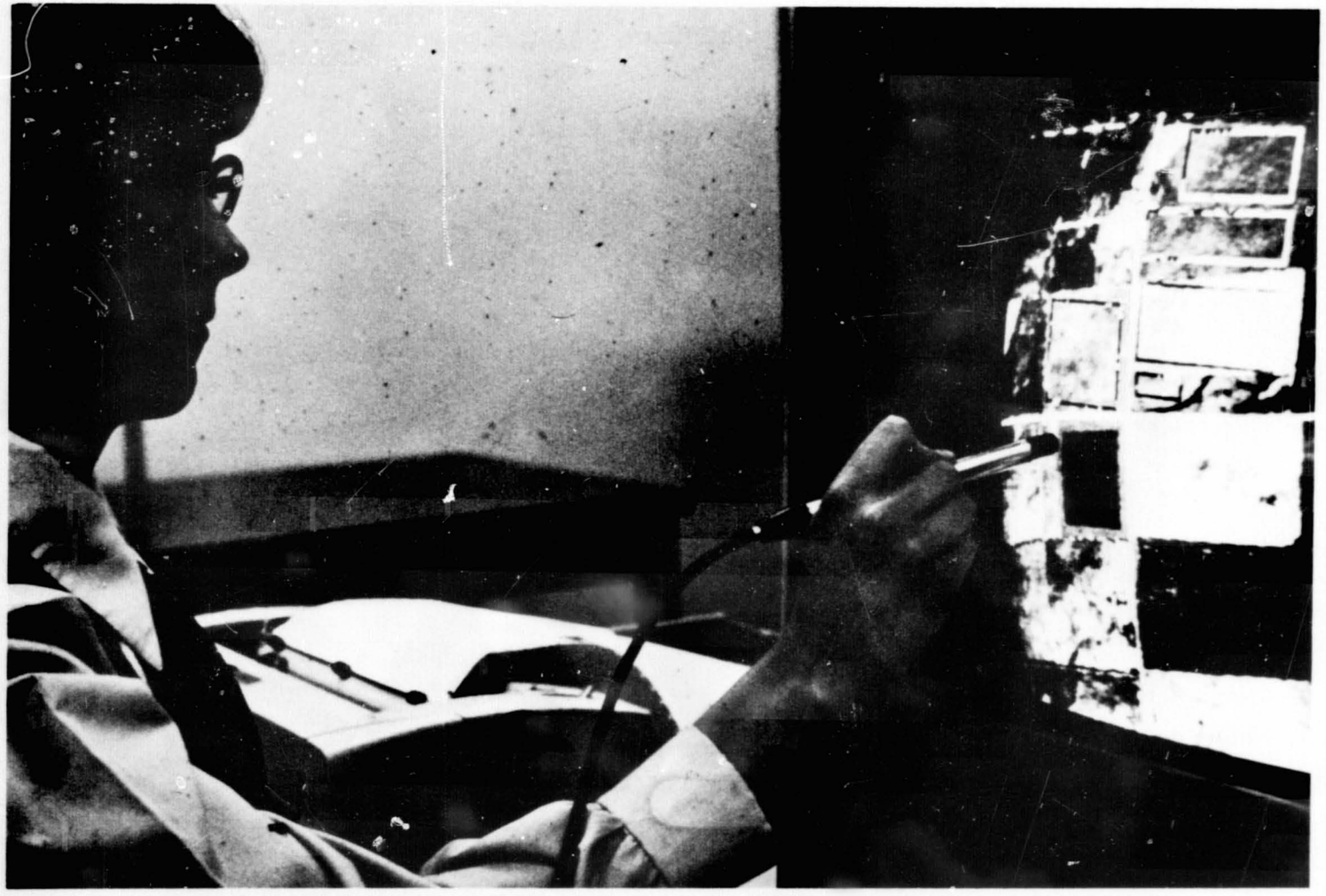

Figure 2. Specifying field boundaries on the digital image-editing display system.

Figure 3. Outlining field boundaries on gray-scale printouts.

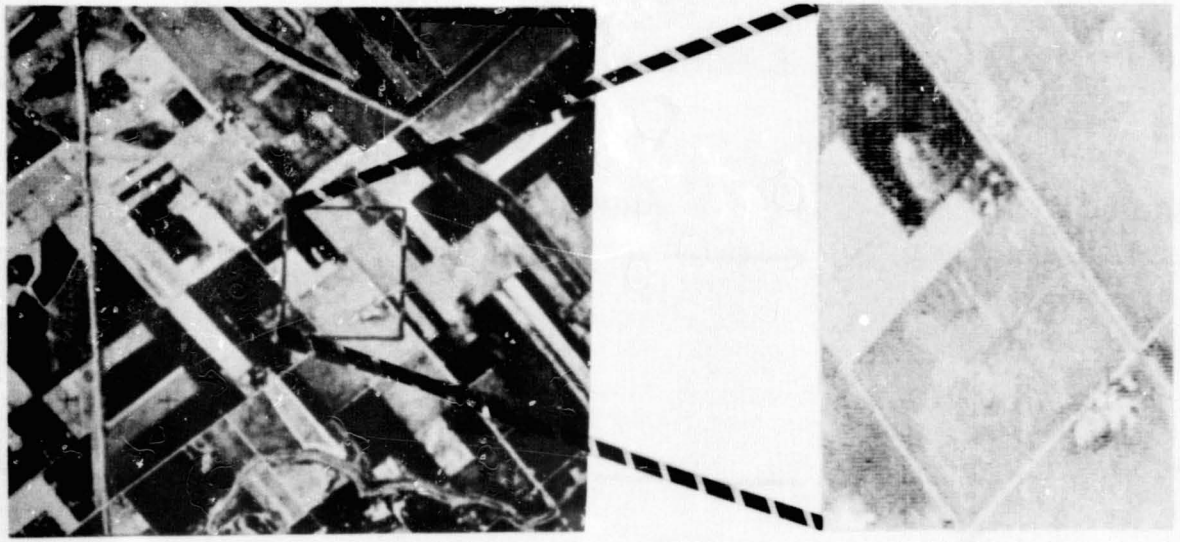

a) Digital display image

b) Computer printout

Figure 4. Map-like display of cluster analysis results.

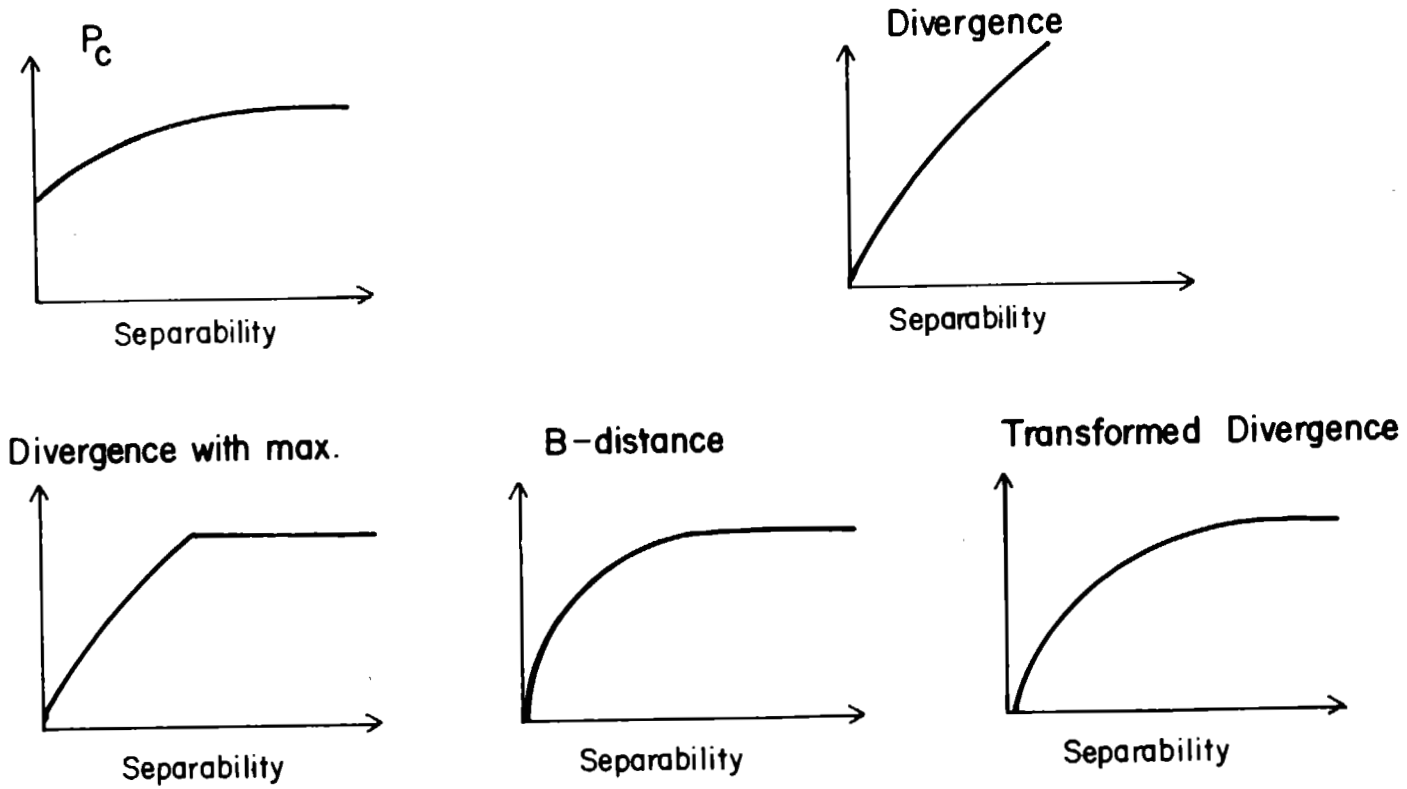

Figure 5. Behavior of probability of correct classification and various measures of statistical separability.

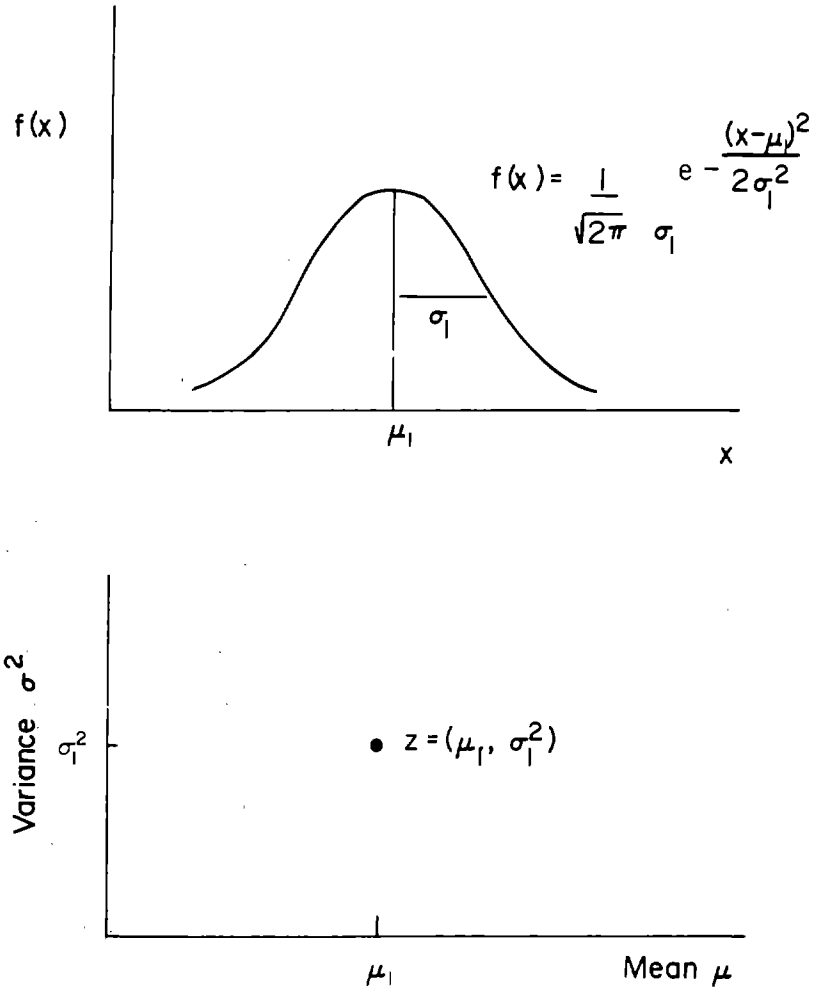

Figure 6. Parameter space representation of a sample (one-dimensional Gaussian case).

SECTION 51

DATA PROCESSING II: ADVANCEMENTS IN LARGE-SCALE DATA PROCESSING SYSTEMS FOR REMOTE SENSING*

by

David Landgrebe and Staff
Laboratory for Applications of Remote Sensing (LARS)
Purdue University
Lafayette, Indiana

INTRODUCTION

In the preceding paper, Dr. Swain described some of the research activities in Data Analysis techniques carried out at LARS/Purdue this past year. This paper continues by summarizing some results obtained from additional data processing research tasks now under study there. Time and space do not permit details. Full descriptions of these projects are reported in LARS reports and in papers in the open literature.

These studies fall into three categories: (1) an examination of the suitability of several sensor types with regard to producing data required for multispectral machine analysis; (2) various types of data preprocessing necessary to prepare such data for analysis in this fashion; and (3) an experiment in how to make this type of technology available efficiently and inexpensively.

COMPARISON OF SENSOR TYPES

There are a large number of different types of sensors capable of producing data as input to machine analysis processors. These sensor types tend to fall into three broad categories: scanners, photography and television. The line scanner tends to be preferred for this type of analysis procedure because it covers greater portions of the spectrum and has greater dynamic range and radiometric precision. However, scanners tend to be expensive, complex to operate and relatively unavailable at this time. Photography, on the other hand, is relatively less expensive and is widely available; it is a very well-developed technology.

---

*In this paper, results from a number of studies are summarized; researchers are identified in the Acknowledgment section.

Television has still different characteristics in this regard, having some of the advantages and disadvantages of both. In order to compare these sensors as sources of data for this type of machine processing and analysis, a scene was selected in which data had been gathered by both a scanner and photographic cameras simultaneously. Classifications with identical classes and training areas were carried out on both types of data. From this scene four different data types were to be compared:

- scanner data;
- black and white multispectral photography;
- color infrared photography; and
- vidicon-scanned color infrared photography.

The scanner data was used directly in this test. The black and white multispectral photography was first scanned, digitized and then the images from the several parts of the spectrum were registered with respect to one another. In the case of the color IR photography, color separations were first obtained and these were then scanned, digitized and registered.

Unfortunately, television data was not collected simultaneously with the other types of data since an airborne television sensor system was not available to us. However, in order to obtain some idea of how television might have performed, the color photography was subjected to a vidicon scanning system* after which it was digitized and registered.

The results of this study are shown in Figure 1 in bar graph form. The results for individual classes are shown on the left with the overall average results shown on the right. In carrying out this study, it was decided to assess the performance based upon the accuracy achieved by the samples used to train the classifier. This is compared to using so-called test samples or samples other than those used to train the classifier. It was felt in so doing that this would minimize the effect of scene variability, one of the other major experimental variables.

In the case of the scanner data, the best four of 15 available spectral bands were selected using the divergence processor. These bands turned out to be 0.44-0.46, 0.58-0.62, 1.0-1.4 and 1.5-1.8 micrometers. The data was collected with the Michigan scanner system. Three bands of black and white photography were available in a 70mm format. The film types and Wratten filters used were: Green, 2402, 58; Red, 2402, 25A; and IR, 2424, 89B. The color photography portion of the experiment was carried out using type 2443 color infrared film in a 9" by 9" format with a Wratten 15 filter.

---

*The vidicon scanning of the photography was accomplished by the IBM Houston Science Center at no cost to Purdue.

It is seen that the classification accuracy as a whole was very high. Thus, a two or three percent difference in overall accuracy is probably significant.

The results do tend to verify what might be expected from a detailed knowledge of the sensor type and processing algorithms, namely, that the scanner produced the highest performance. This was followed by the black and white multispectral photography; performance in this case was only slightly greater than color photography due no doubt to the possibility of achieving slightly greater radiometric precision with a single photographic emulsion as compared to a multiple-layer one. The television-scanned data gave the poorest performance, and while it must be kept in mind that this data contained the variability factors of both the photography and the television sensor, it nevertheless is to be expected that performance of a television sensor for this type of analysis would indeed be somewhat inferior to the others. No corrections were applied to the data with regard to sun angle effect, vignetting or other types of distorting factors.

DATA PREPROCESSING STUDIES

There are a large number of parameters of the sensor and data processing systems which are, at least initially, under the control of the system designer. Such factors as the spectral and spatial resolution, signal-to-noise ratio, the degree to which the signals are calibrated against available standards, and many others have a direct bearing upon the achievable classification accuracy. In order to determine the sensitivity and overall effect of the system with regard to these various parameters, a number of studies are underway at LARS/Purdue. An additional objective of these studies is the determining of suitable techniques by which data preprocessing may be carried out to modify and optimize the data with respect to these parameters. This is especially desirable since no one system design will be universally optimal for all data analysis purposes. Figure 2 shows the overall organization of these studies. They are divided into four broad areas, each of which has several sub-parts. For example, consider the programs in signal-to-noise ratio improvement indicated on the left. By using adjacent scan lines of data it is possible to improve the signal-to-noise ratio but, to some extent, at the expense of spatial resolution. This technique is used to remove or minimize the effect of such random noise as is generated in a scanner detector among other places.

There are many types of systematic noise introduced by sensors. Effects such as vignetting in photography or television where the data is collected in frames or Moire patterns in line scanners are examples

of problems which can be minimized or removed through data processing, but generally at the expense of other parameters in the system. The objective here is to develop suitable techniques to apply theory to practice and to quantify the result of doing so. In the remainder of this section are presented results obtained during the past year by several studies indicated in Figure 2.

SCANNER DATA CALIBRATION STUDY

Consider first a study of methods for the radiometric calibration of scanner data. The results from this study are shown in Figure 3. The data used for this study is from the Michigan scanner system and the 1971 Corn Blight Watch Experiment. With this scanner system the scanner sensors are optically exposed to three different calibration sources for each revolution of the scanning mirror. These are a black level (C_0), a level of fixed illumination (C_1) and a sensor exposed to the solar insolation on the top of the aircraft (C_2). The C_0 or black level calibration is intended to be used to remove any DC drift which may occur during the course of a data gathering mission by establishing a reference level at the output for zero (optical) energy in. It is possible to use either C_1 or C_2 to correct for any changes in system gain and/or any changes in illumination occurring at the top of the aircraft. In actuality, the computer software system used has been arranged in such a way that any two of these three signals can be used to establish calibration of the data in a linear fashion.

When considering data calibration however, one must recognize that calibration levels can only be determined with a signal-to-noise ratio which is finite (that is, less than infinite) just as is the case for the data from the scene itself. Thus, one will be using calibration information of a given signal-to-noise ratio to correct scene data of a given signal-to-noise ratio and depending on the need of the system for calibration, the effect may either improve or degrade the overall performance of the system. The question posed in this study then is: In a given situation does calibration help, and if so, which type helps the most?

Three different data sets were used in this particular test. These data sets are from segments 206, 208 and 215 of the 1971 Corn Blight Watch Experiment.* In each case training samples from a given segment

*Segments 201 through 230 of the 1971 Corn Blight Watch Experiment were distributed in order from north to south along the western third of the State of Indiana. These three segments are therefore from the northern half of the state and are separated by a maximum of about 100 miles. Each segment is approximately 1 by 8 miles.

were selected for a corn vs. noncorn classification. The classification was carried out and then samples from fields other than those used for training were used to test the accuracy to assess the performance.

Shown in Figure 3 are the results of the test with the individual segment accuracies shown on the left and the overall average shown on the right. The overall average does indeed indicate that calibration helps, although note that in segment 215 the "no calibration" control classification provided a higher performance than any of the types of calibration. Again, overall there was indicated a slight preference for using the $C_0 - C_1$ calibration.

Based on the design of the sensor system, the signal-to-noise ratio of the C_1 calibration signal is, in general, poorer than that from the sun sensor C_2. That is to say, given a higher quality signal from the calibration lamp, this slight preference in this case of $C_0 - C_1$ calibration might become an even more pronounced preference. It is important to add however, that in the case of aircraft data, as one collects data from larger and larger areas, variations in solar illumination become more important, and it may become more desirable to use $C_0 - C_2$ calibration in order to achieve highest accuracy. This proved to be the case in the next experiment to be described.

EXTRAPOLATION OF TRAINING SAMPLES

Over how large a geographical area is a given training set valid? This is a very important question. Only a relatively small proportion of the total cost of processing the data at the present time is attributable to the actual analysis calculation itself. This is true whether the analysis is done by analog or digital mode. The expensive portion of the processing remains the training phase of the analysis. Thus, it is important to develop techniques which reduce the complexity and therefore the cost of the training phase and it is also desirable to develop techniques by which a single training of a classifier can be utilized over larger and larger geographical areas. It was an examination of this latter question which was treated in the study to be described now. Many of the details of the study are apparent from the results displayed in Figure 4. The ordinate displays test data accuracy. The abscissa indicates the segment of the 1971 Corn Blight Watch Experiment data from which training was derived. The legend of the graph indicates the segments classified. The following table indicates the distance separating each segment.

Number of Airmiles Separating the
Center of Four Segments of the
1971 Corn Blight Watch Experiment

Segment Number	208	215	230
206	28	90	235
208		68	193
215			126

As expected, it appears to be generally true that the farther one gets from the training sample area the poorer the accuracy. However, there are several factors to be kept in mind in this particular test in considering how rapidly the accuracy deteriorates with distance. First of all, the segments are distributed in a north-south direction. This is the direction of maximum change with regard to seasonal variation. One would expect the growing season to be approximately two weeks further advanced at the southern most segment on a given day than at the northern most. Second, while all data used is from the same mission period of the corn blight watch, it did not prove possible to gather all the data on the same day. Indeed, the data gathering was extended over a 13-day period and, in addition, the data from the north, or least advanced portion of the growing season, was gathered first, with that in the south or most advanced being gathered last. This tended to enhance seasonal variations with regard to crop maturity. All data was gathered between 10:30 and 11:45 a.m. Thus there were only relatively small changes in sun angle. It did prove desirable in this case to use $C_0 - C_2$ calibration. That is, that calibration involving removing DC drift with the black level calibration information and adjusting the overall system gain based upon the indicated solar illumination as determined at the top of the airplane.

These results together with earlier results shown, tend to be encouraging with regard to the extrapolation of training sets particularly in view of the improvement expected when satellite-gathered data becomes available. Perhaps one of the greatest advantages of the satellite, one which is not achievable with an aircraft system, is that data over very large areas can be gathered in a very short time, thus holding as nearly constant as possible many experimental variables of the system such as the sun angle, time of the growing season, etc.

SUN ANGLE EFFECT CORRECTION

Attention has often been drawn to the fact that the reflectance of earth surface materials is very dependent upon the angle of illumination relative to the angle of view. This fact has a pronounced effect upon all types of imagery. The effect on scanner imagery is illustrated in Figure 5. The left image in this figure shows uncorrected data which was gathered by scanner at 10:00 a.m. This data was gathered from an aircraft having a northern heading such that at this hour of the morning the sun was to the right and somewhat to the rear (due to the season and latitude of the flightline) of the aircraft. The fact that the image appears washed out on the left is not an artifact of image reproduction, but sun angle effect which is present in the data.

Briefly, since the line of view is nearly parallel to the illuminating rays of the sun on the left portion of the image, the amount of energy reflected from any given (rough surface) material tends to be greater.

This effect is even more apparent by viewing the average response from a large number of scan lines. Figure 6 shows such a presentation in graphical form. Plotted here is the average response for a large number of columns of data in the imagery plotted versus the column number. For this data set, gathered shortly after 9:00 a.m., the response is clearly greater on the left, or west, portion of the field of view than it is on the right, or east. Figure 7 and 8 show presentations of the same type for data gathered near local noon and late in the afternoon, respectively. Variations of this effect with time of day is readily apparent.

This effect has been known for some time and it is relatively easy to improve the appearance of the imagery by appropriate processing. The most successful technique found to date has been to use a characteristic curve such as Figure 6 to derive appropriate multiplicative correction factors for each column in the data. The results of having applied this technique to the data for the leftmost image of Figure 5 is shown in the center of Figure 5. It is obvious that the appearance of the image is greatly improved. However, a careful inspection of the image will reveal that a vertical line structure has been introduced into it due to the fact that the characteristic curve was not sufficiently smooth. If, prior to applying the correction, this characteristic curve is smoothed appropriately, the result achieved will be as shown in the right-hand image of Figure 5.

Perhaps more important than the appearance of the image, however, is the quality of the data itself. A more quantitative test of the relative effectiveness of this type of correction can be obtained by carrying out a classification of the data set into appropriate classes for the case

of both corrected and uncorrected data. Two examples of the result of doing this are shown in Figure 9. In this case, the results for a corn versus noncorn classification carried out on two different data sets is shown, and in each case the classification of the original versus sun-angle-corrected data is compared. Note that the correction of the data did result in a significant improvement in accuracy for the classification indicated by the two pair of bars on the left. However, the other classification shows a degradation of performance due to data correction. Note that the degradation occurred in the data set collected earlier in the morning, when the sun angle effect would be more severe.

The purpose of this is to illustrate the point that though satisfactory improvement in image appearance is possible, the results with regard to improving data quality are quite mixed. It must be kept in mind that the degree to which the illustrated sun angle effect takes place depends not only upon the angle relationship between the sun, the scene and the observer but also the contents of the scene itself. Individual areas within the scene will display this effect to a greater extent depending on their contents. By the procedure described, although a globally appropriate correction can be made, there is no information available by which to make the correction also locally correct. Since classification is made on a local basis it is local correction that is required. Best overall results can be obtained by defining pairs of classes - one set for the left side of the scene, the other for the right side - but at the expense of training and processing complexity. It is felt, therefore, that the problem is in an unsatisfactory state and a new approach is really needed, one no doubt less empirically based, but based on an appropriate model of the total situation.

DATA COMPRESSION TECHNIQUES

We turn now to the question of data compression. One of the most obvious characteristics of the remote sensing field is the large quantity of data. This data quantity tends to strain system resources especially with regard to data transmission and data storage and retrieval. If means for compressing the data can be found which do not significantly alter the data quality, it would be most valuable. This led us to begin a data compression study and in particular to examine a class of linear transformations for this purpose. Among other advantages, this approach would tend to minimize the amount of additional processing which would be involved.

There exists in the literature a particular signal representation scheme known as the Karhunen-Loeve Orthogonal expansion. Theoretical results available with regard to this expansion suggested a number of advantages and I shall briefly describe the technique. In this

application it amounts simply to a principal components transformation and this is illustrated in Figure 10. Suppose for example, we have some multispectral data in two spectral bands. Since multispectral data is typically correlated from channel to channel it may distribute itself as shown by the oval shaped distribution in this figure. A principal components transformation amounts to defining a new set of axes by taking a linear combination of the original axes. The computation involved is shown by the two equations in the lower part of the figure. The a coefficients in these equations determine the orientation of the new axes relative to the original ones.

A principal components transformation is that particular transformation by which the first new axis, y_1 in the figure, is chosen so as to be oriented along the direction of maximum range or spread of the data as shown in the figure. The second component is chosen perpendicular to the first but in the direction of the next most principal distribution of the data. In higher dimensional cases, succeeding axes continue to be chosen orthogonal to the prior ones but in the direction of maximum remaining range of distribution.

The usefulness of this transformation for the data compression problem comes about because multispectral data, typically being highly correlated between spectral bands, tends to fall in a relatively long, narrow distribution in n-dimensional space. Thus, it is possible to concentrate most of the dynamic variability of the data in a very few number of principal components. This is dramatically illustrated in Figure 11, which is a plot of one measure of the dynamic range of the data after transformation as a function of the principal component number. This data was from 12 spectral bands and it can be seen that after transformation only about 3 coordinates have any appreciable dynamic distribution of data. The concept for data compression purposes is to transform this 12-spectral band data into 12 new components and then discard the, in this case 9, which have essentially no range and therefore no information in them. In this case, a 12 to 3 or 4 to 1 compression ratio would be achieved while incurring only the small error indicated by the sum of the mean square values of the 9 discarded components as compared to the 3 retained ones.

A further compression can also be achieved by a process called "bit allocation." For example, suppose the original 12 band data had been represented to an 8 bit precision in each of the 12 bands; that is, in each band any one of 256 possible gray values is allowed for. This would be 8 bits times 12 bands or 96 bits per multispectral sample.

Again referring to Figure 11, certainly the dynamic range of the first principal component after transformation would be much larger than any of the original spectral bands had been. Therefore, in order to

achieve the same precision of data representation more bits would need to be assigned to this component. However, succeedingly less could be assigned to successive components. It may turn out, for example, that for the 3 most principal components, the dynamic range required in terms of the number of bits might be 9, 6 and 4 allowing for 512, 64 and 16 gray values respectively for the three most principal components. This total new bit allocation of 9 plus 6 plus 4 equals 19 bits and compares with the 8 plus 8 plus 8 equals 24 which might have been used had not bit allocation been considered. This represents not only an additional compression of data but also an improvement in the precision with which the data would be presented since the original 8 bits in the first principal component would not have been adequate to handle properly the larger dynamic range.

Figure 12 shows a block diagram of a test data compression system which has been assembled in order to test this general approach on earth resources multispectral data. The first two blocks indicate the two steps just described; namely, data transformation followed by bit allocation. If it is then desired to recover the original data, the next step would be an inverse transformation followed by a bit allocation, thus transforming the compressed data back to the original coordinate system and the original dynamic range.

Two additional features not previously described have been incorporated into this system. First of all, though the above description of the concept involves compression based only on spectral redundancy, it is possible to use this approach to take advantage of both spectral redundancy and spatial redundancy in the imagery data. It is apparent from the above description that basically the only requirement at the input is for the data to be in the form of a vector representation. The components of the vector may be spectral components as described above, but they may also have been derived by using groups of vectors in spatial proximity to one another. For example, if the data is composed of samples from a 12-band multispectral scanner, inputs to this data compression system could be assembled by taking pairs of adjacent points, thus creating 24-dimensional input vectors. Indeed, the system of Figure 12 is prepared to handle data from an arbitrary number of lines, an arbitrary number of columns and an arbitrary number of channels of adjacent sample points. In this way, in addition to spectral redundancy, spatial redundancy can also be used to achieve higher compression ratios.

Another feature of the system is that other transformations besides the Karhunen-Loeve (principal components) transformation have been implemented with the system. The principal components transformation is a type referred to as a data-dependent transformation in that the precise coefficients for the transformation are computed each time based upon calculations involving the total data set to be transformed. However, any transformation could be used and at least two other transformations

have been examined besides the one just described. These are the standard Fourier (harmonic analysis) transformation and one called the Hadamard transform. The Fourier transform was selected for tests because of its familiarity and the robustness the transformation has shown with regard to a large class of problems extending across the various fields of science. The Hadamard transform, on the other hand, was selected because of its extreme convenience since the Hadamard functions and, therefore, the coefficients involved, are always either ones or zeros, thus making a digital implementation of this transform extremely simple and efficient from the computational standpoint. Both of these two transforms are non-data dependent; that is, they require no prior computation of scene statistics before proceeding with the transformation. In addition to these two, an "average" Karhunen-Loeve transform could be used based on scene statistics from a so-called average scene. This would be another means of eliminating a need for a precalculation of scene statistics at the cost of some degradation from optimum performance.

In addition to data compression for data storage and retrieval purposes, a procedure such as the above could have several other advantages. For example, in Figure 12 the data transformation output could be used directly for feature selection and classification purposes. Assuming 12-dimensional original data, one problem immediately to be faced in preparing to analyze the data set is which spectral bands will be best in a given classification. A somewhat lengthy computational procedure is available for determining the optimum subset of spectral bands desirable; however, the data in principal components form can be used directly in that the first n-principal components tend always to produce classification accuracies which are at or above the accuracy performance obtainable by the same number of optimally chosen original spectral bands. Thus, in addition to accomplishing data compression, this scheme shows promise for eliminating the need for the optimum feature selection computation. This property of the transformation has been known for some time and has been used previously by other researchers elsewhere.

Further, since after data transformation the coordinate system, and therefore the components involved, have been oriented to have maximum dynamic range, if an image is constructed using the data from the first principal component at this point, the image will have greater dynamic range and therefore greatest scene contrast of any possible image presentation of the data. One is guaranteed of having greater image contrast than any one of the original spectral bands could have. This provides imagery useful in determining, for example, boundaries in the scene and manually determining differences between any two materials. Figure 13 shows images constructed from data using the first, second, third and twelfth principal components. These images were produced by attempting to spread whatever dynamic range is present in the data over the full range of the contrast available in the photographic film. Notice that the scene contrast of the first principal component image is markedly greater than that in the third

and slightly greater than that in the second. Notice also that the twelfth principal component has essentially no image detail at all.

How does one determine the effectiveness of a proposed data compression scheme? The questions which must be asked are: how much distortion does the compression scheme introduce into the data and how much does this distortion affect the potential classification accuracy and the image quality. Figure 14 gives the rate distortion characteristics for this compression scheme and therefore shows the relationship of the degree of compression obtained to the amount of distortion introduced. The distortion is assessed by determining the mean square difference between the original image and the compressed and reconstructed image. In this case, the original data was available at eight bits-per-sample precision. In this case, the lower and upper curves are bounds on possible performance. The lower curve represents a best performance theoretical limit based upon information theory considerations after appropriate assumptions. The upper curve on the other hand, is the result achieved by simply truncating the number of bits per sample in the data. In between them, then, lies the performance characteristics for the three transformations under consideration. The Karhunen-Loeve clearly provides the best performance. However, keep in mind that it is a data dependent transformation. The Fourier and Hadamard transforms show the penalty of achieving non-data dependency. These are the performance characteristics based upon using a rectangular region out of the image of size 8 samples by 8 samples by 2 spectral bands to construct the vector which undergoes the transformation. This appears to be a near optimal choice of combination between spectral and spatial redundancy.

Figure 15 shows the results of carrying out classification tests on the compressed data. A test classification was carried out using various numbers of features. In the case of the original data, the optimal spectral bands were first determined in each case. On the other hand, in the case of the principal components data, components were added in order as higher dimensional classifications were desired, thus indicating the lack of necessity for the calculation of optimal spectral bands in this case. Notice that the principal component classifications were always at least as high and usually higher in performance compared to the same number of components of original data. Notice also that the classification with three spectral bands was approximately as high as that achieved with any number of bands.

And finally, Figure 16 shows the result of carrying out a compression by a factor of eight and then reconstructing the image from the data. This is compared with the image made from the original data. For the small amount of distortion present, keep in mind that with such a procedure if it had originally been required to have 8 digital tapes to store the data, using this procedure only one would be necessary.

TEMPORAL INFORMATION AND THE IMAGE OVERLAY PROCESS

During each of the previous of these annual meetings, we have reported on progress towards achieving a suitable capability for the precision overlaying of one image from a given geographic area onto that of another from the same area. These images may be from different parts of the spectrum and/or from data gathered at a different time. This has proved to be very challenging, primarily since the precision required is better than plus or minus one resolution element; thus, in the overlay process one must cause all local distortions of one image to precisely conform to those of the other.

Though this processing step is likely to be a relatively expensive one in terms of achieving image overlays of this precision, there are a number of important advantages which will accrue as a result. For example, temporal information could be made available to the processor by having images from different time periods registered with respect to one another. Also, the need to correlate ground truth information with data from a new mission can be eliminated by overlaying the new image data onto an image for which the correlation has already been established. And, in the case of airborne scanner data which often contains unexceptably high geometric distortions, these distortions can be removed by simply overlaying them onto an image which is of high geometric quality. By overlaying the new data onto existing maps of areas, procedures could be established whereby the maps could be automatically updated after subsequent analysis of the data.

Before describing new procedures developed this past year for improving overlay quality possible, an example result in the use of temporal information will be shown. This result is given in Figure 17. Data from Missions 43M, 44M, 45M and 46M of the University of Michigan airborne scanner system and the 1971 Corn Blight Watch Experiment gathered over segment 208 were overlayed upon one another. This figure shows the result of carrying out classifications for corn versus non-corn for various subsets of features in this total data set.

First of all, beginning on the left, classifications for each individual mission period were carried out using the best four channels from each mission period as chosen by the divergence processor. It is seen that the performance was relatively high on Mission 43 but dropped considerably by the next mission and then began a slow rise. In addition to indicating that some times of the growing season are better for making these discriminations than others, part of the difference in performance in these four classifications is due to differences in quality of the data due to such factors as weather conditions, etc.

The fifth set of bar graphs indicates the result of using all of the preceding data for a classification; that is, a 16-band classification, each four of which came from a different mission period. Notice that the capability for classifying corn and the overall accuracy was indeed considerably higher in this case.

One additional question has been posed of this data set so far. It was hypothesized that not all 16 channels were necessary; that is, that the data is not really intrinsically 16-dimensional. The last classification was carried out using the best four of the 16 channels. The results show an overall performance down from the previous classification and also down from the results obtained for Mission 43M alone. This would tend to suggest that more than 4 of the 16 bands are indeed significant in this case. Much more needs to be determined about temporal information and its value.

With regard to the overlay procedure itself, a new element has been added to the technique in order that a larger number of different situations can be successfully handled. This work began originally with scanner data in mind. More recently, scanned photography and television imagery have also been successfully overlayed.

Figure 18 shows the steps now used in the overlay procedure. First, initial checkpoints or points of obvious image congruency are marked manually. Based on these checkpoints in the two images to be overlayed, a curve-fitting operation is carried out to find the best fit between the images from this initial information. More specifically, several coefficients in the curve-fitting operation are computed. Next, a fast fourier transform two-dimensional correlation is carried out between the two images over a uniform grid to obtain precision checkpoints. This correlation uses the initial overlay previously determined by the checkpoints in order to minimize the region which must be searched for a maximum of correlation. As a result of this correlation operation, a final overlay function is computed and the two images are then merged to achieve the final overlay of the images.

Figure 19 shows the actual overlay function which would be required for some photographic data from the Apollo 9 S065 experiment. Briefly, frame 3808 from the Lubbock, Texas area was scanned and digitized at a rate of approximately 2100 scan lines by 2100 samples per scan line. Shown here in the two curves is the variation in registration in terms of columns (samples). From the upper curve, it is seen that for channels 1 and 2, the green and red, respectively, when the left edge and right edge of the two images were in proper registration, the center of the frame was out of registration by as much as four samples. On the other hand, from the lower curve comparing channel 1 with channel 3, the green with the infrared respectively, the misregistration in this case was also

by as much as four samples but in the opposite direction. Thus, it would be necessary to change the local distortion of the red and the infrared channels so that it more properly corresponds with the green channel prior to the actual image overlay process. The entire process is, of course, carried out digitally.

ON THE AVAILABILITY OF TECHNOLOGY

One final experiment which is now underway will be described. The problem is as follows: research into techniques for the machine processing of earth resources data has now been underway for several years and significant new technology is now available. How can this technology become available to the user community? In considering this question, it was decided to analyze how this had been accomplished at Purdue between the data processing specialists and user scientists.

The elements for the availability of this technology are hardware, software and the knowledge or training on how to use the system. Hardware, at least in the form of general purpose computers, is readily available, but expensive. The transfer of software is more of a problem. The implementation of a large software system on a new computer is a relatively expensive process requiring special data processing expertise. It is also relatively expensive to maintain the software once it has been implemented.

Insofar as the third element, training, is concerned, it was possible at LARS to give individual attention to training each new staff member in the use of the system. However, for the transfer of technology to a large body of people, this technique would be too expensive and slow. This led to the proposal of a specific experiment in the transfer of technology. The concept is illustrated in Figure 20. It became apparent that the hardware a user scientist needs to have available is a card reader and punch, a typewriter and a line printer, in short, the I/O devices. Thus, it is possible to centralize not only the computational capability, but also the data storage capability required. Such a system would then have the following advantages: (1) full user access to both the data and the processing capability at the user's location; (2) centralization of the expensive portions of the hardware at considerable cost advantages; (3) centralization of software maintenance, again achieving a cost advantage plus a flexibility in updating; and (4) facilitation of training through commonality of data format, terminology and simplicity of communication. As a result of this commonality, standard training materials tailored to the specific system could be developed and the amount of teacher time per pupil could be greatly reduced by relying on training materials. The computer itself can be used for training purposes through computer-aided instruction.

The status of this experiment is as follows. It was authorized by NASA/Headquarters two years ago. On January 1, 1971, an IBM System/360 Model 67 time share system was placed on line in a minimal configuration in order to appropriately prepare the software system. The 1971 Corn Blight Watch Experiment necessitated a delay in the experiment since both the equipment and the personnel involved were required for the Watch. However, recently the final hardware was installed and is now ready. Some training materials are already ready while others are in preparation. The location for the first terminals are now being selected by NASA/HQ. It is expected that the experiment will be underway by the time ERTS is launched.

ACKNOWLEDGMENT

The research summarized herein was supported by NASA under Grant NGL 15-005-112. Grateful appreciation is expressed to NASA for this support. The various individual studies were carried out by Mr. Paul Anuta, Patrick Ready, a graduate student, Mr. Terry Phillips, David Strahorn, a student, Professor Paul Wintz, Dr. Stanton Yao and the author. Mr. Phillips has overall responsibility for coordinating the research projects reported here.

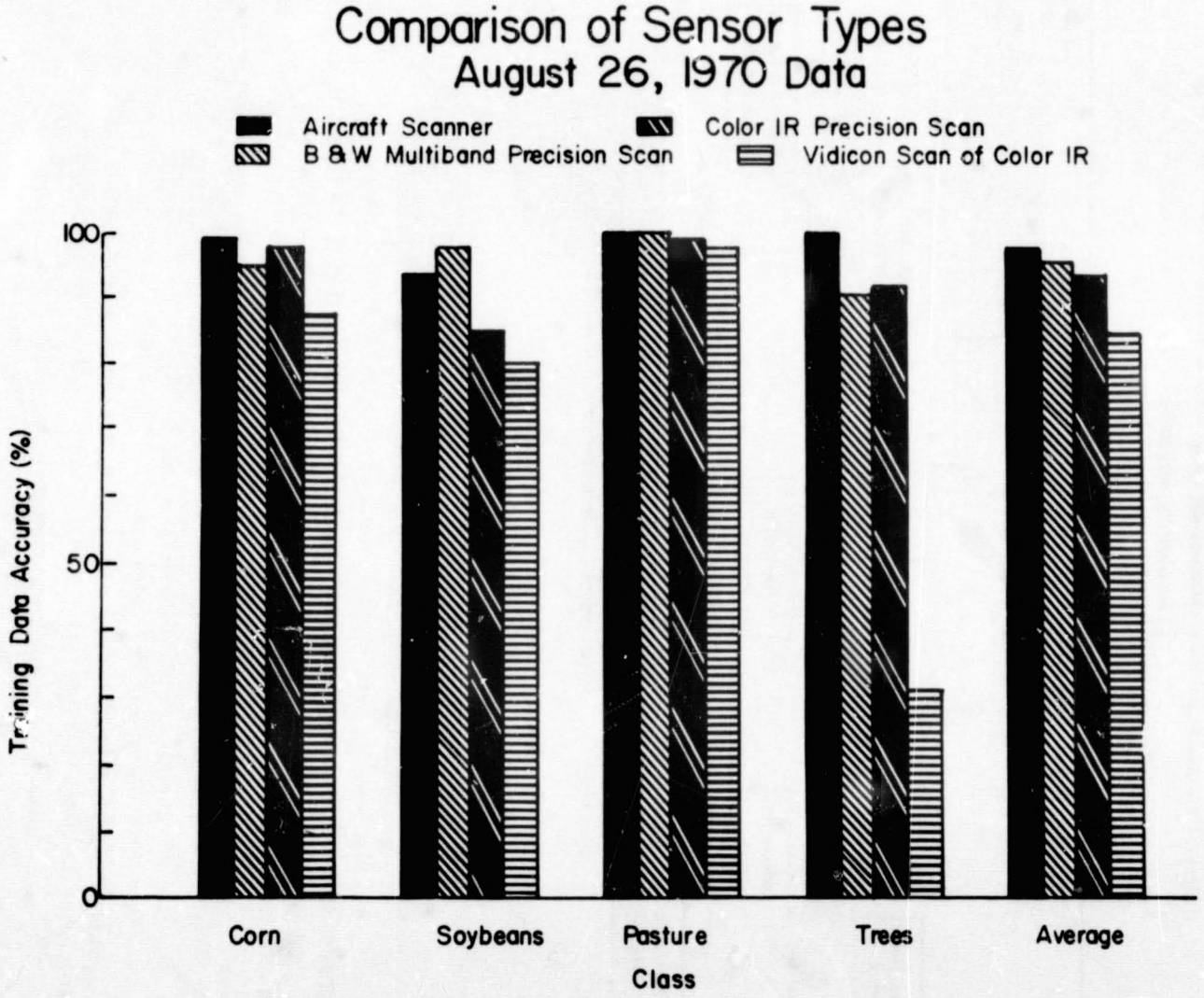

Figure 1.- Results of comparative classifications of multispectral data from four sensor types.

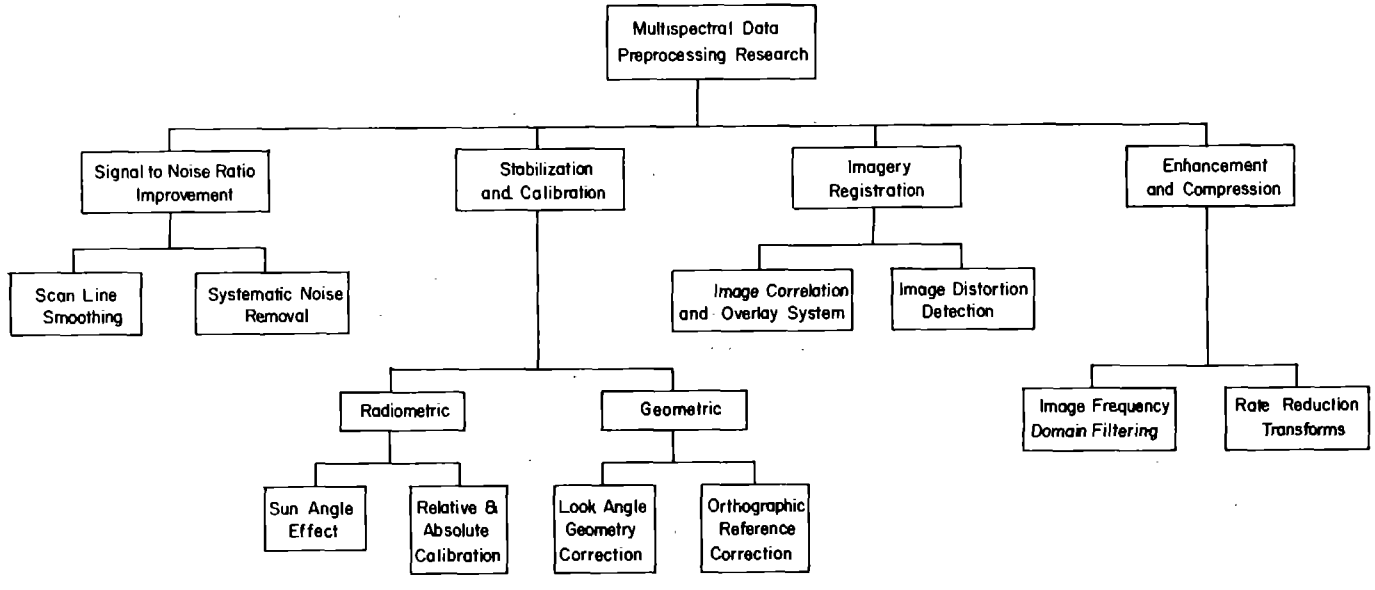

Figure 2.- Organization of multispectral data preprocessing studies being pursued at LARS/Purdue at this time.

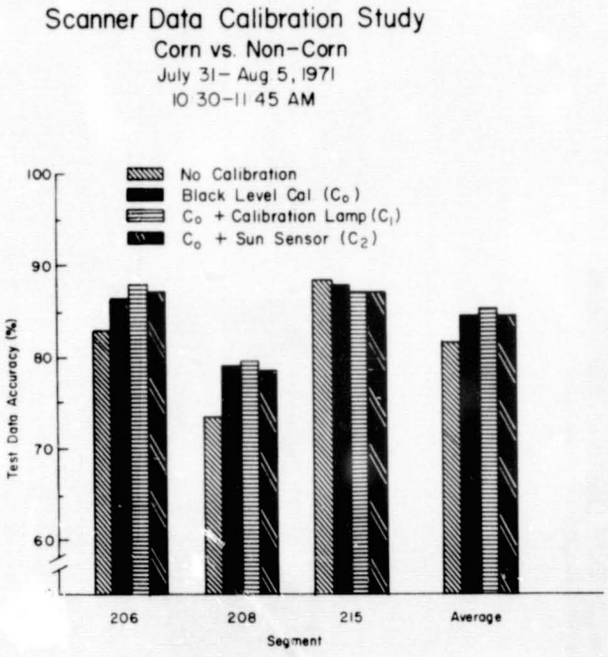

Figure 3.- Results of classifications from three different flightlines comparing four different calibration procedures.

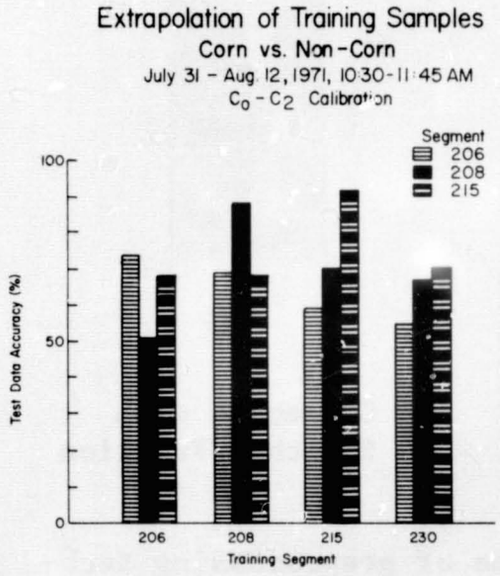

Figure 4.- Results of a test of extrapolating training data from one flightline to another. Segment 206 is more than 200 miles from segment 230, however, several factors, in addition to distance, are significant in this test.

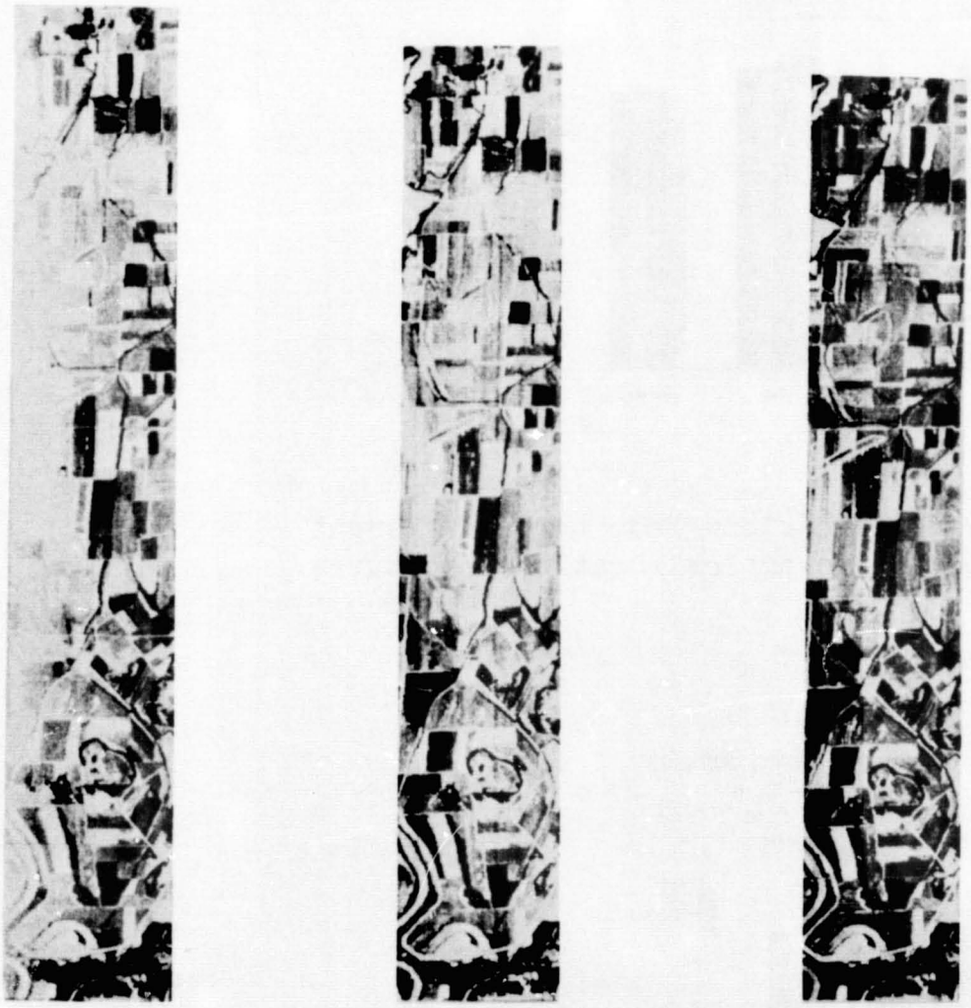

Uncorrected | Corrected | Corrected with Smoothed Function

Figure 5. An illustration of the use of preprocessing techniques to improve the appearance of imagery affected by variation in reflectance due to view angle and sun angle relationships (channel 6, segment 221, mission 42M, July 27, 1971.

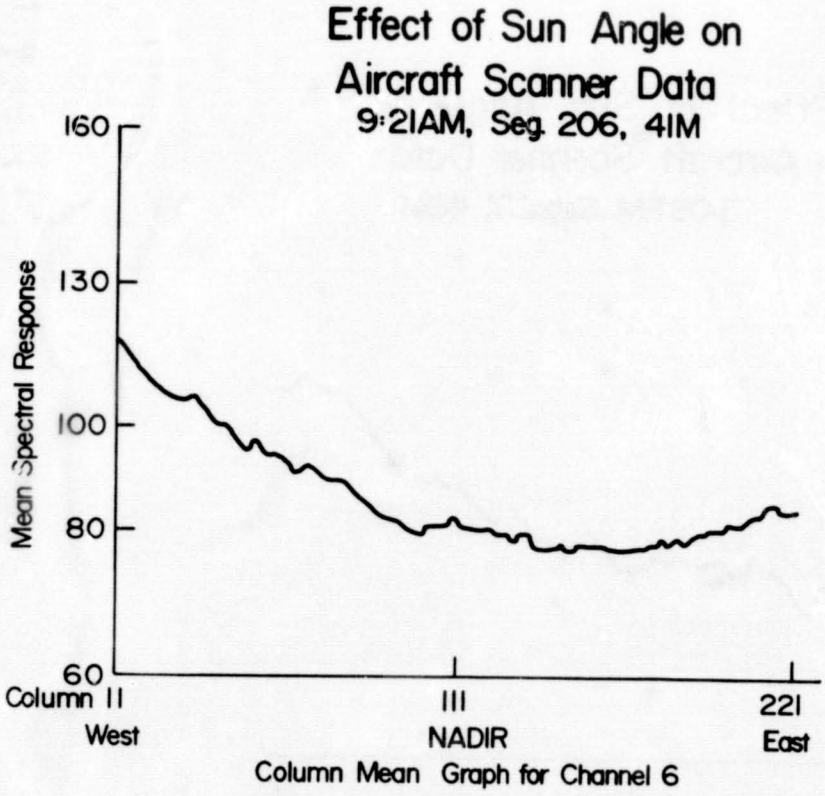

Figure 6.- A graph showing the mean spectral response as a function of view angle for data collected with an early morning sun angle. In this case, sufficient data has been used to nearly average out effects due to individual surface cover materials leaving only the sun angle effect.

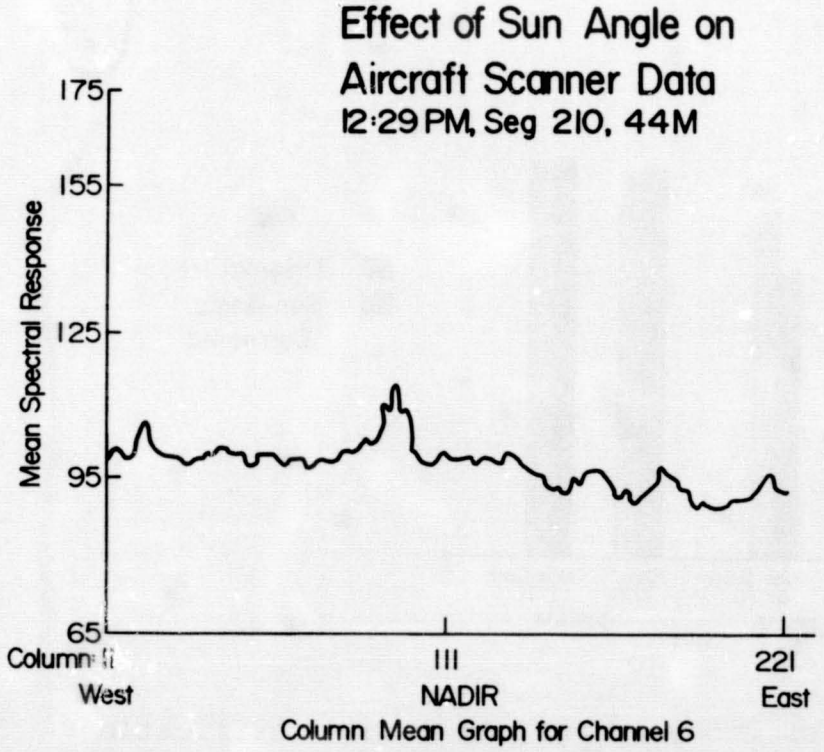

Figure 7.- A graph similar to Figure 6, but for data gathered with a nearly local noon sun angle.

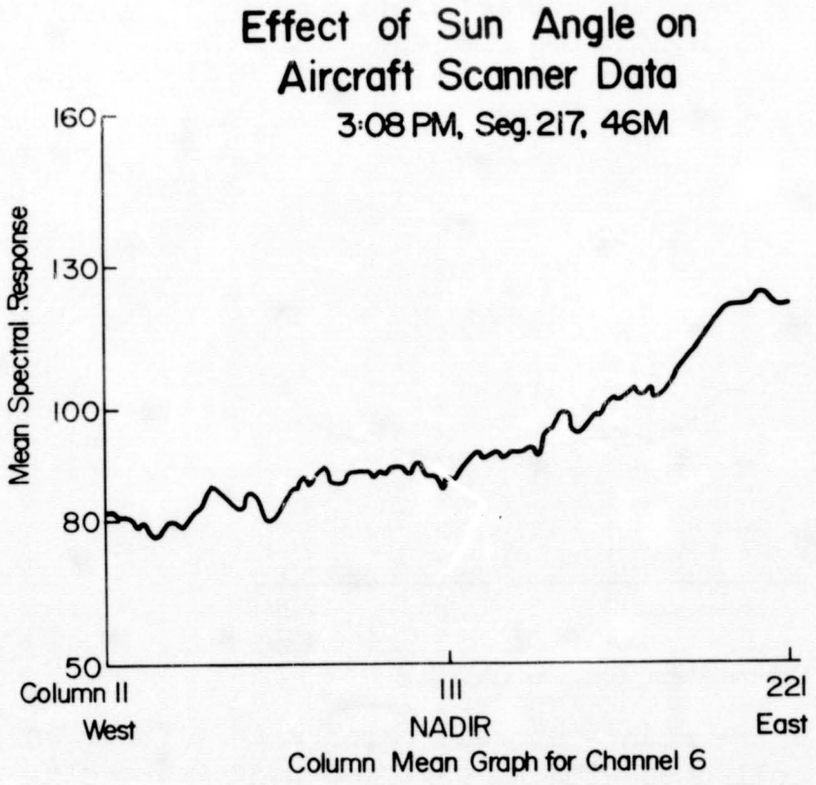

Figure 8.- A graph similar to Figure 6, but for data gathered with a late afternoon sun angle.

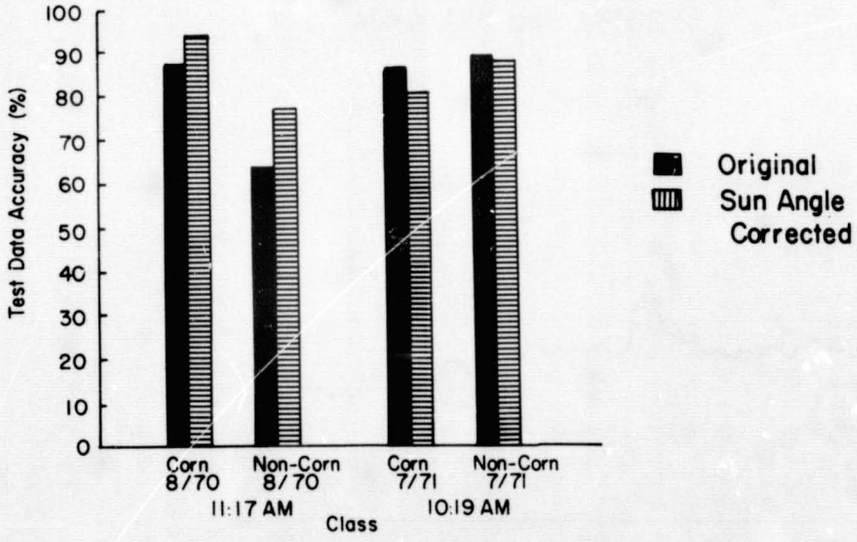

Figure 9.- Results of two corn vs. non-corn classifications carried out on the original data and the sun angle correction procedure used in Figure 5. Though the imagery appearance is obviously improved, the results from the quantitative classification comparison are mixed.

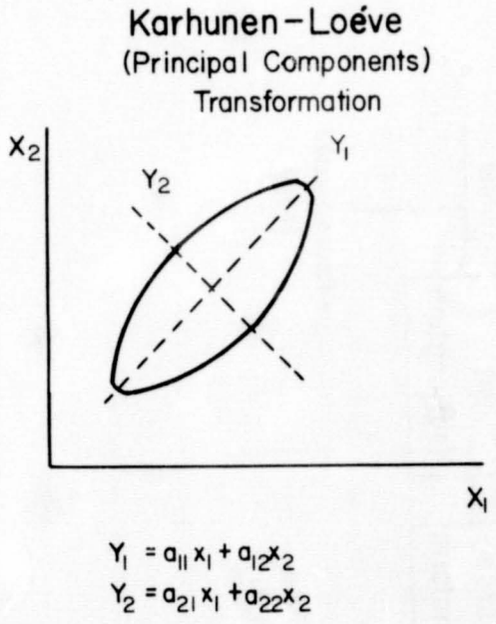

Figure 10.- A sketch of hypothetical bivariant multispectral data illustrating the result of a principal component transformation. X_1 and X_2 were the original coordinate axes; Y_1 and Y_2 are the new ones. The necessary equations are at the bottom.

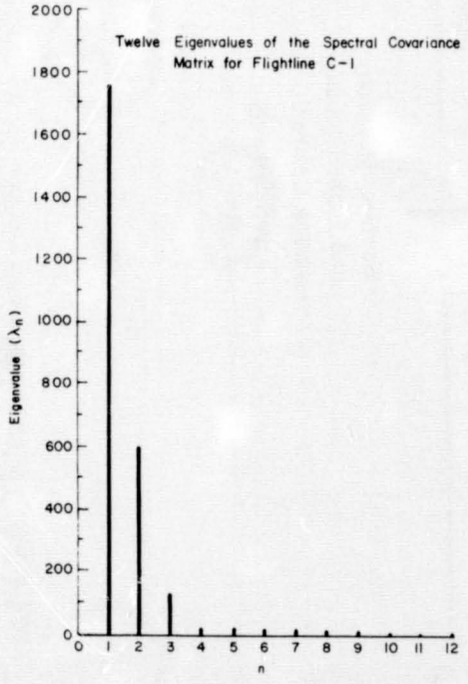

Figure 11.- The eigenvalues of an actual 12-band multispectral data set. An eigenvalue in this case is an indicator of the relative range of the data after principal components transformation. Even though there were 12 bands before transformation, only three appear to have significant range after.

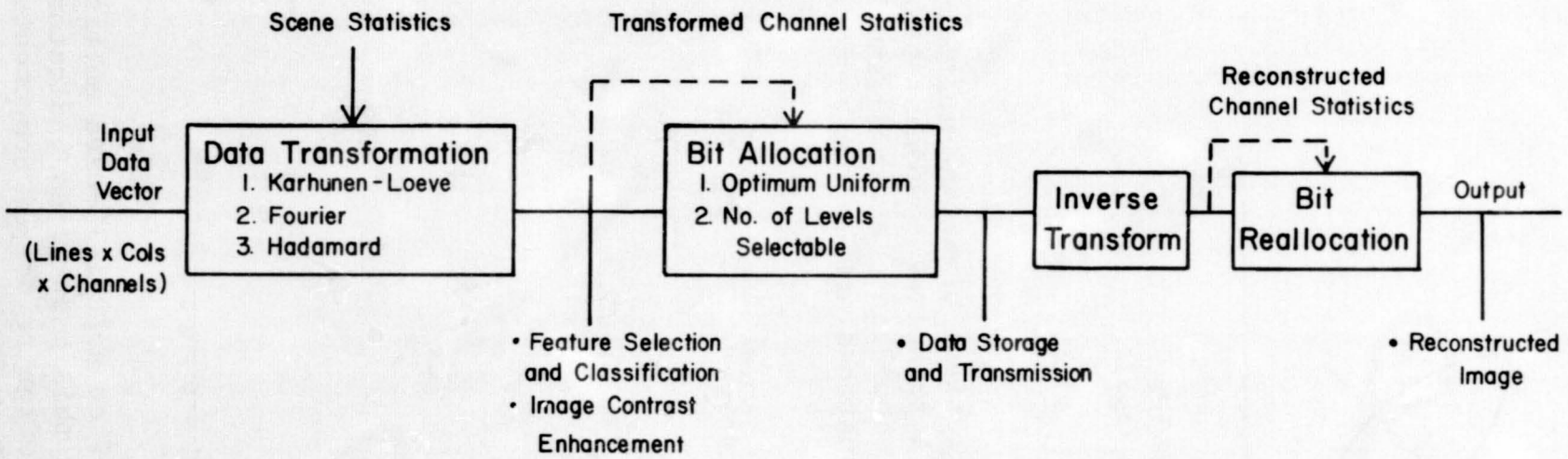

Figure 12.- Organization of a system used to test data compression transforms. Fourier and Hadamard transforms have been implemented in addition to the Karhunen-Loeve.

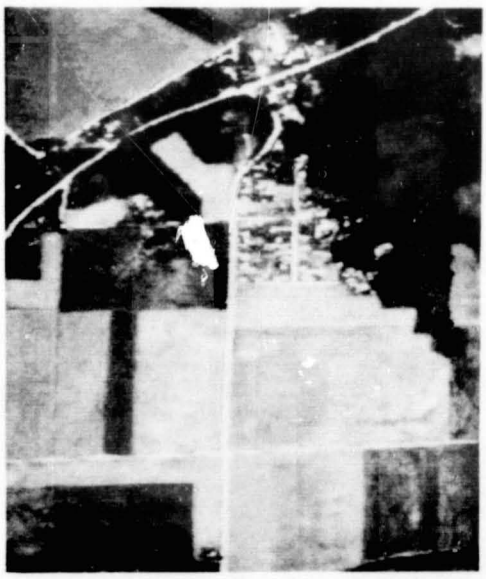

First Component

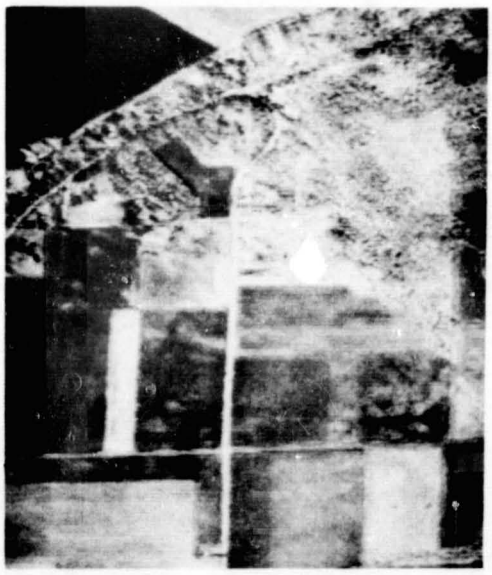

Second Component

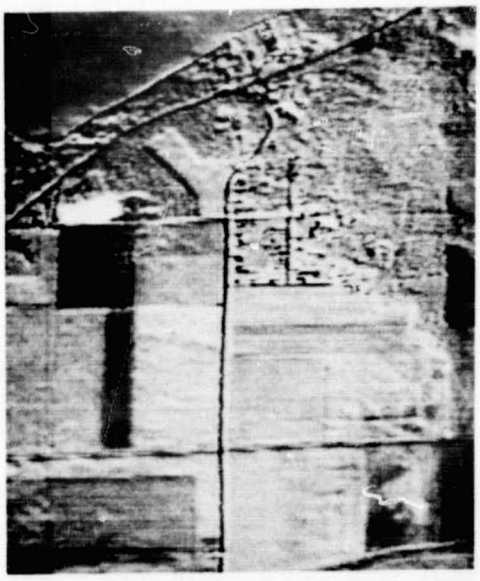

Third Component

Twelfth Component

Figure 13. Images generated after the data has first undergone principal components transform. The first two have higher contrasts than any of the original 12 spectral bands.

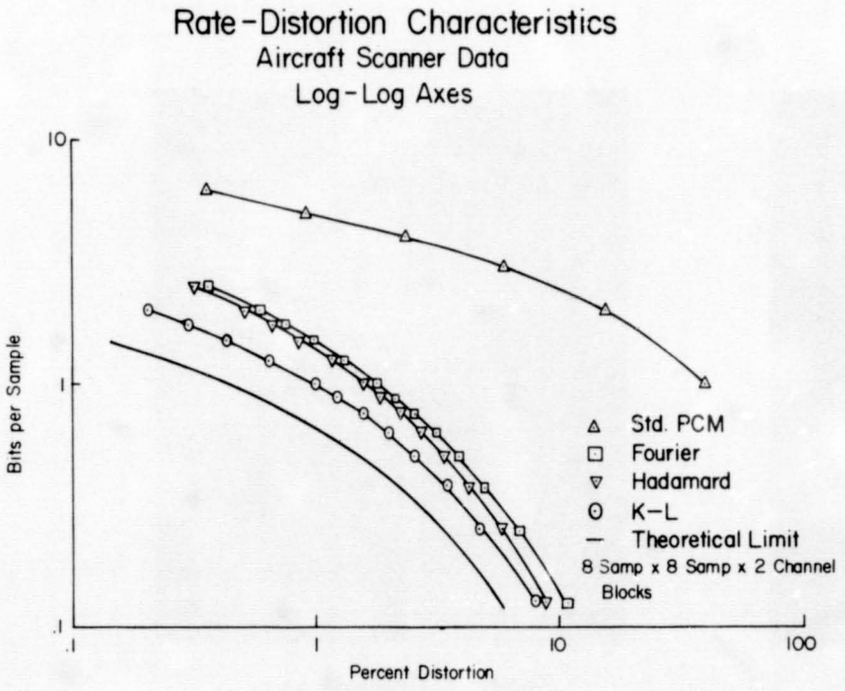

Figure 14.- Comparative rate distortion characteristics for the three transformations tested. Distortion is measured as the mean square difference between the original image and the compressed and reconstructed version.

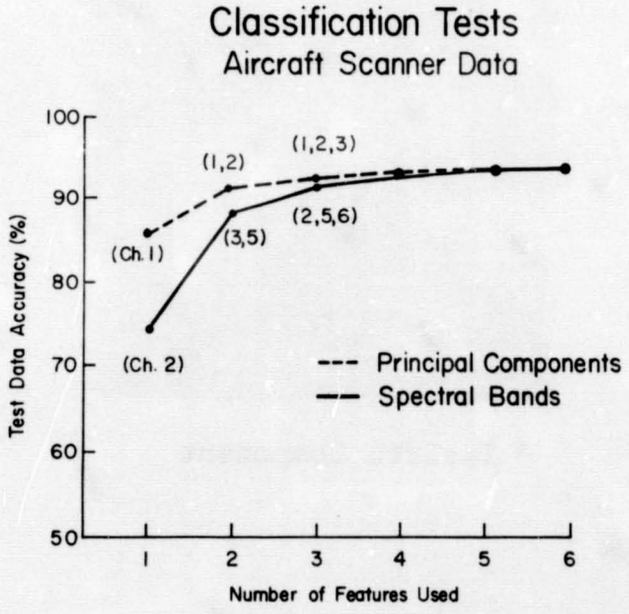

Figure 15.- Comparative results between classifications using original data and identical ones using principal components data. The best subsets of spectral bands were selected using a divergence processor.

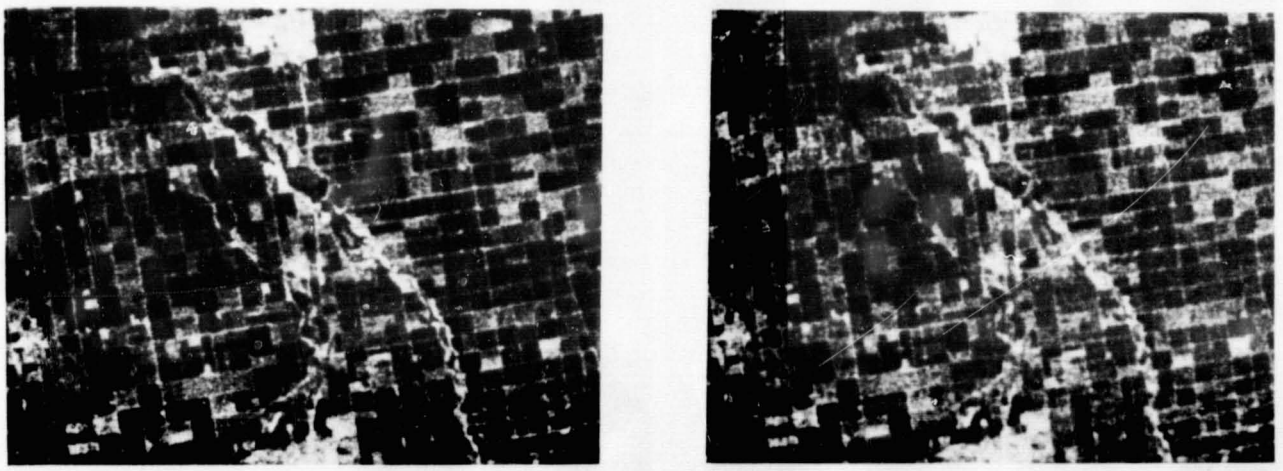

Original

8 X Compression

Figure 16. The results of data compression on image quality. A compression factor of 8 to 1 was used (Apollo 9 Frame No. 3698A).

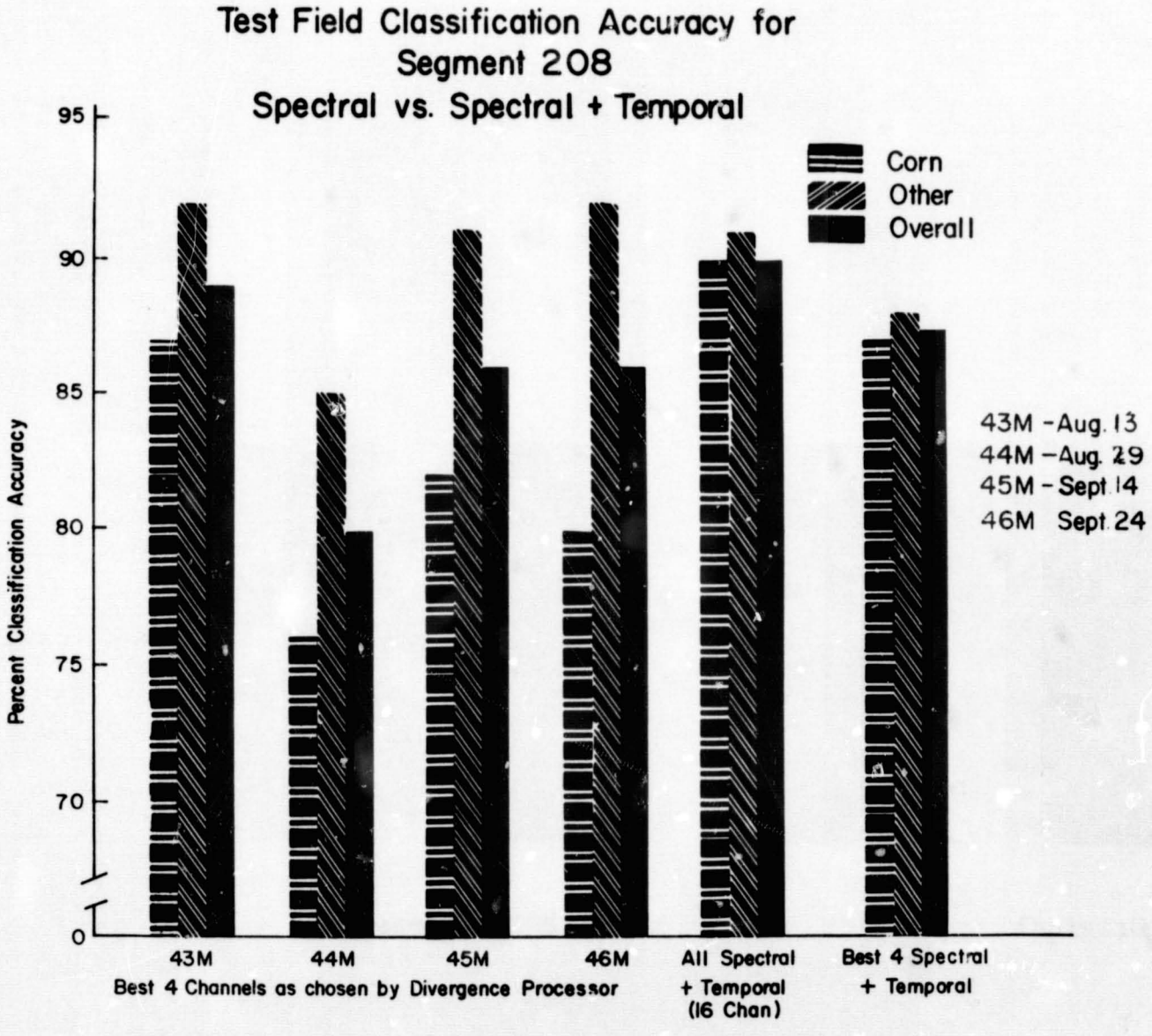

Figure 17.- A group of classification results illustrating the relative value of temporal information. The numbers 43M-46M are mission numbers flown on the dates shown.

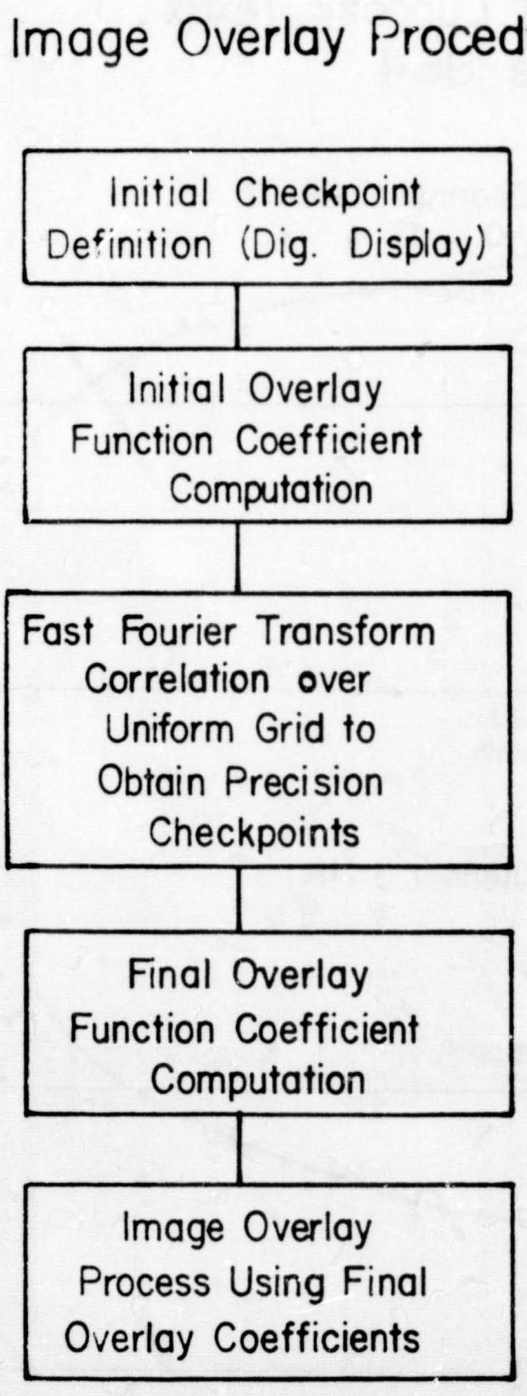

Figure 18.- The steps used in the current image overlay system.

Apollo 9 Digitized Image Correlation

Frame 3808 Lubbock, Texas
Line 1864

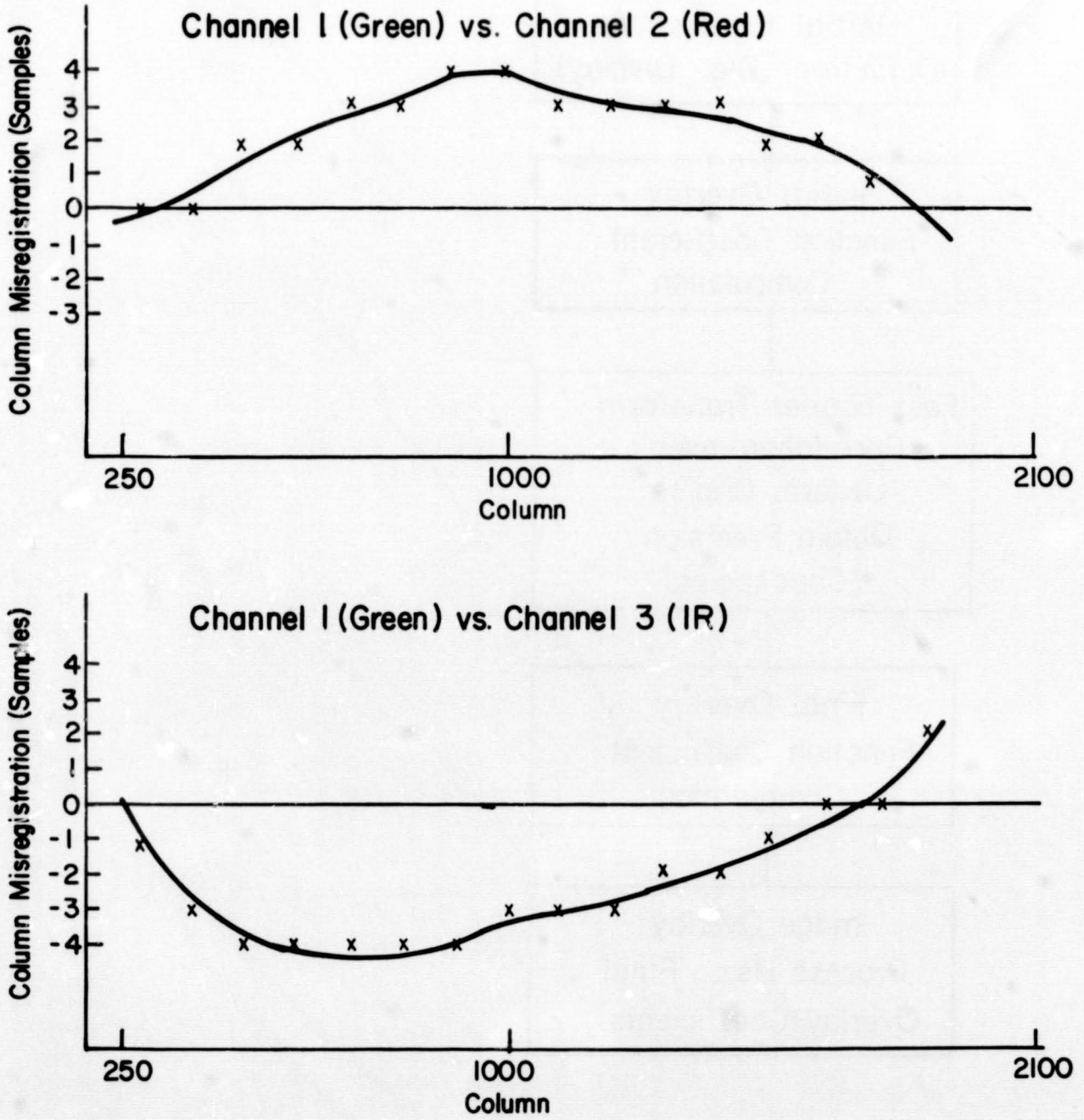

Figure 19.- Curves obtained with the image overlay system. They show that even when the particular frames were properly aligned at the left and right edges, they were as much as four samples (out of 2100) out of alignment in the middle. Thus, before overlaying a translation of the center portion of one image with respect to the other must be carried out in each case.

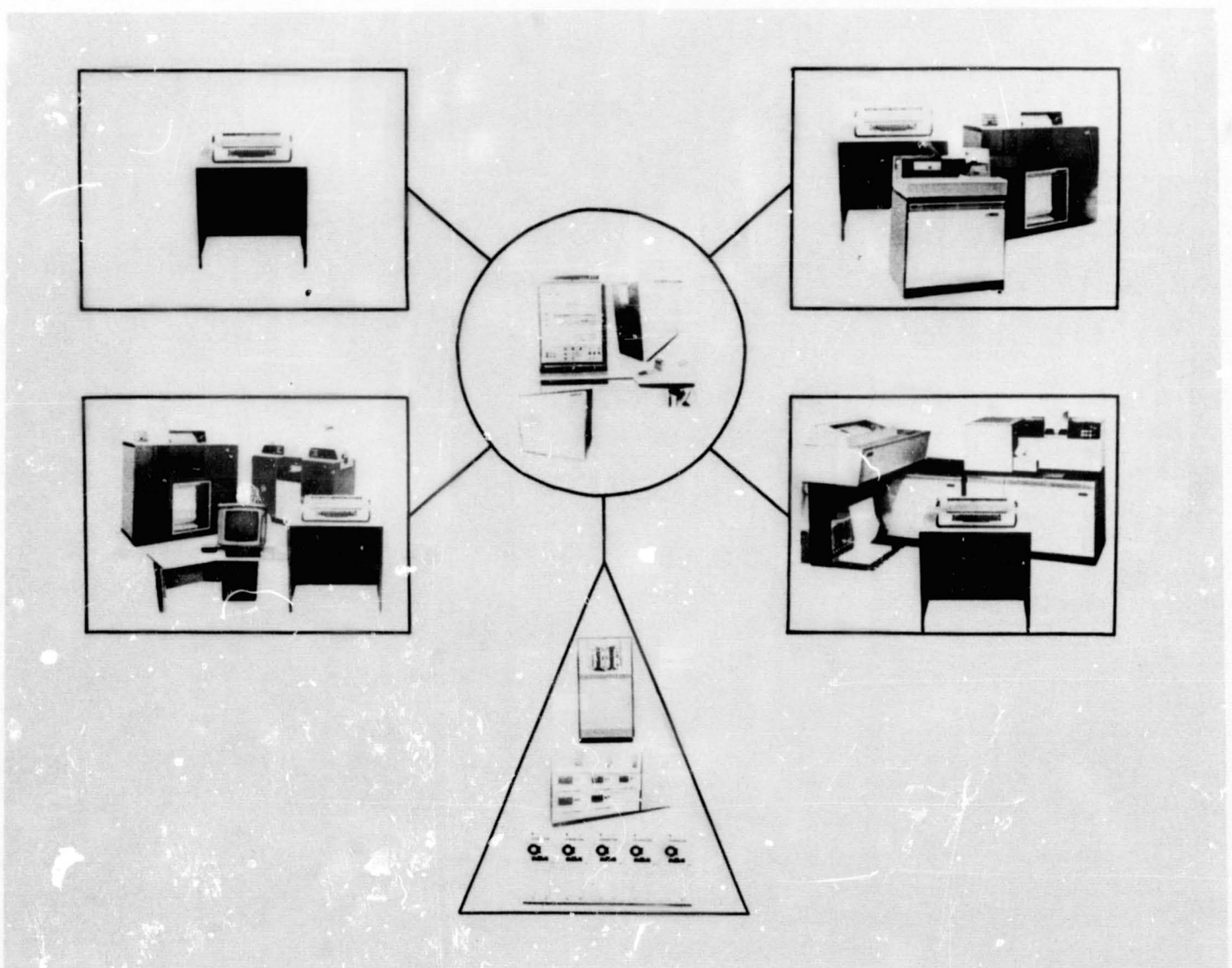

Figure 20.- The layout of equipment for the Multiterminal Processing System Experiment. The experiment will test the feasibility of centralizing the data bank and computational facility while proving input-output and control of that computational facility at multiple remote locations.

OVERVIEW OF THE EARTH RESOURCES PROGRAM OF THE JET PROPULSION LABORATORY

by

Donald P. Burcham
Space Science Program Office
Jet Propulsion Laboratory
California Institute of Technology

INTRODUCTION

The Jet Propulsion Laboratory's applicable experience is that gained under NASA support for the unmanned exploration of the solar system, including remote sensing and the processing and interpretation of the resulting data. At the present time the tasks in Earth Resources consist of two continuing ones under the Manned Spacecraft Center, one just awarded, and two proposals outstanding, as shown on the accompanying figure. The two continuing tasks will have their progress reported by John Blinn, and by David Martin, a co-worker of Walter Brown. My presentation will be very brief in describing what has been proposed on the other three tasks.

FIELD REFLECTANCE SPECTROMETER

The Portable Field Reflectance Spectrometer is a fabrication task for a 20 pound portable instrument including recording to make ground measurements in support of the Geologic Investigation proposal. It will employ a filter wheel to measure terrain spectral reflectivity in the range 0.3 to 2.5 micrometers with 2% or better resolution, and will employ ratio techniques to eliminate sky brightness fluctuations.

THE APPLICATION OF ERTS/EREP IMAGES TO GEOLOGIC INVESTIGATIONS

This proposal includes coinvestigators of Caltech and of USGS and is to exploit orbital multispectral photography plus computer

image processing to test their applicability in geologic mapping and in solving some geologic problems such as the discovery and mapping of geomorphic features of ancient, abandoned drainage systems in northwestern and north-central Arizona.

JPL's Image Processing Laboratory (IPL) is accustomed to applying various computer processes to imaging data, such as: contrast stretching, rubber sheet stretching, band ratios, selective digital Fourier filtering, haze removal, etc. It is sufficiently flexible to apply other processes that may be found desirable, such as those developed by Purdue University.

THE APPLICATION OF ERTS/EREP IMAGES TO A WATER QUALITY MONITORING AND INFORMATION SYSTEM

This proposal includes coinvestigators of the State of California Resources Agency, the Scripps Institution of Oceanography, and Caltech. It proposes an investigation to develop and correlate remote sensing from satellites and aircraft into an effective prototype system for California statewide water quality surveillance. Aircraft overflights, computer enhanced recognition of pollution signatures, ground truth measurements, and data processing will be employed to develop a simplified and automated monitoring system.

The ERTS A data would be used for nine major drainage basins of California having unique water quality influences from waste discharges, thermal contributions, oil spills, turbidity, sea water intrusion, agricultural drainage, toxicity, biostimulation, and eutrophication.

JPL EARTH RESOURCES ACTIVITIES

- CONTINUING TASKS

M W STUDIES	(160-75-03)	JOHN C. BLINN
RADAR RADIOMETER	(160-75-03)	WALTER E. BROWN

- JUST AWARDED TASK

PORTABLE FIELD REFLECTANCE SPECTROMETER (160-75-XX)	ALEXANDER GOETZ

- OUTSTANDING PROPOSALS

APPLICATION OF IMAGES FROM ORBIT TO GEOLOGIC INVESTIGATIONS (ERTS)	ALEXANDER GOETZ
WATER QUALITY MONITORING FROM ORBIT (ERTS)	GUNTHER REDMANN

Figure 1.

SECTION 53

MICROWAVE PROPERTIES OF GEOLOGICAL MATERIALS: STUDIES OF PENETRATION DEPTH AND MOISTURE EFFECTS

by

John C. Blinn III
Jet Propulsion Laboratory
Pasadena, California 91103

Jack G. Quade
University of Nevada
Reno, Nevada 89507

INTRODUCTION

This paper discusses two series of ground based microwave radiometer measurements performed by the Jet Propulsion Laboratory in cooperation with the University of Nevada. The studies were conducted at three wavelengths in a variety of typical sands and gravels. In nature, the microwave radiation from an object is a complex function of composition, moisture and temperature, all as a function of depth, and of surface cover, surface geometry and sky brightness temperature. It is difficult to interpret the microwave signature from a natural site without understanding the effects contributed by each of these individual parameters. Hence, the experiments were controlled to permit examination of the effects of a single parameter at a time on the microwave radiation. The two parameters studied were penetration depth and moisture effects.

Added to the complexity of interpreting the microwave radiation is the problem of measuring it. If radiometer measurements are to be valid independent of measurement system parameters, then they must be absolutely calibrated; that is, effects due to antenna beam energy distributions and systems losses must be removed. This can be a complex operation; however, the experiment designed also permitted a simplified calibration technique. In summary, our experimental approach was to minimize the complexity of the radiometer calibrations, isolate individual target parameters, and make maximum use of existing equipment.

EXPERIMENT DESCRIPTION

The experiments were conducted for three weeks during the summer of 1970 with three dual-polarized microwave radiometers operating at 0.95, 2.8 and 21 cm wavelengths (see Figure 1). The radiometers were mounted four meters above the target on an antenna positioner on the front of a truck. They viewed a controlled target area formed by a 2.4 x 2.4m box with movable sides for accurate variable depth control. The electronics were contained in the truck. The real time data system utilized a PDP8 computer which gathered data from the data/programmer, punched it in raw form, performed real time calculations and outputted calibrated data.

The measurements were made in the vicinity of Pyramid Lake, 80 km northeast of Reno, Nevada. The lake provided a wide variety of naturally sorted and man-made sands and gravels and had low levels of RFI which is particularly important at the 21 cm wavelength.

RADIOMETER CALIBRATION

Two stages of calibration were utilized. A relative calibration valid over the short term (5-15 min) was established by periodically viewing two internal heated sources controlled at approximately 45 and 100°C. This calibration is relative because the antennas with their sidelobes and generally wide beams receive energy from sources other than the target area as indicated in Figure 2. Also, loss in the components up to and including the internal calibration switches modify the incoming radiation. To remove these effects, two point, linear absolute calibrations were accomplished externally by replacing the target area with two sources of known microwave brightness temperature. In this experiment, an aluminum sheet was the "cold" source, and a microwave absorber the "warm" source. Using the internal calibrations only, the temperature predicted for the plate is generally warmer than the correct value, 0°K, as shown in Figure 3.

The result is the use of an incorrect calibration which was off by as much as 50% for these experiments. By forcing the data to fit at the two known external points, a correct absolute calibration for the target area was established. (Note: By forcing a fit to 0°K, sky contributions are also removed. The calibration technique is more fully described in Reference 3.).

Ideally, this is a one time calibration. It was generally accomplished once or twice per experiment. Use of this technique, which greatly simplified the calibration, is subject only to the

condition that the background radiation be invarient during the period between calibrations.

RESULTS: PENETRATION DEPTH

The first series of measurements was to determine the effective depth of radiation for a number of sands and gravels. Measurements were made by viewing a metal plate with varying depths of material placed on it in accurately controlled plane parallel layers. A theory based strictly on intensity of radiation predicts that the microwave brightness temperature, T_B, will increase exponentially with increasing thickness. The penetration depth is twice the thickness required to reach the 1/e extinction point (Reference 1). Consequently, the experiment was devised to use doubling thicknesses starting at one cm. It was quickly found that points did not behave smoothly as expected and the thickness increments were reduced to examine more closely what was happening. As a result, increments as low as 0.8 cm were used over the range 0-32 cm.

The results in Figure 4 show an oscillating behavior, particularily noticeable at 21 cm for this fine sand. The fringe amplitude will disappear with increasing particle size. However, it still exists at 21 cm when particle size is on the order of $\frac{1}{4}$ wavelength as seen in Figure 5.

The results can be modeled theoretically by solving for the reflectivity, which is related to emissivity and hence microwave brightness temperature. Standard textbook solutions of Maxwell's Equations (Reference 2) for reflectivity for plane parallel layered isotropic media yield the theoretical curve shown in Figure 4. Although no attempt was made to optimize a fit, correlation between the two curves is excellent as evidenced by the zero slope at the origin, broader nulls than peaks for the small values of layer thickness, and general agreement in the values of the maxima and minima.

It is noted that the theoretical maxima-minima excursions are greater than the experimental results for larger values of thickness. Since the 21-cm radiometer measurements are not at a single frequency but over a 10% band of frequencies, this "smearing" of the higher-order fringes would be expected and can easily be included in the model.

A two dimensional fit of the data to the model is being studied as a potential method of determining the microwave properties of materials in bulk. Extension of this work could lead to the definition of a technique for remotely determining layer thickness in certain

naturally layered systems such as sea ice. The penetration depth measurements and results are more completely described in Reference 3.

RESULTS: MOISTURE EFFECTS

An independent series of measurements designed to isolate the effect of moisture content in a smooth uniform sand were performed in the same 2.4 x 2.4 m container without the aluminum reflector. The measurements were conducted in a ten cm thickness of material by mixing in calculated amounts of water, smoothing the surface, measuring the brightness temperature at both polarizations, and collecting five samples for determining the moisture content at the four corners and center of the target area. The results for Mono, Pyramid, and Junction Sands are shown in Figures 5 and 6. The horizontal lines represent the spread in values of moisture as a percent of dry weight obtained for the dry five samples. The curves typically show no effect until moisture is above approximately four percent. Brightness temperature then decreases with increasing moisture in a somewhat linear fashion at rates ranging from 1.5 to 4.8°K per 1% change in moisture content (see Table 1 for values). Table 2 lists the properties of the materials discussed in this report.

Wavelength (cm) / Sand	0.95	2.8	21
Mono	1.5	2.4	4.8
Pyramid	2.4	3.4	4.8
Junction	4.5	3.1	3.9

Table 1: Rate of Decrease in Brightness Temperature with Increasing Moisture Content (-°K/1%)

The shorter wavelengths with smaller penetration depths are more sensitive to the surface variations caused by evaporation, water migration, and roughness. This is especially noticeable in the rates and scatter for the data from Mono Sand which was very permeable and hence drained rapidly. Because of the deeper penetration depths at 21 cm, the wooden bottom of the container had an influence on that data. This is particularily noticeable as a "warm" anomaly in the 21 cm data for moistures around 16%.

It was difficult to obtain a perfectly smooth surface for the higher values of moisture. To check the effects of roughness, a rake was passed over the surface parallel to the direction of horizontal polarization. The spacing between the furrows was approximately two cm. As shown in Figure 7, the effects due to moisture essentially disappear at 0.95 and 2.8 cm where the wavelength is on the order of, or shorter than, the furrow spacing. At 21 cm where the furrow spacing is on the order of 0.1 wavelengths, the effect is smaller but still apparent. Vertically polarized data shows similar results.

CONCLUSION

This paper has summarized the results of two of a series of controlled experiments performed in three weeks during the summer of 1970. The first series of experiments to determine penetration depth showed the value of having a modeled response and data reduced in real time for examination in the field. This capability permitted a modification of the experimental approach when the data showed that results did not conform with expectations and lead to a detailed examination of the interference effect discussed herein. The results suggest a radiometric method for measuring the microwave properties of materials in bulk and are applicable to studies of sea ice and other naturally layered media.

The sensitivity of the microwave emission to changes in moisture content has inspired a number of airborne and ground based investigations. Although the effect is dominent under certain conditions, the complicating factors of soil type, roughness, vegetation, etc. seem to govern the conclusions regarding its application at this time. Obviously, the nature of the proposed technique affects the likelihood of its success. For instance, monitoring moisture in a smooth material has a good chance for quick application. While this may not be practical in nature, it may be in process control such as monitoring the curing of concrete.

Concerning applications in the natural environment, experiments which use repeated observations on an area as calibrations for future observations of the same area have a greater chance of success than those which propose remote determination of soil moisture over an unknown area. Consideration of roughness effects and penetration depth indicate the desirability of using longer wavelength radiometers for soil moisture and certain other applications.

REFERENCES CITED

1. Conel, J. E., Microwave Emission from Granular Silicates: Determination of the Absorption Coefficient from Plate Measurements and the Effects of Scattering, Jet Propulsion Laboratory TM 33-458, October 1970.

2. Stratton, J. A., Electromagnetic Theory, McGraw-Hill Book Co., Inc., 1941.

3. Blinn, J. C. III, Conel, J. E., and Quade, J. G., Microwave Emission from Geologic Materials: Observation of Interference Effects, Submitted for publication.

TABLE 2. Summary of Materials Studied

Material	Mineralogy		Particle Sizes, mm		Density		Surface Characteristics
	Minerals	%	Mean	σ	Bulk	Specific	
Mono sand (lake shore deposit)	Glass Devitrified glass Quartz Potash feldspar Iron oxide Elements less 1%	68 16 8 4 1 3	0.46	0.26	1.25	2.25	Coarse-grained
Junction sand (windblown)	Plagioclase Quartz Iron oxide Biotite Volcanic chips Elements less 1%	38 35 5 13 12 7	0.12	0.042	1.20	2.49	Very fine-grained
Pyramid Sand (river deposit)	Quartz Plagioclase Iron oxide Hornblende Lithic Frags. Elements less 1%	45 35 5 3 8 4	0.24	0.10	1.37	2.41	Very fine-grained
Gravel ≃ 5 cm	Welded tuffs Olivine basalts Rhyolites Andesites Highly silicified rhyolites and tuffs	30 20 20 20 10	30-50		1.17		Broken, irregular

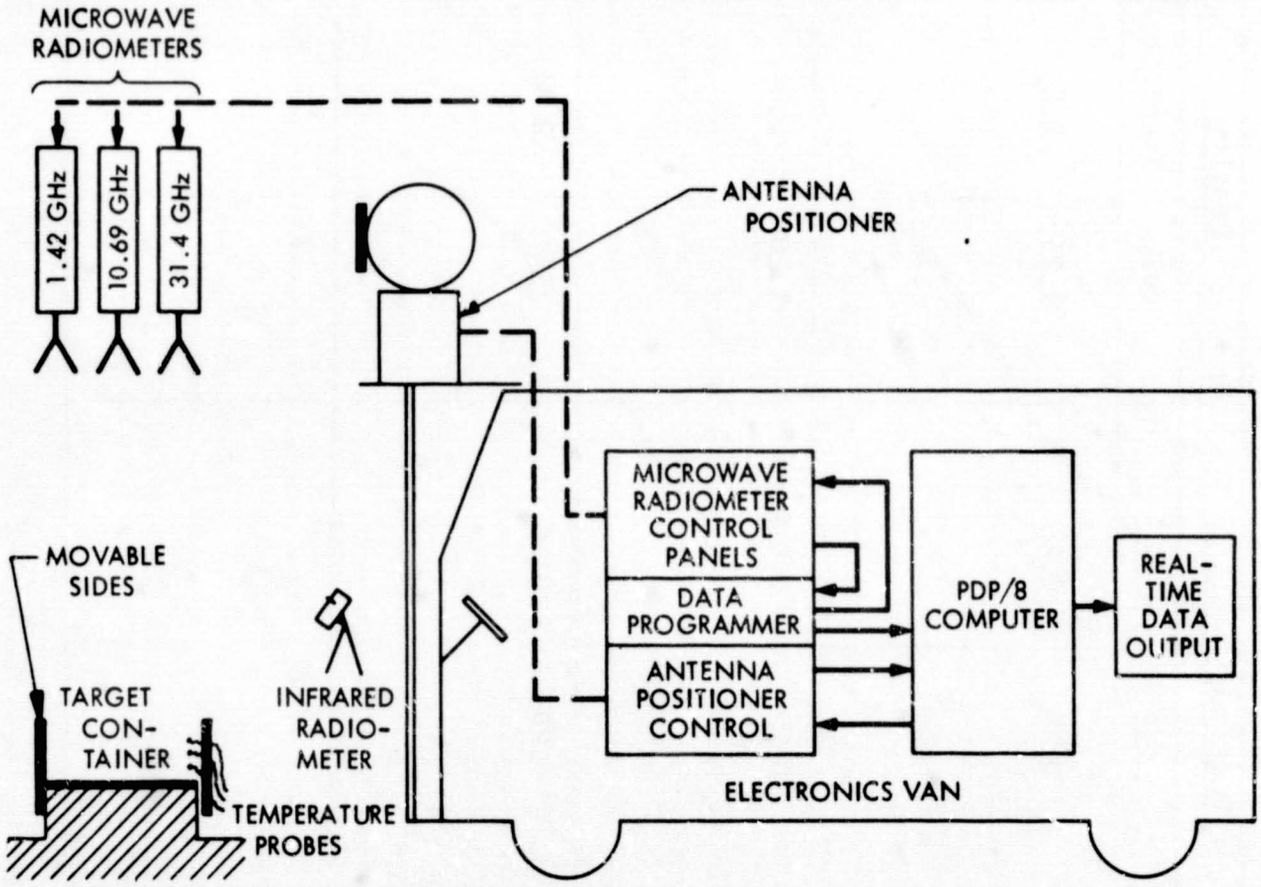

Figure 1. Microwave Radiometric Field Experiment Configuration

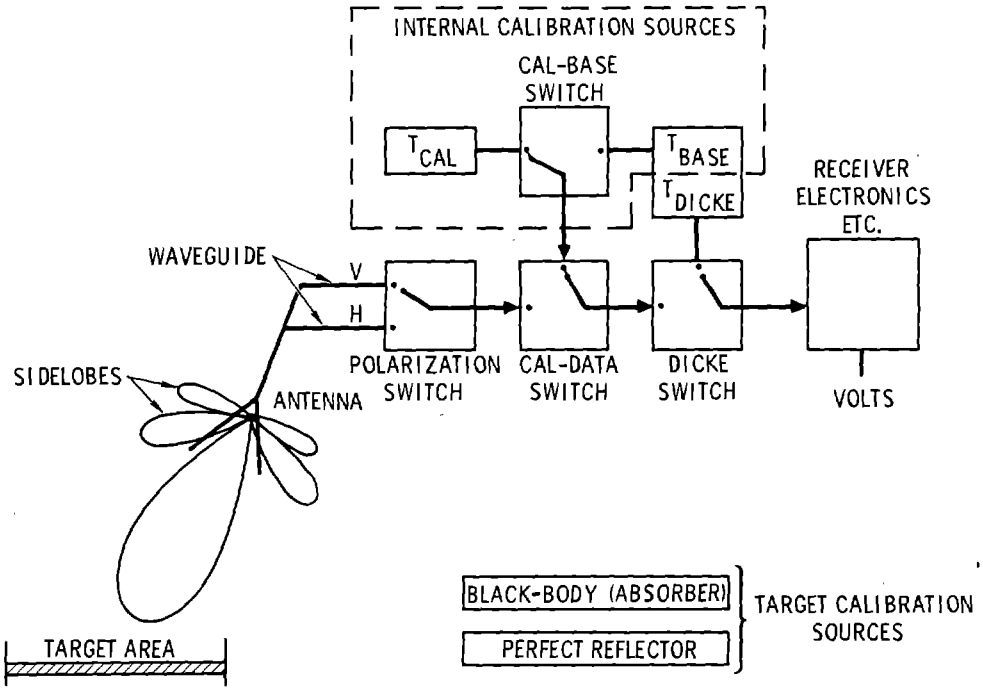

Figure 2. The Calibration Problem

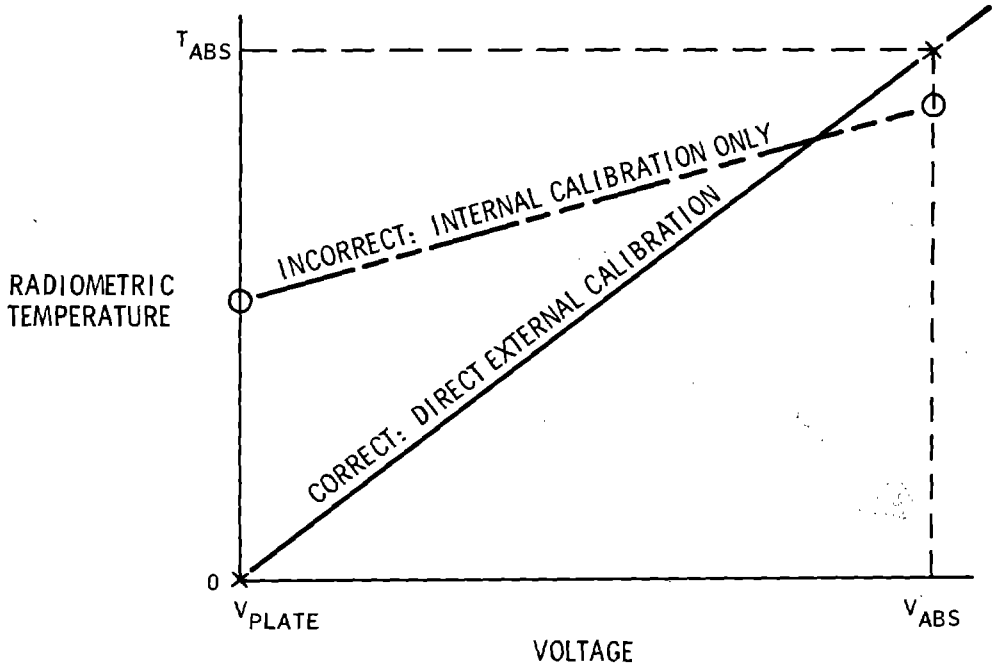

Figure 3. Target Calibration Curves

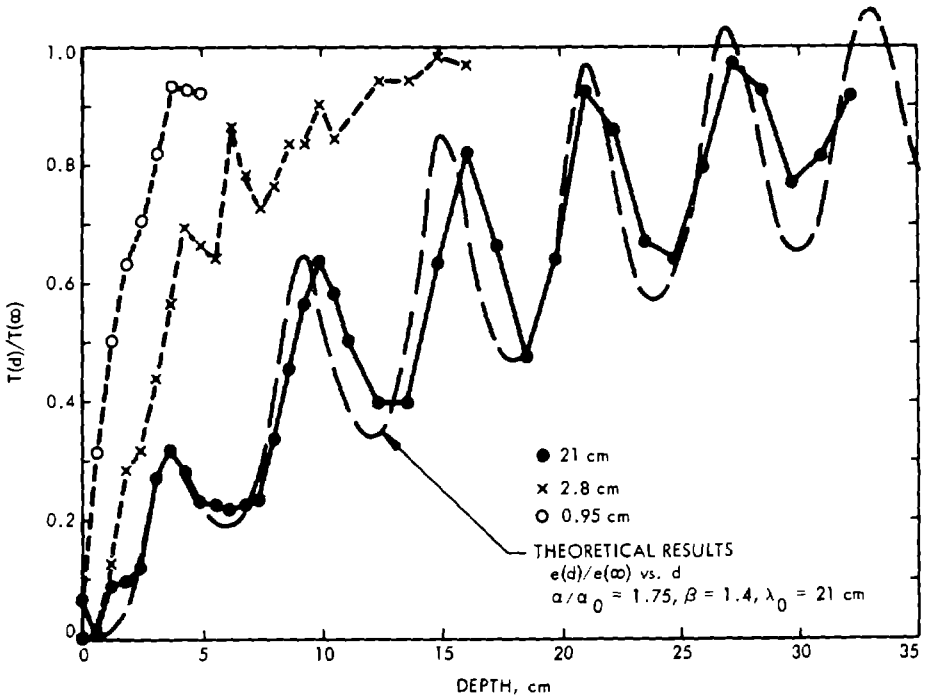

Figure 4. Plate Measurements for Junction Sand

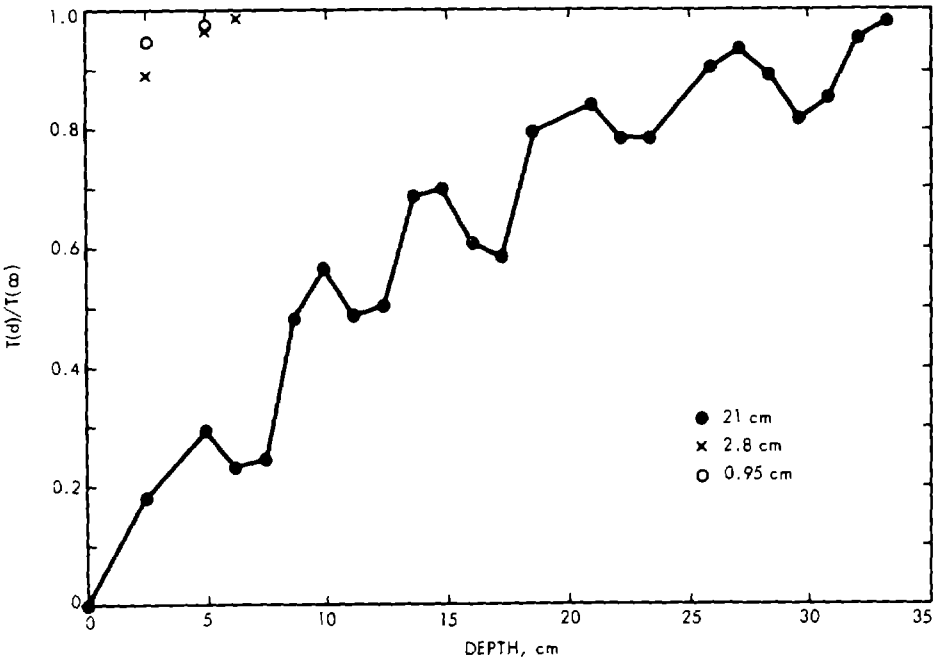

Figure 5. Plate Measurements for 2.5-10 cm Gravel

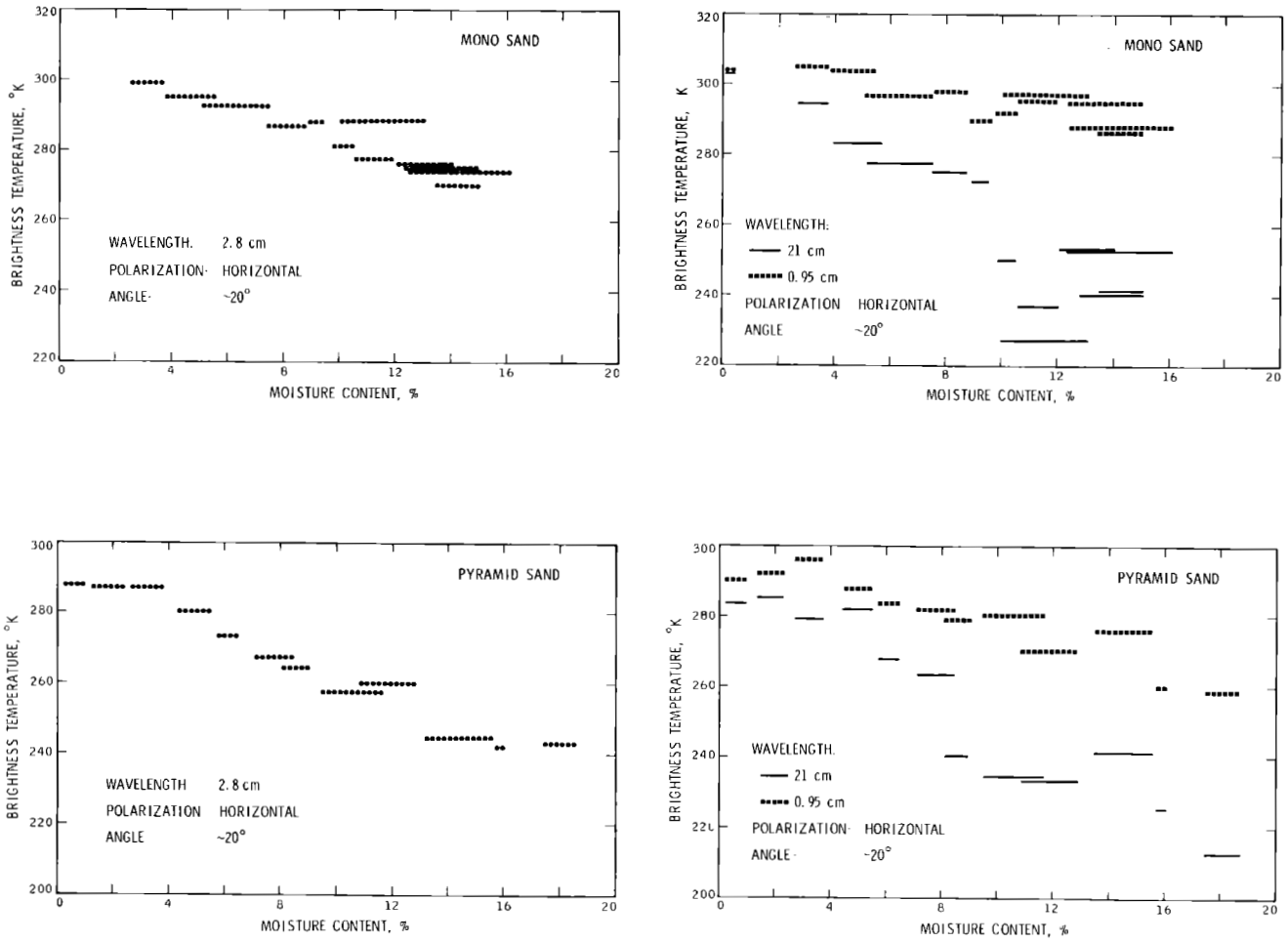

Figure 6. Moisture Effects in Mono and Pyramid Sands

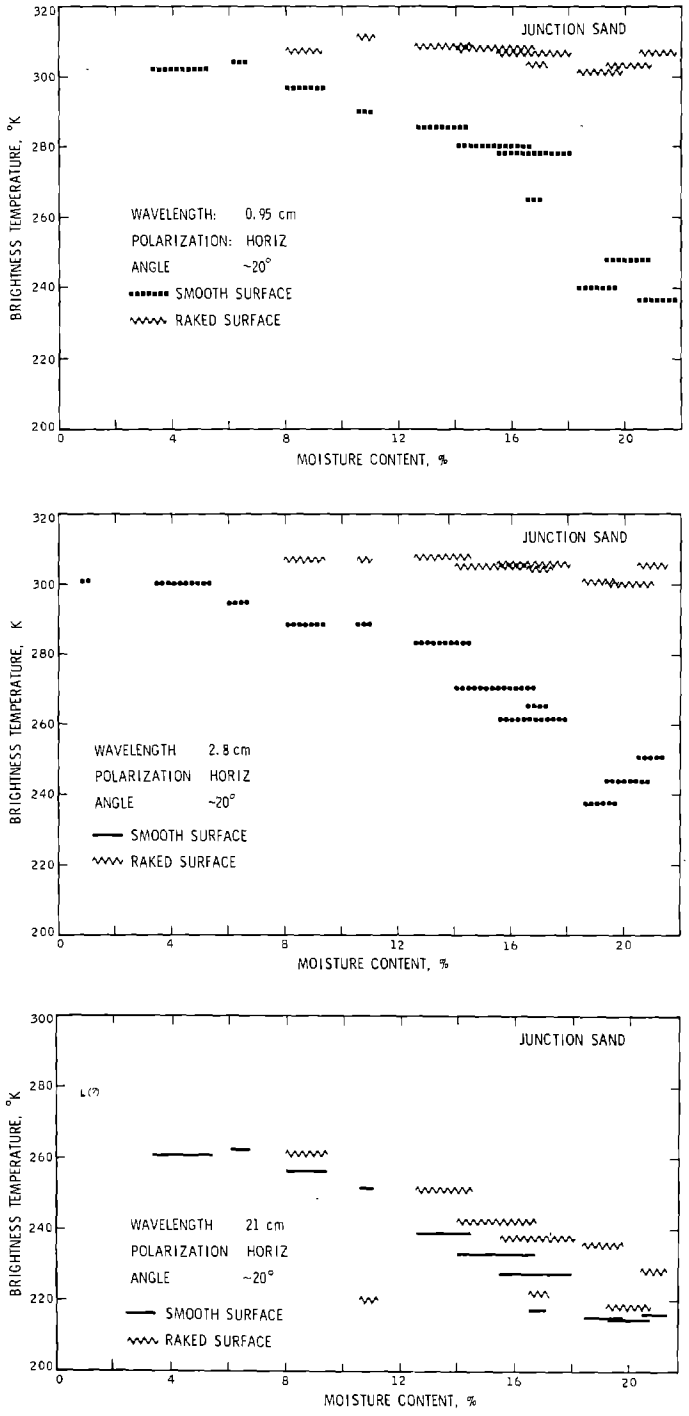

Figure 7. Moisture Effects for Smooth and Rough Junction Sand

SECTION 54

POLARIZATION EFFECTS WITH A COMBINED RADAR - RADIOMETER

by

David Martin
Space Sciences Division
Jet Propulsion Laboratory
Pasadena, California

INTRODUCTION

The purpose of this report is to describe a unique microwave sensor. The device uses a coherent X-band radar, a radiometer at the same wavelength and an antenna with a polarization that can be varied electronically. This microwave sensor was developed to acquire polarization signature information about various surfaces in both the active and passive mode simultaneously. One application for the sensor is expected to be the location and identification of plant life.

DESCRIPTION OF THE EQUIPMENT

In Figure 1 the equipment is shown mounted on an aerial platform truck for access to targets in their natural state. The boom height is 10 meters. The antenna parabola is 1.2 meters in diameter and can be positioned to any selected angle of incidence. The advantages of this approach are that the interpretation of the data will be aided by removing uncertainties concerning the geometry, surface conditions and equipment for the active and passive measurements. Furthermore, the detailed polarization measurements will provide a polarization signature for improved surface characterization.

Figure 2 is a simplified block diagram of the equipment which is shared by both the passive and active measurement functions. The center frequency is 8505 Megahertz. An integral part of the antenna is the polarizer. The orientation of the electric field vector can be rotated electronically with the polarizer. This may be compared to an optical polarimeter in which a polarized plate is rotated to analyze the polarization effects of an optically active sample. The radar transmitted signal has a separate polarizer in order to control the polarization of the illumination as well as of the received signal. The receiver is a superheterodyne, solid state design, with an IF bandwidth of 320 MHz and IF center

frequency of 1215 MHz. The system noise figure of 8 dB is achieved with a low noise TWT mounted on the antenna. The IF signals are routed to either the radar or radiometer detectors by a special transfer switch which provides greater than 90 dB isolation and minimizes the switching transients. The data conditioning function will be described later.

The operator can select from 5 modes of time sharing and 16 switching rates. Figure 3 is an example of Mode 1 and the 1 KHz switching rate sequence of data acquisition. In Mode 1 the radar is on for 2 μ sec in each radiometer switching cycle. This mode is applicable for studying nearby objects so the echo returns within the 2 μ sec time interval. In Mode 2 the radar is on for 500 pulses then the radiometer for the equivalent time. Mode 4 is radar only and Mode 5 is radiometer only. The maximum PRF is 5000 pulses per second and the minimum is 312. The polarization scan switching rate is either at the PRF or after 8000 pulses by operator selection.

The polarization control, Figure 4, is achieved by adding equal amplitude right and left circularly polarized waves in the feed horn, resulting in a radiated linear polarized wave. The phase shift in one of the paths can be digitally selected by actuating latching ferrite phase shifters of 22.5, 45, 90 or 180 electrical degrees, thus varying the angular orientation of the resultant linearly polarized wave. There are 16 polarization states which will rotate the electric vector in $11\frac{1}{4}$ degree increments for a total of 180°. The circulators separate the transmit and receive signal paths. The reference and phase shifted signals are converted to right and left circular polarized waves in the orthomode transducer and 90° delay section. Figure 5 is a photo of the polarization network, Serial No. 1. It is about 20cm wide. The maximum scan rate is 5000 polarization changes per second.

The polarization data conditioning function may be explained with the aid of Figure 6. The transfer switch connects the IF signal to either the radar or the radiometer channel. The signal is coherently detected and amplified. The operator selects the delay of the sample gate to correspond to the range to the target. A 50 nanosecond sample of the echo is held and read in to the 16 channel processor. The 16 FET read in switches operate synchronously with the antenna polarization switches. The radiometer has a second balanced mixer amplifier in order to filter the radar center frequency. A detector recovers the Dicke switched signal which is amplified and synchronously detected at the PRF. This signal is filtered in individual channels synchronized with polarization.

The read out rate is 8 seconds per channel when operating at the 1 KHz PRF. Each filter is reset after being read out. For slow polarizations scan the read in and out are at the same time, for the fast scan 8000 read ins occur for each read out. Figure 7 is an example of analog data recording of the radar and radiometer outputs with slow and fast polarization scan. The first scan is at the slow rate and the next 2 scans are fast. The polarization state 3 corresponds to vertical and state 11 to horizontal polarization. Figure 8 is an example of a radar echo as observed with a sampling oscilloscope. The 100 nanosec transmitter pulse is blanked by the receiver protector switch.

PRELIMINARY RESULTS

The radiometer was calibrated with hot and cold loads. The configuration for this calibration is shown in Figure 9. The variable attenuator provides a check on the linearity by accounting for the loss factor A at the selected attenuations. After the hot and cold load calibration the waveguide switch is switched to the antenna. The antenna temperature response as seen through the polarizer is given in Figure 10. The polarizer loss is 1.2 dB and it is thermally controlled to 323^{o}K. With this calibration the radiometric temperature seen by the antenna is related to the voltage output of the radiometer. The radiometric temperature observed while looking at an asphalt surface at an incidence angle of 70^{o} and scanning the polarization at the slow rate is shown in Figure 11. The radar and radiometer measurements were time shared at the 1 KHz switching rate in Mode 1.

The radar is calibrated with reflectors of known or calculated radar cross-section. A Luneberg lens reflector of 24.3 dB square meter cross-section produced the amplitude shown in Figure 12. The darker curve is the cosine function with arbitrary amplitude and phase to indicate how close the measured points are to the cosine function. After removing the reflector the radar amplitude of the background is recorded. The radar data is shown in voltage units as measured. The radar backscatter voltage for asphalt at 70^{o} incidence angle, slow polarization scan is seen in Figure 13. The radar data was taken at the same time as the radiometer data of Figure 11. One curve is for the case of transmitting vertically polarized and the other for transmitting horizontally polarized waves. If the amplitude of the sine and cosine coherent detectors are squared and added, the relative echo power as a function of polarization is obtained. Although the angle of polarization is measured, the direction of the electric vector is not. For example with horizontal polarization the vector may be pointing left or right. Thus all polarization states are included in 180 degrees of vector angular rotation and in a polar

plot the points are symmetrical about the origin. Polarization signatures based on the data in Figure 13 are shown in Figures 14 and 15. These are polar plots of polarization angle verses relative echo power obtained by observing an asphalt surface at an incidence angle of 70°. The radar and radiometer measurements were time shared at the 1 KHz switching rate in Mode 1. Interpretation of the data from various surfaces will be the subject of another paper.

SUMMARY

A microwave sensor with an electronically variable polarized antenna has been described. A coherent X-Band radar and a radiometer share the same antenna and receiver at switching rates up to 5000 per second. The antenna polarization can be switched at the same rate for both the transmit and receive independent signal paths. The equipment is mounted on an aerial platform truck and is ready to make measurements in areas of interest for agricultural, geological and hydrological applications of remote sensing. The additional information due to the polarization modulation is expected to aid the identification of surface conditions. The time sharing of the radar and radiometer will ensure that the geometry, the surface conditions and equipment do not change for the active and passive measurements. The sensor will also provide new information about the relationship between surface reflectivity and emissivity.

Figure 1. The radar radiometer is mounted on an aerial platform truck for access to areas of interest for remote sensing applications. The Luneberg lens and corner reflectors provide calibration targets for radar calibration.

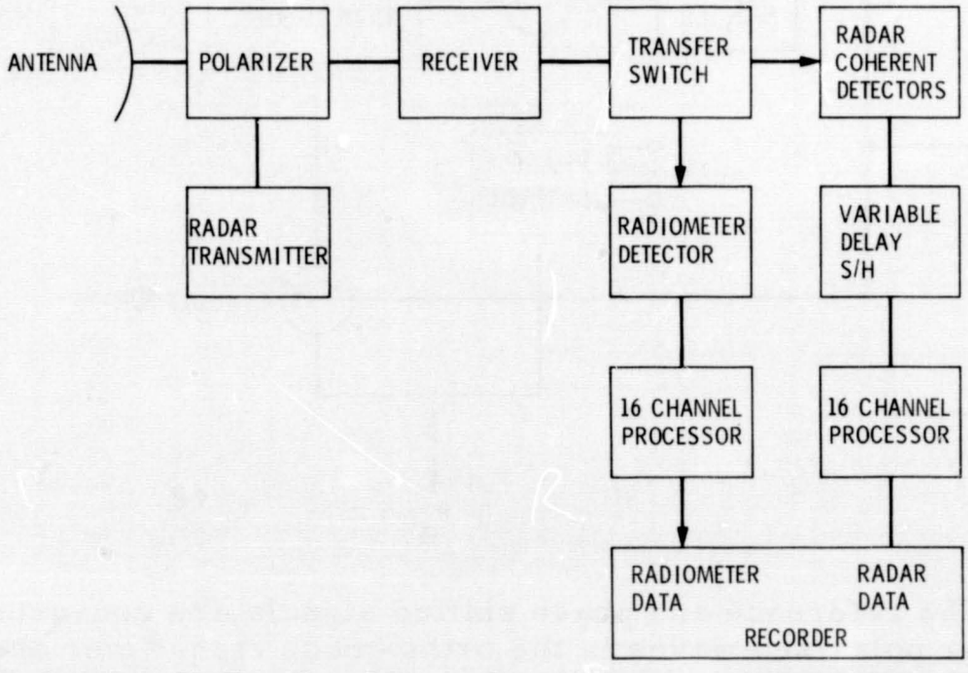

Figure 2. A coherent X-Band pulse radar is time shared with a radiometer. The antenna polarization can be modulated to identify the target polarization signatures for both the radar and the radiometer.

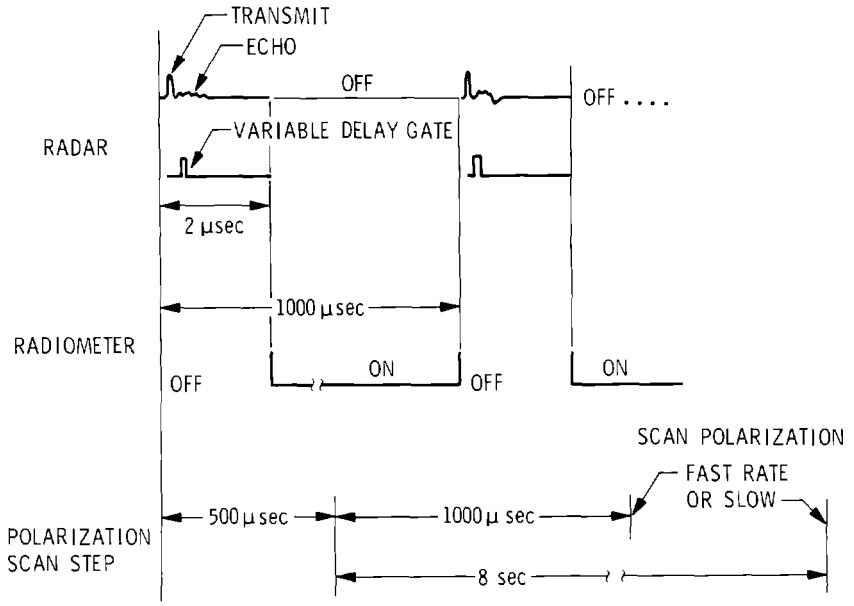

Figure 3. The operator can select from 5 Modes of time sharing and 16 switching rates. This is an example of pulse to pulse time sharing at 1 KH_Z. Polarization scan step can be either at the PRF or after 8000 pulses.

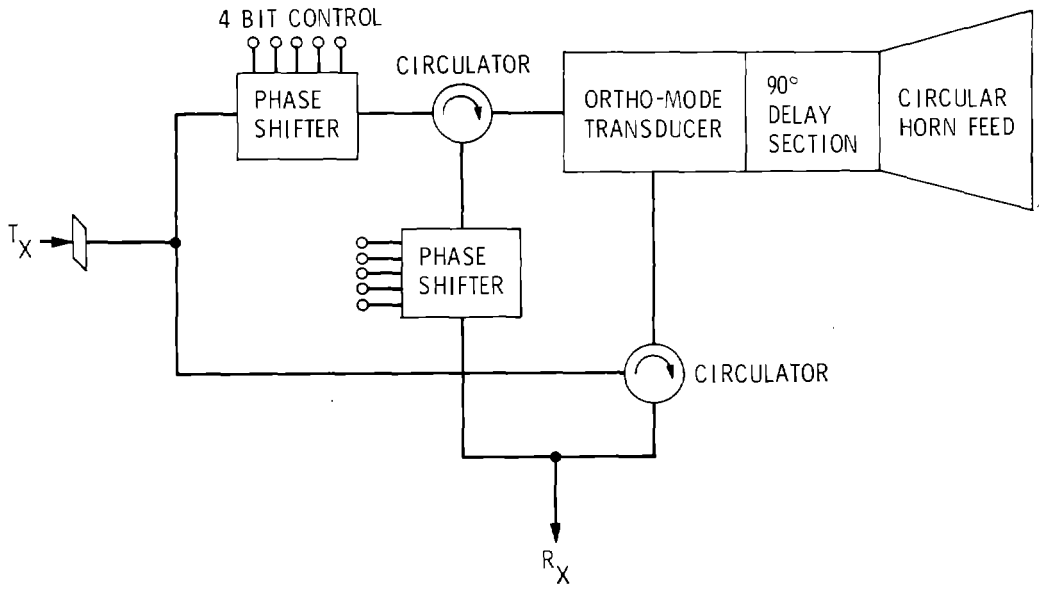

Figure 4. The reference and phase shifted signals are converted to right and left circular polarized waves in the ortho-mode transducer and 90° delay section. The sum of the two waves is a linearly polarized wave with the angular orientation a function of the phase shift. The 16 states rotate the electric vector 180° in 11 1/4° steps.

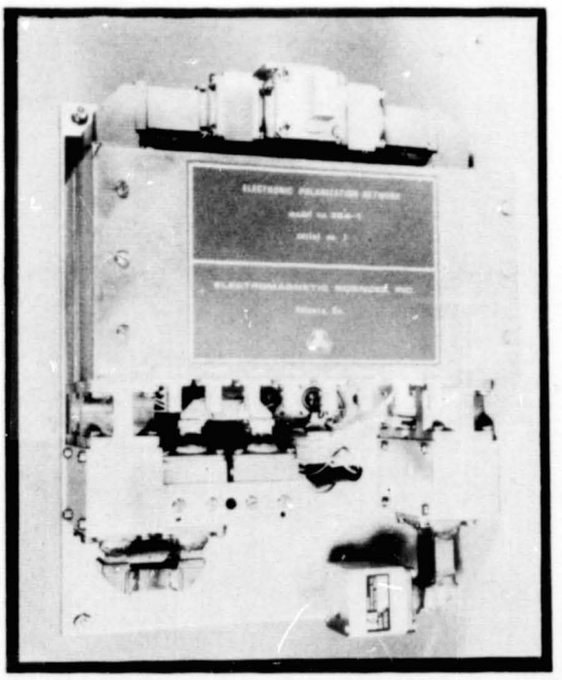

Figure 5. The ferrite phase shifters and X-Band waveguide network provide the antenna polarization control. Sixteen linear polarization states can be scanned at rates up to 5000 changes per second independently for the transmitted and received signals.

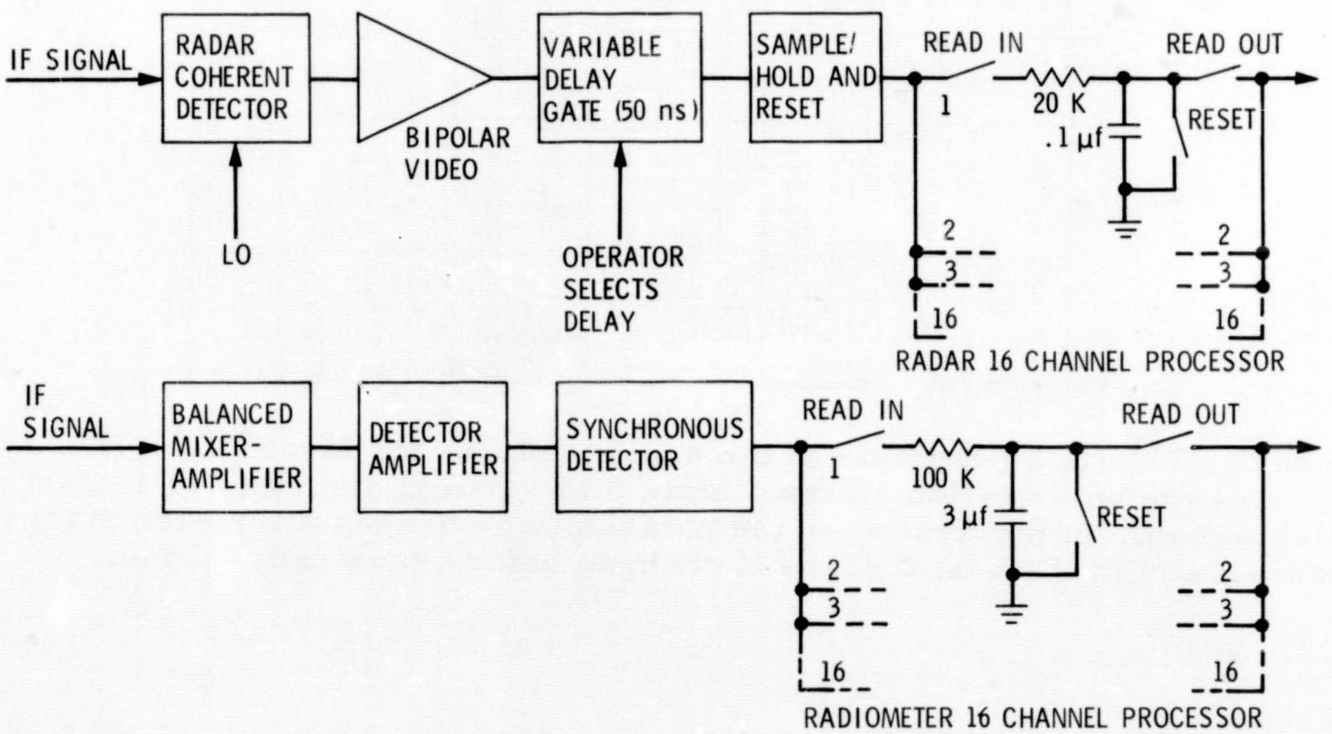

Figure 6. The IF signal from the receiver is switched to either the radar or the radiometer detector. There are 16 filters synchronized with the polarization scan. Each filter is reset after being read out.

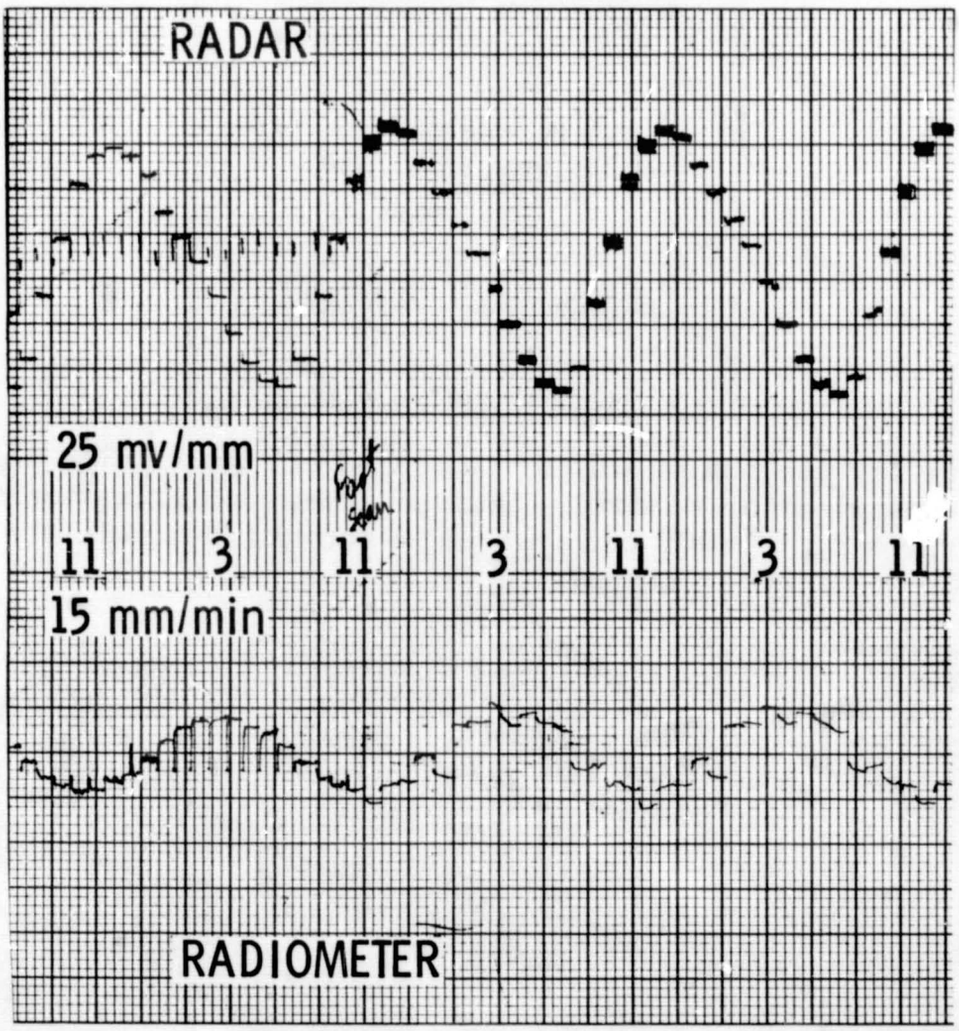

Figure 7. This is an example of the analog voltage for Mode 1 at 1 KHz while scanning the polarization states. State 3 is vertical and state 11 is horizontal polarization. In the first scan the polarization changes after each state is read out and in the next 2 scans it changes before each radar pulse.

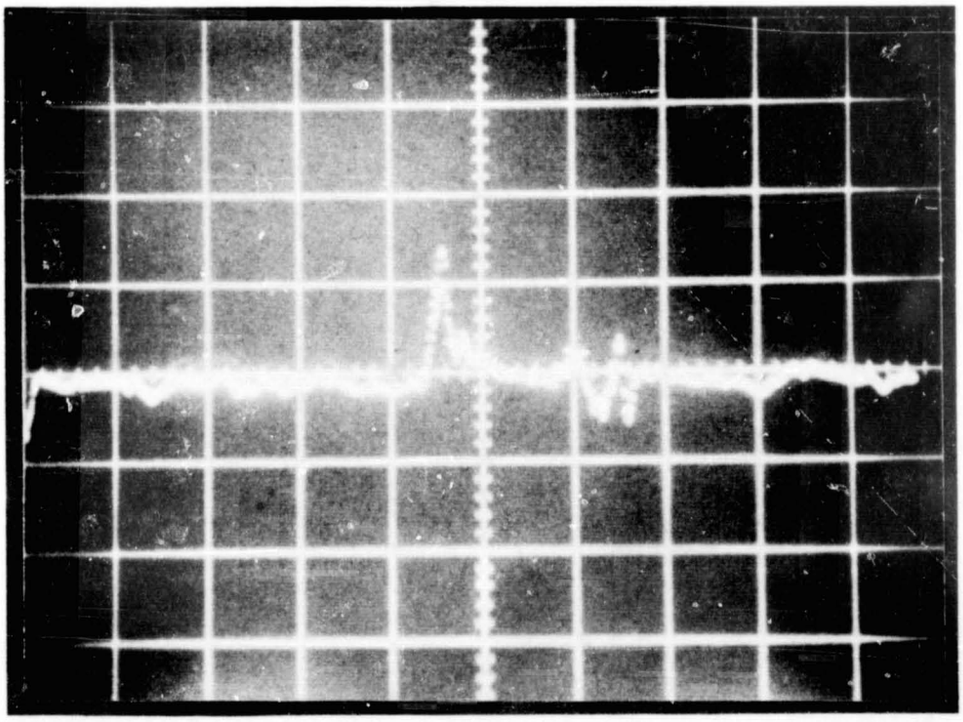

Figure 8. The 100 nanosec wide transmitted pulse is blanked by the receiver protector. The coherent echo is from a gravel surface at an incidence angle of 60°.

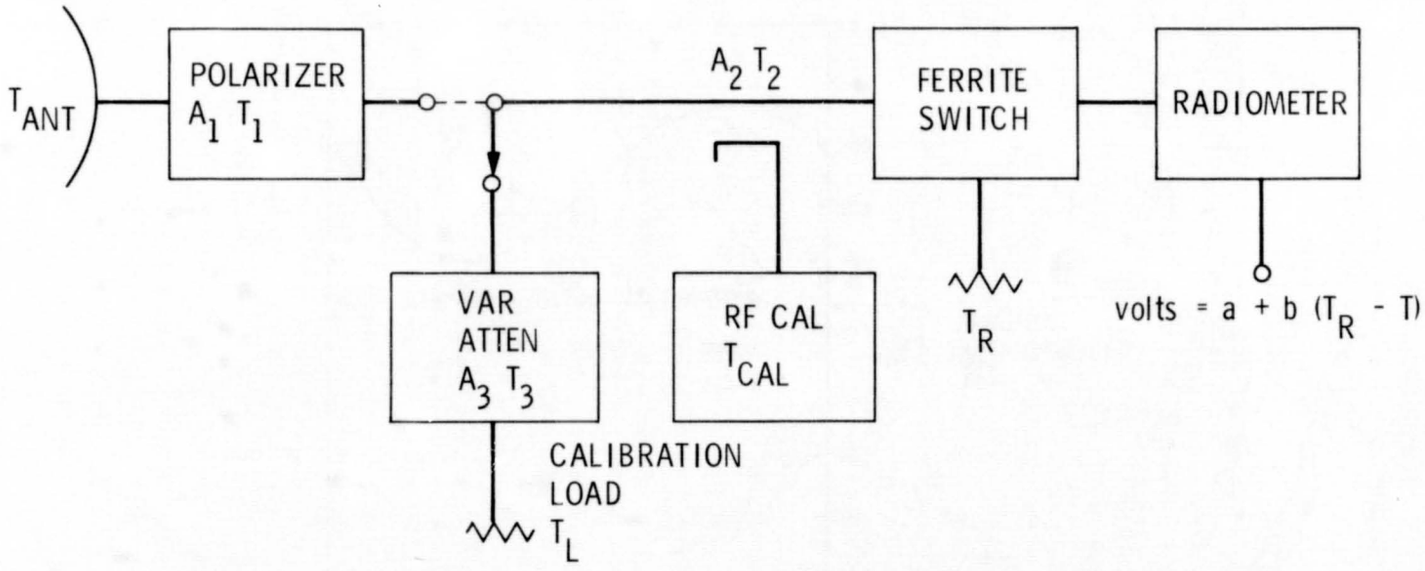

$$T_{APPARENT_1} = A_2 \left[A_3 T_L + (1 - A_3) T_3\right] + (1 - A_2) T_2$$

$$T_{APPARENT_2} = A_2 \left[A_1 T_{ANT} + (1 - A_1) T_1\right] + (1 - A_2) T_2$$

Figure 9. A waveguide switch on the antenna is switched to hot or cold loads for the radiometer calibration. The variable attenuator checks the linearity. A noise diode provides a calibration source in the field.

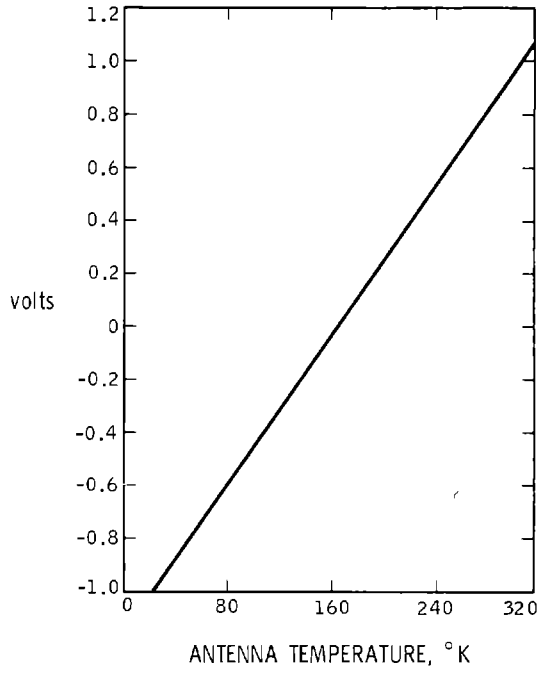

Figure 10. The radiometer output voltage as a function of antenna temperature is obtained by the calibration procedure.

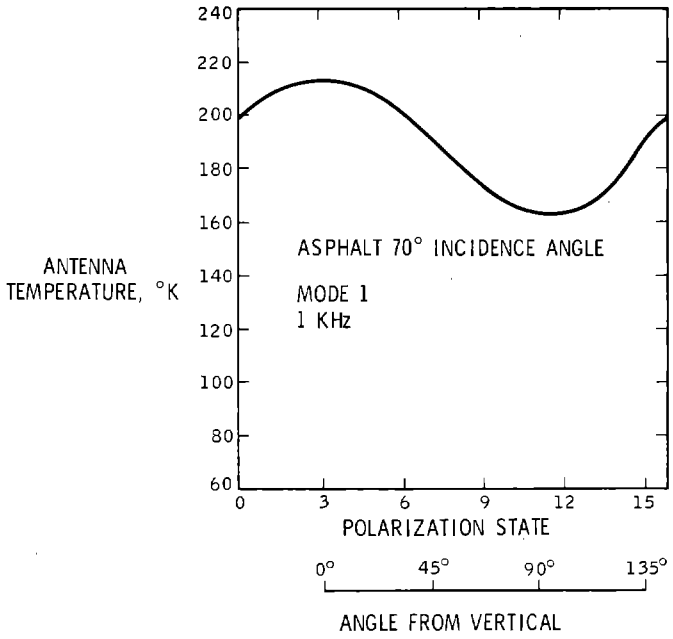

Figure 11. This radiometric temperature was obtained for an asphalt surface observed at a 70° incidence angle while operating in Mode 1 at 1 KHz with slow polarization scan.

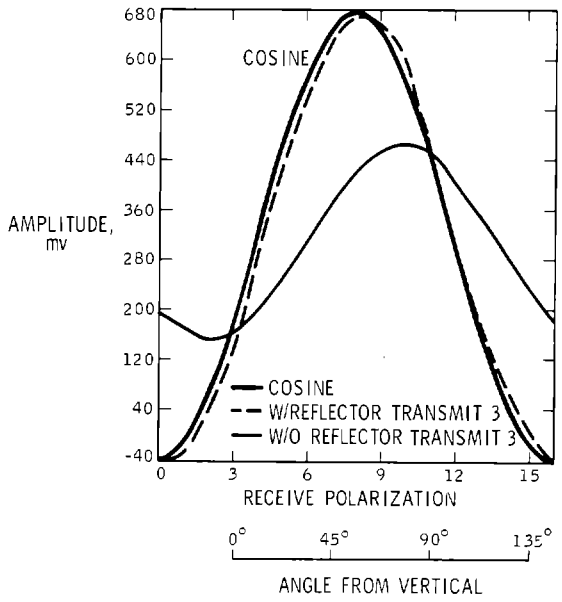

Figure 12. The radar signal obtained with a Luneberg lens reflector is compared to the background signal without the reflector and to a cosine function of arbitrary amplitude and phase.

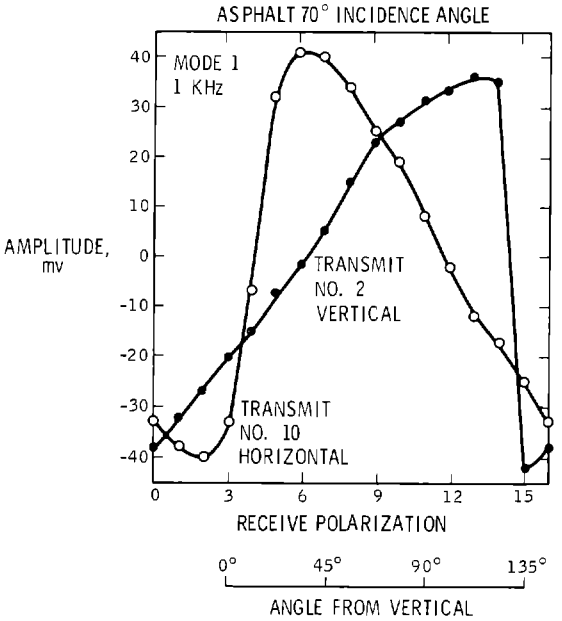

Figure 13. These radar backscatter amplitude curves were obtained for an asphalt surface observed at a 70° incidence angle while operating in Mode 1 at 1 KHz with slow polarization scan. The radar transmitted polarization was horizontal for the open points and vertical for the filled points.

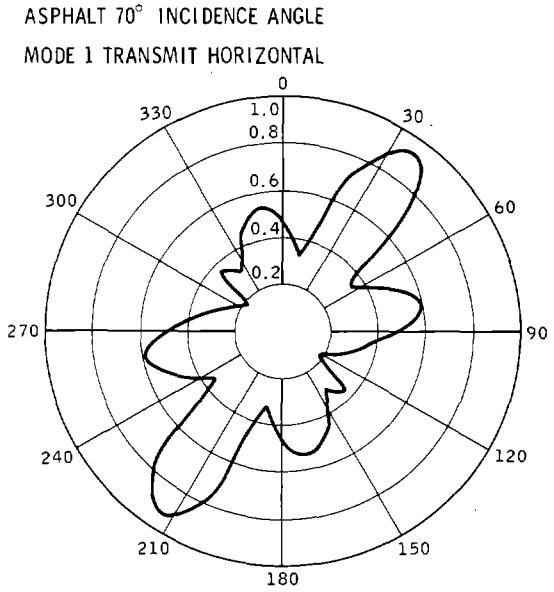

Figure 14. The relative power is plotted as a function of received polarization angle for an asphalt surface observed at a 70° incidence angle while operating in Mode 1 at 1 KHz with slow polarization scan, transmit horizontal polarization.

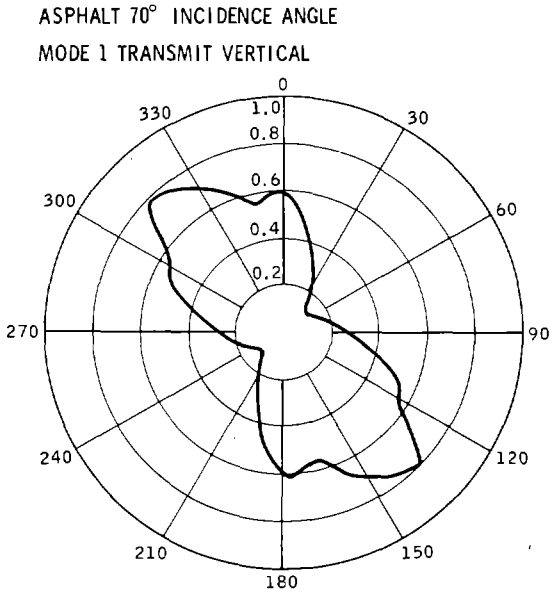

Figure 15. The relative power is plotted as a function of received polarization angle for an asphalt surface observed at a 70° incidence angle while operating in Mode 1 at 1 KHz with slow polarization scan, transmit vertical polarization.

☆ U. S. GOVERNMENT PRINTING OFFICE: 1972—770-624